GRANITOID GEOCHEMISTRY AND LATE ARCHEAN CRUSTAL EVOLUTION IN THE CENTRAL SLAVE PROVINCE

WILLIAM JAMES DAVIS

NOTICE

The quality of this microform is heavily dependent upon the quality of the original thesis submitted for microfilming. Every effort has been made to ensure the highest quality of reproduction possible.

If pages are missing, contact the university which granted the degree.

Some pages may have indistinct print especially if the original pages were typed with a poor typewriter ribbon or if the university sent us an inferior photocopy.

Reproduction in full or in part of this microform is governed by the Canadian Copyright Act, R.S.C. 1970, c. C-30, and subsequent amendments.

AVIS

La qualité de cette microforme dépend grandement de la qualité de la thèse soumise au microfilmage. Nous avons tout fait pour assurer une qualité supérieure de reproduction.

S'il manque des pages, veuillez communiquer avec l'université qui a conféré le grade

La qualité d'impression de certaines pages peut laisser à désirer, surtout si les pages originales ont été dactylographiées à l'aide d'un ruban usé ou si l'université nous a fait parvenir une photocopie de qualité inférieure.

La reproduction, même partielle, de cette microforme est soumise à la Loi canadienne sur le droit d'auteur, SRC 1970, c. C-30, et ses amendements subséquents

Granitoid Geochemistry and Late Archean Crustal Evolution in the Central Slave Province.

A thesis submitted to the School of Graduate
Studies in partial fulfillment of the requirements for the degree of
Doctor of Philosophy

Department of Earth Sciences
Memorial University of Newfoundland
May 1991

St. John's Newfoundland

ISBN 0-315-73311-X

Canada

Abstract

The Contwoyto-Nose Lakes area in the central Slave Province is a Late Archean granite-greenstone terrain consisting of metavolcanic (Central Volcanic Belt) and metasedimentary rocks extensively intruded by syn- to post-deformation granitoid rocks. The latter, representing over 65% of exposed crust in the area, were emplaced between 2616 and 2585 Ma, post-dating the earlier (*ca.* 2670-2650 Ma) assemblage by more than 35 m.y.

Plutonic rocks in the area are subdivided into 8 suites. Four of the suites are strongly deformed and recrystallized, and are temporally linked to the supracrustal assemblage (van Breemen *et al.*, 1990). These include: 1) hornblende diorites of the Central Volcanic Belt (CVB) Suite; 2) quartz porphyritic trondhjemitic plutons of the Gondor Suite; 3) biotite tonalites to monzogranites of the Wishbone Suite; and, 4) biotite tonalites of the Olga Suite. Two suites, the Siege and Concession, are interpreted to have been emplaced syn- to late- during the regional metamorphism and deformation, whereas the Yamba and Contwoyto Suites post-date this event. The Siege Suite consists of leucocratic biotite tonalite. The Concession Suite is predominantly tonalite but ranges from hornblende diorite to biotite granodiorite compositions. These rocks define prominent aeromagnetic highs and commonly form composite bodies. In many cases, plutons are tabular-shaped, with long dimensions parallel to the regional foliation (S_2). Two samples have yielded U-Pb ages of 2608±1 and 2608+5/-3 Ma. The Yamba Suite consists dominantly of red weathering, biotite monzogranites and associated pegmatites. The Contwoyto Suite, on the other hand, contains primary muscovite and biotite (± tourmaline) and is grey-green weathering. Pegmatites are a ubiquitous feature of the suite. One sample of the Yamba and 3 samples of the Contwoyto Suite have yielded U-Pb ages within error of *ca.* 2582-2585 Ma.

Rocks of the CVB are calc-alkaline and most have trace element characteristics diagnostic of rocks formed in modern supra-subduction zone settings. The felsic plutonic suites include low-Al_2O_3 (Gondor, Wishbone Suites) and high-Al_2O_3 (Olga Suite) trondhjemites. The former have high abundances of HFSE and REE and are compositionally similar to rocks from Phanerozoic ophiolites, ridges and island arc

settings. They are interpreted to have formed by low pressure, partial melting of mafic protoliths leaving a pyroxene- and plagioclase-dominated residue. In contrast, the high-Al_2O_3 trondhjemites have steep REE patterns with low abundances of the HREE and are interpreted to have formed by melting of garnet-bearing mafic protoliths.

The Siege Suite has characteristics of high-Al_2O_3 trondhjemites and may also have formed by partial melting of garnet-bearing mafic crust. The Concession Suite is calc-alkaline and varies from metaluminous to weakly peraluminous with increasing SiO_2 content (50-72 wt%). The suite is characterized by high contents of Sr (up to 1600 ppm), Ba (up to 2000 ppm), and Ce (up to 170 ppm), high $(Ce/Yb)_N$, low Rb/Sr (<0.3), no or small negative Eu anomalies and pronounced negative Nb anomalies. Mafic samples are most enriched in trace elements; Sr, Ba, Y and the REE show a continuous decrease with increasing SiO_2. Although the REE characteristics are consistent with those predicted in melts of garnet-bearing mafic crust, the chemical variation within the suite cannot be accounted for by variable degrees of melting of basalt. The tonalites can however, be related to the mafic end members by assimilation and fractional crystallization (amphibole-plagioclase dominated) processes. The composition of potential parental magmas is similar to some high-Mg andesites (HMA; *e.g.* sanukitoids, bajaites) derived from melting hydrated enriched peridotite. The juvenile $\epsilon_{Nd(t)}$ values measured for the suite limit the mantle enrichment event to the 200 m.y. preceding magmatism. The HFSE characteristics suggest mantle enrichment may have been subduction-related.

Post-deformation plutonic suites are high SiO_2 (68 to 78 wt%) and peraluminous. The Yamba Suite is K_2O-rich with high Rb/Sr ratios and strongly negative Eu and Sr anomalies relative to enriched REE patterns. The Contwoyto Suite is, in general, less potassic and more strongly peraluminous. REE patterns are variable, probably reflecting the evolution of fluid phases and pegmatite formation. $\epsilon_{Nd(t)}$ values for both suites exhibit a wide range from positive (+3.7) to negative values (-5.1). The Contwoyto Suite has been modelled as partial melts of dominantly metasedimentary protoliths, possibly similar to the exposed turbidite sequences. The origin of the Yamba Suite is more equivocal. The spatial association with the earlier mantle-derived

Concession Suite and their compositional similarity to granites of hybrid origin suggest that they may be products of the mixing and homogenization of mantle-and crust-derived materials. The negative $\epsilon_{Nd(t)}$ values for some of these rocks require that the crustal component had a significant pre-history (> 400 m.y.).

Nd isotopic data from representative rock types along an E-W traverse at 65° N across the central part of the province reveal distinctly different characteristics in the east compared to the west. Supracrustal and plutonic rocks from the east have positive $\epsilon_{Nd(t)}$ values consistent with juvenile sources and formation remote from significantly older crust. In contrast, samples of post-deformation granites west of 110°30'W have negative $\epsilon_{Nd(t)}$ values. The Nd isotopic data for these granitoid rocks reflect the presence of mixed crustal sources dominated by Mid to Early Archean crust or derivative sediments. The asymmetric pattern defined by the Nd isotopic data suggests the presence of distinct crustal blocks beneath the Slave Province, as predicted by models proposing tectonic assembly of the province through accretion of juvenile crust to an older continental mass.

The secular evolution in the mineralogy and geochemistry of the plutonic suites reflects a change from dominantly mantle- to crustal-derived plutonism. Igneous rocks of the early assemblage are interpreted to be remnants of an allocthonous island arc terrane, which was accreted to a continental block during the late Archean deformation. Crustal shortening and thickening during collision caused melting of previously subduction-modified mantle to generate HMA magmas, possibly by the detachment of the lower part of the lithosphere (e.g. Houseman *et al.*, 1981). Intrusion of these mantle-derived magmas into the crust, in combination with crustal thickening, caused crustal melting and the generation of peraluminous granites. The nature and evolution of the granitoid rocks is comparable to features of more recent collisional orogenic belts. This interpretation suggests that the tectonic and related igneous processes leading to crustal stabilization in the Late Archean Slave Province were relatively similar to those in modern orogenic belts, which implies a continuity in process for the last 2.7 Ga.

Acknowledgements

I would like to express my thanks to my supervisors Dr. B.J. Fryer, Dr. T. Rivers and Dr. G. Dunning for their participation. Dr Fryer was particularly generous in supporting my research activities and providing financial support during the last 6 months. NSERC is thanked for financial support in the form of a 1967 Scholarship. I am particularly indebted to Dr. J. King (GSC) for tremendous field and logistical support, as well as enthusiasm. Dr. G.A. Jenner introduced me to the analyses of Nd isotopes and provided many stimulating arguments. Dr O. van Breemen (GSC) dated the plutonic rocks in support of this project, and was always interested in my evolving ideas on the evolution of the Slave Province. Dr J. Mortensen provided ages for the Central Volcanic Belt. Dr E. Hegner (GSC now at Universitaat Tubingen) analysed some of the samples for Nd isotopes and provided his unpublished data from the eastern Slave Province which were used in Chapter 7. His comments on my interpretation of the Nd isotopic data were appreciated. Dr H. Longerich is thanked for his contagious enthusiasm and help with all things analytical.

The assistance of mapping colleagues Janet King, Carolyn Relf, Tim van Nostrand, Mike Wingate, Janien Schwartz, Ron Avery, Debbie Macphedron, Anne Seguin and Debra Lemkow during the coarse of the three field seasons was greatly appreciated. Gert Andrews is thanked for performing the major element analyses, Geoff Veinnot for assistance with XRF analyses, and Dr. Simon Jackson for ICP-MS analyses. Pam King, Pat Horan and Bill Gosse were always helpful in the laboratory. Daryl Clarke is thanked for computer assistance, especially with NEWPET during its formative years. Wilf Marsh provided photographic services. Members of the general office staff were always helpful and accomodating.

I would also like to thank my fellow graduate students for their advice, assistance and friendship. In particular the residents of the S.J. Carew basement corridor during the long winter of 90-91; in order from west to east, Jereon van Gool, David Pitman, Steve Edwards, Adam Szibinski and David van Everdingen.

Most importantly I thank my wife, Heather Ballantyne for putting up with my summer absences, the lack of time to do fun things and the duration of this project.

Table of Contents

List of Figures

List of Tables

List of Abbreviations and Symbols

Ab	Albite
Allan	Allanite
Amph	Amphibole
An	Anorthite
Apat	Apatite
Bt	Biotite
Bulk D	$\sum_{i=1}^{n} Kd_i \cdot M_i$ where M_i = modal amount and Kd_i = partition coefficient for phase i.
CHUR	Chondritic uniform reservoir
Cpx	Clinopyroxene
CVB	Central Volcanic Belt
$\epsilon_{Nd(t)}$	Initial Nd composition of sample relative to CHUR (Appendix 3)
$f_{Sm/Nd}$	147Sm/144Nd of sample relative to CHUR value (Appendix 3)
HFSE	High Field Strength Elements
HMA	High-Mg andesite
HREE	Heavy rare earth elements (Ho-Lu)
HTLP	High temperature/low pressure
K-spar	Alkali feldspar
Kb	kilobar
K_d	partition coefficient
LFSE	Low field strength elements
LILE	Large ion lithophile elements
LREE	Light rare earth elements (La-Nd)
MORB	mid-ocean ridge basalt
MREE	Middle rare earth elements (Sm-Dy)
Na-HMA	Na-rich high-Mg andesite
Oliv	Olivine
Opx	Orthopyroxene
Or	Orthoclase
Plag	Plagioclase
PLM	Pellatt Lake Monzogranite
Pre-YKS	Rocks predating the Yellowknife Supergroup
REE	Rare earth elements
T_{DM}	Depleted mantle model age (Appendix 3)
Titan	Titanite
WM	Wolverine Monzogranite
YKS	Yellowknife Supergroup

Chapter 1

Introduction

1.1 Granitoid Rocks and Continental Crust Formation

Continental crust is formed as a consequence of orogenic processes. During the Phanerozoic and Proterozoic, crust-formation is thought to have dominantly occurred along convergent continental margins by tectonic accretion of crustal material, metamorphism and syn- to post-deformation magmatic intrusion and underplating. These processes are closely linked to lateral plate movements and subduction. A large percentage of the present mass of continental crust was formed during the Late Archean (Taylor and McLennan, 1985), however, there remains no consensus on how and in what type(s) of tectonic setting(s) this may have occurred. Did Late Archean crust develop in response to plate tectonic processes fundamentally similar to those observed today (Kroner, 1991; Nisbet, 1987; Burke *et al.*, 1976) or were crust-forming processes in the Late Archean unique to the early history of the Earth? The answer to this question is fundamental to understanding the Earth's chemical and tectonic evolution.

The generation of granitoid rocks is one of the principal mechanisms which differentiates and stabilizes continental crust, as orogenic belts of all ages consist of large volumes of granitoid rocks. Since many granitoid rocks are derived wholly, or in part, from partial melting crustal rocks (Pitcher, 1987), the study of their petrogenesis and isotopic systematics can provide useful constraints on the composition and nature of the underlying crustal section. Specifically, petrogenetic models of granitoid rocks can be used to evaluate the nature and composition of source regions (mid to lower crust), the relative involvement of mantle and crustal material and the extent of recycling of old crust (Vidal, 1987; Allègre and Ben Othman, 1980; Farmer and DePaolo, 1983; 1984; Bennett and DePaolo, 1987). The relationship of plutonism to deformational and metamorphic events, and changes in pluton chemistry with time reflect changes in the compositional or thermal structure of the crust and upper mantle in response to tectonic processes. This, in turn, imposes constraints on the roles of processes such as lateral

accretion of crustal blocks, crustal thickening due to collision and crustal heating due to magmatic underplating. Understanding the nature and evolution of plutonism is an important constraint in understanding crust formation and in reconstructing the tectonic evolution of an orogenic belt.

Granitoid rocks make up a significant portion of the exposed crust in the Late Archean Slave Province (Figure 1.1), however, their origin is presently poorly constrained. The petrogenesis of these granitoid rocks has not been used to constrain, nor has it been fully incorporated within, tectonic hypotheses for the development of the Province. This information is particularly relevant because it may be used to address the contrasting hypotheses currently proposed for the tectonic development of the province: 1) ensialic rifting (Henderson, 1981; Easton, 1985; Thompson, 1989); or 2) tectonic assemblage by accretion similar to modern subduction-related tectonics (Kusky, 1989; Hoffman, 1986; Fyson and Helmstaedt, 1988). The models predict different crustal structures (Figure 1.2), which may be reflected in the granite geochemistry. In particular, the identification of distinct lower crustal blocks analogous to those observed in modern accretionary margins (Farmer and DePaolo, 1983). Establishing if the Slave Province was formed by lateral accretion has important implications not only for the tectonic history of the province but also in establishing whether a continuity in crust-formation processes exists, at least from the Late Archean to the present.

1.2 Subject and Scope of the Thesis

This thesis reports the results of an integrated field, geochemical and isotopic study of granitoid rocks generated during the major Late Archean crust forming event in the central Slave Province. The purpose of the study is to document and evaluate the nature and evolution of granitoid magmatism leading to stabilization of crust, and to use this information to examine broader tectonic questions concerning the evolution of the province. The study area, within the Contwoyto Lake-Nose Lake area (NTS 76E and west half of 76F; Figure 1.3), is well situated to address some of the problems outlined above as it extends more than 150 km across the structural trend of the province, from areas close to documented outcrops of 'basement' rocks in the west to areas with no

evidence for older rocks in the east. Additional sampling, to the east and west of the area of detailed study, completes a transect of the province. This transect crosses a proposed suture between an older crustal block (refered to as the Anton Terrane by Kusky, 1989) in the west and newly-formed, accreted crust in the east (Contwoyto Terrane; Kusky, 1989; Figure 1.3). In addition, the eastern margin of the area adjoins an area for which a granitoid geochemical database presently exists (Hill and Frith, 1982) - this study essentially completes the first geochemical traverse across the province.

The specific purposes of this study are therefore to:

1) Characterize the intrusive rocks within the central part of the Slave Province in terms of their field relationships, petrography, geochemistry and Neodymium (Nd) isotopic composition.

2) Use whole-rock major, trace and rare earth element (REE) data to evaluate the petrogenesis of the rocks and, employing Nd isotopes, to examine the relative contributions of mantle and crustal components, and thereby, infer the crustal residence time of the source regions.

3) Utilize the above data to evaluate the more general problem of the crustal evolution of the central Slave Province, and test the ensialic rift and accretionary tectonic models.

1.3 Organization of the Thesis

The thesis consists of four parts.

1) Chapters 2 and 3 establish the geological framework upon which the geochemical studies are based. Chapter 2 presents a brief summary of the geology of the Slave Province. Chapter 3 describes the results of the field studies; the setting and regional geology of the study area, the rationale for subdivision of plutonic rocks into suites and the field and petrographic characteristics of each suite. The subdivision of plutonic rocks serves as a framework for presentation and discussion of the geochemical data in following chapters. The field work was done in

conjunction with a regional mapping project of Dr. Janet King (Geological Survey of Canada). The author spent a total of nine months mapping in collaboration with Dr. King.

2) Chapters 4 through 6 present the geochemical data, each chapter corresponding to a temporally distinct event as described in Chapter 3. Chapter 4 describes volcanic rocks and those plutonic rocks interpreted to be syn-volcanic. Chapter 5 describes the syn- to late-deformation plutonic suites and Chapter 6 the post-deformation plutonic suites. Each chapter is self contained; all the geochemical data available for each suite is presented and petrogenetic models are constructed and discussed.

3) Chapter 7 presents the results of a Nd isotopic tracer study undertaken to test the proposed tectonic models for the development of the province.

4) Chapter 8 integrates the results presented in previous chapters and discusses their implications for the crustal evolution and tectonic development of the central Slave Province.

Figures are located at the end of each of the respective chapters. Tables are included within the text.

Appendix 1 describes the sample preparation procedures, analytical techniques and states the precision and accuracy of the various analytical procedures used in this study. The full geochemical database and sample locations are presented in Appendix 2. Nd isotope analytical procedures and nomenclature are given in Appendix 3. Partition coefficients and trace element modelling techniques are discussed in Appendix 4. Trace element normalizing values for primitive mantle, chondrite and mid-ocean-ridge basalt reservoirs are listed in Appendix 5.

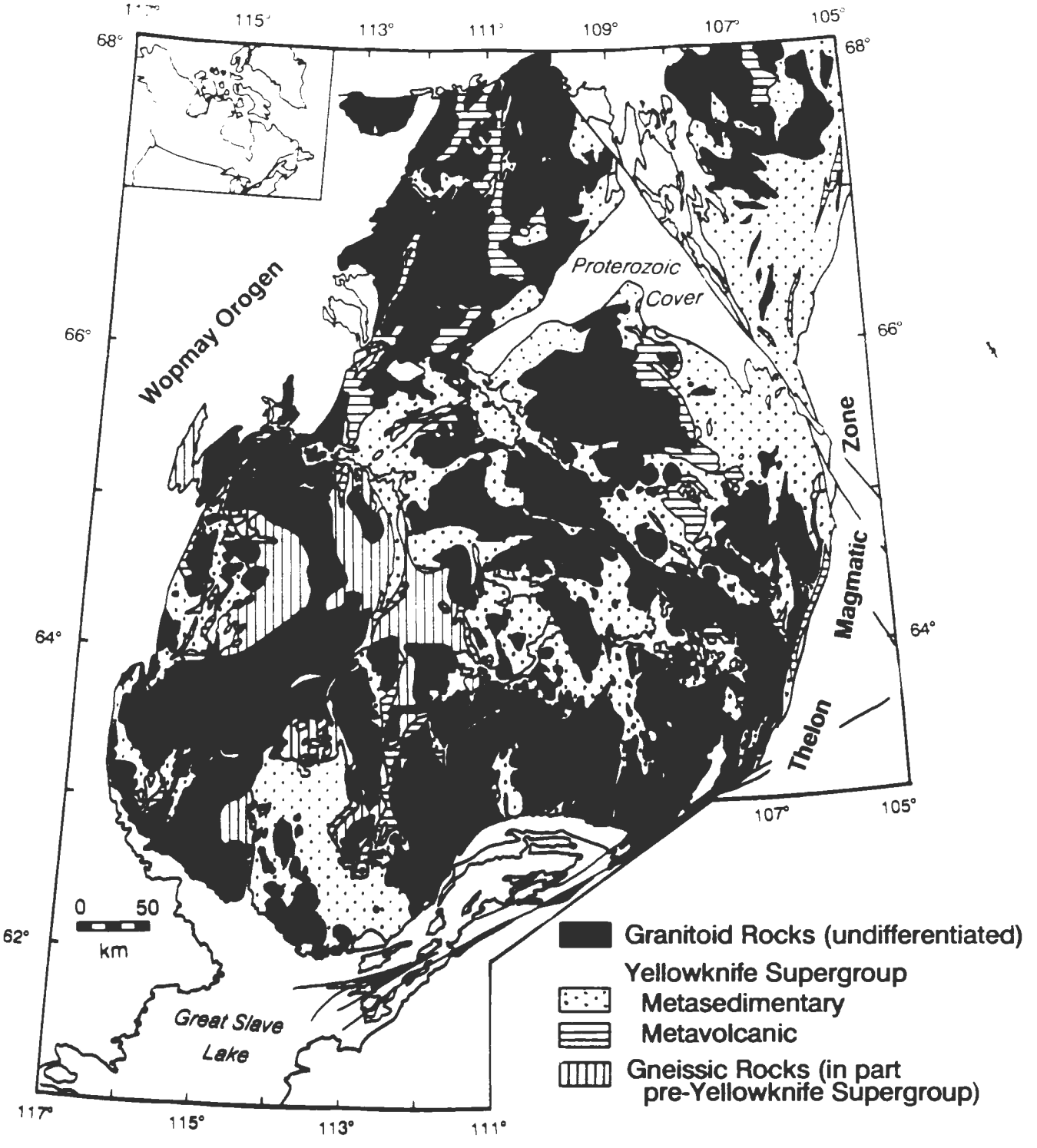

Figure 1.1. Simplified geological map of the Slave Province showing four principal lithological units (after Hoffman, 1989). Location map in inset.

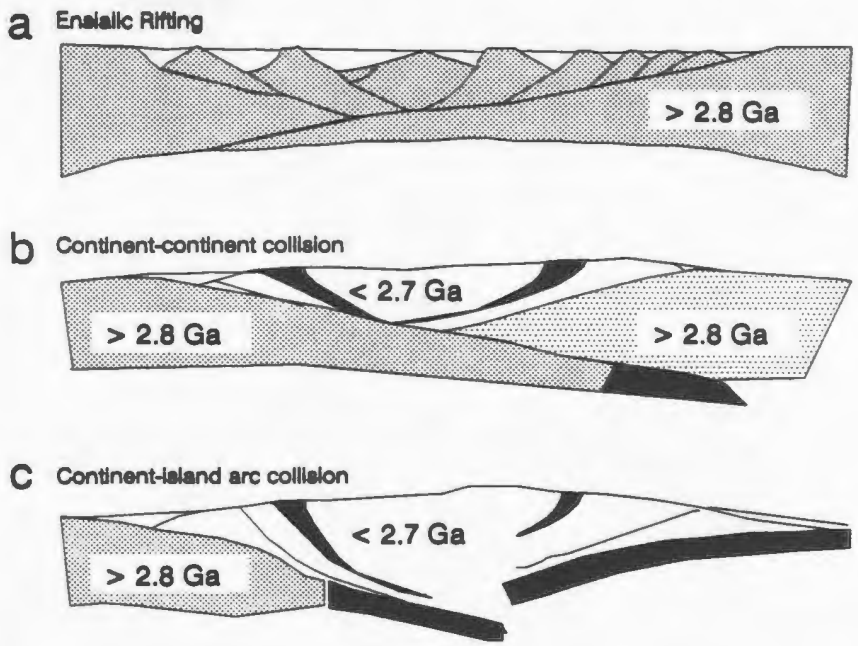

Figure 1.2. Schematic representation of crustal sections predicted by different tectonic models proposed for the evolution of the Slave Province. The ca. 2630-2580 granitoid rocks are not shown.

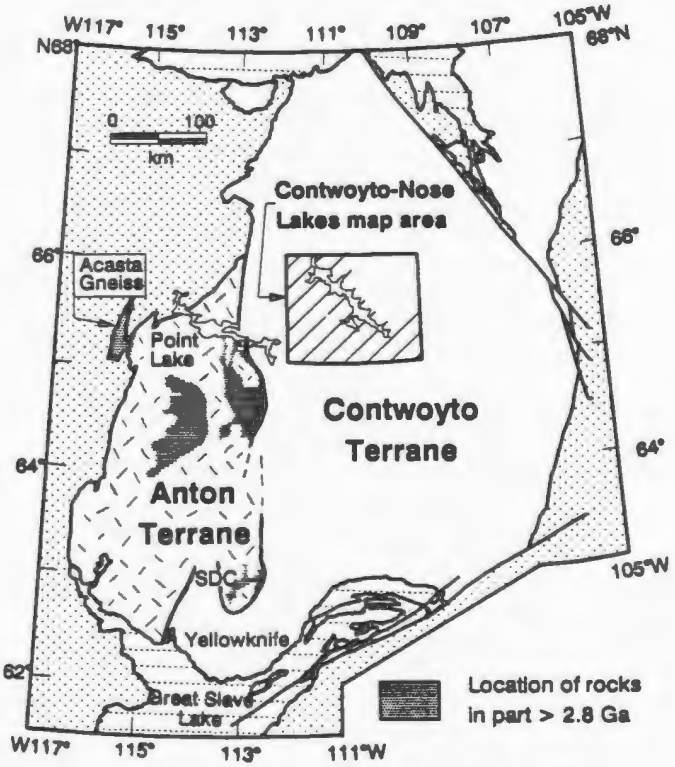

Figure 1.3. Location of the Contwoyto-Nose Lakes study area (NTS 76E and southwest quadrant of 76F)(cross hatched field). Anton and Contwoyto Terranes and terrane boundary are shown as proposed by Kusky (1989, 1991). SDC = Sleepy Dragon Complex.

Chapter 2

Geology of the Slave Province

2.1 Introduction

The Slave Structural Province is an Archean (2.7 - 2.5 Ga) granite-greenstone terrane which occupies an area of 190,000 km² in the northwestern Canadian Shield (Figure 1.1). The province is bounded to the east by the Thelon Tectonic Zone (TTZ) and to the west, the Wopmay Orogen, both early Proterozoic orogenic belts (Hoffman, 1989).

2.2 Regional Geology

The geology of the Slave Province (Figure 1.1) is typical of Archean granite-greenstone terranes (*e.g.* Condie, 1981) and consists of sedimentary (generally turbiditic) and volcanic sequences intruded by granitoid rocks. Recent summaries of various aspects of the geology of the Slave Province have been presented by Henderson (1985), Fyson and Helmstaedt (1988), Hoffman (1989), Thompson (1978) and Padgham (1981, 1985). The province can be broadly subdivided into three geological groups: 1) syn- to post-deformation granitoid rocks; 2) supracrustal rocks (metasedimentary, metavolcanic and syn-volcanic plutons) included in the Yellowknife Supergroup (YKS); and 3) pre-Yellowknife Supergroup rocks.

2.2.1 Post-Yellowknife Supergroup Granitoid Rocks

Approximately 50% of the province is composed of Late Archean granitoid rocks ranging in composition from gabbro to syenogranite. The majority of the plutons were emplaced between 2630 and 2580 Ma (Figure 2.1; van Breemen and Henderson, 1988; van Breemen *et al.*, 1987a, b; 1990; Henderson *et al.*, 1987). Field characteristics (King *et al.*, 1988, 1989, 1990; Hill and Frith, 1982; Henderson, 1985), in conjunction with detailed geochemistry (Davis *et al.*, 1990; Hill and Frith, 1982; Frith and Fryer, 1985) and geochronology (references above) allow a simplified, but effective two-fold subdivision of granitoid rocks: 1) syn- to late-deformation, metaluminous to weakly peraluminous, biotite and hornblende diorite to granodiorite (low K) and; 2)

post-deformation, peraluminous, biotite ± muscovite tonalite to syenogranite (high K). The available U-Pb ages indicate that the two plutonic groups were emplaced sequentially with only limited temporal overlap (Figure 2.1).

2.2.2 Yellowknife Supergroup Rocks

Supracrustal rocks outcrop in over twenty geographically separate belts, comprising 50% of the area of the province (Figure 1.1). Supracrustal rocks are collectively grouped as the Yellowknife Supergroup (YKS) owing to lithological similarities throughout the province (Henderson, 1970). In contrast to some other greenstone belt terrains (*e.g.* Superior Province) sedimentary rocks predominate, making up approximately 80% of the supracrustal sequences. In general, the sedimentary rocks are comprised of monotonous sequences of turbidites of mixed volcanic-plutonic provenance (Henderson, 1981). Locally quartzite, conglomerate, carbonate and iron formation are present. Volcanic and syn-volcanic plutonic rocks consist of both tholeiitic bimodal series (*e.g.* Yellowknife; Condie and Baragar, 1974; Cunningham and Lambert, 1989) and calc-alkaline intermediate series (*e.g.* Hackett River; Ewing, 1979; Frith, 1987). The tectono-stratigraphic relationship of sedimentary rocks to volcanic rocks is not well documented.

Present U-Pb geochronology indicates that volcanic rocks formed over a 65 m.y. time period from approximately 2715 to 2650 Ma (Figure 2.1; Mortensen *et al.*, 1988; Isachsen *et al.*, 1990; Henderson *et al.*, 1987; Frith and Loveridge, 1982; van Breemen *et al.*, 1987a; MacFie *et al.*, 1990). There are insufficient, detailed studies of individual volcanic belts to document regional age variations within the province. Mortensen *et al.*, (1988) suggested, on the basis of a single age determination of a felsic porphyry at Point Lake (2827 Ma), that an older supracrustal sequence may exist at Point Lake.

The metasedimentary turbidite rocks are not dated and are only constrained to be older than *ca.* 2630 Ma, the age of the oldest syn-deformation plutonic rock intruding the sedimentary rocks. Limited detrital grain studies indicate that the metasedimentary rocks contain zircons equivalent in age to the volcanic rocks and one sample from the

western part of the province contains a minor fraction from an older (> 3.0 Ga) component (Shärer and Allègre, 1982). The turbidites could have been deposited at any time between the age of associated volcanic rocks and the time of deformation and plutonism.

The supracrustal rocks are deformed by multiple sets of isoclinal folds, cleavages and faults that have been re-folded by regional, open cross-folds (Relf, 1989; Fyson and Frith, 1979; Fyson and Helmstaedt, 1988). Metamorphism is of the low pressure/high temperature type, with grade ranging from greenschist to upper amphibolite facies (Thompson, 1978; 1989). The age of metamorphism is not precisely constrained. Monazite in a pre-Yellowknife Supergroup gneiss (2989 Ma, U-Pb zircon) has been dated at 2600 Ma, and has presumably been reset by the Late Archean metamorphism (Frith and Loveridge, 1982). Similarly, metamorphic monazite from the Sleepy Dragon Complex yield ages of 2588 Ma (James and Mortensen, 1991).

2.2.3 Pre-Yellowknife Supergroup Rocks

Exposures of Mid to Early Archean rocks, pre-dating the YKS, are so far restricted to the western margin (west of approximately 112°30' W) of the province (Figure 1.1; Baragar and McGlynn, 1974; Hoffman, 1989). The rocks consist of banded amphibolitic-tonalitic gneisses, tonalitic gneisses, and massive tonalites to granites (Davidson, 1972; Easton, 1985; Henderson, 1985). Geochronologic studies have identified a range of ages between 2840 and 3960 Ma (Figure 2.1; Krogh and Gibbons, 1978; Nikic *et al.*, 1980; Henderson *et al.*, 1982, 1987; Chamberlain *et al.*, 1984; Frith *et al.*, 1986; Bowring *et al.*, 1989a, b). The range in ages suggests that the "basement" was not stabilized at one time but is made up of a complex collage of Late, Mid and Early Archean rocks. The relationship of these rocks to each other is not constrained. In addition, their relationship to the overlying YKS rocks is not clearly established. These rocks have been interpreted to be autochthonous basement to the YKS (Stockwell, 1933; Baragar and McGlynn, 1974; Easton 1985), however, in most

cases the contacts between the gneisses and the YKS are faulted and they could equally well be structurally juxtaposed (Kusky, 1989, Lambert and van Staal, 1987; James, 1990).

2.2.4 Summary of Geological Evolution

1) Early gneisses and granitoid rocks range in age from 2.82 to 3.96 Ga, 150 to 1200 m.y. older than the volcanic rocks of the greenstone belts.

2) Volcanism occurred over a 65 m.y. period from 2715 to 2650 Ma. Available data are insufficient to document regional age differences between volcanic belts.

3) Sedimentary rocks are only constrained to be older than *ca.* 2630 Ma, the age of the oldest syn-deformation plutonic rock intruding the sedimentary rocks. Limited detrital grain studies indicate that the metasedimentary rocks contain zircons equivalent in age to the volcanic rocks and one sample from the western part of the province contains a very minor fraction from an older (>3.0 Ga) component (Shärer and Allègre, 1982).

4) Syn- to post-deformation plutonism occurred across the Slave Province from 2.63 to 2.58 Ga, post-dating volcanism by 30 to 135 m.y. On the basis of the present data set, plutonism occurred contemporaneously across the province and there is no indication of a migration of intrusive activity across the region with time.

2.3 Tectonic Models Proposed for the Development of the Slave Province

Tectonic models currently proposed to explain the geological evolution outlined above can be separated into two contrasting types: ensialic rifting (Henderson, 1981; Easton, 1985; Thompson, 1989), and; continental margin or island arc/marginal basin accretionary processes (Folinsbee *et al.*, 1968; Hoffman, 1986; Fyson and Helmstaedt, 1988; Kusky, 1989). The latter hypothesis is strictly analogous to processes of crustal stabilization observed along convergent margins today. Rift (or plume-related) and accretionary models have both been proposed to explain Late Archean granite-greenstone terranes from throughout the world (Kroner, 1991; de Witt and Ashwal, 1986). Unfortunately, at least in the Slave Province, the stratigraphic and

structural information on a province-wide scale has proven insufficient to unambiguously distinguish between the models. Basement/cover unconformities, the underpinnings of rift models, are in contention. Structural elements generally associated with tectonic accretion, *ie.* melanges, ophiolites and major thrust faults, have been proposed, but are also not well documented (Helmstaedt *et al.*, 1986; Kusky, 1989a,b; King *et al.*, 1989b).

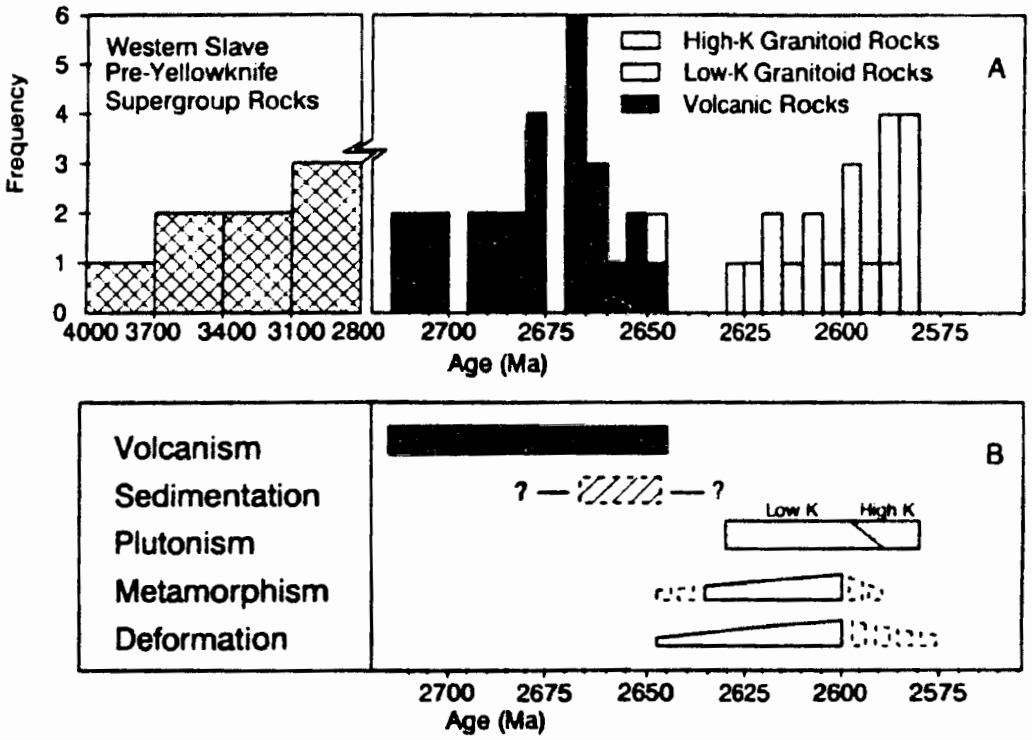

Figure 2.1. A) Frequency diagram of published U-Pb zircon and monazite ages from the Slave Province (sources of data: van Breemen et al., 1987a, b; 1990; Bowring quoted in Padgham, 1985; Culshaw and van Breemen, 1990; Lambert and Henderson, 1980; Frith and Loveridge, 1982; Frith et al., 1986; Krogh and Gibbons, 1978; Bowring and van Schmus, 1984; Nikic et al,. 1980; Henderson et al., 1982, 1987; Isachsen et al., 1990; Mortensen et al., 1988; Bowring et al., 1990a, b; Mortensen pers comm. 1991). B) Interpreted timing of geological events in the Slave Province based on the U-Pb geochronology.

Chapter 3

Regional Geology and Description of Plutonic Suites in the Contwoyto-Nose Lakes Area

3.1 Introduction

The objectives of this Chapter are to: 1) summarize the regional geology of the Contwoyto-Nose Lakes area, central Slave Province, with particular emphasis on setting the geological framework for discussion of the plutonic rocks; 2) present the methodology used to subdivide the plutonic rocks into suites; 3) describe the field characteristics (composition, principal mineralogy, textures, fabrics, intrusive style, relationships to regional structural elements, relative chronology, spatial distribution and abundance) of each of the eight plutonic suites; and 4) summarize the results of U-Pb geochronology (van Breemen *et al.*, 1990) within the previously described framework. The chapter provides the geological framework upon which later petrogentic interpretations are based.

The field work was carried out over three summers (1987-89) within the regional mapping project of Dr. J.E. King of the Geological Survey of Canada. U-Pb geochronology in support of the field studies was done by Dr. O. van Breemen of the Geological Survey of Canada.

3.2 Regional Geology Contwoyto-Nose Lake Area

3.2.1 Previous Work

Previous work in the area was limited to 1:500,000 scale helicopter reconnaissance mapping (Fraser, 1964), 1:250,000 scale mapping of the western portion of the area (Bostock (1980) and 1:50,000 scale mapping of the area immediately around the Lupin mine site (Tremblay, 1976). Regional scale maps of areas adjoining the southern (Folinsbee, 1949) and western (Frith, 1987) map boundaries are also available. Relf (1989; 1990) has presented summaries of the structural and metamorphic history of the

supracrustal rocks at Contwoyto Lake. Preliminary results of 1:100,000 scale mapping of the area (Figure 3.1) supporting the current study are reported in (King *et al.*, 1988; 1989a; 1990).

3.2.2 Geological Overview of the Area

The geology of the Contwoyto-Nose Lakes area consists of an older tectono-stratigraphic assemblage of deformed and metamorphosed volcanic, plutonic and sedimentary rocks (Yellowknife Supergroup) which has been extensively intruded by a younger assemblage of syn- and post-deformation plutonic rocks (Figure 3.1, 3.2). Sedimentary rocks make up approximately 30%, volcanic rocks 5% and plutonic rocks 65%, of the area mapped (Figure 3.2). There is no evidence for rocks predating the supracrustal rocks, although older rocks are exposed at Point Lake, 40 km west of the area (Stockwell, 1933; Easton, 1985). Figure 3.2 is a schematic summary of the geological evolution of the area which serves as a guide to the brief geological summary below.

3.2.3 The Older Tectono-Stratigraphic Assemblage

Yellowknife Supergroup Rocks

The Yellowknife Supergroup within the area consists of metavolcanic rocks and two formations of metasedimentary rocks (Contwoyto Fm. and Itchen Fm.; Bostock, 1980) belonging to the Cogead Group (Henderson, 1988). For reasons described below, a number of plutonic rocks are also considered part of this older assemblage.

The metavolcanic rocks principally outcrop within an elongate zone in the centre-west of the map area, termed the Central Volcanic Belt (CVB; Bostock, 1980). The belt comprises mafic, intermediate and felsic lavas and pyroclastic rocks with a high proportion of intercalated epiclastic rocks. These latter rocks include turbiditic sediments, conglomeratic debris deposits, and tuffaceous rocks of unknown origin (Bubar and Heslop, 1985; King *et al.*, 1988). A characteristic feature of the belt is the high proportion of epiclastic rocks (King *et al.*, 1988). The internal stratigraphy of the belt has not been mapped in detail.

Metasedimentary rocks of the Coghead Group occur above the volcanic rocks (Bostock, 1980). The relationship (*ie.* stratigraphic or tectonic) between volcanic and sedimentary formations is poorly constrained (King *et al.*, 1988). Both the Contwoyto and Itchen Formations comprise intercalated psammitic and pelitic beds which have structures indicative of deposition by turbidity currents (Bostock, 1980; King *et al.*, 1988; Relf, 1989) and all facies are distal. Bostock (1980) subdivided the rocks into formations on the basis of the presence (or absence) of stratigraphic iron formation. The Contwoyto Formation was defined as containing iron formation (Bostock, 1980). King *et al.* (1988; 1989a) also suggested that the Itchen formation is generally thicker bedded (0.1 to 1 m) than the Contwoyto Formation. Stratigraphic thickness of the formations cannot be determined owing to complex deformation. The stratigraphic and sedimentologic relationship between the two formations is unconstrained (King *et al.*, 1988; Relf, 1989; 1990).

3.2.4 Structural History

Detailed descriptions of structural elements within the area have been given by King *et al.* (1989a) and Relf, (1989; 1990). Structural elements are assigned to four groups:

D1 pre-thermal-peak isoclinal folding (F1), faulting and development of penetrative axial planer cleavage (S1).

D2 syn-thermal-peak isoclinal folding (F2), development of an axial planar cleavage (S_2) and limb-parallel faulting. The S_2 surface generally transposes S1 and is typically the dominant tectonic fabric throughout the map area.

D3 post-thermal-peak open folding (F3) and crenulation cleavage development. These structures are domainal with axial traces oriented NE or NW.

D4 brittle-plastic strike slip faulting along dominantly NE structures. These faults cut all Archean lithologies and may be associated with Proterozoic deformation (King *et al.*, 1989a).

3.2.5 Metamorphic History

Metamorphic grade ranges from sub-biotite (lower greenschist facies) to sillimanite/partial melt (upper amphibolite facies). Most of the area is above the sillimanite isograd (Figure 3.1). Textural relationships indicate that peak metamorphic mineral growth post-dates S_1 and is synchronous with S_2 (Relf, 1989). Pressure-temperature estimates range from 2 to 6 kbar and 400° to 700°C (Relf, 1990; Wingate, 1990). High temperature/low pressure metamorphism is typical of the Slave Province in general (Thompson, 1978; 1989).

Metamorphic grade does not increase in spatial association with individual plutons, however plutonic rocks generally outcrop in those areas above the sillimanite isograd. Plutonic bodies that are presently exposed in the center of metamorphic thermal highs in fact post-date the time of peak metamorphic conditions.

3.3 Subdivision of the Granitoid Rocks in the Area

Plutonic rocks have been subdivided into eight suites (Figure 3.2, 3.3); four of which are associated with the early tectono-stratigraphic assemblage. Usage of the term *suite*, in conformity with the recommendations of the North American Stratigraphic code (1983), is entirely descriptive and does not imply any specific genetic relationships.

Plutons were subdivided in the field based on their petrographic characteristics, summarized in chart form in Figure 3.4, mutual cross-cutting relations and their relationship to the regional deformation structures. The methodology for subdivision is outlined in Figure 3.3.

Rock names conform to the recommendations of Streckheisen (1976) (see Figure 3.7). The terms syenogranite and monzogranite are synonymous with granite A and granite B. Rock names were based on visual estimates of modal mineralogy in the field, which were subsequently supported by thin section observations and mesonorm calculations.

3.3.1 Criteria Used to Constrain Relative Timing of Intrusion to Regional Deformations

The following criteria were used to establish the timing of intrusion relative to the regional peak metamorphic deformation event (D2).

Plutons are considered to predate deformation if their metamorphic grade and extent of recrystallization are similar to their host rocks, they contain the regional deformation fabrics (*ie.* S_2), and they do not truncate or contain xenoliths with tectonic fabrics not found in the pluton.

Syn-deformation intrusion is difficult to precisely constrain, however in this study, syn-deformation intrusion is presumed if an intrusive body both utilizes and contains structural surfaces observed in the host rocks. Commonly these plutons contain xenoliths which contain the regional S_2 surface. These plutons have undergone variable amounts of recrystallization but are significantly less recrystallized than the pre-deformation plutons.

Post-deformation intrusions cross-cut regional deformation structures, are generally not foliated, contain foliated xenoliths, overprint syn-deformation metamorphic assemblages, and have a granitic texture.

It is important to note that all of the plutonic rocks have been subjected to some deformation. At least some of the post-deformation plutons have been affected by the D_3 event and locally are folded and may contain weak foliation surfaces. The nomenclature (*ie.* pre-, syn-, post-) used in this thesis refers specifically to the D_2, peak metamorphic deformation event as defined by King *et al.* (1989a).

A relative chronology of intrusion can be devised based on regionally consistent crosscutting field relationships and xenolith suites; schematically in Figure 3.5.

3.3.2 Summary of U-Pb Geochronology

U-Pb geochronology in support of the field work was done by O. van Breemen of the G.S.C.. Representative samples of all the principal suites, excepting the Central Volcanic and Wishbone Plutonic Suites, have been dated (Table 3.1).

Table 3.1 Summary of U-Pb zircon and monazite ages determined for the Plutonic Suites (from van Breemen et al., 1990).

Plutonic Suite	Sample	Rock Type	Age (Ma)
Gondor	D221-87	Q-P Porphyry	2660.4 +0.9/-0.5[z]
Olga	D072a-87	Bt Tonalite	2650 ±5[z]
	D072a-87	Bt Tonalite	2649 ±2[z]
Siege	D217-87	Bt Tonalite	2605-2616[z]
Concession	D218-87	Hb-Bt qtz Diorite	2608 ±1[z]
	D110-88	Bt Tonalite	2608 +5/-3[z]
Yamba	D078a-87	Bt Monzogranite	2582 ±4[m]
Contwoyto	D216-87	Bt-Mu Monzogranite	2585±5[m]
	K193-88	Bt-Mu Monzogranite	2581 +9/-5[m]
	K308-87	Pegmatite	2584 ±4[m]

errors quoted are 2 sigma
z - age determined on zircon
m - age determined on monazite

The principal subdivision of plutonic rocks into two groupings (Figure 3.3) based on the extent of recrystallization and relationship to regional deformation is supported by the geochronologic data. Plutonic rocks that have been extensively recrystallized are older than 2650 Ma; in contrast, weakly or non-recrystallized plutonic rocks are younger than 2616 Ma. Thus, the subdivision corresponds to a temporal gap of at most 34 m.y.

Plutonic rocks spatially associated with the CVB, and interpreted to be temporally related to development of the volcanic belt yield ages slightly younger than that of the dated CVB rhyolite (Mortensen *et al.*, 1988). The Gondor porphyry has been dated at 2660 Ma, and two units of the Olga Suite are both dated at 2650 Ma. These ages,

although slightly younger than the single age from the CVB do overlap with ages determined from volcanic rocks and coeval plutonic rocks from elsewhere in the Slave Province (Figure 2.1).

The subdivision of the younger plutonic rocks into syn- and post- deformation suites is also supported by the available age dating. Samples of plutonic rocks considered to be syn-deformation (*ie.* the Concession and Siege Suites) range in age from 2608 to a maximum of 2616 Ma. In contrast, samples (n=4) of post-deformation plutonic suites (Yamba and Contwoyto) yield ages (monazite) between 2590 and 2580 Ma. The present data from the Contwoyto-Nose Lakes area indicates a time gap on the order of 15 to 20 m.y. between the syn- and post-deformation suites. However, when these data are considered in the context of data available from the whole of the Slave Province, the time gap between the syn- and post-deformation suites is not apparent (van Breemen *et al.*, 1991) and the younger granitoid plutonism appears to be a continuous event from 2630 to 2580 Ma.

The following descriptions of the plutonic suites are presented in a sequence of relative younging based on the field observations and geochronology.

3.4 Plutonic Suites Associated with the Older Tectono-Stratigraphic Assemblage

3.4.1 Central Volcanic Belt Suite

Rocks assigned to this suite are restricted to areas within the Central Volcanic Belt (Figure 3.1). This suite comprises metamorphosed (no relict igneous texture), foliated (commonly lineated) hornblende gabbro to quartz diorite. The metamorphic mineral assemblage is similar to that of the host volcanic rocks. Individual bodies occur as sills, dykes and irregular small plutons on the scale of metres to hundreds of metres in size within the volcanic stratigraphy. In many cases intrusive bodies, particularly sills, are difficult to distinguish from volcanic lithologies. None of these bodies has been mapped out in detail.

Based on their similar metamorphic mineral assemblage, and spatial association with the volcanic belt they are interpreted to be syn-volcanic intrusions. This suite has not been dated, however, felsic volcanic rocks within the associated volcanic belt have been dated at 2667±2 Ma (Mortensen *et al.*, 1988).

3.4.2 Gondor Plutonic Suite

The Gondor Suite comprises quartz-plagioclase porphyritic rocks concentrated in the southwest portion of the CVB, where they intrude the structurally lower portions of the volcanic belt (Figure 3.1).

Lithology

These rocks are all porphyritic and consist of variable proportions of rounded to euhedral quartz and plagioclase phenocrysts (1-4 mm) within a fine grained siliceous granophyric matrix (Figure 3.6a, b). Quartz phenocrysts are distinctly blue coloured. The fine grained matrix makes mineralogical classification difficult, but the rocks are dominantly tonalite on the basis of mesonorm mineralogy (Figure 3.7). Ragged biotite clots are present locally although in most cases they are replaced by chlorite. The phenocryst assemblage is similar to that observed in felsic volcanic rocks within the CVB.

Pluton Morphology, Nature of Contacts and Age

Rocks of this suite make up an extensive dyke and sill network (<1m to 10 m) within the southwestern part of the CVB. Individual bodies range in width from less than 1 m to 10's of m and are continuous along strike . The dykes are concentrated around and extend out from the western and northern margins of a larger body of porphyry, termed the Gondor Porphyry on Figure 3.1. Because of very poor exposure in the area, the form and internal character of this body is unconstrained.

Contacts with host rocks are very sharp. Locally internal and external breccias are developed. The breccias consist of angular fragments of country rocks or porphyritic rocks within a compositionally similar matrix. The angularity of the fragments suggests a

hydrofracturing mechanism. The breccias are similar to those described from ophiolite-related plagiogranites (*e.g.* Lewisporte, Bay of Islands; Malpas, 1979) and may imply high volatile contents at the time of intrusion.

The penetratively deformed nature of the suite and its close spatial association with the volcanic belt suggest that the suite is predeformation and temporally related to the volcanic rocks. The U-Pb zircon age of 2660±1 Ma determined from one sample, intruding the basal part of the volcanic belt is 7 m.y. younger than that determined for the adjacent felsic volcanic rocks (van Breemen *et al.*, 1990; Mortensen *et al.*, 1988).

3.4.3 Wishbone Plutonic Suite

The Wishbone Plutonic Suite comprises massive to foliated, red weathering tonalite to granodiorite and monzogranite. Rocks of this suite principally outcrop in three areas: within the core of the Wishbone dome (Figure 3.1); as smaller bodies west of Contwoyto Lake and in the eastern part of the map area between Nose and Ghurka Lakes (Jaeger Monzogranite, Figure 3.1).

Bodies within the Wishbone Dome have been previously described by Tremblay (1976). He considered the more intensely foliated rocks of the Wishbone Dome to be a leucocratic granoblastic gneiss, which he interpreted to be transitional to more massive granitoids by a process of *in situ* granitization. Bostock (1980) described the bodies within the dome as gradational between felsic tuffs and granitoids. All of these rocks are considered here to be deformed granitoid bodies.

Lithology

Rocks of the Wishbone Suite are typically equigranular, medium-grained (2-8 mm) tonalite to monzogranite. A typical weathered outcrop surface is shown in Figure 3.8. The rocks consist of anhedral plagioclase (50%), quartz (25-30%) and variable proportions of microcline (5-25%). Biotite is the principal mafic mineral (amphibole is extremely rare) and makes up less than 10% of the rock. All rocks are extensively recrystallized, well foliated and locally contain distinctive polycrystalline quartz

aggregates and magnetite porphyroblasts (2-5 mm). The foliation surface is defined by alignment of biotite and the flattened shape of quartz and plagioclase grains. Locally the rock has a lineation defined by elongate quartz grains.

The Jaeger Monzogranite (Figure 3.1) is distinctly more potassic than most bodies within the Wishbone Dome area (Figure 3.7). The body is extensively intruded by irregular bodies of medium to coarse grained alkali feldspar-rich veins and pegmatites at all scales. Owing to the extent of deformation, the relationships between the phases are not clear. The potassic veining is, however, predeformation and not related to younger potassic plutonism. The more potassic composition of the Jaeger Monzogranite and some of the bodies within the Wishbone Dome may be the result of intrusion and metasomatism by these veins.

Pluton Morphology, Nature of Contacts and Age

The original morphologies of plutons of this suite are unconstrained. Within the Wishbone Dome, a number of petrogaphically distinct phases are observed, however the exposure is insufficient to map contacts between the phases. The size and form of individual bodies is thus unknown. The present shape of the Wishbone Dome is considered to be the result of post-emplacement deformation rather than a primary bulbous form (King *et al.*, 1989a).

The poor exposures of this suite provide little information concerning the nature of contacts with host rocks. In all cases where contacts are observed, the host rock is volcanic. Small, (<1 m) to km-scale, angular xenoliths of orthogneiss, most likely correlative with volcanic rocks, commonly occur within the plutons. They are particularly abundant in the Jaeger Monzogranite (King *et al.*, 1990). In the Wishbone Dome, a large area of intermediate volcanic rock occurs within the core of the body, however it cannot be determined if this is a large xenolith or a downfolded roof pendant (Bostock, 1980). The limited exposures suggest contacts are sharp and that stoping occurred during intrusion.

The granitoids along the north-eastern margin of the Wishbone dome locally contain a mineral lineation defined by elongate quartz grains. Unfortunately most of this area is poorly exposed and frost-heaved. It is possible that this part of the contact is tectonic, not intrusive, although this cannot be clearly shown.

Samples of this suite have not been dated by U-Pb geochronology. The following characteristics suggest that the plutons of the Wishbone Suite intruded prior to major deformation and metamorphism.

1) All samples are extensively recrystallized, retaining few primary igneous textures.

2) The foliation in the rocks is generally concordant with the regional S_2 surface in the surrounding host rocks (Figure 3.1).

3) Host rocks are restricted to those of the early tectono-stratigraphic assemblage (*ie.* metavolcanic and metasedimentary).

3.4.4 Olga Plutonic Suite

The Olga Plutonic Suite consists of massive to gneissic, grey to white weathering, medium grained biotite quartz diorite to tonalite. This unit constitues less than 1% of the area mapped and is largely restricted to the core of a structural dome centred on Olga Lake in the center-west of the map sheet (Figure 3.1; King *et al.*, 1988). Other possible occurrences include scattered remnants as xenoliths within rocks of the Wishbone Suite and as septa within banded gneisses.

Bostock (1980) originally interpreted this unit as recrystallized felsic volcanic tuffs. Felsic tuffs are a common host rock at Olga Lake, however these rocks are reinterpreted here to be intrusive. Evidence in support of this interpretation is: 1) compositionally similar rocks occur as sills intruding the volcanic rocks (Figure 3.9); 2) individual layers are compositionally homogeneous at a scale of cm to metres and contacts between layers are extremely sharp (Figure 3.10), 3) internal contacts are locally discordant to the regional foliation surface and are at high angle to overall layering (Figure 3.10).

Lithology

Rocks of this suite are massive to gneissic, white-weathering biotite tonalite to quartz diorite. Rocks are equigranular, consisting of anhedral interlocking crystals of plagioclase and quartz (0.5-1 mm), with rare interstitial microcline (<10%) and subhedral biotite (0.5-1 mm). Accessory minerals include apatite, zircon, secondary epidote and chlorite. Porphyroblastic magnetite (1-5 mm) is characteristic. The gneissosity is defined by: 1) original compositional layering attributed to multiple intrusion of sills; and 2) subsequent deformation and foliation development. Compositional layering is present at the 10 cm to 1 m scale. Differences between the different phases reflect varying proportions of biotite and quartz.

Pluton Morphology, Nature of Contacts and Age

The shape of the Olga tonalite is unconstrained as the base of the body is not observed. Internal contacts within the Olga tonalite suggest that it is made up of numerous sill or sheet-like bodies, on the scale of metres to tens of metres.

In most cases, original contact relationships are obscured by intrusion of younger plutons. The only location where the Olga Suite is observed to be in contact with older rocks is north of Olga lake where tonalitic sills intrude the structurally overlying metavolcanic rocks of the CVB (Figure 3.9). A zone, extending less than one km above the Olga tonalite, is characterized by the occurrence of numerous sills of tonalite within mafic to intermediate volcanic rocks. In places layering is at a relatively fine scale on the order of 10 cm or less, but thicker layers of 1 to 3 m are also present.

Layered mafic/felsic orthogneiss, similar to rocks found within the contact zone described above, occur as xenoliths within younger plutonic rocks in the eastern part of the map area (King *et al.*, 1990). Formation of these layered orthogneisses may have occurred by a similar process to that suggested for the contact zone north of Olga Lake. If this correlation is correct then rocks of the Olga Suite are not restricted to the Olga Lake area, but are regionally more widespread. Nonetheless, as presently exposed they represent an areally minor plutonic unit.

Rocks of the Olga Suite are spatially associated with metavolcanic rocks; in all cases where intrusive relationships are observed the host rock is metavolcanic. The similar extent of recrystallization and deformation of the Olga Suite and metavolcanic rocks argues that both experienced the regional deformation and metamorphic events. The suite is constrained to be pre-deformation. Two samples of this suite have been dated at ca. 2650 Ma, 17 m.y. younger than the associated volcanic rocks.

3.5 Syn-Deformation Plutonic Suites

3.5.1 Concession Plutonic Suite

Plutons belonging to this suite occur throughout the map area. Figure 3.11a shows the spatial distribution and informal names assigned to individual plutons or groups of plutons. Generally rocks of the Concession Suite have high magnetic susceptibilities (M-type granitoids of Ishihara (1977) and define prominent anomalies on residual magnetic anomaly maps (Figure 3.11b). These data have been used to interpolate map boundaries beneath areas of extensive glacial till cover.

Lithology

The Concession Plutonic Suite is comprised of strongly to weakly foliated, mesocratic plutons ranging in composition from hornblendite to granodiorite. Continuous gradations occur between the different rock types. The predominant lithology is tonalite (Figure 3.12).

Hornblendite

This rock type is relatively rare, occurring as a marginal facies to the Concession Pluton (see below), as well as smaller dyke or plug-like bodies within the metasedimentary rocks (*e.g.* south-east of Wishbone Dome). The rocks are black to green coloured, melanocratic, consisting of 60 to 90% subhedral amphibole and pyroxene (2-20 mm), with interstitial plagioclase and/or quartz. Amphibole is the dominant mafic phase although irregular cores of orthopyroxene indicate that amphibole, in part, replaces orthopyroxene. One sample contains 30-50% euhedral prismatic orthopyroxene grains

(enstatite; 2V=50°; +ve) some of which are contained within oikocrysts of pale brown amphibole. Amphibole both overgrows and replaces orthopyroxene. The Mg-rich nature of the orthopyroxene indicates crystallization from an Mg-rich liquid.

Diorites, Quartz Diorites, Tonalites and Granodiorites

These rocks consist of varying proportions of the minerals plagioclase, quartz, amphibole, biotite and microcline. The rocks are generally equigranular and medium grained, although porphyritic (hornblende and plagioclase) varieties do occur (Figure 3.13). Plagioclase (andesine to oligoclase) occurs as subhedral to anhedral prismatic grains. Zoning is not prominent. Quartz occurs as strained interstitial anhedral crystals. Microcline, where present, is dominantly interstitial. Hornblende is the dominant (10-30%) mafic mineral in the more mafic rocks, with the proportion of biotite increasing with increasing quartz content. The amount of biotite is secondarily related to the extent of deformation. Hornblende occurs as pale to dark green, sub to anhedral crystals, containing abundant inclusions of blebby quartz and euhedral apatite. Biotite is present in most rocks, forming subhedral crystals, and is commonly the only mafic mineral in rocks of granodiorite composition.

The rocks contain a large number of accessory minerals, including apatite, zircon, titanite, allanite, epidote and oxides. Allanite is a characteristic trace mineral, forming large, euhedral metamict grains, often rimmed by epidote (Figure 3.14). Titanite occurs as both primary subhedral grains and as a secondary mineral associated with the breakdown of amphibole to biotite and opaques. Epidote is also associated with this subsolidus reaction. It is difficult to establish petrographically if epidote was also a primary magmatic phase. Low metamorphic pressures recorded for the host rocks (<5 kb; Relf, 1990) suggest that the plutons crystallized at crustal depths near or above the epidote stability field (5-8 kb; Liou, 1973; Zen and Hammerstrom, 1984).

Rocks have variably developed foliations, ranging from strongly foliated and recrystallized to weakly or nonfoliated. The foliation is principally defined by the

alignment of biotite some of which is secondary after hornblende. Amphibole and plagioclase also show alignment, but little evidence of penetrative recrystallization. This fabric may in part be late magmatic as suggested by Hill (1980).

Monzodiorites, Quartz Monzonites and Monzogranites

These rocks are more potassic than average for the suite. They usually contain subhedral phenocrysts of microcline (3-10 mm) (Figure 3.15) and are biotite-rich, seldom containing significant amounts of hornblende. Very few of these bodies outcrop in the map area and they have not been studied in detail. King *et al.* (1991) report large bodies in the NE quadrant of the Nose Lake Mapsheet (not included within this study).

Pluton Morphology

As shown on the geology and aeromagnetic relief maps (Figure 3.11) rocks of this suite form discrete small to medium sized clusters on the scale of one to many tens of km in surface dimension. Generally, individual clusters are made up of numerous intrusions. Tabular, sheet- or dyke-like intrusions as well as ovoid bodies have been documented.

Tabular bodies occur at all scales, although they are most easily recognized where they are small. The smaller bodies typically form layer parallel sills within generally steeply dipping, foliated host rocks. Good examples occur within gneisses south of the Southern Diorite (Figure 3.16) and around the Wishbone Dome. The apparent thickness of these bodies ranges from less than one metre to one km and the strike length ranges up to 5 or more km.

Some of the larger bodies, such as the Southern Diorite, are also interpreted to form layer parallel, tabular bodies (Figure 3.17). A partial cross-section through the Southern Diorite is afforded by the shallow dip of host rocks folded across the Olga dome, providing a small amount of structural relief. The form of the pluton is distinctly tabular, with a minimum thickness on the order of two km. This is the place where a reasonable estimate of the three dimensional form of a pluton can be made.

Many plutons have ovoid or circular outcrop patterns (eg. Concession, Crane, SE Concession), similar to plutons to the east of the study area described by Hill and Frith (1982). These plutons tend to have the long dimension parallel to the regional foliation surface and the regional foliation wraps around the intrusion (King *et al.*, 1990). The extent of these bodies at depth cannot be determined.

Internal Variations Within Plutons

Bodies of the Concession Suite show mineralogical and textural variations both at the outcrop and map scale. Large areas (km^2) of relatively homogeneous rock occur (*ie.* parts of the Southern Diorite), however, more typically plutonic bodies are amalgamations of many compositionally and texturally distinct lithologies. Intrusive relationships can often be documented between the different phases. Four or more distinct phases, each with sharp contacts, may be observed within a single outcrop. In most cases, variations from one outcrop to the next are non-systematic and the nature of the transition between outcrops is considered to be intrusive. Similar field relationships are noted in monzodiorite and tonalite rocks in the Archean Superior Province (*e.g.* Stern *et al.*, 1989).

Examples of systematically zoned plutons include the Concession Pluton and the SE Concession Pluton. Bostock (1980) first noted that the Concession Pluton consists of hornblendites and diorites along the north and west margins and a relatively homogeneous quartz diorite in the interior (Figure 3.18). Most of the mafic marginal zone consists of amphibole cumulate rocks. These rocks are in turn intruded by dioritic to quartz dioritic rocks which vein and disaggregate the earlier cumulate rocks, incorporating clots and individual minerals of amphibole into the intruding rock (Figure 3.19). Rocks immediately adjacent to the cumulates are more mafic than those in the core, possibly as a result of the incorporation of cumulate minerals. Rocks which contain cumulate or excess amphibole can be recognized on geochemical grounds (Chapter 5).

Similar intrusive relationships are observed within the composite SE Concession Pluton. In this body, dioritic rocks outcrop within the core of a small body of tonalite. The compositional zoning, from diorite core to tonalite margin, is a result of multiple

intrusion, not in situ differentiation. Dykes of the diorite are common in the tonalite as are xenoliths of tonalite in the diorite. The quartz and plagioclase phenocryst content of the diorite increases with proximity to areas containing abundant tonalite xenoliths.

Other examples of zoned plutons in the area (*e.g.* dykes east of the Wishbone dome; the pluton north of Virgin lake) are also composite intrusions. Continuously zoned plutons such as the Uist Pluton of the Kegan Intrusive Suite to the east of the map area described by Hill (1980) have not been identified.

Microdiorite Enclaves

Microdiorite enclaves (Didier, 1973) are a ubiquitous feature of the suite. Two general types of enclaves are observed: 1) non-porphyritic or amphibole and/or plagioclase porphyritic, fine grained diorites to quartz diorites and 2) medium to coarse grained hornblendites. The former are much more common and are similar to microdiorite enclaves described by Vernon (1983). The best exposures of these enclaves occur along the shoreline of Nose Lake (King *et al.*, 1990). Possible origins include magma mingling (Vernon, 1983) or quench cumulates (R. Flood, pers. comm., 1990). If the former then physical interaction, and possibly mixing between magmas of different compositions is implied. The second type of enclave is interpreted to be xenoliths of hornblende cumulates entrained during intrusion, similar to the hornblendites observed along the margins of the Concession Pluton described above.

Evidence for Timing of Intrusion

The following field relationships are interpreted to suggest that intrusion of this suite occurred during the peak metamorphic regional compressive deformation.

1) Plutons intrude parallel to, and are typically elongate along the regional syn-metamorphic S_2 surface. Dyke orientations are strongly controlled by the regional anisotropy as defined by S_2. Since there is no evidence for transposition, these features suggest that S_2 was already developed at the time of intrusion.

2) The majority of plutons contain a foliation surface, defined by the alignment of biotite, hornblende and plagioclase and in extreme cases flattening of quartz and feldspar. This foliation is generally concordant with the regional S_2 surface. Correlation of this internal fabric with S_2 suggests intrusion pre or syn-D2 deformation. There is however little evidence for extensive recrystallization, and the foliation may have been imposed during a late magmatic stage (*e.g.* Hill, 1980). The much lower degree of recrystallization, in comparison to plutons of the Olga and Wishbone Suites, suggests that the Concession Suite may not have experienced the same intensity of deformation as the earlier suites. The variable development of the foliation from one pluton to the next could be interpreted in terms of relative (with respect to deformation) time of emplacement. However, since these foliations are variably developed within a single pluton, this may be more characteristic of heterogeneous strain than time of emplacement.

3) There is no evidence for large scale truncation of regional tectonic fabrics by the intrusions.

U-Pb zircon ages for two samples of this suite are similar both yielding *ca.* 2608 Ma ages.

3.5.2 Siege Plutonic Suite

Rocks of the Siege Plutonic Suite form a large irregular shaped body in the central part of the map area (Figure 3.1). A smaller satellite body outcrops immediately to the west of the main body, and many sills occur within the paragneiss belt along the southern margin of the pluton. The suite constitutes the main part of the Central Batholith of Bostock (1980).

Lithology

The rocks are massive, medium grained (1-3 mm), white weathering, leucocratic (< 5% biotite) tonalite to granodiorite (Figure 3.20). A typical sample consists of 40-60% equant, sub to anhedral plagioclase, 5-25% interstitial anhedral microcline, 20-30% anhedral strained and polygonized quartz, and 2% sub to anhedral biotite. Apatite is a

common accessory phase, and is visible in hand sample as small blue crystals. Large (2-4 mm) porphyroblasts of magnetite are common. Chlorite, epidote and muscovite are typical alteration minerals. Plagioclase is saussuritized, locally replaced by microcline and in places rimmed by fine muscovite along grain boundaries. Biotite is commonly altered to chlorite.

In many locations the rock is hybrid, consisting of two distinct phases; a bioite tonalite as described above and a mafic-free leucocratic granodiorite to monzogranite. The latter occur as irregular diffuse veins and amoeboid patches within the former. Magnetite porphyroblasts are preferentially contained within the more potassic phase.

Nature of Contacts with Host Rocks

The Siege Plutonic Suite intrudes rocks of the Concession, Wishbone and Olga Suites and volcanic rocks along its northern and western margins and metasedimentary rocks to the south and east. Contacts with host rocks may be sharp, but are typically more complex, consisting of a marginal facies containing abundant host rock xenoliths transitional into an intensely veined host rock. The marginal facies is an intrusive migmatite or diatexite composed of various xenoliths, schlieren and biotite-rich folia within a tonalite to granodiorite matrix. Bostock (1980) interpreted this contact to be gradational, reflecting *in situ* granitization. The intrusive contact zone may be 10 metres to 100's of metres broad. The mixed xenolith zones are not restricted to the contacts, but also occur within the central part of the body.

The strongly veined host rocks along the western margin are complexly folded (Figure 3.21). The fold patterns cannot be correlated with structures outside the immediate contact zone. One possibility is that the folds formed, at least partially, as a result of intrusion. Intrusion of this suite certainly involves stoping, as witnessed by the abundance of xenoliths, but may also have a component of diapirism or in situ ballooning (Bateman, 1985) causing deformation of the surrounding migmatized aureole (King et al. 1988). Softening of the host rocks by intrusion of magma and heating may have facilitated intrusion and deformation. Deformation associated with intrusion has not been studied in detail.

Evidence for Relative Timing of Intrusion

The pluton contains xenoliths of earlier plutonic rocks of the Olga and Concession Suites, as well as metavolcanic and metasedimentary rocks. The xenoliths commonly contain veins of tonalite compositionally similar to the host rock which occur parallel to the interpreted S_2 surface. Tonalite veins within the xenoliths are commonly isoclinally folded, although there is no evidence for folding within the pluton external to the xenolith. This relationship suggests that veining and folding occurred during emplacement, and the xenoliths were incorporated as the magma engulfed its contact zone. The fact that veins occur preferentially along the S_2 surface within the host rocks and xenoliths suggests that S_2 was already developed at the time of intrusion. The presence of a weak foliation within the pluton (locally defined by the alignment of biotite) concordant with S_2 suggests that emplacement occurred late in D_2.

van Breemen *et al.* (1990) reported U-Pb data for zircons from the Siege Pluton; however a precise age has not been determined because of inheritance. Of the five fractions analyzed, two show evidence of inheritance, while three others are discordant but define a line which intersects concordia at 2616±2 Ma. This age is in conflict with the field observation that the Siege Tonalite intrudes the Southern Diorite since the Southern Diorite has been precisely dated at 2608±1 Ma. As discussed by van Breemen *et al.* (1990), it is possible that the age of the Siege Tonalite could be up to several million years younger than 2608 Ma and the older age reflects the inherited component. If the age of 2616 is correct then this imples that either the Siege Tonalite or the Southern Diorite are composite bodies which formed over a protracted period of time (>8 m.y.).

3.6 Post-Deformation Plutonic Suites

3.6.1 Yamba Plutonic Suite

The Yamba Plutonic Suite principally outcrops as two large bodies within the southern portion of the map area. The Wolverine Monzogranite (WM) occupies an area of close to 1500 km^2 around Yamba Lake (Yamba Batholith of Bostock, 1980) and extends a further 15 km to the south (Folinsbee, 1949). The Pellatt Lake Monzogranite

(PLM) is a similar sized body located 30 km to the east of the WM. The two bodies are divided by a septa of mixed paragneiss and Concession Suite granitoids. In addition to these two larger bodies many smaller bodies occur throughout the central and southern part of the map area.

Lithology

The suite is dominantly monzogranitic with lesser amounts of granodiorite and syenogranite (Figure 3.12). Outcrops are typically massive, well jointed and pale pink to red weathering. Rocks are medium to coarse grained (2-10 mm), equigranular to microcline porphyritic, with a granitic texture (Figure 3.22). A typical rock consists of 25-40% plagioclase, 25-35% quartz, 25-40% microcline, 5% biotite, 0-5% myrmekite and trace amounts (<1%) of muscovite, apatite, opaque, monazite and zircon. Variation in the plagioclase/microcline ratio reflects, in part, local concentration of microcline phenocrysts. Plagioclase is generally equant, medium grained (2-4 mm) and anhedral to subhedral. Smaller euhedral crystals with albite rims are common inclusions in microcline phenocrysts. Myrmekite and/or albitic selvedges are common at boundaries between plagioclase and microcline. Quartz is equant and anhedral, commonly with serrated boundaries against plagioclase and microcline. Grains are strained but not polygonized. Microcline occurs as both anhedral interstitial grains and as subhedral phenocrysts (2-7 mm) with inclusions of plagioclase, apatite and biotite. Microcline phenocrysts are common, in places making up 5 to 30% of the rock. Microcline crystals are perthitic, consisting of 10-15% of relatively coarse lamellae of albite. Locally the long axes of phenocrysts define a shallowly dipping lineation, which is subparallel to contacts. In places the rocks contain segregations or pods of microcline rich (± magnetite) material interpreted to represent late stage movement of potassic fluids. Euhedral biotite comprises 2 to 15% of the rock. Muscovite is locally present but is generally secondary except for occurrences within pegmatites. Garnet is a local accessory phase and is common in pegmatites, along with tourmaline. The occurrence of garnet, tourmaline and muscovite in pegmatites is related to host rock lithology. They are generally present if the host rock is sedimentary and absent if the host is igneous.

Rocks are weakly to moderately altered. The alteration consists of saussuritized plagioclase, chloritized biotite, and secondary growth of muscovite after microcline. Replacement of plagioclase by microcline occurs in small patches.

Hornblende syenites and quartz syenites, occur associated with Yamba Suite monzogranites in one small area along the eastern margin of the WM. The relationships of these rocks to the monzogranites are not known owing to very poor exposure in the area. These rocks have not been investigated in detail here.

Pluton Morphology

Rocks of the Yamba Plutonic Suite outcrop both as large mapscale bodies (*ie.* Wolverine and Pellatt Lake Monzogranites) and as smaller dyke, sill and irregularly shaped bodies. Dykes and sills (10 cm to 10's m wide) are ubiquitous throughout the central part of the map area. They are particularly common intruding plutons of the Concession Suite. Bostock (1980) described these intensely intruded areas as hybrid rocks. In places, dykes and sills may constitute up to 80% of the outcrop area (Figure 3.23) and many of the medium sized bodies (1-10 km) in map view are amalgamations of compositionally similar dykes and sills. Internal contacts within these bodies are readily observed but difficult to map out owing to similar characteristics and lichen cover.

The morphology of larger bodies such as the Wolverine and Pellatt Lake Monzogranites cannot be determined on available data. These large masses are internally complex consisting of numerous texturally variable phases of compositionally similar magmas. Both sharp and transitional contacts are observed. Although exposure is generally good, the often subtle differences between the various phases could not be mapped out at the scale of this project. It is not clear if large masses such as the Wolverine Monzogranite represent dyke and sill complexes as described above, or represent the consolidated products of a single large magma chamber.

The size of bodies shows some correlation with the metamorphic assemblages in the adjacent host rocks: the largest bodies are associated with migmatized host rocks whereas

the dyke and sill complexes occur in lower grade rocks. Since the granites are younger than the metamorphic mineral assemblages recorded in their host rocks, it is not clear if the different intrusive styles are directly related to the depth of intrusion within the crust.

Nature of Contacts with Host Rocks

The orientations of the dyke and sill complexes described in the previous section are strongly governed by the anisotropy of the host rocks (principally the S_2 surface). This has been well documented in the area southwest of Olga lake (King *et al.*, 1988). Here, the regional foliation in the host rocks is relatively shallow and the Yamba Suite bodies occur as large, shallowly dipping sills concordant with S_2 and interconnected by steep dykes.

The intrusion of the dyke swarms has had very little effect on the orientation of regional deformation surfaces (principally S_2; King *et al.* 1988; 1989a). Trains of xenoliths within large granitoid bodies, ranging in size from 10's of m to km in scale effectively map out both lithologic contacts and large scale structural features (King *et al.* 1988). This is particularly evident in the central and northern parts of the map area. Similar relationships, termed '*ghost stratigraphy*' by Pitcher (1970) have been documented in Andean batholiths, and are associated with intrusion in extensional settings. This intrusive style suggests that the rocks were intruded during brittle fracturing and stoping of wallrocks and probably reflects high level exposures of the magmatic system.

In the southern part of the map sheet, the contacts with host rocks are more complex. In places they are razor sharp as in the dyke and sill complexes described above; however more characteristically the contact with the host rock is marked by a relatively diffuse zone of intense veining and microcline metasomatism up to several hundred metres wide. Monzogranitic and pegmatitic veins, ranging in width from one cm to several m pervasively intrude the host rocks. Often the monzogranitic veins appear disconnected from the main body of granite, occurring as irregular pods within the host

rocks. In places, discrete veins are not observed, however the host rocks, generally tonalite of the Concession Plutonic Suite, contains significant amounts of medium grained microcline crystals, implying fluid metasomatism.

Locally within one km of the contact, the monzogranites have a schlieric or gneissic texture (Figure 3.24). Schlieren consist of mafic (biotite ± hornblende) rich and mafic poor (microcline rich) layers intercalated on a scale of centimetres. These 'mixed' rocks are interpreted as remnants of hybridized host rocks, in particular diorites and tonalites of the Concession Plutonic Suite. Particularly good exposures occur at the northern contact of the Wolverine Monzogranite with tonalites of the Concession Suite and more locally along the eastern contact along the eastern shore of Yamba Lake. In addition, the textures are common within the Pellatt Lake Monzogranite which contains a high proportion of dioritic to tonalitic xenoliths (shown as filled squares on Figure 3.1). Although the origin of this texture has not been investigated in detail, the correlation between the diffuse, transitional contact zone described above and these rocks suggests hybridization by fluids and melts derived from the monzogranite. It is therefore speculated that part of the larger monzogranite bodies of the Yamba Suite contain, at least locally hybridized host rocks, dominantly of the Concession Plutonic Suite. In sampling for geochemistry these rocks were avoided.

Evidence for Timing of Intrusion

Plutons of the Yamba Suite intrude all other rock types, although their field relationship to the Contwoyto Suite is not established (see below). The rocks are not penetratively deformed and show no evidence of having experienced the regional D_2 deformation and metamorphism. The regional S_2 surface partly controls intrusive style but is also truncated by the intrusions. Intrusion is therefore interpreted to post-date the peak metamorphic and deformation event in the area. Suitably oriented granitic and pegmatitic sills and dykes are openly folded by the D3 folding event. Intrusion is bracketed to occur between these two deformation events.

A single sample of the Yamba Plutonic Suite from the Wolverine Monzogranite has been dated (U-Pb on monazite) at 2582±4. This provides a minimum age for the time of regional metamorphism and D_2 deformation in the area.

3.6.2 Contwoyto Plutonic Suite

The Contwoyto Plutonic Suite outcrops throughout the map area with the larger bodies concentrated in the north and east. Rocks of the Contwoyto Suite make up the large granitoid region northwest of the Lupin mine site (Contwoyto Monzogranite on Figure 3.1; Contwoyto Batholith of Bostock (1980) and Tremblay (1976)). Plutons assigned to this suite are also present in the central region near Olga Lake, in the south, east of Yamba Lake and in all areas east of Contwoyto Lake. The Contwoyto and Yamba Suites are largely spatially separate and only overlap in the southern part of the map sheet.

Lithology

Rocks of the Contwoyto Plutonic Suite range from tonalite to monzogranite, largely overlapping the compositional field of Yamba Suite rocks, but including a greater proportion of tonalitic to granodioritic rocks (Figure 3.12). Rocks are massive, white to grey-green weathering, equigranular, and fine grained to pegmatitic. A typical Contwoyto Suite rock is comprised of 30% quartz, 35-40% plagioclase, 20-25% microcline, 2-10% biotite and 2-10% muscovite. In contrast to the Yamba Plutonic Suite, two primary micas, muscovite and biotite, are usually both present. The proportion of microcline is variable, ranging from less than 10% to greater than 70% in coarse grained pegmatitic patches. The rock is locally microcline porphyritic although not as prominently as in the Yamba Plutonic Suite. Plagioclase occurs as equant, sub to anhedral grains; compositional zoning is not prominent although secondary sausuritization may preferentially alter cores of grains. Twin lamellae are occasionally kinked or displaced. Quartz shows two habits; anhedral small round grains (0.25 to 1 mm), commonly as inclusions in plagioclase and microcline, and as larger irregular, often interstitial, grains up to 3 or 4 mm. Quartz is strained and occasionally larger grains are polygonized. Microcline occurs as anhedral interstitial grains and as sub to anhedral oikocrysts (2-5

mm) containing abundant inclusions of round quartz grains, euhedral plagioclase (with albitic rims) and biotite. Perthitic texture is well developed. Biotite is euhedral to ragged and distinctly dark reddish-brown in colour. Zircon inclusions with associated metamict haloes are common in biotite. Biotite is commonly altered to chlorite (± oxides, prehnite). Muscovite occurs as euhedral, random to oriented individual crystals, sometimes intergrown with biotite. Muscovite is also observed overgrowing plagioclase and microcline and these crystals are presumed to be subsolidus. Apatite is a common accessory mineral, readily observed in hand sample as large (1-3 mm) euhedral aquamarine crystals. Tourmaline is locally common, both in equigranular granites and in associated pegmatites. Euhedral monazite and zircon are common. Sillimanite is observed intergrown with quartz and muscovite in rosettes within pegmatites (Figure 3.25).

Pegmatites, both internal and external to plutons are extremely common (Figure 3.26). Pegmatites are usually associated with the larger masses of granites (*e.g.* Contwoyto Monzogranite), but also occur as extensive dyke swarms in metasediments isolated from exposures of granite. In this respect they resemble pegmatites associated with the Prosperous Granite in the Yellowknife area (Henderson, 1985; Cerny and Meintzer, 1985; Kretz *et al.*, 1989a,b). Most of the pegmatites have a simple mineral assemblage consisting of variable proportions of microcline, quartz, albite, biotite, muscovite, tourmaline, apatite, garnet, ±sillimanite. Detailed mineralogical studies of the pegmatites were not undertaken.

Pluton Morphology

The Contwoyto Plutonic Suite exhibits a similar dyke and sill style of intrusion to that of the Yamba Suite described above. Larger bodies of the Contwoyto Suite (*e.g.* Contwoyto Monzogranite), which in map pattern appear lobate, in detail are made up of multiple intrusions of compositionally similar but texturally distinct phases, ranging from fine grained to pegmatitic (King et al. 1988). Contacts between phases are extremely sharp. These large bodies do not represent the remains of large magma bodies, rather they

are amalgamations of many small intrusive bodies. In some areas (*e.g.* along the northwest shore of Contwoyto Lake, north of the Lupin Mine site) the pluton is made up entirely of coarse grained tourmaline-muscovite pegmatite.

Nature of Contacts With Host Rocks

Contwoyto Suite rocks most commonly intrude metasedimentary rocks of the YKS although they are also found intruding rocks of the Concession Plutonic Suite. Contwoyto Suite rocks are not observed to intrude Yamba Suite Rocks. Metasedimentary host rocks are generally at or above the cordierite isograd. Intrusion into lower grade rocks is less common although this may, in part, reflect the limited outcrop area of low grade rocks within the map area. Henderson (1985) noted a similar relationship between the two mica, Prosperous Lake Granite and metamorphic isograds in the Yellowknife-Hearne Lake Area, as did Culshaw and van Breemen (1990) for two mica granites in the Tinney Hills area. The occurrence of these two mica granites dominantly above the cordierite isograd is a feature common throughout the Slave Province. The granites in the Contwoyto Lake area are not causally linked to the metamorphism.

Contacts with host rocks are typically sharp. As an example, the contact between rocks of the Contwoyto Monzogranite and metasedimentary rocks east of the Lupin Mine site consists of a narrow (<100 m), marginal zone of sharply bounded, layer parallel sills of granite. Although locally concordant the contact is discordant on a regional scale. In some places the contact is marked by one or more layer parallel vertical sills within the metasediments, external to the main body of granite. Tourmaline is common in both the granites and schists along the contact zone (see Kretz *et al.*, 1989a, b for discussion of similar features around the Prosperous Granite in Yellowknife). Screens and discontinuous septa of metasediments are abundant throughout the body at all scales (Figure 3.27). A '*ghost stratigraphy*' is preserved within these xenolith trains. Metasedimentary xenoliths grade from discrete sharply bounded angular fragments showing little interaction with the melts, to diffuse ghost-like biotite-rich schlieren

(Figure 3.28). All the gradations in xenolith preservation can be observed in a small area and are interpreted to reflect various degrees of assimilation and hybridization. In general the larger xenoliths are less assimilated than smaller enclaves.

Although in many areas the metamorphic isograds parallel the contact of the larger granitoid bodies, in detail the granitoids are discordant and cross-cut isograd surfaces, implying post-metamorphic intrusion. Metamorphic isograds can be mapped within larger areas of granite by the assemblages recorded in the metasedimentary enclaves (King *et al.*, 1990). Contact metamorphic effects have only been documented around one pluton, where sillimanite overgrows the regional S_2 surface (Relf, 1990).

Evidence for Timing of Intrusion

Of all the plutonic suites described above, the timing of the Contwoyto Suite is most enigmatic. In most cases, intrusion of the Contwoyto Suite utilizes pre-existing surfaces (S_2) and crosscuts metamorphic isograds. These observations infer a post-D_2 timing for the suite, in accord with the relatively young (2580-2590 Ma) U-Pb monazite ages reported in van Breemen *et al.*, 1990, and described below. This simple interpretation however fails to account for: folds and boudins of granitoid veins within metasediments; and the presence of a foliation defined by biotite and or muscovite in some bodies which is regionally concordant with S_2. Whether these features are a result of D_3 or subsequent deformation cannot be easily demonstrated, in part because these events are difficult to characterize within the map area (Relf, 1990). It is possible that some of the Contwoyto Suite was intruded during the waning of D_2 deformation in the area.

Lithologic Comparison to the Yamba Plutonic Suite

The Yamba and Contwoyto Plutonic Suites show considerable overlap in the relative timing of intrusion as well as modal mineralogy, both suites being dominated by rocks of monzogranite composition (Figure 3.12). The two suites are, in most cases, relatively easy to distinguish in the field. Some of the characteristic differences between the suites are listed in Table 3.2. The weathering characteristics of the two suites are particularly distinctive on a regional scale and together with the occurrence of two primary micas in the Contwoyto Suite allow the two suites to be distinguished.

Table 3.2. Characteristic petrographic differences between the Yamba and Contwoyto Plutonic Suites.

Characteristic	Yamba Plutonic Suite	Contwoyto Plutonic Suite
Weathering colour	Red-pink	White-grey-green
Microcline Phenocrysts	Very common	Less common
Primary Mica	Biotite	Biotite and muscovite
Biotite Colour (optical)	Brown	Reddish-Brown
Pegmatites	Common	Extremely common
Tourmaline	Only in pegmatites	in granites and pegmatites
Aluminosilicate	Uncommon, garnet locally	Sillimanite & garnet in pegmatites

3.7 Chapter Summary

1) Plutonic rocks are subdivided into 8 suites on the basis of petrographic and field observations. Four of the suites predate the regional metamorphism and deformation (D_2) and are spatially associated with volcanic rocks of the CVB. The four other suites were intruded syn- to post- the peak metamorphic/deformation event. The subdivisions proposed here, based on field relationships, are supported by available U-Pb geochronology (van Breemen *et al.*, 1990).

2) Plutonic rocks associated with the older tectono-stratigraphic assemblage consititute a very small proportion of rocks within the area and are dominantly low-K felsic rocks.

3) Plutonic rocks of the younger assemblage define an evolution in composition with time of intrusion. The two older suites, Concession and Siege, were intruded synchronously with or late in a regional compressive event (D_2), accompanied by low pressure/high temperature metamorphism.

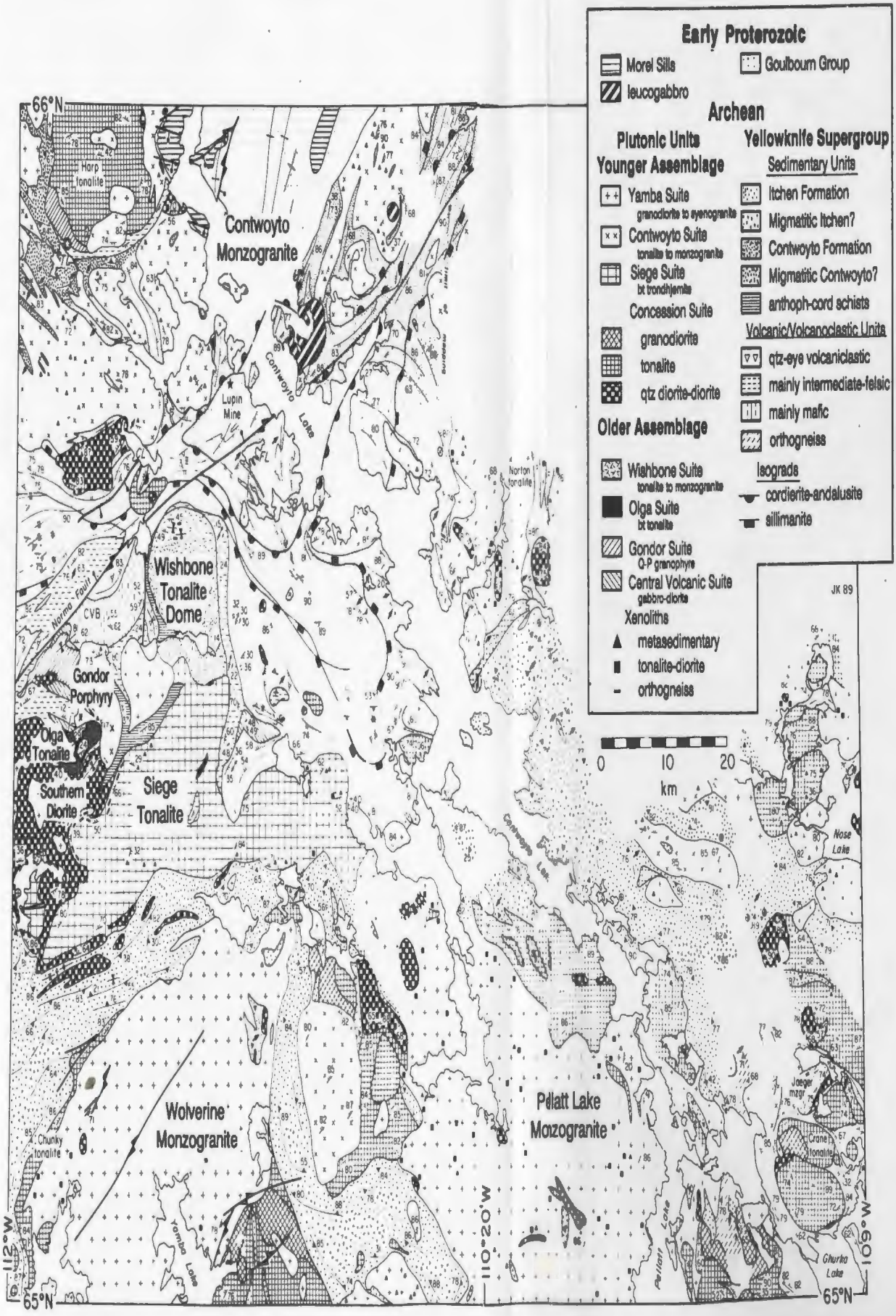

Figure 3.1 Geological map of the Contwoyto-Nose Lakes study area (NTS 76E and SW quadant of 76F, from King et al, 1990). Location of map shown on Figure 1.3

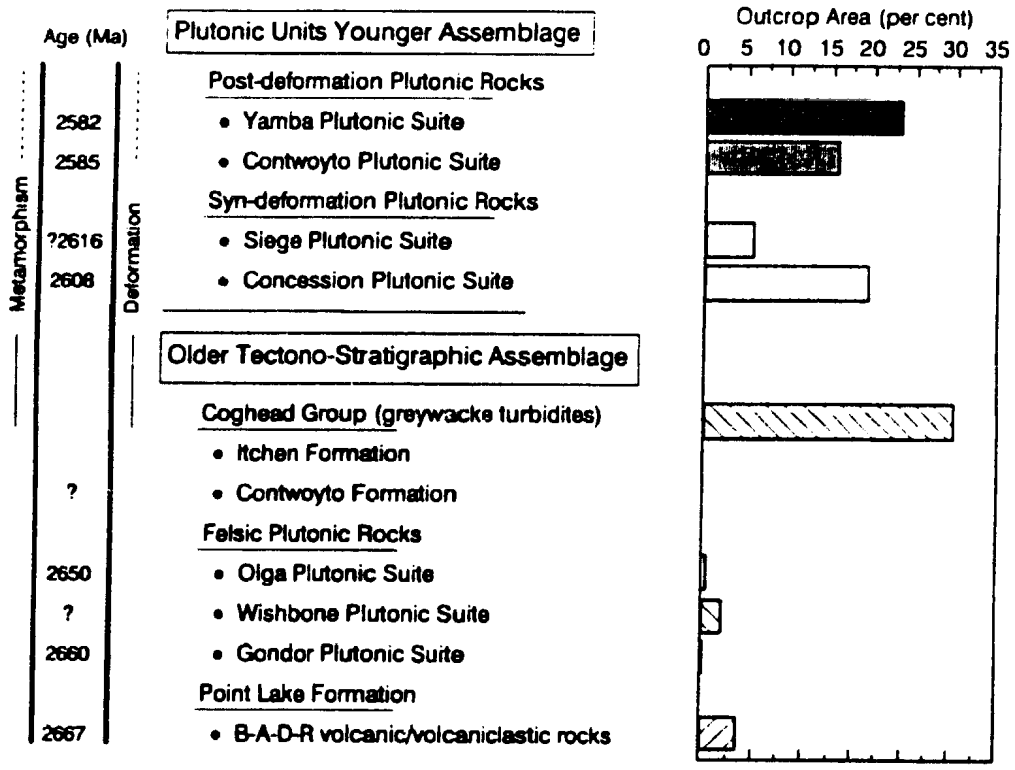

Figure 3.2. Schematic summary of the principal geological units. Outcrop area of the units calculated by point counting (n=1000) the geological map (Figure 3.1). No estimates of volume are made. U-Pb ages from van Breemen et al. (1990) (Table 3.1).

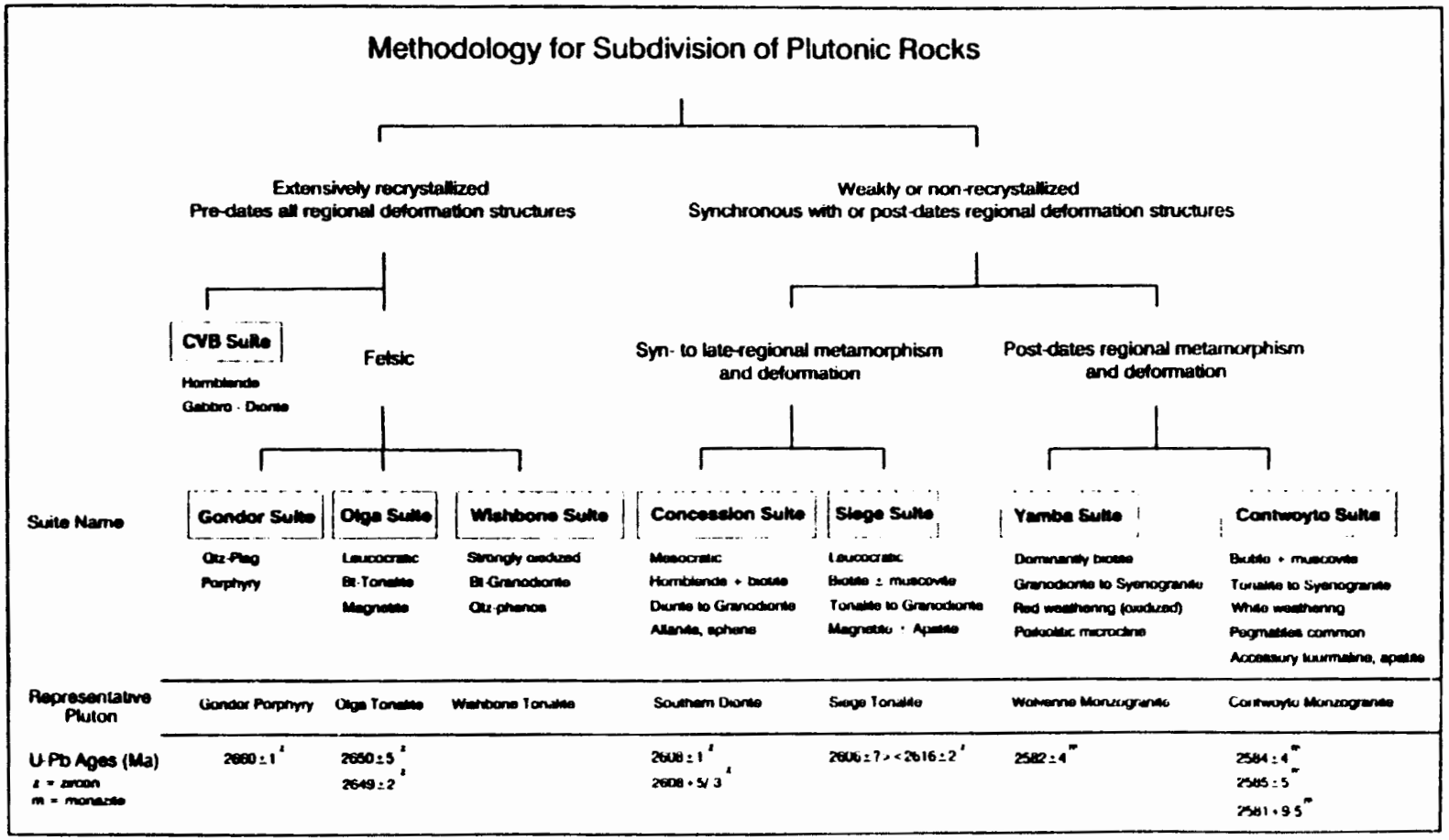

Figure 3.3. Flow diagram outlining the criteria used to subdivide the plutonic rocks into eight suites. Location of representative plutons are shown on Figure 3.1.

Plutonic Suite	Texture	Grainsize	Phenocrysts	Amphibole	Biotite	Muscovite	Titanite	Apatite	Zircon	Monazite	Allanite	Oxide	Tourmaline	Garnet	Sillimanite	Chlorite	Epidote	
Central Volc. Belt	R	M	-	☐	☐		☐	☐	☐			☐				☐ p		
Gondor	I/R		QP		☐	☐ s		☐	☐	☐						☐ p		
Wishbone	I/R	M	Q		☐	☐ s		☐	☐		☐	☐ s				☐ p		
Olga	R	FM	-		☐			☐	☐			☐ s		☐		☐ s	☐ s	
Concession	I/R	M	-	☐	☐		☐	☐	☐		☐	☐				☐ s	☐ s	
Siege	I/R	M	-		☐	☐ s		☐	☐			☐ s				☐ s	☐ s	
Yamba	I	M/C	K		☐	☐ s		☐	☐	☐		☐	☐ p	☐		☐ s		
Contwoyto	I	F-C	-		☐	☐		☐	☐	☐		☐	☐	☐ p	☐ p	☐ s		

Legend
I - Igneous
R - Recrystallized
F - Fine
M - Medium
C - Coarse
Q - Quartz
P - Plagioclase
K - K-spar
S - Secondary
p - in pegmatite
☐ Characteristic
☐ Common
☐ Rare

Figure 3.4. Summary of petrographic characteristics of the plutonic suites.

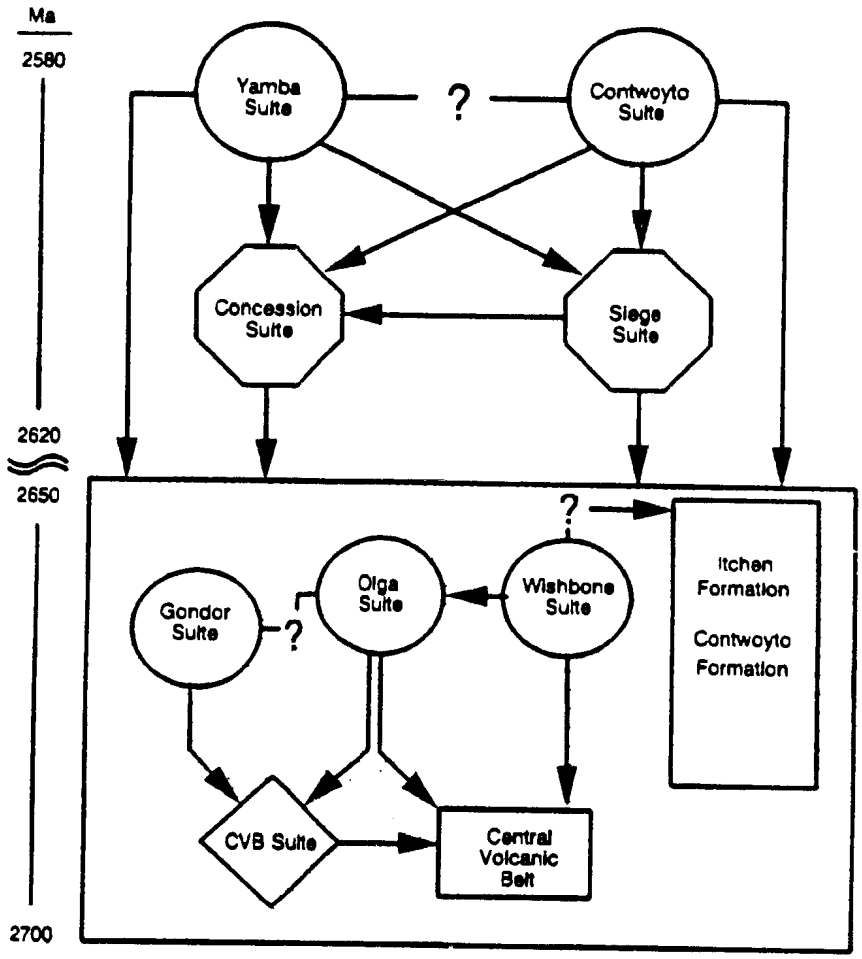

Figure 3.5. Schematic representation of intrusive relationships amongst the plutonic suites as determined from cross-cutting relationships and xenolith suites. Arrowheads indicate intrusive contact established, with the head pointing to the host rock.

Figure 3.6. A) Typical texture (weathered surface) of Gondor Plutonic Suite. (Gondor Porphyry, Figure 3.1). Note large quartz phenocrysts. Scale bar in cm.

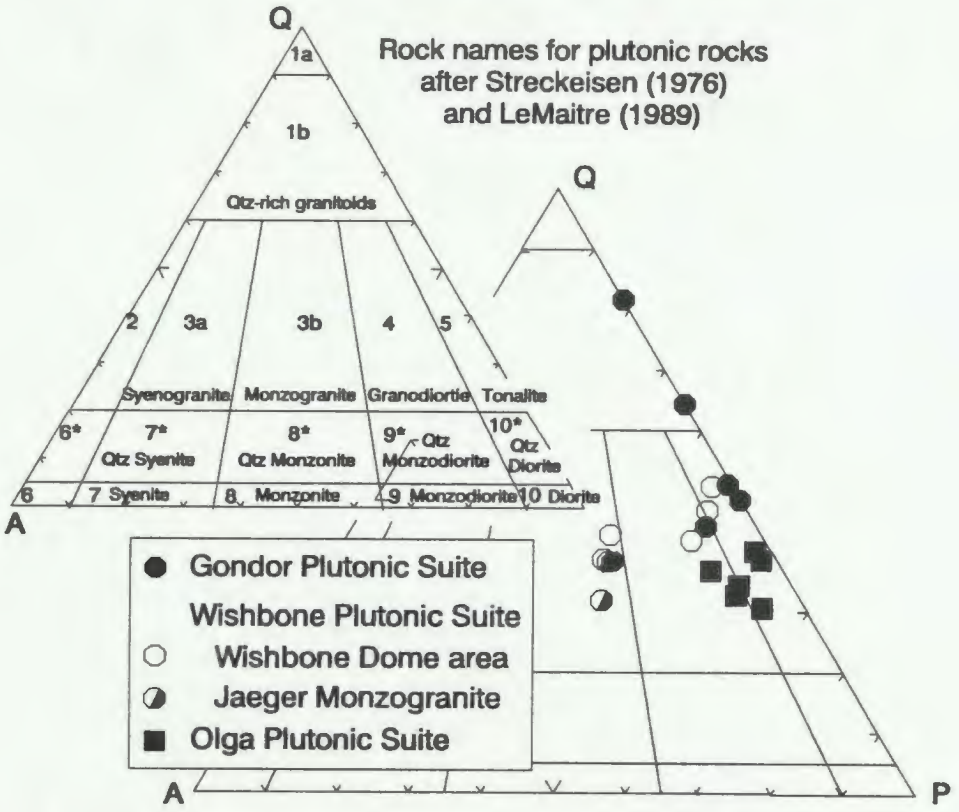

Figure 3.7. Quartz-plagioclase-alkali feldspar (QAP) mesonorm diagram for plutonic rocks associated with the older tectono-stratigraphic assemblage. Rock names following Streckheisen (1976) and LeMaitre (1989) are shown in inset.

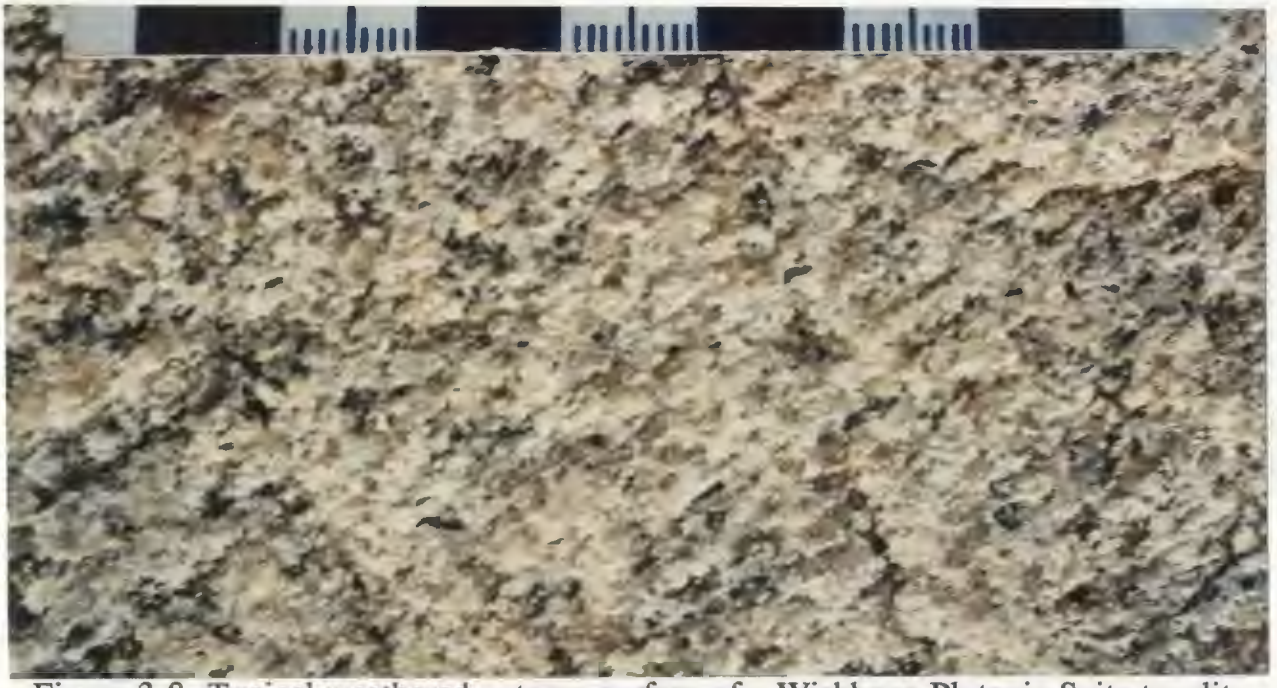

Figure 3.8. Typical weathered outcrop surface of a Wishbone Plutonic Suite tonalite, Wishbone Dome area. Scale in cm.

Figure 3.9. Tonalite sill of the Olga Plutonic Suite intruding the overlying mafic volcanic rocks of the Central Volcanic Belt.

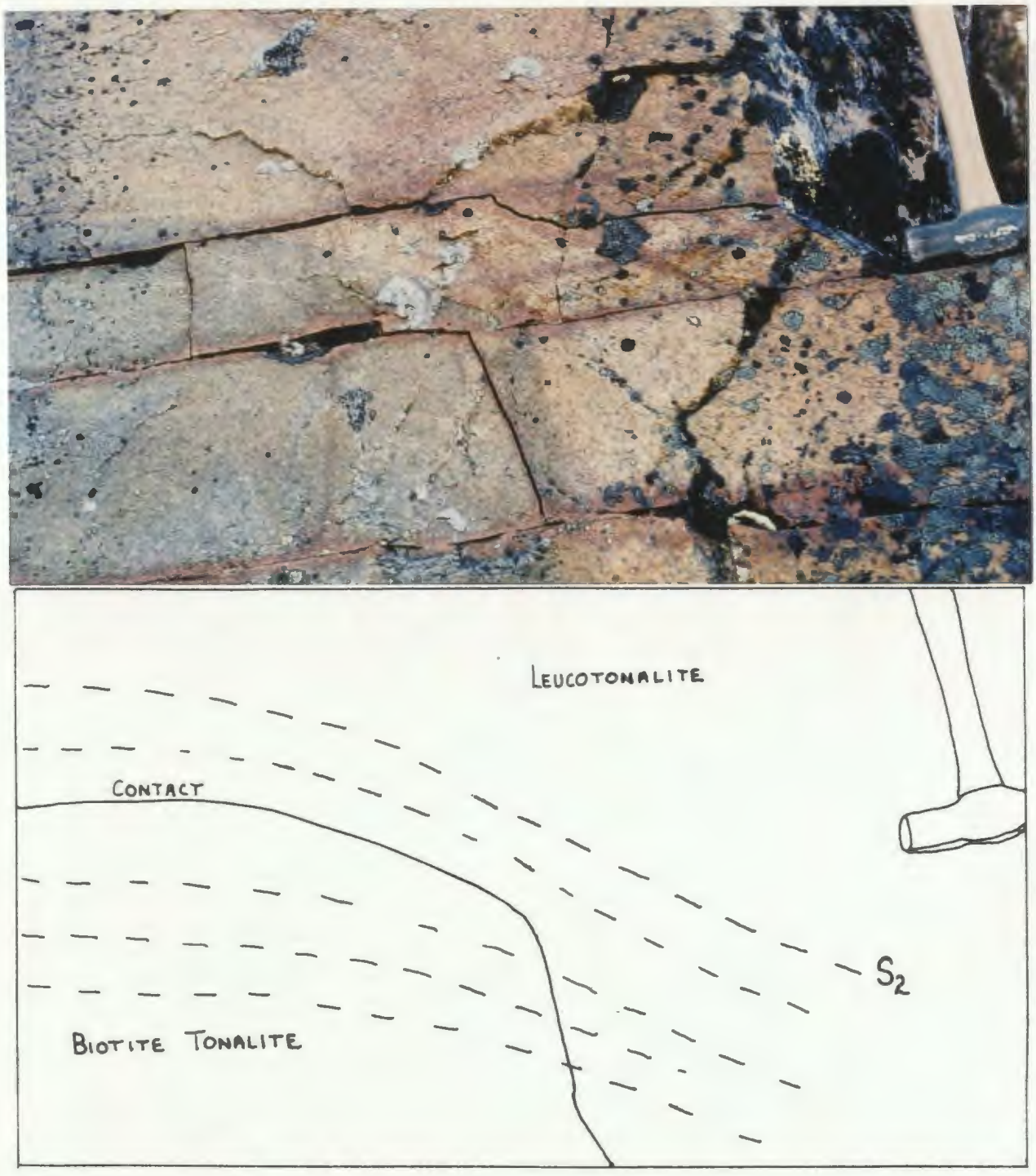

Figure 3.10. A) Contact between two tonalites of the Olga Plutonic Suite. Foliation surface (S_2), highlighted in the accompanying line drawing cuts across the contact at a high angle. Both of the phases shown in this photo have been dated within error of 2650 Ma (van Breemen *et al.*, (1990), Table 3.1).

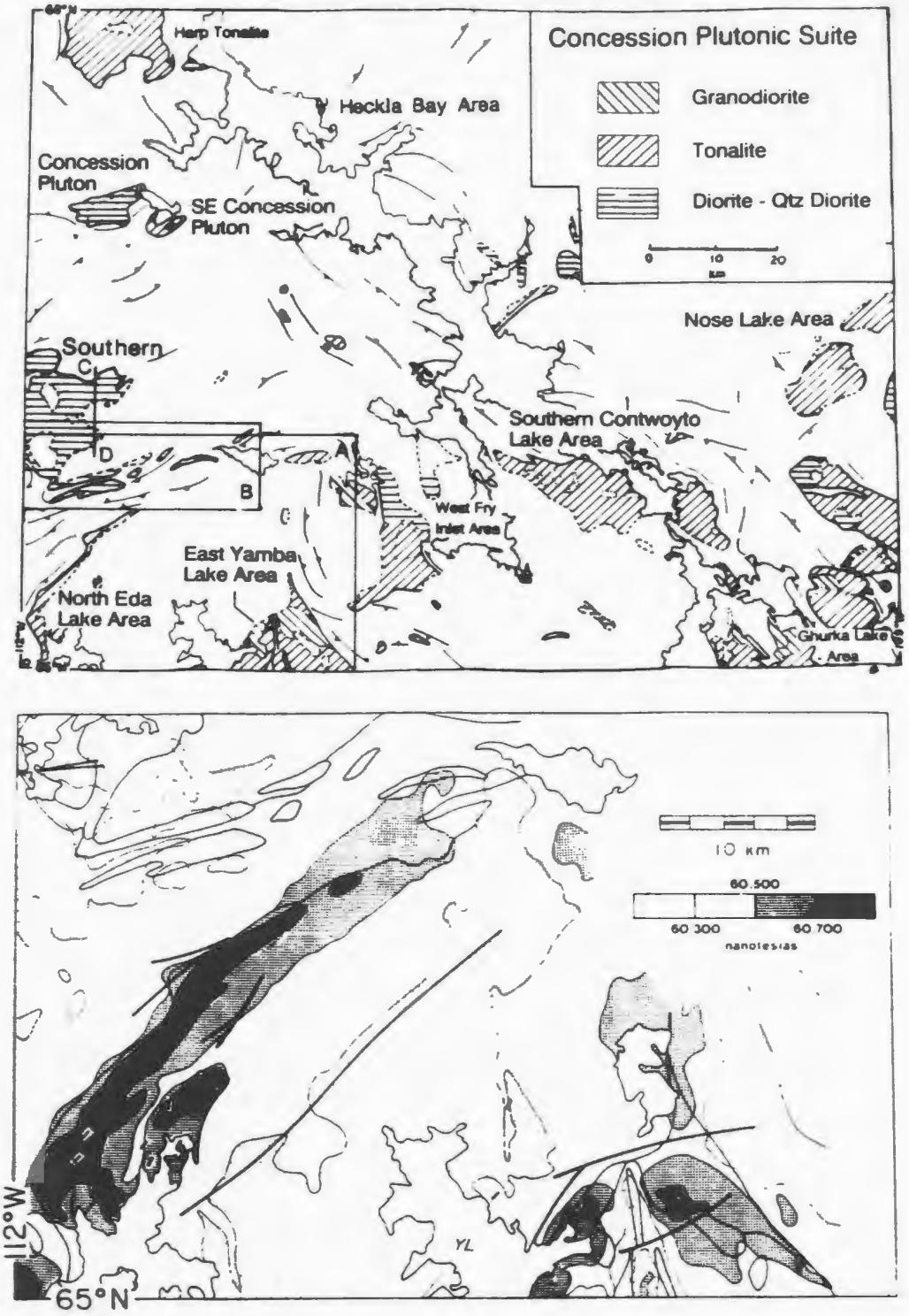

Figure 3.11 A) Regional distribution of rocks of the Concession Plutonic Suite. Names refer either to individual plutonic bodies or to geographical areas. B) Residual magnetic anomaly map of the southwest corner of the map sheet (location outlined by Box A on Figure 3.11A) modified from GSC aeromagnetic map 7206G (King et al., 1989). Magnetic highs correspond with location of Concession Suite plutons (compare also with Figure 3.1). Heavy lines are Proterozoic faults; thinner lines are geological contacts.

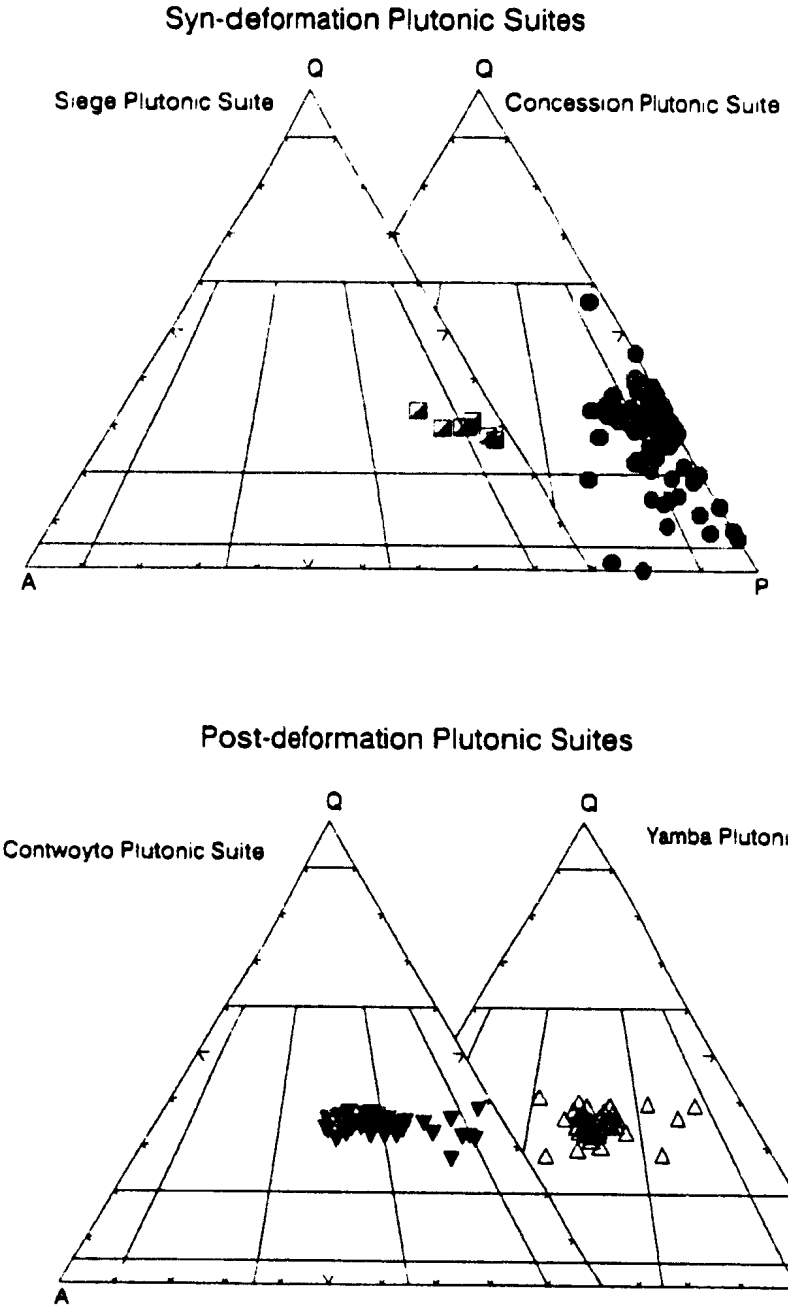

Figure 3.12. QAP mesonorm diagram for syn-deformation and post-deformation plutonic rocks.

Figure 3.13. Typical textures of weathered surfaces of rocks of the Concession Plutonic Suite. A) Strongly foliated hornblende-biotite quartz diorite, intruded by younger (*ca.* 2585 Ma) pegmatite. B) Sharp intrusive contact between different phases. C) massive hornblende biotite quartz diorite. D) Swarm of elongate, microdiorite enclaves within hornblende-biotite tonalite at Nose Lake.


A
A
B
CENTIMETRE
B
INCH
C
D

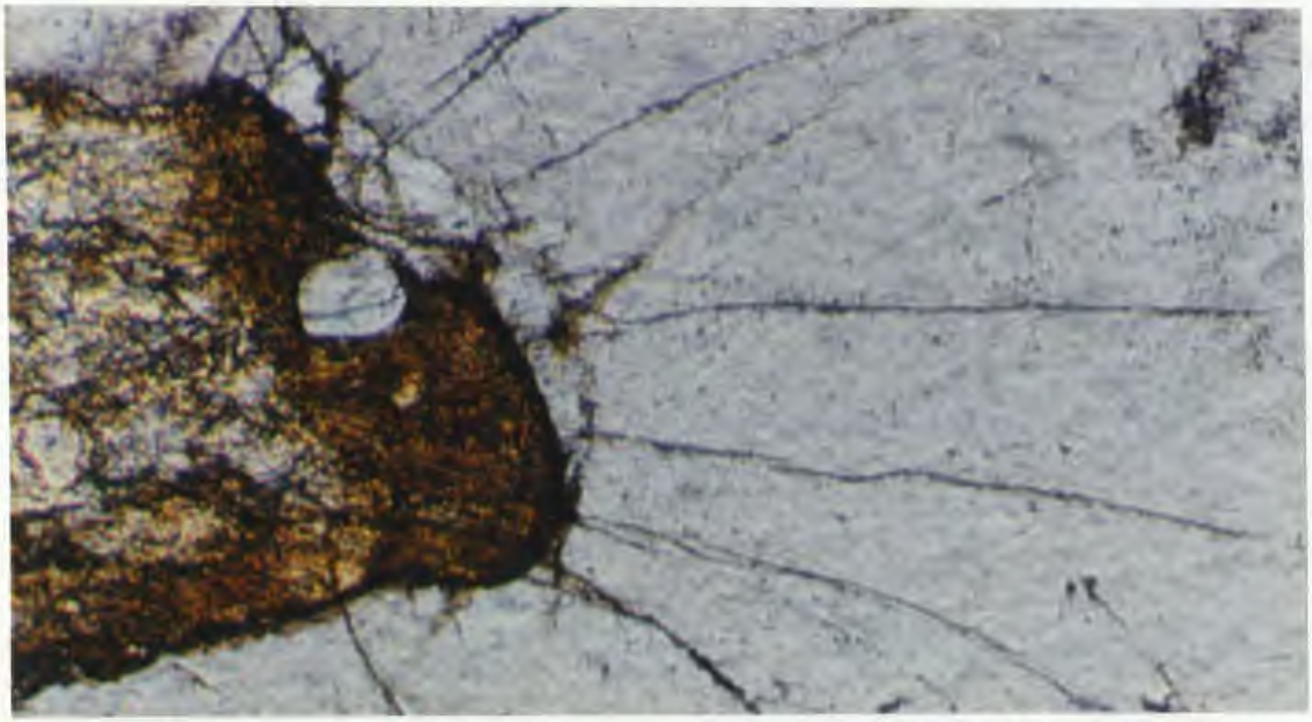

Figure 3.14. Photomicrograph of metamict allanite crystal rimmed by epidote, Concession Plutonic Suite. Width of photo = 1.5 mm.

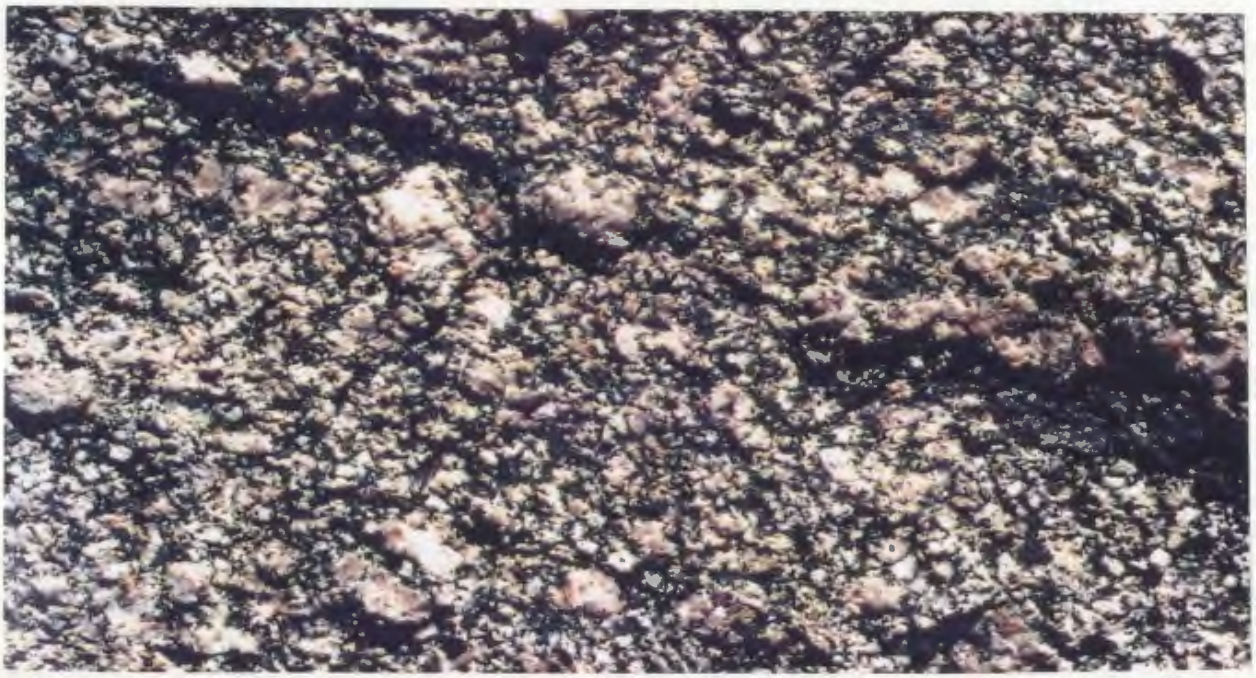

Figure 3.15. Weathered surface, foliated, K-spar porphyritic biotite monzodiorite, Concession Plutonic Suite. True scale.

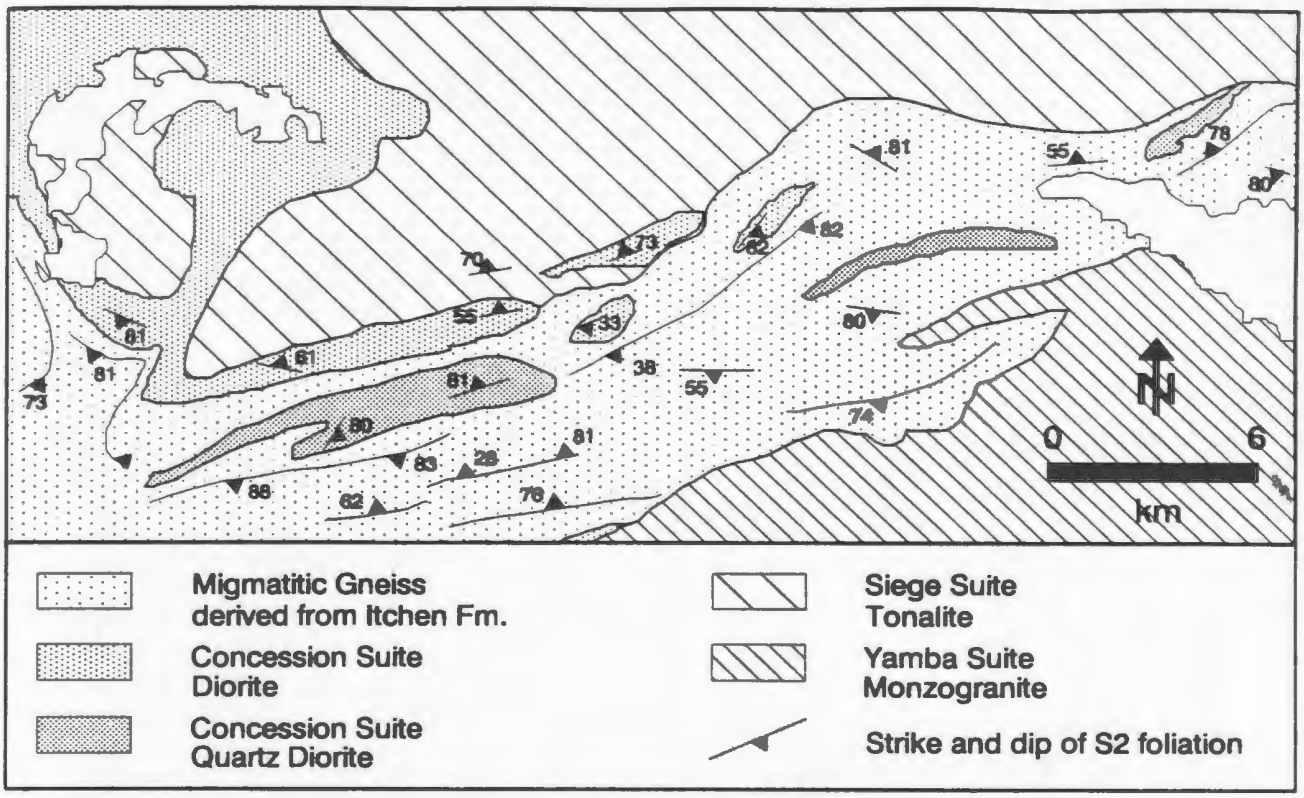

Figure 3.16. Map showing layer parallel bodies of diorite and quartz diorite of the Concession Suite intruded within paragneisses of the YKS. The plutons are elongate parallel to, and contain a foliation surface concordant with the regional S_2 surface in the host gneisses. Location indicated by Box B, Figure 3.11A.

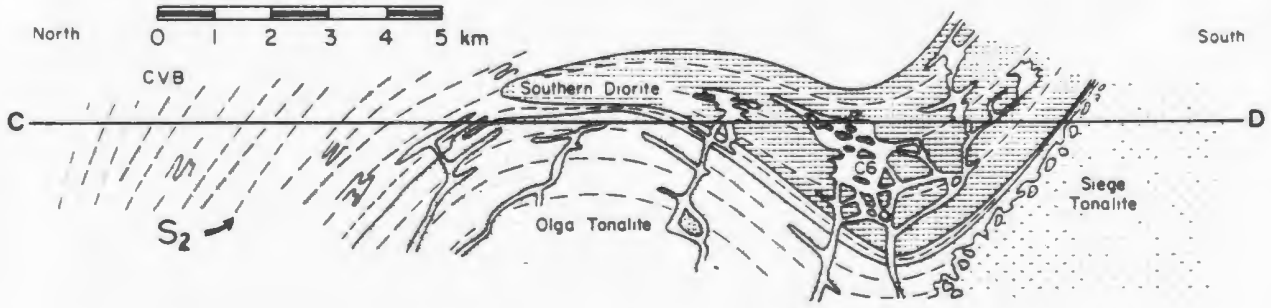

Figure 3.17. Interpreted geological cross section of the Southern Diorite in the Olga Lake area. Section line (C-D) shown on Figure 3.11A. Southern Diorite forms large tabular sheet near or at the contact between the CVB and the Olga Tonalite. Bodies intruding the Southern Diorite (labelled C6) are undifferentiated post-deformation granites.

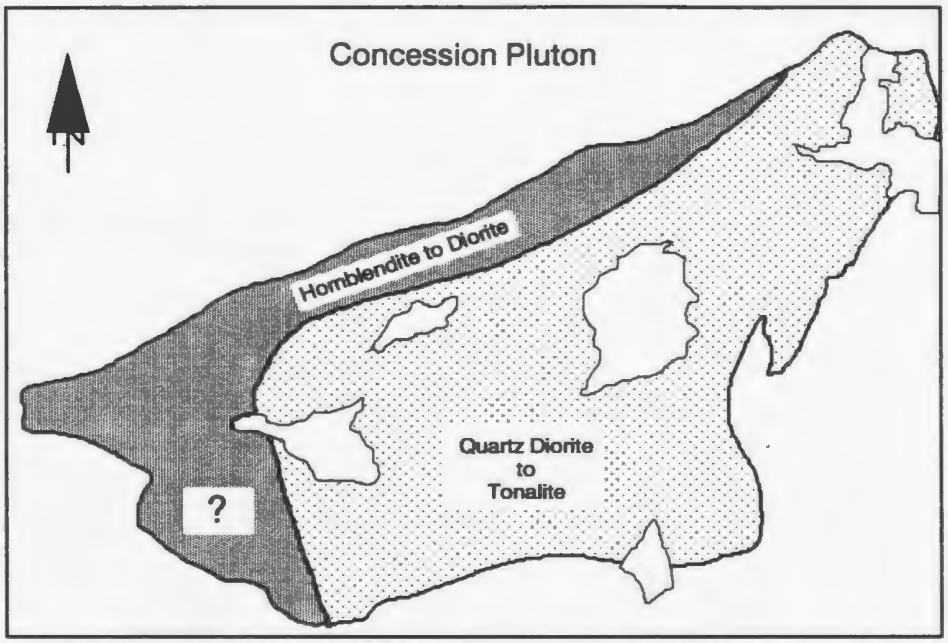

Figure 3.18. Map of the Concession Pluton showing marginal zone of mixed diorite and hornblendite and a relatively homogeneous core of quartz diorite and tonalite. The contact between the different phases are intrusive (see Figure 3-19).

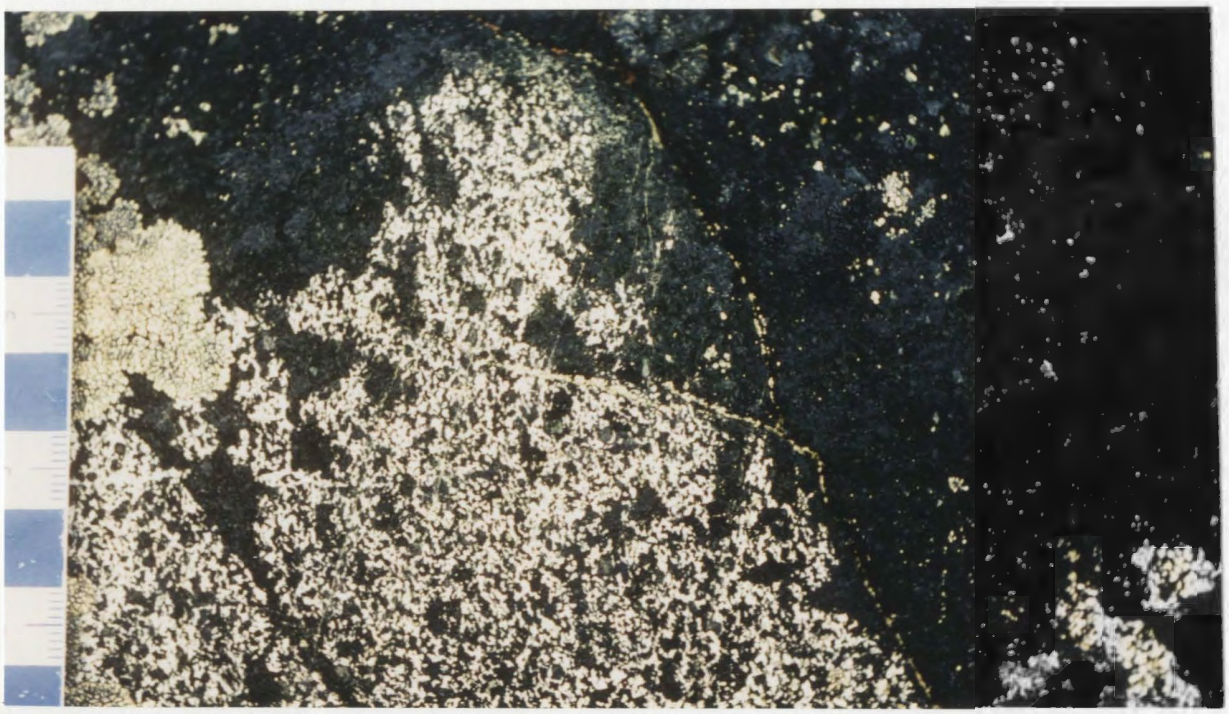

Figure 3.19. Hornblendite within marginal zone of the Concession Pluton being disaggregated by and incorporated within intruding diorite.

Figure 3.20. Typical weathered outcrop surface of a tonalite of the Siege Plutonic Suite. Brownish coloured quartz is characteristic of this suite. ▬ = 1 cm

Figure 3.21. Intrusive contact between the Siege Tonalite and rocks of the Olga Plutonic Suite. The host rocks have been intimately veined by the intruding tonalite prior to folding. The fold geometry within the immediate contact zone (10 to several 100 m wide) does not correlate with regional structures and is presumed to be related to intrusion of the tonalite.

Figure 3.22. Characteristic weathered outcrop surface of rocks of the Yamba Plutonic Suite. A) Equigranular texture, Pellatt Lake Monzogranite. B) Microcline porphyritic monzogranite, Wolverine Monzogranite. Scale in cm.

Figure 3.23. Aerial photograph of dykes of Yamba Suite monzogranite within quartz diorite of the Concession Suite. Pale areas are Yamba Suite rocks, dark areas are enclaves of the Concession Suite. Field of view approximately 250 m.

Figure 3.24. Gneissic texture in granitoids at the eastern margin of the Wolverine Monzogranite. The texture is interpreted to originate by hybridization of Concession Suite tonalites by potassic fluids discharged from the Wolverine Monzogranite during emplacement and cooling.

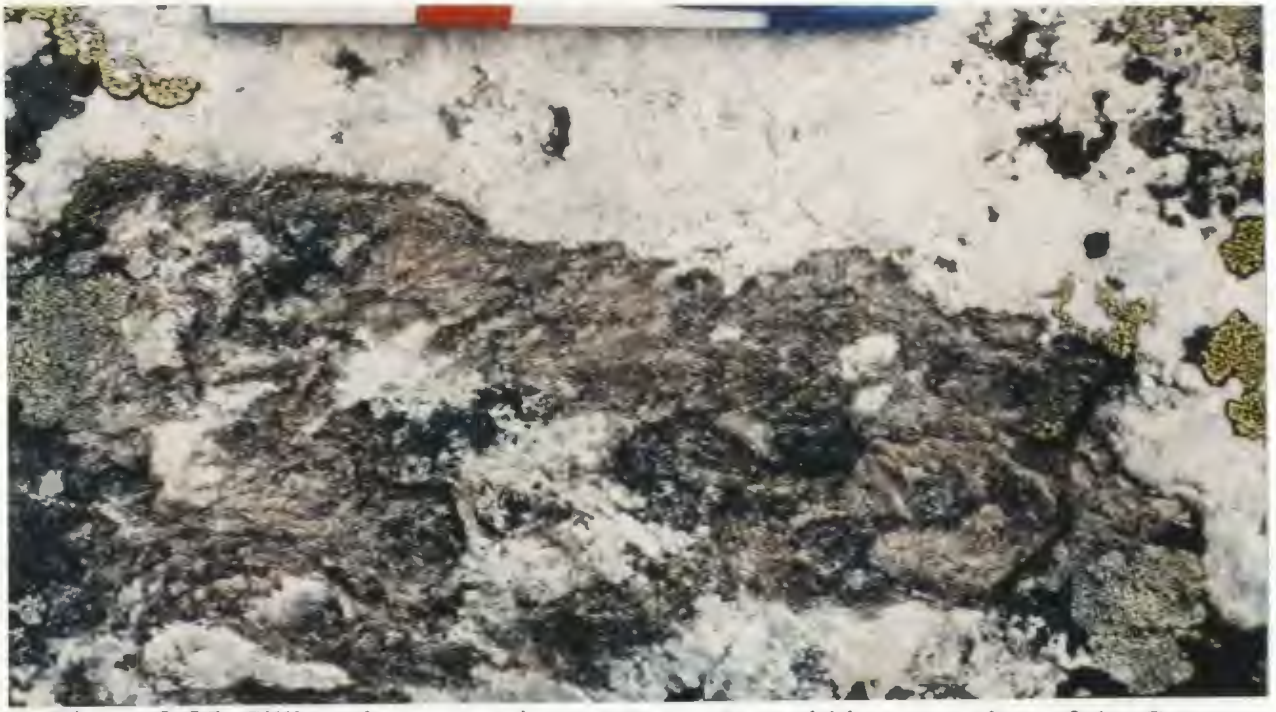

Figure 3.25. Sillimanite-muscovite-quartz rosettes within pegmatites of the Contwoyto Plutonic Suite, Contwoyto Monzogranite, northeast of the Lupin mine site.

Figure 3.26. Contact between fine to medium grained monzogranite and pegmatite in the Contwoyto Monzogranite. Sharply bounded internal pegmatites are a characteristic feature of the Contwoyto Plutonic Suite. Scale in cm.

Figure 3.27. Sharply bounded rafts of metasedimentary rocks (dark areas) within the Contwoyto Monzogranite. Large xenoliths have undergone very little rotation, as indicated by the continuous trace of the S2 surface from enclave to enclave.

Figure 3.28. Biotite-rich schlieren within Contwoyto Monzogranite interpreted to be residual from assimilated host metasedimentary rocks. Scale in cm.

Chapter 4
Geochemistry and Petrogenesis of the Central Volcanic Belt and Pre-Deformation Plutonic Suites

4.1 Introduction

This chapter describes the geochemistry of, and discusses petrogenetic constraints on the origin of igneous rocks associated with the early assemblage; including volcanic and plutonic rocks of the Central Volcanic Belt and the Gondor, Wishbone and Olga Plutonic Suites. All of these rocks pre-date regional deformation and metamorphism and were emplaced within a 20 m.y. period between 2670 and 2650 Ma. This time period is coincident with formation of many other volcanic belts within the Slave Province (Mortensen *et al.*, 1988).

Rocks of the early assemblage consist of three main groups:
1) a basalt-andesite-dacite-rhyolite volcanic series of the Central Volcanic Belt (CVB) and intrusive rocks of the CVB Plutonic Suite; 2) high-SiO_2, low-Al_2O_3 felsic rocks of the Gondor and Wishbone Plutonic Suites and rhyolites of the CVB; and 3) moderate-SiO_2, high-Al_2O_3 trondhjemites of the Olga Plutonic Suite. This tripartite division differs from the divisions based on field characteristics (Chapter 3), with the Gondor and Wishbone Suites grouped together because of their similar geochemical characteristics.

The chapter is organized as follows:

1) the geochemical characteristics of each of the three groups will be presented in sequence, followed by; 2) a brief discussion of the petrogenesis and evolution of each of the groups.

4.2 Presentation of Geochemical Data

4.2.1 The Central Volcanic Belt and Associated Mafic Plutonic Rocks

The data presented below do not form a comprehensive study of the volcanic belt. Relatively few samples were analyzed and the data serve only as a reconaissance study of the broad geochemical characteristics of the belt. Detailed studies of Archean (*e.g.*

Thurston and Fryer, 1983) as well as younger greenstone belts (*e.g.* Swinden *et al.*, 1990) serve to illustrate the complexity of rock types that may be found within an individual volcanic belt.

Representative chemical analyses of CVB volcanic rocks and the associated CVB Plutonic Suite are presented in Table 4.1. Selected major elements are plotted on Harker diagrams in Figure 4.1. The samples are dominantly calc-alkaline (Figure 4.1d, 4.2), and range in composition from 50 to greater than 80 wt% SiO_2. The calc-alkaline designation for these rocks is based on major element criteria, which, in some cases, may be altered by secondary processes such as metamorphism and metasomatism. Although this possibility cannot be evaluated for the samples discussed here, the more extensive major element data set of Bubar and Heslop (1985), also suggests a dominantly calc-alkaline character and a continuous range in SiO_2 for the least altered samples of the CVB. Lithological mapping (King *et al.*, 1988) indicates a continuous compositional range with a high abundance of intermediate rock-types; a characteristic of calc-alkaline rock series.

Volcanic rocks are subdivided into two groups: 1) a basalt-andesite-dacite series; and, 2) high-SiO_2 rhyolites. The former have $SiO_2 < 70$ wt% with moderate to high Al_2O_3 ($> 15.5\%$) in contrast, the latter have $SiO_2 > 75\%$ and distinctly lower Al_2O_3 (< 13 wt%; Figure 4.1f). The high-SiO_2 rhyolites are compositionally similar to plutonic rocks of the Gondor and Wishbone Suites and will be discussed with them below.

Discussion of trace elements is restricted to those considered to be least affected by alteration and metamorphism (*e.g.* Ludden *et al.*, 1982); in particular the rare earth elements (REE) and high field strength elements (HFSE).

Distinctive geochemical features of the mafic and intermediate rocks include: low Ti; $(Th/Nb)_N$ and $(La/Nb)_N$ ratios greater than one; and moderate to high $(Ce/Yb)_N$ (Table 4.1; the subsript $_N$ indicates chondrite normalized values, Appendix 5). Sample D054b-87, a gabbro of the CVB has $(Th/Nb)_N$ less than one but $(La/Nb)_N$ greater than

Table 4.1 Representative anhydrous analyses of rocks from the Central Volcanic Belt

	Mafic and Intermediate Rocks							High-Si Rocks		
Sample	D054b 87	D052 87	R051 87	D206 87	D237 87	D219 87	D052a 87	D084a 87	D220 87	K299 87
	Intr.	Volc.	Intr.	Volc.	Volc.	Volc.	Volc.	Volc	Volc	Volc
SiO2 (wt%)	49.7	50.1	58 8	60.0	60.9	67.0	67.7	78.2	78.9	81 6
TiO2	1.02	0.66	0.74	0.98	1.10	0.57	0 61	0 28	0 00	0 13
Al2O3	17.8	16.0	15.9	17.2	15.9	15 6	16 2	10.9	11 4	9 76
FeO*	9.10	9 83	7.78	6.12	7.08	5.17	4 28	3 11	1 98	1 53
MnO	0.16	0.17	0.13	0.16	0.14	0.06	0 08	0 02	0 03	0 02
MgO	6.89	8.21	4.38	4 24	3.23	2.19	1 43	1 96	2 30	1 59
CaO	11.47	11.12	7.50	6 37	6 98	1 22	3.73	0 65	1 05	0 39
Na2O	2.83	2.64	3.56	4.11	4 30	7.13	4.24	4 68	2 73	2 10
K2O	0.86	1.08	1.07	0.53	0 14	0.80	1.65	0 20	1 60	2 85
P2O5	0.24	0.18	0.11	0.37	0.21	0.25	0 16	0 02	0 00	0 00
LOI	0.87	1.16	0.97	1.09	0.31	1 86	0.67	1 22	2 93	1 21
Mg#	57	60	50	55	45	43	37	53	67	65
Trace elements in parts per million										
Cr	119	17	nd	177	27	dl	dl	dl	dl	dl
Ni	121	42	nd	90	16	dl	dl	dl	dl	dl
Sc	31	43	nd	25	26	11	8	3	dl	dl
V	237	254	nd	195	183	51	56	dl	dl	dl
Zn	82	84	nd	78	87	66	62	29	15	dl
Rb	16	25	31	8	0	11	90	3	32	53
Ba	93	53	nd	91	14	201	302	30	199	624
Sr	329	282	193	161	192	144	235	53	53	137
Ga	18	15	nd	15	16	15	19	13	21	11
Nb	6.7	1.1	12.3	10.0	10.2	13 8	8.4	16 0	19.8	22 4
Zr	72	35	165	173	222	265	189	338	267	272
Y	18	13	36	24	30	29	11	36	31	42
Th	0.40	0.43	3.06	2.01	3.21	3.82	3.24		6 78	7 22
La	12.5	20.9	21.2	25.4	24.9	30.5	15 8	25.2	45.3	30 5
Ce	29 1	51.6	49.6	61	55.9	70	34.8	52.7	101	72
Pr	3.98	8.19	6.3	7.8	6.9	8 5	4.11	7.4	11.5	8 6
Nd	16.7	39.2	26.4	32.8	28 4	33.5	16.0	29 0	42 2	32 7
Sm	3.64	10.1	5 81	6.1	5.79	5.97	2.95	6 0	7 3	5 89
Eu	1.23	5.17	1.13	1.96	1.66	1 69	0.94	1.12	1.14	0 90
Gd	3.29	10.4	6.3	5.47	5.98	5.32	2.79	5 65	5.99	5 65
Tb	0.51	1.67	1.00	0 77	0 91	0.74	0 38	0.87	0 67	0 88
Dy	3.20	10.3	6.3	4 39	5 63	3.80	2.09	5.33	3.24	5 05
Ho	0.67	2.18	1.35	0.87	1.18	0.74	0.43	1.05	0.62	1.13
Er	1.76	5.74	3.71	2.26	3 24	2.01	1.10	2.99	1.72	3 32
Tm	0.26	0.81	0.55	0.30	0.46	0.31	0.16	0.42	0.28	0 51
Yb	1.67	5.53	3.71	2.01	3.15	2.20	1 03	2 70	2.06	3 80
Lu	0.24	0.82	0.56	0.29	0.47	0.33	0.16	0.40	0.33	0 59
Selected ratios										
Ti/Zr	85.	114.	26.9	34.0	29.6	12.9	19.4	5.0		2 8
Zr/Nb	10.8	31.7	13.4	17.3	21.8	19.2	22.4	21.2	13.5	12 2
Zr/Y	4.0	2.6	4.6	7.1	7.3	9.2	17.1	9.4	8.5	6 5
$(La/Nb)_N$	1.9	19.6	1.8	2.6	2.5	2.3	1.9		2.35	1.40
$(Th/Nb)_N$	0.5	3.5	2.2	1.8	2.8	2.5	3.4		3.06	2.88
$(Ce/Yb)_N$	4.51	2.42	3.5	7.9	4.6	8.3	8.8		12.7	5.0
Eu/Eu*	1.09	1.55	0.57	1.03	0.86	0.91	1.00		0.53	0.48

Abbreviations: Intr. = intrusive rocks of the Central Volcanic Belt Plutonic Suite; Volc. = volcanic rocks; dl = below detection limit; nd = not determined.

one. Mid-ocean ridge basalt normalized REE patterns are LREE enriched, with negative Nb anomalies, no significant Eu anomalies and flat, slightly depleted HREE patterns (Figure 4.3).

Ni abundances (Table 4.1) are lower than expected in primary mantle melts and therefore, all samples are considered to be fractionated. Incompatible trace elements (Th, Ce, Zr, Y) increase from basalts through andesites (Figure 4.4), consistent with typical calc-alkaline fractionation series (*e.g.* Gill, 1981).

A single isotopic analysis of a mafic sill gives an $\varepsilon_{Nd(t)}$ value of +3.1 calculated at 2667 Ma (Table 7.1; see Appendix 3 for discussion of Nd isotope nomenclature). This value is similar to estimates of Late Archean depleted mantle (Machado *et al.*, 1986; Shirey and Hanson, 1986).

4.2.2 The Felsic Rocks

Felsic granitoid and volcanic rocks make up a significant portion of the early assemblage in the area. Two types of felsic rocks are observed: 1) high-SiO_2, low-Al_2O_3 rocks many of which are enriched in Y and HFSE; and 2) moderate-Si, moderate-Al rocks with lower Y and HFSE (Figure 4.5). The former type includes felsic volcanic rocks and the Wishbone and Gondor Plutonic Suites. The latter type includes rocks of the Olga Plutonic Suite. The subdivision is similar to the high-Al_2O_3, low-Al_2O_3 tonalite subdivision of Arth (1979).

The Wishbone and Gondor Plutonic Suites - Low-Al_2O_3 Felsic Rocks

Chemical compositions of rocks of the Gondor and Wishbone Plutonic Suites are presented in Table 4.2 and high-SiO_2 volcanic rocks in Table 4.1. The rocks are weakly to strongly peraluminous and dominantly plot as trondhjemites and granites in O'Conner diagrams (Figure 4.6a and b). The three groups share a number of major element characteristics (Figure 4.7), including; high to very high-SiO_2, low Al_2O_3, generally high Na_2O, and low P_2O_5. Scatter in the major element data may reflect metamorphic or metasomatic affects. In particular, the wide range of values and high K_2O content of some of the rocks of the Wishbone Plutonic Suite (*e.g.* Jaeger

Table 4.2 Representative anhydrous analyses of the Gondor, Wishbone and Olga Plutonic Suites

Sample	D085b 87	D205a-87	D221 87	D327 87	D227 89	D038 89	D040 89	D072a 87	D[illegible]	[illegible]
Plutonic Suite	Gondor	Gondor	Gondor	Wishbone	Wishbone	Wishbone (J)	Wishbone (J)	Olga	Olga	Olga
SiO2 (wt%)	77.1	75.9	79.9	78 4	75 8	78 0	77.6.4	75 0	72 5	73 5
TiO2	0.24	0.21	0.08	0 32	0 36	0.08	0.04	0 04	0 36	0 28
Al2O3	12.3	11.7	11.6	11.5	12 9	12 2	12.3	15 1	14 8	[illegible]
FeO*	2.31	4 76	1.34	2 41	2.17	0 34	1 12	0 62	2 66	1 25
MnO	0.03	0.06	0.03	0 05	0.03	0.02	0.02	0 04	0 04	0 [illegible]
MgO	0.42	3 32	0.70	0 41	0.36	0.03	0.11	0 14	0.72	0 41
CaO	1.21	0 56	0.87	1 72	1 96	0 55	0 72	2.31	2 86	2 14
Na2O	4.62	2.34	4 81	4.03	4 13	4 07	3.85	5 33	4 69	[illegible]
K2O	1.79	1.16	0 67	1.19	2.27	4.12	4 21	1 40	1 24	[illegible]
P2O5	0.00	0.00	0.00	0 03	0.03	0.00	0 00	0 00	0 12	[illegible]
LOI	0.91	2.15	0.80	0 42	0.82	0.48	0.55	0 68	0 50	0 39
Mg #	24	55	48	23	23	6	15	29	33	41
Trace elments in parts per million										
Sc	3	dl	dl	3	nd	dl	nd	dl	nd	dl
Zn	13	56	14	21	nd	10	nd	3	nd	24
Rb	43	19	12	37	nd	132	nd	32	43	49
Ba	487	241	197	269	nd	591	nd	530	nd	7[illegible]
Sr	68	18	40	120	nd	20	nd	485	282	53[illegible]
Ga	16	20	21	14	nd	22	nd	16	nd	19
Nb	27.1	27.4	36 2	19.5	nd	28 7	32	1 2	5 0	1 [illegible]
Zr	313	328	231	266	nd	131	nd	66	235	83
Y	84	77	131	50	nd	79	101	1	7	[illegible]
Th	9.71	nd	9.41	4 34	nd	10.1	12.3	0 89	5 06	[illegible]
La	66	nd	86	25 1	47.6	nd	13 3	6 61	28 2	3 43
Ce	151	nd	179	48	98	nd	34 3	13 1	53	7 [illegible]
Pr	18.45	nd	23.73	5 54	11.1	nd	5.01	1 45	5 55	0 99
Nd	73	nd	95	20.4	38.9	nd	22 8	5 24	18 3	3 54
Sm	14.7	nd	20.1	4 33	7.1	nd	9 0	0 82	2 59	0 78
Eu	1.80	nd	2.94	1.20	1.00	nd	0.54	0 18	0 68	0 23
Gd	14.8	nd	21 2	4.95	6 6	nd	12.5	0 57	1 97	0 61
Tb	2.38	nd	3.74	1.04	0.97	nd	2.38	0.07	0 24	0 09
Dy	14.9	nd	23.6	7.66	6.1	nd	16.7	0.34	1 27	0 46
Ho	3.20	nd	4.93	1.80	1 26	nd	3.7	0 08	0.27	0 10
Er	8.77	nd	12.83	5.35	3.72	nd	11 4	0 18	0 68	0 24
Tm	1.29	nd	1.91	0 81	0.56	nd	1 75	0.02	0.10	0 03
Yb	9.69	nd	12.84	5.29	3.62	nd	11 4	0 16	0 69	0 20
Lu	1.31	nd	1 82	0.70	0.52	nd	1.64	0.03	0 12	0 03
Selected ratios										
Ti/Zr	4 6	3.8	2.1	7 3		3.7		3.7	9.2	5 7
Zr/Y	3.7	4.3	1.8	5.3		1.7		119.3	34 9	47 5
Y/Nb	3.1	2.8	3.6	2.8		2.8		0 4	1.3	1 8
$(Th/Nb)_N$	3.2		2.3	2.0				6.4	8.9	2 8
$(Ce/Yb)_N$	4.5		3.6	2.4	7.0		0.78	21.2	19.9	9 2
$(Gd/Yb)_N$	1.38		1.34	0.76	1 47		0.89	2 91	2.33	2 49
Eu/Eu*	0.37		0.44	0.79	0.31		0.11	0.81	0.92	1 02

Samples of Wishbone Suite marked with (J) are for the Jaeger Monzogranite, others from Wishbone Dome area dl = below detection limit, nd = not determined. Cr, Ni, V, below detection for all samples.

Monzogranite) and the high-SiO_2 volcanic rocks may be due to potassic metasomatism. As described in Chapter 3, the Jaeger Monzogranite is cut and metasomatized by potassic veins and its major element composition is unlikely to be a primary igneous feature. Samples which plot in the granite field (C) of Figure 4.6b are suspected of being K metasomatized.

The high SiO_2 (>77 wt%), low Al_2O_3 (<14 wt %) and generally high Na_2O (>4 wt%) contents are similar to quartz-keratophyres, trondhjemites and plagiogranites commonly associated with ophiolites, island arcs and ocean ridges (Table 4.3; Gill and Stork, 1979; Coleman and Donato, 1979; Thy *et al.*, 1990). Although in some cases rocks of these compositions have been shown to be of metasomatic origin, geochemical and petrographic arguments for igneous origins have been discussed by numerous authors (Coleman and Donato, 1979; Gill and Stork, 1979). Since the rocks are weakly altered (chloritized and sausseritized), and metamorphosed it is difficult to evaluate this question in this case. Bubar and Heslop (1985) described the chemical effects of alteration of volcanic rocks in the CVB, primarily related to hydrothermal massive sulfide mineralization, and concluded that Si and Na metasomatism is not a common alteration feature. Although a metasomatic origin cannot be clearly eliminated, and it is recognized that the extremely high SiO_2 contents may indicate some silicification, the general characteristics, particularly the distinctive trace element characteristics described below, are considered to be of igneous origin.

High contents of the HFSE, Nb, Zr and Y are particularly characteristic of the Gondor Suite. Rocks of the Gondor Suite have the highest Y contents, ranging from 75 to 135 ppm. The range in Y content occurs within rocks that only vary between 77 and 80 wt% SiO_2 (Figure 4.8). Samples of the Jaeger Monzogranite (Wishbone Suite) also have high Y and Nb but much lower Zr. Two samples of the Wishbone Suite from the Wishbone Dome area have slightly lower Y (34 - 50 ppm) similar to values determined for felsic volcanic rocks. The increase in Y within and between the different suites

Table 4.3 Comparison of Low Al2O3 Felsic Rocks to Recent Rocks

						Ophiolite - related				Island arc - related			Ridge - related	
	1	2	3	4	5	6	7	8	9	10	11	12	13	14
Sample	Wishbone	Gondor	CVB	CVB	Exp Melt	Oman	Karmoy	Sparta	Canyon	Fiji	Fiji	Fiji	Red Sea	Iceland
	D327 - 87	D065B - 87	D084A - 87	K299 - 87	Comp	OM - 32	Visnes	Complex	Mountain	Wainimala	Undu	Undu	Granophyre	Rhyolite
SiO2	78 39	77 09	78 20	81 63	73 07	73 01	75 28	78 36	72 55	74 46	79 59	75 28	69 17	
TiO2	0 32	0 24	0 28	0 13	0 67	0 47	0 26	0 24	0 58	0 36	0 20	0 50	0 23	
Al2O3	11 46	12 28	10 88	9 76	13 92	13 40	11 71	12 09	12 49	13 93	10 42	13 53	13 30	
FeO*	2 41	2 31	3 11	1 53	3 59	3 44	4 38	1 64	5 70	2 10	2 25	2 38	6 63	
MnO	0 05	0 03	0 02	0 02	0 1	0 13	0 05	0 04	0 15	0 11	0 05	0 01	0 17	
MgO	0 41	0 42	1 96	1 59	0 83	1 00	0 25	0 04	2 54	0 48	0 28	0 34	0 65	
CaO	1 72	1 21	0 65	0 39	3 4	3 00	2 41	1 38	0 76	0 58	1 76	2 48	2 66	
Na2O	4 03	4 62	4 68	2 10	3 43	5 30	5 50	4 51	5 05	6 50	4 09	4 72	4 40	
K2O	1 19	1 79	0 20	2 85	0 85	0 12	0 14	1 68	0 03	1 40	1 17	0 64	2 56	
P2O5	0 03		0 02		0 15	0 12	0 02	0 01	0 15	0 07	0 18	0 14	0 23	
LOI	0 42	0 91	1 22	1 21		1 33	0 94	0 96		1 17	2 32	1 85	1 08	
Rb	37	43	3	59		5				15	6	8	87	
Ba	269	487	30	624		64			23	300	123	90	440	
Sr	120	68	53	137		114	113			120	97	108	148	
Nb	19 5	27 1	16 0	22 4			11 9				1 3	1 2		
Zr	266	313	338	272		108	549			224	119	177	665	
Y	50	84	36	42			110			68	52	561		
Th	4 34	9 71	4 32	7 22		0 4		2 66	0 16	2 51	0 40	0 50		
La	25 99	65 90	25 17	30 52		4 00	15 15	11 78	2 09		7 82	76 18	34 79	
Ce	48 18	150 84	52 65	72 54		12 00	45 55	29 98	8 13		23 06		102 32	177 80
Pr	5 54	18 45	7 41	8 59							3 51	41 10		
Nd	20 38	73 32	28 99	32 65			32 46		8 52		17 04	210 49	61 39	90 32
Sm	4 33	14 69	6 05	5 89		3 80	10 04	5 36	3 39		6 82	71 17	13 30	21 00
Eu	1 20	1 80	1 12	0 90		1 10	1 51	1 05	0 76		2 00	8 42	3 07	2 59
Gd	4 95	14 83	5 65	5 65			12 51				5 81	81 19		17 98
Tb	1 04	2 38	0 87	0 88		1 00		1 34	0 95		0 89	12 03	2 56	
Dy	7 66	14 94	5 33	5 05			15 12				6 01	70 16		19 13
Ho	1 80	3 20	1 05	1 13							1 30	15 64		
Er	5 35	8 77	2 99	3 32			10 45				3 61	37 09		11 21
Tm	0 81	1 29	0 42	0 51										
Yb	5 29	8 69	2 70	3 80		4 90	8 16	7 22	4 00		3 01	27 06	16 37	10 55
Lu	0 70	1 31	0 40	0 59		0 80	0 93	1 18	0 63				2 05	

1. Wishbone Suite; 2. Gondor Suite; 3 – 4 Felsic volcanic rocks, CVB; 5. Partial melt of basalt, Beard and Lofgren, 1989;
6. Plagiogranite, Oman ophiolite, Coleman and Donato, 1979; 7. Plagiogranite, Karmoy ophiolite, Pedersen and Malpas, 1984
8. Trondhjemite, Sparta Complex, Phelps, 1979; 9 Quartz–keratophyre, Canyon Mountain ophiolite, Gerlach et al., 1981;
10 – 12. Miocene volcanic rocks, Fiji, Gill and Stork, 1979; 13 Red Sea, Miocene granophyre, Coleman and Donato, 1979
14. Iceland rhyolite, O'Nions and Gronvold, 1973

correlates with increases in Nb, Ga, LREE, and HREE and decreases in Zr and TiO_2 (Figure 4.8). The large variations in trace element content both within and between different suites occur at near constant SiO_2.

The primitive mantle normalized REE patterns of the three groups are generally similar in shape although the abundances vary (Figure 4.9a, b). Overall they are moderately fractionated ($(Ce/Yb)_N$ 2-5), with fractionated LREE, relatively flat HREE and negative Eu anomalies. REE patterns are generally subparallel and abundance correlates with Y and Nb content. Rocks of the Gondor Suite have the highest abundances of the REE and felsic volcanic rocks the lowest.

No Nd isotopic data are available for rocks of these suites.

The Olga Plutonic Suite - High-Al Trondhjemite

Representative analyses of the Olga Suite are presented in Table 4.2. All samples have high SiO_2 (72 to 76 wt%), Na_2O (4 to 6 wt%), and Na_2O/K_2O (>2); moderate Al_2O_3 (14 to 16 wt%); and low TiO_2, FeO*, and MgO. The rocks are subalkaline, weakly peraluminous (Figure 4.6a) and plot in the trondhjemite field in an O'Connor diagram (Figure 4.6b). The Olga Suite has lower SiO_2 and higher CaO, Al_2O_3 and P_2O_5 relative to the Wishbone and Gondor Suites (Table 4.2). They resemble typical high Al_2O_3 trondhjemites of Barker (1979)

The rocks are characterized by low Rb (<50 ppm), moderate to high Sr (300-500 ppm) and Ba (300 - 700 ppm) and low transition metal contents. In contrast to the Wishbone and Gondor Suites, Nb and Y abundances are extremely low.

The REE are strongly fractionated ($(Ce/Yb)_N$ from 9 to 21), with variable enrichment of LREE and depletion of the HREE (Figure 4.9b). The REE patterns show little or no Eu anomaly and have a distinct concave up curvature in the HREE. All of the samples have negative Nb and Ti anomalies, and positive Zr anomalies relative to the MREE (Figure 4.9b). Normalized REE patterns are typical of high-Al trondhjemites (Arth 1979).

Two samples from one intrusive unit have higher abundances of TiO_2, P_2O_5, Zr, Y, Nb, Th, and REE. The difference in REE abundance does not significantly affect the shape of the normalized REE patterns. The abundances of these trace elements correlate with the modal abundance of biotite, apatite and magnetite in the samples. Correlation of Zr, Th and P contents with REE abundance suggests that zircon and apatite may be the principal REE-bearing mineral phases. Differences in the trace element chemistry between the samples can be accommodated by models involving subtraction of the observed accessory mineral phases; zircon (Zr, Th, HREE), apatite (P, REE), and biotite (Ti, Nb). Apatite and zircon grains typically occur as inclusions within biotite crystals, therefore removal or addition of biotite would also remove zircon and apatite from the melt. The absence of samples intermediate between the two groups precludes rigourous tests of this hypothesis.

Two samples of the Olga Suite yielded $\epsilon_{Nd(t)}$ values of +1.1 and +3.5 calculated at the U-Pb age of 2650 Ma (Table 7.1). These values are similar to estimates of Late Archean depleted mantle values and to the single analysis of a mafic rock from the CVB presented above. They indicate that the source of the Olga Suite had depleted mantle-like Nd isotopic compositions at 2650 Ma.

Classification of Trondhjemite Rocks

The two-fold subdivision of the felsic rocks, described above, is similar to the high and low Al_2O_3 classification for trondhjemites proposed by Arth (1979) and shown in Figure 4.10a.

Low-Al_2O_3, high-SiO_2 incompatible element enriched volcanic and intrusive rocks similar to the Gondor and Wishbone Suites are common in Archean greenstone belts (Paradis *et al.*, 1988; Thurston and Fryer, 1983; Shirey and Hanson, 1986; Arth 1979) and share characteristics of trondhjemites and plagiogranites associated with ophiolite complexes (Malpas, 1979; Pedersen and Malpas 1984; Coleman and Donato, 1979; Phelps, 1979; Menzies *et al.*, 1980; Beard and Day, 1987; Gerlach *et al.*, 1981), recent

island arcs (Gill and Stork, 1979) and oceanic ridges (O'Nions and Gronvold, 1973; Thy *et al.*, 1990). Chemical compositions of representative analyses from these settings are compared to the low-Al_2O_3 felsic rocks from this study in Table 4.3.

The REE chemistry of modern examples of these rocks is diverse (Figure 4.10b), but is generally characterized by: high HREE abundances; convex up HREE patterns; and negative Eu anomalies. The major difference between most modern and Archean examples is the higher abundance of LREE in Archean rocks. Most of the Phanerozoic examples have $(Ce/Sm)_N$ values of less than one. In contrast, most Archean examples, including the rocks discussed above, have values greater than one. However, modern rocks with LREE-enriched patterns have been described from Iceland (O'Nions and Gronvold, 1973), the Red Sea (Coleman and Donato, 1979) and Fiji (Gill and Stork, 1979).

The trondhjemites of the Olga Suite are geochemically similar to high-Al, low Y 'continental' trondhjemites of Arth 1979. Recent examples of these rocks are commonly associated with magmatic arcs developed on thick segments of crust (>30 km) (e.g.the San Juan Province of the Western USA (Zielinski and Lipman, 1976) and in central America (*e.g.* Drummond and Defant, 1990)).

4.3 Petrogenesis

4.3.1 Central Volcanic Belt and Associated Mafic Plutons

The limited number of analyses do not permit a detailed discussion of the petrogenesis of the mafic and intermediate rocks of the Central Volcanic Belt. However, the following points can be made.

1) The low Nb content relative to La, enriched LREE patterns and low HREE of the samples with less than 61 wt% SiO_2, relative to mid-ocean ridge basalts (Figure 4.3) are characteristics of modern subduction-related rocks (Figure 4.11; Kay, 1980; Gill, 1981). Sample D054b-87 has a low $(Th/Nb)_N$ ratio uncharacteristic of island arc magmatism. The Th value has been reproduced in duplicate, and if primary implies a non-arc or back-arc origin. As in modern examples of these rocks, the trace element

characteristics are considered to reflect complex multi-component mixing (mantle, subducted sediments and oceanic lithosphere), melting and fractionation processes in the mantle wedge and crust overlying a subducting oceanic plate (Kay, 1980; Arculus and Powell, 1986; Gill, 1981).

2) Fractionation trends defined by the samples (including those presented by Bubar and Heslop, 1985) are similar to those observed in modern calc-alkaline volcanic series (Gill, 1981); reflecting crystal fractionation, assimilation and mixing processes within the crust.

4.3.2 Petrogenesis of the Low Al_2O_3 Felsic Rocks - CVB Rhyolites, and the Gondor and Wishbone Suites

Petrogenetic models must explain: 1) the large volumes of felsic rocks; 2) the apparent lack of associated intermediate or cumulate rocks; and, 3) the extreme enrichment in the HREE, Y, Zr, Nb.

Low Al_2O_3 tonalite/trondhjemite rocks are generally considered to be derived either from partial melting of basaltic protoliths or the end products of fractional crystallization of mafic parental compositions (Barker, 1979; Coleman and Donato, 1979; Gerlach *et al.*, 1981; Pedersen and Malpas, 1984). An origin by liquid immiscibility has also been suggested; however the absence of suitable, FeO-rich mafic end members and the relative volumes of liquids involved largely precludes this model as a viable alternative (Pedersen and Malpas, 1984).

Although fractional crystallization is a preferred model to generate many low-Al_2O_3 trondhjemites it seems inadequate to account for the trondhjemites under discussion here. Figure 4.5 highlights a compositional gap between the low Al_2O_3 felsic rocks and the moderate to high Al_2O_3 mafic to intermediate rocks. The compositional gap suggests the felsic rocks are probably unrelated to the basalt-andesite-dacite series by crystal fractionation.

The low Al_2O_3 felsic rocks are characterized by large within- and intra-suite variations in REE and HFSE contents. These variations occur at virtually constant SiO_2

and are largely decoupled from the major element chemistry. Extreme enrichments in the HFSE and REE during the final stages of fractionation of felsic systems are commonly documented in high-SiO_2 volcanic and plutonic rocks (*e.g.* Hildreth, 1981; Miller and Mittlefehldt, 1984; Cerny *et al.*, 1985). Processes capable of producing such trace element enriched liquids may include combinations of both crystal fractionation and liquid and volatile complexing (*e.g.* Hildreth, 1981; Cerny *et al.*, 1985; Miller and Mittlefeldt, 1984; Whalen *et al.*, 1987). Similar models have been discussed for other Archean examples (*e.g.* Paradis *et al.*, 1988; Thurston and Fryer, 1983).

Studies of these fractionation processes are best made in fresh glassy volcanic rocks, not in the metamorphosed Archean examples described here. All that can be concluded is that the nature of chemical variation within these rocks is comparable with the complex fractionation processes proposed for other high-SiO_2 magmatic systems. In the following discussion, it is assumed that the least fractionated samples are those with the lower HFSE and REE abundances

Origin of the Least Fractionated Rocks by Partial Melting Mafic Protoliths

Anhydrous and hydrous partial melting of basalt at both high and low pressure may yield liquids which are broadly tonalitic/trondhjemitic in character (Stern and Wyllie, 1978; Huang and Wyllie, 1986; Ellis and Thompson, 1986; Beard and Lofgren, 1989; Helz, 1976). The major element chemistry of the melt is very sensitive to P_{H_2O}, fO_2 and initial source composition (Helz, 1976; Beard and Lofgren, 1989). Under water excess ($P_{H_2O} = P_{tot}$) conditions (*ie.* residual amphibole), melts are strongly aluminous in comparison to natural rocks (Helz, 1976; Beard and Lofgren, 1989; Ellis and Thompson, 1986). In contrast, melts produced by low pressure dehydration melting closely approximate the bulk compositions of natural low-Al_2O_3 trondhjemites and tonalites (Figure 4.12).

Table 4.3 and Figure 4.12 show the compositions of the felsic rocks to be comparable to the major element compositions of liquids produced by basalt-melting experiments. SiO_2 contents of the experimental liquids are generally lower than values

in the natural rocks, possibly owing to the effects of later, high level fractionation discussed above, or silicification. The first order control on experimental melt composition is P_{H2O}. Low Al_2O_3 compositions are produced only under water-deficient conditions (Figure 4.12). Beard and Lofgren (1989) reported a second order dependency on protolith composition. For example, the K_2O content of the melt is critically dependent on the K_2O content of the source. The ranges in K_2O content determined in the Wishbone Suite and the felsic volcanic rocks (1-4 wt%) are comparable to those in Icelandic rhyolites (*e.g.* Thy *et al.*, 1990). In the latter case, the range of values are attributed to differences in mafic source compositions (Thy *et al.*, 1990). It is considered unlikely that the K_2O content is of primary origin in the felsic rocks of this study.

Quantitative trace element models have been made to evaluate the applicability of the experimental basalt melting studies described above. The results are not unique and serve only to show the general potential of this process. The models were evaluated by inverting the equilibrium batch melting equation (Arth, 1976) to solve for the trace element Bulk D values of the residual assemblage. Solving the equations in this manner tests for rather than assumes the residual mineralogy (see explanation of this technique in Appendix 4). Unfortunately, the parental liquid compositions cannot be well constrained, because of the effects of high-level fractionation processes. In the models, the parental composition is assumed to be similar to the least fractionated samples (*ie.* those with lowest REE and HFSE contents: Wishbone Suite - D327-87, and felsic volcanic rocks K299-87, Table 4.2). Two different source rock compositions were used in the modelling: 1) basalt with trace element abundances at 10 times primitive mantle values; and 2) a LREE-enriched source similar to a gabbro (D054b-87) from the CVB. The degree of melting was varied from 1 to 20 wt%, although only the results for 5 and 20% are shown. Results are presented in Figure 4.13.

The Bulk D values required to yield appropriate liquid compositions are weakly fractionated, and have positive Eu anomalies. Most elements show incompatible behaviour regardless of the degree of melting (Figure 4.13). The results of the inverse

modelling can be compared with Bulk D values, calculated from published Kd values (Appendix 4), and using appropriate experimentally determined residual assemblages (Figure 4.13e). The general shape of the Bulk D patterns is not particularly sensitive to changes in Kd values for individual minerals although the absolute values obviously are. Pattern shape is most sensitive to changes in the relative abundances of residual minerals.

The calculated Bulk D values are consistent with a low pressure (below garnet stability field (< 8 kb; Green, 1982) residual assenblage consisting of clinopyroxene, orthopyroxene and plagioclase (Assemblage A, Figure 4.13), similar to that documented in the melting experiments of Beard and Lofgren (1989). Plagioclase in the residuum predicts the positive inflection in the Bulk D values at Eu. Positive inflections for Nb may either reflect the effect of clinopyroxene or amphibole (Kd values are poorly constrained), a Nb-bearing residual phase (titanite, rutile, oxide), or an initial Nb anomaly in the source rock.

The results of the trace element modelling allow for parental liquids to the low-Al_2O_3 felsic rocks to be partial melts of basaltic sources at low pressures (*e.g.* Thy *et al.*, 1990). High level fractionation processes subsequently produced the strong enrichment of the REE and HFSE.

4.3.3 Petrogenesis of High-Al Felsic Rocks - the Olga Plutonic Suite

Petrogenetic models must address the following characteristics: 1) the relatively uniform, trondhjemite composition; 2) the lack of evidence for contemporaneous intermediate or mafic magmatism; 3) the high $(Ce/Yb)_n$ ratios; 4) the low HREE abundances with concave up normalized patterns; 4) the absence of negative Eu anomalies; 5) positive Zr anomalies relative to the MREE; and 6) the juvenile Nd isotopic compositions.

The absence of compositionally suitable mafic or intermediate members suggests that this suite is unlikely to be derived from volcanic rocks of the CVB by fractional crystallization. The lack of significant negative Eu anomalies and the high Sr

abundances would be unusual features in tonalitic magmas derived by low pressure fractionation from typical basalts. Additionally, the Olga Suite may be up to 20 m.y. younger than the mafic and intermediate rocks they intrude.

The most characteristic trace element feature of this suite is the steep normalized REE patterns with convex up curvatures within the HREE. Models generally proposed to explain this pattern in tonalitic rocks involve partial melting of dominantly meta-basaltic rocks at eclogite, granulite or amphibolite grade (Arth and Hanson, 1975; Jahn *et al.*, 1981; Martin, 1985; 1987; Hunter *et al.*, 1978; Barker, 1979; Rudnick and Taylor, 1986). Experimental data supporting such models (in terms of major element composition), to varying degrees of success, have been reported by numerous authors (Helz, 1976; Stern and Wyllie, 1978; Ellis and Thompson, 1986; Huang and Wyllie, 1986).

Melting of mafic source rocks was tested by inverting the batch melting equation to calculate the Bulk D values required to derive a sample of the Olga Suite from a source with trace element composition of 10 times primitive mantle values. The method is similar to that described above. The calculated Bulk D values of the residuum are plotted in Figure 4.14a. The steep slope of the Bulk D pattern is similar to Bulk D patterns predicted for eclogites and garnet-amphibolites (Figure 4.14b) and suggests derivation from a garnet-bearing residuum.

In order to explain the pattern without garnet as a significant residual mineral phase requires the source composition to be LREE-enriched and to have a Gd/Yb ratio similar to that of the tonalite itself (Rudnick and Taylor, 1986). Since Archean mafic rocks with these trace element characteristics are not common (Sun, 1984) it is most likely that garnet was a stable residual phase.

Garnet stability on the liquidus in basaltic systems is strongly dependent on pressure and P_{H_2O} (Green, 1982). It is stable at depths greater than 25 km and 45 km under hydrous and anhydrous conditions respectively (Green, 1982). Appropriate residual assemblages could therefore be stable in the lower crust or upper mantle.

It is not possible to unambiguously differentiate between crustal and mantle depths of melting. Plagioclase stability is restricted to crustal depths and has a limited overlap with garnet, especially under hydrous conditions (Green, 1982). Residual plagioclase may result in negative Sr and Eu anomalies, neither of which are documented in the Olga Suite. However, since plagioclase would be the major contributor to the liquid it could have been totally consumed during non-modal melting, or its effect could be balanced by other residual phases.

The occurrence of positive Zr anomalies may also be a clue to the nature of the residual assemblage. Available Kd data suggest that clinopyroxene may retain Nd and Sm preferentially to Zr in the source, resulting in a positive Zr anomaly in the liquid. For example, eclogite melting , with 80% residual clinopyroxene results in a marked Zr anomaly similar to that required in the partial melting models (Figure 4.14b). This correspondence could suggest that clinopyroxene is a major residual phase, and thus favours a granulite or eclogite source. Ambiguity in the Kd values and the effect of other residual accessory minerals makes more definitive interpretations impossible.

An alternative interpretation of the positive Zr anomalies, not favoured here, is that the rock contains an inherited zircon component. In sample D072b-87 the Zr anomaly represents an excess of approximately 200 ppm Zr. Assuming stochiometric zircon contains on the order of 450,000 ppm Zr, an addition of less than 0.05 wt% zircon could account for the excess Zr. Heaman *et al.*, (1990) report HREE abundances in zircons from mafic and felsic rocks on the order of 10^3 to 10^4 times chondrite values. Assuming Yb abundance in the inherited zircon of 442 ppm (2000 * chondrite) results in the addition of approximately .22 ppm Yb to the rock, or 33 wt% of the total Yb in the rock. Subtraction of this amount of zircon would steepen the REE pattern considerably but would not otherwise change the interpretation concerning the role of garnet during partial melting. However, there is no evidence of zircon cores or inheritance in the U-Pb data of the sample with the greatest amount of Zr (van Breemen *et al.*, 1990). If the rock contains an inherited Zr component then it is not significantly older than the rock itself.

The positive $\epsilon_{Nd(I)}$ values for these rocks suggest that the mafic protolith was relatively juvenile. However, this does not provide an unequivocal constraint for the age of the protolith. Derivation of the tonalites by partial melting of eclogite or garnet-amphibolite will strongly fractionate $^{147}Sm/^{144}Nd$ in the melt relative to the source during melting and calculation of Nd model ages, based on the measured $^{147}Sm/^{144}Nd$ ratio, is meaningless. The protolith could have had a near chondritic $^{147}Sm/^{144}Nd$ ratio, as in the model above, and its $^{143}Nd/^{144}Nd$ composition would diverge rather slowly from that of the depleted mantle. Using the values assumed in this model, the mafic source could be significantly older than the 2650 Ma age of the tonalites (see Jahn *et al.*, (1984) for further discussion). The Nd data is therefore inconclusive in constraining the age of the protolith.

Considering the close spatial and temporal association with volcanism, it is simplest to derive the Olga Suite by partial melting the lower part of the CVB crust. The low HREE, high $(Ce/Yb)_N$ and positive Zr anomalies are consistent with a residual eclogite or garnet granulite source mineralogy. Garnet on the liquidus requires that melting of the crust occurred at depths greater than 25 km (Green, 1982). A thick crust for the CVB is consistent with the LREE enriched, calc-alkaline composition of the CVB volcanic rocks, which in modern environments are characteristic features of arcs constructed on thicker crust (Gill, 1981). Since most of the volcanic and related mafic plutonic rocks have negative Nb anomalies, the negative Nb anomalies in the Olga Suite rocks may be a feature inherited from the source. Alternatively, titanite or other Nb-bearing minerals could be stable residual phases during partial melting at crustal conditions (Green and Pearson, 1987).

4.4 Chapter Summary

Within the period from 2667 to 2650 Ma, a number of different rock types were generated. The age control on this time period is relatively poor because only single samples of representative rocks have been dated. Basaltic and andesitic volcanic rocks have not been dated and are assumed to be similar in age to the associated rhyolites.

The potential range in ages of the individual suites is unconstrained and it is possible that some or all events overlapped in time. The total age range of 17 m.y. is not large relative to the age of modern volcanic arc systems (Gill, 1981).

Basaltic and andesitic rocks of the CVB have many geochemical similarities to modern calc-alkaline orogenic basalts and andesites. By analogy, they most likely were derived by the partial melting of subduction-enriched mantle, followed by crustal fractionation, assimilation and mixing. More detailed studies are required to test this hypothesis. Low Al_2O_3 felsic volcanic rocks appear to be genetically unrelated, and may have been derived by crustal anatexis leaving a plagioclase and pyroxene dominated residua (*e.g.* Beard and Lofgren, 1989). Mafic rocks of the CVB are the most likely protolith.

Rocks of the Gondor and Wishbone Suites intruding the volcanic belt are similar, in terms of major elements, to the low-Al_2O_3 rhyolitic rocks of the CVB, and are also modelled as low pressure partial melts of basaltic protoliths. The extreme enrichment in incompatible trace elements may be due to subsequent high-level fractionation processes, typical of high-SiO_2 felsic magmatic systems (Hildrith, 1981; Cerny *et al.*, 1985; Whalen *et al.*, 1987). In this respect it is interesting to note that the extrusive rocks are less fractionated than plutonic rocks, as was demonstrated for extrusive and correlative intrusive rocks in the Abitibi greenstone belt by Paradis *et al.* (1988).

The age difference of 7 m.y. between the high-SiO_2 rhyolites (2667 Ma ± 1) and the Gondor Suite (2660 ± 1 Ma) is based on a single determination of each group. The Wishbone Suite has not been dated. In any case generation of low-Al_2O_3 felsic magmas occurred over a timespan of at least 7 m.y. and possibly represents a recurring petrogenetic process. Plutonic rocks of similar composition and age (*ca.* 2650 Ma) have also been described from the Yellowknife greenstone belt (Amacher Granite; Meintzer, 1987).

High-Al_2O_3 trondhjemites of the Olga Suite are distinct from all the earlier rocks. There is no evidence within the CVB for extrusive rocks of comparable composition; however Ewing (1979) described rhyolites of similar compositon from the Hackett

River volcanic belt 150 km to the east of the study area. The rocks can be modelled as high pressure (> 8 kbar) partial melts of basaltic source rocks within the lower crust or upper mantle. A crustal origin requires a thick crustal section at *ca.* 2650 Ma (> 25 km) consistent with the calc-alkaline characteristic of the slightly older volcanic belt. The close spatial and temporal association with the volcanic rocks suggests that they may represent melts of the lower portion of the CVB crust.

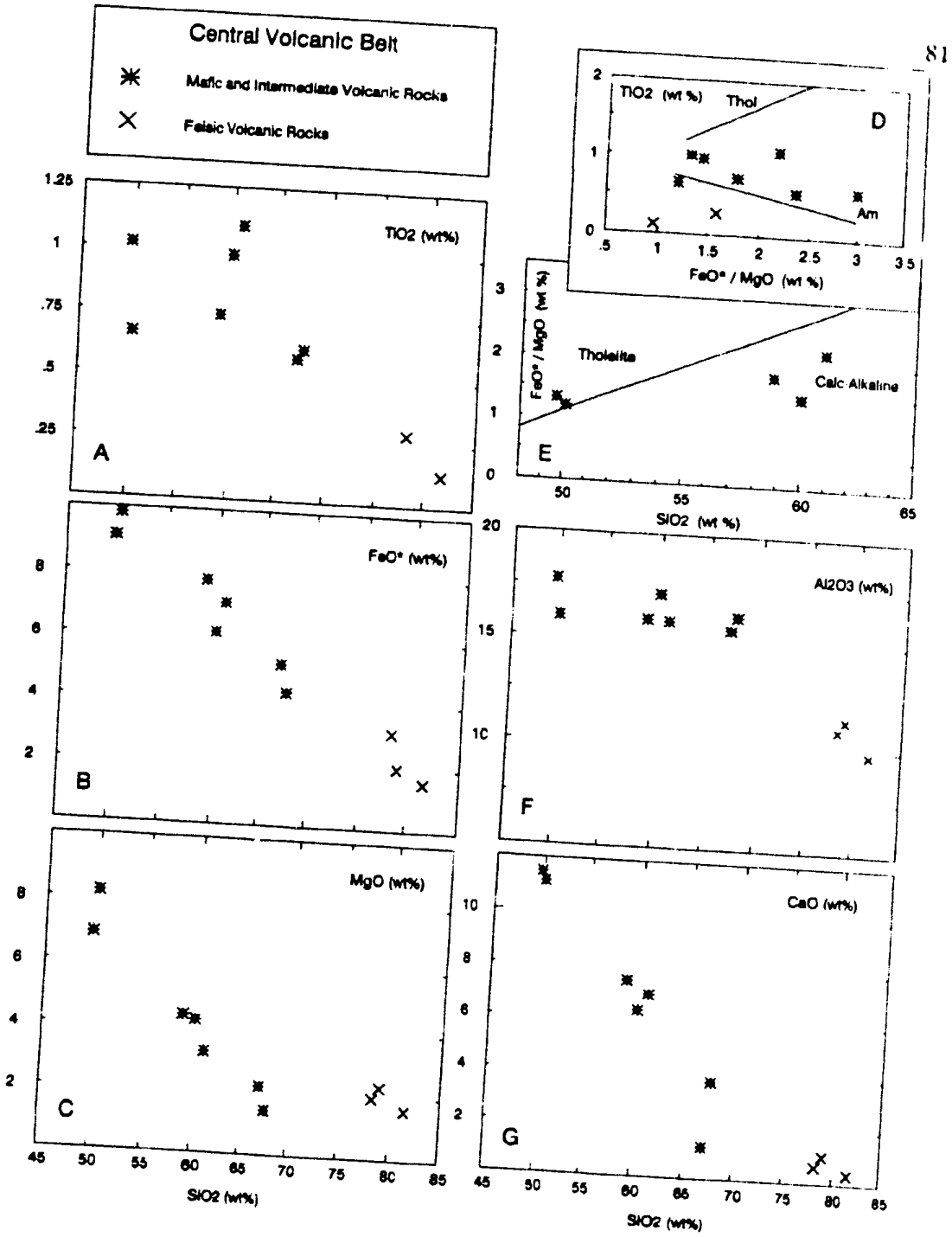

Figure 4.1. Major element variation diagrams for rocks from the Central Volcanic Belt (CVB). Fields for tholeiitic and calc-alkaline rocks shown in (D) and (E) are from Miyashiro, 1974.

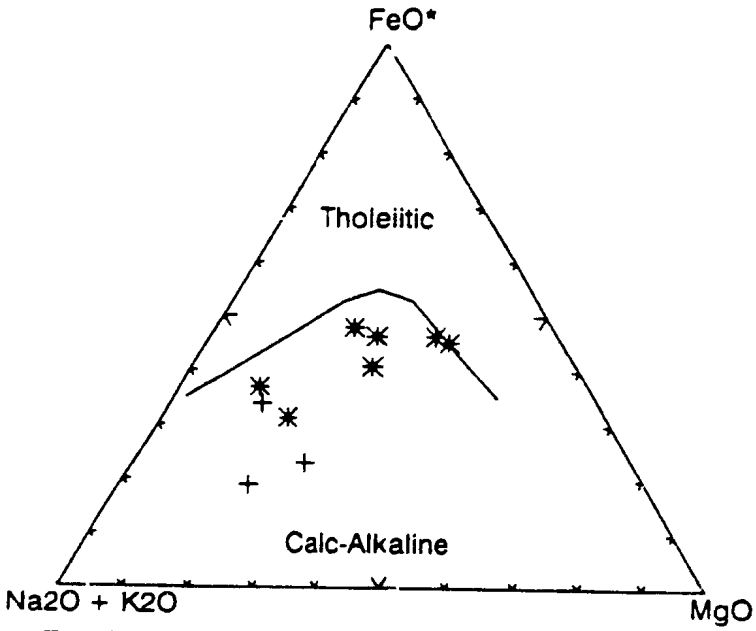

Figure 4.2. AFM diagram of rocks from the CVB. Symbols as in Figure 4.1. Calc-alkaline and tholeiitic fields from Irvine and Baragar, 1971.

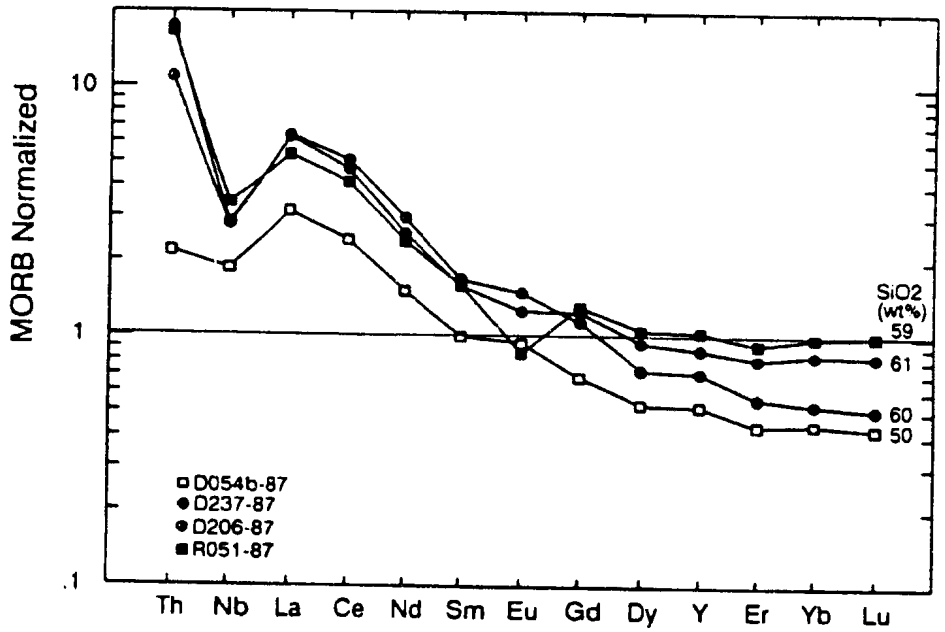

Figure 4.3. Mid-ocean ridge basalt normalized, extended REE diagram for mafic and intermediate rocks from the CVB. Sample D054b-87 is a mafic plutonic rock (CVB Plutonic Suite).

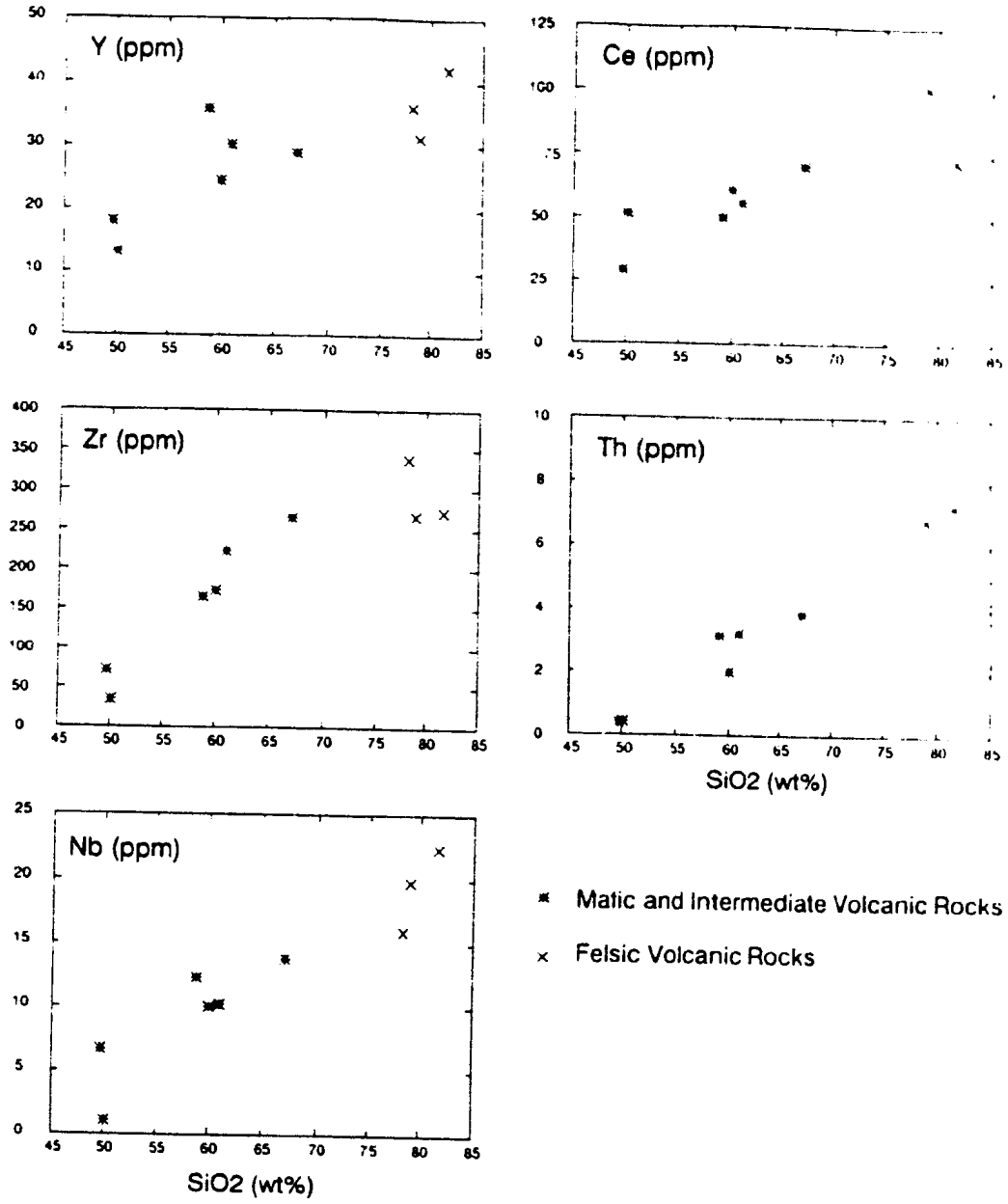

Figure 4.4. Trace element variation diagrams for rocks from the CVB.

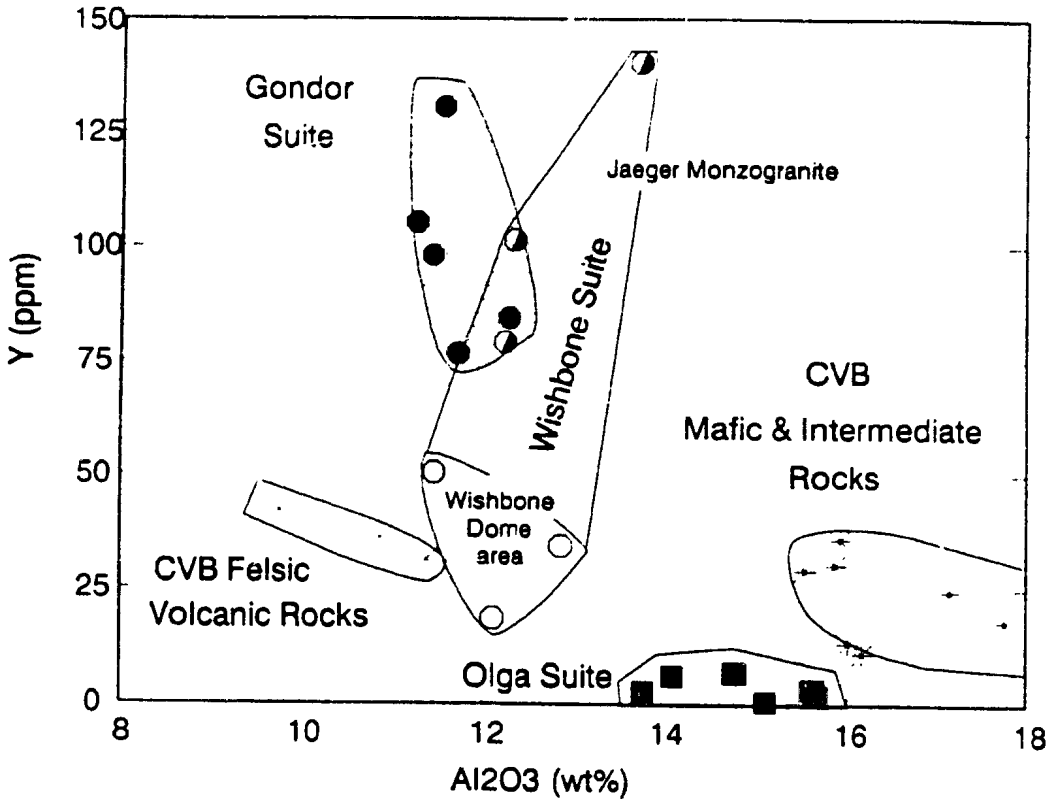

Figure 4.5. Plot of Y against Al_2O_3 showing two distinct groups of felsic rocks: 1) Low Al_2O_3 with moderate to high Y (the Wishbone and Gondor Plutonic Suites and felsic volcanic rocks, and; 2) high Al_2O_3, low Y rocks of the Olga Plutonic Suite.

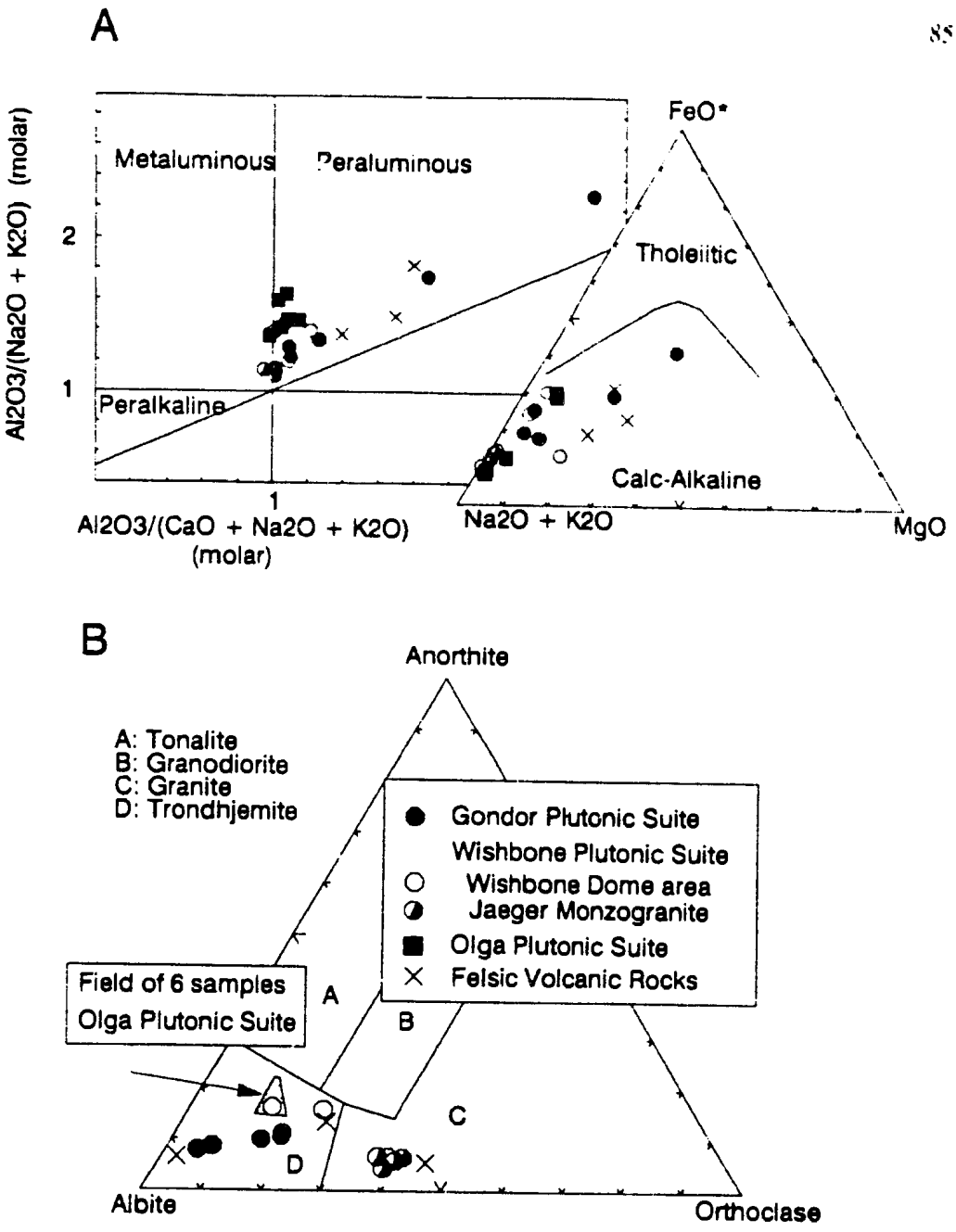

Figure 4.6. A) AFM diagram and molar A/CNK vs. A/NK diagram for the felsic rocks. A=Al_2O_3; C=CaO; N=Na_2O; K=K_2O. B) Classification of the low Al_2O_3 felsic rocks based on normative albite (Ab), orthoclase (Or) and anorthite (An), Barker (1979) after O'Conner (1965). Symbols for both diagrams shown in B.

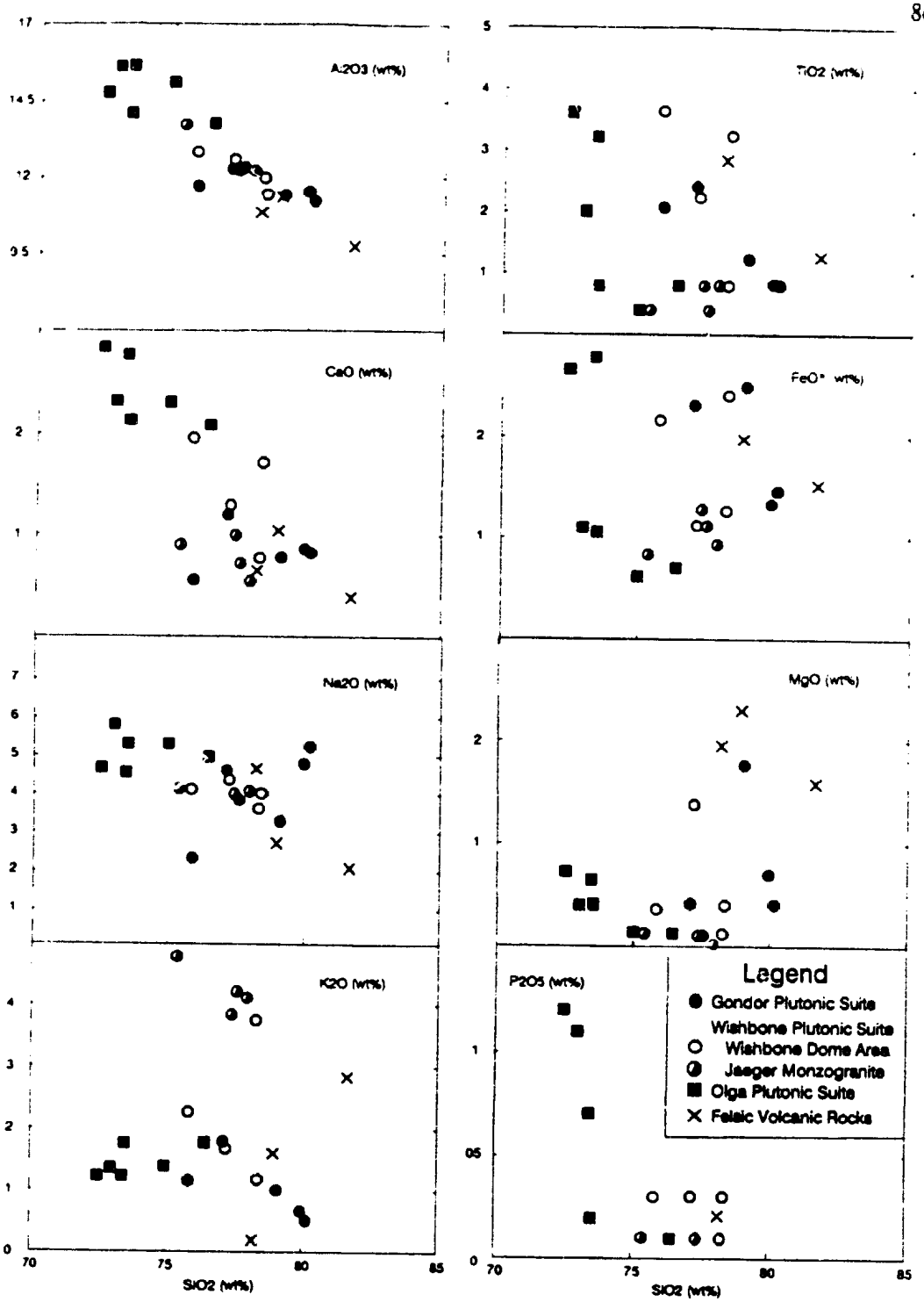

Figure 4.7. Major element Harker diagrams for the felsic rocks.

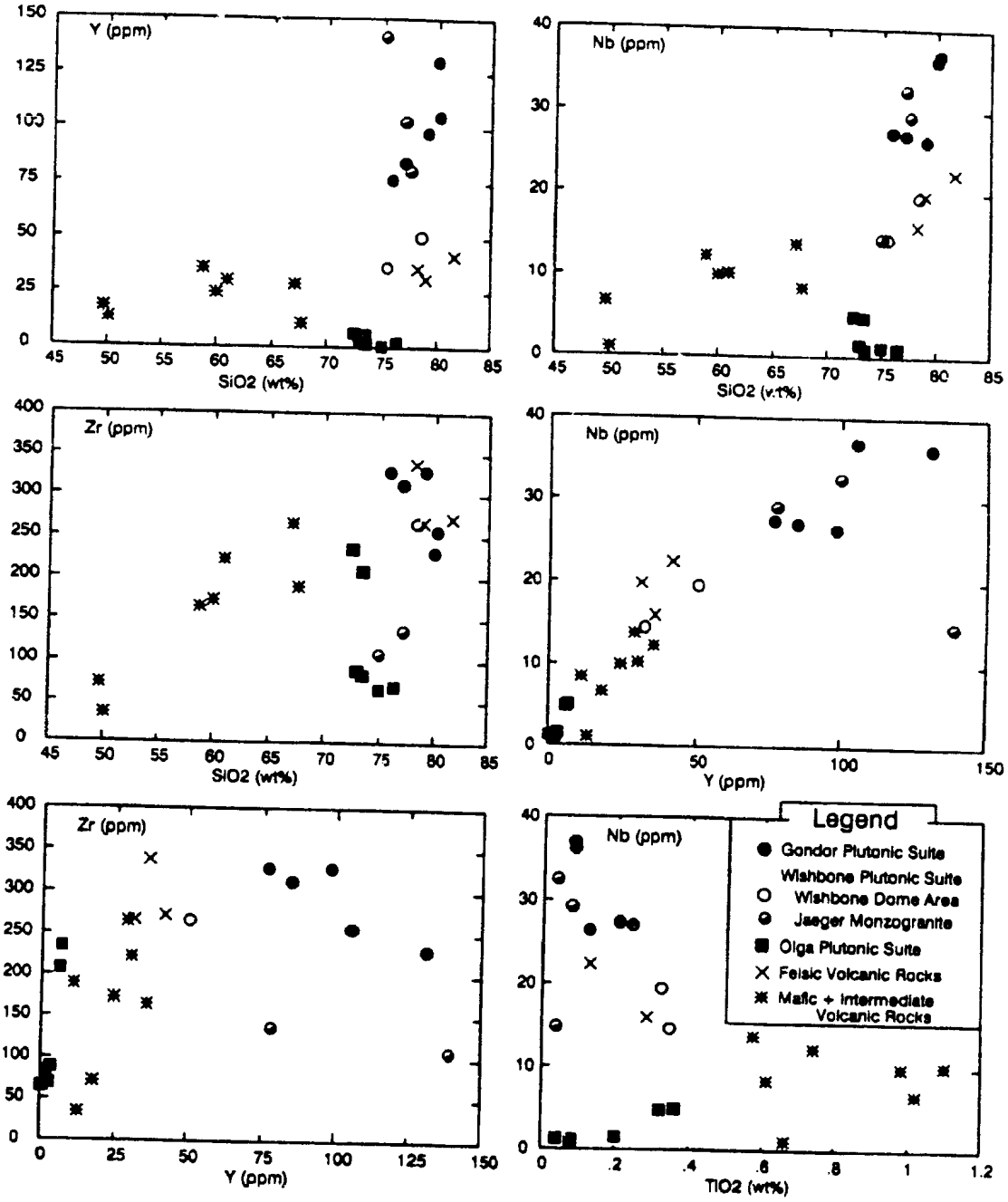

Figure 4.8. Trace element variation diagrams for the felsic rocks.

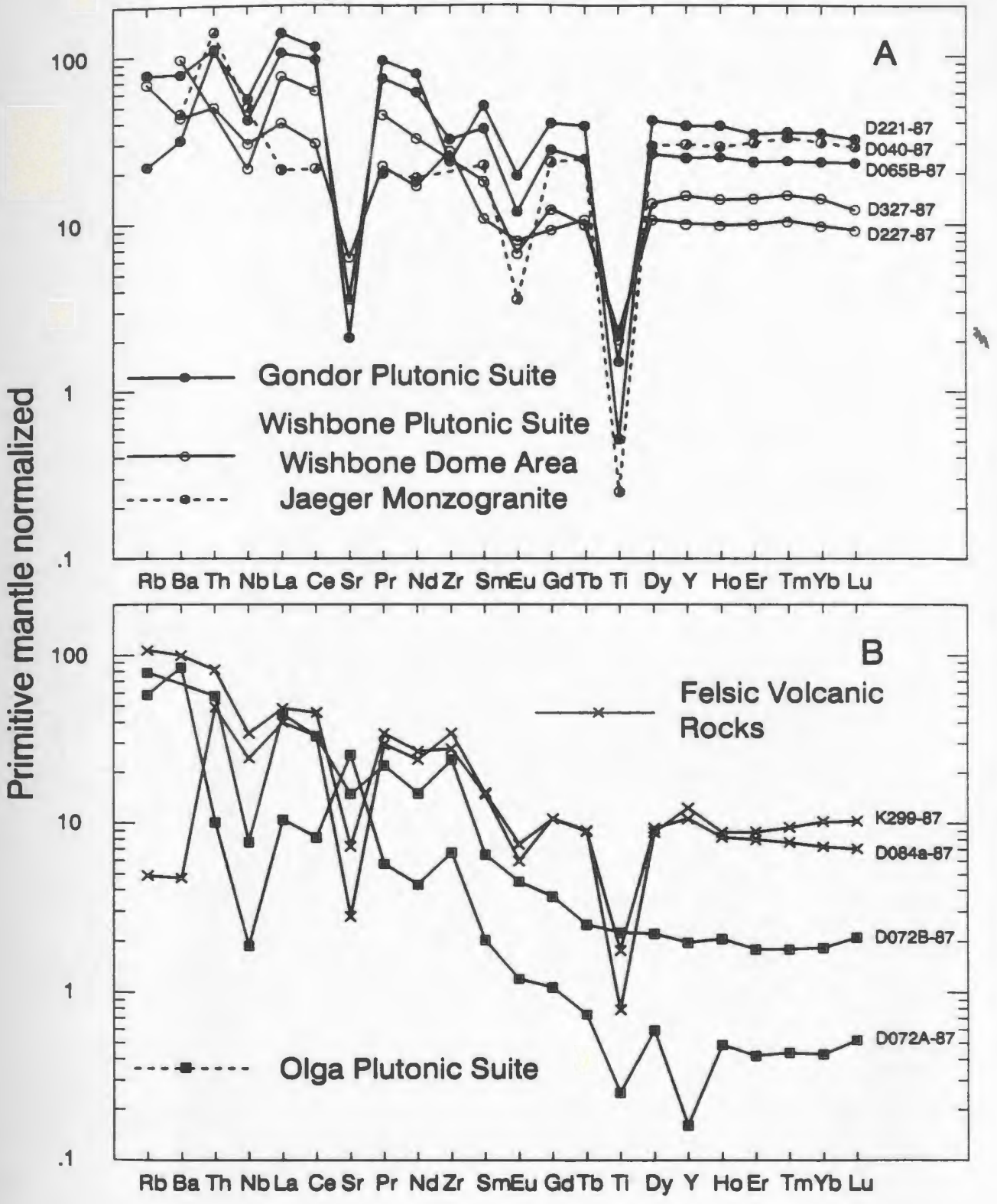

Figure 4.9. Primitive mantle normalized extended REE diagram for the felsic rocks: A) Gondor and Wishbone Suites; B) felsic volcanic rocks and Olga Suite.

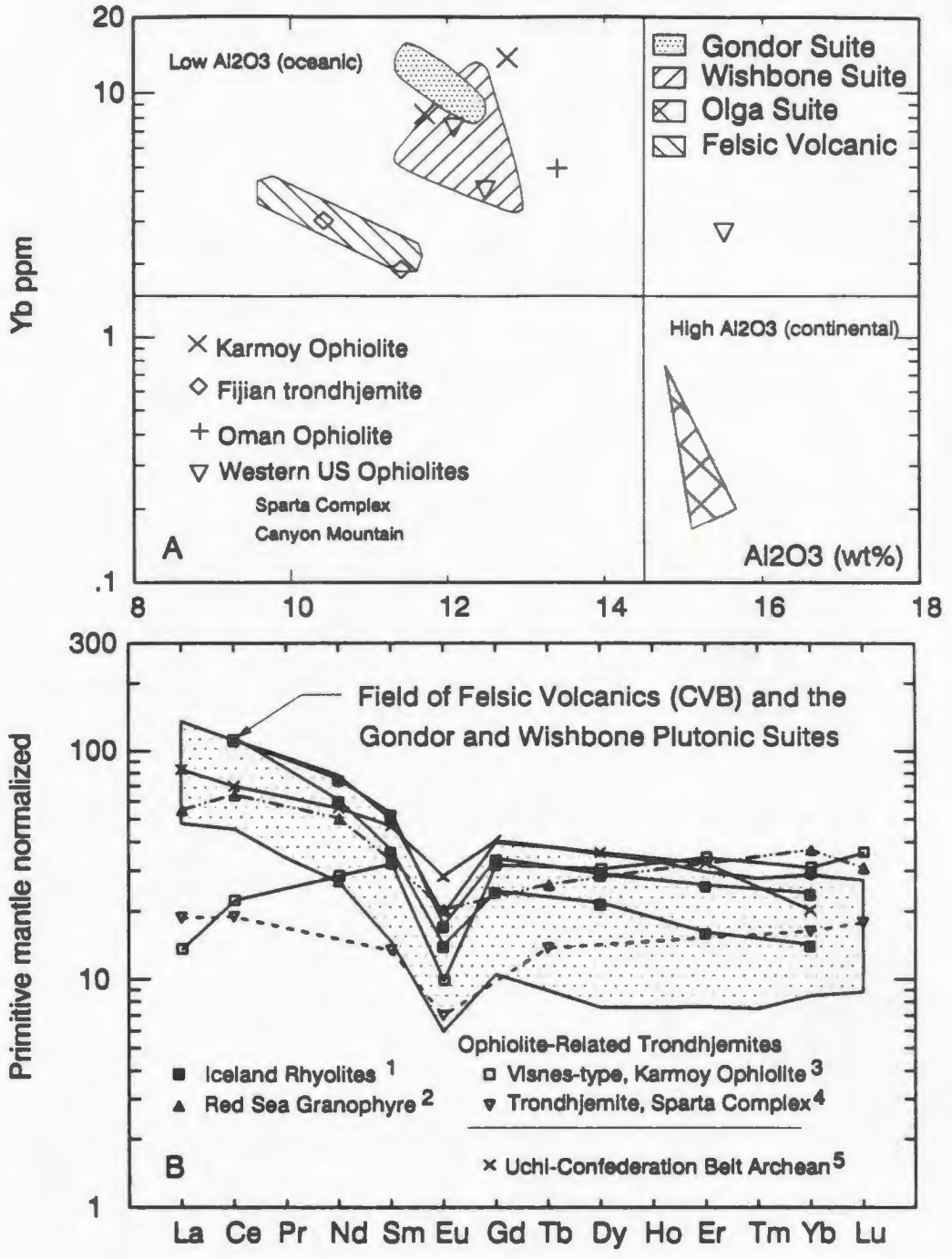

Figure 4.10. A) Al_2O_3 *vs.* Yb diagram comparing the low Al_2O_3 felsic rocks to ophiolite and island arc-related plagiogranites and dacites. Fields for oceanic and continental trondhjemites are shown following Arth (1979). Data sources: Oman - Coleman and Donato, 1979; Fiji- Gill and Stork (1979); Karmoy - Pedersen and Malpas (1984); Sparta- Phelps (1979); Canyon Mountain- Gerlach *et al.* (1981). B) Primitive mantle normalized REE diagram comparing the felsic volcanic rocks, and the Wishbone and Gondor Plutonic Suites to ophiolite-related or oceanic trondhjemites. 1. O'Nions and Gronvold (1973); 2. Coleman and Donato (1979); 3. Pedersen and Malpas (1984); 4. Phelps (1979) 5. Thurston and Fryer (1983).

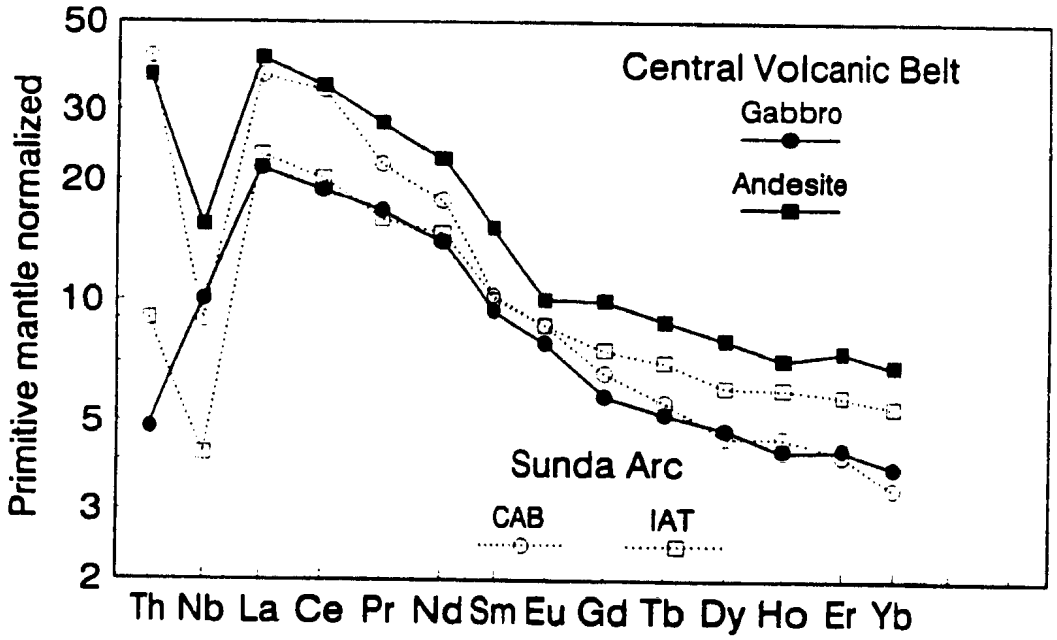

Figure 4.11. Primitive mantle normalized extended REE diagram comparing mafic and intermediate rocks from the Central Volcanic Belt to island arc basalt and andesite from the Sunda arc (data from Whitford *et al.*, 1979).

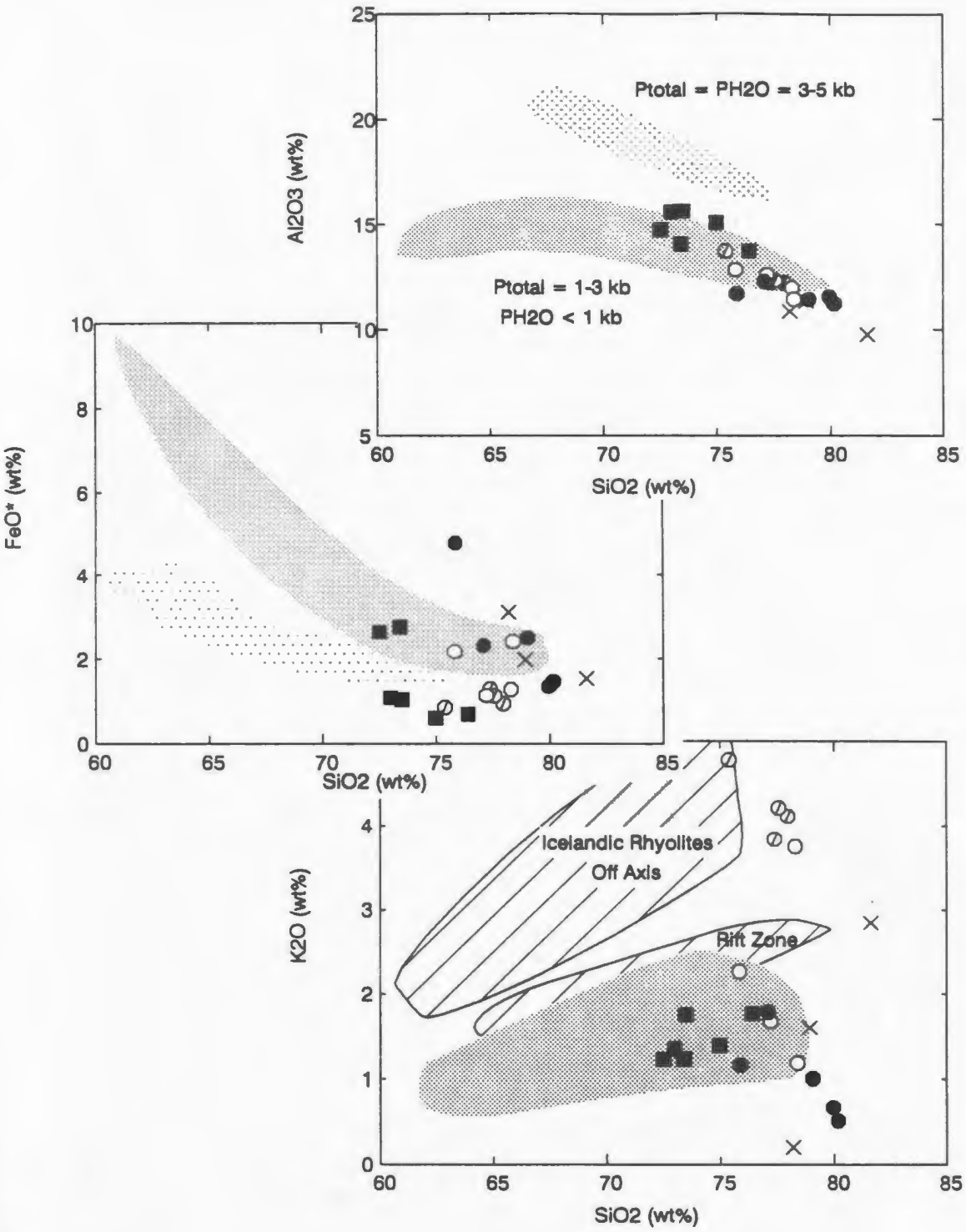

Figure 4.12. Compositions of experimental melts produced by water-saturated (heavy stippled field) and undersaturated melting (lighter stipple) of basalt (after Beard and Lofgren, 1989; Thy et al., 1990). Fields for Icelandic rhyolites from Thy et al. (1990). Symbols as in Figure 4.7.

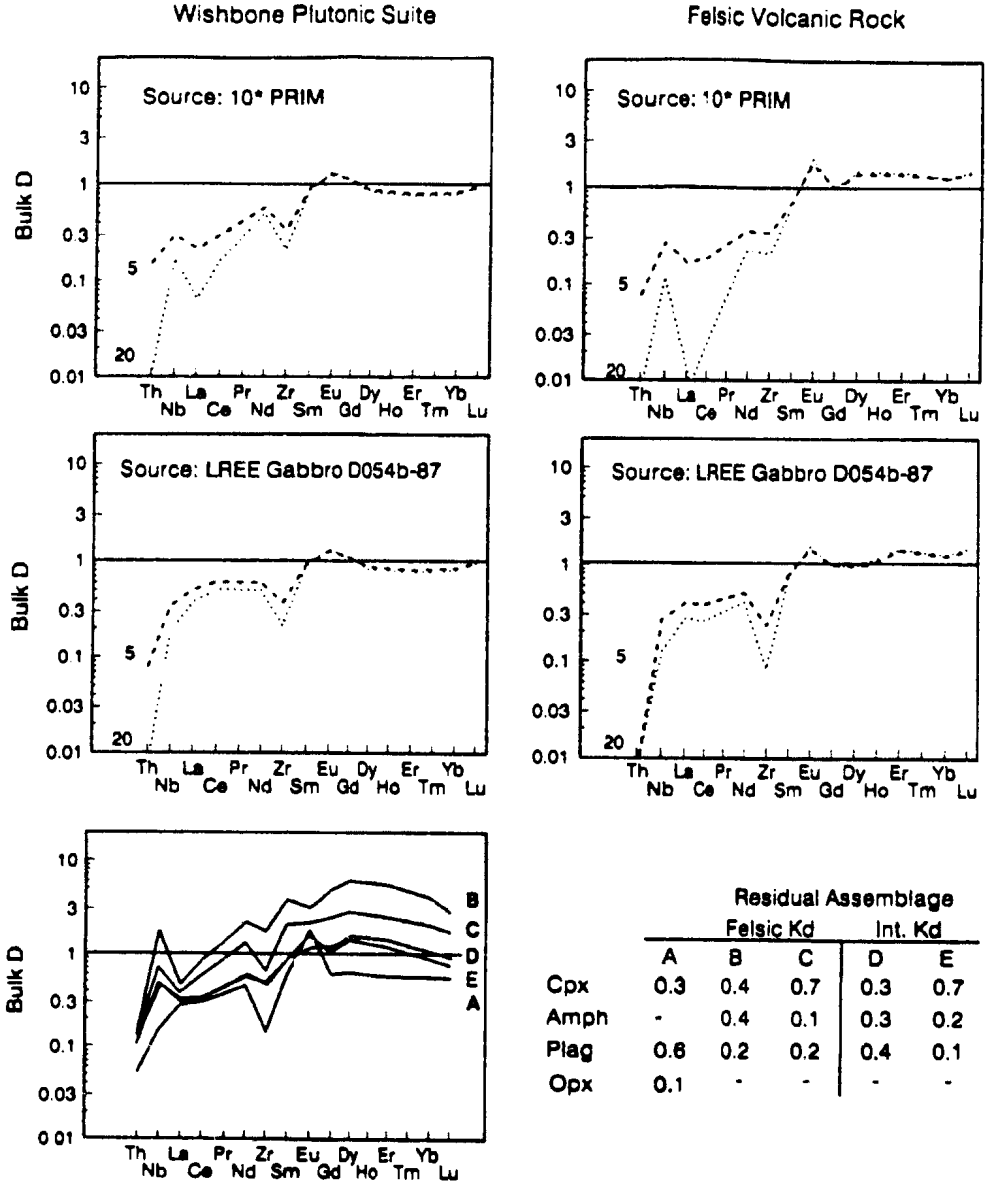

Residual Assemblage

	Felsic Kd			Int. Kd	
	A	B	C	D	E
Cpx	0.3	0.4	0.7	0.3	0.7
Amph	-	0.4	0.1	0.3	0.2
Plag	0.6	0.2	0.2	0.4	0.1
Opx	0.1	-	-	-	-

Figure 4.13. Calculated Bulk D values required to produce the trace element contents of low Al_2O_3 trondhjemites (Wishbone (D327-87 and felsic volcanic rocks - K299-87) by batch melting basaltic source rocks. See Appendix 4 for discussion of methodology. Dotted lines are for 5% melting, dashed lines are for 20% melting. Bulk D patterns shown in E were calculated assuming Kd values for felsic rocks (Appendix 4) and the residual mineral assemblages shown in the adjacent table. Bulk $D = E\ Kd_iM_i$, where M_i is the percentage of a given mineral and Kd_i is the partition coefficient for that mineral. The residual assemblages were selected to approximate the results of experimental basalt melting studies referenced in the text.

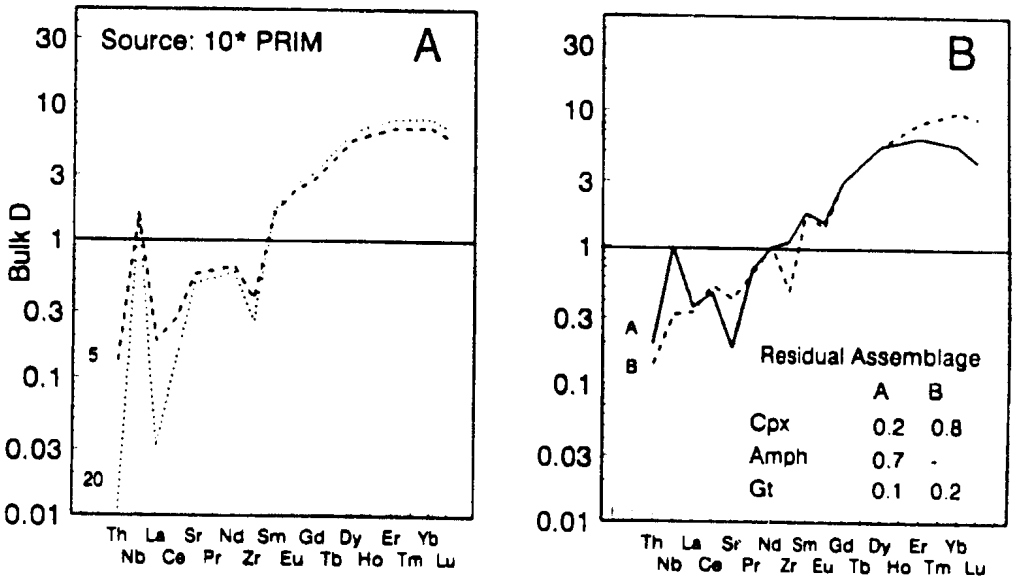

Figure 4.14. A) Calculated Bulk D values required to produce the trace element contents of a high Al_2O_3 trondhjemite of the Olga Plutonic Suite (D072b-87) by batch melting basaltic source rocks. See Figure 4.13 for further description. B) Bulk D values predicted for eclogite and garnet amphibolite residual assemblages assuming Kd values appropriate for felsic compositions (Appendix 4).

Chapter 5

Geochemistry and Petrogenesis of Syn-Deformation Plutonic Suites

5.1 Introduction

This chapter presents geochemical data on samples of the Concession and Siege Plutonic Suites. Both suites were emplaced synchronous with, or late in the peak metamorphic and deformation event at *ca.* 2600-2616 Ma (van Breemen *et al.*, 1990). They are at least 34 m.y. younger than the volcanic and synvolcanic plutonic suites discussed in the previous chapter.

Although close in age, the two suites are interpreted below to have different origins. The Siege Suite consists entirely of trondhjemitic rocks and is likely of crustal origin. In contrast, the Concession Suite ranges in composition from diorite through granodiorite and is interpreted to reflect a mantle input into the crust, followed by fractionation and assimilation within the crust.

5.2 Geochemistry of the Concession Suite

Representative analyses are shown in Table 5.1 and the full data set of eighty analyses is presented in Appendix 2.

The chemistry of some of the analysed samples is considered to be dominated by a cumulate component, primarily amphibole, but in some cases plagioclase. Cumulate rocks have been identified, in part, using Figure 5.1, a plot of Al_2O_3 vs. SiO_2. This diagram is an effective indicator of accumulation of low-Al_2O_3 mafic phases such as amphibole, orthopyroxene, clinopyroxene, and olivine, as well as plagioclase, a high-Al_2O_3 phase. The cumulate rocks include all hornblendites, much of the mafic margin to the Concession Pluton (Figure 3.18), as well as many but not all cognate xenoliths. The cumulate samples are not shown on many of the following classification figures, although they are shown on the Harker diagrams and will be discussed later in the chapter in relation to the petrogenesis of the suite.

Table 5.1 Representative analyses of the Concession Plutonic Suite

	HIGH MG# GROUP								LOW MG# GROUP		
Sample	D154b-87	A280-87	D203-87	D277-88	D260-88	D023-87	D218-87	D142-88	D172c-87	D173-87	D172-87
Pluton or Area	Concess. Pluton	Concess. Pluton	Concess. Pluton	S Contw. Lake	S Contw Lake	Southern Pluton	Southern Pluton	East Yamba Lake	SE Conc Pluton	SE Conc Pluton	SE Conc Pluton
SiO2	53.3	60.4	64.7	65.3	69.9	56.3	59.0	61.0	59.2	65.4	69.3
TiO2	0.94	0.58	0.49	0.57	0.38	0.86	0.73	0.69	1.65	0.78	0.62
Al2O3	16.0	16.7	16.2	16.1	15.6	18.0	18.0	16.9	14.4	16.3	15.5
FeO*	8.26	5.11	4.20	4.34	2.90	6.65	5.51	5.18	11.61	5.67	3.82
MnO	0.13	0.09	0.07	0.08	0.06	0.10	0.08	0.08	0.14	0.06	0.05
MgO	6.38	4.23	3.18	2.54	1.53	4.45	3.66	3.45	1.82	1.60	1.08
CaO	7.67	5.35	4.24	4.78	2.45	6.30	5.56	5.15	5.19	3.51	2.53
Na2O	4.32	5.09	4.40	4.50	4.75	4.53	4.94	4.54	3.59	4.14	4.14
K2O	2.33	2.18	2.33	1.37	2.23	2.32	2.16	2.70	1.58	2.20	2.82
P2O5	0.61	0.25	0.16	0.37	0.24	0.48	0.39	0.31	0.85	0.28	0.14
LOI	0.70	0.69	0.65	1.15	0.81	1.04	0.39	0.70	0.98	0.73	0.68
Mg#	58	60	57	51	48	54	54	54	22	34	33
Trace elements in parts per million											
Cr	113	102	95	40	dl	44	53	28	dl	6	dl
Ni	75	68	50	8	dl	31	26	12	dl	1	dl
Sc	24	15	11	13	4	17	13	15	13	8	5
V	231	123	106	104	167	150	145	116	~1	64	38
Zn	97	66	56	67	46	92	72	65	159	83	56
Rb	62	53.5	52.4	45.6	134	84	61	93	35.6	61	69
Cs	10.1	4.01	2.53	nd	nd	nd	1.13	nd	1.77	nd	nd
Sr	1535	1243	1085	809	569	1129	1128	997	461	423	313
Ba	1173	1034	1078	632	688	781	911	1181	427	706	599
Ga	23	24	19	23	21	23	21	23	26	23	22
Pb	9	8	9	nd	nd	nd	nd	nd	7	nd	nd
Y	22	12	10	16	14	24	19	20	45	16	19
Zr	143	174	163	178	157	229	235	231	182	227	155
Nb	6.6	5.5	5.2	6.2	7.8	11.1	9.2	8.5	29.2	11.9	9.5
Th	1.93	4.59	6.40	7.88	7.73	0.01	7.95	10.53	4.17	0.14	4.41
U	0.40	1.03	0.98	nd	nd	nd	nd	nd	0.98	nd	nd
Rare earth elements in parts per million											
La	71	32.5	30.9	70	43.2	63	51.1	70	38.0	38.3	23.9
Ce	159	72	67	142	88	150	114	147	94	82	51.3
Pr	19.7	8.7	7.7	17.2	10.7	18.8	14.5	18.4	12.9	9.7	6.3
Nd	83	34.6	29.9	66	41.7	77	55.7	72	58.5	38.7	25.3
Sm	15.0	6.0	4.76	9.9	7.1	13.4	9.4	12.7	13.2	7.1	5.32
Eu	3.59	1.24	1.21	2.19	1.38	2.63	2.25	3.03	3.84	1.70	1.09
Gd	12.0	5.06	4.20	5.60	4.46	8.7	6.3	8.3	11.8	5.39	4.67
Tb	1.22	0.51	0.38	0.66	0.60	1.01	0.78	1.03	1.67	0.72	0.65
Dy	5.65	2.44	2.00	3.27	2.69	4.91	3.88	4.84	9.1	3.68	3.51
Er	2.18	1.20	0.90	1.36	0.99	2.14	1.80	2.01	4.13	1.71	1.54
Ho	0.95	0.47	0.38	0.56	0.42	0.86	0.73	0.87	1.70	0.69	0.68
Tm	0.28	0.15	0.12	0.18	0.13	0.29	0.46	0.26	0.54	0.22	0.20
Yb	1.64	1.06	0.82	1.11	0.76	1.81	1.60	1.75	3.23	1.32	1.29
Lu	0.24	0.15	0.13	0.15	0.10	0.28	0.24	0.26	0.43	0.18	0.20
Selected ratios											
K/Rb	314	338	370	249	139	230	295	241	368	299	340
Rb/Sr	0.04	0.04	0.05	0.06	0.23	0.07	0.05	0.09	0.08	0.14	0.22
Ba/Sr	0.76	0.83	0.99	0.78	1.21	0.69	0.81	1.18	0.92	1.67	1.91
Ba/La	16.6	31.8	34.9	9.0	15.9	12.3	17.8	16.9	11.2	18.4	25.1
La/Nb	10.7	5.9	6.0	11.3	5.5	5.7	5.6	8.2	1.3	3.2	2.5
Ti/Zr	39.7	19.8	18.0	19.2	14.6	22.5	18.6	17.9	54.4	20.7	23.8
$(Ce/Yb)_N$	25.1	17.6	21.0	33.3	29.9	21.4	18.1	21.9	7.5	16.1	10.3
Eu/Eu*	0.82	0.69	0.83	0.90	0.75	0.74	0.90	0.90	0.94	0.84	0.67

REE, Th, Pb and Cs determined by ICP-MS all other trace elements determined by XRF. nd = not determined, dl = below detection limit.

Rocks of the Concession Suite show a considerable range in Mg# at a specific FeO* content (Figure 5.2). This is particularly apparent for the more mafic compositions and suggests the presence of at least two different groups or end members. The two groups define independant, but sub-parallel trends on an AFM diagram (Figure 5.3).

The majority of plutons in the study area are of the high Mg#-type. Occurrences of the low Mg# group are presently restricted to two plutons (Harp and SE Concession) as well as a number of small sill/dyke bodies SE of the Wishbone Dome. Samples from the eastern part of the field area, between Nose and Ghurka Lakes, have intermediate Mg#, possibly implying a continuous variation between the groups. The rocks are petrographically similar and cannot be distinguished in the field.

Both groups plot predominantly in the calc-alkaline field of the AFM diagram (Figure 5.3) although some samples of the low Mg# group plot within the tholeiitic field. Most samples are calc-alkalic as originally defined by Peacock (1931) (*ie.* CaO=Na2O+K2O at SiO_2 between 56 and 61 wt%), with the exception of low Mg# samples from the Harp Pluton which are calcic. Samples range from metaluminous to weakly peraluminous with increasing SiO_2 (Figure 5.4) and plot mainly within the tonalite and granodiorite fields of the O'Conner diagram (Figure 5.5).

5.2.1 Major Element Chemistry

Major element chemical variation is shown in Harker diagrams in Figure 5.6. Symbols used on these diagrams refer either to individual plutons (*e.g.* Concession Pluton) or to the geographical areas shown on Figure 3.11. The cumulate rocks identified from Figure 5.1 are not subdivided by area.

Samples range from less than 50 % SiO_2 to slightly over 70%, however most samples with less than 55 wt% SiO_2 contain a cumulate component. The dominant composition is between 60 and 70 wt% SiO_2, mafic rocks being less common.

Samples of the high Mg# group are characterized by moderate to high Al_2O_3, low TiO_2, high MgO relative to FeO*, high CaO and P_2O_5, high Na_2O and moderate but

variable K_2O. Na_2O/K_2O ratios exceed one except in monzodiorites. With the exception of the alkaline earths, major elements are linearly correlated with SiO_2 (Figure 5.6), especially for compositions greater than 56% SiO_2. CaO, TiO_2, MgO and FeO* all show strong linear trends with SiO_2. Scatter, at compositions less than 56% SiO_2, can be attributed to cumulate origins for these rocks. Major element abundances and co-variation are typical of calc-alkaline, I-type plutonic suites (*e.g.* Pitcher, 1983).

Samples of the low Mg# group show a similar range in SiO_2 content to the high Mg# group but have higher TiO_2, and lower Mg# for a given SiO_2 content (Figure 5.6). Low SiO_2 samples (< 60 wt%) from the SE Concession Pluton have lower K_2O contents relative to the high Mg# samples of similar SiO_2 content. Samples of tonalite from the Harp Pluton also have lower K_2O than typical tonalites of the high Mg# group. The abundances of other major elements are indistinguishable at similar SiO_2 contents. Variation trends tend to converge at higher SiO_2 contents making chemical differences difficult to see. Fewer low Mg# group samples, particularly of intermediate compositions, result in poorer definition of the major element trends. Given this limitation, the overall data trends appear similar to those described for the high Mg# group.

5.2.2 Trace Element Chemistry

The variation of selected trace elements is shown in Harker diagrams in Figure 5.7.

Low Field Strength Elements

The high Mg# group has high Ba (500-1500 ppm) and Sr (500-1500 ppm) and moderate to low Rb (< 180ppm) contents. Sr and to a lesser extent Ba abundance both decrease with increasing SiO_2. Rb shows considerable scatter but in general increases with SiO_2. Rb/Sr ratios are low and increase with increasing SiO_2. Ba/Sr ratios are high (> 1), and K/Rb are moderate (250 to 500).

The low Mg# group has distinctly lower Sr abundances. Ba and Rb contents overlap those of the high Mg# group but trend towards lower values (Figure 5.7), resulting in lower Ba/Sr and higher Rb/Sr ratios.

Transition Elements

Ni, Sc, V and Zn have moderate to low abundances which decrease with increasing SiO_2 (Figure 5.7). With the exception of cumulate samples, Ni abundances are less than 100 ppm (generally less than 20ppm) suggesting that even the most primitive samples are not primary mantle melts.

High Field Strength Elements

Zr content ranges from 130 to 250 ppm. Zr abundance shows little change from 55 to 65 wt% SiO_2, then tends to decrease with increasing SiO_2. Y content is less than 25 ppm, except for some samples of the low Mg# group, and generally decreases with increasing SiO_2. Zr and Y contents overlap between the two groups, although Y tends to be higher in the low Mg# group. Nb contents are low in the high Mg# group (< 15 ppm), but higher values (30 ppm) are common in the low Mg# group. In general the HFSE of the two groups show considerable overlap, with the low Mg# group having higher abundances (particularly Nb).

Rare Earth Elements

Primitive mantle normalized REE patterns for the high Mg# group are shown in Figure 5.8. The patterns are characterized by high abundances of LREE, low HREE, no or small negative Eu anomalies, and high to extremely high $(Ce/Yb)_N$ (10-120). The normalized patterns are slightly sinusoidal, with concave down LREE (La-Sm) and concave up MREE and HREE. Pattern shapes are generally similar over the full SiO_2 range (Figure 5.9), with only minor crossing of patterns (Figure 5.8). Differences in the slope (*ie.* $(Ce/Yb)_N$) or concavity (*ie.* $(Dy/Yb)_N$) of the patterns with increasing SiO_2 (Figure 5.10a, b), occur within the regional data set but are less, or not, apparent at the scale of individual plutonic bodies or geographical areas.

The highest abundance of REE occur within the most mafic samples and in general all the REE decrease with increasing SiO_2 content (Figure 5.7, 5.9, 5.10d). The HREE show a stronger negative correlation with SiO_2 than do the LREE.

Primitive mantle normalized REE diagrams for the low Mg# group are shown in Figure 5.11. The samples have similar REE patterns to those described above but in general show less enrichment in the LREE and have lower $(Ce/Yb)_N$ (see also Figure 5.10a).

Selected trace elements are plotted on normalized extended REE diagrams in Figure 5.12. The diagrams show the high abundances of the LFSE and LREE, and the steep slope and curvature of the REE pattern described above. Relative to the LFSE and REE, the HFSE elements Nb and Ti ($\pm$ Zr) show distinctly negative anomalies. Normalized Sr abundance is generally comparable to that of Sm, however both positive and negative anomalies occur. Positive Sr anomalies are common in samples from the Concession Pluton.

Small but consistent trace element differences between the groups are evident from Figure 5.12. In particular, the lower abundances of LREE and Sr, and the higher abundances of Nb. The size of the Nb anomaly ($(La/Nb)_N$) is smaller in the low Mg# group.

5.2.3 Regional and Local Scales of Chemical Variations

The fact that the data set includes samples collected from a number of individual plutons over a wide geographical area results in within-suite chemical variation at two scales: the regional and the local. Local is used to refer to either a single plutonic body or a geographically restricted area. The geochemical characteristics illustrated in Figure 5.12 are shared by most samples at the regional scale, however, in detail, samples from individual plutons show distinct major and trace element characteristics.

The variation of Sr with SiO_2 provides a good example of regional chemical variations. This is shown in Figure 5.13 in which samples are grouped according to geographical area. The abundance of Sr at 60 wt% SiO_2 differs between a particular

pluton or geographic region. For example, the Concession pluton has distinctly higher Sr than do other plutons such as the Southern pluton, or those from the Yamba Lake area. Samples from the Yamba Lake area, on the other hand, have lower Y and HREE abundances and higher $(Ce/Yb)_N$ (Figure 5.8, 5.10a). The regional variations in pluton chemistry show no systematic distribution within the field area. As expected for samples taken over a large region, the suite cannot be related by a single fractionation, partial melting or mixing process. However, the similarities in both the trends and abundances of major and trace elements over the area, implies common genetic relationships within the group as a whole.

5.2.4 Radiogenic Isotopes

Neodymium

Ten samples of the Concession Suite have been analyzed for their Nd isotopic composition. Results are presented in Table 5.2 .The high and low Mg# groups have similar isotopic compositions and the total range in $\epsilon_{Nd(t)}$ values (0.4 to 2.7) is small relative to estimated total reproducibility of values (± 1 epsilon unit; Appendix). Regression of the total data set yields an errorchron age of 2610 $\pm$146 Ma (Figure 5.14a, within error of the ca. 2608 Ma age determined by U-Pb on zircons on two of the samples (van Breemen *et al.*, 1990).

Plots of $\epsilon_{Nd(t)}$ versus indices of fractionation (*e.g.* Mg#, SiO_2) show no clear correlation (Figure 5.14b). The range in $\epsilon_{Nd(t)}$ is small relative to estimated errors. The positive $\epsilon_{Nd(t)}$ values require that the source region for the samples experienced a long term, LREE depleted history.

Strontium

Bostock (1980) reports whole rock Sr isotopic data from samples of the Concession Suite along the western margin of the Wolverine Monzogranite. Recalculation of this data, using decay constants from Steiger and Jäger (1978) and the U-Pb zircon age (2608 Ma; van Breemen *et al.*, 1990) of a sample in close proximity to those analyzed by Bostock (1980), yields initial $^{87}Sr/^{86}Sr$ values of approximately

Table 5.2 Sm-Nd Isotopic Data, Concession and Siege Plutonic Suites

Sample	Rock Type	Lat	Long	Nd (ppm)	Sm (ppm)	$^{147}Sm/^{144}Nd$	$^{143}Nd/^{144}Nd$[a]	ϵ Nd(i)[b]	Age[c] (Ma)	T_{DM} (Ma)
Concession Plutonic Suite										
High Mg# Group										
D119-88	Bt Qtz Diorite	65° 03'	111° 08'	52.60	10.07	0.1100	0.511285	2.7	2610	2728
D253-88	Hb-Bt Diorite	65° 16'	109° 58'	56.39	9.45	0.1040*	0.511165	2.4	2610	2752
D152b-87	Hb-Bt Diorite	65° 43'	111° 44'	56.70	11.06	0.1172	0.511382	2.2	2610	2767
D201a-87	Hb-Bt Tonalite	65° 43'	111° 40'	32.16	6.41	0.1019	0.511118	2.2	2610	2768
" "	" "	"	"	"	"	0.1073	0.511118	0.4	2610	2903
D278-88	Hb-Bt Diorite	65° 19'	110° 07'	55.54	11.44	0.1264	0.511529	2.0	2610	2783
D218-87	Hb-Bt Qtz Diorite	65° 26'	111° 51'	54.89	9.22	0.1045	0.511099	0.9	2607[1]	2860
D110-88	Bt Tonalite	65° 13'	111° 41'	41.21	6.22	0.08770*	0.510809	0.9	2608[1]	2862
D121a-88	Bt Qtz Diorite	66° 02'	111° 07'	67.45	9.70	0.09079	0.510851	0.7	2610	2878
Low Mg# Group										
D172b-87	Bt Tonalite	65° 40'	111° 31'	34.78	7.97	0.1368	0.511713	2.1	2610	2776
D172-87	Bt Tonalite	65° 40'	111° 24'	25.27	5.32	0.1304*	0.511494	-0.1	2610	2934
Siege Plutonic Suite										
D217-87	Bt Trondhjemite	65° 22'	111° 40'	4.98	0.86	0.1114	0.511226	1.1	2610	2849
D044-87	Bt Trondhjemite	65° 24'	111° 45'	1.51	0.38	0.1382	0.511634	0.1	2610	2926

[a] Internal precision is better .000015 2 SEM

Ratios are normalized to $^{146}Nd/^{144}Nd$ = .7219 $^{143}Nd/^{144}N$ = .511860 ± 20 for La Jolla during period of study. All samples analysed at G.S.C.

[b] $\epsilon_{Nd(i)}$ = [($^{143}Nd/^{144}Nd_{sample}$ / $^{143}Nd/^{144}Nd_{BE}$ Bulk Earth) - 1] * 10^4 where (i) = age of sample. Present day values Bulk Earth $^{143}Nd/^{144}N$ = .512638; $^{147}Sm/^{144}Nd$ = .1967.

[c] Published U-Pb zircon or monazite ages are designated by superscripts as follows [1] van Breeman et al., 1990; [2] van Breeman et al., 1987a; [3] Mortenson et al., 1988; [4] Krogh and Gibbons, 1978; [5] van Breeman et al., 1987b. Ages for other samples are estimated values discussed in text.

* $^{147}Sm/^{144}Nd$ determined by ICP-MS. Estimated error ± 2%. 1% for ratios determined by ID.

• Samples 1-13, 18a, 30-33, 44-49, 51-52, 54, 56-58 chemistry done at G.S.C. All other samples done at Memorial University.

0.7020. This value is similar to estimates of Late Archean depleted mantle (*e.g.* Machado *et al.*, 1986). The Sr isotopic data is in accord with the Nd isotopic data; both indicate derivation of the suite from a source(s) which was isotopically similar to the contemporaneous depleted mantle.

5.2.5 Summary of Geochemical Characteristics of the Concession Suite

The following are the salient chemical features of the Concession Suite.

1) Two chemical groups are recognized on the basis of MgO and FeO* content: 1) a high Mg# (>50 at SiO_2 <60%); and,2) a low Mg# group (<50 at SiO_2 < 60%).

2) The two groups both show a continuous range in SiO_2 from 53 to 72 wt% SiO2. The majority of samples, with less than 55 wt% SiO_2 contain cumulate amphibole and/or plagioclase.

3) Major elements, CaO, FeO*, MgO, and TiO_2, decrease in a linear fashion with SiO_2. K_2O contents are moderate and Na_2O/K_2O ratios are high.

4) Samples of the high Mg# group have high abundances of Sr, Ba, LREE, low HREE, high $(Ce/Yb)_N$, low Rb/Sr, little or no Eu anomalies and pronounced negative Nb anomalies relative to Th and La. Samples of the low Mg# group have lower abundances of Sr and REE and generally lower $(Ce/Yb)_N$, and higher abundances of HFSE.

5) The lower SiO_2 samples are generally the most enriched in trace elements; Sr, Ba, LREE, HREE and Y all decrease with increasing SiO_2.

6) Isotopic compositions (Sr and Nd) are similar to estimated values of the contemporaneous depleted mantle.

5.3 Geochemistry of the Siege Plutonic Suite

The Siege Suite is restricted to one large irregular plutonic body within the central part of the field area. Analyses of seven representative samples (Table 5.3), covering a large area of the pluton, show extremely limited chemical variation. The rocks are trondhjemitic (Figure 5.15), weakly peraluminous (Figure 5.16) and are

Table 5.3 Representative analyses of the Siege Plutonic Suite.

Sample Name	D044-87	D119-87	D136-88	D217-87	D319c 87	D104 88	V284 88
Rock Type	Trondhj.	Trondhj.	Trondhj.	Trondhj.	Trondhj.	Trondhj.	Trondhj.
SiO_2	74.0	73.0	72.5	72.5	72.3	72.0	71.4
TiO_2	0.08	0.04	0.16	0.10	0.08	0.16	0.16
Al_2O_3	15.5	15.7	16.1	16.2	16.8	16.5	16 8
FeO*	0.65	0.93	1.01	0.93	0.67	1.23	1.06
MnO	0.02	0.02	0.01	0.03	0.01	0.02	0.02
MgO	0.22	0.36	0.40	0.29	0.22	0.41	0.41
CaO	1.94	2.34	3.26	2.89	2.69	2.79	3.15
Na_2O	4 38	5.41	5.34	5.45	6.23	5.52	6.06
K_2O	2.~3	2.16	1.20	1.57	0.87	1.44	0.90
P_2O_5	0.'2	0.05	0.00	0.05	0.04	0.02	0.02
LOI	0.55	0.31	0.69	0.31	0.73	0.54	0.54
Mg Number	38	41	41	36	37	38	41
Trace elements in parts per million							
V	dl	4	10	dl	dl	13	5
Zn	10	18	6	11	15	11	13
Rb	62.5	41.2	37.4	39.1	15.9	30 8	26.9
Ba	484	984	337	712	202	674	332
Sr	469	548	538	531	742	512	540
Ga	16	17	18	16	19	20	20
Y	2.7	0.3	0.6	3.3	0.0	0.4	0.8
Nb	2.4	0.8	1.1	1.9	1.3	1.7	2.3
Zr	71.3	82.6	88.5	82.8	105	101	86.3
La	2.15	3.83	3.10	5.43	3.35	nd	nd
Ce	3.71	6.71	5.37	11.41	6.46	nd	nd
Pr	0.40	0.71	0.54	1.28	0.68	nd	nd
Nd	1.52	2.58	1.97	4.84	2.44	nd	nd
Sm	0.38	0.54	0.35	0.88	0.50	nd	nd
Eu	0.16	0.14	0.15	0.17	0.19	nd	nd
Gd	0.36	0.39	0.21	0.87	0.33	nd	nd
Tb	0.07	0.05	0.03	0.10	0.04	nd	nd
Dy	0.48	0.23	0.18	0.50	0.22	nd	nd
Ho	0.10	0.04	0.04	0.10	0.05	nd	nd
Er	0.31	0.13	0.14	0.28	0.14	nd	nd
Tm	0.05	0.02	0.02	0.04	0.02	nd	nd
Yb	0.36	0.14	0.13	0.25	0.14	nd	nd
Lu	0.06	0.03	0.02	0.04	0.03	nd	nd
Th	0.14	0.41	0.50	6.12	nd	nd	nd
Selected ratios							
K_2O/Na_2O	0.49	0.40	0.22	0.29	0.14	0.26	0.15
K/Rb	323	436	265	334	452	389	277
Rb/Sr	0.13	0.08	0.07	0.07	0.02	0.06	0.05
Ba/Sr	1.03	1.79	0.63	1.34	0.27	1.32	0.61
Ba/La	225	257	109	131	60		
La/Nb	0.89	4.84	2.75	2.82	2.52		
Ti/Zr	6.8	3.0	11.0	7.3	4.7	9.5	11.3
(Ce/Yb)n	2.7	12.5	10.6	11.7	12.1		
Eu/Eu*	1.35	0.00	1.73	0.60	1.42		

REE and Th determined by ICP-MS all other trace elements determined by XRF. nd = not determined, dl = below detection limit.

characterized by a limited range in SiO_2 content (71.5 to 74 wt%), moderate to high Al_2O_3 (> 15 wt%) and high Na_2O (>5.0%) contents with Na_2O/K_2O ratios greater than 2.

As described in Chapter 2, samples of the Siege Suite are heterogeneous on the handsample scale, consisting of variable proportions of two petrographic components: a biotite-bearing tonalite phase pervasively mixed with a relatively younger leucocratic tonalite. The latter often contains magnetite prophyroblasts and blue-green apatite. Samples collected for analyses were selected to minimize the amount of the leucocratic component. The two phases have not been separated and analyzed separately.

The suite has low to moderate abundances of LFSE (Rb< 65 ppm; Ba 200-1000 ppm; Sr 500-750 ppm); extremely low contents of HFSE (Nb<2.5 ppm; Y<4 ppm); and, low abundnaces of REE. Normalized REE patterns have a positive slope in the LREE and flat to slightly concave up HREE patterns (Figure 5.17). The patterns (excepting sample D044-87) are subparallel with slightly positive to negative Eu anomalies. Sample D044-87 has a flatter pattern and higher HREE. It also has higher P_2O_5, which together with the higher HREE may reflect a higher apatite content.

An extended REE plot is shown in Figure 5.18. The normalized values of the LFSE are much higher and relatively decoupled from those of the LREE. Positive Sr anomalies are prominent. Nb is relatively depleted in contrast to Zr which has a distinctly positive anomaly. These differences lead to the extremely fractionated HFSE ratios (*e.g.* Ti/Zr) shown in Table 5.3.

$\epsilon_{Nd(t)}$ values calculated for two samples range from +0.1 to +1.1 (Table 5.2; Figure 5.14b). These values overlap the lower range of $\epsilon_{Nd(2.6)}$ values of rocks of the older tectono-stratigraphic assemblage described in Chapter 6. van Breemen *et al.*, (1990) discuss U-Pb isotopic evidence for an inherited zircon component in sample D217-87. The precise age of the inherited component is poorly constrained but is at least as old as 2650 Ma.

5.4 Origin and Evolution of the Concession Plutonic Suite

The primary criteria which must be met by potential petrogenetic models for the Concession Suite is the ability to account for large volumes of tonalite with apparently lesser volumes of chemically related granodiorite, quartz diorite and diorite at high crustal levels (< 12 km). Petrogenetic processes capable of meeting this criteria include: 1) variable degrees of partial melting of basaltic precursors (Helz, 1976; Green and Ringwood, 1968; Stern and Wyllie, 1978; Huang and Wyllie, 1986; Holloway and Burnham, 1972; Green, 1982); 2) fractional crystallization of parental mafic liquid, either crustal or mantle in origin (Green and Ringwood, 1968; Arth, 1976; Stern and Hanson, 1990); 3) assimilation of crust by mantle-derived magmas, concomitant with fractional crystallization (AFC), (DePaolo, 1981); and 4) mixing (unmixing) of mafic and felsic magmas (McBirney, 1980). Mixing can be considered as a special case of the AFC process in which crystal fractionation has a negligible effect.

Crustal melting, fractional crystallization and unmixing models have each been proposed, at different times, for correlative plutonic rocks to the Concession Suite elsewhere in the Slave Province (Green and Baadsgaard, 1971; Drury, 1979; Meintzer, 1987; Hill and Frith, 1982; Frith and Fryer, 1985).

For the purposes of the following discussion the processes listed above are grouped into two first order possibilities: 1) an entirely crustal origin (*e.g.* partial melting of basalt); or, 2) a mantle origin followed by crustal processes (*e.g.* fractionation, crustal assimilation, mixing).

5.4.1 Evaluation of Models Deriving the Suite From Crustal Sources

This section will address two questions: 1) can magmas of appropriate composition be derived entirely from crustal melting; and 2) if so, what then is the origin of the chemical variation observed within the suite?

Tonalites from Mafic Crust: A Brief Review of Experimental Contraints

Experimental phase relationships of basaltic and tonalitic rocks theoretically permit the generation of calc-alkaline tonalites and associated rock types by partial

melting of basaltic precursors at both crustal and mantle pressures (Green and Ringwood, 1968; Stern and Wyllie, 1978; Huang and Wyllie, 1986; Ellis and Thompson, 1986; Beard and Lofgren, 1989; Helz, 1976). Experimental partial melts of basaltic rocks generated under water undersaturated conditions most closely approximate the weakly meta-aluminous compositions of natural calc-alkaline rocks, such as the Concession Suite (*e.g.* Ellis and Thompson, 1986; Huang and Wyllie, 1986). However it should be noted that experimental studies have not been successful, to date, in exactly reproducing the full range of compositions of natural calc-alkaline rock series (see Huang and Wyllie, 1986; Ellis and Thompson, 1986). The range of SiO_2 compositions from diorite through tonalite, corresponds to degrees of melting ranging from 50 to 10%, respectively, depending on melting conditions (*e.g.* Stern and Wyllie, 1978, Helz, 1976). Dioritic compositions (55 to 60 wt% SiO_2) would require relatively high temperatures of melting, certainly greater than 900°C (Helz, 1976).

Predicted residual assemblages vary depending on the pressure, amount of water, and degree of melting. At crustal pressures (< 15 kb), tonalite melts may coexist with amphibole, clinopyroxene, Fe-oxides, ±olivine, ±garnet under water-saturated conditions (Helz, 1976; Holloway and Burnham, 1972; Green and Ringwood, 1968; Huang and Wyllie, 1986), and with clinopyroxene, garnet, ±amphibole, ±plagioclase, ± quartz and oxides under anhydrous or water deficient conditions (Huang and Wyllie, 1986). Amphibole is not stable at pressures greater than 30 kbars with clinopyroxene and garnet dominating the assemblage at higher pressures.

Based on phase relationships and available experimental studies, potential crustal source rocks to the suite could include mafic rocks metamorphosed to amphibolites, garnet-amphibolites, garnet-granulites or eclogites.

Accepting that the range in bulk compositions could be generated by basalt melting models, then, within-suite variation could be due to: variable numbers of parental compositions derived from variable degrees of melting source rocks; mixing

between high and low degree melts; fractional crystallization starting from a 'parental' high degree melt (*ie.* diorite) with or without assimilation; or unmixing or accumulation from a 'parental' low degree melt (*ie.* tonalite).

The viability of these processes and the basalt melting hypothesis will be tested using trace element systematics.

Evaluation of Basalt Melting Models Using Trace Element Systematics

Garnet and amphibole are both minerals which strongly fractionate the REE and melting garnet or amphibole bearing mafic rocks will produce large to extreme fractionations in the REE content of the resulting liquid. The high $(Ce/Yb)_N$ ratios, low abundances of HREE and concave up HREE patterns characterstic of the Concession Suite (Figure 5.8) are predicted features of tonalites derived from partial melts of basalts leaving either a garnet-amphibolite, garnet-granulite or eclogite residuum (*e.g.* Arth and Hanson, 1975; Rudnick and Taylor, 1986; Gromet and Silver, 1987; Martin, 1986; Defant and Drummond, 1990; see also Chapter 4).

The predicted effect on the REE contents of melts derived by batch partial melting leaving an eclogite, garnet amphibolite or amphibolite residuum are shown in Figure 5.19 (see Table 5.4 for details of melting parameters used in the calculations). Since both garnet and amphibole fractionate the REE, the variable degrees of melting required to yield the range of rock types observed (10 to > 40%), should result in rocks with REE patterns of variable slope. This is particularly true if garnet is a significant residual phase. Crossing REE patterns are expected as the mafic rocks, representing higher degrees of melting, should have lower $(Ce/Yb)_N$ ratios and lower abundances of Ce compared with more SiO_2-rich samples (*ie.* lower degree melts).

This is not what is observed in the data set. Measured REE patterns are subparallel, and the highest abundance of both the LREE and HREE occur in the most mafic samples of the suite, contrary to predictions of variable melting models. Only if all of the REE behaved compatibly and the Kd values decreased during melting would the more felsic melts be less enriched in Ce than mafic rocks. Accessory mineral phases with large Kd values for the REE (*e.g.* apatite, titanite) may be stable residual

Table 5.4. Parameters used in non-modal batch melting calculations.

	Amphibolite		Garnet Amphibolite		Eclogite	
	Source(%)	Melt(%)	Source(%)	Melt(%)	Source(%)	Melt(%)
Plagioclase	25	50	20	50	-	-
Hornblende	60	50	20	50	-	-
Clinopyroxene	15	-	48	-	80	80
Garnet	-	-	12	-	20	20

Estimates of source and melt modes: (1) amphibolite (Helz, 1976); (2) garnet amphibolite (Huang and Wyllie, 1986; Lambert ad Wyllie, 1972); (3) eclogite (Stern and Wyllie, 1978; Ellis and Thompson, 1986).

phases during partial melting of basalt (Green and Pearson, 1987; Watson and Harrison, 1984) and could significantly increase the Bulk D values for the REE. However even under these conditions, the bulk D of the residual assemblage is still expected to fractionate the REE as apatite and titanite fractionate the MREE relative to the LREE and HREE, in a fashion similar to amphibole.

To produce the very high abundance of Ce in mafic rock types of the Concession Suite requires an extremely LREE enriched basaltic source with high $(Ce/Yb)_N$. For example, a source similar in composition to the average Archean tholeiite of Taylor and McLennan (1985)(AT, Figure 5.19) requires extreme fractionation to even approximate the lowest abundances of Ce observed in the rocks (Figure 5.19). Even if a relativley enriched basaltic source composition is assumed (*e.g.* D054b-87), the high abundances of Ce in the mafic rocks cannot be achieved unless the degree of melting is extremely low ($< 10\%$). Such low degree melts of basalt will not be dioritic in composition, as required by the data.

Additional problems with the basalt melting hypothesis include:

1) The lack of a significant Eu anomaly and the high Sr contents of the Concession Suite preclude plagioclase as a significant residual phase during melting. Sr is therefore predicted to behave incompatibly, with the highest abundance in the lower degree melts. The reverse relationship is observed as Sr is most enriched in diorites not tonalites (Figure 5.13). Additionally, in order to get the very high abundances of Sr

(> 1000 ppm) by melting typical basaltic rocks (*e.g.* 300 ppm) requires degrees of melting of less than 15% (Stern *et al.*, 1989). As pointed out above, such low degree melts would not be dioritic or quartz-dioritic in composition.

2: Abundances of "compatible" (*e.g.* Ni) vs "incompatible" (*e.g.* Rb) elements do not follow paths predicted by partial melting models (Figure 5.20). The rapid decrease in Ni compared to the more moderate increase in Rb are more characteristic of fractional crystallization and/or assimilation-fractional crystallization processes.

3) Partial melting of basalt produces liquids with lower Mg# and Ni abundances than the protolith (Green and Ringwood, 1968; Stern and Wyllie, 1978). The high Mg# and Ni abundances of the most mafic members of the Concession Suite require that the source rocks had Mg# > .6 and relatively high Ni (> 100 ppm) abundances. On average, volcanic rocks exposed in the Slave Province do not have these primitive characteristics (Cunningham and Lambert, 1989; Goodwin, 1988; Lambert, 1988). Ultramafic sequences are extremely rare. Volcanic rocks that are presently exposed may not, however, be representative of mafic protoliths in the lower crust.

Given the experimental uncertainty in generating the full range of observed compositions (*e.g.* Ellis and Thompson, 1986; Huang and Wyllie, 1986) and the inability to predict within-suite trace element variations, the hypothesis that all members of the suite are related by variable degrees of partial melting must be rejected. Further, the high Ce and Sr compositions of the mafic endmember of the suite cannot be accounted for by any simple crustal melting model.

Since the full range of compositions cannot be generated through variable degrees of basalt melting, this also eliminates the possiblilty that the suite represents mixing between different crustal melts. Clearly, in order for mixing models to be practical in this case, crustal melting must be able to generate appropriate end member compositions.

Frith and Fryer (1985) proposed that the parental magma to the Regan Intrusive Suite in the Beechey Lake area, immediately east of the present study area was tonalitic in composition, not dioritic. They suggested that the related quartz diorites and diorites

represented various accumulates of nonliquid compositions. Unmixing and accumulation of mafic crystals from a 'parental' tonalite could generate a range of more mafic compositions. Conceptually this is not disimilar to the restite unmixing models of Chappell and White (1974). The more mafic rocks need not, however, include residual materials, they could be cumulates of early formed crystals, or even immiscible liquids.

There are two major problems with this hypothesis:

1) The presence of plagioclase and/or hornblende porphyritic, fine grained mafic dyke rocks provide petrographic evidence that mafic rock types are not all cumulate in origin. If unmixing is an important process it is unlikely to occur by the physical separation and accumulation of crystals. There is no evidence to support an immiscible relationship between tonalites and the more mafic rocks.

2) The unmixing model fails to account for the chemical variation of the REE within the suite. Unmixing of a residuum dominated by plagioclase and hornblende will result in rotation of the REE pattern (not observed) and an increase in the MREE relative to the LREE and HREE in mafic rock types. Positive Eu anomalies may or may not develop depending on the relative Kd values and proportions of plagioclase and amphibole (*e.g.* Arth *et al.*, 1978). As with the basalt melting models, crossing REE patterns are predicted unless the Kd values for amphibole are high (>2 for all elements), or apatite, titanite or other accessory REE rich minerals are also separated. The $(Dy/Yb)_N$ ratio, a monitor of the extent of MREE fractionation, should increase with increasing proportions of cumulate amphibole, titanite and apatite (see Figure 5.21 and discussion below). It has previously been shown that the MREE are not significantly fractionated with variation in SiO_2 content (Figure 5.10).

3) The predicted Ba and Rb contents of cumulate rocks, based on published Kd values for amphibole and plagioclase, are extremely low in comparison to values measured in the diorites. The predicted values are, however, similar to measured values in cumulate rocks, which, as shown in Figure 5.8, generally have low Ba and Rb (as well as Sr) compared to the mafic rock types. Minerals capable of concentrating these

elements (*e.g.* biotite, k-spar) in the mafic rocks are not abundant, or in the case of K-spar are absent from the most mafic rocks. It is therefore unlikely that the LFS element abundances can be predicted by crystal unmixing models.

5.4.2 Models of Crustal Differentiation of Mantle-Derived Magmas

The inability to derive the mafic rock types of the suite from crustal melting suggests a mantle origin for the suite. None of the samples of the Concession Suite have compositions in equilibrium with mantle rocks (*ie.* Mg#> ; Ni > 100 ppm). All samples must therefore have undergone some fractionation. This will be discussed below.

Two possibilties will be considered for the within-suite chemical variation: 1) differentiation due to fractionation and; 2) differentiation due to assimilation of crust combined with fractional crystallization (AFC, DePaolo, 1981). Deriving intermediate compositions through mixing of felsic and mafic endmembers can be considered as a special case of the AFC process.

It is difficult to quantify these processes using a regional database because of 'second order' effects such as variable parental compositions, differences in fractionating assemblage and mixing of variably fractionated magmas. In order to minimize these effects, the following discussion will be restricted to samples from a single plutonic body, (Concession Pluton) which shows a range in composition. The style of chemical variation within this body is typical of rocks of the Concession Suite as a whole, including both the high and low Mg# groups and the conclusions drawn below are probably applicable in a general sense for the suite as a whole.

Major Element Within-Suite Variation

The potential effect of fractional crystallization (FC) and assimilation fractional crystallization (AFC) processes on major element compositions has been modelled using the least squares mixing equation of LeMaitre (1979). The models assume: a parental compositon similar to sample D154b-87; fractionation of minerals observed in the rocks (prinicipally amphibole and plagioclase); and assimilation of a felsic crustal

component similar in composition to the Siege Tonalite. The Siege Tonalite was selected as the assimilant because it may represent a felsic crustally-derived liquid, approximately contemporaneous with the Concession Suite. Mineral compositions are taken from Hill (1980) and Davis (1985).

The least squares mixing models have been subdivided into two stages, in order to allow for changing mineral assemblages with fractionation. The first stage of the model covers the interval from 53 to 60 % SiO_2, the second stage from 60 to 65 wt% SiO_2, the dominant compostion of the suite. A third stage from 65 to 70 wt% SiO_2 has not been modelled in detail.

Results of Least Squares Mixing Models

Fractionation models dominated by amphibole and plagioclase yield acceptable solutions to least squares mixing equations (Table 5.5).

The first stage of the model involves 48% fractionation dominated by amphibole followed, in the second stage, by an additional 34% fractionation dominated by plagioclase. The total amount of crystal fractionation required to reproduce the range of SiO_2 compositions (53 to 66 wt%) is 58%. The initial stage requires large degrees of amphibole fractionation because it is the predominant low-SiO_2 phase observed in the mafic rocks and separation of a low-SiO_2 phase is required to increase SiO_2 in the liquid. Biotite is less common in mafic lithologies and spinel phases are rare in the more mafic samples and absent from cumulate rocks. The model can accomodate fractionation of small amounts of biotite. Orthopyroxene is observed in some cumulate rocks and as cores to amphibole, however its high SiO_2 content would cause little change in SiO_2 content of the resulting liquids. Orthopyroxene could on the other hand, reduce the Ni and Mg# values from those in equilibrium with mantle rocks, during an earlier period of fractionation.

Models which include assimilation of high SiO_2 material in combination with fractionation also produce acceptable solutions. As shown in Table 5.5, AFC models require significantly less crystal fractionation than fractional crystallization alone. The ratio of assimilated material to fractionated material is relatively high (2 to 3) which

TABLE 5.5 Results of least squares mixing calculations, Concession Pluton.

STAGE 1

Fractional Crystallization

	Wt%	SIO2	TIO2	AL2O3	FE2O3	MNO	MGO	CAO	NA2O	K2O	P2O5
REACTANTS USED											
D154B-87	100.0	53.3	0.9	16.0	8.3	0.1	6.4	7.7	4.3	2.3	0.6
PRODUCTS USED											
A280-87	51.9	60.0	0.6	16.6	5.7	0.1	4.2	5.3	5.1	2.2	0.3
HORNBLENDE 1	34.0	45.7	1.5	11.4	16.5	0.3	10.6	12.3	1.0	0.8	0.0
PLAG AN 40	12.8	58.5	0.1	25.9	0.2	0.1	0.1	8.1	6.9	0.2	0.0
APATITE	1.0	0.0	0.0	0.0	0.0	0.0	0.0	57.1	0.0	0.0	42.9
FE OXIDE	0.3	0.0	7.0	0.0	92.5	0.5	0.0	0.0	0.0	0.0	0.0
ESTIMATED COMPOSITIONS											
REACTANTS		53.3	0.9	16.0	8.3	0.1	6.4	7.7	4.3	2.3	0.6
PRODUCTS		54.2	0.8	15.8	8.8	0.2	5.8	8.6	3.9	1.4	0.6
DIFFERENCES		-0.9	0.1	0.2	-0.5	0.0	0.6	-0.9	0.5	0.9	0.0

RESIDUAL SUM OF SQUARES = 3.3

Fractional Crystallization and Assimilation (Mixing)

	WT%	SIO2	TIO2	AL2O3	FE2O3	MNO	MGO	CAO	NA2O	K2O	P2O5
REACTANTS USED											
D154B-87	100.0	53.3	0.9	16.0	8.3	0.1	6.4	7.7	4.3	2.3	0.6
PRODUCTS USED											
HORNBLENDE 1	11.5	45.7	1.5	11.4	16.5	0.3	10.6	12.3	1.0	0.8	0.0
PLAG AN 40	0.4	58.5	0.1	25.9	0.2	0.1	0.1	8.1	6.9	0.2	0.0
APATITE	1.1	0.0	0.0	0.0	0.0	0.0	0.0	57.1	0.0	0.0	42.9
SIEGE	-35.6	72.4	0.1	16.2	1.0	0.0	0.3	2.9	5.5	1.6	0.1
TONALITE											
A280-87	122.6	60.0	0.6	16.6	5.7	0.1	4.2	5.3	5.1	2.2	0.3
ESTIMATED COMPOSITIONS											
REACTANTS		53.3	0.9	16.0	8.3	0.1	6.4	7.7	4.3	2.3	0.6
PRODUCTS		53.3	0.8	16.1	8.4	0.1	6.3	7.6	4.4	2.2	0.8
DIFFERENCES		0.0	0.1	0.0	-0.2	0.0	0.1	0.1	-0.1	0.2	-0.2

RESIDUAL SUM OF SQUARES = 0.1

STAGE 2

Fractional Crystallization

	WT%	SIO2	TIO2	AL2O3	FE2O3	MNO	MGO	CAO	NA2O	K2O	P2O5
REACTANTS USED											
A280-87	100.0	60.0	0.6	16.6	5.7	0.1	4.2	5.3	5.1	2.2	0.3
PRODUCTS USED											
HORNBLENDE 2	15.7	48.3	0.7	8.0	16.5	0.3	12.5	12.2	0.8	0.7	0.0
PLAG AN30	24.5	60.9	0.0	24.4	0.0	0.0	0.0	6.5	7.9	0.4	0.0
APATITE	0.0	0.0	0.0	0.0	0.0	0.0	0.0	57.1	0.0	0.0	42.9
FE OXIDE	1.0	0.0	7.0	0.0	92.5	0.5	0.0	0.0	0.0	0.0	0.0
D203-87	58.8	64.7	0.5	16.2	4.2	0.1	3.2	4.2	4.4	2.3	0.2
ESTIMATED COMPOSITIONS											
REACTANTS		60.0	0.6	16.6	5.7	0.1	4.2	5.3	5.1	2.2	0.3
PRODUCTS		60.5	0.5	16.8	6.0	0.1	3.8	6.0	4.6	1.6	0.1
DIFFERENCES		-0.5	0.1	-0.1	-0.4	0.0	0.4	-0.7	0.4	0.6	0.1

RESIDUAL SUM OF SQUARES = 1.5

Fractional Crystallization plus Assimilation (Mixing)

	WT%	SIO2	TIO2	AL2O3	FE2O3	MNO	MGO	CAO	NA2O	K2O	P2O5
REACTANTS USED											
A280-87	100.0	60.0	0.6	16.6	5.7	0.1	4.2	5.3	5.1	2.2	0.3
PRODUCTS USED											
HORNBLENDE 2	5.8	48.3	0.7	8.0	16.5	0.3	12.5	12.2	0.8	0.7	0.0
PLAG AN30	16.5	60.9	0.0	24.4	0.0	0.0	0.0	6.5	7.9	0.4	0.0
APATITE	0.1	0.0	0.0	0.0	0.0	0.0	0.0	57.1	0.0	0.0	42.9
FE OXIDE	0.6	0.0	7.0	0.0	92.5	0.5	0.0	0.0	0.0	0.0	0.0
SIEGE	-32.1	72.4	0.1	16.2	1.0	0.0	0.3	2.9	5.5	1.6	0.1
TONALITE											
D203-87	109.1	64.7	0.5	16.2	4.2	0.1	3.2	4.2	4.4	2.3	0.2
ESTIMATED COMPOSITIONS											
REACTANTS		60.0	0.6	16.6	5.7	0.1	4.2	5.3	5.1	2.2	0.3
PRODUCTS		60.2	0.6	17.0	5.8	0.1	4.1	5.5	4.4	2.1	0.2
DIFFERENCES		-0.1	0.0	-0.3	-0.1	0.0	0.1	-0.2	0.7	0.0	0.0

RESIDUAL SUM OF SQUARES = 0.6

would require that the assimilated crust was hot at the time of intrusion (*e.g.* DePaolo, 1981; Sparks, 1986). The interpretation of a crustal origin for the Siege Tonalite (see below) and the close temporal relationship to metamorphism argues for locally high temperatures in the crust during plutonism.

Simple mixing models, without fractionation can also yield appropriate major element solutions for intermediate compositions (not shown). However, the more felsic samples diverge significantly from calculated values.

In summary, the solutions to major element least squares mixing equations suggest that the major element chemical variation within the suite can be reproduced by assimilation of anywhere from zero to 30% crustal material, resembling the Siege Tonalite, and involving anywhere from 30 to 60 % fractional crystallization.

Within-Suite Trace Element Variation

The results of the major element models have been used to evaluate the trace element variation within the suite. Trace element systematics have been modelled using standard equations for fractional crystallization and AFC (*e.g.* Arth, 1976; DePaolo, 1981), and published mineral Kd values (Appendix 4). The mineral proportions used in the trace element modelling are given in Table 5.6. The rational for the use of accessory mineral phases is given below.

Table 5.6. Fractionating mineral assemblages used in trace element modelling calculations.

	Model A				Model B			
	Fractional Crystallization		Assimilation Fractional Crystallization		Fractional Crystallization		Assimilation Fractional Crystallization	
Mineral (wt%)	1	2	1	2	1	2	1	2
Hornblende	74	39	78	25	70	39	78	25
Plagioclase	25	60	20	74	27	59	20	75
Apatite	1.0	1.0	1.0	1.0	2.0	1.0	1.0	1.0
Titanite	0.5	0.5	0.5	0.5	0.5	1.0	0.5	0.5
Allanite	0.1	0.1	0.1	0.1	0.1		0.5	

Table 5.7 presents the calculated bulk D values required to account for the measured trace element variations within each of the two stages described above. The values were determined by inverting the standard fractionation equation (Arth, 1976), using measured values for the final (Cf) and initial compositions (Co), and solving for D assuming degrees of fractionation determined by the major element solutions. The bulk D values determined in this fashion are equivalent to the integrated value over the fractionation interval.

Table 5.7. Estimated Kd values required for fractional crystallization models in accord with major element solutions.

	Samples			Required Bulk D Values			Calculated Bulk D values	
	D154b-87	A280-87	D203-87	Stage 1 f = 0.6	Stage 2 f = 0.7	Total f = 0.4	Stage 1	Stage 2
Cr	113	102	95	1.15	1.21	1.19	22	12
Ni	75	68	50	1.14	1.87	1.44	5.9	3
Sc	24	15	11	1.65	1.82	1.81	9	5
V	231	123	106	1.91	1.42	1.85	24	12
Rb	62	54	o2	1.19	1.09	1.18	0.04	0.02
Ba	1173	1034	1078	1.18	0.88	1.09	0.11	0.13
Sr	1535	1243	1085	1.30	1.38	1.38	0.64	1.2
Nb	6.6	5.5	5.2	1.26	1.18	1.27	1.68	1.23
Zr	143	174	163	0.71	1.18	0.85	1.04	0.56
Y	22	12	10	1.89	1.48	1.86	2.59	1.74
Th	1.9	4.6	6.4	-0.25	0.07	-0.31	0.33	0.26
La	70.8	32.5	30.9	2.12	1.14	1.90	1.57	1.56
Ce	159	72.3	66.9	2.14	1.22	1.95	1.72	1.62
Pr	19.7	8.7	7.7	2.19	1.3[illegible]	2.02	2.03	1.85
Nd	82.8	34.6	29.9	2.26	1.41	2.11	2.24	2.1
Sm	15.0	6.0	4.8	2.31	1.66	2.25	2.59	2.54
Eu	3.6	1.2	1.2	2.53	1.07	2.19	2.51	3.19
Gd	12.0	5.0	4.2	2.24	1.52	2.14	2.77	2.7
Tb	1.2	0.51	0.38	2.25	1.82	2.27	-	
Y	5.8	2.4	2.0	2.21	1.56	2.13	3.00	2.92
Ho	0.95	0.47	0.38	2.02	1.61	2.01	-	
Er	2.2	1.2	0.90	1.86	1.81	1.97	2.67	2.42
Tm	0.28	0.15	0.12	1.89	1.64	1.92	-	
Yb	1.6	1.1	0.82	1.63	1.70	1.75	2.09	1.51
Lu	0.24	0.15	0.13	1.67	1.39	1.66	1.94	1.30

Required Kd values calculated by solving equation 6 of Arth (1976), using measured values for initial (C_o) and final compositions (C_f) and assuming the degree of fractionation consistent with major element solutions (Table 5.5). Stage 1 assumes C_o = D154b-87 and C_f = A280-87, Stage 2 assumes C_o = A280-87 and C_f = D203-87. Calculated Kd values are based on mineral assemblages shown in Table 5.6 (Model A) and intermediate Kd values (Appendix 4).

The Bulk D values for the REE determined by this method are higher than would be predicted for amphibole and plagioclase dominated assemblages assuming published Kd values. This suggests either: 1) the Kd values used for amphibole are too low; or 2)

the separation of REE-rich accessory phases (*e.g.* titanite, allanite, apatite, zircon). All of these accessory phases are common in the rocks and because of their high Kd values for the REE they may have an important effect on REE systematics.

Effect of Accessory Phases on REE Systematics

The effect on REE patterns of small amounts of fractionation of titanite, apatite, allanite and zircon are shown in Figure 5.21b. Although published REE Kd values for these minerals show considerable variation, the REE behave coherently as a group and the relative effect of each of these minerals is predictable. Changes in the absolute values of the Kd will dominantly affect the magnitude, not the style, of REE fractionation.

As can be seen from Figure 5.21b fractionation of apatite and titanite results in a decrease in all REE, and a strong relative depletion of the MREE. This type of fractionation is not dissimilar to that caused by amphibole (Figure 5.21a). Fractionation of these two phases will, therefore, have the effect of increasing the apparent Kd values of amphibole.

In contrast, allanite and zircon produce different types of REE fractionation (Figure 5.21b). Zircon strongly depletes the HREE relatively to the LREE (Heaman *et al.*, 1990) and allanite strongly depletes the LREE relative to the HREE (Brooks et al., 1981). The potential for allanite, observed in all rocks with greater than 56% SiO_2, to control the LREE content of the rocks should not be underestimated. Figure 5.21b shows the effect of fractionating 0.5 wt% allanite from a typical sample of the Concession Suite. All elements lighter than Eu show a strong depletion, however, the HREE are less affected. As previously noted, the LREE correlate with Th abundance in the rocks, elements which are all strongly concentrated in allanite. Compare this with the effect of small amounts of allanite fractionation (Figure 5.21b) and it suggests that allanite may be one of the controls on the LREE budget of the rocks.

Crossing LREE patterns are not, however, commonly observed within the data set (Figure 5.9). This imposes limits on the extent of allanite fractionation. Allanite

fractionation must be much less extensive, than 0.5 wt% shown in Figure 5.21b. Small amounts of allanite could be responsible for minor variations in LREE, and contribute to the high bulk D values for the REE that are required by FC models (see Table 5.7).

The high bulk D values shown in Table 5.7 , particularly for the LREE, can be accomodated by the fractionation of the REE-rich accessory phases mentioned above, in addition to hornblende and plagioclase. The REE Bulk D values calculated from published Kd values, taking into account the effect of small amounts of these accessory phases, are shown in Table 5.7. The proportions of amphibole, plagioclase, and apatite are based on the major element solutions (Table 5.5 and 5.6), whereas, the proportion of titanite and allanite are based on their abundance relative to apatite estimated from thin section. The latter estimates are not precise. The Bulk D values calculated using published Kd values approximate, in general, the magnitude of the required bulk D values (Table 5.7). However, achieving this integrated D value, over the full range of fractionation, would require a relatively delicate balance in the proportions of the fractionating phases (particularly accessory phases) and in the variation in Kd over a large range in SiO_2 content and temperature. Whether this balance is feasible is not clear.

Fractional Crystallization Models

The major element solutions for simple fractional crystallization (FC) predict large amounts (40%) of amphibole fractionation, particularly in the first stage of the model. The FC model can accomodate certain aspects of the trace element chemistry of the suite, for example, the Ni and Rb variation shown in Figure 5.20. It has difficulties, however, in accounting for the REE and LFSE (Ba, Sr) variations.

Figure 5.22 shows REE contents measured in hornblendites or hornblende-rich diorites, interpreted to be amphibole-dominated cumulate rocks, normalized to the most mafic non-cumulate composition (*ie.* 'liquid' composition). The cumulate rocks show relative depletions in LREE, and significant enrichments in MREE and HREE with a

marked concave down pattern. The shape of the patterns is similar to measured Kd patterns of amphibole in tonalites (*e.g.* Gromet and Silver, 1983; Sawka, 1988) supporting a cumulate origin for these rocks.

Based on the REE patterns of these amphibole cumulate rocks and published Kd values for amphibole in intermediate liquids, extensive amphibole fractionation, as required in the first stage of the FC model, should cause rotation and steepening of the REE with a pronounced depletion of the MREE with progressive fractionation (Figure 5.21a).

The MREE depletion predicted by amphibole-dominated fractionation can be seen in Figure 5.23, which plots the calculated results of the first stage of the fractional crystallization model normalized to the starting 'parental' composition. The 'target' composition, in this case sample A280-87 (SiO_2 = 60 wt%), is shown as a dashed line. The fractionating assemblage used in this calculation is given in Table 5.6 (Model A). The FC model results in REE patterns which are more strongly fractionated in the MREE than those observed in the data set.

High bulk D values are also required for Ba and Sr to account for their compatible behaviour throughout the series (Table 5.7). This requirement is particularly problematic through the first stage of the model in which plagioclase fractionation is strongly subordinate to amphibole and the predicted bulk D values for Sr and Ba should both be considerably less than unity. Figure 5.24 is a diagram of Ba against Sr for rocks of the Concession Pluton. Superimposed on this diagram are the trends predicted for the two stages of the FC model assuming fractionating assemblages shown in Table 5.6. The results of AFC models, described below, are shown for comparison. The FC models predict increasing Ba and Sr contents through the first stage of the model. Sr becomes compatible in the second stage, as plagioclase becomes the dominant fractionating phase.

The decrease in Ba and Sr contents is not compatible with the compositions of the cumulate rocks which, for the most part, have low Ba and Sr (Figure 5.24). Separation of these cumulate rocks will drive residual liquids to higher Sr and Ba. We are

therefore, left with the paradox that the observed cumulate rocks do not have the appropriate LFSE or REE (or for that matter major element chemistry) required to shift the liquids along appropriate descent lines. Cumulate rocks exposed as marginal phases or as cognate xenoliths within plutons cannot account for the observed fractionation trends, arguing against processes of *in situ* differentiation at this level. Stern and Hanson (1991) noted a similar paradox in considering the origin of chemical variations in diorite-tonalites for the Superior Province.

Assimilation Fractional Crystallization Models

The problems encountered by the FC model are considerably reduced or eliminated in AFC models in which a high SiO_2 component is assimilated or mixed in, during fractionation (DePaolo, 1981). The trace element characteristics of the assimilant cannot be uniquely determined, however, it should have the following characteristics: 1) REE abundances lower than mafic rocks of the Concession Suite; 2) no significant Eu anomalies; 3) low Sr and Ba abundances; and 4) mantle-like Nd isotopic compositions.

The first requirement is needed to explain the decreasing REE abundances with increasing SiO_2 observed within the suite, but more importantly, assimilation of such a component will not result in significant crossing of REE patterns in resulting magmas. The low Sr and Ba are required to account for the decreasing abundances of these elements with fractination, as outlined above. This requirement is not as critical if biotite is a fractionating phase. The requirement that the crustal assimilant has a radiogenic Nd isotopic composition and non-radiogenic Sr reflects the overall juvenile isotopic character of the Concession Suite and the absence of significant changes in Nd isotopic composition with degree of fractionation. The crustal assimilant cannot be derived from a significantly older (>200 m.y.) LREE-enriched crustal source.

The trace element and isotopic characteristics described above are similar to those of the Siege Tonalite, which has been used as the assimilant in the AFC models. They

are not the characteristics of the slightly younger Yamba and Contwoyto Plutonic Suites described in the following chapter, some of which are derived from significantly older crust (Chapters 6 and 7).

AFC models were evaluated using equations of DePaolo (1981) and assuming assimilant and mineral proportions consistent with major element solutions (Table 5.5). The assimilant to fractionation ratio (r) was varied from 0 (simple fractional crystallization) to 3. The model assumes constant Bulk D values over the fractionation interval.

Figure 5.25 is a plot of calculated compositions compared to measured values. The results of the fractional crystallization models are also shown on this figure for comparison. The diagrams highlight the problems with the simple fractionation models described above. Particularly, the inability to predict the behaviour of Sr and Ba, and the excess depletion of MREE, caused by the large amounts of amphibole fractionation. In contrast, AFC processes, which require lower degrees of amphibole fractionation more closely fit the measured abundances. This is most notable through the first stage of the model (Figure 5.25a). SiO_2 content increases rapidly without large amounts of amphibole fractionation, and rocks of intermediate composition do not have strongly fractionated REE patterns. The potential of the AFC model to approximate the within-suite variation is seen in plots of Ba *vs.* Sr (Figure 5.24) and $(Ce/Yb)_N$ *vs.* Ce_N (Figure 5.26).

The details of any modelling of this type are clearly open to discussion as to the choice of fractionating assemblage and Kd values used, and the composition of the assimilant. As an example, small changes in the fractionating assemblages (particularly accessory phases) result in somewhat different results. An example of this is shown in Figure 5.26 which highlights differences in the predicted variation of Ce and Yb caused by small variations in the relative abundances of the fractionating phases (see Table 5.6, Model A and B). Models can be fine tuned, by arbitrarily choosing appropriate parameters to yield acceptable solutions. There is significant flexibility in modelling magmatic systems which contain a large number of accessory phases. Additionally,

any model can be made more complicated by considering the effects of true open system behaviour which includes mixing and magma replenishment in addition to fractional crystallization and assimilation (*e.g.* Defant and Neilson, 1990). The complexity of natural processes preclude uniquely determined fractionation paths, particularly in open systems. Recognizing these considerable limitations and that the models presented are simplifications of natural processes, chemical variation within the suite can be reasonably accommodated by AFC processes.

Origin of Regional Variations

As described earlier, individual plutonic bodies may have distinctive major or trace element contents at a given SiO_2 content. The concept of a single liquid line of descent is clearly invalidated on a regional scale, if not on a local scale. Multiple differentiation trends could reflect:

1) compositional differences in 'parental' magmas owing to compositionally different source regions or different melting conditions (Stern *et al.*, 1989)

2) variations in the details of the AFC process (compositions, rates, Bulk D)

3) mixing of differentiated and primitive magmas (*e.g.* Defant and Neilson, 1990)

4) any combination of the above.

Quantitative evaluation is difficult owing to the complexity and multiplicity of the processes involved. Differences in assimilation rates, different compositions of assimilant, variation in fractionating assemblage and bulk D values could all contribute to different fractionation trends. Additionally, true open system behaviour, involving magma mixing and periodically replenished magma chambers has not been explicitly considered (*e.g.* Defant and Neilson, 1990). Superposition of magma mixing of variably fractionated magmas results in non-liquid descent lines for both major and trace elements (Defant and Neilson, 1990). Field evidence of textures interpreted to originate from mingling between mafic and more felsic magmas was reported in

Chapter 2, and magma mixing and mingling could account for some of the regional variation. Alternatively, some of the diffences may reflect different parental compositions.

5.4.3 Summary

A unique solution explaining all of the chemical variation observed in the suite cannot be determined. This reflects both limitations inherent in simple models and the fact that the evolution of this suite involves superposition of more than one process. Within these limitations the following conclusions can be made:

1) Members of the Concession Suite are unlikely to be related by variable degrees of melting of basaltic source rocks at any pressure.

2) The general trends of within-suite chemical variation within the Concession Pluton can be modelled by open system behaviour involving fractional crystallization and crustal assimilation (AFC). Regional variation in pluton chemistry suggests that magmas have had varied evolutions reflecting: 1) different parental compositions; 2) unique differentiation histories, and; 3) the effects of mixing variably fractionated magmas.

3) The magmas did not interact significantly with older, LREE enriched crust.

5.4.4 The Origin of Parental Magmas to the Concession Suite

Parental magmas to the high Mg# group are characterized by andesitic compositions, with relatively high Mg# (>55), high Sr, Ce, and $(Ce/Yb)_N$ and low HREE contents. Magmas parental to the low Mg# group have lower Mg# (<50) and lower abundances of Sr, and the LREE. The following discussion will be focusssed on the origin of the high Mg# group.

Martin (1987) has suggested that calc-alkaline rocks with high $(Ce/Yb)_N$ ratios similar in composition to the Concession Suite are predominantly an Archean rock-type, whose origin is closely linked to the higher thermal conditions postulated to exist during the Archean. These higher thermal conditions could have led to extensive crustal melting in subduction zones and production of high $(Ce/Yb)_N$ tonalites. Although

arguably less predominant, volcanic and plutonic rocks with these same chemical characteristics occur in calc-alkaline rock series of all ages (*e.g.* Drummond and Defant, 1990; Defant and Drummond, 1990). For example, andesites, and their plutonic equivalents, with chemical characteristics similar to those of the Concession Suite occur in some recent continental margin arcs (*e.g.* Cascades, Condie and Swanson, 1973; Ewart, 1982; Peninsular Ranges Batholith, Gromet and Silver, 1987; Southern Volcanic Zone, Chilean Andes, Hildreth and Moorbath, 1988; Hickey *et al.*, 1986; Northern Volcanic Zone, Andes, Rogers and Hawkesworth, 1989) and in post-subduction 'collisional' zones such as the Papua New Guinea Highlands (Johnson *et al.*, 1978); Iran (Dostal 1978) and Turkey (Pearce *et al.*, 1990). The unusual combination of evolved and primitive chemical signatures is also characteristic of some arc-related high-Mg andesites (HMA) (*e.g.* Saunders *et al.*, 1987; Tatsumi and Ishizaka, 1982; Kay, 1978; Stern *et al.*, 1984; Shirey and Hanson, 1984).

There are three general models proposed to account for high Sr, high $(Ce/Yb)_N$ andesites:

1) derivation from subcrustal sources which have undergone variable degrees of slab enrichment and mantle melting (Saunders *et al.*, 1987; Johnson *et al.*, 1978; Stern *et al.*, 1989; Shirey and Hanson, 1984) or variable interaction with subcontinental lithosphere (Hickey *et al.*, 1986)

2) generation from 'normal' arc basalts by fractional crystallization (garnet, amphibole, pyroxene, olivine) and/or partial melting of underplated crust at garnet amphibolite or eclogite grade (Green, 1982; Gromet and Silver, 1987) within zones of melting, assimilation, storage and homogenization (MASH) at the base of the crust (*e.g.* Hildreth and Moorbath, 1988)

3) melting of subducted slab at eclogite grade followed by equilibration with mantle (Defant and Drummond, 1990; Stern *et al.*, 1984; Kay, 1978).

Derivation from Enriched Mantle Sources

Shirey and Hanson (1984) and Stern *et al.* (1989) have recently compared primitive Archean monzodiorites from the Superiour Province to high-Mg andesites from the Setouchi Volcanic Belt, termed sanukitoids (Tatsumi and Ishizaka, 1982a) and suggest a direct mantle origin for the Archean rocks. The term high-Mg andesite (HMA) refers to magmatic rocks which have intermediate SiO_2 (53-60 wt%), high Mg# (>60) and high Ni and Cr contents (>100 ppm). Table 5.8 shows the least fractionated samples of the Concession Suite to be compositionally similar to the monzodiorites from the southwestern Superior Province, as well as some recent HMA variously named alkaline low Ca boninites (Type IIb, Crawford *et al.*, 1989), bajaites (Saunders *et al.*, 1987), and sanukitoids. Because of their high alkali contents, particularly Na, these HMA rocks will be referred to as Na-rich high-Mg andesites (Na-HMA).

Na-HMA rocks are characterized by: high SiO_2 (56-59 wt%), Mg# (>60), Ni (>100ppm), Sr (up to 2500 ppm), Ce (up to 150 ppm) and $(Ce/Yb)_N$ (up to 30), and high Na_2O (>3%, Na_2O/K_2O > 1) and very low CaO/Al_2O_3 (<0.55) and HREE contents. Compared to other HMA (*e.g.* boninites) they are strongly enriched in LILE (particularly Na, Sr and the LREE). Although the major element compositions are similar, Na-HMA can have a range of trace element contents. For example, Figure 5.27 highlights a number of chemical differences between sanukitoids and bajaites previously noted by Rogers and Saunders (1989). In particular, sanukitoids are less enriched in LILE and have typical calc-alkaline K/Rb ratios. The REE are less fractionated and the HREE patterns are flat compared to those of the bajaites.

Mafic rocks of the Concession Suite, as well as the Superior Monzodiorites, are most similar to the bajaite-type Na-HMA characterized by high Ba, Sr and fractionated HREE. Samples from the Concesssion Pluton have the characteristic positive Sr anomalies of these Na-HMA. Rb contents of the Concession rocks are however higher

Table 5.8 Comparison of Concession Plutonic Suite to high-Mg andesites.

	Concess. Suite	Concess. Suite	Average Superior	Bajaite	Sanukitoid	PNG	Boninite	Exp. Melt Pyrolite	Exp. Liq. Ton.-Per.
	1	2	3	4	5	6	7	8	9
SiO2 (wt%)	56.34	53.35	56.07	58.23	56.80	56.46	58.43	55.50	59.5
TiO2	0.86	0.94	0.71	1.20	C.69	0.85	0.17	2.50	0.80
Al2O3	17.96	16.00	14 88	16.38	15.26	14.49	11.35	12.30	17.9
FeO*	6.65	8.26	7.08	4.40	6.10	6.27	8.57	7.10	5.30
MnO	0.10	0.13	0.12	0.07	0.12	0.10	0.12	0.10	0.10
MgO	4.45	6.38	6.85	5.86	9.17	7.07	11.40	9.30	4.10
CaO	6.30	7.67	7.65	6.57	7.01	8.26	7.76	10.40	6.20
Na2O	4.53	4.32	4.04	4.95	3.16	3.42	1.74	2.00	3.90
K2O	2.32	2.33	2.23	1.79	1.69	2.58	0.51	0.50	2.20
P2O5	0.48	0.61	0.36	0.55	0.00	0.50		0.00	
Mg Number	54	58	63	70	73	67	70	70	58
CaO/Al_2O_3	0.35	0.48	0.51	0.40	0.46	0.57	0.68	0.85	0.35
Cr	44	113	352	245			832		
Ni	31	75	154	152			205		
Rb	84	62	60	10	60		10		
Ba	781	1173	1214	956	303	1166	-		
Sr	1129	1535	1229	2186	235	994	71		
Nb	11	7	-	5	20	6	-		
Zr	229	143	111	211		223	19		
Y	24	22	-	9	15	19	5		
Ce	150	159	97	66.2	30.3	122	2.15		
Yb	1.81	1.64	1.6	.72	1.45	1.52	.67		
Rb/Sr	.07	.04	.05	.005	.26	-	.14		
K/Rb	230	314	309	1469	232	-	423		
Ba/Sr	.69	.76		.44	1.3	1.2	-		
Ti/Zr	23	40		34	-	23	54		
Ce/Yb	21	25	15.5	24	5.4	21	0.8		
Eu/Eu*	.74	.82	-	1.03	.83	.94	.73		

SAMPLE DESCRIPTION: (1) and (2) mafic samples of Concession Plutonic Suite, D023-87 and D154b-87; (3) average of 11 Archean diorites and monzodiorites from the southwestern Superior Province from Stern et al., 1989; (4) high-Mg andesite from Baja, Ca. termed Bajaite by Saunders et al., 1987 (SB.8.1); (5) high-Mg Andesite from Setouchi volcanic belt, sample 7201-705b, (Kushiro and Sato, 1978); (6) high-mg andesite from Papua New Guinea, Victory andesite (Johnson et al., 1978); (7) high-Mg andesite from Bonin Island - Boninite (Jenner, 1983); (8) melt composition (28% liquid) calculated to be in equilibrium with pyrolite - 40% olivine (cpx, opx, ol) at 10 kbar, 1000°C, water saturated (Green , 1976); (9) experimental glass composition in the tonalite-peridotite-H_2O system (90/10 tonalite/peridotite, 15 kbar, 1100°C, 10% H_2O).

than typical for bajaites, resulting in typical calc-alkaline K/Rb ratios, unlike the extremely high values characteristic of the bajaites. In this respect they are similar to sanukitoids.

In contrast to monzodiorites from the Superior Province, and NA-HMA, samples of the Contwoyto Suite do not exhibit Mg#, or Ni abundances compatible with direct mantle derivation. However, fractionation of only 5-10% olivine and orthopyroxene will reduce Ni from primitive, mantle-derived values, to the 50-100 ppm range of the parental magmas of the Concession Suite. Olivine is not an observed phenocryst phase, however it may have been an early fractionating phase which reacted out. Mg-rich orthopyroxene is observed in mafic cumulate rocks. The high Mg# group of the Concession Suite may represent slightly fractionated equivalents of high-Mg andesites.

Models for the Origin of Na-Rich High Mg Andesites

The high Ni and Mg# of little fractionated, Na-HMA are thought to represent direct partial melts of hydrated peridotite (Tatsumi and Ishihaki, 1982b; Shirey and Hanson, 1984; Saunders *et al.*, 1987; Stern *et al.*, 1989). Stern *et al.*, (1989) have argued that the combination of high SiO_2, LILE, Ni and Mg# is unlikely to result from fractionation, contamination or mixing involving basaltic, komatiitic or lamprophyric magmas and crust (*e.g.* Sparks, 1986). In accord with this, isotopic data for samples from Baja, Ca. argue against extensive crustal interaction for these magmas (Saunders *et al.*, 1987). The Na-HMA do not resemble rocks interpreted to be crustally contaminated komatiites (*e.g.* Arndt and Jenner, 1985; Sun *et al.*, 1989).

Experimental studies on primitive Na-HMA from the Setouchi volcanic belt indicate that they could be in equilibrium with peridotite (harzburgite or lherzolite) at relativley shallow depths (30-50 km), and high temperature (> 1100°C) and water contents (7 wt % at 14 kbar). Note that garnet is not an observed liquidus phase under these conditions. High SiO_2 melts with broadly similar major element chemistry have also been derived through hydrous pyrolite melting experiments (*e.g.* Nichols, 1974; Green, D.H. 1976, Table 5.8).

Based on these experimental studies, and the primitive compositions of Na-HMA, these rocks may be derived by melting hydrated peridotite (*e.g.* Shirey and Hanson, 1984; Stern *et al.*, 1989; Saunders *et al.*, 1987; Rogers and Saunders, 1989). In the case of the NA-HMA from Baja, Rogers and Saunders (1989) have documented primitive rocks (Mg# > 65) with a range of SiO_2 contents up to 60 wt%, and suggest that these reflect a wide range of near-primary magma compositions generated from the mantle. The full range of possible melt compositions that could be derived from hydrated peridotite remains poorly constrained.

The high LILE contents of Na-HMA are thought to reflect mantle enrichment prior to, or simultaneous, with melting (Crawford *et al.*, 1989; Saunders *et al.*, 1987; Rogers and Saunders, 1989; Shirey and Hanson, 1984; Stern *et al.*, 1989; Tatsumi and Ishihaka, 1982b). This has led to two stage models for the origin of Na-HMA: 1) development of a moderately to strongly refractory mantle source by extraction of melts; and 2) subsequent enrichment (H_2O, Sr, Ba, LREE) of this depleted mantle prior to, or simultaneously with, melting.

The necessity for an enriched mantle source can be demonstrated by consideration of Figure 5.28. This diagram plots the calculated Bulk D values required in order to generate melts with the trace element characteristics of sample D154b-87 from a relatively fertile mantle source (*ie.* MORB reservoir). Successful models require extremely small degrees (< 0.5%) of melting in order to reproduce the high abundances of incompatible elements observed in the rocks. Additionally, the residual assemblage must be capable of fractionating HFSE (in particular Nb) from REE, and $(Ce/Yb)_N$. Although extraction of small degree melts from the mantle may be theoretically possible (MacKenzie, 1984), these melts will be silica undersaturated, not saturated like the Na-HMA. Additionally, fractionation of Nb is unlikely to occur as a result of melting non-enriched mantle sources, even at very low degrees of melting. Garnet would be required to fractionate the REE, in disagreement with the experimental data indicating a garnet-free residuum.

Garnet would not be a required residual phase if the source was LREE-enriched. Figure 5.29 shows the calculated abundances of trace elements required in a mantle source to derive a melt with the trace element characteristics of parental rock of the Concession Suite, assuming moderate degrees of melting (10 and 20%) of a harzburgite source residuum (*ie.* amphibole and garnet-free residuum). The normalized trace element patterns of the source, calculated by this method, resemble, in shape but not abundance, those of the parental magmas. Even if garnet occurs as a residual phase the Sm/Nd ratio would not be significantly fractionated, unless the degree of melting is very small (comparable to the Bulk D of one of the elements), or a zone refining process concentrates incompatible elements (*e.g.* Hawkesworth *et al.*, 1987). The enrichment and fractionation of the REE is, therefore, considered to be dominantly a mantle source characteristic, not a result of melting processes.

Assuming that the source represents a two component mixture consisting of variably depleted mantle and an enriched component (*e.g.* Frey and Green, 1974), then the incompatible trace element content of the mixed source will be dominated by the enriched component and the compatible element contents (*e.g.* Ni) will be dominated by the mantle component. The enriched component must, therefore, have a similar normalized incompatible trace element pattern (though not abundance) as the calculated mantle source composition shown in Figure 5.29.

The normalized trace element pattern of the enriched component is superficially similar to patterns of some mantle xenoliths, including both hydrous (*e.g.* pargasitic peridotite) and non-hydrous types (Frey and Green, 1974; Kempton, 1987) as well as alkaline volcanic rocks (*e.g.* ocean island basalts, kimberlites), calc-alkaline lamprophyres, and small volume melts of eclogite (Figure 5.30).

In contrast to most mantle xenoliths and alkaline rocks, the enriched component has a relative HFSE depletion - a depletion characteristic of the 'subduction component' in modern island arc systems (Gill, 1981). Mantle metasomatism above Benioff zones may occur by a number of processes including dehydration of subducted oceanic crust

and pelagic sediments, or partial melting of sediments and mafic crust (*e.g.* Wyllie, 1984). The generation of melts and fluids in subduction zones depends on the thermal conditions of both the mantle and downgoing plate (Wyllie, 1984). Whether the metasomatising agent is a melt or a fluid cannot be easily determined by their chemical fingerprint, as both may be capable of transporting the LILE (*e.g.* Eggler, 1987; Tatsumi *et al.*, 1986). Fluid-mineral-melt partition coefficients required to address this issue remain very poorly constrained (*e.g.* Eggler 1987; Tatsumi *et al.*, 1986).

Saunders *et al.* (1987) and Rogers and Saunders (1989) have considered, in some detail, the source of the enriched component in Na-HMA (*ie.* bajaites). They argue that the relative fractionation of element pairs, particularly the high K/Rb ratios observed in bajaites cannot be produced within a fluid phase, or through partial melting of mafic crust at eclogite grade. They attribute many of the chemical features to stabilization of, and equilibration of metasomatizing fluids with amphibole within the mantle. In their model, the mantle would behave as a chromatographic separation column, preferentially retaining those elements stable in the pargasitic mantle assemblage (Na, Ba, Sr, REE) during metsomatism. Those elements not compatible with such an assemblage would pass through the mantle into the crust. Breakdown of paragasite and mantle melting, caused by a later thermal event, releases elements temporarily stored in the mantle, thereby enriching the resulting Na-HMA magma. Melting a pargasitic mantle would account for the Na-rich nature of the magmas, along with their high LREE, Sr, and Ba but low Rb contents. It is particularly effective in producing the high K/Rb ratios of bajaites (Saunders *et al.*, 1987).

A slab melting model has been invoked to explain some Na-HMA in modern settings, including those from the Aleutians (Kay, 1978), Isla Cook (Stern *et al.*, 1984; Puig *et al.*, 1984) and elsewhere (Defant and Drummond, 1990). Geochemical arguments presented in section 5.4.2 mitigate against a direct derivation from an eclogite source for diorites of the Concession Suite. Kay (1978) postulated that the Aleutian Na-HMA inherited their incompatible trace element characteristics from small volume, slab-derived eclogite melts (see also Defant and Drummond, 1990, Stern *et*

al., 1984; Puig *et al.*, 1984) which reacted and equilibrated with the overlying mantle peridotite during ascent. As shown by Carrol and Wyllie (1989) and Johnston and Wyllie (1986) reaction of tonalite with peridotite increases and then buffers the Mg# and compatible element content of the siliceous melt. The reaction is likely to cause crystallization of orthopyroxene and garnet or amphibole (P_{H2O} dependant) from the melt, and assimilation of orthopyroxene and olivine. Liquids experimentally produced by these reactions have major element compositions comparable to rocks of the Concession Suite (Table 5.8).

The Mg# of liquids produced in these experimental studies are buffered at values of approximately Mg60. These values are similar to those observed in the Concession Suite but are much lower than observed in primitive Na-HMA (Mg > 70). If the assumption that Na-HMA with lower Mg# (< 60) are genetically related to the more primitive varieties then this mechanism, on its own seems unlikely. In addition, it is not clearly established that small volume slab melts (*e.g.* 3%, Kay, 1978) will be physically and thermodynamically able to ascend through the mantle while continuously reacting with peridotite wallrock. This is particularly true if the melt is water-saturated (*e.g.* Wyllie and Sekine, 1982). The tonalite melt may completely react out during ascent producing garnet or amphibole-mica peridotite (Sekine and Wyllie, 1982a.b). Such a process could be responsible for generating the enriched mantle source described above, which could then be melted during a subsequent thermal event, to produce primary Na-HMA. This will be discussed in Chapter 8.

Is a Refractory Mantle Source (RMS) Required in NA-HMA petrogenesis?

Crawford *et al.* (1989) have postulated that Na-HMA are derived from extremely refractory mantle sources (RMS)- sources more refractory than those which produce boninites. Their argument is based on the high SiO_2 and extremely low CaO/Al_2O_3 ratios (< .55) characteristic of these rocks (Table 5.8).

RMS are generated by repeated extraction of melts rich in basaltic components from the mantle, leaving an increasingly refractory mantle residuum (Duncan and Green, 1980). Compared to melts of more fertile mantle (*e.g.* MORB or Archean

tholeiite) those derived from RMS have lower CaO/Al_2O_3 and higher Al_2O_3/TiO_2 and CaO/TiO_2 ratios and lower abundances of incompatible trace elements (*e.g.* LILE, Zr, Ti, P, Y, HREE) than melts of more fertile mantle (Sun and Nesbitt, 1978; Falloon *et al.*, 1989).

Samples of the Concession Suite and Na-HMA in general, have very low CaO/Al_2O_3 ratios, consistent with derivation from a highly RMS (Figure 5.31). Unlike boninites, which are generally accepted to be derived from RMS, the high TiO_2 and relatively low, MORB-like (or Archean tholeiite-like) ratios of Al_2O_3/TiO_2 and CaO/TiO_2 suggest derivation from relatively fertile mantle materials which were not extensively depleted in the past (Tatsumi and Ishihaka, 1982b; Tatsumi and Maruyana, 1989). In support of this, Stern *et al.*, (1989) have shown that the FeO-MgO systematics of Archean Na-HMA are consistent with derivation from relatively fertile mantle sources (*e.g.* pyrolite). Additionally, the trace element abundances of Zr and P in Na-HMA are much higher than predicted for melts from refractory mantle, although the low Y and HREE would be consistent with derivation from RMS.

The contradictory major and trace element indicators of source fertility, described above, argue against the use of inverse geochemical techniques to assess the fertility of the mantle source of Na-HMA. This is because the chemistry of the rocks may largely be controlled by mantle enrichment events, not only previous melting events. As one possible example of this phenomenon, Figure 5.31 shows the effect on the CaO/Al_2O_3 ratio of binary mixing between a fertile mantle source and a siliceous liquid (*e.g.* slab-derived tonalite), to simulate enrichment of the mantle by slab-derived melts (*e.g.* Wyllie, 1984). Because the CaO/Al_2O_3 ratio of siliceous eclogite-derived melts is very low relative to mantle ratios, mixing and reaction will rapidly reduce the CaO/Al_2O_3 ratio of the mantle source without significantly affecting the TiO_2 content, or the CaO/TiO_2 or Al_2O_3/TiO_2 ratios. The low CaO/Al_2O_3 in this case reflects a mixed mantle source rather than a refractory source. The effect of other types of mantle metasomatism (*ie.* fluid processes) on these ratios cannot be estimated, however CaO/Al_2O_3 ratios in many mantle xenoliths generally decrease with increasing trace

element enrichment (Kempton, 1987). Because significant major and trace element changes accompany mantle metasomatism, elemental abundances and ratios characteristic of Na-HMA may be telling more about the nature of the mantle enrichment process than the pre-enrichment source composition.

As noted above, the HREE abundances of the rocks are lower than predicted for melts derived from a garnet-free MORB or Archean tholeiite mantle source. This requires that: 1) garnet be a residual mantle phase; or 2) the mantle source was depleted in HREE relative to typical MORB or Archean tholeiite mantle sources. Figure 5.29 illustrates that the abundances of the HREE in the calculated mantle source overlap those of a MORB-mantle reservoir, assuming the Na-HMA rocks are derived by moderate degrees of melting (20%, *e.g.* Green, 1973). Hybridization by eclogite-derived melts or fluids could also contribute to the low HREE contents of the source, and garnet need not, therefore, be a residual phase in order to account for the low HREE contents.

To summarize, the mantle source to the Concession Suite may be a depleted, but relatively fertile (*ie.* cpx present), hydrated and chemically modified, garnet-free mantle. The source is not required to be extremely refractory as suggested by Crawford *et al.*, (1989).

Timing of the Mantle Enrichment Event

An estimate of the maximum age of the mantle enrichment event can be made using Nd isotopic data. Metasomatic changes in the $^{147}Sm/^{144}Nd$ ratio of the mantle source will produce changes in its Nd isotopic composition in the long term. This is shown on a diagram of $f_{Sm/Nd}$ vs $\varepsilon_{Nd(t)}$ (Figure 5.32), a modification of a standard isochron diagram. As described by DePaolo (1988) and Shirey and Hanson (1986) changes in the $^{147}Sm/^{144}Nd$ ratios ($f_{Sm/Nd}$) result in vertical movements on this diagram (assuming the enrichment process does not recycle Nd from older crustal sources). The time integrated effects of these changes result in changes in the ε_{Nd} value and produce

horizontal movements on the diagram. In the simplest case, isotopic evolution lines are shown as straight lines on this diagram as on isochron diagrams. Note that this assumes that the enriched component and the mantle component had similar $\epsilon_{Nd(t)}$ values.

The absolute decrease in ϵ_{Nd} of the mantle source depends on both the amount of fractionation and the time since the fractionation event occurred. If the large decrease in $f_{Sm/Nd}$ resulting from the mantle enrichment event described above significantly preceded magmatism, the enriched mantle source would have had sufficient time to evolve horizontally to lower ϵ_{Nd} values. If the enrichment occurred only a short time prior to magmatism there would be insufficent time for changes in ϵ_{Nd} values to have occurred.

This technique is applied to the samples of the Concession Suite in Figure 5.32. An important unknown is the pre-enrichment Nd isotopic composition of the mantle source. Estimates of the ϵ_{Nd} values for the Late Archean depleted mantle are generally within the range of +1.2 to +3.5 units (stippled region on Figure 5.32). The value of +3.5, assumed in positioning the array of isochron lines on Figure 5.32, is the highest value measured for volcanic rocks in the Slave Province. The array of isochron lines will shift to the left or right depending on the ϵ_{Nd} value of the mantle. The depleted mantle value can be thought of as the initial ratio in a standard isochron diagram. Most of the data for the Concession Suite lies within the range of depleted mantle ϵ_{Nd} values and all except one lie within the region of 100-200 m.y. If a lower value for the depleted mantle is assumed (*e.g.* 2.5), then most samples would lie within the 100 m.y. isochron of this value.

The mantle enrichment event is therefore restricted to have occurred within the 200 m.y. prior to the magmatism. This should be considered a maximum value because it assumes a high value of +3.5 for depleted mantle (basalts in the Slave Province range from -2.1 to +3.5; see Chapter 7), and that the change in $f_{Sm/Nd}$ did not affect the isotopic composition of the source (i.e. no recycling of older crust). The age

of the enrichment event is therefore considered to be younger than 2800 Ma and possibly contemporaneous with the magmatism at *ca.* 2600 Ma. The Concession Suite cannot be derived from an old enriched lithospheric source.

Relationships between the Low Mg# and High Mg# Groups

As described above, the low Mg# group have distinctly higher Ti, Nb, and lower Sr, Ce and $(Ce/Yb)_N$ compared to rocks of the high Mg# group, with equivalent SiO_2 contents. Although it cannot be shown in all cases, the chemical differences between the two groups appear to extend back to the mafic compositions. Stern *et al.*, 1989 noted similar chemical differences within the monzodiorite rocks from the southwestern Superior Province. In that case, Stern *et al.* (1989) had more primitive samples (*ie.* high Ni, Mg#) and were able to relate the differences to mantle source composition. Some of the range in chemistry within the Concession Suite could also be caused by primary differences in 'parental' composition. This would require a mantle source with variable Mg# (Stern *et al.*, 1989); the high Mg# rocks being derived from higher Mg# mantle. Since the high Mg# rocks are also more enriched in LILE this requires that the more depleted mantle source was also more enriched in LILE as suggested by Stern *et al.* (1989). The small number of primitive samples of either of the two groups precludes evaluation of this or other possibilities.

Alternative Petrogentic Models

Differentiation of 'normal' arc basalts at the crust-mantle boundary

Andesites with high LILE and $(Ce/Yb)_N$, similar to the Concession Suite, may evolve from 'normal' arc basalts by high pressure fractionation and/or assimilation of garnet-pyroxene-amphibole assemblages at the base of the crust (Green, 1982; Gill, 1981). Hildreth and Moorbath (1988) have recently discussed this hypothesis in detail and suggest that zones of "melting, assimilation, storage and homogenization" which they refer to by the acronym (MASH), develop "in the lowermost crust or mantle crust transition where basaltic magmas that ascend from the mantle wedge become neutrally buoyant, induce local melting, assimilate and mix extensively, and either crystallize completely or fractionate to the degree necessary to re-establish buoyant ascent.

Magmas ascending from such zones may range from evolved basalt to dacites." MASH zones operate as filters and buffers to ascending mantle magmas and have been proposed as the origin of calc-alkaline magmas (*e.g.* Keleman, 1990; Carrol and Wyllie, 1989).

Quantitative assessment of this model is difficult owing to both the complexity and multiplicity of the processes involved. Hildreth and Moorbath (1988) have discussed possible effects on the trace element characteristics of resulting magmas. Fractionation of garnet-pyroxene assemblages and assimilation of partial melts of crustal material in equilibrium with garnet (including differentiates of earlier intrusions) can both increase the $(Ce/Yb)_N$ and decrease the Yb content of the resulting magmas. However in order to increase the Sr content to very high levels (> 1500 ppm) requires special conditions (*e.g.* Stern, 1990): 1) extensive fractionation of minerals with low Kd^{Sr} values; and 2) extensive assimilation of high Sr material. Hildreth and Moorbath (1988) argued for assimilation of high Sr lower crust to produce andesites with Sr contents in excess of 600 ppm in southern Chile.

Extensive filtering within the lower crust will produce low Ni fractionated magmas at surface. MASH zones within ultramafic host rocks (*ie.* cumulate or upper mantle rocks) may buffer Mg# and Ni abundances (Kelemen 1990; Carrol and Wyllie, 1989), but are unlikely to produce compositions in chemical equilibrium with peridotite (*ie.* Mg# > 70, Ni > 150 ppm), as extreme Mg enrichment is buffered by orthopyroxene saturation (Keleman, 1990). If the rocks are related to high Mg# and Ni parents such as Na-HMA then they are unlikely to develop by crustal contamination and mixing with mantle melts as shown by Stern *et al.*, (1989).

5.5 Origin and Evolution of the Siege Plutonic Suite

Rocks of the Siege Suite are compositionally similar to high-Al trondhjemitic rocks (Arth, 1979; Barker, 1979). The rocks geochemically similar to those of the Olga Suite (Figure 5.18), and they may also be derived from partial melting of basaltic source rocks or derivative sediments, leaving a plagioclase-free residuum (see Chapter 4, Figure 4.14).

The extremely low abundance of REE and in particular HREE (< 1 times primitive mantle) require either a source residuum mineralogy capable of concentrating HREE (amphibole, garnet, zircon, apatite, titanite, or other) or depletion of HREE by fluids or volatiles (CO_2-bearing (Collerson and Fryer, 1978) prior to, during, or subsequent to, the melting event. The extreme ratios of HFSE (*e.g.* Ti/Zr, Zr/Nb) relative to those commonly observed in mafic and intermediate rocks could reflect a residual Ti-bearing, REE-enriched phase.

The available data cannot be interpreted in a simple petrogenetic model. Field observations presented in Chapter 3 indicate that petrogenetic models must take into account assimilation of host rocks and late-magmatic separation of a melt or fluid phase (leucocratic phase?). Data are not available to qualitatively assess the latter process and establishing an entirely igneous origin for this suite cannot be done at this time. With these caveats, the most likely origin of the Siege Suite is through melting of mafic rocks in the lower crust.

5.6 Chapter Summary

Magmatism spanning the time of maximum regional shortening and peak metamorphism includes: 1) the intrusion of mantle-derived high-Mg andesites into the crust; and 2) crustal melting to yield trondhjemite plutons. The proposed HMA parents to the Concession Suite are similar to some Na-rich HMA, including bajaites and sanukitoids. Differentiation of these mantle-derived magmas within the crust to produce the dominant tonalite composition, occurred by fractionation (amphibole-plagioclase dominated; ?early orthopyroxene) combined with assimilation of crustal melts, possibly similar in composition to those of the Siege Suite. Mixing of more, and less,S fractionated magmas may also have contributed to some of the chemical variation. The Siege Suite is similar in composition to the older Olga Suite, and could be derived by a similar process of eclogite melting.

The mantle source for the Concession Suite was enriched in LILE relative to mantle sources for typical Archean tholeiites. The enriched component has HFSE anomalies similar to those charactersistic of modern subduction systems. Enrichment

of the mantle source is restricted to have occurred within the 200 m.y. prior to magmatism. By analogy with modern examples of Na-HMA, enrichment may have occurred by transport of elements in a fluid or siliceous melt derived from a subducting slab. As discussed in Chapter 8, this need not, however, imply active subduction at the time of magmatism.

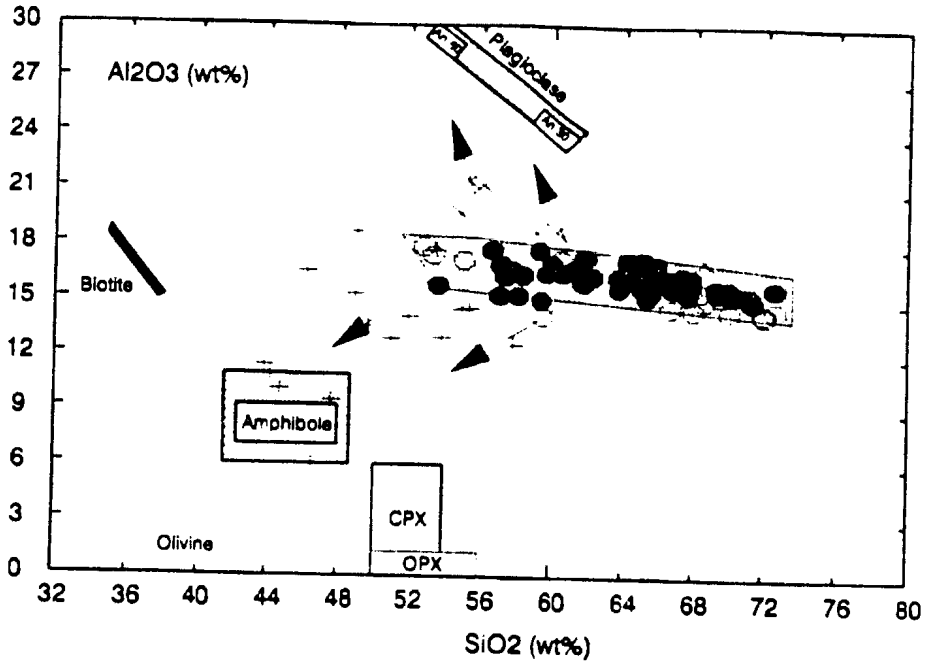

Figure 5.1. Al_2O_3 *vs.* SiO_2 for rocks of the Concession Plutonic Suite. Compositional fields for the principal rock forming minerals are taken from (Hill, 1980; Deer *et al.*, 1966). All minerals except biotite have Al_2O_3 contents distinct from those of the whole rocks. Accumulation of amphibole (± orthopyroxene, clinopyroxene, olivine) leads to lower SiO_2, low Al_2O_3 compositions (arrows shown). Accumulation of plagioclase leads to high Al_2O_3 intermediate SiO_2 rock compositions. Biotite has similar Al_2O_3 content to the magma composition. Samples which plot off of the data array (shown as crosses) contain either high proportions of modal amphibole (below data array) or plagioclase (above data array).

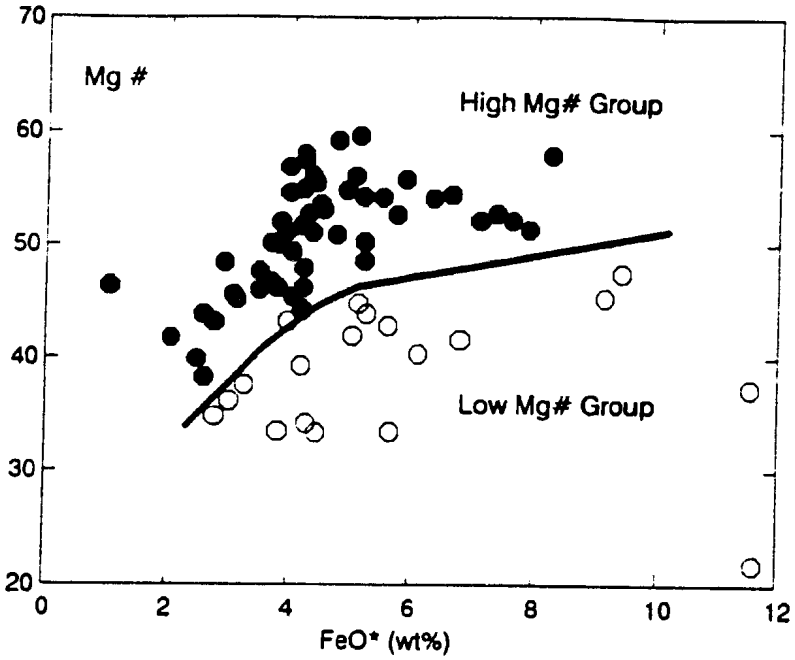

Figure 5.2. Subdivision of the Concession Plutonic Suite into high and low Mg# groups.

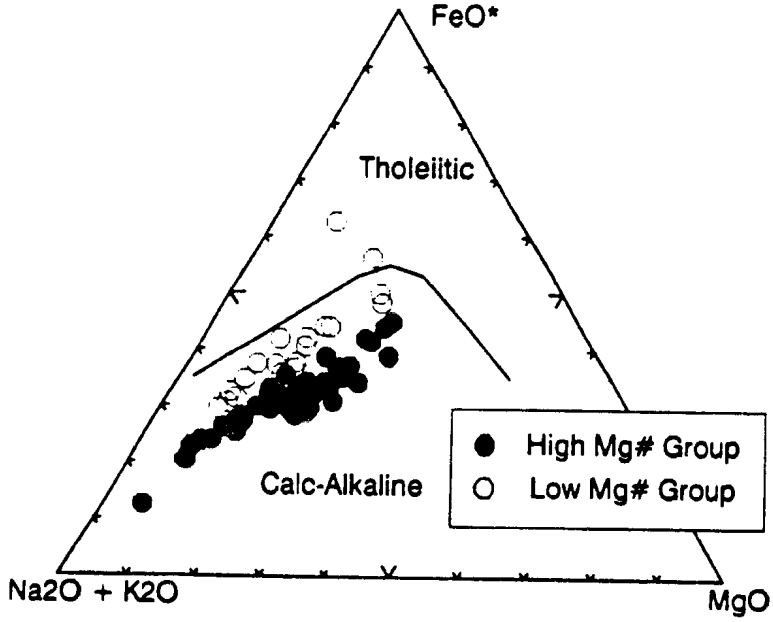

Figure 5.3. AFM diagram for the Concession Plutonic Suite. Filled symbols represent high Mg# group, open symbols the low Mg# group. Tholeiitic and calc-alkaline fields from Irvine and Baragar (1971).

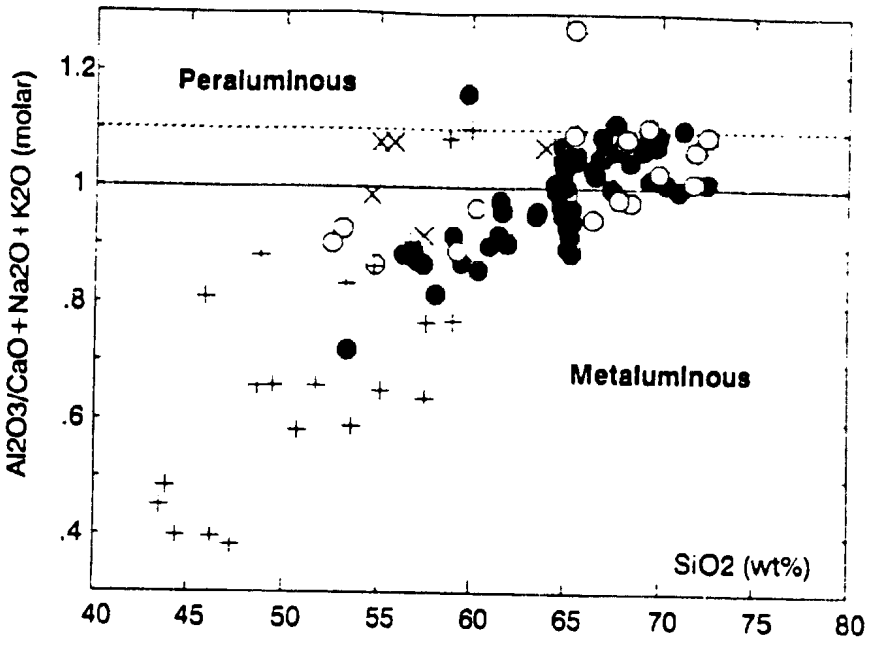

Figure 5.4. SiO_2 *vs.* $Al_2O_3/CaO+Na_2O+K_2O$ (Molar). Amphibole cumulate rocks are shown as +; plagioclase cumulate rocks as X. Other symbols as in Figure 5.3.

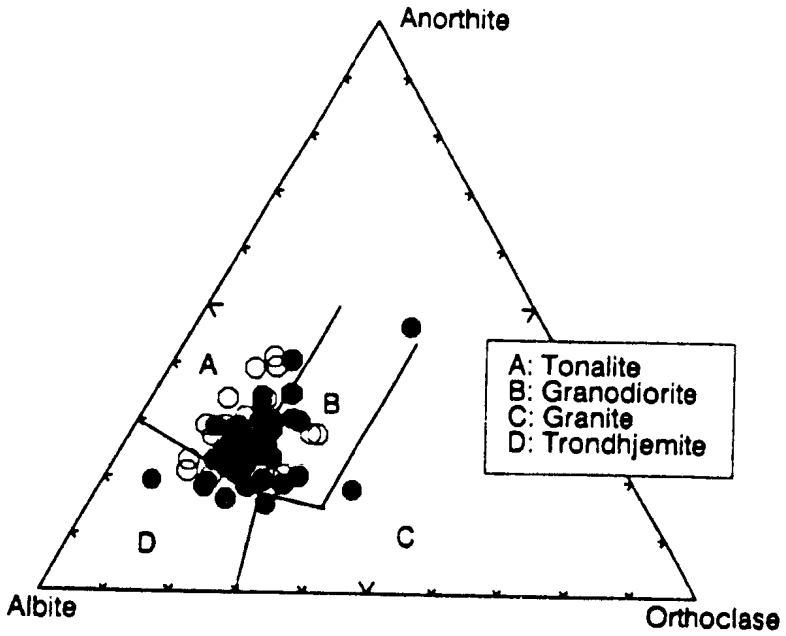

Figure 5.5. Classification of the Concession Plutonic Suite based on CIPW albite, anorthite and orthoclase. Fields from Barker (1979) after O'Conner (1965). Symbols as in Figure 5.3.

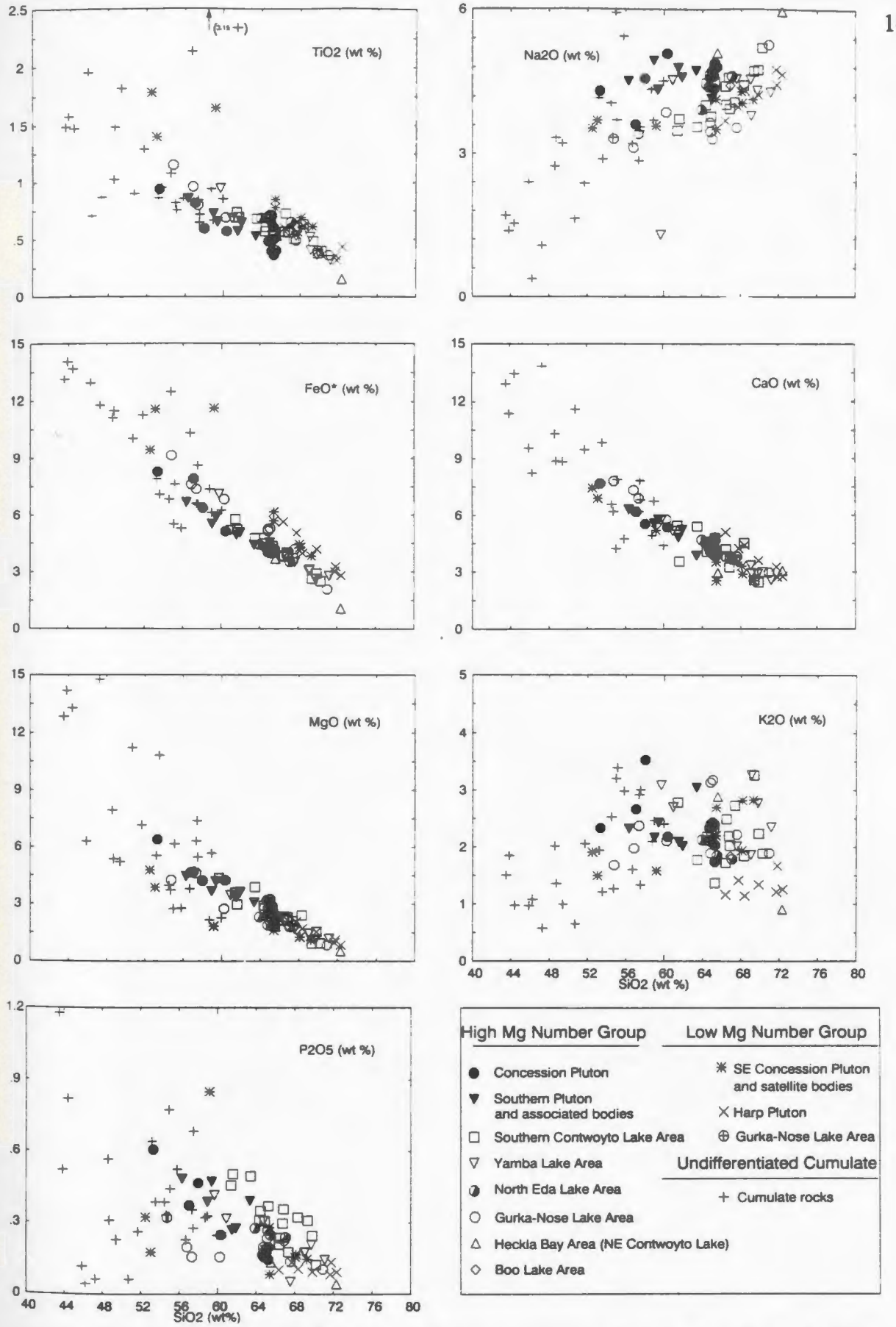

Figure 5.6. Major element Harker variation diagrams, Concession Plutonic Suite.

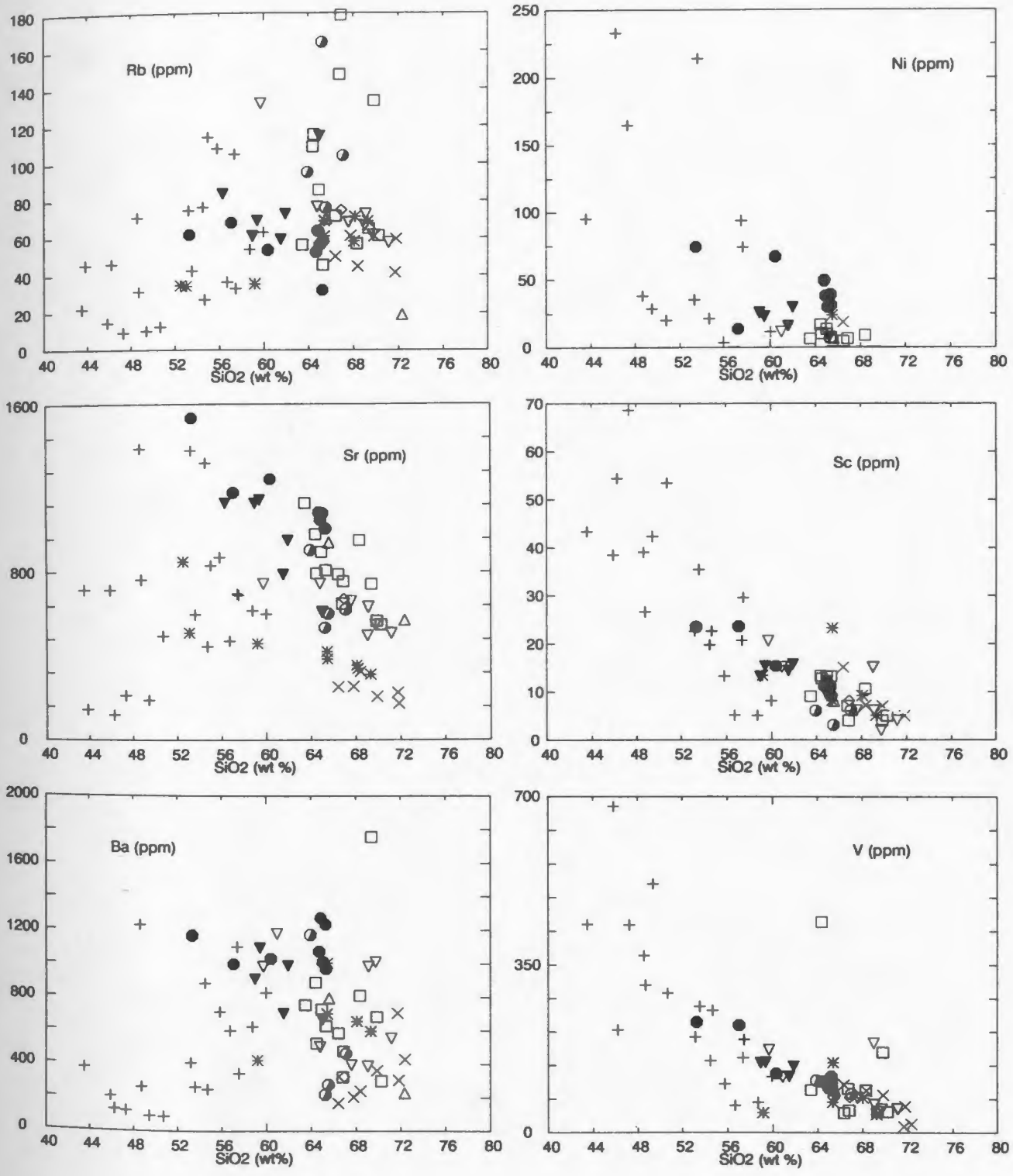

Figure 5.7. Trace element Harker variation diagrams, Concession Plutonic Suite. Symbols as in Figure 5.6.

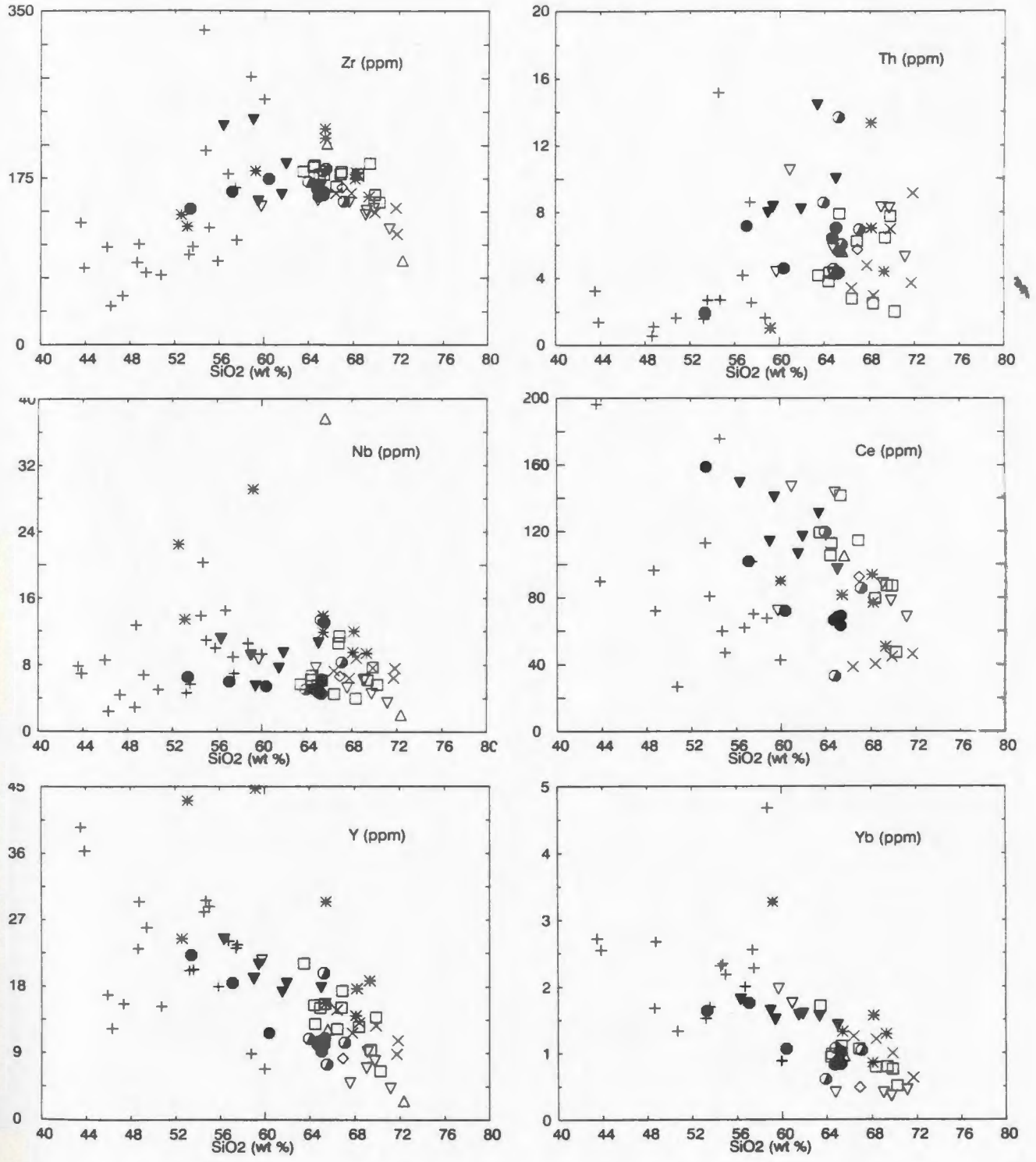
Zr (ppm)
Th (ppm)
Nb (ppm)
Ce (ppm)
Y (ppm)
Yb (ppm)
SiO2 (wt %)

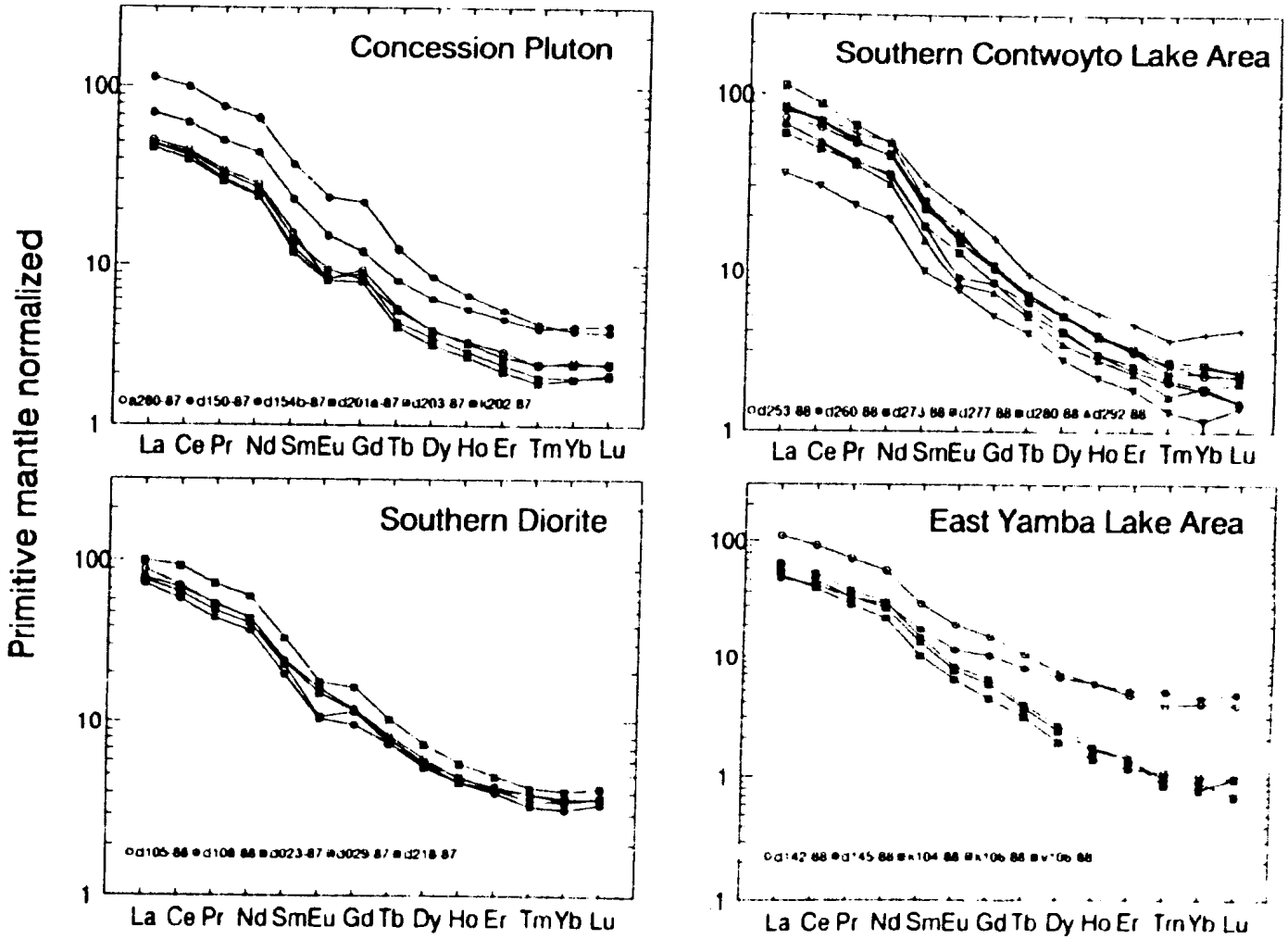

Figure 5.8. Primitive mantle normalized REE diagrams, high Mg# group, Concession Plutonic Suite. Each plot includes only samples from individual plutons or geographical areas. Figure 3.11 serves as a location map.

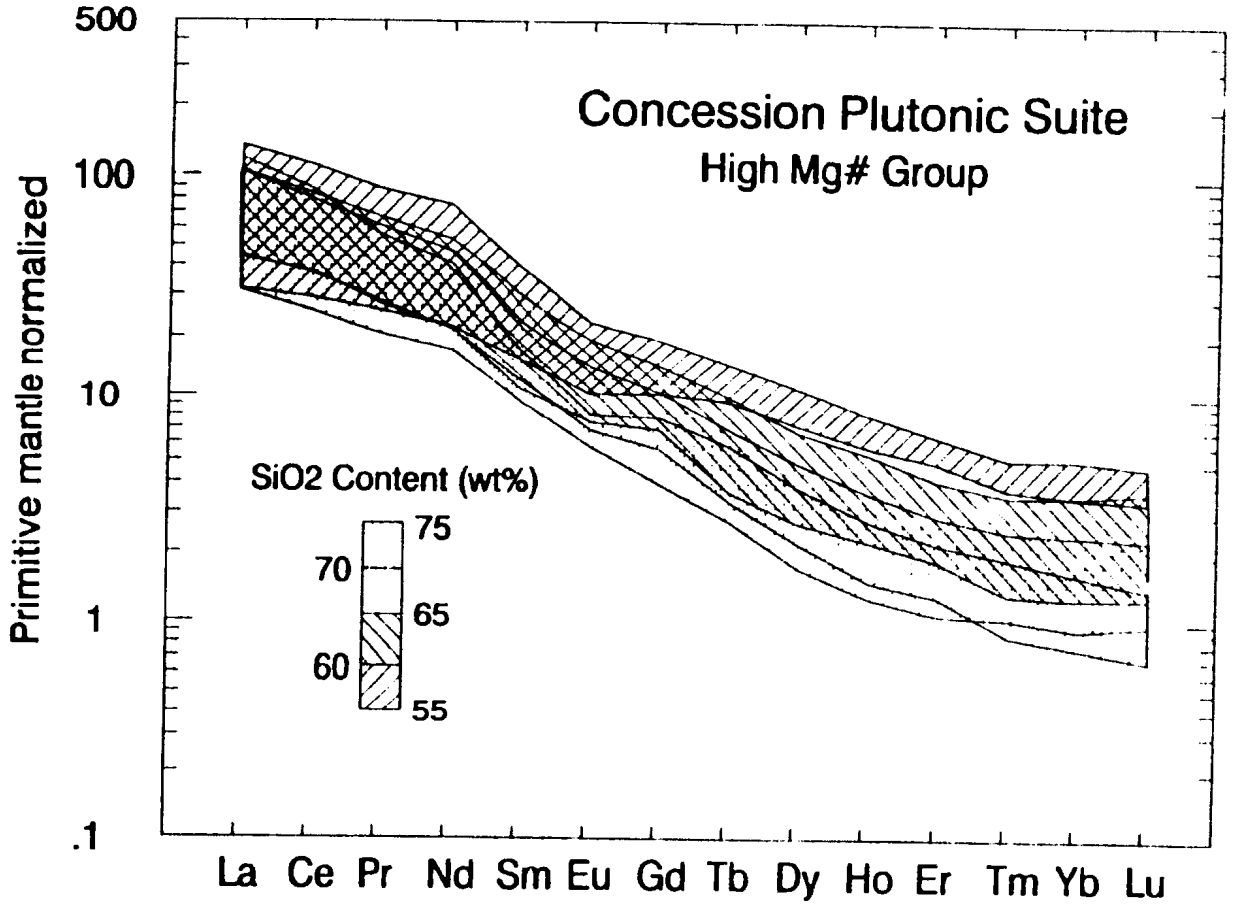

Figure 5.9. Primitive mantle normalized REE diagram of the high Mg# group, Concession Plutonic Suite rocks grouped according to SiO_2 content.

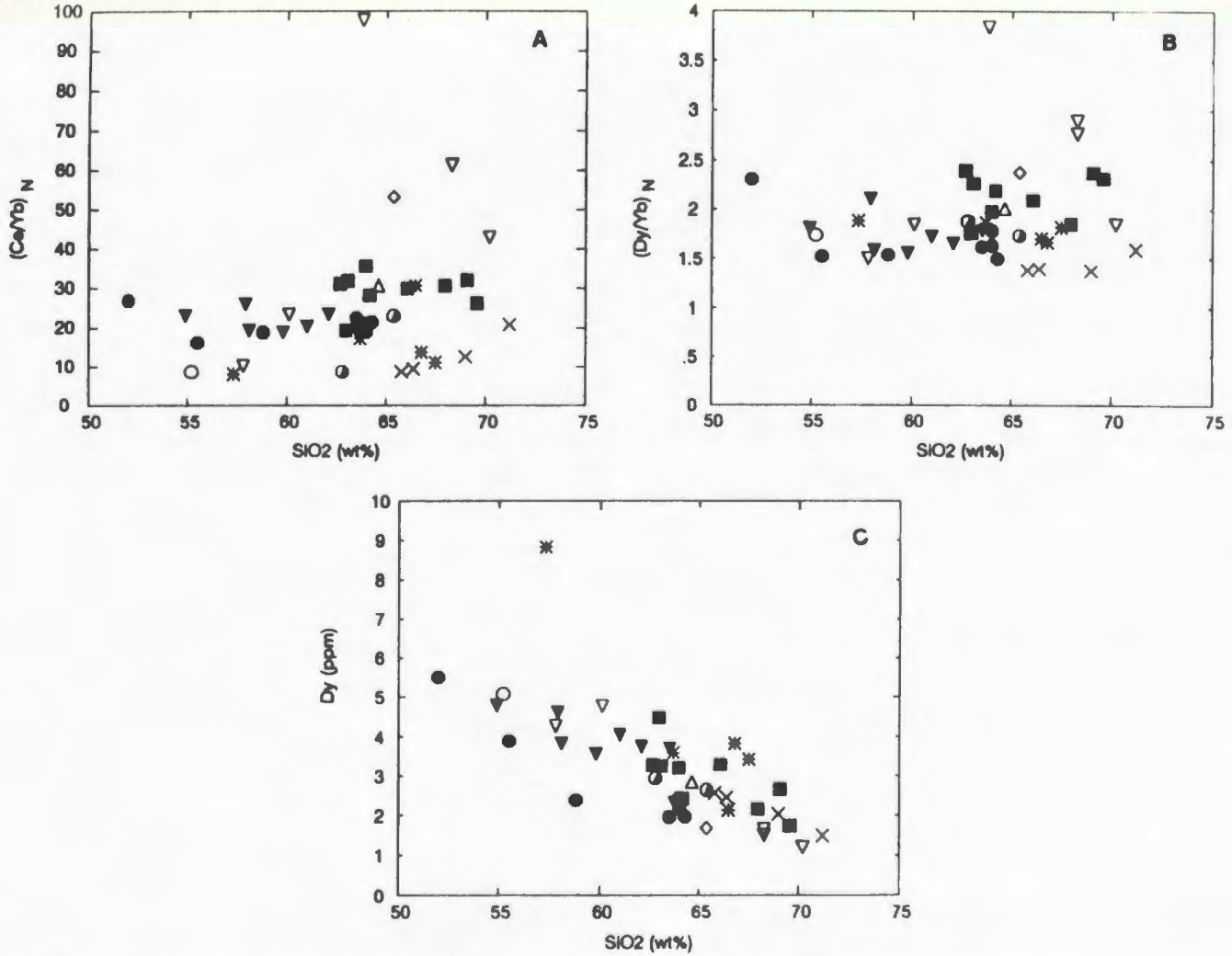

Figure 5.10. Plots of (A) $(Ce/Yb)_N$, (B) $(Dy/Yb)_N$ (C) Dy *vs.* SiO_2. REE ratios show regional variations but exhibit little change with increasing SiO_2 content. Symbols as in Figure 5.6.

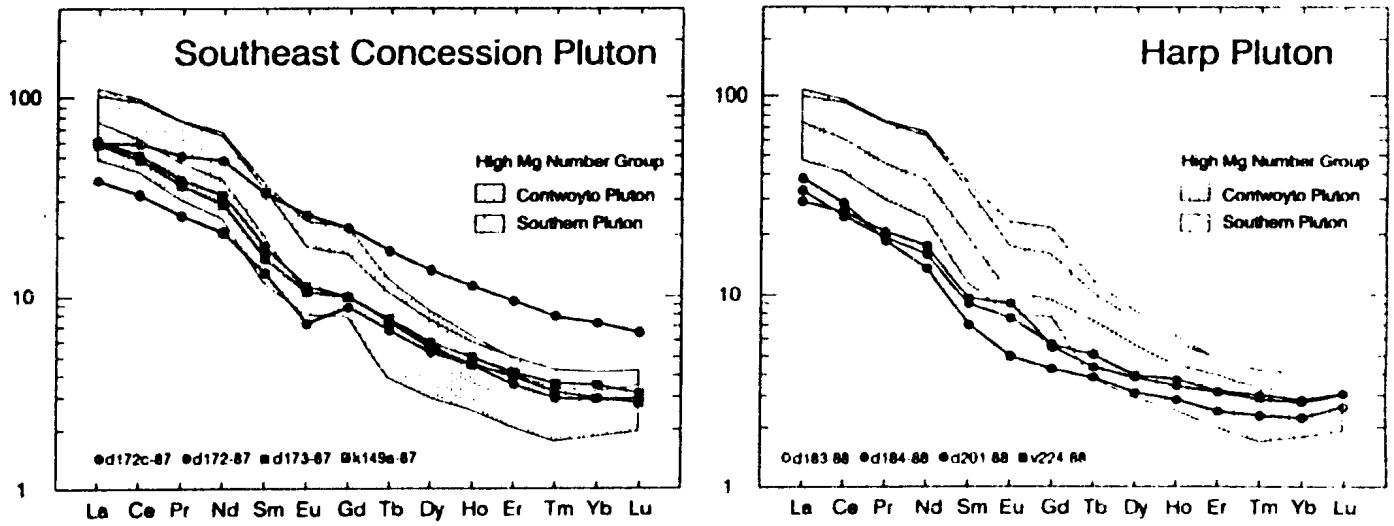

Figure 5.11. Primitive mantle normalized REE diagrams for rocks of the low Mg# group, Concession Plutonic Suite. Fields for two plutons of the high Mg# group are shown for comparison.

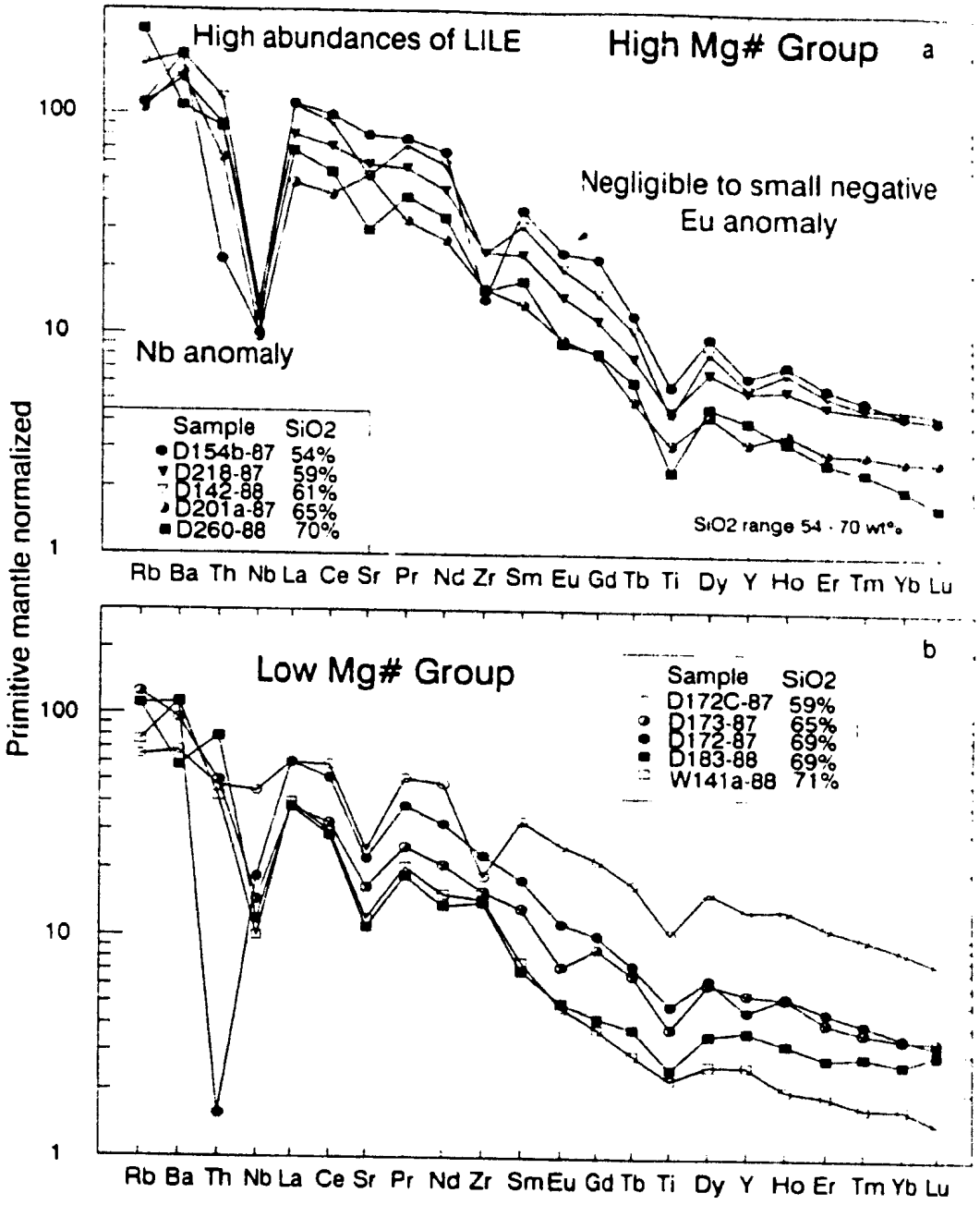

Figure 5.12. A) Primitive mantle normalized extended REE diagram illustrating the high abundances of LILE, LREE, strong negative Nb anomalies and low HREE characteristic of the high Mg# group, Concession Plutonic Suite. B) Primitive mantle normalized REE diagram for the low Mg# group.

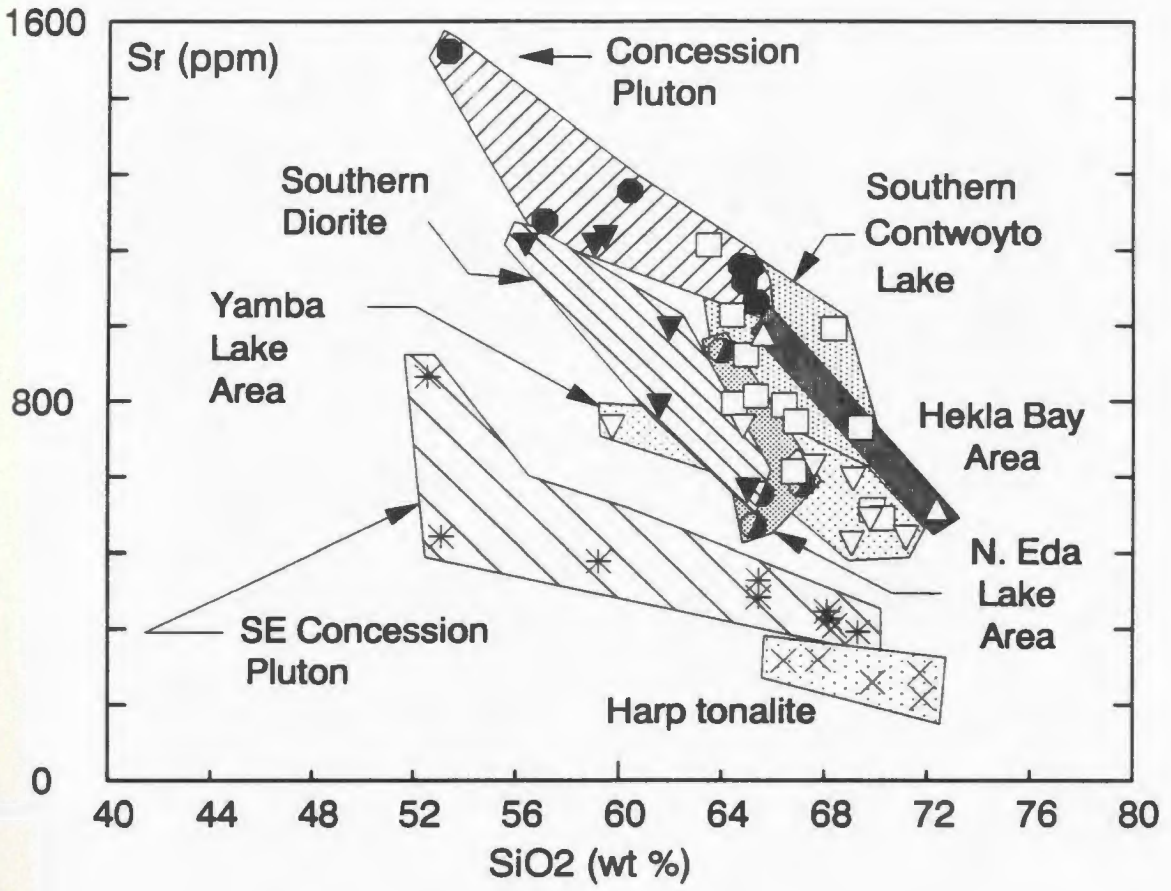

Figure 5.13. Sr *vs.* SiO_2 showing regional variations in Sr content at a given SiO_2 content. Note low Mg# groups have low Sr. Symbols as in Figure 5.6.

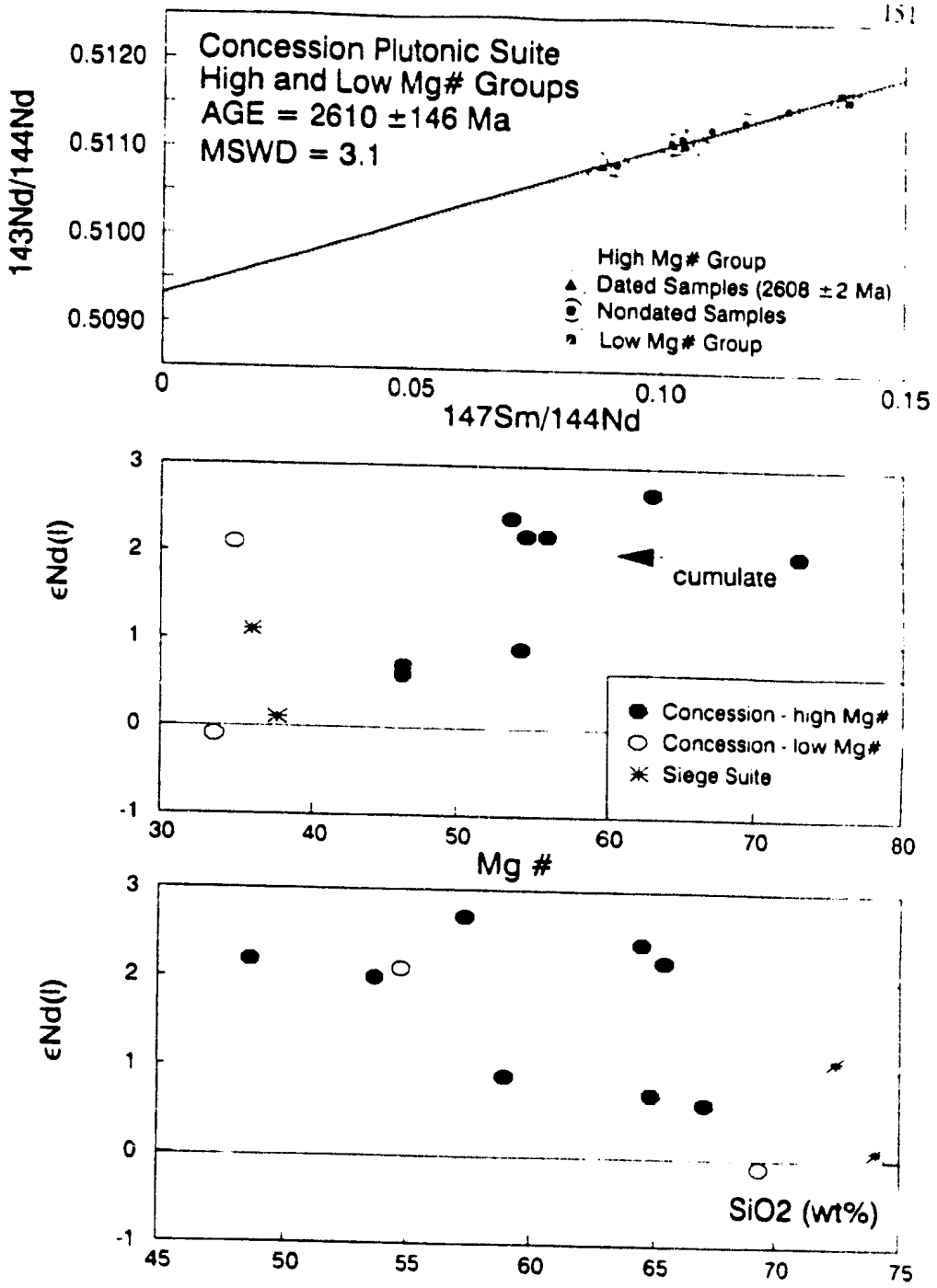

Figure 5.14. A) $^{147}Sm/^{144}Nd$ *vs.* $^{143}Nd/^{144}Nd$ isochron plot. Regression line (solid) calculated following Ludwig (1980). Dashed line is calculated using the U-Pb zircon ages (2608 ±2 Ma) determined for two of the analyzed samples (van Breemen *et al.*, 1990). B) $\epsilon_{Nd(I)}$ *vs.* Mg#. C) $\epsilon_{Nd(I)}$ *vs.* SiO_2.

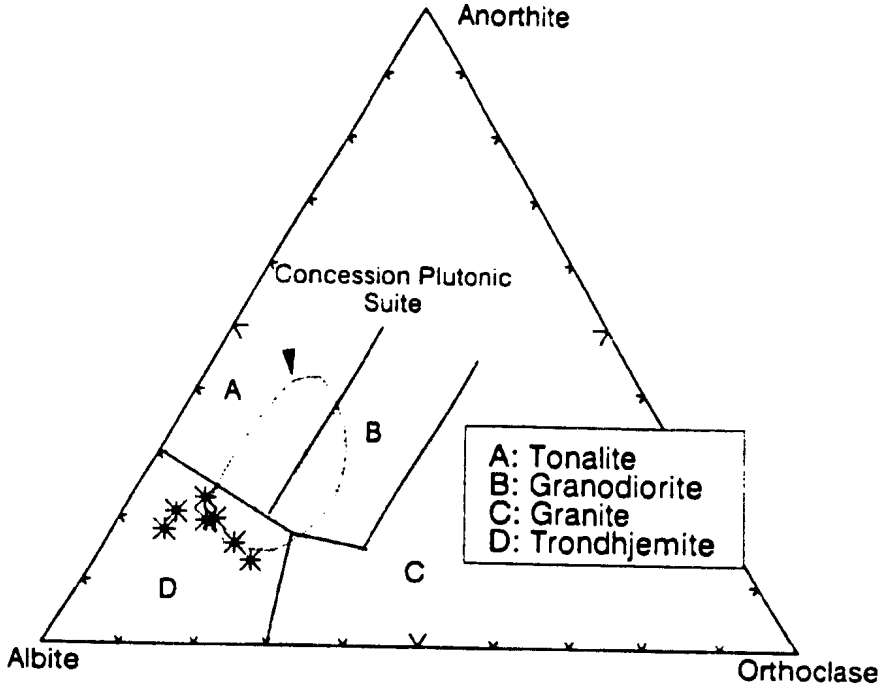

Figure 5.15. Plot of CIPW normative Ab-An-Or for the Siege Plutonic Suite. Field of Concession Suite shown by stippled area.

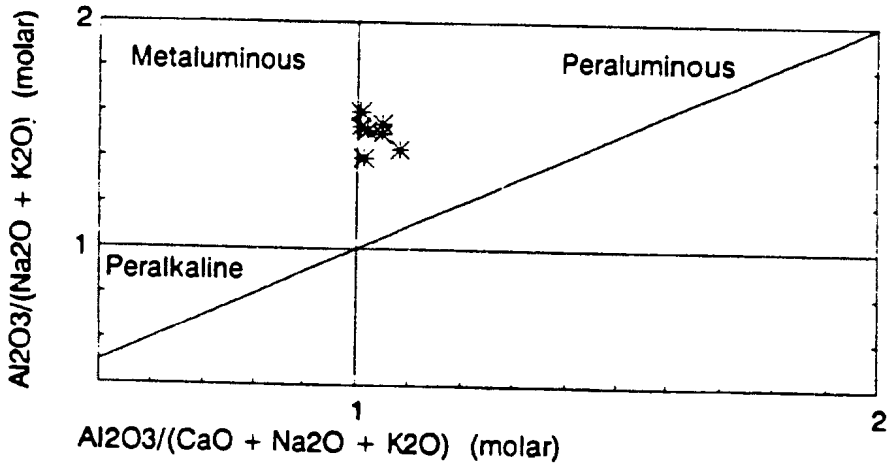

Figure 5.16. $Al_2O_3/(CaO+Na_2O+K_2O)$ *vs.* $Al_2O_3/(Na_2O+K_2O)$ plot showing the weakly peraluminous composition of the Siege Plutonic Suite. All values molar.

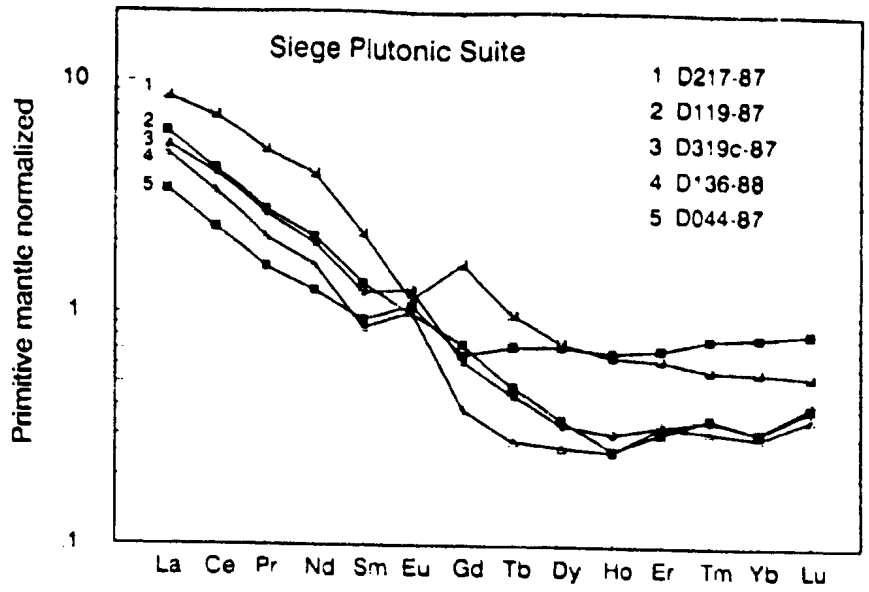

Figure 5.17. Primitive mantle normalized REE diagram for rocks of the Siege Plutonic Suite.

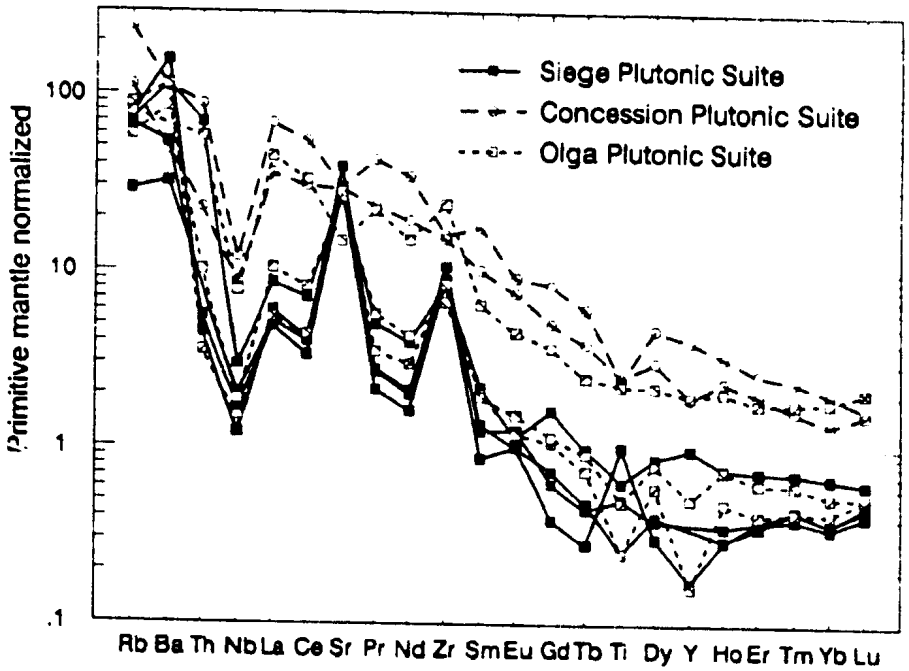

Figure 5.18. Primitive mantle normalized extended REE diagram comparing rocks of the Siege Suite to trondhmjemites and tonalites of the Olga and Concession Suites. The Siege Suite is most similar to the Olga Suite, in particular the positive inflections at both Sr and Zr.

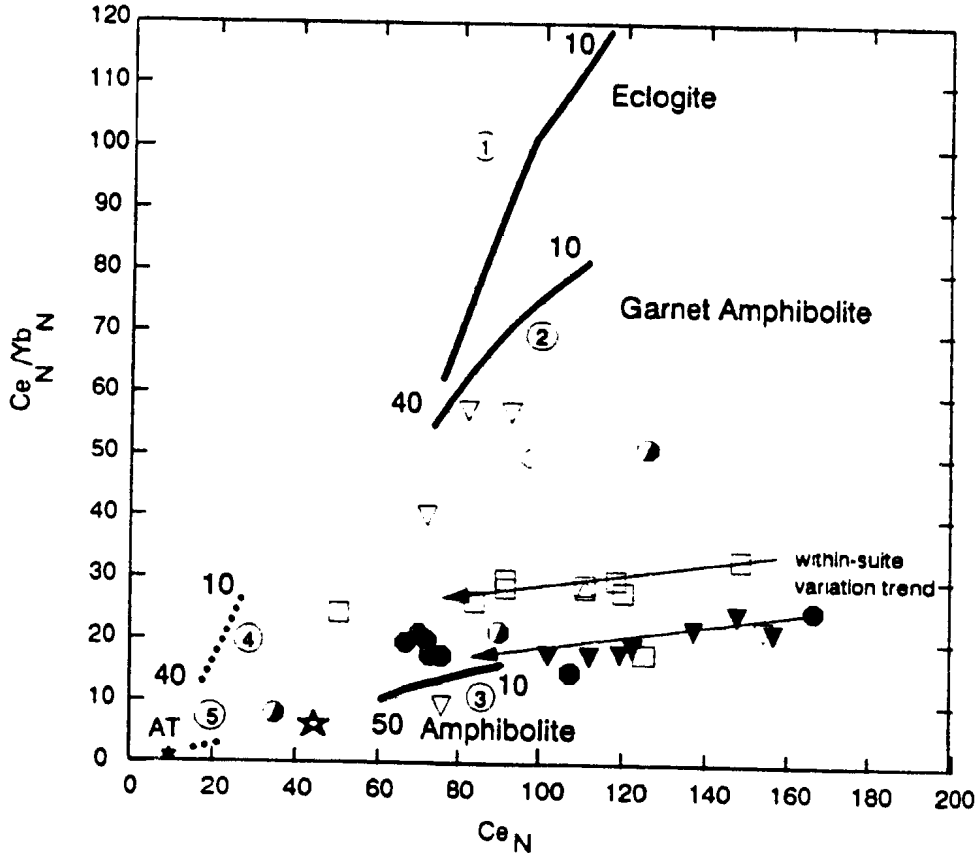

Figure 5.19. $(Ce/Yb)_N$ *vs.* Ce_N for rocks of the high Mg# group. Solid curves show the effect of non-modal batch melting of a LREE enriched source composition (star) at (1) eclogite , (2) garnet amphibolite and (3) amphibolite grade (see Table 5.3 for detailed parameters). Dashed curves show similar calculations for (4) eclogite and (5) amphibolite assuming the average Archean tholeiite source composition (Taylor and McLennan, 1985). Numbers at ends of curves indicate degrees of melting required to generate range of major element compositions from diorite through tonalite (Stern and Wyllie, 1978; Helz, 1976). Symbols as in Figure 5.6.

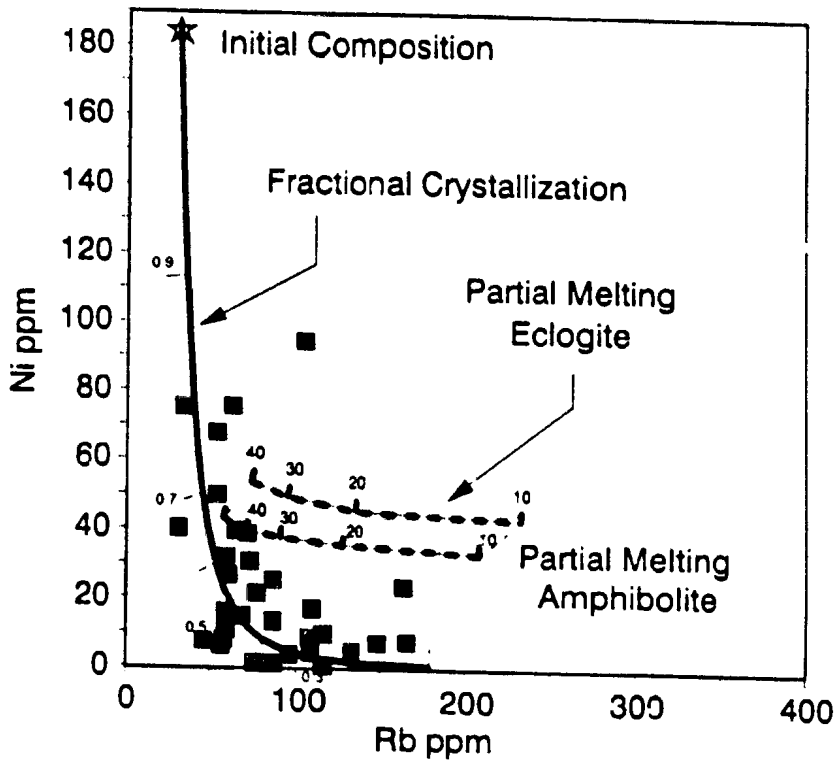

Figure 5.20. Ni *vs.* Rb. Squares are undifferentiated samples of the Concession Suite. Dashed curves show the effect of non-modal batch melting of mafic source (composition shown by star) at eclogite and amphibolite grade (see Table 5.3). Solid curve is the trend defined by fractional crystallization dominated by amphibole and plagioclase (see Table 5.5).

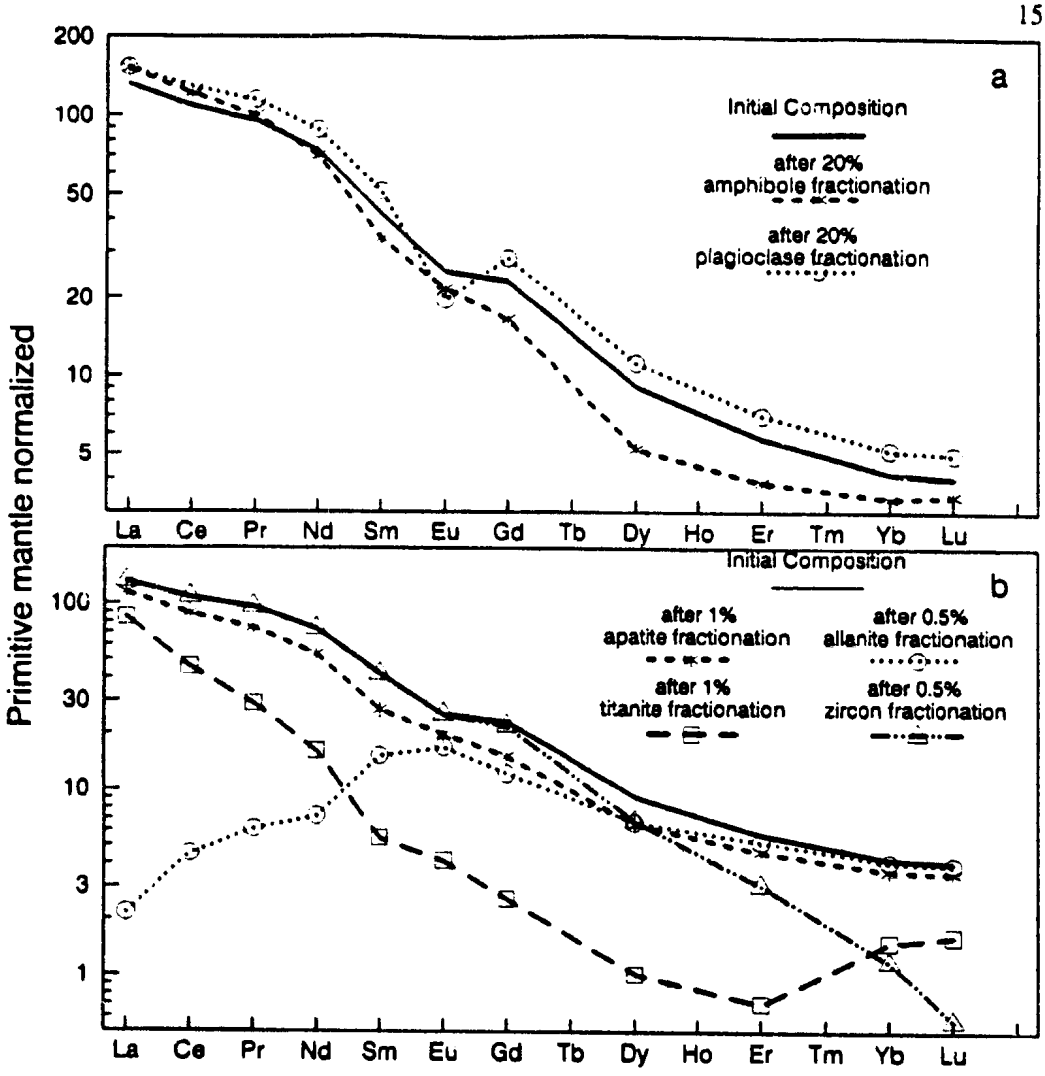

Figure 5.21. Primitive mantle normalized REE diagrams illustrating the effect of fractional crystallization of primary and accessory mineral phases based on published Kd values for intermediate composition melts (Appendix 3). A) diagram showing the effect of 25% fractional crystallization of amphibole and plagioclase. Amphibole fractionation causes depletion of the MREE and HREE and LREE enrichment, resulting in rotation of the pattern and an increase in the Ce/Yb ratio and a decrease in the Dy/Yb. Plagioclase does not significantly fractionate the REE (except Eu) and results in an overall increase in REE. B) diagram showing the effects of small amounts of fractionation of the accessory phases allanite, apatite, titanite and zircon. Allanite strongly depletes the LREE, apatite and titanite the MREE, and zircon the HREE.

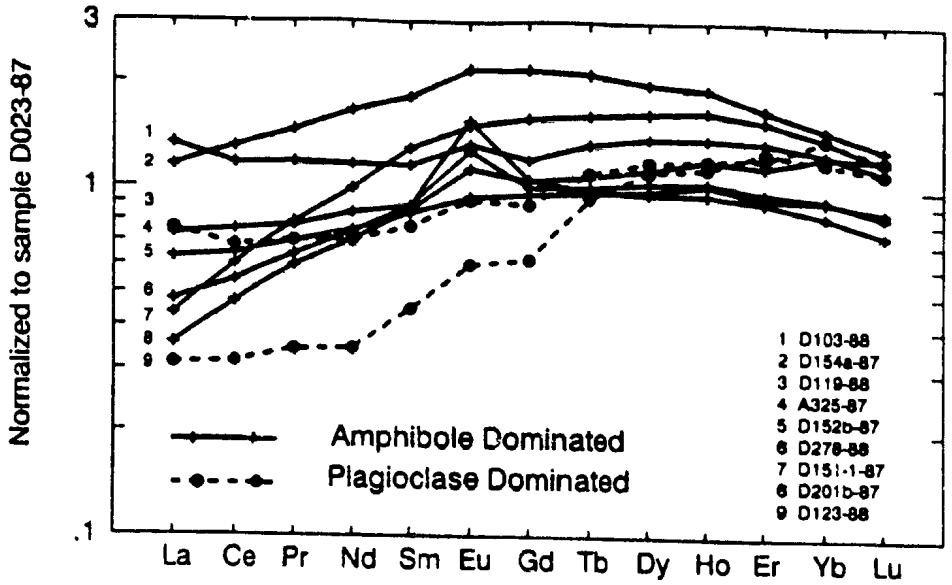

Figure 5.22. Normalized trace element contents of cumulate rocks. Samples normalized to sample D023-87, a diorite considered to be non-cumulate. The concave-down REE patterns are similar in shape to empirically determined Kd patterns of amphibole in tonalites (e.g. Gromet and Silver, 1983; Sawka, 1988).

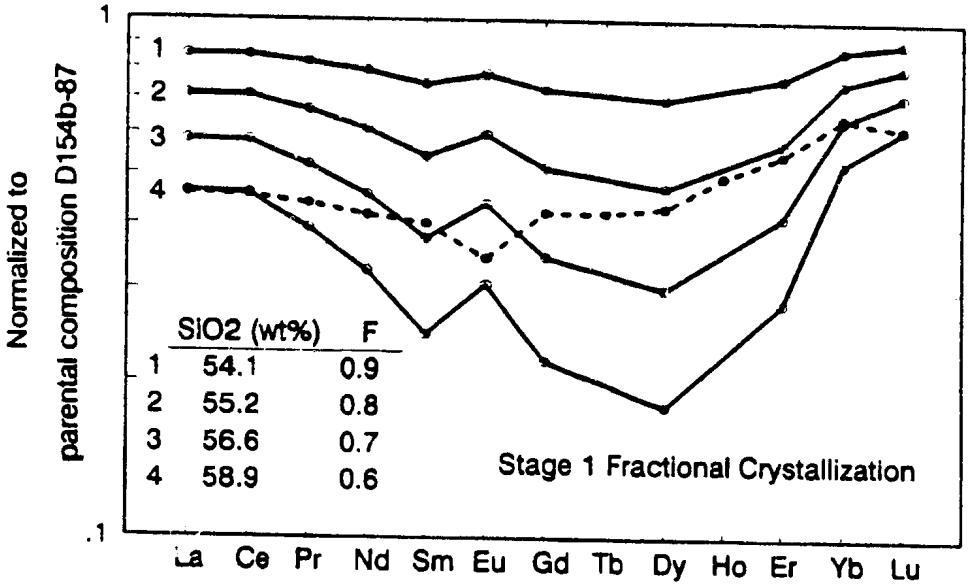

Figure 5.23. Normalized REE diagram of values calculated by the Stage 1 crystal fractionation model. Calculated values (solid lines) are normalized to the parental composition (D154b-87; horizontal line at 1). Dashed line indicates the normalized values of the 'target' composition (A280-87). Calculated MREE abundances are excessively depleted relative to those in the target composition.

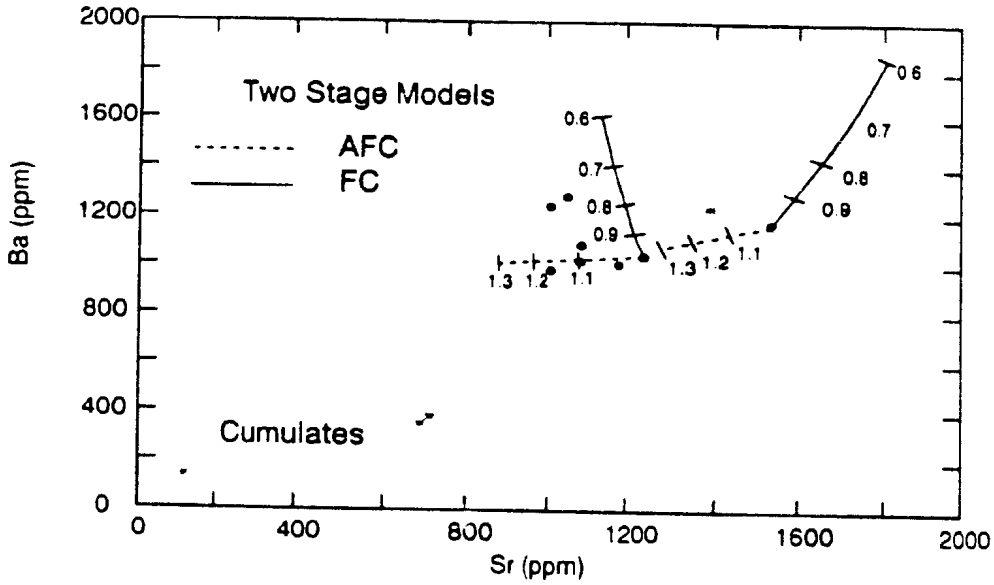

Figure 5.24. Ba *vs.* Sr diagram showing increasing Sr and Ba abundances predicted by fractionation models.

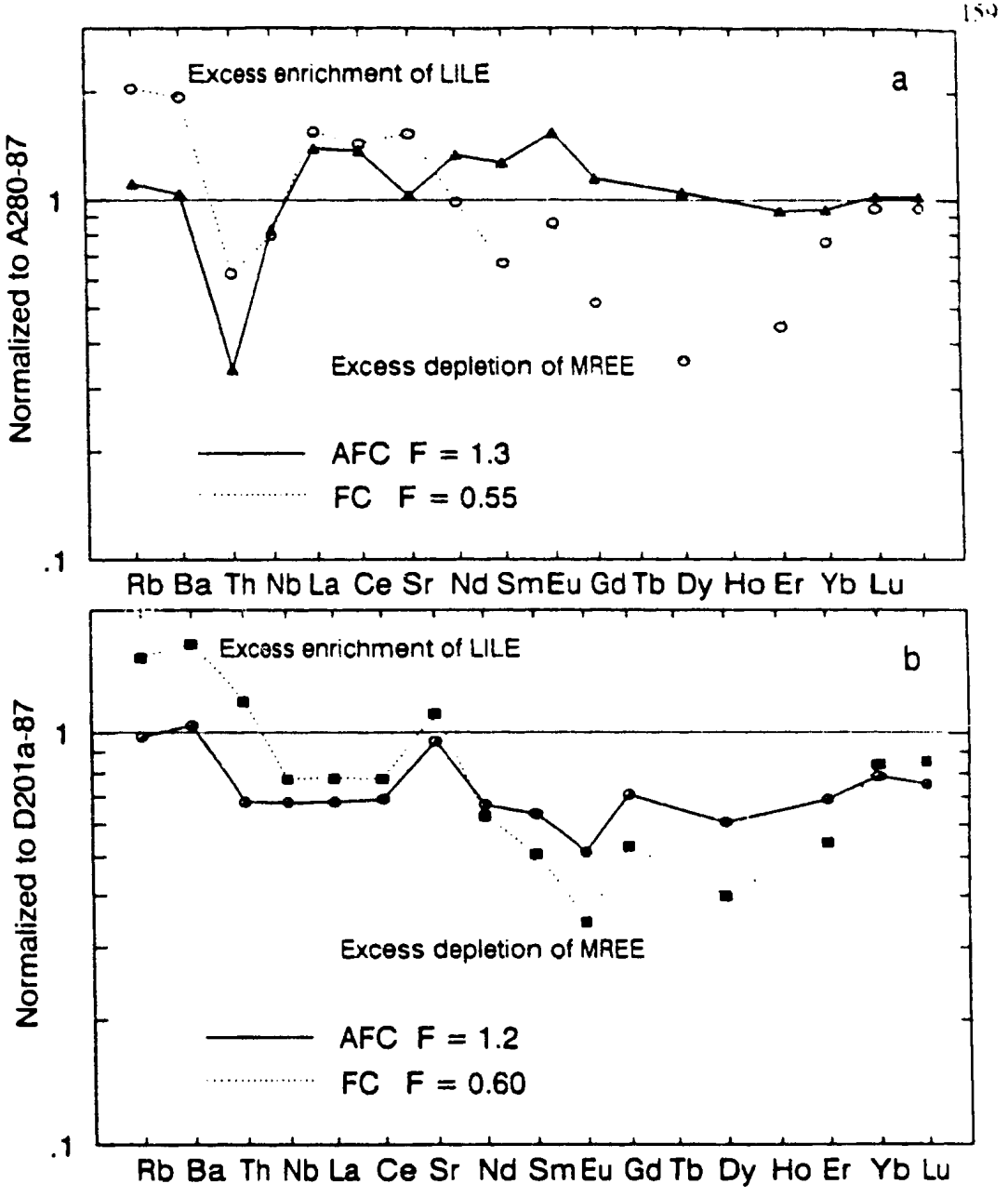

Figure 5.25. Comparison of the results calculated by the fractional crystallization and assimilation-fractionation models. Diagram is constructed by normalizing the calculated trace element abundances to the measured abundances of the target composition. A perfect fit between model and observed values defines a straight line with a normalized value of 1. The degree of fractionation plotted corresponds to values appropriate to the SiO_2 content of the target rock. A) Stage 1, B) Stage 2.

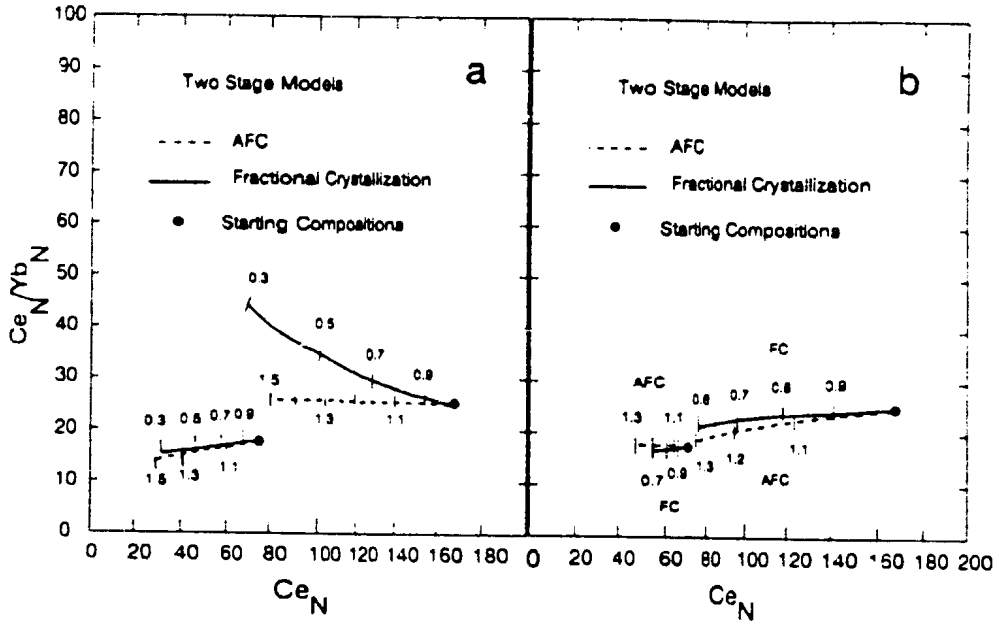

Figure 5.26. Results of quantitative modelling calculations plotted as $(Ce/Yb)_N$ v Ce_N. Solid lines are for fractional crystallization, dashed lines assimilation-fractionation. Numbers refer to degree of fractionation, which in the case of crystal fractionation are volume ratios (final/initial), assimilation-fractionation are mass ratios (final/initial). Measured data points are shown on a comparable diagram in Figure 5.19. The fractionating assemblage is different in A than B, details of the models are given in Table 5.5.

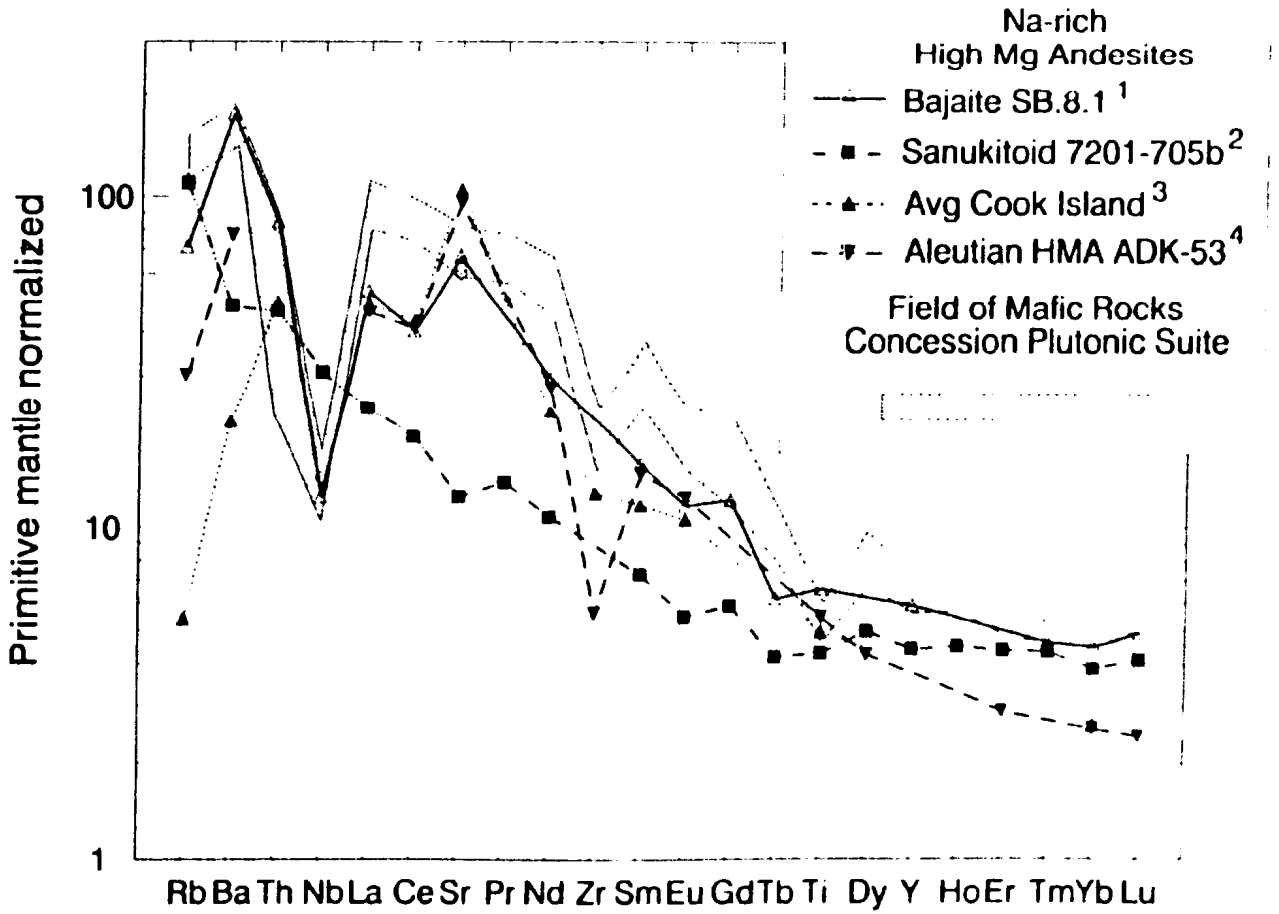

Figure 5.27. Primitive mantle normalized REE diagram comparing the composition of mafic samples of the Concession Plutonic Suite (samples D023-87; D154b-87) to some high magnesium andesites (sanukitoids, bajaites).

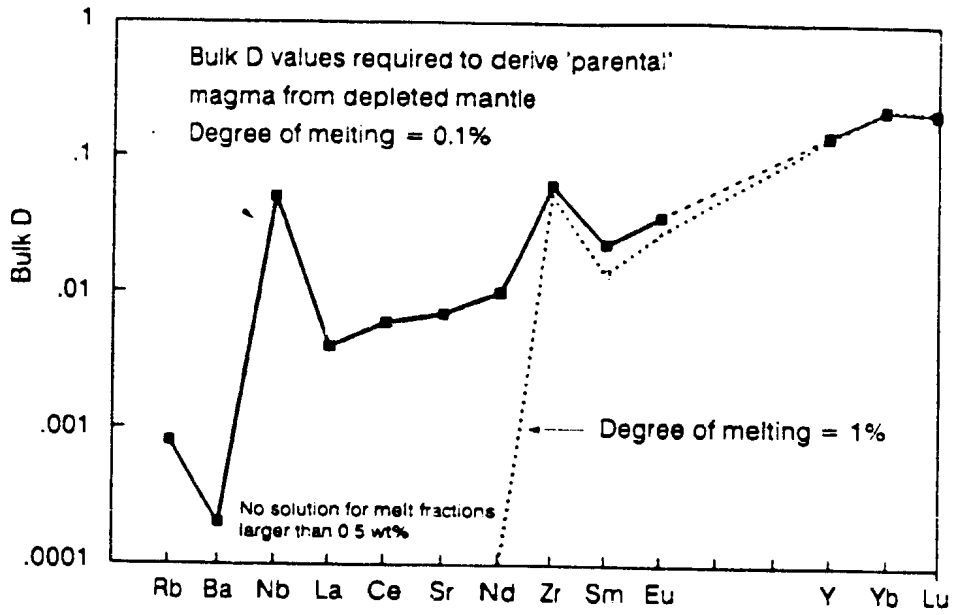

Figure 5.28. Calculated Bulk D values required to derive parental composition of the Concession Plutonic Suite from a MORB reservoir source by batch melting, leaving a harzburgite residuum.

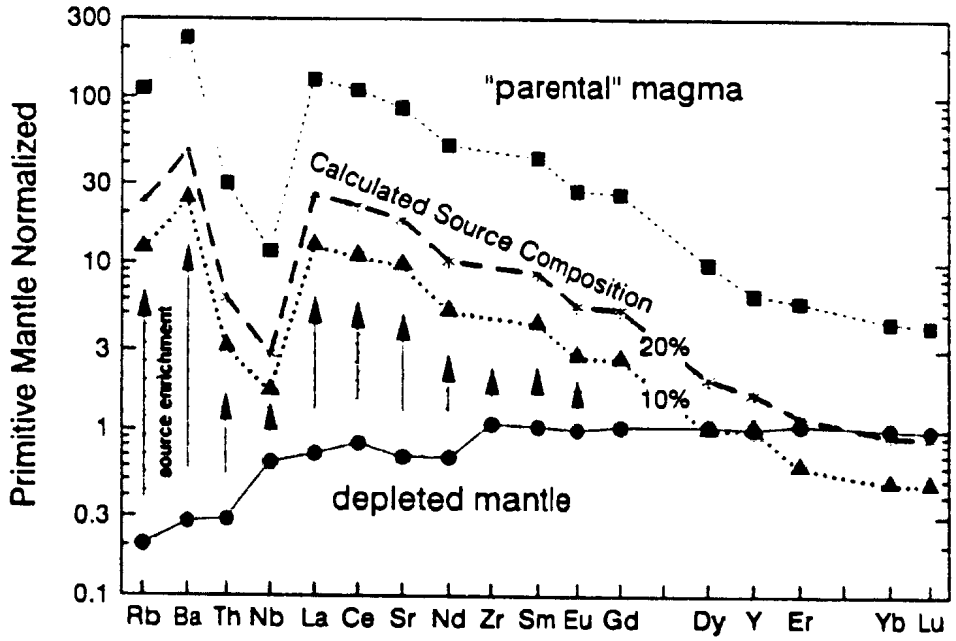

Figure 5.29. Primitive mantle normalized diagram illustrating the composition of an enriched mantle source required to generate primitive members of the Concession Suite (squares) assuming 10% (asterix) to 20% (triangles) batch melting with a harzburgite residuum. Depleted mantle source shown by circles.

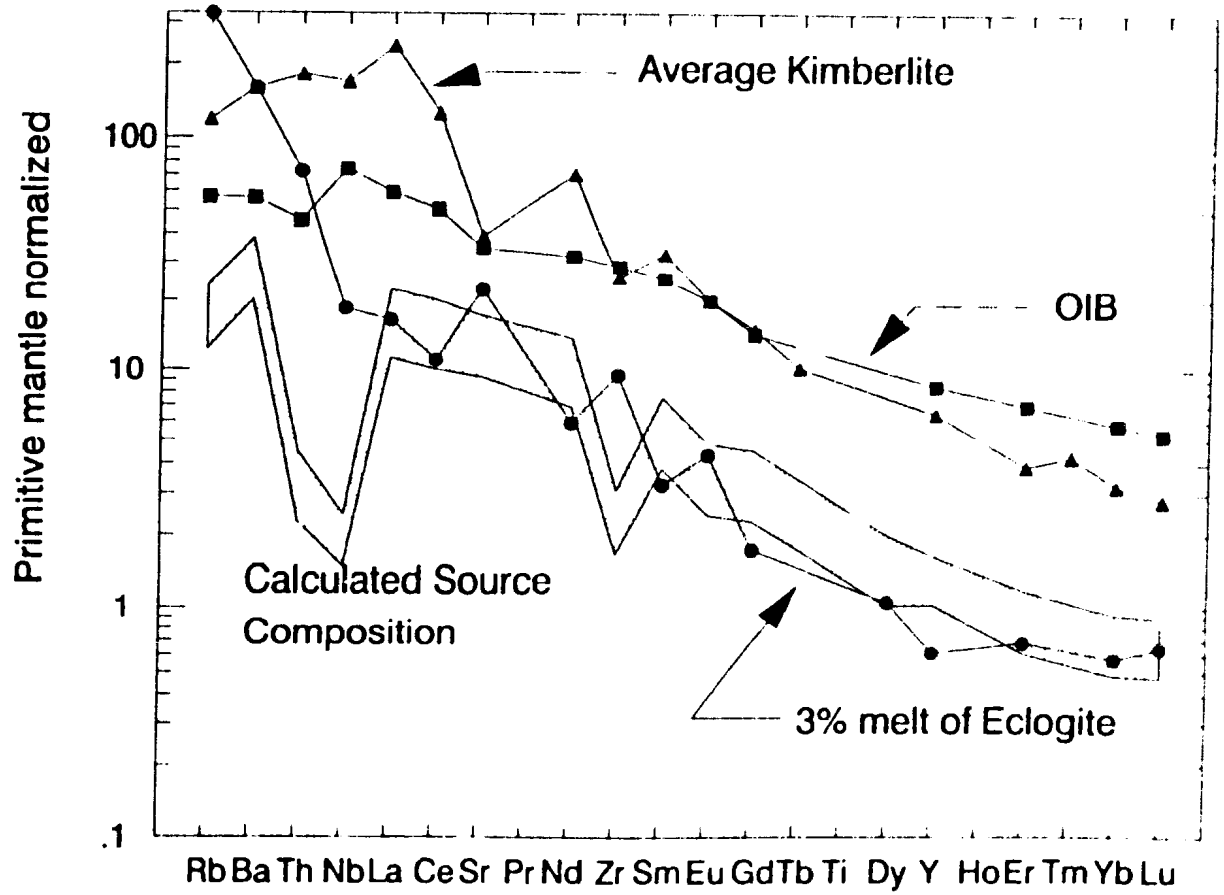

Figure 5.30. Primitive mantle normalized extended REE diagram comparing the calculated composition of the enriched mantle source to measured ocean island basalts (Sun, 1990),average kimberlite (Wedepohl and Muramatsu, 1979) and small volume (3%) melts of eclogite (Kay, 1978).

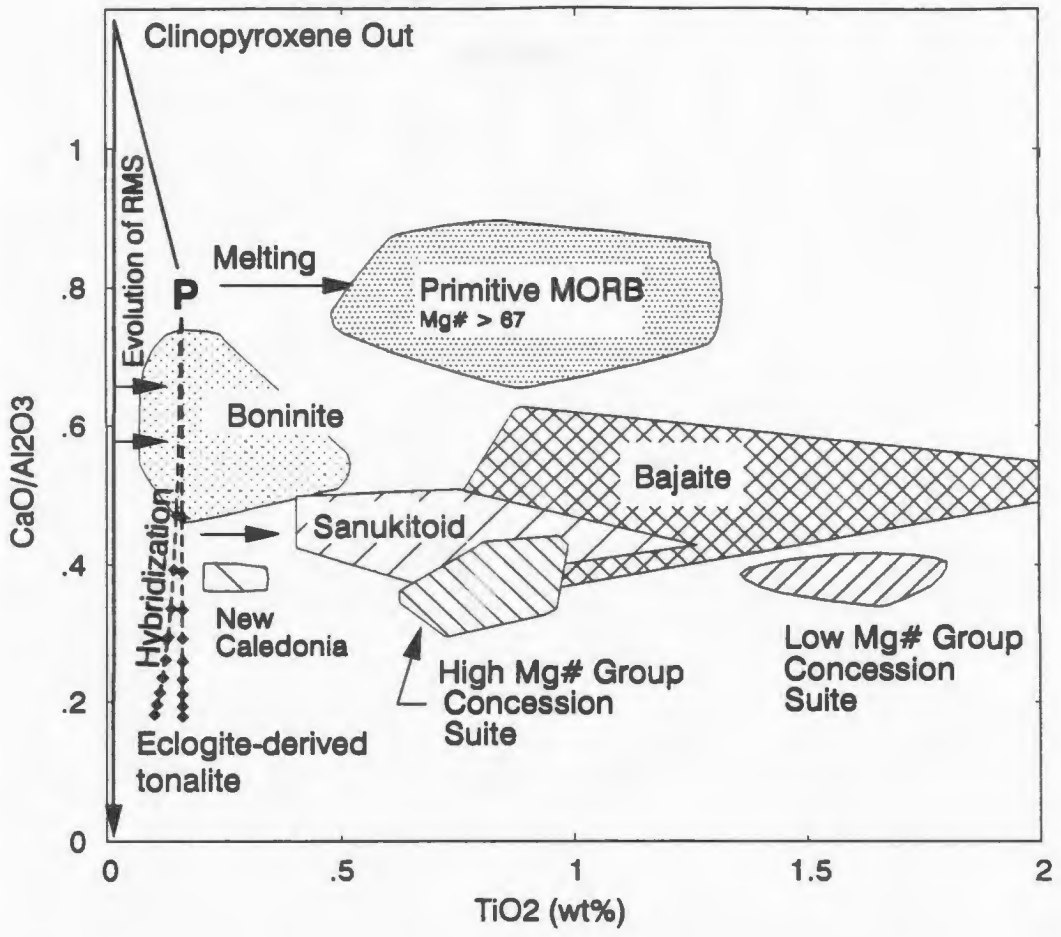

Figure 5.31. Plot of CaO/Al_2O_3 against TiO_2. Fields for primitive mid-ocean ridge glasses (Mg# > 67); boninites; bajaites; sanukitoids and mafic rocks of the Concession Suite are shown. Capital P = primitive mantle value (Maaloe and Aoki, 1977). The solid line indicates the path followed by increasingly depleted mantle. The curve initially increases in Ca/Al_2O_3 ratio with decreasing TiO_2 until clinopyroxene is exhausted at which point the CaO/Al_2O_3 decreases rapidly (Falloon, 1989). The low CaO/Al_2O_3 ratios in boninites reflect derivation from cpx-free sources (Crawford *et al.*, 1989). The CaO/Al_2O_3 ratio can alternatively be reduced by mantle hybridization. This is shown by the dashed lines labelled mixing, which show the effects of simple two component mixing between the primitive mantle (P) and tonalites derived from eclogite melting. The latter does not significantly reduce the TiO_2 content of the mantle and can account for the MORB-like TiO_2 contents and Al_2O_3/TiO_2 and CaO/Al_2O_3 ratios (Tatsumi and Ishizaka, 1982) of sanukitoids, bajaites and rocks of the Concession Suite.

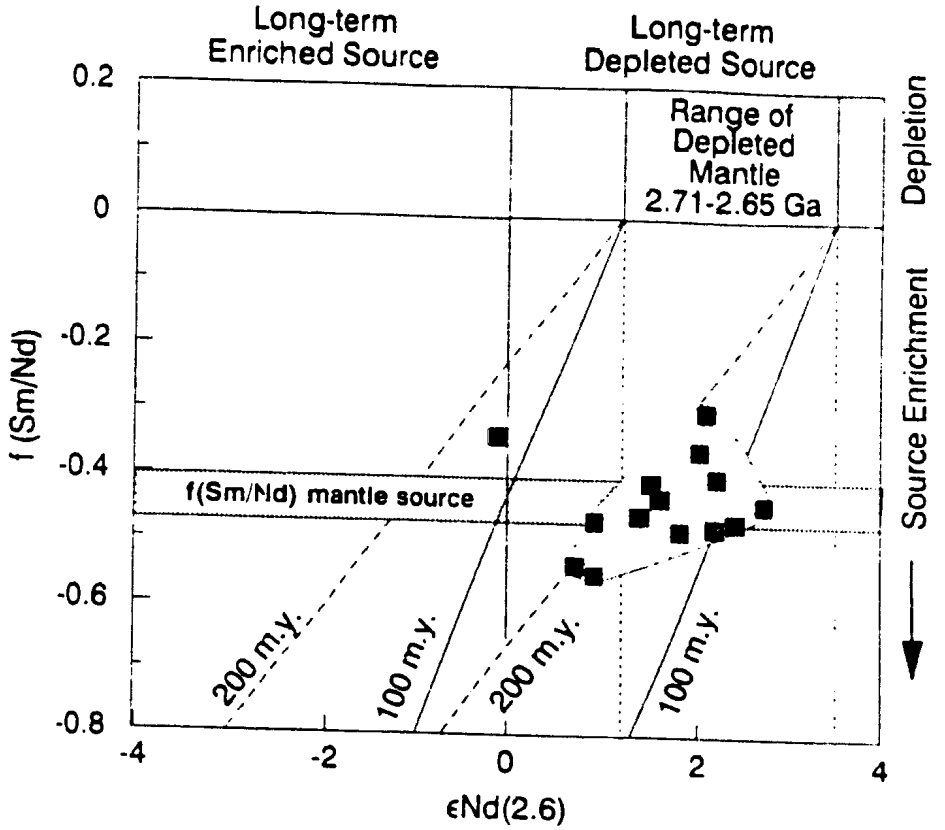

Figure 5.32. $\epsilon_{Nd(I)}$ *vs.* $f_{Sm/Nd}$ diagram for rocks of the Concession Plutonic Suite. $f_{Sm/Nd} = (^{147}Sm/^{144}Nd_{sample}/^{147}Sm/^{144}Nd_{CHUR})-1$ and reflects the degree of LREE enrichment or depletion in the sample. Negative values are LREE enriched relative to CHUR. The rate of change of $\epsilon_{Nd(I)}$ depends on $f_{Sm/Nd}$ (greater for more negative values) and the magnitude of the change is a product of $f_{Sm/Nd}$ and time. A group of samples with the same initial ϵ_{Nd} value but variable $f_{Sm/Nd}$ will evolve at different rates and define isochron lines on this diagram. This is shown by the time lines labelled 100 and 200 my which assume an $\epsilon_{Nd(I)}$ value of +3.5. This value is equivalent to the initial ratio in a standard isochron diagram. The stippled area indicates a possible range of $\epsilon_{Nd(I)}$ values for the Late Archean depleted mantle estimated from the range of values determined for volcanic rocks within the central Slave Province (see Table 7.1) and the Superior Province (Shirey and Hanson, 1986; Machado *et al.*, 1985). The horizontal band represents the $f_{Sm/Nd}$ value of the enriched mantle source to the Concession Suite determined in Figure 5.31. A mantle source with this $f_{Sm/Nd}$ value will rapidly evolve to more negative ϵ_{Nd} values. The majority of the samples have $\epsilon_{Nd(I)}$ within the range of the depleted mantle field and cannot be derived from a long term (>200 my) enriched mantle source.

Chapter 6

Geochemistry of the Post-Deformation Plutonic Suites: the Yamba and Contwoyto Suites

6.1 Introduction

Post-deformation granitoids of the the Yamba and Contwoyto Suites are the most abundant rocks exposed in the area, constituting over 40% of the region mapped. The two granite suites are contemporaneous (*ca.* 2585 Ma, van Breemen *et al.*, 1990), yet exhibit distinct petrographic and field characteristics. This chapter presents geochemical data which support the subdivision of the post-deformation granites proposed in Chapter 3, and suggests that these reflect distinct origins for the suites.

6.2 Review of Field Relationships and Sample Coverage

Rocks of the Yamba Suite principally outcrop in the southern part of the map area, forming two large intrusive complexes, the Wolverine Monzogranite (WM), centred around Yamba Lake, and the Pellatt Lake Monzogranite (PLM), to the west of Pellatt Lake (Figure 3.1). The two bodies are separated by septa of high grade migmatitic gneisses and syn-deformation plutonic rocks of the Concession Suite. In addition, smaller bodies occur as dykes and sills intruding volcanic rocks in the Olga Lake and Central Volcanic Belt areas. Both the Wolverine and Pellatt Lake Monzogranites are spatially associated with rocks of the earlier Concession Suite, and intrude some of the highest grade rocks in the field area.

The Contwoyto Suite is present throughout the map area, with the largest bodies located in the NW quadrant near the Lupin mine site (Contwoyto Batholith of Bostock (1980); Contwoyto Monzogranite, Figure 3.1), and to the east of Contwoyto Lake. The rocks dominantly intrude metasedimentary rocks of the Itchen and Contwoyto Formations. Metamorphic grade of the host rocks is above the cordierite isograd.

The majority of samples of the Yamba Suite are of the Wolverine Monzogranite and bodies in the Olga Lake area. Data for five samples of the Pellatt Lake Monzogranite are also reported. Samples of the Contwoyto Suite are dominantly of the

Contwoyto Monzogranite and from smaller bodies in the Olga Lake area. A smaller number of samples are from east of Contwoyto Lake and the southern part of the map area.

6.3 Presentation of Geochemical Data

Representative major and trace element analyses are presented in Table 6.1. The full data set is given in Appendix 2.

6.3.1 Major Element Chemistry

Yamba Plutonic Suite

The majority of samples of the Yamba Suite are monzogranites with lesser amounts of granodiorite and syenogranite. The rocks dominantly plot in the granite field of the modified O'Conner diagram (Figure 6.1). All samples are silica rich (SiO_2 between 68 and 78 wt%) and weakly peraluminous (Figure 6.2; 6.3). Salient major element features are high K_2O (>4%) contents, high K_2O/Na_2O (1-3), and generally low abundances of Al_2O_3 (< 15%), FeO* (<2%), MgO (< 0.5%), CaO (< 2.5%) and TiO_2 (<0.5%)(Figure 6.3). With the exception of K_2O and Na_2O, major elements decrease in an approximately linear fashion relative to increasing SiO_2.

Contwoyto Plutonic Suite

The Contwoyto Suite is more chemically heterogeneous than the Yamba suite, consistent with the observed mineralogical and textural variations described in Chapter 2. Samples are SiO_2 rich (69 to 78 wt%), and on average more strongly peraluminous than the Yamba Suite (Figure 6.2). This is in accord with its more aluminous modal mineralogy (Chapter 2). Comparatively, this suite generally has higher Al_2O_3, Na_2O and P_2O_5 and lower K_2O, MgO and TiO_2 concentrations (Figure 6.3).

Table 6.1. Representative anhydrous analyses of rocks of the Contwoyto and Yamba Suites.

	Contwoyto Plutonic Suite						Yamba Plutonic Suite					
							High Y			Low Y		
Sample	D199 -88	D128a -87	D241 -88	R037 -89	D216 -87	D350b -87	D078a -88	D135 -88	D117 -87	R051e -88	D056 -89	D153 -89
Name												
Area	Contw. Monzogr	Contw. Monzogr	Heckla Bay	Ghurka Nose Lake	Olga Lake area	Windy Lake	Wolv. Monzogr	Wolv. Monzogr	Wolv. Monzogr dyke	N. Wolv. Monzogr	Pellatt Lake Monzogr	Pellatt Lake Monzogr
Mineralogy	Bt Mu	Mu-T	Bt	Mu-Bt	Mu-Bt	Mu-Bt	Bt	Bt	Bt	Bt	Bt	Bt
Texture	eq	eq	eq	eq-p	eq-p	eq-p	eq-kx	eq-kx	fgr	kx	eq	eq
SiO2	72.9	75.7	72.5	75.8	75.2	74.1	74.3	74.3	72.9	70.1	73.2	72.8
TiO2	0.28	0.08	0.32	0.00	0.12	0.12	0.20	0.24	0.28	0.37	0.16	0.24
Al2O3	14.9	14.0	15.3	14.1	14.5	14.7	13.9	13.8	13.66	15.7	14.8	14.8
FeO*	1.76	0.40	1.77	0.34	0.95	1.14	1.38	1.68	2.51	2.42	1.03	1.53
MnO	0.02	0.02	0.04	0.01	0.02	0.03	0.01	0.02	0.02	0.03	0.01	0.02
MgO	0.54	0.07	0.75	0.12	0.23	0.35	0.30	0.36	0.51	0.81	0.35	0.54
CaO	1.11	0.63	1.38	0.99	0.88	0.89	1.20	1.14	1.17	2.17	0.67	0.79
Na2O	4.13	4.59	4.92	4.28	3.79	4.35	3.34	3.29	2.76	4.24	3.51	3.49
K2O	4.21	4.25	2.92	4.35	4.30	4.13	5.35	5.13	6.05	4.06	6.19	5.61
P2O5	0.18	0.28	0.05	0.04	0.04	0.12	0.04	0.02	0.08	0.16	0.11	0.15
LOI	0.66	0.49	0.69	0.52	0.63	0.51	0.54	0.46	0.79	0.40	0.57	0.87
Trace elements in parts per million												
Cr	8	dl	6		dl	dl	dl	dl	dl	3	6	dl
Ni	dl	dl	dl		dl	dl	dl	dl	dl	dl	dl	dl
Sc	dl	dl	dl		dl	dl	dl	dl	dl	dl	dl	dl
V	13	dl	28		dl	dl	10	16	27	43	13	9
Zn	20	14	15		16	29	8	16	26	45	22	48
Rb	112	280	112		191	238	186	185	198	85	125	252
Ba	612	153	613		291	547	680	688	909	871	476	596
Sr	158	39	232		119	118	85	80	101	342	100	136
Ga	24	17	22		18	19	18	17	18	19	18	23
Nb	7.3	5.0	4.9		13.3	11.3	10.4	14.1	12.2	2.9	2.4	10.7
Zr	144	24	121		58	93	143	176	302	246	119	137
Y	10	7	6	4	22	7	23	18	23	5	6	2
Th	8.05	1.04	7.20	3.02	13.5	16.5	44	59	85	36	15.1	28.4
Rare earth elements in parts per million												
La	25.0	2.63	21.7	6.8	13.4	26.3	54.6	67.	119	67	28.7	32.4
Ce	47.1	6.00	38.0	13.3	26.3	49.9	103.	129.	215	140.	63.	77.
Pr	6.1	0.77	4.43	1.47	2.99	5.04	10.55	13.13	22.9	15.76	7.53	9.80
Nd	22.9	2.94	15.9	5.34	10.3	16.6	35.9	44.1	78	55.7	28.2	37.1
Sm	4.16	0.79	2.68	1.30	2.48	2.98	6.04	7.3	11.5	8.0	5.18	8.0
Eu	0.63	0.13	0.44	0.30	0.20	0.43	0.46	0.54	.62	1.17	0.50	0.54
Gd	2.60	0.66	1.92	1.08	2.28	2.66	4.48	5.54	7.1	4.09	3.12	4.67
Tb	0.34	0.11	0.25	0.13	0.45	0.24	0.76	0.84	0.87	0.31	0.31	0.44
Dy	1.55	0.56	1.30	0.72	2.85	1.05	4.25	4.23	4.33	1.08	1.47	1.53
Ho	0.25	0.10	0.22	0.13	0.57	0.16	0.82	0.72	0.74	0.15	0.23	0.21
Er	0.64	0.29	0.58	0.37	1.46	0.36	2.11	1.63	1.67	0.34	0.59	0.50
Tm	0.07	0.04	0.07	0.04	0.20	0.06	0.27	0 18	0.22	0.05	0.07	0.06
Yb	0.47	0.35	0.51	0.28	1.27	0.33	1.73	1.23	1.40	0.26	0.41	0.26
Lu	0.05	0.05	0.07	0.04	0.18	0.06	0.25	0.18	0.20	0.06	0.06	0.05
Selected Ratios												
K_2O/Na_2O	1.0	0.9	0.6	1.0	1.1	0.9	1.6	1.6	2.2	1.0	1.8	1.6
FeO*/MgO	3.2	5.7	2.4	2.8	4.1	3.2	4.5	4.7	4.9	3.0	2.9	2.8
K/Rb	311	126	216		187	144	239	230	254	395	411	185
Rb/Sr	0.7	7.2	0.5		1.6	2.0	2.2	2.3	2.0	0.2	1.2	1.8
Ba/Sr	3.9	4.0	2.6		2.4	4.6	8.0	8.6	9.0	2.5	4.8	4.4
Sr/Y	16	5	39		5	18	4	4	4	71	18	61
Zr/Th	18	23	17		4	6	3	3	4	7	8	5
Ti/Nb	233	97	398		55	64	117	104	139	759	400	137
Zr/Y	15	3	20		3	14	6	10	4	51	21	61
$(Ce/Yb)_n$	26.0	4.4	19.2	12.2	5.4	39.6	15.4	27.2	100	137	39.7	77.8
Eu/Eu*	0.58	0.53	0.60	0.78	0.25	0.47	0.27	0.26	0.21	0.62	0.38	0.27

Code: WM = Wolverine Monzogranite; Bt = biotite; Mu = muscovite; T = tourmaline; Cord = cordierite; eq = equigranular; p = pegmatitic; kx = microcline prophyritic; fgr = fine grained. Major elements by AA. REE and Th determined by ICP-MS, other trace elements by XRF. nd = not determined, dl = below detection limit.

6.3.2 Trace Element Chemistry

Selected trace elements are plotted against SiO_2 in Figure 6.4.

Yamba Plutonic Suite

The Yamba Suite exhibits a wide range (1 to 80 ppm) and a bimodal distribution of Y abundances (Figure 6.5). Y is therefore useful to subdivide the suite into two groups; a high (Y > 12 ppm), and a low (Y < 12 ppm) group. The two groups have generally similar major element compositions (Figure 6.3), however the low Y group tends to have more variable K_2O/Na_2O, and lower FeO*/MgO ratios (Figure 6.5).

During the course of the field mapping, some, but not all, of the low Y samples were recognized as a separate lithodeme. These rocks have alkali feldspar phenocrysts similar to those in the high Y group but also have well formed, equant plagioclase crystals characteristic of the Concession Suite. Some, but not all, have higher biotite contents.

The high Y group occurs dominantly in the western part of the study area, within the Wolverine Monzogranite and other small bodies in the Olga Lake area. The low Y group occurs: 1) along the northern margin and 2) within the southeastern extension of the Wolverine Monzogranite south of the map sheet boundary (Lac des Gras, Folinsbee, 1949); and, 3) throughout the Pellatt Lake Monzogranite (PLM). To date, samples of the high Y group have not been identified within the PLM, however the total number of samples analyzed from this large complex is small.

The high Y group has low Sr (< 100 ppm), high Rb (> 150 ppm) and variable Ba (> 300 ppm) contents, low abundances of transition elements, and variable to high abundances of HFSE and Th (Figure 6.4). The low Y group has higher Sr (100-400 ppm) and lower Rb, Th and Nb contents, resulting in lower Rb/Sr and Ba/Sr ratios and higher K/Rb, Sr/Y, and Zr/Y ratios (Table 6.2).

The high Y group are variably LREE-enriched with large negative Eu anomalies (Figure 6.6a, b, c). Minor crossing of patterns may reflect the effect of REE-rich accessory minerals observed in the rocks (*e.g.* monazite, zircon). A small subset of

Table 6.2. Average values of the Contwoyto, Yamba and Concession Suites

	Contwoyto Monzogranite	Yamba High Y Wolvenne	Yamba Low Y Wolverine	Yamba Low Y Pellatt	Concession High Mg#	Concession Low Mg#
n	18	29	10	5	8	5
SiO_2	73.0 ±1.5	74.2 ±1.4	73.5 ±2.2	73.7 ±0.85	70.1 ±1.1	71.0 ±1.2
TiO_2	0.23 ±0.12	0.23 ±0.10	0.26 ±0.12	0.20 ±0.08	0.38 ±0.10	0.43 ±0.10
Al_2O_3	15.1 ±0.5	13.8 ±0.50	14.3 ±0.91	14.4 ±0.49	15.7 ±0.24	14.8 ±0.36
FeO*	1.61 ±0.60	1.66 ±0.59	1.49 ±0.56	1.39 ±0.30	2.58 ±0.61	3.41 ±0.52
MnO	0.02 ±0.01	0.02 ±0.01	0.02 ±0.01	0.02 ±0.01	0.04 ±0.01	0.05 ±0.01
MgO	0.63 ±0.33	0.40 ±0.17	0.48 ±0.24	0.49 ±0.13	1.13 ±0.32	1.10 ±0.23
CaO	1.36 ±0.68	1.14 ±0.32	1.44 ±0.65	1.05 ±0.52	2.84 ±0.28	2.96 ±0.39
Na_2O	4.33 ±0.46	3.23 ±0.31	3.52 ±0.57	3.64 ±0.33	4.70 ±0.61	4.44 ±0.24
K_2O	3.59 ±1.07	5.26 ±0.70	4.96 ±1.13	5.00 ±1.15	2.31 ±0.74	1.66 ±0.60
P_2O_5	0.17 ±0.09	0.07 ±0.05	0.09 ±0.05	0.13 ±0.04	0.18 ±0.07	0.11 ±0.03
Rb	104 ±41	196 ±32	126 ±55	164 ±56	67 ±29	58 ±10
Ba	510 ±138	640 ±205	953 ±294	632 ±214	741 ±472	494 ±185
Sr	190 ±97	88 ±27	235 ±117	166 ±85	578 ±73	230 ±52
Ga	21 ±3	18 ±2	18 ±2	20 ±2	21 ±1	20 ±2
Nb	6 ±2	14 ±4	5 ±3	7 ±3	5 ±2	8 ±1
Zr	122 ±42	166 ±83	158 ±67	126 ±22	141 ±27	138 ±14
Ti	1470 ±707	1361 ±606	1559 ±712	1173 ±467	2298 ±622	2559 ±677
Y	8 ±3	23 ±8	7 ±2	3 ±2	8 ±3	13 ±4
Th	7 ±3	46 ±16	25 ±16	15 ±7	6 ±2	6 ±2
Ce	49 ±10	170 ±61	85 ±42	72 ±7	57 ±36	36 ±21
Yb	0.4 ±0.2	1.4 ±0.3	0.0 ±0.0	0.38 ±0.07	0.4 ±0.3	0.7 ±0.5
Rb/Sr	0.7 ±0.5	2.4 ±0.7	0.8 ±0.6	1.3 ±0.7	0.1 ±0.1	0.3 ±0.1
Ba/Sr	3.0 ±1.4	7.4 ±1.5	4.7 ±2.0	4.2 ±1.0	1.2 ±0.6	2.1 ±0.6
K/Rb	300 ±76	233 ±37	353 ±69	270 ±82	314 ±89	249 ±57
Sr/Y	23 ±15	4.1 ±1.8	39 ±24	53 ±25	94 ±53	19 ±4
Zr/Th	16.3 ±7	3.7 ±1.5	7.4 ±3.6	10.5 ±5.5	30.2 ±20.2	26.6 ±10.7
Ti/Nb	294 ±257	107 ±62	366 ±217	204 ±112	449 ±75	324 ±49
Zr/Y	15.3 ±6.6	7.8 ±4.2	25.6 ±15.3	51.3 ±24.4	21.2 ±6.8	11.5 ±2.9
Ce/Yb_N	30 ±10	32 ±10	83 ±42	52 ±15	40 ±13	14 ±4
Eu/Eu*	0.58 ±0.19	0.28 ±0.05	0.62 ±0.03	0.59 ±0.28	0.87 ±0.10	0.82 ±0.11

Average values for Concession Suite rocks only include samples with greater than 69 wt% SiO_2.

samples from the Wolverine Monzogranite have higher abundances of Y (> 50 ppm). LREE abundances in these samples are similar to typical Wolverine samples, but the abundances of the MREE and HREE are higher and have a flatter slope with slightly concave down curvature (Figure 6.6c).

The two samples with the highest abundances of Th and the LREE are fine grained granite dykes, one intruding the Wolverine Monzogranite, the other the Siege Tonalite north of the WM (Figure 6.6c). These rocks have lower SiO_2 but otherwise similar major element chemistry to the more common coarser grained phases (Table 6.1; Figure 6.3). Th shows a large within-suite variation, which is paralleled by other trace elements (*e.g.* Zr, Ce; Figure 6.7). The covariation of these elements may indicate REE-rich accessory mineral control (*e.g.* zircon, monazite) on the trace element budget.

The low Y group are also LREE-enriched but have smaller negative to positive Eu anomalies and lower abundances of the HREE (Figure 6.6d, e). They also tend to have higher abundances of Sr and Ba. In this respect they resemble the REE patterns of granodiorites of the Contwoyto Plutonic Suite (compare Figure 6.6d with 5.8).

Contwoyto Plutonic Suite

The LFSE concentrations in the Contwoyto Suite overlap those in the Yamba Suite, but Rb and Ba contents tend towards lower values (Figure 6.4). Sr and Ba generally decrease with increasing SiO_2, in contrast, K and Rb increase. Ratios involving these elements are more variable than in the Yamba Suite. Ga abundances are moderate (18-30 ppm), but generally higher than in the Yamba Suite, and are not correlated to SiO_2 content. HFSE elements are generally lower, but do overlap average concentration levels in the Yamba Suite. Zr abundance decreases systematically over a SiO_2 range of 70 to 76 wt% SiO_2. Y does not correlate with Zr content. The Nb abundance shows no clear correlation with that of other elements. Th abundances are much lower in comparison to the high Y group of the Yamba Suite. There are,

however, indications of locally high abundances of Th from detailed aeroradioactivity surveys (possibly in pegmatites) (G.S.C. aeroradiaoctivity survey). Th abundance does not correlate with other elements (*e.g.* Ce, Zr), as it does in the Yamba Suite.

The abundance of REE within the suite is extremely variable. Two 'endmember' types of REE patterns are observed (Figure 6.8). The first type has high total abundances of LREE, with small to moderate negative Eu anomalies and high $(Gd/Yb)_N$ (Figure 6.8a). The second type has lower total abundances of REE, flatter patterns (*ie.* lower $(Ce/Yb)_N$ and $(Gd/Yb)_N$) and variable positive to strongly negative Eu anomalies (Figure 6.8b, c, d). REE patterns intermediate to these types have also been measured.

The former type are more common and are characteristic of non-pegmatitic, fine to medium grained, biotite-muscovite granites. The low REE abundance type is associated with: 1) smaller dykes or sills isolated from large outcrop areas of granite; 2) muscovite-rich pegmatitic samples; and 3) some tourmaline granites. Similar REE patterns are commonly documented in fractionated leucogranites, pegmatitic leucogranites and pegmatites (*e.g.* Shearer et al., 1984, Cerny and Meintzer, 1988; Muecke and Clarke, 1981; Vidal et al., 1982; Searle and Fryer, 1985).

6.3.3 Isotope Geochemistry

Neodymium isotopic compositions for samples from the immediate study area are given in Table 6.3. Additional data for correlative granitoid rocks from outside the map area are presented in Chapter 7.

Yamba Plutonic Suite

Samples of the Yamba Plutonic suite have $\epsilon_{Nd(t)}$ values ranging from +2.9 to -5.1 (Figure 6.9). The $\epsilon_{Nd(t)}$ values show a systematic regional variation. Samples from the Wolverine Monzogranite, and other plutons to the west, have negative values, in contrast, to samples from the Pellatt Lake Monzogranite and other bodies to the east, which have positive values. This spatial variation is discussed in Chapter 7.

Table 6.3. Sm-Nd Isotopic Data, Post-Deformation Plutonic Suites

Sample[a]	Rock Type	Lat	Long	Nd[b] (ppm)	Sm[b] (ppm)	$^{147}Sm/^{144}Nd$[c]	$^{143}Nd/^{144}Nd$[d]	$\epsilon_{Nd(t)}$[e]	Age[f] (Ma)	T_{DM} (Ma)
Yamba Plutonic Suite										
D153-89	Bt Granite	65° 10'	109° 44'	45.47	9.16	0.1218	0.511508	2.9	2590	2697
D224-88	Bt Granite	65° 27'	112° 25'			0.1002	0.510833	-3.1	2590	3139
D078a-88	Bt Granite	65° 11'	111° 37'	44.09	7.26	0.1060	0.510858	-4.6	2582[1]	3181
D238-87	Bt Granite	65° 30'	112° 05'	19.52	3.11	0.0970*	0.510682	-5.0	2590	3280
D135-88	Bt Granite	65° 05'	111° 39'	44.09	7.26	0.1048	0.510807	-5.1	2590	3292
Contwoyto Plutonic Suite										
R037-89	Bt-Mu Granite	65° 14'	109° 12'	4.62	1.07	0.1397	0.511808	2.8	2590	2705
D199-88	Bt-Mu Granite	65° 52'	111° 38'	22.61	4.13	0.1131	0.511202	-0.2	2590	2925
D207-88	Bt-Mu Granite	65° 49'	111° 14'	23.98	4.71	0.1258	0.511415	-0.2	2590	2931
K193-88	Bt-Mu Granite	65° 49'	111° 25'	15.08	2.72	0.1140	0.511170	-1.1	2585[1]	2992
D216-87	Bt-Mu Granite	65° 28'	111° 40'	10.15	2.43	0.1434	0.511515	4.2	2585	3220
D295-88	Bt-Mu Granite	65° 53'	110° 38'	12.74	2.80	0.1374	0.511410	-4.3	2590	3222

[a] Samples D153-89, R037-89 chemistry analyzed at G.S.C. by E. Hegner. All other samples done at Memorial University.

[b] Nd and Sm concentration data for samples analyzed at Memorial University determined by ICP-MS (5% error). Data from GSC determined by isotope dilution (1% error)

[c] Samples analysed at GSC (0.5% error); at Memorial (1% error). Values marked with asterix (*) determined by ICP-MS at Memorial (3% error).

[d] Internal precision is better than external precision of $2 * 10^{-5}$.
Ratios are normalized to $^{146}Nd/^{144}Nd = .7219$ $^{143}Nd/^{144}N = .511862 \pm 19$ for La Jolla during period of study. All samples analysed at G.S.C.

[e] $\epsilon_{Nd(t)} = [(^{143}Nd/^{144}Nd_{(t)sample}/^{143}Nd/^{144}Nd_{(t)\ Bulk\ Earth}) - 1] * 10^4$ where (t) = age of sample. Present day values Bulk Earth $^{143}Nd/^{144}N = .512638$; $^{147}Sm/^{144}Nd = .1967$.

[f] Published U-Pb zircon or monazite ages are designated by superscripts as follows [1] van Breemen et al., 1990;

Wanless and Loveridge (1978) report Sr isotopic data for four samples of the Yamba Suite from the Wolverine Monzogranite. Recalculation of this data, assuming a crystallization age of 2585 Ma (van Breemen *et al.*, 1990) and decay constants from Steiger and Jäger (1977), yields initial $^{87}Sr/^{86}Sr$ ratios from 0.6929 to 0.7040. The initial ratio correlates with the Rb/Sr ratio; high Rb/Sr samples have the lowest initial $^{87}Sr/^{86}Sr$ values. The extremely low values indicate that post-crystallization modifications have occurred in the Rb/Sr system, which does not permit interpretation of the whole rock ratios.

Contwoyto Plutonic Suite

Samples of the Contwoyto Suite have $\epsilon_{Nd(I)}$ values ranging from +2.8 to -4.3 (Figure 6.9). Systematic east-west differences are similar to those described for the Yamba Suite. The isotopic composition does not vary in a systematic fashion with other chemical characteristics of the rocks. For example, samples with Type I REE patterns (*e.g.* D295-88) have similar $\epsilon_{Nd(I)}$ to those samples with type II patterns (*e.g.* D216-87). This indicates that the isotopic composition is not simply a function of the fractionation process.

The negative $\epsilon_{Nd(I)}$ values determined for samples of both suites require a contribution from significantly older crustal sources. Figure 6.9 shows that the integrated average age of the crustal source of those granites with the most negative values may be greater than 400 Ma older than the crystallization age. This assumes average crustal $^{147}Sm/^{143}Nd$ values ($f_{Sm/Nd}$ = -0.40) (Taylor and McLennan, 1985) for the protolith and a depleted mantle value of +3.5 at 2.6 Ga (see Appendix 3).

6.3.4 Classification of the Suites

Granitic rocks have eluded simple classification schemes, reflecting the complexity and diversity of granite petrogenesis. Pitcher (1983; 1987) has pointed out that different granite types can be recognized and that these may be characteristic of different tectonic settings (*e.g.* Cordilleran margins, continental collision zones). The plethora of different granite classification schemes (cf. Barbarin, 1990), reflect

fundamental differences of opinion on the petrogenesis and tectonic significance of granitic rocks. The commonly used classification of I-, S- and A-type granites assumes dominantly crustal sources for most granites, and that the nature of the crust (*ie.* igneous or sedimentary) is reflected in the composition and mineralogy of the granite (Chappell and White, 1974; White and Chappell, 1983). Alternative schemes, such as that recently proposed by Barbarin (1990), assume an important mantle component in the petrogenesis of some granitoid rocks, and thus crustal (C-type), mantle (M-type) and mixed or hybrid (H-type) granites are defined. Classification of the plutonic suites using these different schemes are shown in Table 6.4.

Table 6.4. Classification of the Contwoyto, Yamba and Concession Plutonic Suites according to different schemes.

	Plutonic Suite		
Scheme	Contwoyto	Yamba	Concession
Pitcher (1983, 1987)	Hercynotype	Caledonian-type	Caledonian-Andinotype
Chappell and White (1974); White and Chappell (1983)	S-type	I-type (±S)	I-type
Barbarin (1990)	Crustal	Crustal-Hybrid	Hybrid
Petrographic	C_{ST} - C_{CI}	C_{CI} - H_{LO}	H_{LO} - H_{CA}
Mineralogical	C_{ST} - C_{CI}	C_{CI}	H_{LO} - H_{CA}
Major elements	C_{ST} - C_{CI}	C_{CI} - H_{LO}	H_{LO} - H_{CA}
Intrusive Style	C_{ST} - C_{CI}	C_{ST} - C_{CI}	

C_{ST} = two-mica leucogranites, ?thrust related, dominantly crustal source; C_{CI} = peraluminous intrusive granitoids, dominantly crustal source; H_{LO} = mixed origin (crust + mantle), potassic calc-alkaline granitoids (high K-low Ca); H_{CA} = mixed origin (crust + mantle), calc-alkaline granitoids (low K-high Ca); S-type = sedimentary source rocks; I-type = igneous source rocks.

The Contwoyto Suite shares geological, petrographic, and mineralogical traits with the Hercyno-type or continental collisional granitoid type (*e.g.* Pitcher, 1987). In particular, the high SiO_2 contents, peraluminous compositions, primary muscovite, common occurrence of tourmaline, monazite and apatite, and rapid changes in textural

facies and abundant pegmatites are characteristic features of this granite type (*e.g.* Vidal *et al.*, 1984; Cerny and Meintzer, 1988). These characteristics are indicative, in part, of S-type granites (sedimentary-derived) as defined by Chappell and White (1974) or the C-type of Barbarin (1990). There is a general consensus that this type of granite is dominantly crustally derived, most likely from sedimentary protoliths.

Classification of the Yamba Suite is more equivocal. The suite has characteristics similar to the Caledonian-type granites of Pitcher (1983), and has features of both I- and S-type granites. However, the absence of primary muscovite or peraluminous minerals argues against an S-type classification (*s.s.*, White *et al.*, 1986). The suite shows characteristics of both crustal and hybrid granites as defined by Barbarin (1990) (Table 6.4).

6.4 Origin and Evolution of the Yamba and Contwoyto Plutonic Suites

Magmatic differentiation in granitic systems is extremely complex owing to the multiplicity of processes capable of affecting the composition of the rock (Miller *et al.*, 1988; Pitcher, 1987; Wall *et al.*, 1987). These include crystal-liquid-fluid partitioning during partial melting and crystallization, entrainment and unmixing of restite material (*e.g.* Chappell and White, 1974), crystal fractionation, particularly of accessory phases enriched in trace elements, assimilation, magma mixing, variable and heterogeneous source terrains, and the exsolution of fluid phases, generation of pegmatites and subsolidus alteration processes (*e.g.* Cerny *et al.*, 1985). It is not possible to quantitatively constrain all or indeed any of these processes.

In addition to the complexity of petrogenetic process inherent in granite systems, the regional nature of the sampling in this study precludes systematic evaluation of differentiation processes within a single magmatic system. The following sections, therefore, present a qualitative assessment of within-suite chemical variation and the potential roles for some of the differentiation processes listed above. Quantitative models serve only to highlight the potential effects of a particular process, they cannot yield unique solutions, and are undoubtedly poor simulations of the actual processes involved.

6.4.1 Within-Suite Chemical Variation

Major and trace element contents of samples of the Yamba and Contwoyto Suites define distinct groups, or subparallel trends on most variation diagrams (Figure 6.3, 6.4). The two suites are unlikely, therefore, to be related by a simple process such as fractional crystallization, mixing, or variable partial melting of similar source rocks. Separate origins are consistent with the field data showing that the suites are not spatially associated, and do not form composite batholiths. The Contwoyto Suite is spatially associated with supracrustal rocks, while the Yamba Suite commonly intrudes rocks of the Concession Suite (*e.g.* Wolverine Monzogranite). There is no field evidence to petrologically link the two suites at the present level of exposure.

The style of within-suite trace element variation is different in the two suites. For example, in the Yamba Suite, elements such as Th and Y are extremely variable, but in the Contwoyto Suite they are uniformly low (Figure 6.7). P_2O_5 contents vary significantly in the Contwoyto Suite but not in the Yamba Suite (Figure 6.7). Perhaps the most distinctive difference between the suites is the style of REE variation. The LREE-depleted, low abundance REE patterns (Type II) are only documented in rocks of the Contwoyto Suite. In the Yamba Suite, the LREE show large absolute variations but LREE fractionation (*e.g.* $(Ce/Sm)_N$) is minor. As outlined below these differences in within-suite elemental variation may reflect differences in the relative importance of the differentiation processes responsible for the chemical fractionations.

Fractionation of the REE in the Contwoyto Suite occurs by a decrease in the LREE abundance which results in lower $(Ce/Yb)_N$ patterns with little or no change in SiO_2 contents. HREE may increase or maintain abundance with the development of small positive to large negative Eu anomalies (*e.g.* Figure 6.8b). Decreasing LREE contents, $(Ce/Sm)_N$ and $(Ce/Yb)_N$ are characteristic features of the Archean 'fertile' granite association (Cerny *et al.*, 1985; Cerny and Meintzer, 1988) as well as many leucogranites (*e.g.* Vidal *et al.*, 1982; Searle and Fryer, 1985; Muecke and Clarke,

1981). This type of REE variation is generally attributed to fractionation of REE-enriched accessory mineral phases, or the evolution of a fluid phase which complexes the REE.

REE-enriched accessory minerals can produce extreme effects on the REE content of felsic igneous rocks (*e.g.* Schaltegger and Krahenbuhl, 1990; Mahood and Hildreth, 1983; Miller and Mittlefehldt, 1984; Sawka, 1988). The accessory minerals apatite, zircon and monazite (± garnet and tourmaline) all occur in samples of the Contwoyto Suite and the differences in the measured REE patterns could reflect separation or accumulation of one or more of these REE-rich phases. One prediction of this hypothesis is that the contents of trace elements common to a particular accessory mineral, will covary. For example, monazite and apatite are phosphate minerals, rich in Th, as well as the REE (Miller and Mittlefelhdt, 1984; Schaltegger and Krahenbuhl, 1990). Zircon has high contents of Zr, Y and the REE (± Th) (Heaman *et al.*, 1990). Fractionation of these phases should, therefore, result in sympathetic variations in Zr, REE, Th and P_2O_5. However, the abundance of Zr in the rocks does not correlate simply with Y or HREE contents, nor do the REE correlate with P_2O_5 or Th as would be expected by apatite- or monazite-controlled fractionation. The common accessory phases cannot be directly responsible for REE fractionation, although they may have some smaller effect. The possible occurrence of other REE-enriched phases (*e.g.* thorite, chernovite, polycrase, Schaltegger and Krahenbuhl, 1990) cannot be evaluated at this time.

The abundance of pegmatites, rapid variations in grain size, occurrence of primary muscovite, and tourmalinization and muscovitization of host sediments provide ample evidence for the presence and mobility of fluid phases during the evolution of the Contwoyto Suite. REE variation in leucogranites is commonly thought to be strongly affected by complexing of REE in a fluid phase (*e.g.* Vidal *et al.*, 1982; Cerny *et al.*, 1985). REE may be transported as complex anions (F^-, Cl^-, CO_3^{2-}, BO_3^{2-}) in the fluid phase (Flynn and Burnham, 1978; Collerson and Fryer, 1978). This can result in overall depletion of REE in the melt, large Eu anomalies (both negative and positive) as

well as kinked REE patterns atypical of crystal-melt partitioning (*e.g.* Cerny and Meintzer, 1988; Walker et al., 1984). These REE features are similar to the fractionated and depleted REE patterns characteristics of some of the Contwoyto Suite granites, particularly the tourmaline-bearing granites and granites associated with external pegmatites (*e.g.* Figure 6.8b,c,d). Fluid processes could also be responsible for the variability in P_2O_5 and LFSE (*e.g.* Rb, Na_2O) contents . As pointed out by Cerny and Meintzer (1988), quantitative modelling of these processes is unrealistic, given the present state of knowledge.

The considerable chemical heterogeneity, and the complexity of the differentiation processes seriously impedes reconstruction of a parental magma composition(s), a reliable estimate of which is required to constrain the nature of the source region to the granites. Cerny and Meintzer (1988) suggest that in the Archean 'fertile' granite association, the least fractionated samples are those with higher K/Rb, LREE and $(Ce/Yb)_N$, as differentiation of the suite generally leads to decreasing LREE with increasing HREE and decreasing $(Ce/Yb)_N$. This same type of differentiation is common to the Contwoyto Suite. The majority of the samples analyzed in this study have high LREE, low HREE contents and moderate Eu anomalies, characteristics of the 'least fractionated' samples described by Cerny and Meintzer (1988).

Within-suite variation in the Yamba Suite (high Y group) is different than observed in the Contwoyto Suite, namely: 1) the REE patterns in the Yamba Suite are less variable than those in the Contwoyto Suite, without significant LREE fractionation; and, 2) trace elements enriched in accessory minerals (*e.g.* Th, Ce and Zr) demonstrate positive correlations with each other (Figure 6.7).

Most of the major and LFS element variation observed within the Wolverine Monzogranite can be accounted for by 25 wt% fractionation of the principal rock forming minerals (Table 6.5; Figure 6.10). This model, however, fails to explain the large range of values, and correlation of Zr, Th and LREE contents. These trace element correlations may reflect accessory mineral control (*e.g.* separation or accumulation of zircon or Th-rich phase). This could be a residual phase from melting

(*ie.* restite) or of magmatic origin. Th, Zr and the LREE contents also correlate with those of SiO_2, Ti, Ba, $\pm$Nb and V. The concentration of these latter elements is most likely controlled by biotite and feldspars, suggesting that separation or accumulation of the accessory minerals occurred in concert with fractionation of biotite and feldspar.

Table 6.5. Results of least squares mixing calculations (LeMaitre, 1979), Wolverine Monzogranite, high Y group.

Fractional Crystallization											
	Wt%	SIO2	TIO2	AL2O3	FE2O3	MNO	MGO	CAO	NA2O	K2O	P2O5
REACTANTS USED											
D114-87	100.0	70 55	.53	14.60	2.93	0 02	0.72	1.50	3 03	5.88	0 24
PRODUCTS USED											
D134-88	77.49	75 65	.16	13.11	1.28	.01	0.33	0.85	2.96	5.63	0 02
Plag AN 17	9.02	63.97	0 0	22.61	.25	0 0	0.0	3.2	9.87	0 05	0.0
K-spar	5.23	65.19	0.0	18.29	0.0	0.0	0 0	0 15	0 86	15.52	0 0
Biotite	7.51	36.45	2.90	17.84	25 56	0.33	6.71	0 0	0.0	10.21	0 0
Apatite	0.76	0.0	0.0	0.0	0.0	0.0	0.0	57.1	0.0	0 0	42 9
ESTIMATED COMPOSITIONS											
REACTANTS		70.55	.53	14.60	2.93	0.02	0.72	1 50	3.03	5 88	0 24
PRODUCTS		70.53	.34	14 50	2.93	0.03	0.76	1.39	3 22	5 94	0 34
DIFFERENCES		0 02	0.18	0.10	0.0	-0.01	0.04	0 11	0.19	0.06	0 10
RESIDUAL SUM OF SQUARES = 0.11											

If fluid processes were important in the Concession Suite, their effects are less apparent in the Yamba Suite, consistent with the textural differences between the suites.

6.4.2 Origin of the Contwoyto Plutonic Suite

Partial Melting of Metasedimentary Rocks

Granites with the characteristics of the Contwoyto Suite are commonly modelled as partial melts of metasedimentary source rocks (Vidal *et al.*, 1982; Miller, 1985; Pitcher, 1987). Metasedimentary protoliths have been proposed for compositionally and petrographically similar granites from elsewhere in the Slave Province (*e.g.* Prosperous Granite,Drury, 1979; Meintzer, 1987; two-mica granites, Hackett River area, Frith and Fryer, 1985), as well as Archean leucogranites from other provinces

(*e.g.* Day and Weiblen, 1986). Turbidite sequences represent a relatively large component of the crust in the Slave Province and thus represent a reservoir of sufficient volume to generate the significant volumes of granite observed.

It is well accepted that peraluminous granites can be produced through partial melting of sedimentary source rocks (Patino-Douce and Johnston, 1990, LeBreton and Thompson, 1988; Vielzeuf and Holloway, 1988; Miller, 1985; Clemens and Vielzeuf, 1987). Recent experimental studies emphasize the importance of biotite dehydration reactions in generating large volumes of peraluminous granite (Patino-Douce and Johnston, 1990, LeBreton and Thompson, 1988; Vielzeuf and Holloway, 1988). Importantly, melting occurs under water undersaturated conditions thought to be appropriate for the mid to lower crust.

Melting may occur through the reaction:

$$\text{biotite} + \text{plagioclase} + \text{aluminosilicate} + \text{quartz} = \text{melt} + \text{garnet} \pm \text{alkali Feldspar}$$

At lower pressures cordierite rather than garnet is the residual phase (*e.g.* Green, T.H. 1976; Vielzeuf and Holloway, 1988). Melt proportions exceeding 50% can be produced over a fairly limited temperature interval of 800°-900°C at 7-13 kb (see Table 6.6). Quartzo-feldspathic metagraywackes approximate the most fertile source compositions (Patino-Douce and Johnston, 1990, Clemens and Vielzeuf, 1987). Metagraywackes are the single most abundant, pre-granite rock type presently exposed in the Slave Province.

The high melt fractions generated through biotite dehydration reactions exceed that theoretically required to mobilize and separate melts from their source regions (*ie.* exceed the rheological critical melt fraction, *e.g.* Wickham, 1987; Miller *et al.*, 1988; Arzi, 1978). Since melts produced through this reaction are water undersaturated, they are able to separate and ascend to higher structural levels, intruding lower grade metamorphic rocks as have the Contwoyto Suite granites.

Table 6.6. Average compositions of the Contwoyto and Yamba Monzogranites compared to compositions of experimental melts of sedimentary rocks.

Sample Name	Contwoyto Monzogr.	Yamba Wolv. high Y	7-875 PD	7 975 PD	13-900 PD	13 950 PD	10 875 VH	10 900 VH
Melt%			29	66	24	42		
SiO2	73 00	74.21	73.79	74.41	73 69	73 51	73 20	71 30
TiO2	0.23	0.23	0.14	0.54	0.30	0.28	0.30	0.60
Al2O3	15.06	13.79	15.72	13.81	15.29	14.51	16.10	16 10
FeO*	1.61	1.66	1.75	2.09	1.63	1.50	1.50	1.90
MnO	0.02	0.02	0.00	0.06	0.02	0.04	0.00	0.00
MgO	0.63	1.66	0.37	0.91	0.44	0.37	1.00	1.30
CaO	1.36	0.40	0.37	0.41	0.23	0.11	0.40	1.60
Na2O	4.33	3.23	1.87	0.89	1.94	1.30	3.10	3.00
K2O	3.59	5.26	5.94	6.71	6.40	8 29	4 40	4 20
P2O5	0.17	0.07	0.05	0.07	0.05	0.10	0 00	0.00
H2O			4.09	2.98	7.14	5.33	3.74	3.50

Average values of Contwoyto and Yamba Plutonic Suites taken from Table 5.2. Numbers of experimental melts are coded as follows: the number before the hyphen refers to the pressure in kbars; that following the hyphen the temperature (°C). PD = Patino Douce and Johnston, 1990, VH = Vielzeuf and Holloway, 1988.

Migmatites exposed in the study area commonly have melanosome assemblages consisting of corderite, sillimanite, biotite, plagioclase ±quartz, ±garnet, ±alkali feldspar (Wingate, 1990). Wingate (1990) describes mineral relationships within migmatites of the Itchen Formation (north of the WM) consistent with the biotite dehydration reaction:

$$\text{biotite} + \text{sillimanite} + \text{quartz} = \text{melt} + \text{cordierite}$$

Melting conditions in these migmatites are estimated to be high temperature (800°C) and relatively low pressure (5-6 kb), consistent with the occurrence of residual cordierite rather than garnet (*e.g.* Green T.H., 1976). Since the granites are not directly associated with migmatite zones, the actual source region for the Contwoyto Suite is not exposed, and must be at greater depths in the crust.

Cordierite is a common but not ubiquitous mineral in sedimentary derived granites (*e.g.* White *et al.*, 1986) and many migmatites in the Slave Province contain cordierite in their leucosome (Wingate, 1990; Folinsbee, 1949). However, cordierite (or garnet)

is not observed as phenocrysts (xenocrysts) in the granites, although garnet is present in pegmatites. This suggests that if cordierite was an important residual phase during melting it was removed from the melt during or subsequent to magma segregation (Zen, 1989). Cordierite may have reacted out with increasing water activity during crystallization and decompression, to produce the observed muscovite, quartz and microcline assemblage (Zen, 1989; Clemens and Wall, 1988).

Experimental melts produced by biotite dehydration reactions are compositionally similar to the average value of 'least fractionated' samples of the Contwoyto Suite (Table 6.6; Patino-Douce and Johnston, 1990; Vielzeuf and Holloway, 1988). The higher Na_2O contents in the Contwoyto Suite compared to the experimental liquids probably reflects different protolith compositions. According to Chappell and White (1974), sedimentary-derived granites should have low Na_2O contents because of the loss of Na_2O during surficial weathering and sedimentation processes. The Na_2O contents in rock of the Concesion Suite are much higher than in typical S-type granites, as defined by Chappell and White (1974; White and Chappell, 1983). However, metasedimentary rocks exposed in the Slave Province are chemically immature (*ie.* low Al_2O_3/Na_2O, Easton, 1985; Jenner *et al.*, 1981; Appendix 2) and Na_2O-rich. Since they are not themselves Na-deficient, they could yield relatively high-Na granites.

Yellowknife Supergroup Metasedimentary Rocks as Protoliths

Nd Isotopic Constraints

Isotopic data are particularly useful in evaluating possible and impossible crustal sources. The Contwoyto Suite exhibits a wide range of $\epsilon_{Nd(t)}$ values, ranging from +2.8 to -4.3 (Table 6.3). The process responsible for generating these granitic rocks must, therefore, be capable of producing petrographically and geochemically similar rocks from isotopically distinct sources. The $\epsilon_{Nd(2.6)}$ values of Contwoyto Suite rocks fall within the range of compositions determined for Yellowknife Supergroup rocks (Table 7.1; Figure 6.11). It is, therefore, possible to generate the range in measured $\epsilon_{Nd(2.6)}$ values by variable mixtures of an isotopically heterogeneous metasedimentary source. An example of this is shown in Figure 6.12 which assumes the simplest

possible case, a two component mixture of: 1) metasedimentary rocks similar to a pelite sample from Point Lake ($\epsilon_{Nd(2.6)}$ = -6.7); and, 2) an average value of the metasedimentary rocks with juvenile isotopic compositions from the central and eastern parts of the province. Insignificant amounts to over 80% of the component with negative $\epsilon_{Nd(2.6)}$ values are required to reproduce the range in $\epsilon_{Nd(2.6)}$ values. The relative percentages of the end members calculated in this fashion is critically dependant on their isotopic compositions and Nd contents. These values are not well defined for either end member. Mixing of these different components could occur during sedimentation, during deformation or as a result of melting and coalescence of different magma batches. The actual process will be more complicated than this simplistic model, possibly involving a number of different crustal components, with different Nd isotopic compositions and abundances.

This model requires that metasedimentary rocks with negative $\epsilon_{Nd(t)}$ values, similar to those of the pelite sample from Point Lake, would be required to occur beneath at least the western part of the field area in order to account for those granites with $\epsilon_{Nd(t)}$ values of less than -1. The single analyses from the eastern most part of the area (R037-89) would not require this component (See Chapter 7).

The Nd isotopic compositions of the Contwoyto Suite granites are, therefore, consistent with their derivation from isotopically heterogeneous metasedimentary rocks similar to those exposed at the current erosional level. Oxygen isotope studies could better constrain the role of sedimentary rocks. This data is not available for the Contwoyto Suite but data is published for compositionally similar rocks from the southern Slave Province (Prosperous and Buckham Plutons). $\delta^{18}O$ values for these granites have high values (9-11 per mille), interpreted to reflect a significant metasedimentary component (Meintzer, 1987).

Trace Element Constraints

Compositions of metasedimentary rocks in the area are given in Appendix 2. Rocks range in composition from 55 wt% SiO_2, in the pelites, to up to 70 wt% SiO_2 in quartz-rich metagraywackes. The samples are LREE-enriched with high $(Ce/Yb)_N$ and

no or small Eu anomalies (Figure 6.13). These characteristics are generally similar to published data for metasedimentary rocks from Yellowknife and Point Lake (Meintzer, 1987; Jenner *et al.*, 1981; Easton, 1985).

The trace element characteristics of YKS sedimentary rocks are compared to granites of the Contwoyto Suite in Figure 6.13. Compared to representative YKS sedimentary rocks, the granites have lower LREE, higher HREE, lower $(Ce/Yb)_N$ and larger negative Eu anomalies. Residual Bulk D values of selected trace elements, required to derive the granites from the metasedimentary rocks, are shown in Figure 6.14. These values were calculated by assuming an equilibrium batch melting model with variable melt fractions from 10 to 50%. The Bulk D values for the REE in the residuum are relatively high and increase from La to Yb. Discontinuities at Eu and Sr (*ie.* higher Kd values than adjacent elements) are present and their magnitude varies depending on the assumed source composition. This implies residual feldspar, or subsequent feldspar fractionation.

The calculated Bulk D values for the REE are too high to be consistent with a residual assemblage of biotite, plagioclase, alkali feldspar and quartz, and additional residual phases with high Kd values are required. This is a common problem in models deriving granites from metasedimentary source rocks (*e.g.* McCarthy and Haskey, 1976; Vidal *et al.*, 1982; Miller *et al.*, 1988) and can be explained by a number of processes:

1) the compositions of the granites are not representative of the melts because of the effect of post-melting fractionation processes;

2) the composition of metasedimentary rocks is inappropriate or was modified during metamorphism preceding or simultaneously with melting; and

3) the residual mineralogy includes minerals with high Kd values for the REE (*e.g.* garnet, zircon, apatite, monazite, allanite, titanite; amphibole).

Accepting the extremely large uncertainties involved in estimating all parameters of a partial melting model (parental composition, source composition, residual mineralogy, Bulk D values), partial melting of metasedimentary rocks similar in

composition to the YKS can be considered as a viable model. Assessing the involvement of other crustal rock types (*ie.* Pre-YKS Gneisses, earlier plutonic rocks of the Concession Suite) in the generation of the Contwoyto Suite requires additional reliable isotopic data (Sr, Pb, O) from both granitic and potential source rocks.

6.4.3 Origin of the Yamba Plutonic Suite

Large batholiths of biotite-bearing, K-rich granites similar to the Yamba Suite are abundant in many Archean terrains (*e.g.* Arth and Hanson, 1975, Day and Weiblen, 1986, Cerny *et al.*, 1987; Condie, 1981; Martin and Querre, 1984), including both sediment dominated terrains, such as the Slave Province, and volcanic dominated terrains such as the many belts in the Superior Province. Petrogenetic models proposed for these granites include:

1) partial melting of metagraywacke (e.g Arth and Hanson, 1975; Drury, 1979);

2) partial melting of tonalite-trondhjemite-granodiorite terrains (Day and Weiblen, 1986; Moorbath *et al.*, 1981; Cerny *et al.*, 1987) including plutonic rocks similar in composition to the Concession Suite (Shirey and Hanson, 1986); and

3) hybridization of mantle-derived melts by mixing and/or assimilation of partial melts of older crust (tonalite-trondhjemite-granodiorite) (Martin and Querre, 1984; Gariépy and Allègre, 1985).

Crustal Melting Models

Deriving the Yamba Suite from metasedimentary protoliths seems unlikely since the petrological and compositional differences between the Contwoyto and Yamba Suite rocks preclude their derivation by variable degrees of melting of compositionally similar protoliths. The major element compositions of experimental melts of metasedimentary rocks show little pressure dependence (*e.g.* Patino-Douce and Johnston, 1990) and the trace element chemistry of the two suites cannot be simply related by varying degrees of partial melting or entrainment of restite material from a similar source. Rather the petrological and geochemical differences suggest derivation from different source rocks or through different genetic processes. This is consistent

with the less peraluminous compositions of, and absence of primary muscovite in, the Yamba Suite rocks. The Yamba Suite resemble fractionated or contaminated I-type or hybrid granites (*e.g.* White *et al.*, 1986; Miller, 1985; Barbarin, 1990) not sedimentary-derived granites.

Models which derive the suite from remelting igneous rocks of the 20 m.y. older Concession Suite or older volcanic sequences (*ie.* hypothesis 2, above) fail to account for the negative $\epsilon_{Nd(I)}$ values determined for some samples of the suite. The Concession Suite in the Contwoyto Lake area has juvenile $\epsilon_{Nd(2.6)}$ values but is intruded by Yamba Suite rocks which have negative $\epsilon_{Nd(2.6)}$ values (Figure 6.11). An additional component with negative $\epsilon_{Nd(2.6)}$ values is required and the Yamba Suite cannot, therefore, be derived by remelting juvenile igneous crust underplated during the earlier magmatic events. Volcanic sequences (ca. 2650-2670 Ma) also have juvenile $\epsilon_{Nd(2.6)}$ values and do not occur in sufficient volume, at least as presently exposed, to account for the large volumes of granite generated.

The only other potential crustal protolith, known from surface exposures is the Pre-YKS rocks. These rocks satisfy some, but not all, of the radiogenic isotope requirements. Their range of $\epsilon_{Nd(2.6)}$ values overlap the more negative values of the Wolverine Monzogranite and other samples from the western part of the area (Figure 6.11). They don't however have the positive ϵ_{Nd} values required to account for the sample from the Pellatt Lake Monzogranite (+2.9) or those further to the east (Chapter 7). They are thus unlikely to be the sole protolith to the suite.

Crustal Hybridization of Mantle-derived Magmas

The relative timing of intrusion of the mantle-derived Concession Suite, peak metamorphism and intrusion of the Yamba Suite allows for a direct genetic linkage, in which all three represent the evolving manifestation of a single tectono-thermal magmatic event. In the immediate study area, the two suites appear to be discontinuous events separated by a time gap on the order of 20 m.y. (van Breemen *et al.*, 1990). However, a discontinuous relationship between the magmatic events is less apparent when considered in the regional context of the Slave Province (van Breemen *et al.*,

1991). Biotite granites, petrographically similar to the Yamba Suite, are generally younger but do overlap in age with rocks of the Concession Suite (van Breemen *et al.*, 1991). In some areas tonalites are younger than microcline megacrystic biotite granites (*e.g.* Culshaw and van Breemen, 1990). There is no evidence for regional variations in intrusive age. The potential for sequential but overlapping emplacement of the Concession and Yamba Suites suggests a continuum or evolution in chemistry of plutonic rocks from early, dominantly tonalite magmatism, to later, dominantly granitic magmatism. Similar compositional evolution is common to many calc-alkaline batholith systems (*e.g.* Pitcher, 1987).

The field and geochronological relationships are consistent with the Yamba Suite being generated through assimilation of, or mixing between, crustal melts and more mafic magmas of the Concession Suite - a common model to explain granites in calc-alkaline batholiths (DePaolo, 1981; Barton, 1990; Pitcher, 1987).

Figure 6.15 compares the abundances of selected trace elements in the Concession Suite to those in the Yamba Suite. The within-suite chemical variation defined by rocks of the Concession Suite (labelled AFC Trend 1 on Figure 6.15) does not lead directly to compositions typical of the Yamba Suite. This requires that the fractionating assemblage and/or the composition of the assimilant changed. Since the trace element differences are linked to isotopic differences, at least for samples from the Wolverine Monzogranite, the change in the differentiation trends cannot be simply linked to closed system fractionation processes. An assimilant consisting of older crustal component is required. The Yamba Suite is therefore not simply an extreme product of the same processes that generated the Concession Suite, rather its petrogenesis must involve different crustal rock types. This implies secular variations in the nature of crustal contamination.

Nature of the Assimilant

Establishing the nature and composition of the assimilant remains an open ended problem. To generate the high Y granites from diorites of the Concession Suite the AFC process must: 1) increase contents of Rb, K, Th, Y, HREE, and Ba; 2) decreases contents of Sr, P, Ti, Zn, and V; and 3) develop large negative Eu anomalies.

The assimilant, therefore, must have high contents of K, Rb, Ba, Th and Y in order to produce the high abundances observed in the granitic rocks relative to the tonalites. The requirement for high Rb, K, and Ba is especially true if biotite is a significant fractionating phase because of its high Kd values for these elements. Plagioclase (or K-spar) must be a significant fractionating and/or residual phase to account for the significant decrease in Sr and the large negative Eu anomalies. Th-bearing accessory minerals (*ie.* monazite, allanite, thorite) must not be important fractionating or residual phases in order to account for the high Th and little fractionation of the LREE. Xenocrysts or restite grains could increase Th and the LREE. Minerals with high Kd values for Y and the HREE (*e.g.* amphibole, zircon, garnet) cannot be significant residual or fractionating phases because of the similar or higher abundances of these elements in the granite.

None of the potential protoliths known from the Slave Province have significant negative Eu anomalies, and therefore bulk assimilation of any of these materials will not generate the large anomalies observed in the granites. Eu anomalies can be generated by crustal melting leaving a plagioclase-rich residuum. For this reason, assimilation of crustal melts, rather than bulk assimilation processes, are favoured.

These observations constrain the source of the assimilant as follows.

1) The assimilant is unlikely to be a melt derived from an amphibolite residuum particularly if garnet is stable (*e.g.* mafic lower crust, or source of Siege or Olga Suite). This is because this assimilant would have low Y and relatively high Sr. Furthermore K and Rb contents in tonalites derived from basalt melting are low (*e.g.* the Olga and Siege tonalites).

2) The assimilant is unlikely to be derived from depleted (K, Th, Rb) granulitic lower crust (*e.g.* Taylor and McLennan, 1985), such as crustal residues from earlier melting events which may have generated the Pre-YKS granitoid rocks.

3) The assimilant is, however, likely to be derived from a plagioclase-rich protolith. This could include partial melts of metagraywackes, metavolcanic rocks and pre-Yellowknife tonalite gneisses and granitoids.

The chemical differences between the high and low Y groups could be accounted for by one or more of the following: 1) the composition of the assimilant was different; 2) the ratio of assimilant to fractionation differed; or, 3) the fractionating assemblage differed. The Nd isotopic difference between the sample of the Pellatt Lake low Y granite and the Wolverine high Y granites suggests that, as a minimum, different assimilants may be involved.

Nd Isotopic Test of the AFC Model

Simple AFC models (DePaolo, 1981) can account for the $\epsilon_{Nd(t)}$ values of the Wolverine Monzogranite provided the following approximations are met:

1) the initial magma has an $\epsilon_{Nd(t)}$ value of +1.0;

2) the assimilant has an $\epsilon_{Nd(t)}$ of -10;

3) the assimilant and initial magma have similar Nd contents.

The assimilant, at least in the western part of the field area, must have had a long-term, LREE-enriched prehistory in order to generate the negative $\epsilon_{Nd(t)}$ values in the granites. In contrast, the assimilant in the east must be young or have a near chondritic Sm/Nd ratio to account for the positive $\epsilon_{Nd(t)}$ value of the Pellatt Lake Monzogranite. Assimilation of this material will effectuate no or little change on the $\epsilon_{Nd(t)}$ value.

Since there is no evidence that the earlier tonalites show systematic regional variations within the Contwoyto Lake area and to the east (Chapter 5 and 7), the crustal component must vary across the field area. The crustal component in the west could

consist of variable mixtures of pre-YKS rocks or sedimentary rocks derived from a similarly aged crust. The crustal components in the west could be derived from the ca. 2650-2700 supracrustal rocks.

6.5 Chapter Summary

Compositional and petrological differences between the two post-deformation granite suites indicate separate origins and evolutionary histories.

The Contwoyto Suite resembles many collisional-type granites (*e.g.* Pitcher, 1987; Barbarin, 1990; Harris *et al.*, 1986), and is considered to be derived through biotite-breakdown, dehydration melting of a heterogeneous metasedimentar source. The source could be similar to the turbidite rocks of the YKS as presently exposed at the surface. Within-suite differentiation occurred by both crystal-melt and fluid-melt processes, the full nature of which cannot be well documented. Differentiation leads to magma compositions relatively depleted in LREE, enriched in HREE and with variable positive or negative Eu anomalies. These features are generally ascribed to fluid processes (*e.g.* Cerny *et al.*, 1985). Nd isotopic data require a range of source compositions. Mixing of these different crustal components (old crust and young crust) could occur either during initial deposition of the sedimentary protoliths, or later through mechanical mixing during deformation, melting and metamorphism. Further isotopic studies on both the granitic rocks and the metasedimentary rocks are required to better constrain these possibilities.

The origin of the Yamba Suite is more equivocal. Compositional differences between it and the Contwoyto Suite are incompatible with it being derived from similar metasedimentary sources. The spatial association of these rocks with the earlier mantle-derived Concession Suite, and their compositional similarity to granites of hybrid origin (*e.g.* Barbarin, 1990) suggest they may be best modelled as products of the mixing and homogenization of mantle- and crust-derived material. This would occur by assimilation of crustal components (probably melts) by mantle-derived magmas similar in composition to diorites of the Concession Suite. The differences between the high and low Y groups may reflect regional differences in the AFC

process, including differences in the composition of the assimilant. The east-west difference in Nd isotopic composition of the rocks indicate assimilation of different crustal rocks, whose spatial distribution argues for a laterally composite crust beneath this part of the Slave Province (see Chapter 7).

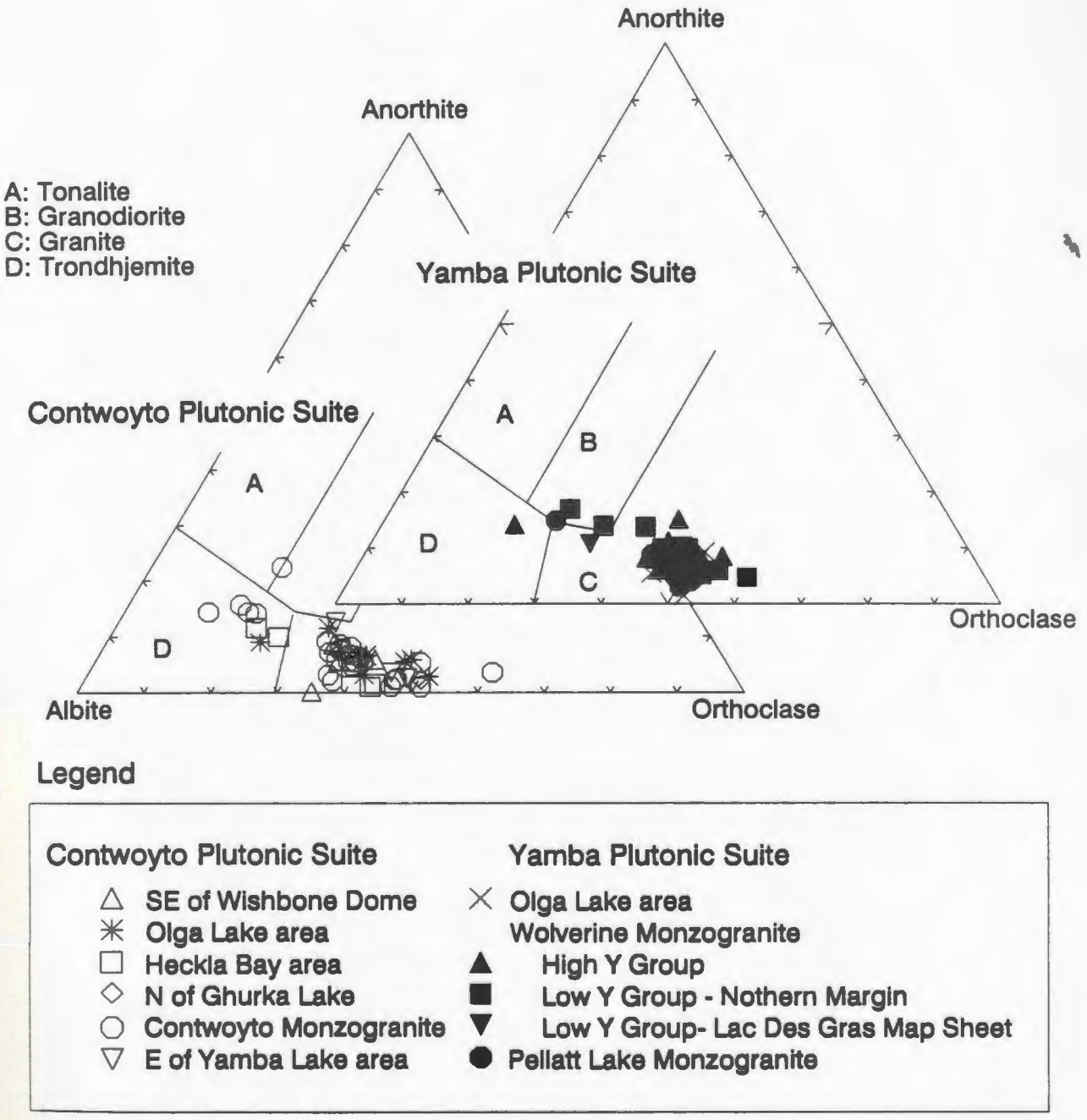

Figure 6.1. Classification of the post-deformation granite suites based on CIPW albite, anorthite and orthoclase. Fields from Barker (1979) after O'Conner (1965).

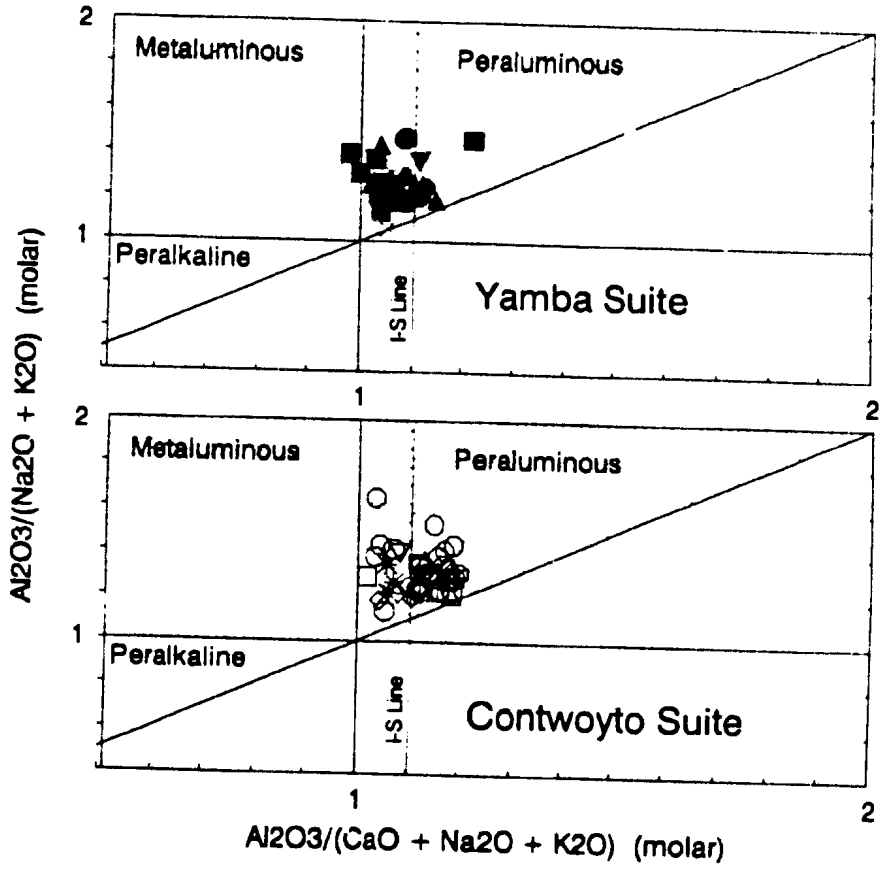

Figure 6.2. Plot of index of peraluminousity [$Al_2O_3/(CaO+Na_2O+K_2O)$] *vs.* peralkalinity [$Al_2O_3/(Na_2O+K_2O$] for the Contwoyto and Yamba Suites. Symbols as in Figure 6.1.

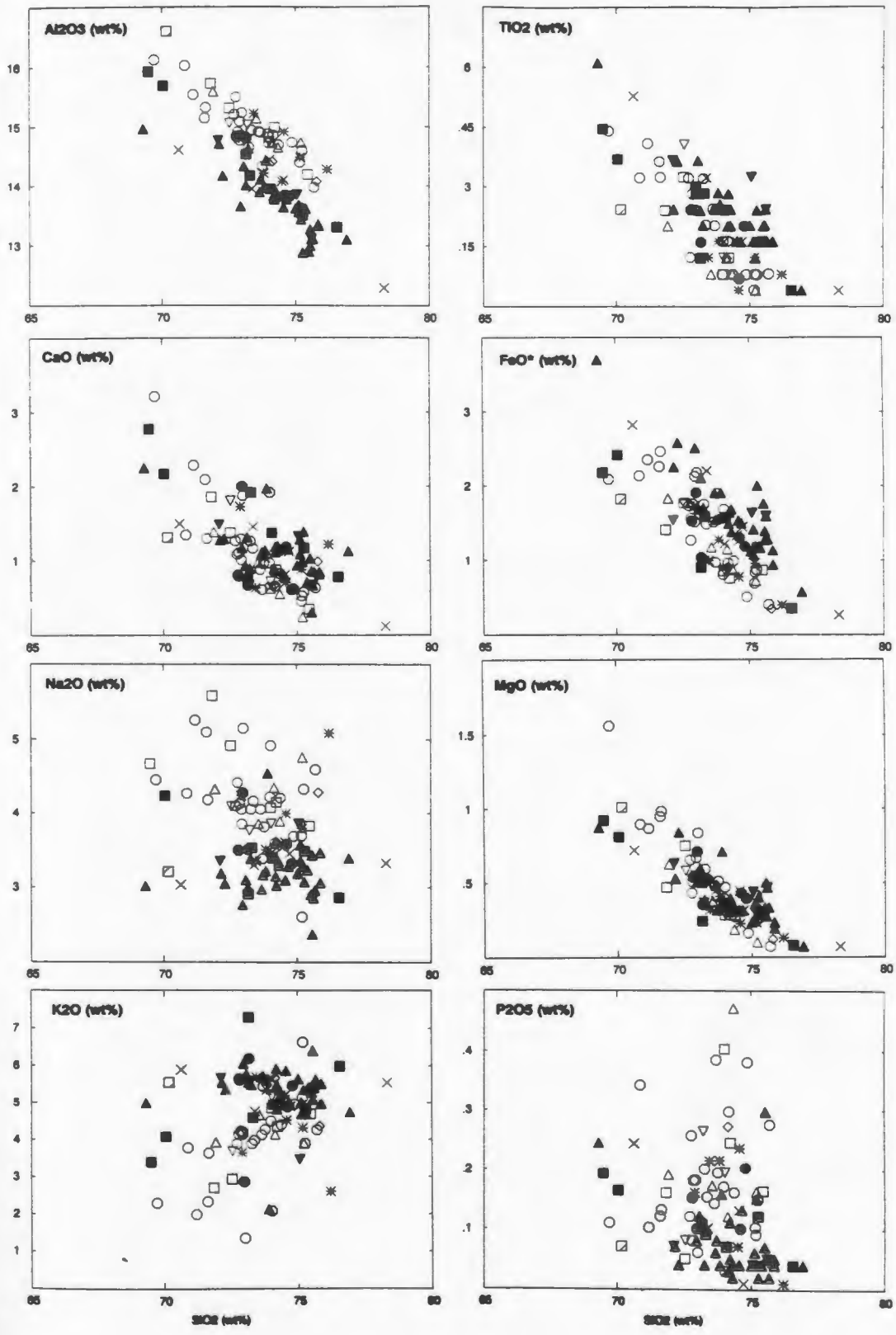

Figure 6.3. Major element Harker variation diagrams, Contwoyto and Yamba Suites. Symbols as in Figure 6.1.

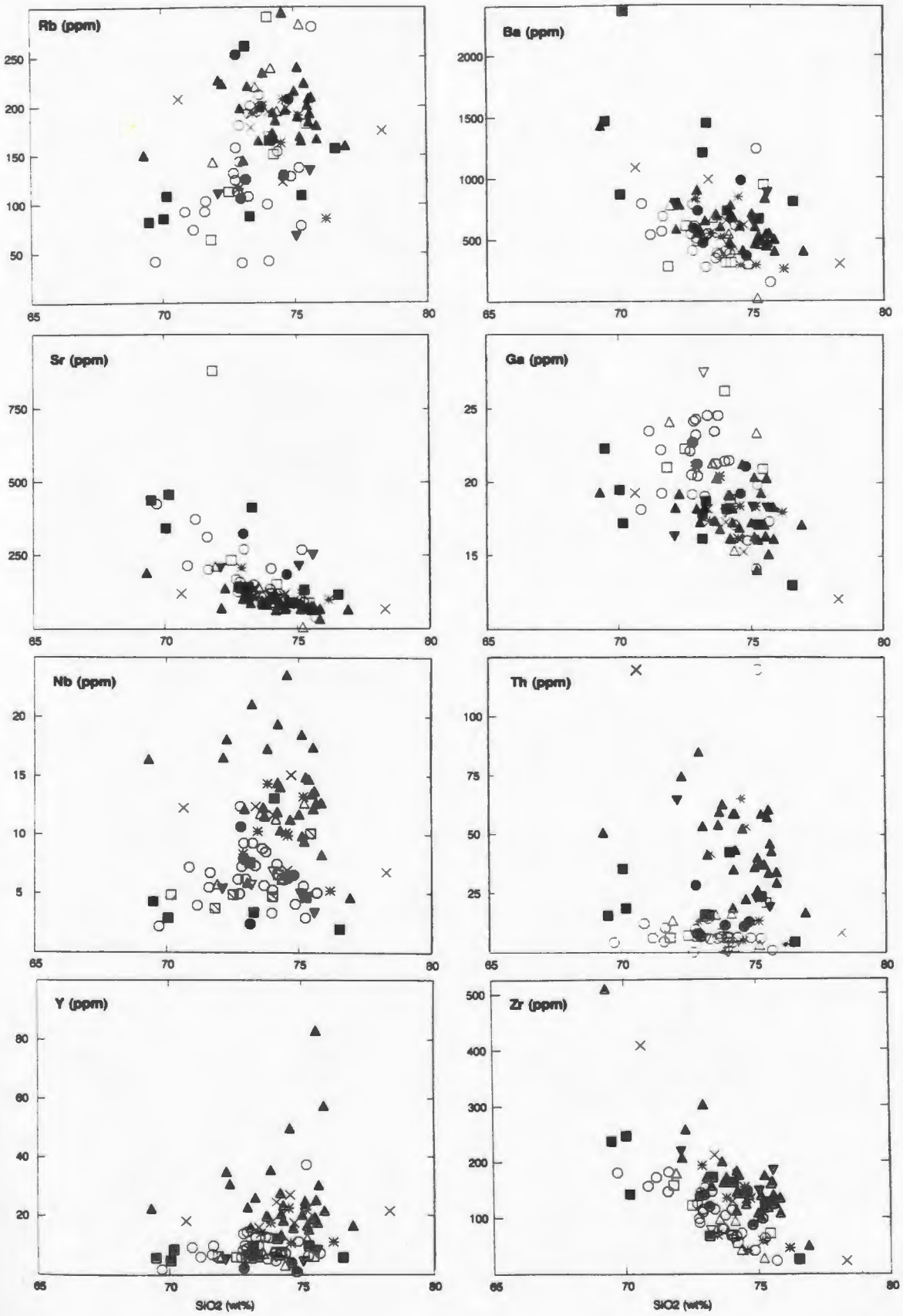

Figure 6.4. Trace element Harker variation diagrams, Contwoyto and Yamba Suites. Symbols as in Figure 6.1..

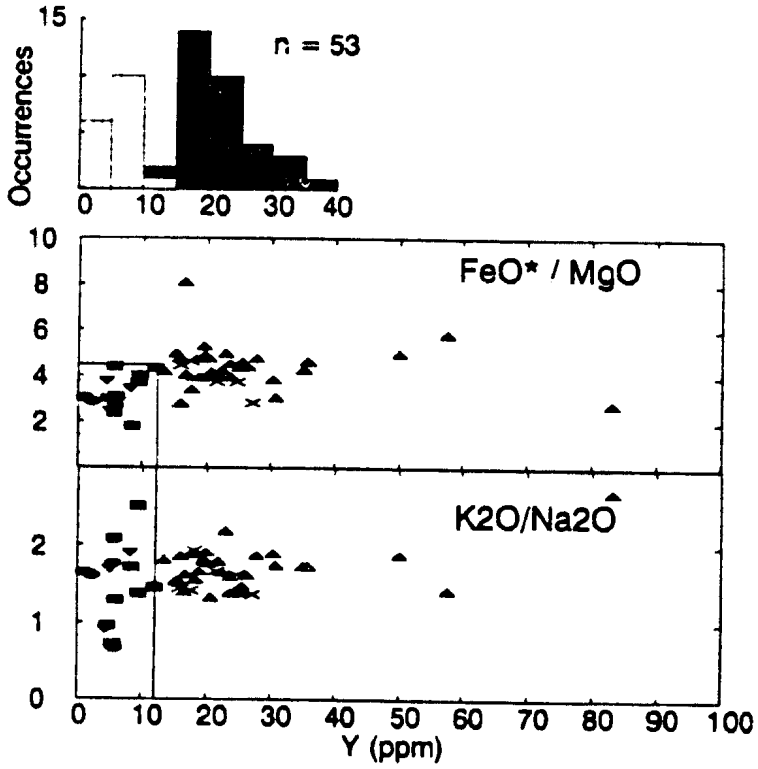

Figure 6.5. Subdivision of the Yamba Plutonic Suite into two groups on the basis of Y content.

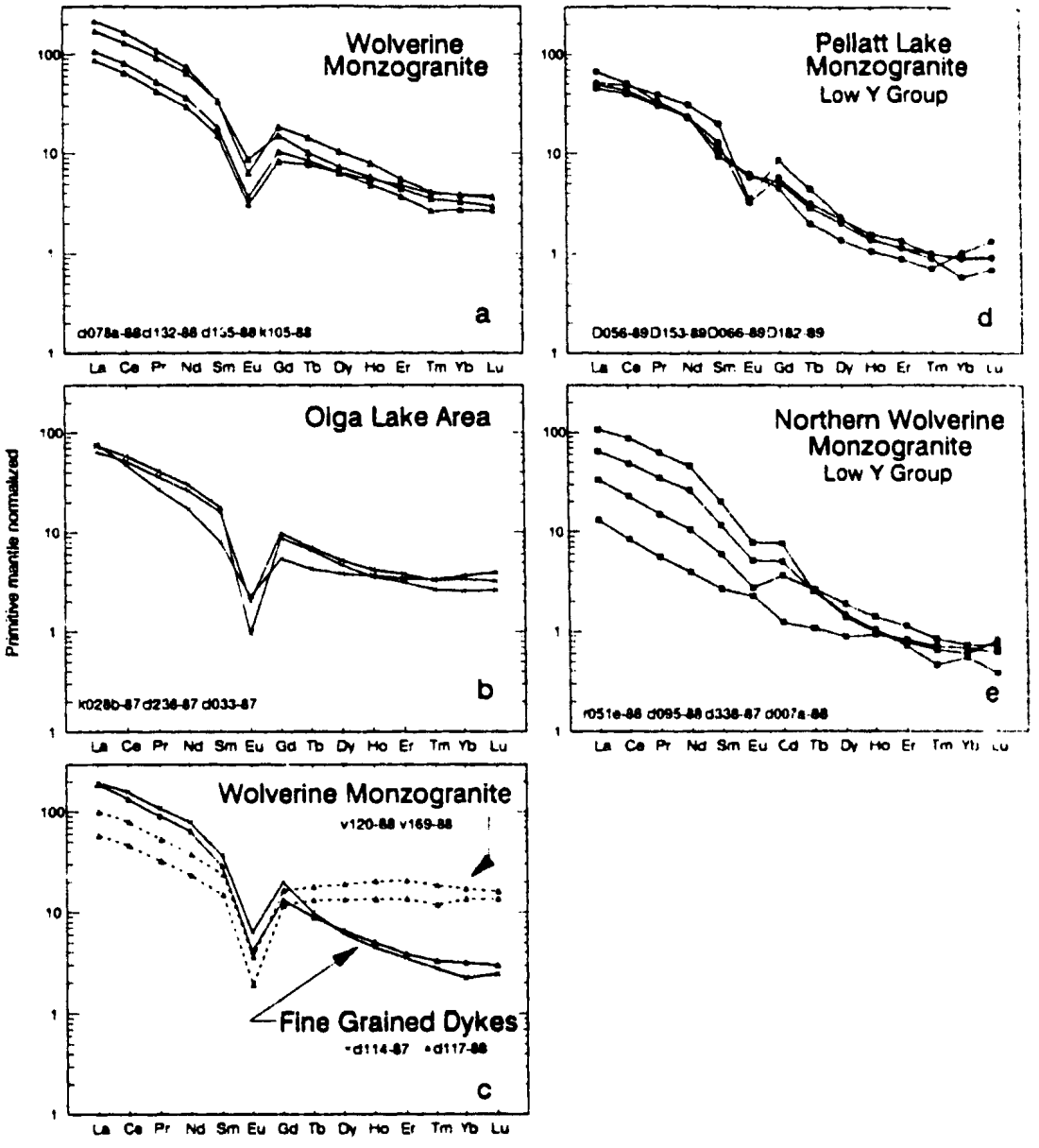

Figure 6.6. Primitive mantle normalized REE diagrams for the Yamba Suite. High Y group - a, b and c. Low Y group - d and e. a) typical Wolverine Monzogranite; b) Olga Lake area; c) fine grained dyke rocks, and high Y samples from the Wolverine Monzogranite; d) Pellatt Lake Monzogranite; e) northern margin Wolverine Monzogranite.

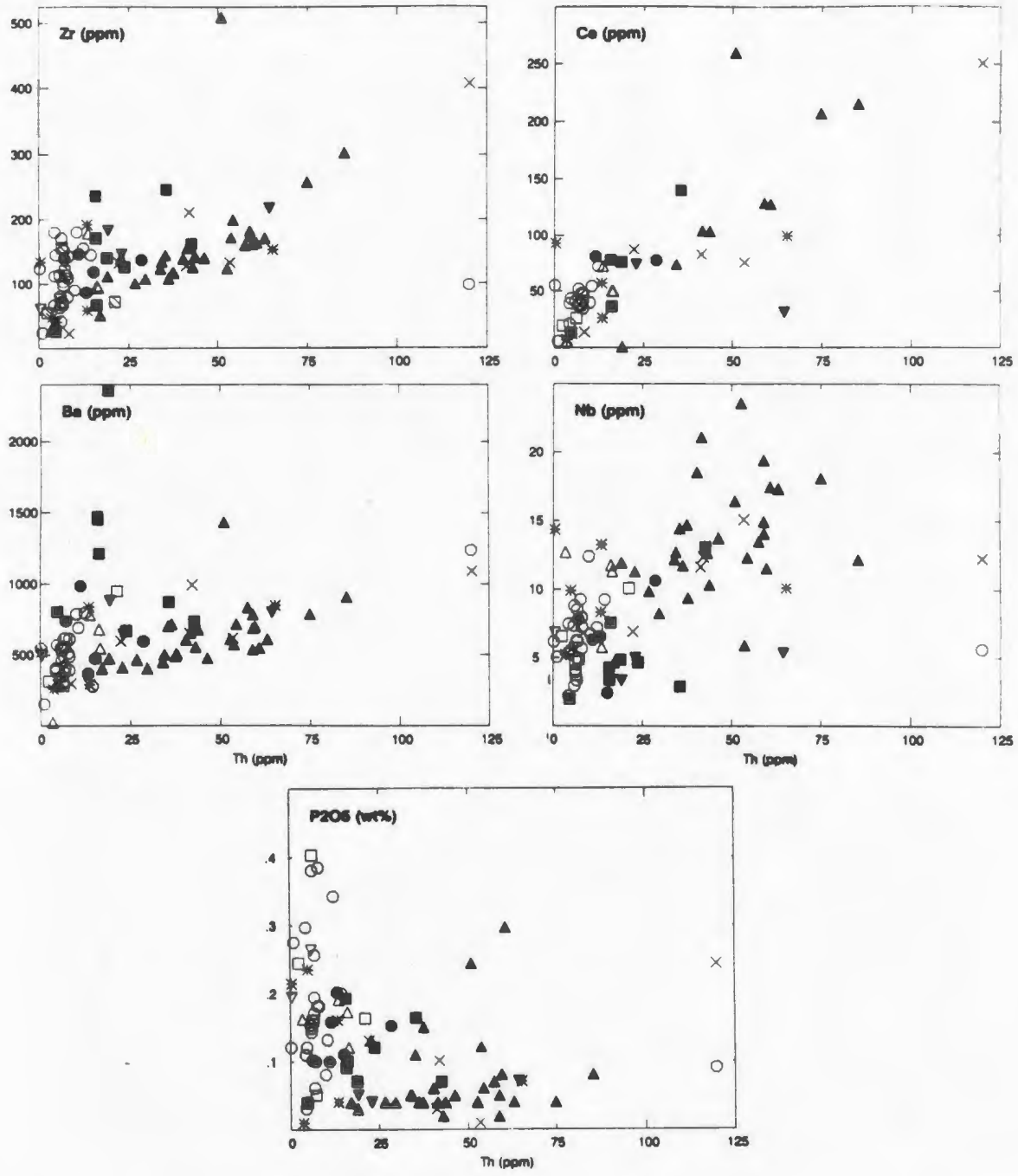

Figure 6.7. Variation of selected trace elements with Th. Symbols as in Figure 6.1.

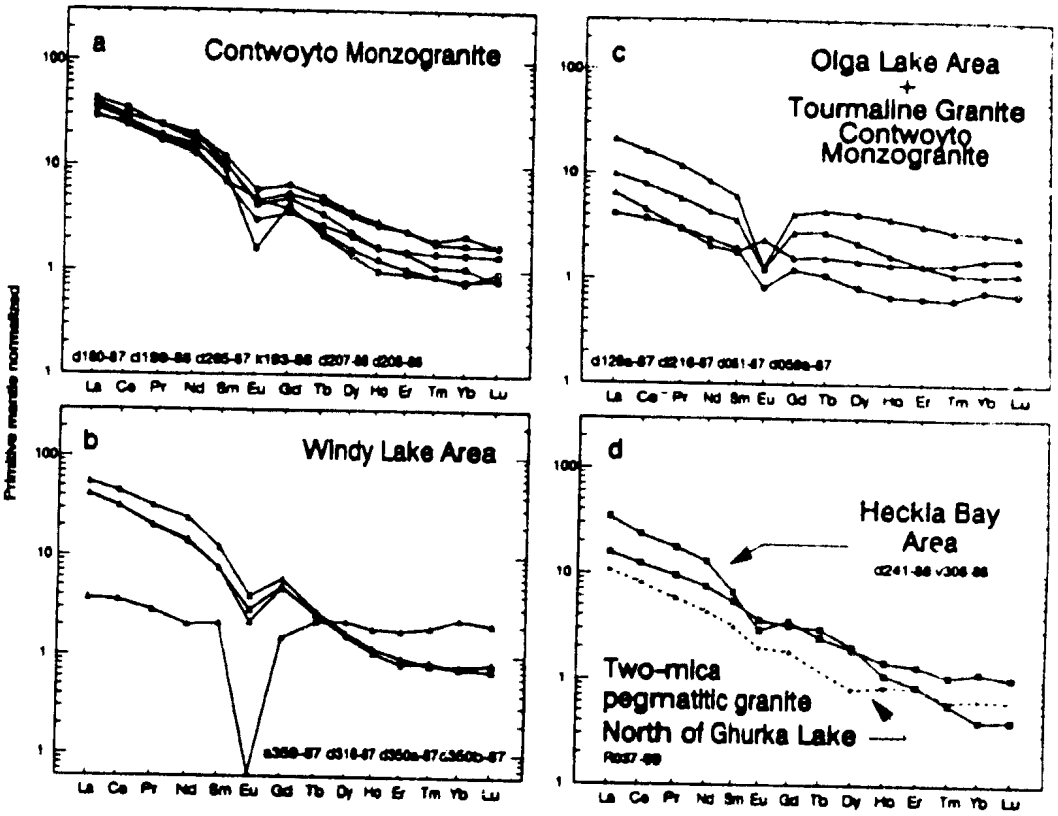

Figure 6.8. Primitive mantle normalized REE diagram for rocks of the Concession Plutonic Suite. a) Contwoyto Monzogranite; b) Windy Lake area; c) Olga Lake area and tourmaline granite from Contwoyto Monzogranite; d) Heckla Bay and north of Ghurka Lake areas.

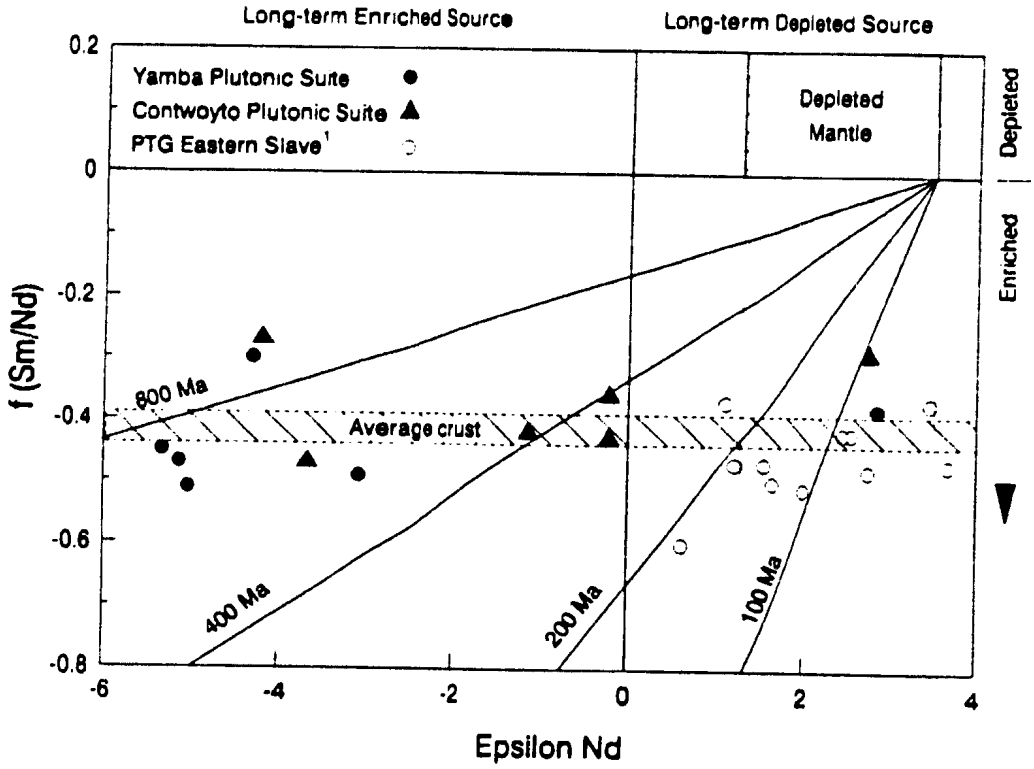

Figure 6.9. $\epsilon_{Nd(I)}$ *vs.* $f_{Sm/Nd}$ for rocks of the Contwoyto and Yamba Plutonic. $f_{Sm/Nd} = (^{147}Sm/^{144}Nd_{sample}/^{147}Sm/^{144}Nd_{CHUR})-1$ and reflects the degree of LREE-enrichment or depletion in the sample. Negative values are LREE-enriched relative to CHUR. See Figure 5.31 for a more detailed description. The time lines labelled 100, 200, 400 and 800 my assume a depleted mantle value of $\epsilon_{Nd(I)} = +3.5$. The hatched horizontal band represents estimated $f_{Sm/Nd}$ values of the continental crust (Taylor and McLennan, 1985). A crustal source with this $f_{Sm/Nd}$ value will rapidly evolve to more negative ϵ_{Nd} values. The most negative $\epsilon_{Nd(I)}$ values measured in the granites require crustal components which have had a long-term LREE pre-history of several hundred million years.

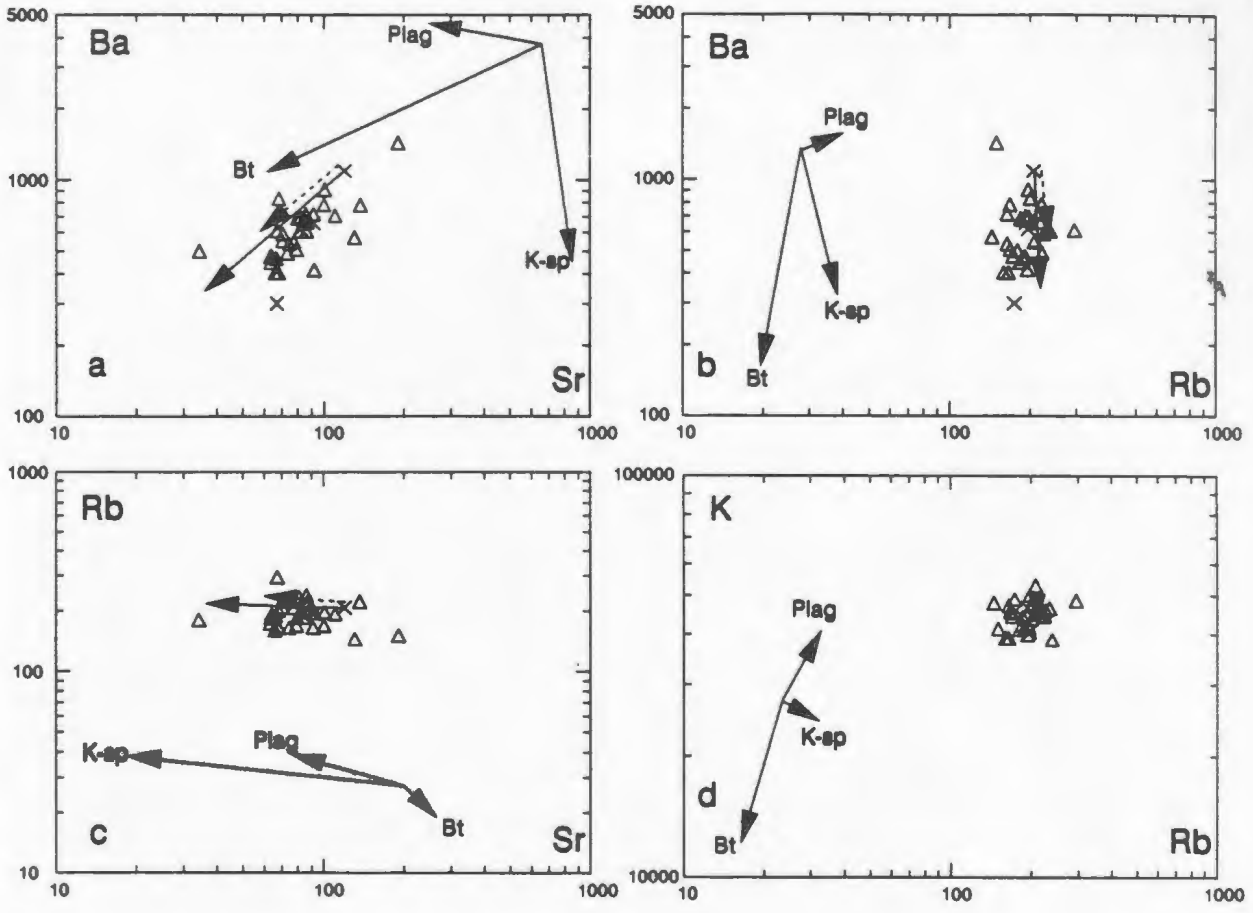

Figure 6.10. Variation diagrams of selected LFSE for the high Y group Yamba Plutonic Suite. a) Ba *vs.* Sr; b) Ba *vs.* Rb; c) Rb *vs.* Sr; d) K *vs.* Rb. Vectors labelled Bt, Plag, K-spar, show the effect of 25% fractional crystallization of biotite, plagioclase and alkali feldspar respectively (Kd values for felsic rocks, Appendix 4). The unlabelled vectors drawn through the data set are the calculated results of fractional crystallization (solid lines) and equilibrium crystallization (dashed lines) based on a fractionating assemblage determined by the major element least squares mixing solutions given in Table 6.5.

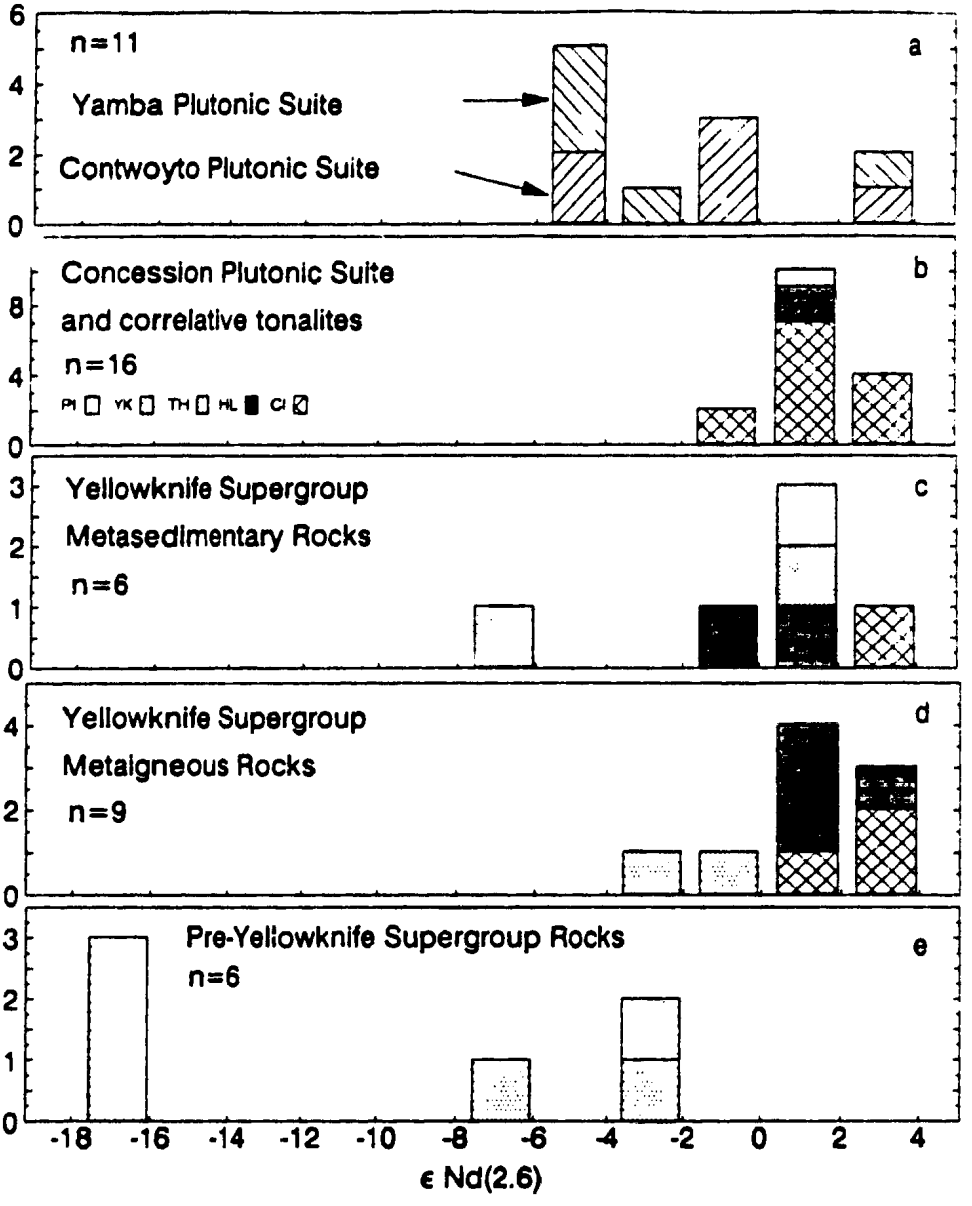

Figure 6.11. Frequency histograms of $\epsilon_{Nd(2.6\ Ga)}$ values rocks of the Concession and Yamba Suites and potential crustal protoliths to the granites. a) Concession and Yamba Plutonic Suites; b) Concession and Siege Plutonic Suites; c) Yellowknife Supergroup metasedimentary rocks; d) Yellowknife Supergroup metaigneous rocks, e) pre-Yellowknife Supergroup rocks. Data from Table 7.1; Dudas, 1989; Stevenson and Patchett, 1990; Bowring *et al.*, 1989. Fill patterns of bars in b through e are coded to geographical area: Point Lake (Pl); Yellowknife (Yk); Tinney Hills, northeast Slave (TH); Healey Lake, eastern Slave (HL); and Contwoyto Lake (Cl).

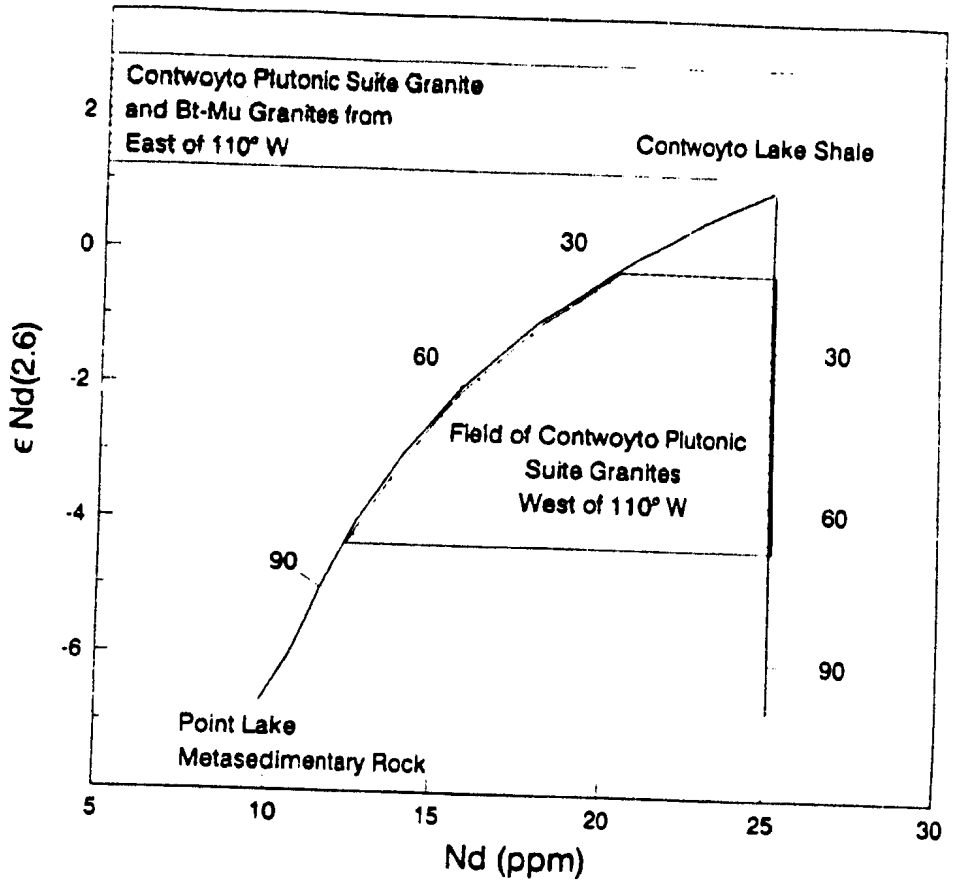

Figure 6.12. Example of two component mixing model to derive the range of $\epsilon_{Nd(I)}$ values observed in the Contwoyto Plutonic Suite. Both endmembers are assumed to be metasedimentary: the component with negative $\epsilon_{Nd(2.6)}$ used is sample D300-89, a pelite from Point Lake; the positive $\epsilon_{Nd(I)}$ is the average of 4 metasedimentary rocks from the Yellowknife Supergroup (Table 7.1). The range in compositions of the Contwoyto Suite shown refers only to ϵ Nd values not to Nd abundance.

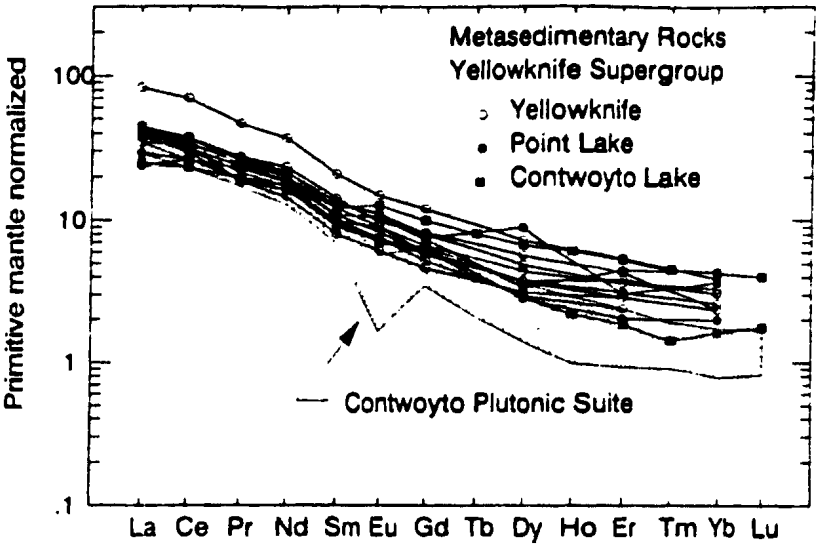

Figure 6.13. Primitive mantle normalized REE abundances of metasedimentary rocks from the Slave Province. Data for samples from the Contwoyto Lake area given in Appendix 2; Yellowknife data from Jenner *et al.* (1981); Point Lake data from Easton (1985). Stippled region shows the field of 'least fractionated' samples of the Contwoyto Monzogranite (Figure 6.8a)

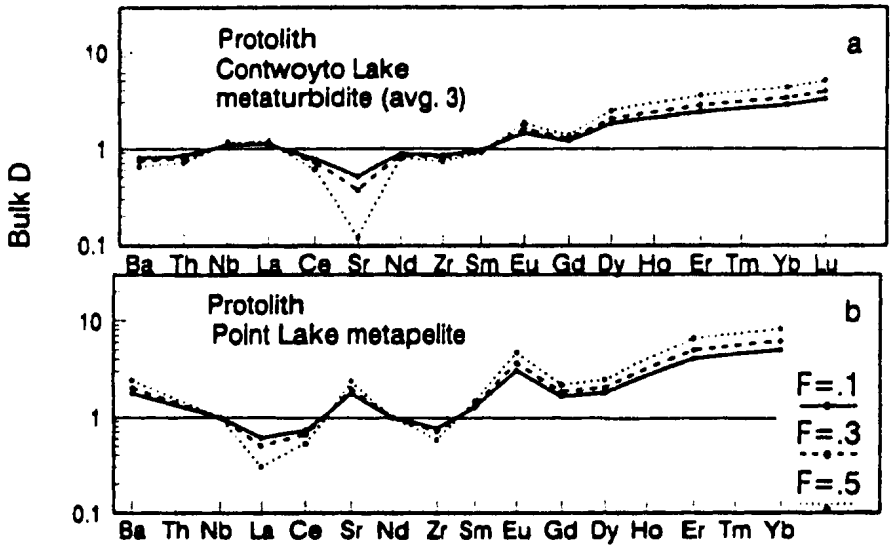

Figure 6.14. Bulk D values required in the source residuum to derive 'least fractionated' samples of the Contwoyto Monzogranite from Yellowknife Supergroup metasedimentary rocks. a) protolith composition taken to be average of three metaturbidite analyses, from 6 km southeast of the Contwoyto Monzogranite. b) protolith composition taken to be average of 3 Point Lake metasediments from Easton (1985).

Figure 6.15. (following page) Comparison of selected trace element contents of the Yamba Suite to rocks of the Concession Suite. Trend labelled AFC 1 indicates the within-suite variation described for the Concession Suite in Chapter 5. Yamba Suite rocks do not occur on this differention trend. Arrows (dashed and solid) labelled AFC Trend 2 are the results of quantitative AFC models (DePaolo, 1981) using the following parameters: assimilant composition (labelled A) taken to be a metasedimentary migmatite leucosome sample K022-88; Bulk D values as shown in upper right corners; ratio of assimilation to fractionation rate of 0.5 (dashed lines) and 1.5 (solid lines). Cross hatched field indicates samples of the low Y group.

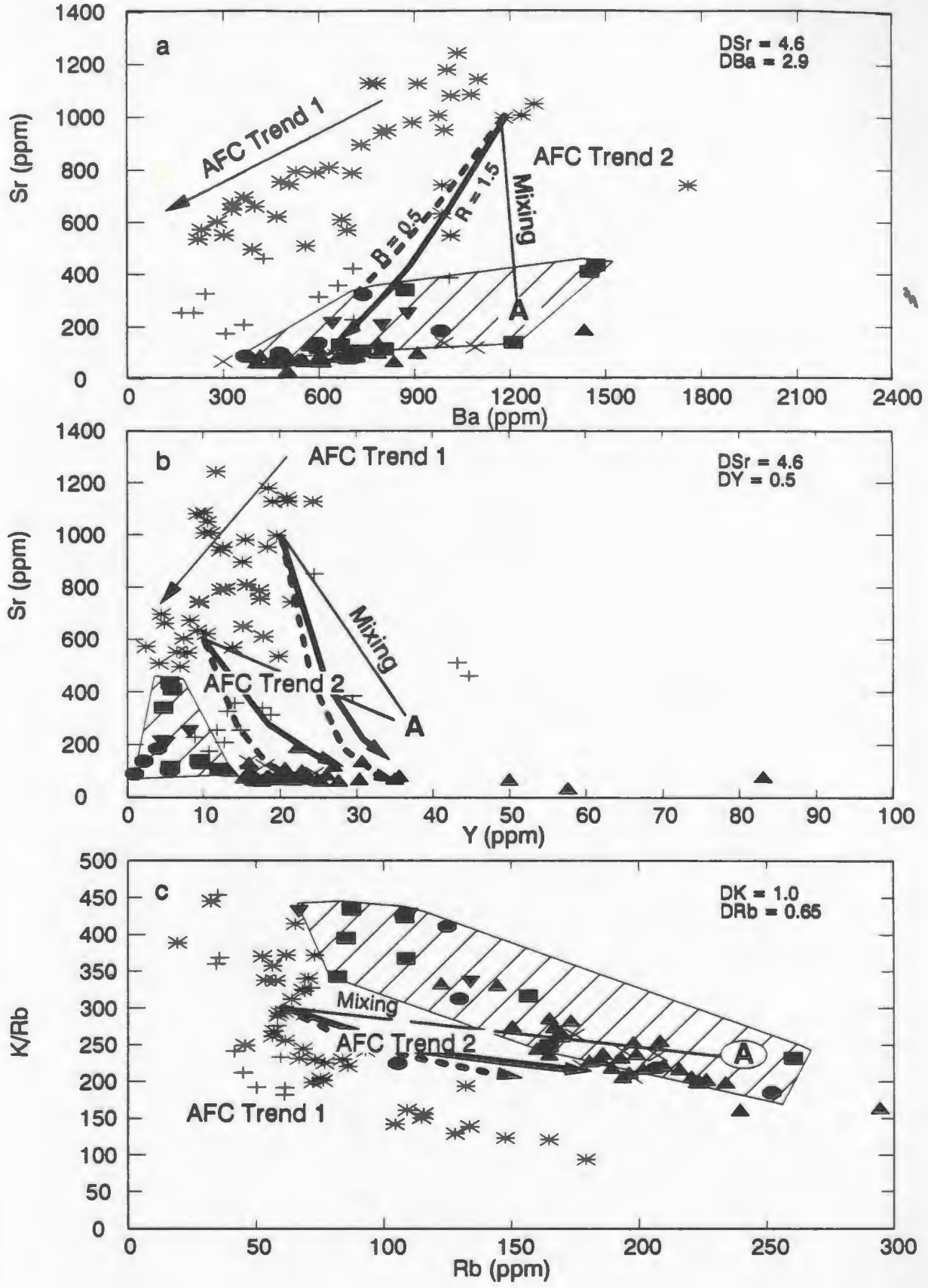
a
DSr = 4.6
DBa = 2.9
AFC Trend 1
AFC Trend 2
R = 1.5
B = 0.5
Mixing
A
Sr (ppm)
Ba (ppm)
b
AFC Trend 1
DSr = 4.6
DY = 0.5
Mixing
AFC Trend 2
A
Sr (ppm)
Y (ppm)
c
DK = 1.0
DRb = 0.65
Mixing
AFC Trend 2
A
AFC Trend 1
K/Rb
Rb (ppm)

Chapter 7

Nd Isotopic Evidence for the Tectonic Assembly of Late Archean Crust in the Slave Province

7.1 Introduction

The Late Archean is recognized as a major orogenic period in earth history during which up to 40% of the present mass of continental crust was formed (Taylor and McLennan, 1985). The processes by which Late Archean crust may have been stabilized, and possible similarities to tectonic evolution of Phanerozoic crust remain unresolved. Growth and stabilization of crust in Phanerozoic orogens dominantly occurs along continental margins during convergent plate interactions by: 1) the tectonic accretion of crustal terranes to a continent; and 2) syn- to post-deformation magmatism (underplating). Terrane accretion results in the structural juxtaposition of crustal rocks of different lithological, geochemical or chronological characteristics (Howell *et al.*, 1985) to form a new crustal segment. Addition of dominantly juvenile material to an older craton results in compositional zonation across strike of the orogenic belt, a feature which may subsequently be reflected in the isotopic and geochemical signatures of syn- to post-accretion granitoid rocks derived in part or entirely from these crustal sources. Granitoid rocks on the oceanic side of an orogen which has evolved in this fashion are generally more juvenile than those on the cratonic side; a feature interpreted to reflect differences in the age and nature of the crustal source (DePaolo, 1981; Farmer and DePaolo, 1983; Liew and McCulloch, 1985; Nelson and DePaolo, 1985; Kistler and Peterman, 1973).

If Late Archean cratons were formed by accretionary plate tectonic processes (*e.g.* Burke *et al.*, 1976; Windley, 1976; Condie, 1981; Kusky, 1989) then systematic variations in the isotopic signatures of granitoid rocks similar to those documented across younger orogens should also be expected. Although there is increasing evidence that some Archean granitoid rocks recycle older crust (Oversby, 1976; Gariepy and Allegre, 1985; Wooden and Mueller, 1988; Jahn *et al.*, 1984; Walker *et al.*, 1986), regionally

systematic isotopic variations in granitoid rocks similar to those described across Phanerozoic and Proterozoic accreted margins have not yet been documented. However, rather than indicating a fundamentally different tectonic process, this lack of isotopic variations (*e.g.* Shirey and Hanson, 1986) may only reflect the shorter crustal residence time or rarity of older continental rocks in the Late Archean (Taylor and McLennan, 1985; Chase and Patchett, 1988). Only those Late Archean orogens for which there is geological and isotopic evidence for the presence of significantly older crust provide an opportunity for identification of accretionary tectonic processes using the isotopic compositions of orogenic granitoid rocks.

In this chapter Sm-Nd isotopic data are presented which document orogen scale, Nd isotopic variations across the Slave Province that satisfy the specific predictions of accretionary tectonic models outlined above. The Slave Province is particularly well suited for isotopic tracer studies because the majority of geological units formed within a short orogenic period between 2.71 and 2.55 Ga, and geological (Stockwell, 1933; Baragar and McGlynn, 1976) and recent geochronological and isotopic studies have documented a significant Mid to Early (2.9 - 3.96 Ga.) Archean crustal history in the western part of the province (Bowring *et al.*, 1989a,b; Dudas, 1989; Henderson *et al.*, 1987, Frith *et al.*, 1986; Krogh and Gibbons, 1978; Nikic et al, 1980). The geology of the province thus provides for the isotopically distinct crustal rock types required to test tectonic models for Late Archean crustal growth using isotopic methods.

7.2 Tectonic Models Proposed For Development of the Slave Province

Tectonic models proposed for the development of the province can be subdivided into three hypotheses:

1) Intracratonic rifting (Henderson, 1981; 1985; Easton, 1985; Thompson, 1989).

2) Continent-continent collision (Fyson and Helmstaedt, 1988);

3) Island-arc microcontinent collision (Kusky, 1989);

All of the models recognize the existence of older cratonic blocks, however, the specific predictions about the nature of the crust beneath the Slave Province are clearly different (Figure 1.2). Intra-cratonic rift and continent-continent collision models require pre-2.7 Ga crust beneath the entire province, and argue for limited crustal growth. In contrast, island-arc microcontinent collision models predict pre-2.7 Ga crust in the western and accreted juvenile crust (2.7-2.65 Ga) in the eastern Slave.

7.3 Location and Description of Samples

The 57 rocks of this study include representative samples of all of the principal lithological units along a transect, sub-perpendicular to the dominant tectonic fabric of the Slave Province (Figure 7.1). Samples from the eastern and northeastern parts of the Slave Province were collected by Dr. J.B. Henderson (G.S.C.), and Dr P. Thompson (G.S.C.), respectively, and analyzed by Dr. E. Hegner (G.S.C., now at Universitat Tubingen). These samples are noted in the footnote to Table 7.1. The other samples were processed by the author.

A total of 43 granitoid rocks (ca 2625-2580 Ma) were analyzed, including 20 samples of syn-deformation and 23 samples of post-deformation granitoid rocks (Figure 7.1). Five of the syn-deformation samples analysed in this study have been previously dated (U-Pb zircon) between 2627 and 2595 Ma; six of the post-deformation samples have been dated (U-Pb zircon and monazite) between 2606 and 2585 Ma (van Breemen *et al.*, 1990; van Breemen and Henderson, 1988; van Breemen *et al.*, 1987a,b; Henderson *et al.*, 1987).

Metavolcanic and syn-volcanic plutonic rocks are from the Central Volcanic Belt (CVB) in the central, and the Back River (BR), Clinton-Colden (CC) and Healey Lake (HL) areas in the eastern Slave Province (Figure 7.1). Dated samples range in age from 2692 to 2650 Ga (U-Pb zircon; Mortenson *et al.*, 1988; van Breemen et al, 1989; van Breemen *et al.*, 1987a; Frith and Loveridge, 1982). Ages of undated samples are constrained by the ages of geographically associated rocks. Uncertainties in the ages of the undated samples are considered to be less than 20 m.y.

Five samples of turbiditic shales and psammites from Point Lake (western Slave), Contwoyto Lake (central Slave), Healey Lake (eastern Slave) and Tinney Hills (north eastern Slave) were analyzed (Figure 7.1). All of the samples are biotite- or chlorite-grade, fine grained pelitic and psammitic turbidites. Sample 45 is a composite sample made up of 10 samples. The depositional age of the sedimentary rocks is considered to be younger than the associated volcanic rocks (ca. 2692-2650) and older than the intruding syn-deformation plutonic rocks (ca. 2630-2600). An age of 2650 Ma is assumed in the calculations below.

Samples of pre-YKS rocks include: 1) the Augustus Granite (3.155 Ga, Krogh and Gibbons, 1978), notable as basement to the well exposed, Late Archean Point Lake unconformity (Stockwell, 1933; Barager and McGlynn, 1976); and 2) a tonalitic gneiss from the Acasta Gneiss (ca. 3.60-3.96, Bowring *et al.*, 1989a,b).

Analytical techniques and the Nd notation used are presented in Appendix 3.

7.4 Results

Sm-Nd isotopic analyses are listed in Table 7.1. Initial $^{143}Nd/^{144}Nd$ ratios were calculated using the measured U-Pb zircon age, or the following inferred age of samples: 2650 Ma for sedimentary rocks; 2610 Ma for syn-deformation and 2590 Ma for post-deformation granitoids. Estimated errors of less than 30 m.y. associated with these ages are insignificant for the purposes of this study. Initial epsilon Nd values, ($\varepsilon_{Nd(I)}$), were calculated using the following reference values for CHUR: $^{143}Nd/^{144}Nd = .512638$; $^{147}Sm/^{143}Nd = 0.1967$. ε_{Nd} values calculated at any time other than the age of consolidation are designated by a subscript, in which the age used for the calculation is given in Ga.

The $\varepsilon_{Nd(I)}$ values are presented in Figure 7.2. Included in Figure 7.2 for reference are the depleted mantle (DM) evolution line of Goldstein and O'Nions (1984). Nd model ages using their parameters yielded a better agreement with the U-Pb ages, whereas those calculated with the model of DePaolo (1988) were in many cases

Table 7.1. Sm-Nd Isotopic Data

	Sample	Rock Type	Lat	Long	Nd[b] (ppm)	Sm[b] (ppm)	$^{147}Sm/^{144}Nd$[c]	$^{143}Nd/^{144}Nd$[d]	$\epsilon_{Nd(t)}$[e]	Age[f] (Ma)	T_{DM} (Ga)
Post-deformation Granitoid Rocks											
1	D197-89	Bt-Mu Granite	65° 07'	107° 18'	61.92	11.91	0.1041	0.511245	3.7	2590	2640
2	Thol 32	Bt-Mu Granite	66° 40'	107° 11'	22.04	4.49	0.1231	0.511559	3.5	2590	2655
3	D153-89	Bt Granite	65° 10'	109° 44'	45.47	9.16	0.1218	0.511508	2.9	2590	2697
4	R037-89	Bt-Mu Granite	65° 14'	109° 12'	4.62	1.07	0.1397	0.511808	2.8	2590	2705
5	Art 100	Artillery Lake Granite	63° 22'	107° 54'	30.79	5.22	0.1024	0.511167	2.8	2596	2710
6	Thel 14	Bt-Mu Granite	64° 05'	107° 17'	41.24	7.82	0.1146	0.511366	2.6	2590	2724
7	Art 113	Bt-Mu Granite	63° 35'	107° 43'	12.40	2.35	0.1144	0.511351	2.5	2606	2742
8	Thel 19	Bt-Mu Granite	64° 14'	107° 52'	28.16	4.50	0.09651	0.511029	2.0	2590	2765
9	Art-142	Smart Gneiss Migmatite	63° 45'	106° 32'	98.40	15.88	0.09751	0.511023	1.6	2590	2798
10	Art 82	Musclow Granite	63° 49'	106° 52'	39.71	6.88	0.1047	0.511136	1.5	2603	2812
11	Thol 43	Bt-Mu Granite	66° 53'	107° 08'	22.32	3.84	0.1040	0.511121	1.2	2585[1]	2817
12	Thel 13	Megacryst. Granodiorite	64° 03'	107° 16'	20.94	4.30	0.1241	0.511452	1.1	2595	2836
13	Thol 24	Granitoid Migmatite	66° 59'	106° 28'	21.08	2.71	0.0778	0.510636	0.6	2590	2871
14	D199-88	Bt Mu Granite	65° 52'	111° 38'	22.61	4.13	0.1131	0.511202	-0.2	2590	2925
15	D207-88	Bt Mu Granite	65° 49'	111° 14'	23.98	4.71	0.1258	0.511415	-0.2	2590	2931
16	K193-88	Bt Mu Granite	65° 49'	111° 25'	15.08	2.72	0.1140	0.511170	-1.1	2585[1]	2992
17	D224-88	Bt Granite	65° 27'	112° 25'			0.1002	0.510833	-3.1	2590	3139
18	D078a-88	Bt Granite	65° 11'	111° 37'	44.09	7.26	0.1060	0.510858	-4.6	2582[1]	3181
19	D216-87	Bt Mu Granite	65° 28'	111° 40'	10.15	2.43	0.1434	0.511515	-4.2	2585	3220
20	D295-88	Bt Mu Granite	65° 53'	110° 38'	12.74	2.80	0.1374	0.511410	-4.3	2580	3222
21	D238-87	Bt Granite	65° 30'	112° 05'	19.52	3.11	0.0970	0.510682	-5.0	2590	3280
22	D135-88	Bt Granite	65° 05'	111° 39'	44.09	7.26	0.1048	0.510807	-5.1	2590	3292
23	D220-88	Bt Granite	65° 22'	113° 17'	35.13	6.72	0.1075	0.510842	-5.3	2590	3307
Syn-deformation Granitoid Rocks											
24	D119-88	Bt Qtz Diorite	65° 03'	111° 08'	52.60	10.07	0.1100	0.511285	2.7	2610	2728
25	D253-88	Hb Bt Diorite	65° 16'	109° 58'	56.39	9.45	0.1040	0.511165	2.4	2610	2752
26	D152B-87	Hb Bt Diorite	65° 43'	111° 44'	56.70	11.06	0.1172	0.511382	2.2	2610	2767
27	D201A-87	Hb-Bt Tonalite	65° 43'	111° 40'	32.16	5.41	0.1019	0.511118	2.2	2610	2769
28	D172b-87	Bt Tonalite	65° 40'	111° 31'	34.78	7.97	0.1368	0.511713	2.1	2610	2776
29	D278-88	Hb-Bt Diorite	65° 19'	110° 07'	55.54	11.44	0.1264	0.511529	2.0	2610	2783
30	Thel 15	Bt-Hb Tonalite	64° 04'	107° 49'	24.82	4.21	0.1026	0.511105	1.8	2616[2]	2804
31	Art 21	Bt-Hb Tonalite	64° 50'	107° 31'	35.48	6.59	0.1123	0.511260	1.6	2622[2]	2822
32	Thel 18	Bt-Hb Tonalite	64° 13'	107° 46'	24.08	4.63	0.1162	0.511324	1.5	2620	2827
33	Thol 23	Bt-Hb Tonalite	66° 51'	106° 35'	35.13	6.12	0.1053	0.511136	1.4	2610	2827

34	D217-87	Bt Trondhjemite	65° 22'	111° 40'	4.98	0.86	0.1114	0.511226	1.1	2610	2849
35	D218-87	Hb-Bt Qtz Diorite	65° 26'	111° 51'	54.89	9.22	0.1045	0.511099	0.9	2607[1]	2860
36	D110-88	Bt Tonalite	65° 13'	111° 41'	41.21	6.22	0.0877*	0.510809	0.9	2608[1]	2862
37	D121a-88	Bt Qtz Diorite	66° 02'	111° 07'	67.45	9.70	0.09079	0.510851	0.7	2610	2878
38	D044-87	Bt Trondhjemite	65° 24'	111° 45'	1.51	0.38	0.1382	0.511634	0.1	2610	2926
39	D172-87	Bt Tonalite	65° 40'	111° 24'	25.27	5.32	0.1304*	0.511494	-0.1	2610	2934
40	D222-88	Bt-Hb Granodiorite	65° 04'	113° 03'	38.19	6.38	0.1019	0.510933	-1.0	2645	3033
41	D218-88	Bt-Hb Granodiorite	65° 21'	113° 37'	66.87	11.63	0.1091*	0.510966	-3.2	2610	3168
42	D219-88	Bt-Hb Granodiorite	65° 21'	113° 36'	53.65	7.29	0.08688	0.510511	-4.6	2610	3273
Yellowknife Supergroup Sedimentary Rocks											
43	D269-89	Contwoyto L Shale	65° 43'	111° 10'	39.33	6.87	0.1056	0.511251	4.0	2650	2666
44	Thel 16	Yellowknife SuperGr.	64° 03'	107° 40'	30.68	5.50	0.1084	0.511184	1.8	2650	2834
45	Art 34	Yellowknife Psammite	63° 53'	107° 26'	24.82	4.25	0.1034	0.511055	0.9	2650	2894
46	T2P 84-375	Yellowknife Shale	Tinney	Hills	31.40	5.64	0.1086	0.511113	0.3	2650	2942
47	D300-89	Point Lake Shale	65° 22'	113° 03'	9.81	2.23	0.1373	0.511276	6.4	2650[1]	3432
Yellowknife Supergroup Volcanic and Syn-Volcanic Plutonic Rocks											
48	Thel 21	Healy Complex	64° 22'	106° 51'	32.07	6.21	0.1171	0.511414	3.6	2675[1]	2723
49	D072b-87	Bt Tonalite	65° 28'	111° 46'	18.18	2.58	0.08268	0.510822	3.5	2650[1]	2707
50	Art-112	Healy Complex Granite	64° 34'	107° 29'	12.26	1.62	0.07968	0.510683	2.2	2679[4]	2824
51	HBA V 20	Healy Complex	64° 22'	106° 53'	21.55	4.27	0.1197	0.511362	1.7	2679[2]	2865
52	D072a-87	Bt Tonalite	65° 28'	111° 46'	5.16	0.80	0.0972	0.510955	1.1	2650	2882
53	Art 130	Rhyolite	63° 56'	107° 20'	23.84	4.14	0.1051	0.511202	3.5	2671[4]	2723
54	D054b-87	Gabbro	65° 29'	111° 48'	16.03	3.5	0.1262	0.511552	3.1	2670	2754
55	77-L1269	Back River Basalt	65° 05'	108° 18'	10.29	3.32	0.1949	0.512669	1.2	2692	2908
Pre-Yellowknife Supergroup Rocks											
56	HBA 673 3	Augustus Granite	65° 14'	113° 04'	77.27	14.55	0.1138	0.511082	3.4	3155[5]	3137
57	D215 88	Acasta Gneiss	65° .5	115° 36'	45.09	5.12	0.06863	0.50954	0.9	3600	3826

[a] Samples 1-13, 30-33, 43-48, 50-51, 53, 55-57 chemistry done at G.S.C. All other samples done at Memorial University

[b] Nd and Sm concentration data for samples analyzed at Memorial University determined by ICP-MS (5% error). Data from GSC determined by isotope dilution (1% error)

[c] Samples analysed at GSC (0.5% error); at Memorial (1% error). Values marked with asterix (*) determined by ICP MS at Memorial (3% error).

[d] Internal precision (2 SEM) is better than external precision of $2*10^{-5}$.
Ratios are normalized to $^{146}Nd/^{144}Nd = .7219$ $^{143}Nd/^{144}N = .511862 \pm 19$ for La Jolla during period of study. All samples analysed at G.S.C.

[e] $\varepsilon_{Nd(t)} = [(^{143}Nd/^{144}Nd_{(Sample)}/^{143}Nd/^{144}Nd_{(t)\ Bulk\ Earth}) - 1] * 10^4$ where (t) = age of sample. Present day values, Bulk Earth, $^{143}Nd/^{144}N = .512638$; $^{147}Sm/^{144}Nd = .1967$.

[f] Published U-Pb zircon or monazite ages are designated by superscripts as follows [1] van Breemen et al., 1990; [2] van Breemen et al., 1987a; [3] Mortenson et al., 1988; [4] Krogh and Gibbons, 1978; [5] van Breemen et al., 1987b. Ages for other samples are estimated values discussed in text.

younger than the crystallization age of the rocks. A field enclosing the $\varepsilon_{Nd(t)}$ evolution trend of previously published basement samples from the western Slave Province (Dudas, 1989; Bowring et al.,1989a) is also shown.

The geographical variation of depleted mantle model ages (T_{DM}) are shown in Figure 7.3. T_{DM} values were calculated by projecting from the initial $^{143}Nd/^{144}Nd$ of a sample along an evolution line of typical crustal $^{147}Sm/^{144}Nd$ (.1100) to intersect the evolution line of depleted mantle. It is therefore linearly correlated to $\varepsilon_{Nd(t)}$ values.

7.4.1 Pre-Yellowknife Supergroup Rocks

The Augustus granite (3.155 Ga; Krogh and Gibbons; 1978) yields an $\varepsilon_{Nd(t)}$ value of +3.4, indicating a time-integrated depleted source. The U-Pb zircon age and a T_{DM} age of ca. 3.1 for this sample are virtually identical (Table 7.1), suggesting a juvenile composition of the pluton. A sample from the 3.6 to 3.96 Ga Acasta Gneiss (Bowring et al., 1989a,b) has a depleted mantle model age of 3.83 Ga. This is similar to the Nd isotopic data reported for two other samples of the Acasta Gneiss by Bowring et al., (1989a).

In addition to the data for Pre-YKS rocks presented here, Dudas (1989) reports $\varepsilon_{Nd(t=2.6)}$ values of -2 to -7.0 for the ca. 2.9 Ga Sleepy Dragon Complex in the southwestern part of the Slave Province (Figure 1.3).

Pre-YKS rocks would have evolved to distinctly negative $\varepsilon_{Nd(t=2.6)}$ values of -2.6 to -17, and recycling of this older crust should be detectable in the isotopic composition of rocks produced during the 2.7 to 2.6 orogenic event.

7.4.2 Yellowknife Supergroup - Volcanic Rocks

Initial ε_{Nd} values for volcanic and syn-volcanic rocks range from +1.2 to +3.6 indicating time-integrated depleted sources. The range of values is similar to estimates of Late Archean depleted mantle (Shirey and Hanson, 1986; Smith and Ludden, 1988). Volcanic rocks thus represent dominantly mantle additions to the crust at ca. 2670-2650 Ma.

There is no apparent correlation of $\varepsilon_{Nd(t)}$ with rock composition, nor is there a difference between samples from the central and eastern Slave. The $\varepsilon_{Nd(t)}$ values for intermediate and felsic volcanic and related plutonic rocks range from +1.7 to +3.6, and are similar to those in metabasaltic rocks ($\varepsilon_{Nd(t)}$ +1.2 and +3.5). Production of rhyolites and synvolcanic tonalites with similar $\varepsilon_{Nd(t)}$ values to associated meta-basalts suggests rapid recycling of mafic to intermediate crust (*e.g.* Shirey and Hanson, 1986; Chauvel *et al.*, 1986).

The Nd isotopic data for the YKS volcanic rocks of this study, however, contrast with those for metabasaltic rocks from the Yellowknife Belt in the southwestestern Slave Province which range from -0.4 to -2.1 (Dudas, 1989). These volcanic rocks may have interacted with a crustal reservoir during their evolution, an interpretation consistent with the ensialic back-arc basin model proposed for the Yellowknife Belt by Helmstaedt and Padgham (1986). The isotopic differences between volcanic rocks from the southwestern, central and eastern parts of the province suggest evolution in different settings, continentally influenced in the southwestern and dominantly oceanic in the central and eastern belts.

7.4.3 Yellowknife Supergroup - Sedimentary Rocks

Nd isotopic compositions of fine grained metasedimentary rocks are considered to reflect the integrated isotopic composition of the source region or provenance area for the sediment. Distinctly positive $\varepsilon_{Nd(t)}$ values of sedimentary rocks (+0.3 to +4.0) in the eastern and central Slave suggests a provenance area dominated by juvenile crust. In contrast, a single sample from the western part of the province has an $\varepsilon_{Nd(t)}$ value of -6.4, indicating a component of older crust in this sample.

The positive values of the samples from the central and eastern areas overlap, but extend to slightly lower values than associated volcanic sequences. The volcanic rocks are considered to be the most likely sources for the sediments. This is consistent with previous interpretations based on detrital grain studies (McGlynn and Henderson, 1970; Henderson, 1981) and trace element geochemistry (Jenner et al., 1981). The Nd data alone cannot, however, completely eliminate the possibility that a small component of

older crust is present within these sediments. For example, a simple binary mixing calculation which assumes the average $\varepsilon_{Nd(I)}$ and Nd abundance of the volcanic rocks to be typical of the dominant sedimentary source material, allows for up to 15 wt% of an old crustal component ($\varepsilon_{Nd(I)}$ -5, Nd=30 ppm) in some of the sediments. This possibility may be resolved by single grain detrital zircon studies.

A shale sample from Point Lake, in the western Slave Province, with an $\varepsilon_{Nd(I)}$ value of -6.4, is clearly derived from different source rocks or different proportions of similar source rocks than the other analyzed Yellowknife Supergroup sediments. The Point Lake shale is the westernmost and only sample of the YKS analyzed in this study which can be documented to presently overlie older, pre-YKS rocks (Henderson, 1985), although presently in tectonic contact (Hoffman, 1989; Kusky, 1990). The $\varepsilon_{Nd(I)}$ value of this sample falls within the range of values characteristic of pre-YKS rocks and it may be partly derived from the older crustal rocks located in the western Slave Province. Schärer and Allègre (1982) reported detrital, single grain zircon $^{207}Pb/^{206}Pb$ ages ranging from 2630 to a minimum of 3130 Ma for a sedimentary rock sample from the same area as D300-87. The majority of zircon grains gave $^{207}Pb/^{206}Pb$ ages of 2630 to 2700 Ma, approximately coincident with the time of major volcanic activity throughout the Slave Province.

If this sedimentary rock contains significant ca. 2670 Ma material, as the detrital zircon ages suggest (Schärer and Allègre, 1982), and if this material has $\varepsilon_{Nd(I)}$ values similar to other volcanic rocks in the Slave Province (-2 to +3.6; this paper, Dudas, 1989) then the average $\varepsilon_{Nd(I=2.6)}$ for the older component must be significantly more negative than the value of -6.4 determined for the sample. Assuming an average crustal $^{147}Sm/^{144}Nd$ ratio for this material requires a depleted mantle model age exceeding 3400 Ma. The only rocks presently known to meet this requirement are the Acasta gneisses (Bowring *et al.*, 1989a,b).

7.4.4 Late Archean Granitoid Rocks

Figures 7.2 and 4 show the $\varepsilon_{Nd(I)}$ values of the syn- and post-deformation plutonic rocks from across the province. East of 110°30' W, both the syn- and post-deformation granitoid rocks have positive $\varepsilon_{Nd(I)}$ within a restricted range from +0.6 to +3.6.and T_{DM} ages within 0 to 250 m.y. of the crystallization age (Figures 7.3 and 7.4). In contrast, granitoid rocks from the western Slave Province include negative values and exhibit a much larger range from +2.7 to -5.3, suggesting involvement of a significantly older crustal component(s).

7.5 Origin of the Isotopic Variations in the Granitoid Rocks

7.5.1 Syn-deformation Granitoids

The syn-deformation, dominantly low-K granitoid rocks have been interpreted to be related to mantle-derived andesitic magmas through assimilation fractional crystallization processes (Hill and Frith, 1982; Davis et al., 1990). Syn-deformation granitoids in the eastern Slave Province with positive $\varepsilon_{Nd(I)}$ values would have assimilated crustal rocks with Nd isotopic compositions similar to their source mantle values and little shift in composition would occur. They represent new mantle-derived additions and recycling of recent crustal additions.

Syn-deformation granitoids between 112° and 110° 30'W have juvenile $\varepsilon Nd_{(I)}$ similar to their host supracrustal rocks, and to the syn-deformation rocks to the east. This is true in spite of the fact that the slightly younger post-deformation granitoids in the same area have negative $\varepsilon Nd_{(I)}$ values (Figures 7.2 and 7.4). The syn-deformation rocks in this part of the province are unlikely to have significantly interacted with older crust.

Samples of syn-deformation granitoids from the Point Lake area, western Slave, have $\varepsilon_{Nd(I)}$ ranging from -4.6 to -1.0, and clearly contain a component derived from a long-term enriched reservoir. They are also more SiO_2 and K_2O-rich than the juvenile syn-deformation plutons suggesting extensive crustal assimilation. To produce the negative $\varepsilon_{Nd(I)}$ values by crust-mantle mixing, requires a crustal component with an $\varepsilon_{Nd(t=2.6)}$ value significantly less than the granitoid itself. An example of a binary mixing

calculation, assuming one endmember characterized by a typical syn-deformation quartz diorite ($\varepsilon_{Nd(T)}$ = +3.0) and a hypothetical crustal endmember is shown in Figure 7.5. The composition of the crustal component in this example is very poorly defined, but regardless of its $\varepsilon_{Nd(T)}$ value, any viable mixing model requires the involvement of a large percentage (>30%) of significantly older crust. This is particularly true given the high Nd contents (>50 ppm) of the syn-deformation diorites (Table 7.1). This suggests the presence of an older crustal reservoir beneath the western Slave Province.

The change in isotopic composition observed in the syn-deformation plutonic rocks suggests increasing contamination of mantle-derived magmas by older crustal rocks from east to west across the Slave Province. The extent of contamination of magma within the crust depends, amongst many things, on the thickness of the crust through which the magma is intruded (Huppert and Sparks, 1986; Hildreth and Moorbath, 1988). The greater extent of contamination of the early plutonic suite at Point Lake may reflect a greater thickness of pre-YKS continental crust at Point Lake, than beneath the central part of the province. Such a geometry could account for the diminishing evidence of crustal interaction towards the east in the syn-deformation suite. More detailed work is required to evaluate this hypothesis.

7.5.2 Post-deformation Granitoids

Post-deformation granites in the eastern Slave Province have $\varepsilon_{Nd(t)}$ values which fall within the range of values determined for metasedimentary and metavolcanic rocks from the eastern parts of the province (Figure 7.2 and 4). The composition and mineral assemblage of these granitoids are consistent with a dominantly crustal origin and the granitoids can be modelled as partial melts of the supracrustal rocks (e.g. Frith and Fryer, 1985). The involvement of an additional component (i.e. depleted mantle) is likely for some of these plutons (see Chapter 6), but is not required by the Nd isotopic data.

Post-deformation granites west of 110° 30'W, require a substantial proportion of isotopically evolved crustal component in their protoliths in order to account for the very negative $\varepsilon_{Nd(T)}$ values (-0.2 to -5.3). Figure 7.4 shows that most of these granites overlap but are concentrated at the higher end of the spectrum of $\varepsilon_{Nd(t=2.6)}$ values of the pre-YKS

rocks from the western part of the province. Also overlapping these values is the shale sample from Point Lake ($\varepsilon_{Nd(t=2.6)}$ = -6.7). The isotopic data can be interpreted in one or more of the following ways: 1) granites are derived entirely from pre-YKS crustal rocks with an average ε_{Nd} value of -3 to-5 (i.e. Sleepy Dragon Complex, -2.6 to -7, Dudas, 1989; Augustus Granite, -2.6, Table 7.1); 2) granites represent variable mixtures of pre-YKS rocks, including extremely evolved rocks such as the Acasta Gneisses, juvenile YKS rocks and depleted mantle; 3) granites are partial melts of sedimentary rocks derived from the pre-YKS rocks (*ie*. similar to the Point Lake shale). The latter possibility is difficult to constrain because the full lateral extent of sediments with these negative $\varepsilon_{Nd(t)}$ values is unconstrained. In any case, old crustal rocks have been extensively recycled during the Late Archean orogeny.

The data provide evidence that plutonism in the eastern Slave Province involved both new crustal addition from the mantle and extensive and rapid recycling of juvenile crust. In this respect, it is similar to plutonism in other Late Archean terranes where crustal recycling is difficult to detect owing to the juvenile characteristics of the crust (e.g. Shirey and Hanson, 1986). In the western Slave, recycling of older crust is required, as is commonly observed in Phanerozoic batholiths.

7.6 Tectonic Implications

The regionally systematic change in $\varepsilon_{Nd(t)}$ values of granitic rocks across the central Slave Province suggests that the mid to lower crust is composite, with ca. 2.7 Ga juvenile crust beneath the eastern and older (> 3.0 Ga) continental crust beneath the western parts of the province (Figure 7.4b). This pattern is consistent with the previously established asymmetry of surface exposures of pre-2.8 Ga continental rocks (Kusky, 1989; Padgham, 1981) and is analogous to isotopic patterns observed across Phanerozoic convergent continental margins. The Nd data support the general applicability of models involving development of the province by collision and tectonic accretion of rocks of dominantly oceanic affinity (e.g island arcs, back arc basin, juvenile sedimentary rocks), represented by rocks of the YK Supergroup, to a continental nuclei represented by the scattered exposures of Mid and Early Archean rocks in the western Slave Province (Kusky, 1989;

Hoffman, 1986). There is no evidence to suggest that older crust existed beneath the entire Slave province prior to 2.7 Ga, as suggested by the intracontinental rift (Henderson, 1985; Thompson, 1989) and continent-continent collision models (Fyson and Helmstaedt, 1988).

Regional differences in the isotopic composition of the volcanic and sedimentary sequences (this paper, Dudas, 1989) suggest that supracrustal assemblages in the Slave Province are unlikely to have evolved within a single tectonic environment. Supracrustal sequences in the western Slave Province (e.g. Yellowknife, Point Lake) have evolved, to varying degrees in association with older crustal rocks (Dudas, 1989; Compston, 1990), whereas, the sequences in the central and eastern Slave Province formed largely in isolation from older crustal rocks. This is predicted by the analogy to accretionary orogens in which a complex collage of genetically unrelated terranes may be juxtaposed during collisional events. Detailed isotopic, geochemical and geochronological studies are required on the individual supracrustal belts to evaluate the nature of their pre-accretion evolution.

In an accretionary model, as suggested above, the lateral change in $\varepsilon_{Nd(t)}$ observed in granitoid rocks requires the presence of crustal suture zone(s) marking the physical boundary between the different crustal blocks. However, there is no known surface expression of a major structure to correlate with the surface trace of the Nd isotopic break defined between 110° and 112°W. A possible explanation is that the suture zone is buried beneath Yellowknife Supergroup rocks which have been thrust over the craton during the collision event as proposed by Kusky (1989). Kusky (1989) proposed that high strain zones at Point Lake represent the surface expression of a major crustal suture which dips moderately to the east beneath the central part of the province. An east dipping suture zone is consistent with the regional structural vergence in the area (Fyson and Helmstaedt, 1988; Kusky, 1989), the absence of suitable crustal structures in the central Slave Province, and Nd isotopic evidence for an apparent westward increase in crustal contamination of the syn-deformation plutonic rocks.

The Nd isotopic results are consistent with the interpretation that the growth and stabilization of Late Archean crust in the Slave Province occurred by tectonic accretion of dominantly juvenile crust to an older continental block(s). Subsequent to collision, mantle- and crust-derived magmatism may have thickened and stabilized the newly formed crustal segment. This model is fundamentally similar to tectonic processes occurring in active orogenic zones today, and implies a continuity of tectonic process from the Late Archean. Recognition of accretion as an important mechanism in the formation of the Slave Craton is a function of the presence of isotopically distinctive, evolved crust and its recycling during the orogenic process. The apparent absence of similar isotopic features in other Late Archean provinces (e.g. Superior Province, Shirey and Hanson, 1986) may reflect the scarcity of significantly older continental crust during the Late Archean (Taylor and McLennan, 1985; Chase and Patchett, 1988; Stevenson and Patchett, 1990). In general, the recognition of continental growth by tectonic accretion in younger orogens is facilitated by the involvement of very old continental crust in the orogenic process.

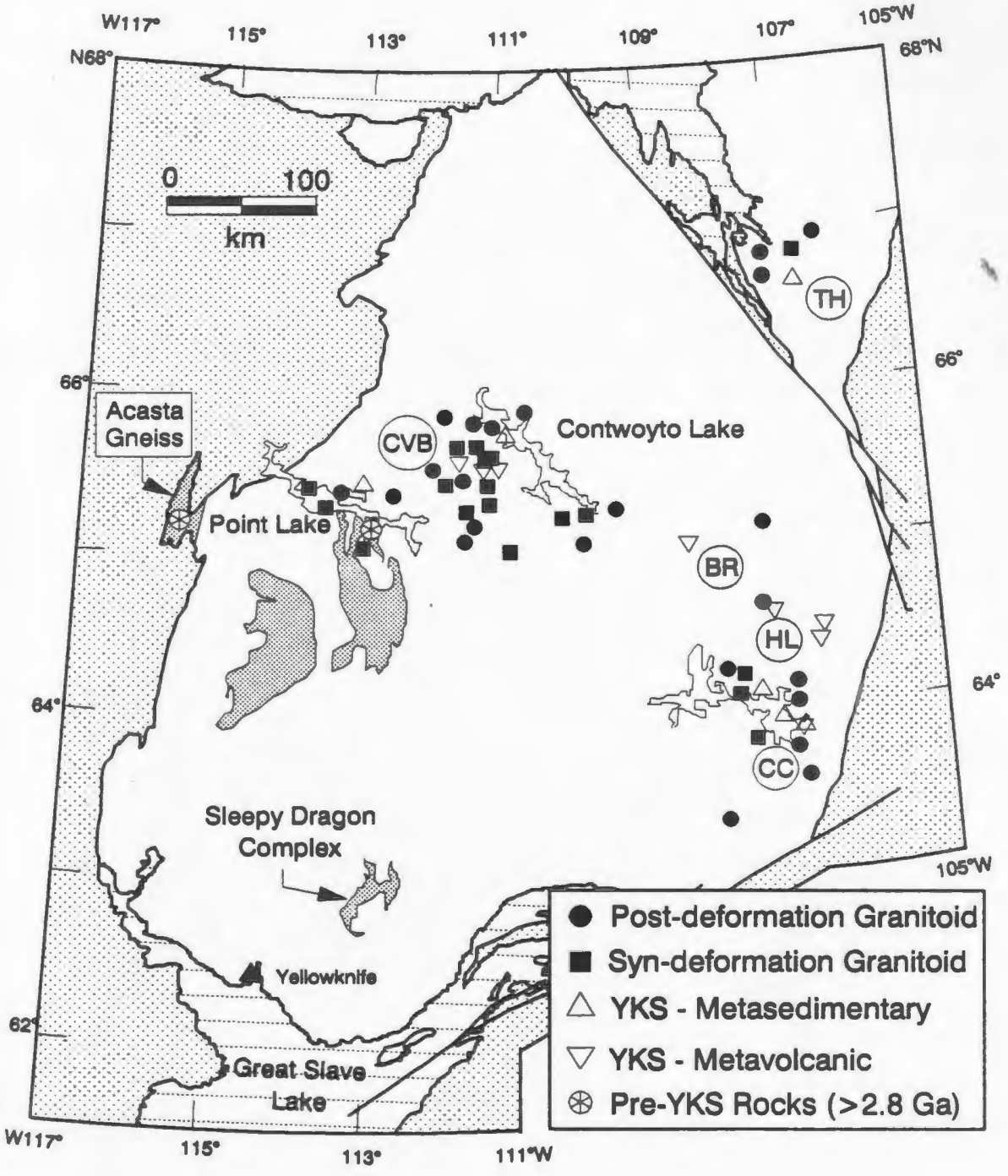

Figure 7.1. Sample localities. Geographic areas referred to in the text are abbreviated as follows: Back River (BR); Clinton Colden (CC); Tinney Hills (TH); Healy Lake (HL); Central Volcanic Belt (CVB). Shaded areas show locations of proven or probable pre-2.8 Ga rocks (after Hoffman, 1989).

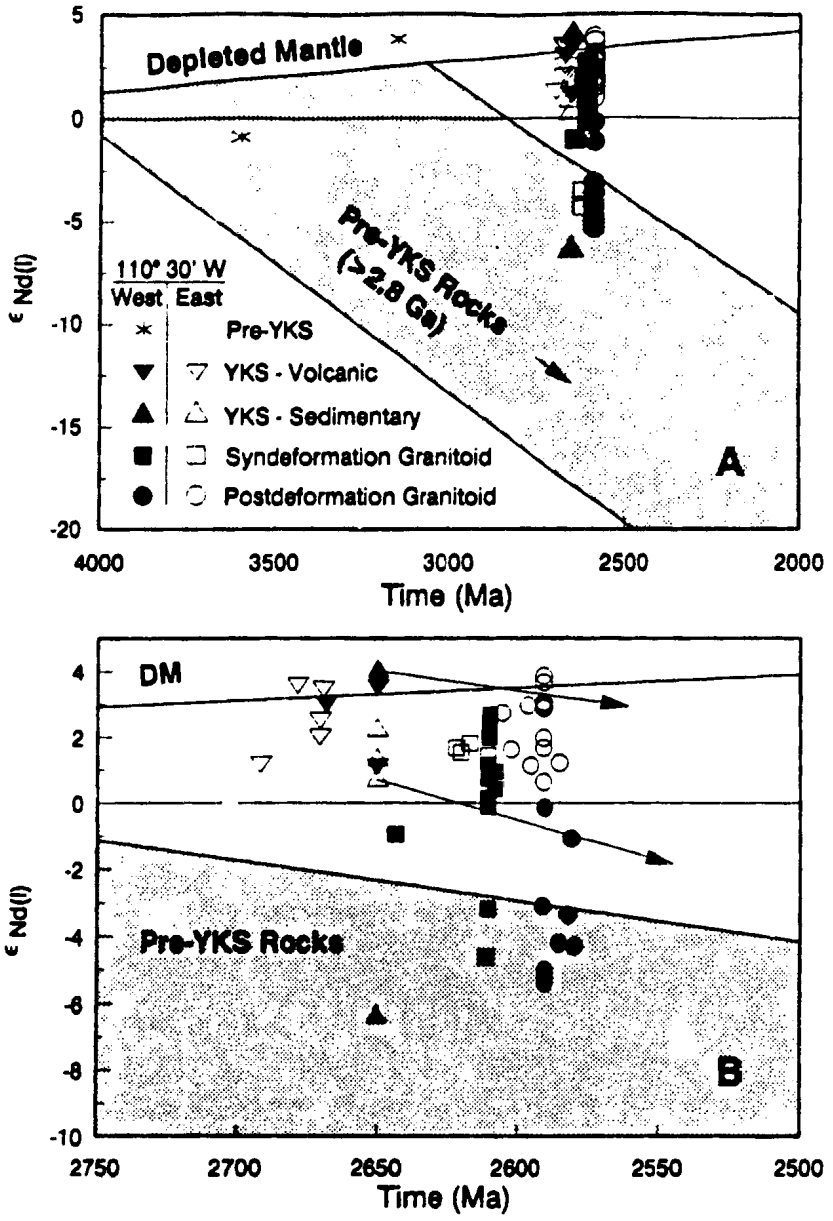

Figure 7.2. A) Plot of $\epsilon_{Nd(I)}$ vs. time of crystallization or deposition of Archean rocks from the Slave Province. Open symbols indicate samples east of longitude 110° 30'W. Filled symbols are west of this longitude. Depleted mantle evolution line from Goldstein and O'Nions (1984). The stippled band contains the isotopic evolution paths of pre-2.8 Ga rocks from the western Slave Province (Bowring et al., 1989a; Dudas, 1989; Table 7.1). B) Detailed view of Nd isotopic data for the principal orogenic time period in the Slave Province. Arrows indicate the isotopic evolution paths of Yellowknife Supergroup rocks from this study. Other features as described above.

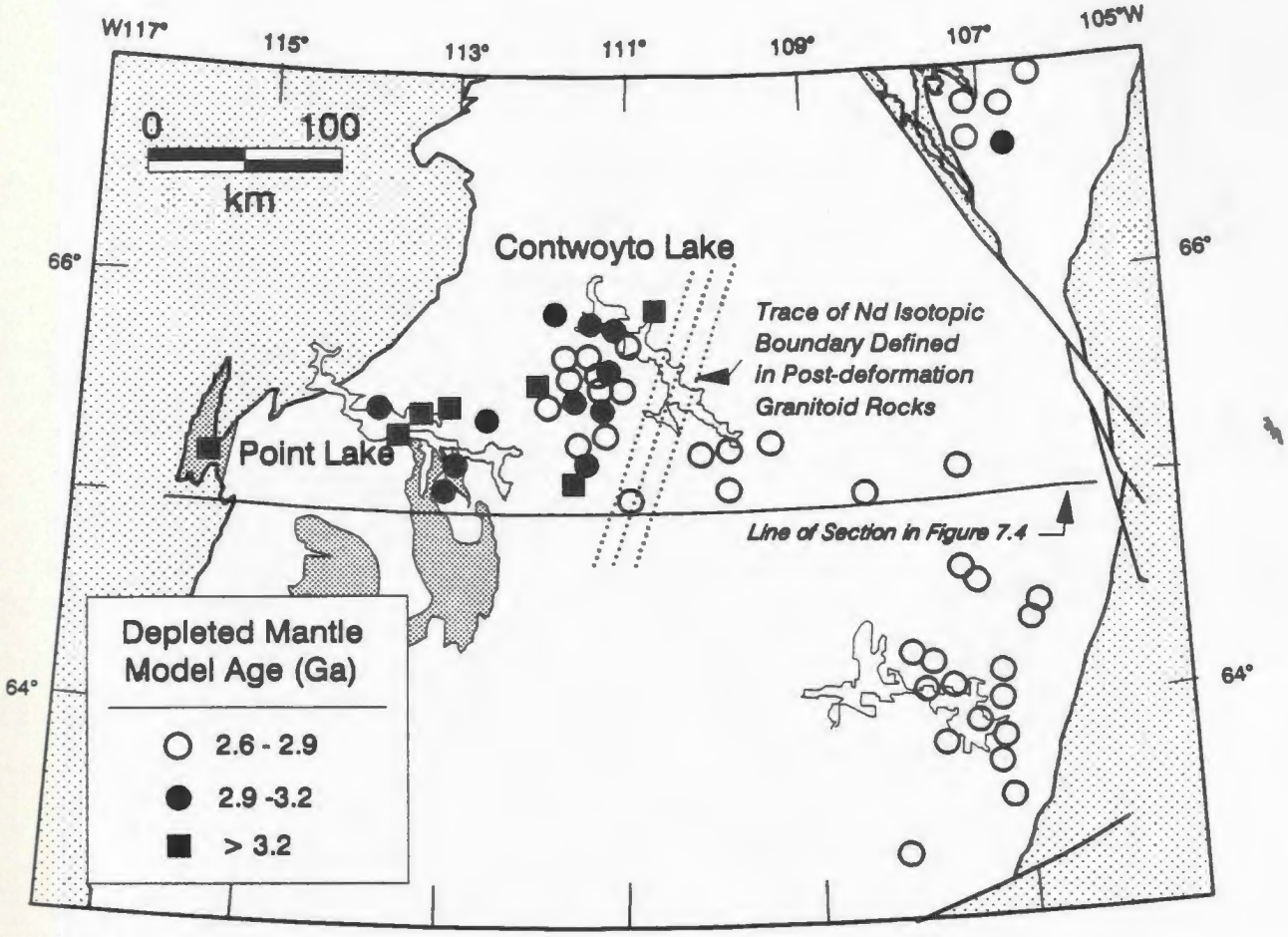

Figure 7.3. Map showing the distribution of T_{DM} values across the Slave Province. Samples are not differentiated by lithology. The eastern extent of postdeformation granitoid rocks with T_{DM} values greater than 2.9 Ga is marked by three dashed lines. The line at 65°N is the section line shown in Figure 6.

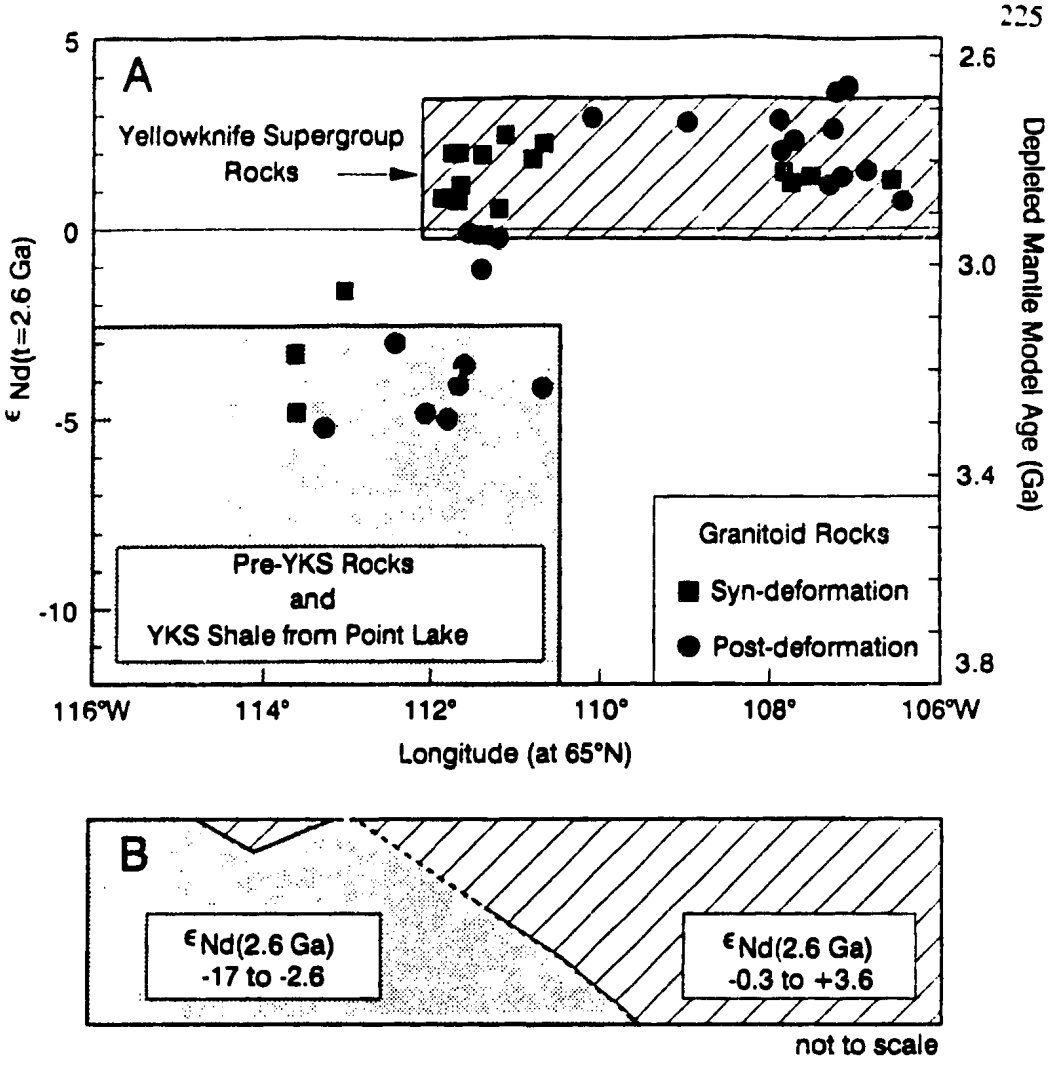

Figure 7.4. A) Variation of $\epsilon_{Nd(2.6)}$ values in syn- and post-deformation granitoid rocks along a transact from 106°W to 116°W at 65°N. The diagram was constructed by projecting the samples to the north or south along longitudinal lines to intersect the section line at latitude 65°N. The hatchered field delineates $\epsilon_{Nd(2.6)}$ values of YKS volcanic and sedimentary rock samples located east of 112°W. The stippled field outlines the $\epsilon_{Nd(2.6)}$ values of pre-Yellowknife Supergroup rocks (this study; Bowring et al., 1989; Dudas, 1989) and includes the value determined for the YKS shale sample from Point Lake. B) Schematic crustal cross section of the Slave Province at 65°N inferred from the $\epsilon_{Nd(2.6)}$ values. The Nd data suggest dominantly juvenile crust in the eastern, and significantly older crust in the western parts of the province. The east dipping suture between the two crustal blocks is inferred from regional structural vergence (Fyson and Helmstaedt, 1988; Kusky, 1989). The suture is not directly correlated with a specific structure at surface.

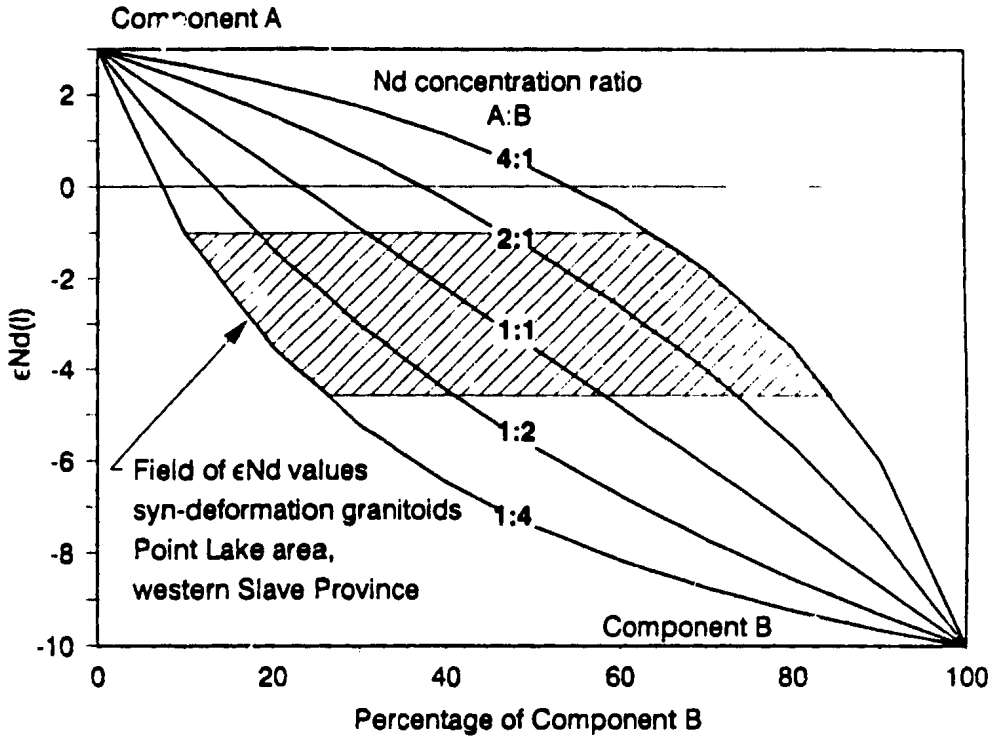

Figure 7.5. Variation in $\epsilon_{Nd(I)}$ produced by two component mixing of a juvenile component (A) similar to syn-deformation diorites in the central part of the province and an old crustal component (B). The crustal component is assumed to have an $\epsilon_{Nd(I)}$ value of -10. The Nd concentration ratio between the two components is likely to be high (A:B > 1) because of the high Nd content of the syn-deformation diorites (> 50 ppm). Hatchered area shows the range of $\epsilon_{Nd(I)}$ values determined for three syn-deformation granitoids from Point Lake.

Chapter 8

A Collisional Model for Plutonism in the central Slave Province

8.1 Introduction

Igneous rocks are derived through melting of the crust and/or mantle, and reflect the transient thermal state of the lithosphere and asthenosphere at the time of the magmatism. The thermal conditions required to cause melting of the crust and upper mantle are intimately linked to deformation and metamorphism of the lithosphere, during either convergent or extensional tectonic events (Thompson and England, 1986; McKenzie and Bickle, 1988; Gill, 1981; Zen, 1990; Barton and Hanson, 1990). The petrogenesis of plutonic rocks, secular changes in their origin and source regions and their relationship to contemporaneous deformation and metamorphism, offer important clues to understanding the tectonic and related magmatic evolution of orogenic belts.

The Contwoyto-Nose lakes area is part of a Late-Archean granite-greenstone terrain consisting of an early assemblage of deformed and metamorphosed volcanic, plutonic and sedimentary rocks (ca. 2667-2650 Ma) extensively intruded by syn to post-deformation granitoid rocks. These granitoid rocks represent 65% of the exposed crust in the area, and were intruded within a short time interval of 30 m.y., post-dating the supracrustal assemblage by 40 to 70 m.y.

Relative field relationships, supported by U-Pb geochronology, indicate a temporal evolution in the composition of the igneous rocks in the area. Rocks associated with the older supracrustal assemblage are dominated by mafic and intermediate volcanic rocks and trondhjemites, derived from melting mantle and mafic source rocks, respectively. The younger plutonic suites evolved from: 1) pre-2600 Ma, mantle-derived, hornblende-biotite diorites, quartz diorites and tonalites of the Concession Suite and mafic-crust-derived trondhjemites of the Siege Suite; to 2) post-2590 Ma, dominantly

crustally-derived, biotite or biotite-muscovite, granodiorites and granites of the Contwoyto and Yamba Suites. These secular changes in the composition of the plutonic rocks are linked to the thermal and structural evolution of the area. The mantle-dominated Concession Suite is associated closely in time with peak high-temperature/low-pressure (HTLP) metamorphism and regional compressional deformation, D2, which the younger granites largely post-date. This evolutionary history is comparable to other regions in the Slave Province (*e.g.* Hill and Frith, 1982; Henderson, 1985; van Breemen *et al.*, 1987a, b).

This chapter presents an attempt to synthesize the data from the granitoid rocks, with the available metamorphic and structural data, to develop a coherent tectonic model for the evolution of the Contwoyto-Nose Lakes area and the Slave Province more generally.

8.2 The Early Tectonostratigraphic Assemblage

The volcanic and coeval mafic plutonic rocks of the Central Volcanic Belt define a continuous calc-alkaline sequence from basalt through dacite (Bubar and Heslop, 1985). Trace element geochemical data indicate that the rocks mostly have $(La/Nb)_N$ and $(Th/Nb)_N$ ratios greater than one, a feature most typical of supra-subduction zone settings in Phanerozoic environments (*e.g.* Gill, 1981). Nb anomalies could equally have developed through contamination of basaltic magmas with continental crust (Arculus, 1987), however, in the case of the Central Volcanic Belt the limited Nd isotopic data do not support significant interaction with older crust.

Determination of the tectonic association of other volcanic belts in the Slave Province is hampered by a paucity of detailed high-precision geochemical data. High-precision data for Nb (or Ta), Th and La, at low abundances, are critical to identify rocks formed in suprasubduction zone settings. The suprasubduction zone setting proposed for the CVB may, however, be shared by some other volcanic belts in the Slave Province. For example, the Point Lake and Red Rock Lake belts have been interpreted to represent island arc and marginal basin volcanic sequences (St Seymour *et al.*, 1988) and volcanic rocks in the Hackett River area are interpreted to be of island arc origin (*e.g.*

Ewing, 1979). Some Yellowknife belt volcanic rocks are characterized by negative Nb and Ta anomalies (Jenner *et al.*, 1981; Goodwin, 1988), suggesting an island arc or back arc origin (*cf.* Helmstaedt and Padgham, 1986). However, Cunningham and Lambert (1989) proposed a plume origin, and Nd isotopic data may indicate an ensimatic origin for the Yellowknife belt (Dudas, 1989).

Fyson and Helmstaedt (1988) drew an analogy between the volcanic belts in the Slave Province and those of the Ordovician Dunnage zone of the Newfoundland Appalachians. This comparison has considerable merits, in particular: the lithologic association of deformed, mafic to felsic metavolcanic belts associated with metaturbidite sequences; the orogen-scale distribution of volcanic belts; the range of ages of volcanic rocks (65 m.y. in the Slave Province, 51 m.y. in the Dunnage zone; Dunning *et al.*, 1987; 1991); and the range and diversity of the geochemistry of the volcanic rocks. Volcanic rocks in the Dunnage Zone indicate derivation from supra-subduction zone tectonic settings (back arc basins, island arcs), as well as non-arc settings (ocean islands, ocean ridges) (*e.g.* Swinden *et al.*, 1990; Jenner and Fryer, 1980; Dunning *et al.*, 1991).

Emplacement and juxtaposition of the volcanic and sedimentary rocks in the Dunnage Zone occurred by obduction and accretion during closure of the Iapetus ocean. A similar tectonic evolution has been proposed for at least some of the volcanic belts in the Slave Province by Kusky (1989, 1990), Hoffman (1986), and Fyson and Helmstaedt (1988). Geological relationships, unequivocally demonstrating autochthonous origins for the volcanic belts in the Slave Province have not been documented, whereas the structural style preserved within the supracrustal sequences is comparable to modern accreted orogenic belts (*e.g.* Fyson and Helmstaedt, 1988; King and Helmstaiedt, 1989; Kusky, 1990, 1991).

The Nd isotopic data presented in Chapter 7 support models for the tectonic emplacement of at least some of the volcanic belts in the Slave Province. This is demonstrated particularly well for the Central Volcanic Belt. The Nd isotopic data for this belt are juvenile, supporting a dominantly ensimatic origin; and U-Pb data on zircons do not show inheritance of significantly older components (van Breemen *et al.*, 1990;

Mortensen *et al.*, 1988). However, the younger granites which intrude the volcanic rocks (*ie.* Yamba and Contwoyto Suites) have negative $\varepsilon_{Nd(t)}$ values and must contain a significant component of older crust, indicating that the volcanic belt was overlying older crust at the time of granite intrusion (ca. 2585 Ma). The absence of any indication of this older crust in the volcanic rocks or the associated metasedimentary rocks during their formation argues that the belt formed isolated from, and was later tectonically emplaced onto the older continental crust. Note that some supracrustal belts in the western part of the Slave Province have isotopic compositions indicating interaction with older crust (*e.g.* Yellowknife, Dudas, 1989; Point Lake, this study). These supracrustal belts may have formed within or adjacent to continental crust, perhaps in marginal basin settings, like the Rocas Verdes of southern Chile (Tarney *et al.*, 1976) as suggested by Helmstaedt and Padgham (1986).

Hoffman (1986) suggested that most volcanic and sedimentary rocks of the Slave Province form part of a single accretionary prism complex. The arc adjacent to which this accretionary prism formed is not recognized. Kusky (1989) argued that there are two fundamentally different origins for the volcanic sequences in the province. Volcanic belts in the western Slave Province (*e.g.* Yellowknife, Point Lake, Central Volcanic Belt) include oceanic sequences deformed within an accretionary prism complex, whereas volcanic belts in the eastern part of the province (*e.g.* Hackett River) form part of the adjacent volcanic arc. Geochronological data do not support this simple two-fold model since volcanic rocks in the inferred volcanic arc are of the same age or older than volcanic rocks withir the adjacent accretionary prism (Mortensen *et al.*, 1988). Unfortunately, the details of these models are far more sophisticated than can be realistically tested by the available field, geochemical or isotopic data. This is well illustrated by the complex evolution of tectonic events demonstrated for the Dunnage Zone by the combination of high precision geochronological and geochemical studies. Understanding the pre-deformation evolution of the Slave Province requires more detailed isotopic, geochemical and field studies.

8.2.1 Deformation and Metamorphism

Supracrustal rocks have accommodated regional compression by multiple generations of isoclinal folding, cleavage development and faulting (King and Helmstaedt, 1989; Kusky and DePaor, 1991; Fyson and Helmstaedt, 1988; Relf, 1990). The regional foliation surface is typically a thermal-peak penetrative cleavage. Different relationships between this surface and folds in different areas of the province imply diachronous, and multiple development of folds, cleavages and faults (King and Helmstaedt, 1989; Fyson, 1978). Kusky (1989, 1990) and King and Helmstaedt (1989) suggest that the regional structural style is similar to Phanerozoic fold and thrust belts developed in accretionary prism settings and links the deformation to accretion of the supracrustal rocks.

Metamorphism in the province is characterized by high-temperature, low-pressure (HTLP) assemblages (Thompson, 1978; 1989). Thompson (1989) pointed out that the regional isograds display both concordant and discordant relationships to structural trends, indicating peak thermal metamorphism was synchronous with the main compressional deformation in some parts of the province (*e.g.* Contwoyto-Nose Lakes; Relf, 1990) and post-dated this event in other parts. The absolute timing of metamorphism is only locally constrained by radiometric dating. U-Pb metamorphic monazite ages have been determined in two samples of pre-Yellowknife Supergroup gneisses from different areas of the province and yield ages of ca. 2600 Ma (Frith and Loveridge, 1982) and ca. 2588 Ma (James and Mortensen, 1991). These ages are in agreement with estimates of the timing of peak metamorphism and compression obtained from the timing of intrusion of associated plutonic rocks (*e.g.* Culshaw and van Breemen, 1990; van Breemen *et al.*, 1990).

Younger post-metamorphic, extensional and transtensional structures, occur but are not as well described as the compressional features. Recent work by James (1990) in the Sleepy Dragon area, southwest Slave Province has documented detachment faults around the core of older basement rocks which he interprets as a metamorphic core complex, resulting from post-compression extension (*e.g.* Armstrong, 1982). The extensional

faults in the area cut granitic rocks that are time correlative with the Contwoyto and Yamba Suites, indicating at least local extension occurred after ca 2588 Ma (James pers comm 1991). Extensional faults also cut younger granitoids in the Point Lake area, although there are no age data available to constrain the age of faulting (J. Henderson, pers. comm., 1991).

Elliptical domes, usually cored by gneissic, syn-volcanic plutonic rocks have been described in many areas of the Slave Province (*e.g.* Olga and Wishbone Domes, Contwoyto Lake area; King *et al.*, 1988; Hanimoor Gneiss Complex, Beechey Lake area; Frith, 1987). The origin of these domal structures has been attributed to fold interference (Relf, 1990; King et al., 1988) is unknown but the possibility that they are related to post-compression extension, similar to that documented for the Sleepy Dragon Complex should be tested.

Another indicator that extension and unroofing occurred soon after regional compression in the Slave Province is the conglomerates of the Jackson Lake Formation at Yellowknife. This formation is interpreted to have formed on top of the Yellowknife Belt, in fault-controlled basins (Helmstaedt and Padgham, 1986). The conglomerate contains non-foliated granitoid clasts, similar to the post-2650 Ma granitoids in the area. One clast has been dated at 2609±6 Ma (Isachsen and Bowring, 1989) providing a maximum age for the deposit. This age is younger than some of the surrounding granitoid rocks and suggests that rapid decompression and erosion of crust occurred at some time after ca. 2609 Ma.

Metamorphic data in the Contwoyto-Nose Lakes area also indicate post-deformation (D2) decompression. Post-thermal peak metamorphic assemblages associated with D_3 open folds (*ie.* post ca. 2585 Ma granite), indicate lower pressures than thermal peak assemblages (Relf, 1991). Wingate (1990) has proposed relatively rapid uplift following regional shortening. Using mineral assemblages and reactions, in conjunction with some geothermometry and geobarometry he proposed decompression

from 6 to 2 kbar during the interval from 2608 Ma to 2588 Ma. The age constraints are derived from igneous rocks which intrude the migmatites, not from the metamorphic assemblages themselves.

In summary, deformation and metamorphism in the Slave Province includes: 1) regional compression, shortening and thickening of crust, synchronous with or immediately followed by peak thermal metamorphism; followed by decompression and at least local extension soon after cessation of regional compression (Figure 8.1).

8.3 Evolution of Plutonism

Granitoid rocks in the Contwoyto-Nose Lakes area change systematically in composition and mineralogy with time of intrusion (Figure 8.2), a secular variation which parallels the structural and metamorphic evolution of the province.

The early to syndeformation, Concession Plutonic Suite (ca. 2610 Ma) is dominated by calc-alkaline, hornblende-biotite tonalite with lesser amounts of diorite, quartz diorite and granodiorite. Rocks range from metaluminous to peraluminous compositions (Figure 8.2d) with increasing SiO_2. The suite is relatively Mg rich, with high Ba, Sr and $(Ce/Yb)_N$; low Rb/Sr (Figure 8.3a) and negligible to small Eu anomalies (Figure 8.3b). Accessory minerals include, magnetite, titanite, allanite, zircon, apatite, and possibly primary epidote. The plutons contain magnetite and define prominent aeromagnetic highs.

The approximately contemporaneous Siege Plutonic Suite consists of leucocratic, low-K and Rb/Sr (Figure 8.3a, c), high Al_2O_3 biotite trondhjemite.

The two postdeformation suites are dominantly peraluminous granites (s.s.), with SiO_2 contents greater than 70 wt% (Figure 8.3). Mafic lithodemes are not directly associated with either suite. The Yamba Suite is biotite-bearing, with rare accessory garnet, (± muscovite), and is characterized by high Rb/Sr, K_2O, and large negative Eu anomalies (Figure 8.3). The contemporaneous Contwoyto Suite is more leucocratic, contains biotite and muscovite and accessory aluminous phases (garnet, tourmaline, ±

sillimanite). Pegmatitic facies are very common implying high volatile contents. The Contwoyto Suite is more peraluminous, has lower K_2O and Rb/Sr, and smaller, but still negative Eu anomalies compared to the Yamba Suite (Figure 8.3).

The accessory mineral suites of the peraluminous granites are different from those of the earlier Concession Suite. Titanite and allanite are absent in the younger granitoids, whereas, monazite is common. Zircon occurs in all suites but in the younger suites metamict cores are present, possibly indicating an inherited component not observed in the earlier Concession Suite (van Breemen *et al.*, 1990). Oxide minerals are rare and the plutons define aeromagnetic lows.

Nd isotopic compositions vary systematically with the geochemical and mineralogical trends. Initial ε_{Nd} values of the syndeformation plutons show limited variation (+0.1 to +2.7) and are similar to estimates of contemporaneous depleted mantle (Figure 8.3). In contrast $\varepsilon_{Nd(t)}$ values determined for the younger granites have variable, positive to strongly negative, values (Figure 8.3). In addition to the temporal changes, the $\varepsilon_{Nd(t)}$ values in the younger granites are geographically controlled; samples from the western part of the area have negative values and contain a component of old (>3.3 Ga) crust, whereas samples from the east show no evidence for recycling of older crust.

The temporal trend in $\varepsilon_{Nd(t)}$ values (Figure 8.2) supports the major and trace element data (*e.g.* high SiO_2, K_2O, Rb/Sr and negative Eu anomalies), which together indicate an increasing crustal component in the intrusions with time. Greater crustal involvement is also reflected in decreasing oxidation (*ie.* decreasing magnetic susceptibility), increasing volatile contents (*e.g.* pegmatites, tourmalinization) and changes in the accessory mineral assemblage (*e.g.* titanite and allanite vs. monazite and zircon with cores). These secular changes are interpreted to reflect changes in the source regions and petrogenetic process, from mantle- to crust-dominated melting as a function of crustal thickening and heating during and following collision of crust.

The mantle-derived Concession Plutonic Suite is closely linked in time to peak metamorphism and compression. Metamorphism in the Contwoyto-Nose lakes area is dominated by regionally extensive HTLP conditions (Relf, 1990), characteristic of the

Slave Province as a whole (Thompson, 1978; 1989). This type of metamorphism is typical of many Archean terrains (Condie, 1984; Perkins and Robinson, 1985) and requires very high upper crustal geothermal gradients (>35°C/km). HTLP belts of all ages are spatially associated with areas of abundant granitoid intrusions (*e.g.* Ernst, 1974; Miyashiro, 1973).

8.4 A Collisional Model For Evolution of Plutonism and Metamorphism in the Slave Province.

Sandiford (1989) and Loosveld and Etheridge (1990) have recently proposed that HTLP metamorphic belts develop in some collisional orogenies as a result of post-collision detachment of some or all of the mantle lithosphere. The models are based on a theoretical hypothesis of the behaviour of the mantle portion of the lithosphere during lithospheric shortening events (Houseman *et al.*, 1981). Houseman *et al.* (1981) proposed that during collision, the entire lithosphere, including both crustal and mantle portions, thickens in response to regional shortening events, causing downward protrusion of cold, dense mantle lithosphere into the convecting asthenosphere. The thickened lithosphere, and in particular the basal thermal boundary layer separating the asthenosphere from the cooler, rigid part of the lithosphere, is predicted to become unstable, and separate and sink into the underlying convecting asthenosphere. The net effect of this will be to thin the lithosphere and introduce hot asthenospheric material to shallower depths, causing rapid warming of the overlying crust and mantle. These conditions would promote the formation of HTLP metamorphic belts, according to Sandiford (1989) and Loosveld and Etheridge (1990). Houseman *et al.* (1981) argued that under certain conditions, detachment of the boundary layer could occur simultaneously with the shortening event. They also allowed for the extreme possibility of the total detachment of the lithosphere.

A predicted consequence of the lithospheric detachment model is that it will induce uplift and extension of the lithosphere following release of compressive strain (Sondor *et*

al., 1987; England and Houseman, 1988). The timing of extension depends on the thermal condition of the lithosphere and could occur anywhere from 0 to 100 m.y. following release of compressive strain (Sondor *et al.*, 1987).

8.4.1 Sequence of Intrusive Events in the Central Slave Province

The main points of a collisional model for the evolution of magmatism in the Slave Province are shown in Figure 8.4. 1) The early (ca. 2715-2650 Ma), pre-collisional stage involved the generation of volcanic and associated plutonic rocks in a range of tectonic settings including island arcs, back arc basins and oceanic ridges. Collision of the various continental blocks and arc terranes occurred between 2650 Ma and 2625 Ma. Subduction processes which preceded, and eventually led to collision, metasomatized lithospheric mantle beneath the fore-arc and arc regions of these disparate terranes. 2) Collision caused lithospheric shortening and thickening, reflected in the folding and faulting of the crustal rocks. Thickening eventually resulted in detachment of the thermal boundary layer (Houseman *et al.*, 1981), upwelling of asthenospheric mantle, and heating of the remaining portion of the lithosphere. Melting of mantle lithosphere, previously enriched by subduction processes during the pre-collisional events, produced high-Mg andesites, the parental magmas to the Concession Suite. Heating of the crust by the effects of crustal thickening, lithospheric detachment and magma intrusion caused HTLP metamorphism over a broad area of the Slave Province. 3) Continued heating of the crust resulted in extensive crustal melting. Mantle-derived melts mixed and assimilated large amounts of crustal material producing hybrid, biotite granites of the Yamba Suite. Muscovite-biotite granites of the Contwoyto Suite represent more sedimentary-protolith dominated melts. Decompression and extension occurred at the same time as intrusion of the granites.

Origin of the Concession Plutonic Suite and Related Rocks

The tonalites and related rocks of the Concession Suite were ultimately derived from a subduction-enriched mantle source (Chapter 5). However, this need not require active subduction as the mantle source to these rocks may have been enriched by subduction processes at some time prior to their generation (*e.g.* Johnson *et al.*, 1978; Gill, 1983; Halliday *et al.*, 1985; Pearce *et al.*, 1990).

Comparison of Plutonic Rocks to Modern Analogues.

One way to derive tectonic information from igneous rocks is to compare their geochemistry to petrologically similar rocks from known tectonic environments (Pearce *et al.*, 1984; Harris *et al.*, 1986; Rogers and Greenberg, 1990). Unfortunately, the relationship between the geochemical characteristics of a suite of rocks and their tectonic association, even in recent environments, is seldom clear (*e.g.* Arculus, 1987). This is particularly true in continental settings where the diversity of potential geochemical reservoirs and processes is great.

Calc-alkaline intermediate intrusive rocks, similar in composition to the Concession Suite are certainly a common product of active subduction zones, particularly in mature or continental arc settings (Gill, 1981). Subduction-related rocks typically have the enrichment of the LILE and relative depletions of some HFSE (*e.g.* Nb) characteristic of the Concession Suite and correlative rocks from elsewhere in the Slave Province (Hill and Frith, 1982; Frith and Fryer, 1985). Figure 8.5a demonstrates the similarity of the Concession Suite to some andesites and tonalites from the continental margin arcs and batholiths of western North and South America. Granitoid trace element discrimination diagrams (*e.g.* Pearce *et al.*, 1984), also indicate an arc affinity for these tonalites. It is therefore tempting to draw a direct tectonic linkage between tonalites of the Concession Suite and contemporaneous subduction beneath the Slave Province, as has been suggested by Hoffman (1986), Fyson and Helmstaedt (1988) and Davis *et al.* (1990).

Calc-alkaline rocks with subduction signatures are not, however, restricted to zones of active subduction but are also common to collisional or post-collisional settings (Figure 8.5b; Gill, 1981; 1983; Pearce *et al.*, 1990). Examples of this association include

Quaternary volcanic rocks from Turkey and western Iran which post-date closure of the Tethys ocean (Innocenti, 1983; Dostal and Zerbi, 1978; Pearce *et al.*, 1990; Zhou, 1985), andesites of Papua New Guinea Highlands which post-date Mesozoic collision of island arc terranes with the Australian continent (Johnson *et al.*, 1978), and calc-alkaline rocks of the Tibetan plateau (Harris *et al.*, 1990). Phanerozoic examples of this association may include the Silurian calc-alkaline magmatism which post-dates closure of the Iapetus Ocean in the Scottish Caledonides (Zhou, 1985). In all of these cases the calc-alkaline rocks resemble continental margin rocks, but they cannot be linked to active subduction.

Since subduction-related settings cannot be discriminated from syn- to post-collision, non-arc associations based exclusively on geochemical arguments (Figure 8.5b), the presence of calc-alkaline intrusions should not be taken as unequivocal evidence for subduction. In order to constrain the tectonic association of the calc-alkaline rocks, their petrogenesis must be considered within the regional metamorphic and structural framework.

Nature and Origin of the Enriched Mantle Source

Mantle overlying subducted oceanic lithosphere can be metasomatized either by fluids derived from dehydration reactions in the slab or through hybridization of the mantle by slab-derived melts (Wyllie, 1984). In mature Phanerozoic subduction systems the slab dehydrates before it can melt (Wyllie, 1984), and the LILE/HFSE enrichment characteristic of subduction-related magmatism is generally considered to reflect transfer of soluble elements (*e.g.* LILE, Si) via a fluid phase into the overlying mantle (*e.g.* Arculus and Powell, 1986; Kay, 1980; Gill, 1981; Tatsumi *et al.*, 1986).

Owing to the higher thermal conditions inferred for the Archean earth (Richter, 1985; Bickle, 1978; Christensen, 1985), attention has been focussed on the potential thermal and dynamic differences between Archean and younger subduction zones and their possible effects on tectonics and magma compositions (Martin, 1986; Drummond and Defant, 1990). Higher mean mantle temperatures during the Archean (Richter, 1985; Bickle, 1978) and more vigorous asthenospheric convection, could result in smaller oceanic plates (*ie.* greater ridge length, Hargrave, 1986), and a younger, and therefore,

hotter average oceanic lithosphere. A hotter oceanic lithosphere, coupled with higher ambient mantle temperatures, are required conditions for slab melting to occur (*e.g.* Wyllie, 1984).

In either case, hydrous mineral phases will be stabilized within the sub-arc mantle, and both the bulk and trace element compositions of the mantle will be modified. Some of the enriched components will be transported through the mantle into the crust via melts or fluids, and some may be removed from the system by asthenospheric convection. However, modified lithospheric mantle, particularly in the fore-arc region and at shallow depths beneath the arc, may not be convectively recycled and will remain coupled to the overlying arc and fore-arc crust (Gill, 1981; Tatsumi, 1986).

The juvenile Nd isotopic compositions indicate that the enrichment of the mantle source to the Concession Suite cannot have taken place more than 200 m.y., and probably less than 100 m.y., prior to the ca. 2600 magmatism (Figure 5.32). This constrains mantle enrichment to a time period between 2600 Ma and 2800 Ma, essentially overlapping the range in ages of the accreted supra-subduction zone terranes. This allows that enriched mantle generated at that time could be the source of the Concession Suite.

Reactivation and Partial Melting of the Enriched Mantle

It is proposed that pre-collision subduction events caused metasomatism and stabilized amphibole in the mantle wedges (*e.g.* Tatsumi, 1986, Wyllie, 1984) underlying the fore-arc and arc zones of *ca.* 2715-2650 Ma island arc terranes. This enriched mantle lithosphere was then subcreted as the overlying supra-subduction zone terranes were accreted, placing subduction-modified mantle beneath the newly stabilized crust.

Melting of this enriched lithospheric mantle occurred during and following collision-related compression and thickening. Melting may have been caused by: 1) thickening of the lithosphere, so that the lower part was depressed below amphibole stability (*ie.* 100 km); and 2) heating of the lithosphere by detachment of the thermal boundary layer (Houseman *et al.*, 1981) and introduction of hot, convecting asthenosphere to shallow depths.

The main points of this model are schematically shown in Figure 8.6. The mantle and crustal portions of the lithosphere both thicken in response to compression. As the lithosphere thickens, amphibole in peridotite breaks down as it is depressed through depths of approximately 100 km (*ie.* 30 kbar; Falloon and Green, 1989; Green, 1973). The amphibole break down reaction releases volatiles, some or all of which migrate to lower pressures, raising P_{H_2O} in the overlying lithosphere and effectively lowering the peridotite solidus (Figure 8.6b). Transport of trace elements with the fluids will further enrich the upper part of the mantle lithosphere. If garnet is formed after amphibole (*e.g.* amphibole = garnet + diopside + volatiles), the REE in the resulting fluids may be fractionated, contributing to the fractionated REE composition of the source region.

Replacement of the detached, thermal boundary layer with hot asthenospheric material will perturb the geotherm, driving it to higher temperatures and eventually intersecting the hydrous peridotite solidus. Melting occurs at the lowest temperature point on the hydrous peridotite solidus, at depths near or below the amphibole-out reaction. The zone of melting is shown by the cross-hatched pattern in Figure 8.6b and c. If the mantle is highly refractory (*ie.* low Al_2O_3), or water saturated, garnet may not be stable after melting (Green, 1973).

The depth of melting inferred from this model is twice that determined by sanukitoid liquidus experiments (Tatsumi, 1982), which suggest segregation pressures less than 14 kbar. If these samples are indeed primary melts, and similar in major element composition to Concession Suite parental compositions, then the melts formed at 100 km depth must have risen to depths of less than 50 km before segregation. Garnet would not be residual at these pressures. Thompson (1989) estimated that the thickness of crust in the Slave Province did not exceed 55 km during collision. This estimate was based on the present crustal thickness of 35 km and the maximum metamorphic pressures exposed at the present erosional surface of <7 kbar. This provides a minimum depth of segregation of 55 km and implies final magma segregation occurred near the base of the crust.

This model is similar in principle to that proposed by Saunders *et al.* (1987) for petrogenesis of bajaites, in California. They suggested that mantle melting occurred following amphibole breakdown reactions in the mantle wedge, accompanying ridge subduction. Fluids released lowered the peridotite solidus and caused melting in already metasomatized mantle. The main difference in the models is the source of the heat. Saunders *et al.* (1987) attributed heating of the sub-arc mantle to ridge subduction, which introduced hot oceanic lithosphere into the subduction zone, raising the isotherms in the overlying mantle (see also Kay, 1978; Drummond and Defant, 1990). In the model proposed here, heating is caused by lithospheric detachment and replacement by hot asthenosphere. The differences in the models indicate the potential for similar rock types to be generated in different tectonic settings (*ie.* subduction- and collision-related).

Timing of Mantle-Derived Magmatism relative to Collisional Events

The timing of magmatism relative to deformation depends critically on when lithospheric detachment occurs (*ie.* early or late during compressive strain). As outlined by Houseman *et al.* (1981), this depends on the rate and amount of convergence, but is also critically dependent on the vigour of asthenospheric convection. Lithosphere beneath orogenic belts with rapid convergence and vigorous asthenospheric convection will detach more easily and more rapidly.

Higher mean mantle temperatures in the Archean, and consequent higher convection rates due to lower viscosities and greater heat dissipation, predict that lithospheric detachment is both more likely to occur and will occur earlier during compressional deformation (*e.g.* Sandiford, 1989). The syn- to late-compressional timing of the Concession Suite and other correlative intrusions in the Slave Province requires that lithospheric detachment occurred simultaneously with thickening and compression.

The timing of mantle-derived magmatism relative to collisional events in more recent collisional orogens is highly variable, suggesting that it may not be simply related to asthenospheric temperatures. In many cases mantle-derived magmatism occurs late during the regional shortening events and is associated with regional extensional features. For example, post-collisional, mantle-derived magmatism in Papua New Guinea is taking

place simultaneously with regional extension and uplift, although the New Guinea Orogenic Belt is still experiencing compression (Johnson *et al.*, 1978; Cooper and Taylor, 1987). In Eastern Anatolia the Quaternary magmatism is associated with transpressional and extensional escape structures associated with collision of the Arabian and Asian plates (Pearce *et al.*, 1990). In the Paleozoic Caledonides, mantle-derived magmatism is associated with extensional or transpressional features following closure of Iapetus (Watson, 1984; Zhou, 1985; Rogers and Dunning, 1990). The structural setting of high Mg monzodiorites and related lamprophyres in the Superior Province is similarly associated with late transpressional faults (Stern *et al.*, 1989).

Calc-alkaline lamprophyres and primitive high-Mg andesites are common to many collisional magmatic belts, in which magmatism is associated with extensional or transpressional faulting (*e.g.* Papua New Guinea Highlands, Johnson *et al.* (1978); Scottish Caledonides, the Appinite Suite, Rogers and Dunning (1990); Superior Province, Stern *et al.* (1989); Baja, Ca. Saunders *et al.* (1987)). This suggests that primitive rock types may preferentially ascend through the crust in extensional settings, aided by crustal scale fault zones. In the Slave Province calc-alkaline lamprophyres have only been reported from the Yellowknife area where they are associated with the major shear zones which host gold mineralization in the area (Webb and Kerrich, 1988). The rarity of these primitive or ultra-mafic rock types in the Slave Province may reflect their intrusion dominantly during the regional compression event, causing such magmas to be trapped within the lower crust, where they fractionated and assimilated crust (*e.g.* Hildreth and Moorbath, 1988), to produce tonalites and related rocks. This would explain the dominance of tonalites with SiO_2 contents of 60 to 65 wt% and the rarity of primitive compositions. Crystallization of these magmas in the lower crust will generate heat to drive metamorphism and the later extensive crustal melting.

8.4.2 Origin of the Granites: the Yamba and Contwoyto Suites and related rocks

The generation of large bodies of peraluminous granite requires elevated, thermal conditions in the middle to lower continental crust in order to induce the large degrees of melting required to mobilize granitic magmas (Wickham, 1987) and/or cause extensive crustal assimilation or mixing with mantle magmas (Barton, 1990). Numerical modelling suggests that these conditions can be met by some combination of crustal thickening (Patino-Douce, 1989; Zen, 1989; Thompson and England, 1984; 1986) or a mantle thermal input into the crust (Foster, 1990; Hyndman and Foster, 1988; Barton,1990; Huppert and Sparks, 1988; Hildreth, 1981). The petrogenesis of these rocks must be closely linked to preceding and synchronous magmatic, tectonic and metamorphic events.

Granites (*s.s.*) are a common feature of collisional orogenic belts. Collisional granites define a wide range of compositions reflecting differences in the composition of source rocks, dynamics of partial melting processes, and the relative involvement of mantle derived material in the granite forming process (*e.g.* Pitcher, 1987). As recently summarized by Pitcher, "... an infinite number of different [granite] types might be generated in response to varying physical parameters and source rock composition". It is indeed remarkable that broad classes of granites can be recognized and that these recur in specific, but complex tectonic associations (Barbarin, 1990; Harris *et al.*, 1986; Pitcher, 1987; Rogers and Greenberg, 1990).

Two broad groups of granites occur in many collisional belts (*e.g.* Harris *et al.*, 1986; Crawford and Wyllie, 1990; Barbarin, 1990). 1) Peraluminous two-mica or aluminosilicate-bearing leucogranites; and 2) weakly peraluminous to metaluminous biotite granites. The former are dominantly derived from partial melting metasedimentary sources (*e.g.* Lefort *et al.*, 1987; Vidal *et al.*, 1982); the origin of the latter is less clear, but they are thought to represent hybrids of mantle and crustal melts (*e.g.* Barbarin, 1990, DePaolo, 1981; Pitcher, 1983, 1987; Didier *et al.*, 1982). The association of these latter granites with high-Mg mafic rocks (e.g. Crawford and Windley, 1990; Fowler, 1988) suggests a causal linkage.

This same granite association is observed within the central Slave Province. The Concession Suite is representative of the two-mica leucogranites and the Yamba Suite the biotite granites. Henderson *et al.* (1982) used a similar two-fold subdivision of granites in the Artillery and Healy Lakes areas, and both two-mica and biotite granites are described from the Yellowknife-Hearne Lake area (Henderson, 1985) and the Beechey lake area (Hill and Frith, 1982). The two granite types are therefore considered to be regionally extensive features of the province.

The large areas of these granites, fully 60% of the area of the Contwoyto-Nose lake map sheets, imply that recycling of pre-existing crust was extensive, and that this dominantly occurred immediately following regional shortening in the area. Crustal melting reflects heating of the crust by a combination of: 1) thermal rebound following crustal thickening during collision; 2) advective heat transfer from the mantle via melts which underplate and intrude within the crust (*ie.* Concession Suite); and 3) heating due to lithospheric detachment. The change from mantle-dominated to crust-dominated magmatism reflects the thermal maturation of the lower part of the crust, as it is progressively heated from below. The development of large partial melt zones, in which greater than 40% melt may be present in the lower parts of the crust, will impede ascent of mantle-derived magmas (*ie.* Concession Suite) and cause mixing and homogenisation of mantle and crustal melts (*e.g.* Hildreth and Moorbath, 1988). Granites of the Yamba Suite may represent these hybrid intrusions. The Concession Suite, dominantly a product of melting metasedimentary protoliths, may not have interacted with the mantle melts to the same extent.

Granites (ca. 2585) are closely linked in time with post-compressional extension in the southern Slave Province (James and Mortensen, 1991). The style of intrusion documented in the central Slave Province is most easily accomodated within an overall extensional setting (particularly the dyke and sill complexes, and the overall 'space' problem). A predicted consequence of crustal thickening, combined with detachment of the mantle lithosphere, is that the crust will extend following release of the compressive strain (Sondor *et al.*, 1987; Wernicke *et al.*, 1987). The timing of extension relative to

the cessation of compression depends on the thermal structure of the lithosphere, warmer lithosphere deforming more easily, with extension starting immediately after the end of compression (Sondor *et al.*, 1987). The collisional model can therefore account for, and predicts an extensional regime during and/or following granite intrusion.

8.4.3 Implications for Subduction Geometry

The model outlined above requires that subduction-modified lithospheric mantle is accreted and at least temporarily stabilized along with the crustal section during collisional orogeny. Fyson and Helmstaedt (1988) and Kusky (1989) proposed that east-directed subduction during collision would account for the dominantly westward structural vergence in the province. Such a geometry implies that subduction-modified mantle should underlie the eastern, but not the western parts of the province. The presence of similarly enriched mantle beneath the older crustal block, west of the suture zone, is more paradoxical.

The detailed geometry of subduction prior to and during collision is highly speculative in the Slave Province and it is equally probable that collision involved many separate plates and subduction systems, as, for example in the southwest Pacific and Mediterranean regions today. Geochronological studies of the pre-YKS rocks in the western Slave Province document rocks with a wide range of ages from 2.85 to 3.96 Ga (Figure 2.1). There are no geological constraints to indicate whether the rocks represent an authochthonous sequence, representing over 1 billion years of continental magmatism and metamorphism, or whether they represent separate crustal blocks which were juxtaposed by accretion in a fashion similar to the Yellowknife Supergroup rocks. It is very possible that multiple terranes, in the sense of Howell *et al.* (1985), are present within the older crustal block. In this case, enriched mantle could have been stabilized beneath the western Slave province by subduction processes during accretion of the ca. 2.85 to 3.9 Ga rocks, potentially at the same time that the eastern Slave Province was accreted. This hypothesis is difficult to test geochemically because rocks in the western Slave have interacted with the older crust and isotopic evidence for derivation of the early

tonalites from older lithospheric mantle may largely be obscured by crustal contamination. In any case there are very few geochemical or isotopic data from tonalites and diorites in the western Slave Province to test specific models at this time.

8.5 Alternative Tectonic Models

8.5.1 The Continental Arc Model

The subduction signature in the Concession Suite rocks could also have originated during active, post-collision subduction (*e.g.* Fyson and Helmstaedt, 1988). Continental margin arcs are also proposed sites of HTLP metamorphism (Miyashiro, 1973; Barton and Hanson, 1989), are commonly associated with terrane accretion, and may define a similar evolution in pluton chemistry (*e.g.* Barton, 1989).

It is instructive to consider the continental margin model relative to the tectonic assembly model outlined in Chapter 7. In particular, the timing and distribution of plutonism, will be examined. Granitoid rocks of the Concession Suite in the Contwoyto Lake area presumably overly an older crustal block, as determined by Nd isotopic data. Time and compositionally correlative tonalites of the Regan and Taylor plutonic Suites in the eastern Slave, occur in the younger block. This requires that calc-alkaline magmatism occurred, simultaneously, within both the underlying and overlying plates (*ie.* on both sides of the suture between the older and younger crustal blocks). This is incompatible with the intrusions being related to the same subduction system that juxtaposed the two blocks, as this would predict subduction related magmatism only on the overlying block, and at some distance from the suture.

A new subduction system would be required in order to generate subduction related plutonism on both sides of the proposed suture following collision. This could occur by: 1) initiation of west directed subduction with the 'new' trench located outboard of the newly accreted juvenile terrain; or 2) east directed subduction with the trench located

west of the older crustal block. The latter hypothesis was favoured by Fyson and Helmstaedt (1988), but depends very much on the width of the older cratonic block. The western limit of this block presently occurs beneath the early Proterozoic Wopmay Orogen at the Wopmay Fault Zone (Hoffman, 1989). If the eastern limit is defined by the Nd isotopic break in the granitoid rocks, then the present width of the older block is less than 300 km. This width would theoretically allow east directed subduction following collision, however the eastern-most intrusions would be 400 km distant from the new trench.

Accounting for the tremendous width of contemporaneous magmatism and metamorphism across the full width of the Slave Province is a major problem of the continental margin subduction model. Broadly contemporaneous tonalite plutonism (and metamorphism) occurred over a width in excess of 400 km across strike of the province between 2625 and 2595 Ma (van Breemen *et al.*, 1991). This is similar in duration, but much wider than modern continental margin batholiths (Pitcher, 1987). Fyson and Helmstaedt (1988) argue that the tremendous width of magmatism could be achieved by shallow subduction and rapid convergence, resulting in plutonism sweeping across the province in only a few tens of million years. The available geochronological data do not support an age progression across the province (van Breemen *et al.*, 1991), nor is there any indication that the present width of the province is a result of post-metamorphic translational or extensional faulting. The magmatism is therefore unlikely to represent a series of coalesced batholithic belts, nor a significantly structurally widened belt. No estimates of post-collisional extension have been made for the province.

The non-linearity and the extreme width of the magmatic belt in the Slave Province is unlikely to reflect unique tectonic processes operative during the Archean (*e.g.* greater plate velocities, different subduction styles) because examples of broad calc-alkaline magmatic belts are also documented in Phanerozoic orogens (*e.g.* Lachland Fold Belt (800 km) Chappell (1984) and the Scottish Caledonides (>250 km), Thirlwall, 1982). The cause of these very broad thermal anomalies remains enigmatic but there is little evidence to link it to active subduction. The collisional setting may better explain the width and non-linearity of the magmatic rocks in these settings.

The situation described above for the Slave Province is comparable to the subduction paradox in the Scottish Caledonides (Thirlwall, 1981; Watson, 1984) and northern Appalachians (Whalen, 1989; David and Gariepy, 1990). Like the Concession Suite, Caledonian granitoids are characterized by high Sr and Ba contents combined with high $(Ce/Yb)_N$. The Caledonian granitoids are linked in time and place with the appinite suite, which represents Mg-rich high SiO_2 magmas similar in composition to Na-HMA (Fowler 1988; Rogers and Dunning, 1990; Stern *et al.*, 1989). The rocks have geochemical characteristics of continental margin batholiths (Thirlwall, 1981), which led to the suggestion that subduction occurred simultaneously with the igneous activity (van Breemen and Bluck, 1981; Thirlwall, 1981).

As in the Slave Province, Silurian magmatism occurs on both sides of the inferred Iapetus suture (*e.g.* Halliday *et al.*, 1985; Watson, 1984), and therefore post-dated closure of Iapetus. Magmatism is associated with a tectonic regime of shortening, transcurrent faulting, and molasse sedimentation (Watson, 1984; Rogers and Dunning, 1990). Although subduction processes cannot be entirely eliminated, the magmatism and tectonism can be accomodated in a collisional to post-collisional tectonic setting as suggested by Watson (1984) and Zhou (1985). This tectonic setting would also be appropriate for the Slave Province.

8.6 Crust Formation Processes in the Central Slave Province

In summary, the formation and stabilization of crust in the central Slave Province occurred by two dominant processes: 1) tectonic assembly of disparate crustal blocks including both juvenile and older crust materials; and 2) collisional and post-collisional magmatism which added to, recycled, and stabilized the new crustal segment. These two processes are fundamentally similar to tectonic and petrogenetic processes associated with the formation and stabilization of orogenic crust in the Proterozoic and Phanerozoic (Patchett *et al.*, 1984; Chauvel et al., 1986; Nelson and DePaolo, 1986; Sampson *et al.*, 1990) and imply a general continuity in petrogentic and tectonic processes during the last 2.7 Ga.

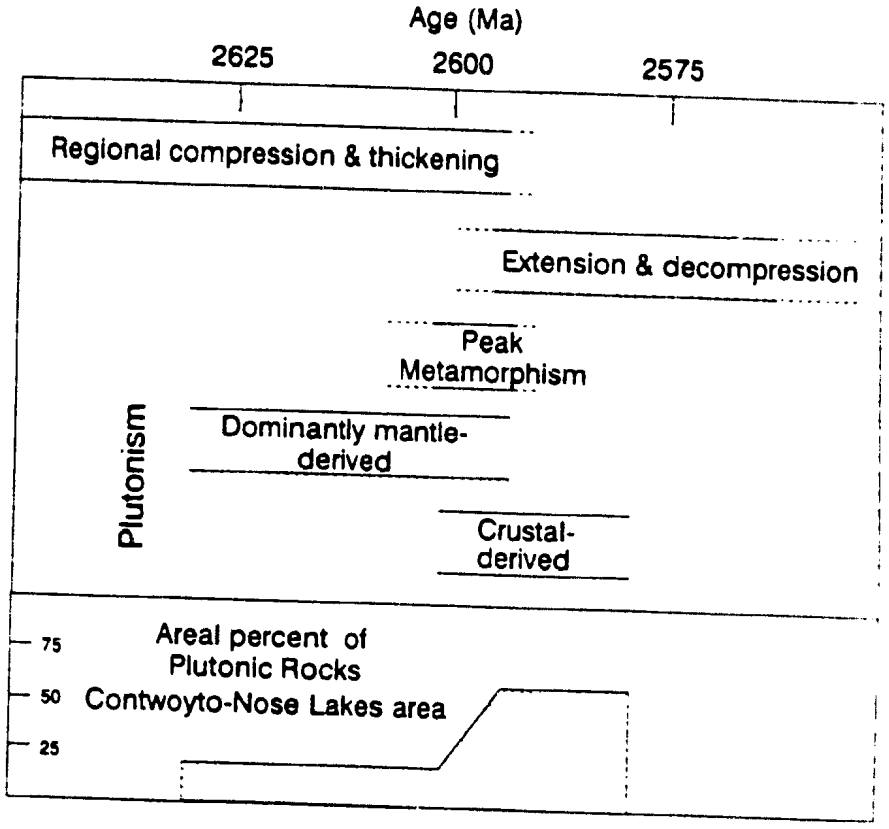

Figure 8.1. Schematic summary of the geological evolution of the area during the time period from 2650 to 2550 Ma.

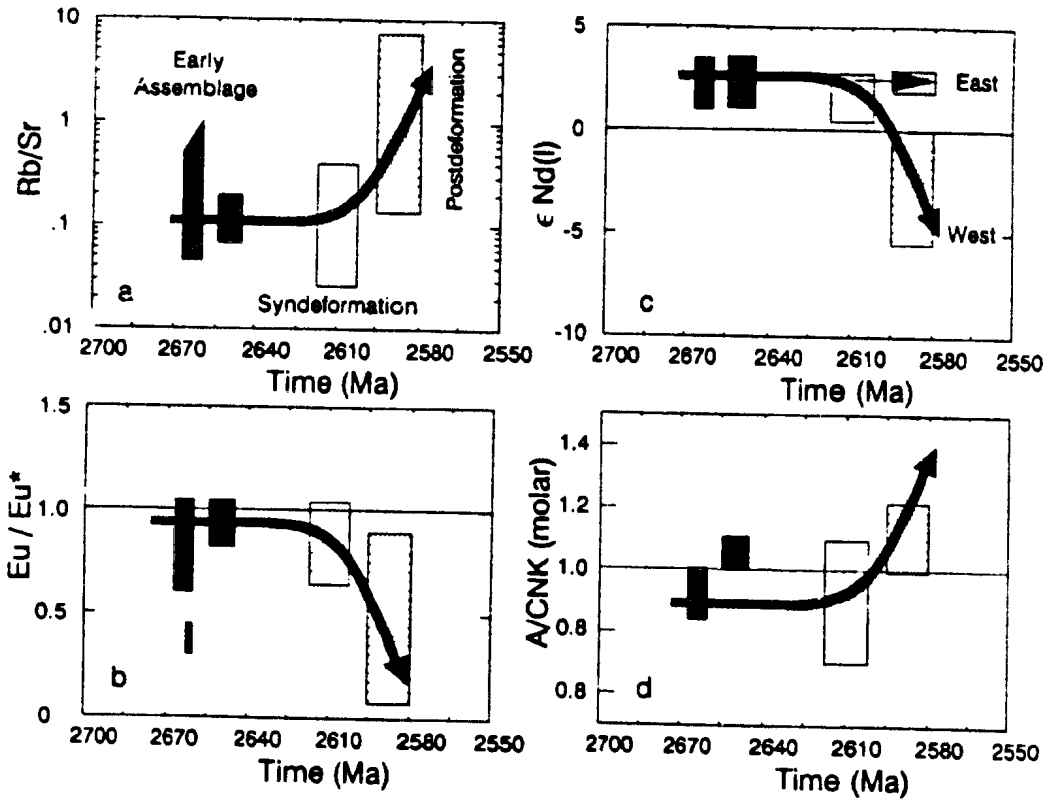

Figure 8.2. Secular evolution in the geochemistry of the igneous rocks in the Contwoyto-Nose Lakes area. Increasing Rb/Sr and peraluminousity (A/CNK) with decreasing Eu anomalies (Eu/Eu*) and $\epsilon_{Nd(I)}$ indicate an increasing crustal component in the rocks with time (indicated by arrow)

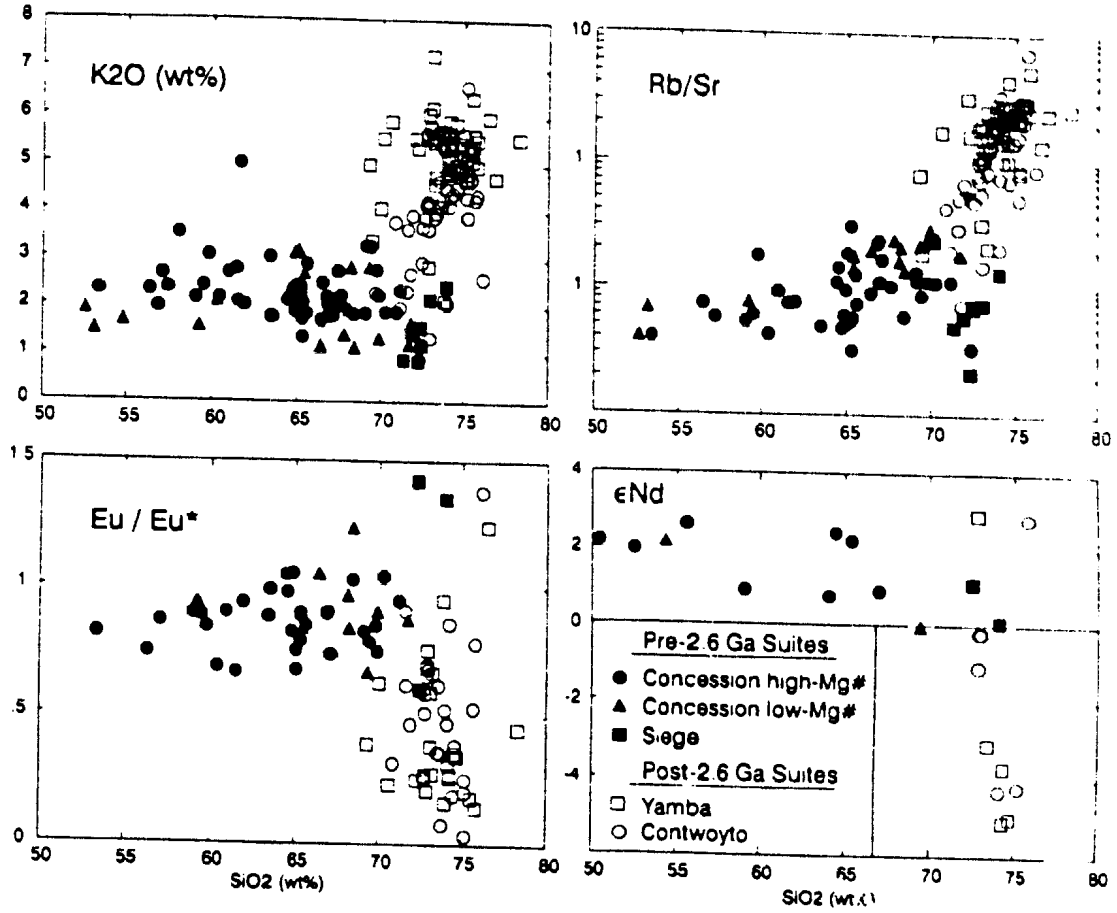

Figure 8.3. Comparison of the composition of the plutonic suites of the younger assemblage.

Figure 8.4. Cartoon depicting the Late Archean tectonic evolution proposed for the Slave Province. A) ca. 2715-2650 Ma. Development of the early tectonostratigraphic assemblage in supra-subduction zone settings, possibly including island arcs, back arc basins and continental marginal basins. The subduction processes enriched the sub-arc mantle wedges (stippled pattern) and eventually led to collision and accretion of the various terranes, including older crustal blocks. B) ca. 2650-2600 Ma. Collision caused regional shortening and thickening of the lithosphere. Melting of subduction enriched mantle (see Figure 8.6 and text for discussion) produced high-Mg andesite magmas, parental to the Concession Suite. Crustal metamorphism is caused by the thermal effects of crustal thickening and heat transfer from the mantle. C) ca. 2600-2580 Ma. Continued heating of the crust caused extensive crustal melting, which resulted in the generation and intrusion of the granites of the post-deformation suites (ie. Contwoyto and Yamba).

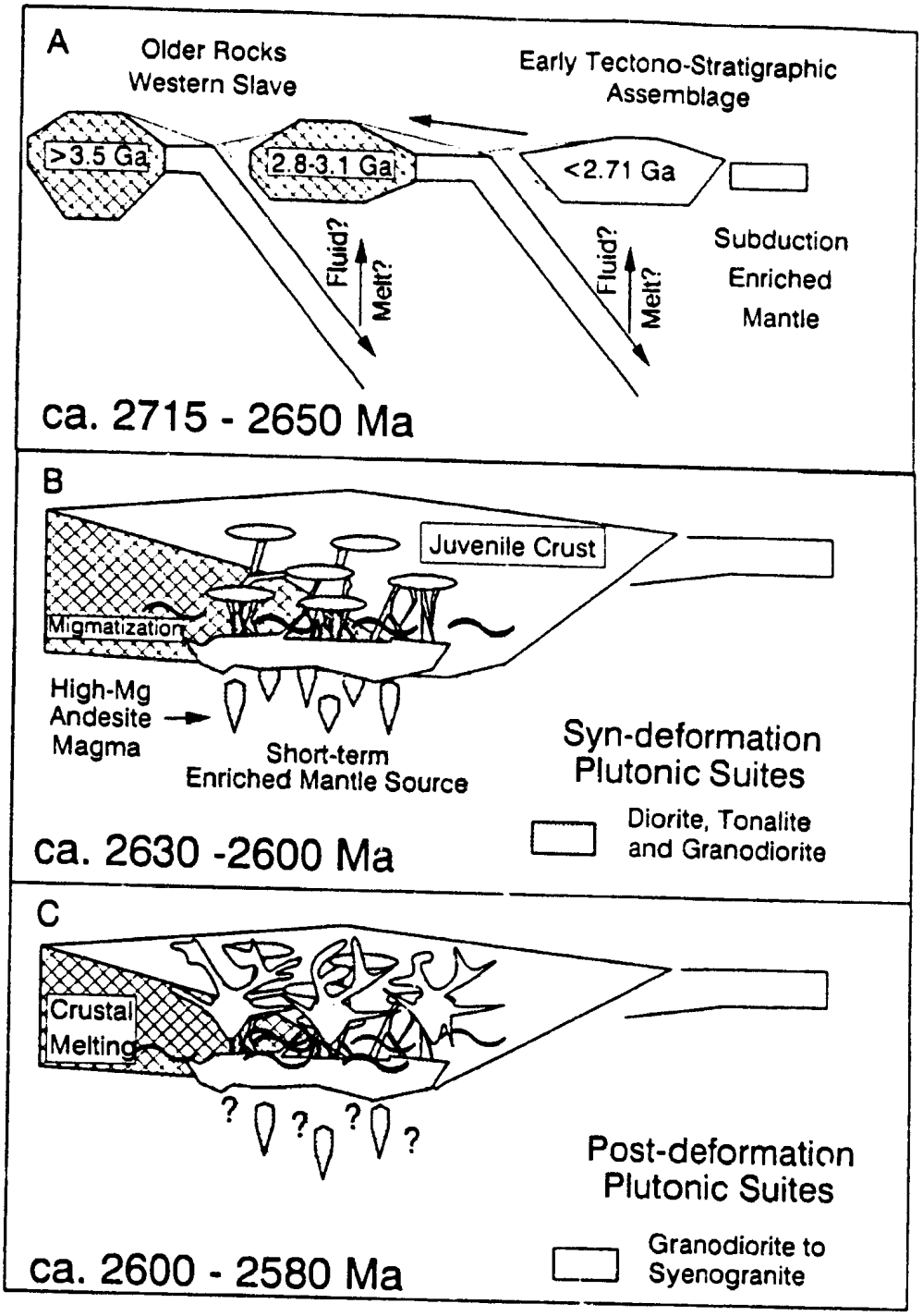
A
Older Rocks
Western Slave
Early Tectono-Stratigraphic
Assemblage
>3.5 Ga
2.8-3.1 Ga
<2.71 Ga
Fluid?
Melt?
Fluid?
Melt?
Subduction
Enriched
Mantle
ca. 2715 - 2650 Ma
B
Juvenile Crust
Migmatization
High-Mg
Andesite
Magma
Short-term
Enriched Mantle Source
Syn-deformation
Plutonic Suites
Diorite, Tonalite
and Granodiorite
ca. 2630 -2600 Ma
C
Crustal
Melting
? ? ? ?
Post-deformation
Plutonic Suites
Granodiorite to
Syenogranite
ca. 2600 - 2580 Ma

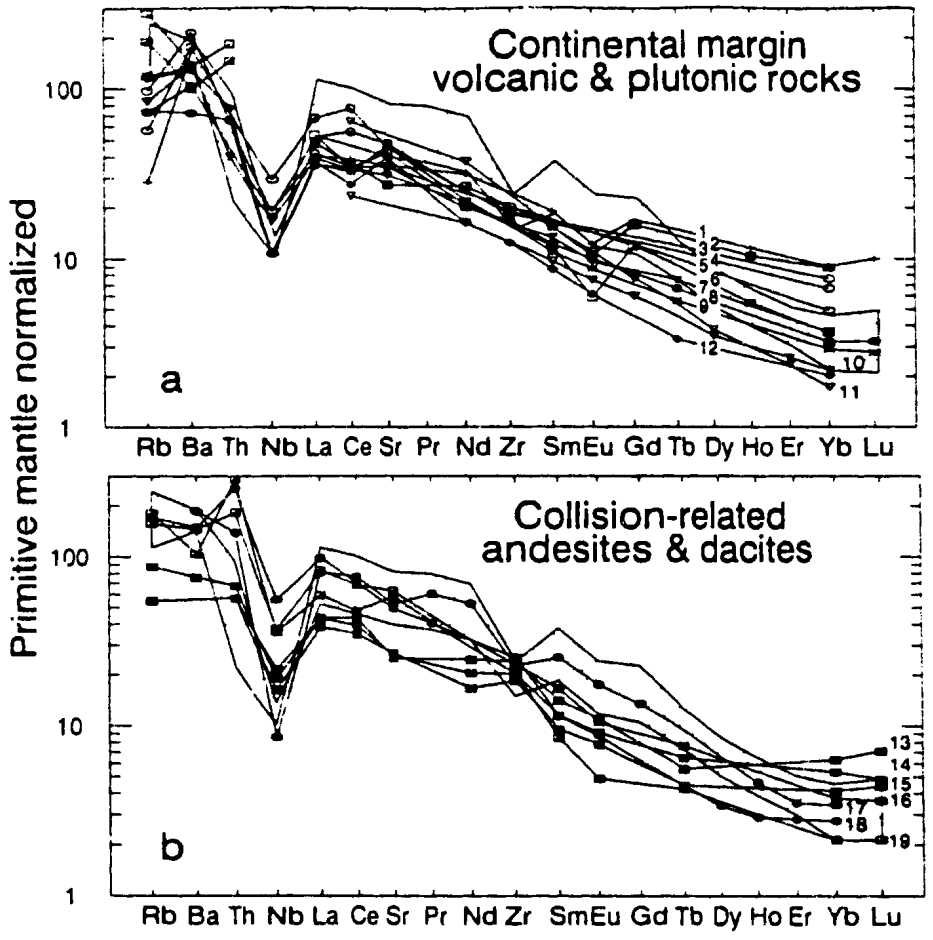

Figure 8.5. Comparison of intermediate (< 63 wt% SiO_2) rocks of the Concession Suite to rocks from continental margin (a) and collisional (b) tectonic settings. 1. north Chilean Andes, Rogers and Hawkesworth, 1988; 2. central Chile Tertiary granite, Lopez-Escobar *et al.*, 1979; 3, 4, 5. average values for Andean, western U.S., and eastern U.S. andesites, respectively, Ewart, 1982; 6. central Chile, Cretaceous granite Lopez-Escobar *et al.*, 1979; 7 central Chile Tertiary granite; Lopez-Escobar *et al.*, 1979; 8. Andean Southern Volcanic Zone, Hickey *et al.*, 1984; 9. andesite, central Chile, Group 3, Dostal *et al.*, 1977; 10 and 11. Peninsular Ranges Batholith, central and western, respectively, Gromet and Silver, 1986; 12. northern Chile Tertiary andesite, Rogers and Hawkesworth, 1988; 13, 14 and 15. eastern Anatolia, Kars and Ararat Quaternary andesites; Pearce *et al.*, 1990; 16 and 19. Iran, Savalon Quaternary andesites, Dostal and Zerbi, 1978; 17 and 18. Papua New Guinea Highlands, Quaternary andesites, Johnson *et al.*, 1978.

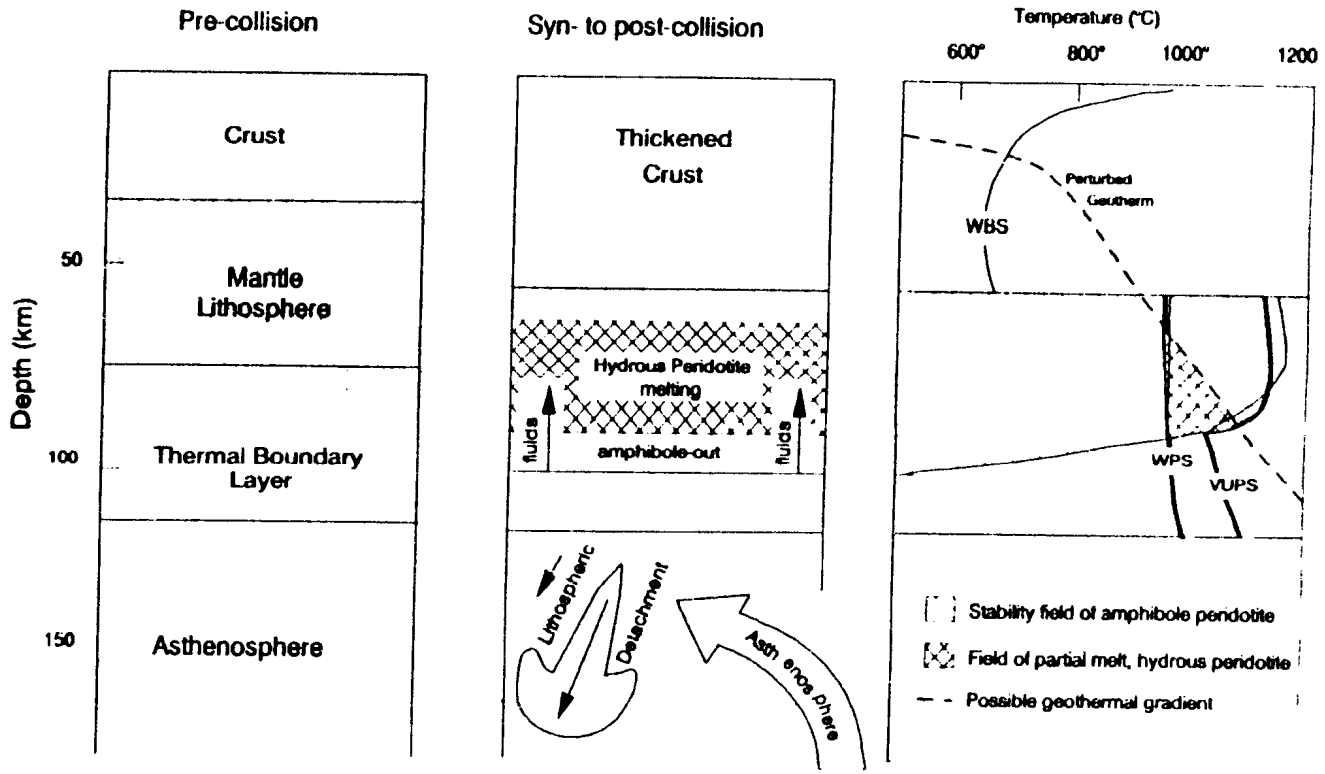

Figure 8.6. Schematic model for the generation of mantle melts during collision. The model assumes that the mantle lithosphere was previously hydrated, and that some part of the mantle lithosphere detaches during thickening of the lithosphere (b), causing upwelling of asthenospheric mantle (b), and rapid heating of the remaining lithosphere (Houseman *et al.*, 1981). The perturbed geotherm (c) may then intersect the wet or volatile undersaturated peridotite solidus, at depths less than 100 km, to produce high-Mg andesite liquids (*e.g.* Green, 1973). WPS = wet peridotite solidus (Green, 1973). VUPS = vapour undersaturated peridotite solidus ($P_{H2O} < 0.2$) (Green, 1973). WBS = wet basalt solidus (Green, 1982). Heavy dashed line is a possible post-collision geotherm. The crustal segment is inferred from observed peak-metamorphic mineral assemblages (Thompson, 1989), the mantle segment is drawn to intersect the lithosphere-asthenosphere boundary at 1300°C.

References

Allègre, C. J., and Ben Othman, B., 1980, Nd-Sr isotopic relationships in granitoid rocks and continental crust development: a chemical approach to orogenesis, Nature, 286, 335-346.

Arculus, R. J., 1987, The significance of source versus process in the tectonic controls of magma genesis, J. Volc. Geotherm. Res., 32, 1-12.

Arculus, R. J., and Powell, R., 1986, Source component mixing in the regions of arc magma generation, J. Geophys. Res., 91, 5913-5926.

Armstrong, R. L., 1982, Cordilleran metamorphic core complexes- from Arizona to southern Canada, Annual Reviews of Earth and Planetary Science, 10, 129-154.

Arndt, N. T., and Goldstein, S. L., 1987, Use and abuse of crust- formation ages, Geology, 15, 893-895.

Arndt, N. T., and Jenner, G. A., 1986, Crustally contaminated komatiites and basalts from Kambalda, Western Australia, Chem. Geol., 56, 229-255.

Arth, J. G., 1979, Some trace elements in trondhjemites-their implications to magma genesis and paleotectonic setting, *in* Barker, F., ed., Trondhjemites, Dacites, and Related Rocks, Elsevier, Amsterdam, 123-132.

Arth, J. G., Barker, F., and Stern, T. W., 1988, Coast Batholith and Taku plutons near Ketchikan, Alaska: petrography, geochronology, geochemistry, and isotopic character, Amer. J. Sci., 288-A, 461-489.

Arth, J. G., Barker, F., Peterman, Z. E., and Friedman, I., 1978, Geochemistry of the gabbro-diorite-tonalite-trondjhemite suite of southwest Finland and its implications for the origin of tonalitic and trondhjemitic magmas, J. Petrology, 19, 289-316.

Arth, J. G., and Hanson, G. N., 1975, Geochemistry and origin of the early Precambrian crust of northeastern Minnesota, Goechim. Cosmochim. Acta, 4, 325-362.

Arzi, A. A., 1978, Critical phenomena in the rheology of partially melted rocks, Tectonophysics, 44, 173-184.

Atherton, M. P., 1990, The coastal batholith of Peru: the product of rapid recycling of 'new' crust formed within rifted continental margin, Geological Journal, 25, 337-349.

Baragar, W. R. A., and McGlynn, J. C., 1976, Early Archean Basement in the Canadian Shield: A Review of the Evidence, Geological Survey of Canada, Paper 76-14.

Barbarin, B., 1990, Granitoids: main petrogenetic classifications in relation to origin and tectonic setting, Geological Journal, 25, 227-238.

Barker, F., 1979, Trondhjemite: Definition, environment and hypotheses of origin, *in* Barker, F., ed., Trondhjemites, Dacites, and Related Rocks, Elsevier, Amsterdam, 1-12.

Barker, F., and Arth, J. G., 1976, Generation of trondhjemitic- tonalitic liquids and Archean bimodal trondhjemite-basalt suites, Geology, 4, 596-600.

Barker, F., Millard Jr., H. T., and Lipman, P. W., 1979, Four low-K siliceous rocks of the western U.S.A., *in* Barker, F., ed., Trondhjemites, Dacites, and Related Rocks, Elsevier, Amsterdam, 401-414.

Barton, M. D., 1990, Cretaceous magmatism, metamorphism, and metallogeny in the east-central Great Basin, The Nature and Origin of Cordilleran Magmatism, *in* Anderson, J.L., ed., Geological Society of America, Memoir 174, 283-302.

Barton, M. D., and Hanson, R. B., 1989, Magmatism and the development of low-pressure metamorphic belts: Implications from the western United States and thermal modelling, Geol. Soc. Amer. Bull., 101, 1051-1065.

Beard, J. S., and Day, H. W., 1987, The Smartville intrusive complex, Sierra Nevada, California: The core of a rifted volcanic arc, Geol. Soc. Amer. Bull. 99, 779-791.

Beard, J. S., and Lofgren, G. E., 1989, Effect of water on the composition of partial melts of greenstone and amphibolite, Science, 244, 195-197.

Ben Othman, D., White, W., and Patchett, J., 1989, The geochemistry of marine sediments, island arc magma genesis, and crust-mantle recycling, Earth Planet. Sci. Lett., 94, 1- 21.

Bennet, V. C., and DePaolo, D. J., 1987, Proterozoic crustal history of the western United States as determined by neodymium isotopic mapping, Geol. Soc. Amer. Bull., 99, 674- 685.

Bibikova, E., Baadsgaard, H., and Folinsbee, R. E., 1986, U-Pb and Sm-Nd dating of gneissic tonalite boulders from a diatreme in the Con mine, Yellowknife, N.W.T., Canada, Terra Cognita Abstracts, 6, 156-157.

Bickle, M. J., 1978, Heat loss from the earth: A constraint on Archean tectonics from the relation between geothermal gradients and the rate of plate production, Earth Planet. Sci. Lett., 40, 301-315.

Bostock, H. H., Geology of the Itchen Lake Area, District of Mackenzie, Geological Survey of Canada, Memoir 391.

Bowring, S. A., King, J. A., Hoish, T. B., Isachsen, C. E., and Podosek, F. A., 1989a, Neodymium and lead isotope evidence for enriched early Archean crust in North America, Nature, 340, 222-225.

Bowring, S. A. Williams, I. S., and Compston, W., 1989b, 3.96 Ga gneisses from the Slave Province N.W.T. Canada, Geology, 17, 971-975.

Le Breton, N., and Thompson, A. B., 1988, Fluid-absent (dehydration) melting of biotite in metapelites in the early stages of crustal anatexis, Contrib. Mineral. Petrol., 99, 226-237.

Brooks, C. K., Henderson, P., and Ronsho, J. G., 1981, Rare-earth partition between allanite and glass in obsidian of Sandy Braes, Northern Ireland, Mineral. Mag., 44, 157-160.

Bubar, D. S., and Heslop, J. B., 1985, Geology of the Gondor volcanogenic massive sulphide deposit, Slave Province, N.W.T., Canadian Institute of Mining and Metallurgy Bulletin, 78, 52-60.

Burke, K., Dewey, J. F., and Kidd, W. S. F., 1976, Dominance of horizontal movements, arc microcontinental collisions during the late per mobile regime, *in* Windley, B.F., ed., The Early History of the Earth, J. Wiley and Sons, New York, N.Y., 113- 130.

Carroll, M. R., and Wyllie, P. J., 1989, Experimental phase relations in the system tonalite-peridotite-H2O at 15 kb: Implications for assimilation and differentiation processes near the crust-mantle boundary, J. Petrology, 30, 1351-1382.

Cawthorn, R. G., and O'Hara, M. J., 1976, Amphibole fractionation in calc-alkaline magma genesis, Am. J. Sci., 276, 309-329.

Cerny, P., Fryer, B. J., Longstaffe, F. J., and Tammemagi, H. Y., 1987, The Archean Lac du Bonnet batholith, Manitoba: igneous history, metamorphic effects and fluid overprinting, Geochim. Cosmochim. Acta, 51, 421-438.

Cerny, P., Meintzer, R. E., and Anderson, A. J., 1985, Extreme fractionation in rare-element granitic pegmatites: selected examples of data and mechanisms, Canadian Mineralogist, 23, 381-421.

Cerny, P., and Meintzer, R. E., 1988, Fertile granites in the Archean and Proterozoic fields of rare-element pegmatites: crustal environment, geochemistry and petrogenetic relationships, *in* Taylor, R.P. and Strong, D.F., ed., Recent Advances in the Geology of Granite-Related Mineral Deposits, Special Volume 39, Canadian Institiute of Mining and Metallurgy, 170-207.

Chamberlain, V. E., Lambert, R. St J., Bradley, M., and Marten, B. E., 1984, U-Pb ages on tonalitic gneisses from the Big Bend area of the Coppermine River, District of Mackenzie, N.W.T., Program with Abstracts, 9, 51.

Chappell, B. W., 1984, Source rocks of I- and S-type granites in the Lachland Fold Belt, southeastern Australia, Phil. Trans. R. Soc. London, A310, 693-707.

Chappell, B. W., White, A. J. R., and Wyborn, D., 1987, The importance of residual source material (restite) in granite petrogenesis, J. Petrology, 28, 1111-1138.

Chappell, B. W., and White, A. J. R., 1974, Two contrasting granite types, Pacific Geology, 8, 173-174.

Chase, C. G., and Patchett, P. J., 1988, Stored mafic/ultramafic crust and early Archean mantle depletion, Earth Planet. Sci. Lett., 91, 66-72.

Chauvel, C., Arndt, N. T., Kielinzcuk, S., and Thom, A., 1987, Formation of Canadian 1.9 Ga. old continental crust I. Nd isotopic data, Can. J. Earth Sci., 24, 396-406.

Christiansen, U. R., 1985, Thermal evolution models for the earth, J. Geophys. Res., 90, 2995-3007.

Clarke, D. B., and Muecke, G. K., 1985, Review of the petrochemistry and origin of the South Mountain Batholith and associated plutons, Nova Scotia, Conference on High Heat Production Granites, Inst. Min. Metall., 41-54.

Clemens, J. D., 1989, The importance of residual source material (restite) in granite petrogenesis: a comment, J. Petrology, 30, 1313-1316.

Clemens, J. D., and Vielzeuf, D., 1987, Constraints on melting and magma production in the crust, Earth Planet. Sci. Lett., 86, 287-306.

Clemens, J. D., and Wall, V. J., 1988, Controls on the mineralogy of S-type volcanic and plutonic rocks, Lithos, 21, 53-66.

Coleman, R. G., and Donato, M. M., 1979, Oceanic plagiogranites revisited, *in* Barker, F., ed., Trondhjemites, Dacites, and Related Rocks, Elsevier, Amsterdam, 149-165.

Collerson, K. D., and Fryer, B. J., 1978, The role of fluids in the formation and subsequent development of early continental crust, Contrib. Mineral. Petrol., 67, 151-167.

Condie, K.C., 1981, Archean Greenstone Belts, Elsevier, Amsterdam.

Condie, K., 1984, Archean geotherms and supracrustal assemblages, Tectonophysics, 105, 29-41.

Condie, K. C., and Baragar, W. R. A., 1974, Rare earth element distributions in volcanic rocks from Archean greenstone belts, Contrib. Mineral. Petrol., 45, 237-246.

Condie, K., and Swanson, D. H., 1973, Compositional variation in three Cascade stratovolcanoes: Jefferson, Rainier and Shasta, Bull. Volc., 37, 205-230.

Cooper, P., and Taylor, B., 1987, Seismotectonics of New Guinea: a model for arc reversal following arc-continent collision, Tectonics, 6, 53-67.

Crawford, A. J., Falloon, T. J., and Green, D. H., 1989, Classification, petrogenesis and tectonic setting of boninites, *in* Crawford, A.J., ed., Boninites and Related Rocks, Unwin Hyman Ltd, London, 2-49.

Crawford, M. B., and Windley, B. F., 1990, Leucogranites of the Himalaya/Karakoram: mplications for magmatic evolution within collisional belts and the study of collision-related leucogranite petrogenesis, J. Volc. Geotherm. Res., 44, 1-19.

Culshaw, N., and van Breemen, O., 1990, A zoned low P-high T complex at the level of anatexis- structural and plutonic patterns in metasediments of the Archean Yellowknife Supergroup, near Bathurst Inlet, N.W.T., Canada, Precambrian Research, 48, 1-20.

Cunningham, M. P., and Lambert, R. St J., 1989, Petrochemistry of the Yellowknife volcanic suite at Yellowknife, N.W.T., Can. J. Earth Sci., 26, 1630-1646.

David, J., and Gariépy, C., 1990, Early Silurian orogenic andesites from the central Quebec Appalachians, Can. J. Earth Sci., 27, 632-643.

Davidson, A., 1972, Granite studies in the Slave Province, Geological Survey of Canada, Paper 72-1A, 109-115.

Davis, W. J., 1985, Geochemistry and Petrology of the Rotoiti and Earthquake Flat Pyroclastic Deposits, unpublished MSc. thesis, University of Auckland.

Davis, W. J., and King, J. E., 1988, Geochemical evolution of plutonism in the central Slave Province, Program with Abstracts, 13, A30.

Davis, W. J., King, J. E., Fryer, B. J., and van Breemen, 1990, Petrogenesis and evolution of Late Archean granitoids in the central Slave Province: implications for the tectonic development of the Slave Province Canada, Abstract Volume. Third International Archean Symposium, Perth.

Day, W. C., and Weiblen, P. W., 1986, Origin of late Archean granite: geochemical evidence from the Vermilion granitic complex of northern Minnesota, Contrib. Mineral. Petrol., 93, 283-296.

de Witt, M. J., and Ashwall, L. D., Workshop on Tectonic Evolution of Greenstone Belts, Lunar and Planetary Institute, Technical Report 86-10, Houston, Texas.

Deer, W. A.; Howie, R. A., and Zussman, J., 1966, An Introduction to the Rock-Forming Minerals, Longman, Harlow, England.

Defant, M. J., and Drummond, M. S., 1990, Derivation of some modern arc magmas by melting of young subducted lithosphere, Nature, 347, 662-665.

Defant, M. J., and Nielsen, R. L., 1990, Interpretation of open system petrogenetic processes: Phase equilibria constraints on magma evolution, Geochim. Cosmochim. Acta, 54, 87-102.

DePaolo, D. J., 1981, A neodymium and strontium isotopic study of the Mesozoic calc-alkaline granitic batholiths of the Sierra Nevada and Peninsular Ranges, California, J. Geophys. Res., 86, 10470-10488.

DePaolo, D. J., 1988, Neodymium Isotope Geochemistry: An Introduction, Springer-Verlag, Berlin.

DePaolo, D. J., 1980, Sources of continental crust: Neodymium isotope evidence from the Sierra Nevada and Peninsular Ranges, Science, 209, 684-687.

DePaolo, D. J., and Farmer, G. L., 1984, Isotopic data bearing on the origin of Mesozoic and Tertiary granitic rocks in the western United States, Phil. Trans. R. Soc. London, A310, 743-749.

DePaolo, D. J., and Wasserburg, G. J., 1976, Nd isotopic variations and petrogenetic models, Geophys. Res. Lett., 3, 249-252.

Didier, J., 1973, Granites and Their Enclaves, Elsevier, Amsterdam.

Didier, J., Duthon, J. L., and Lameyre, J., 1982, Mantle and crustal granite: genetic classification of orogenic granites and the nature of their enclaves, J. Volc. Geotherm. Res., 14, 125-132.

Dostal, J., and Zerbi, Z., 1978, Geochemistry of the Savalon Volcano (Northwestern Iran), Chemical Geology, 22, 31-42.

Drummond, M. S., and Defant, M. J., 1990, A model for trondhjemite-tonalite-dacite genesis and crustal growth via slab melting: Archean to modern comparisons, J. Geophys. Res., 95, 21503-21522.

Drury, S. A., 1979, REE and other trace element data bearing on the origin of Archean granitic rocks from Yellowknife, N.W.T., Can. J. Earth Sci., 24, 809-815.

Dudas, F. O., 1989, Nd isotopic compositions from the Slave craton: the case of the missing mantle, Program with Abstracts, 114, A24.

Dudas, F. O., Henderson, J. B., and Mortensen, J. K., 1990, U-Pb ages of zircons from the Anton Complex, southern Slave Province, Northwest Territories, *in* Radiogenic Age and Isotopic Studies, Report 3, Geological Survey of Canada, Paper 89-2, 39-44.

Duncan, R. A., and Green, D. H., 1980, Role of multistage melting in the formation of oceanic crust, Geology, 8, 22-26.

Dunning, G. R., Kean, B. F., Thurlow, J. G., and Swinden, H. S., 1987, Geochronology of the Buchans, Roberts Arm and Victoria Lake Groups and the Mansfield Cove Complex, Newfoundland, Can. J. Earth Sci., 24, 1175-1184.

Dunning, G. R., Swinden, H. S., Kean, B. F., Evans, D. E., and Jenner, G. A., 1991, A Cambrian island arc in Iapetus: geochemistry and geochronology of the Lake Ambrose Volcanic Belt, Geological Magazine, 128, 1-17.

Dupuy, C., and Dostal, J., 1978, Geochemistry of calc-alkaline volcanic rocks from Southeastern Iran, J. Volc. Geotherm. Res., 4, 363-373.

Easton, R. M., 1985, The nature and significance of pre- Yellowknife Supergroup rocks in the Point Lake area, Slave Structural Province, Canada, *in* Ayres, L.D., Thurston, P.C., Card, K.C., and Weber, W, ed., Evolution of Archean Supracrustal Sequences, Geological Association of Canada Special Paper 28, 153-167.

Eggler, D. H., 1987, Solubility of major and trace elements in mantle metasomatic fluids: experimental constraints, *in* Menzies, M.A. and C.J. Hawkesworth, ed., Mantle Metasomatism, Academic Press, New York, 21-41.

Ellis, D. J., and Thompson, A. B., 1986, Subsolidus and partial melting reactions in the quartz-excess CaO+MgO+Al2O3+SiO2+H2O system under water-excess and water-deficient conditions to 10 kb: some implications for the origin of peraluminous melts from mafic rocks, J. Petrology, 21, 91- 121.

England, P., and Houseman, G. A., 1988, Extension during continental convergence, with application to the Tibetan Plateau, J. Geophys. Res., 94, 17561-17579.

England, P. C., and Bickle, M. J., 1984, Continental thermal and tectonic regimes in the Archaean, J. Geol., 92, 353-367.

England, P. C., and Thompson, A., 1986, Some thermal and tectonic models for crustal melting in continental collision zones, Collision Tectonics, *in* Coward, M.P. and Ries, A.C., ed., Geological Society Special Publication 19, 83-94.

Ernst, W. G., 1974, Metamorphism and ancient convergent continental margins, *in* Burk, C.A. and Drake, C.L., ed., The Geology of Continental Margins, Springer Verlag, New York, 907-919.

Ewart, A., 1982, The mineralogy and petrology of Tertiary-Recent orogenic volcanic rocks: with special reference to the andesitic-basaltic compositional range, *in* Thorpe, R.S., ed., Andesites: Orogenic andesites and related rocks, John Wiley and Sons, New York, 25-95.

Ewing, T. E., 1979, Two calc-alkaline volcanic trends in the Archean: trace element evidence, Contrib. Mineral. Petrol., 48, 1-7.

Falloon, T. J., and Green, D. H., 1987, Anhydrous partial melting of MORB pyrolite and other peridotite compositions at 10 kbar: Implications for the origin of primitive MORB glasses, Mineralogy and Petrology, 37, 181-219.

Falloon, T. J., and Green, D. H., 1989, The solidus of carbonated, fertile peridotite, Earth Planet. Sci. Lett., 94, 364-370.

Farmer, G. L., and DePaolo, D. J., 1983, Origin of Mesozoic and Tertiary granite in the western US and implications for pre- Mesozoic crustal structure. I. Nd and Sr isotopic studies in the geocline of the northern Great Basin, J. Geophys. Res., 88, 3379-3401.

Farmer, G. L., and DePaolo, D. J., 1984, Origin of Mesozoic and Tertiary granite in the western US and implications for the pre-Mesozoic crustal structure. II. Nd and Sr isotopic studies of unmineralized and Cu- and Mo- mineralized granite in the Precambrian craton, J. Geophys. Res., 89, 10141-10160.

Flynn, R. T., and Burnham, C. W., 1978, An experimental determination of rare earth partition coefficients between a chloride-containing vapor phase and silicate melts, Geochim. Cosmochim. Acta, 42, 685-701.

Folinsbee, R. W., 1949, Lac de Gras, District of Mackenzie, Northwest Territories, Map 977A, scale 1:250,000, Geological Survey of Canada.

Folinsbee, R. E., Baadsgaard, H., Cumming, G. L., and Green, D. C., 1968, A very ancient island arc, American Geophysical Union, Geophysical Monograph 12, 441-448.

Foster, D. A., and Hyndman, D. W., 1990, Large-scale crustal anatexis: the importance of subcrustal magma intrusion, EOS, 71, 299-300.

Fowler, M. B., 1988, Ach'uaine hybrid appinite pipes: evidence for mantle-derived shoshonitic parent magmas in Caledonian granite genesis, Geology, 16, 1026-1030.

Fraser, J. A., 1964, Geological notes on the northeastern District of Mackenzie, Northwest Territories, Geological Survey of Canada, Paper 63-40, 16.

Frey, F. A., and Green, D. H., 1974, The mineralogy, geochemistry and origin of lherzolite inclusions in Victoria basanites, Geochim. Cosmochim. Acta, 38, 1023-1059.

Frith, R. A., 1987, Precambrian Geology of the Hackett River Area, District of Mackenzie, Northwest Territories, Geological Survey of Canada, Memoir 417, 61.

Frith, R. A., and Fryer, B. J., 1985, Geochemistry and origin of the Regan Intrusive Suite and other granitoids in the northeastern Slave Province, northwest Canadian Shield, Can. J. Earth Sci., 22, 1048-1065.

Frith, R. A., and Loveridge, W. D., 1982, Ages of Yellowknife Supergroup volcanic rocks, granitoid intrusive rocks and regional metamorphism in the northeastern Slave Province, *in* Current Research, Part A, Geological Survey of Canada, Paper 82-1C, 225-237.

Frith, R. A., Loveridge, W. D., and van Breemen, O., 1986, U-Pb ages on zircon from basement granitoids of the western Slave Province, northwestern Canadian Shield, *in* Current Research, Part A, Geological Survey of Canada, Paper 86-14, 113-119.

Fujimaki, H., 1986, Partition coefficients of Hf, Zr, and REE between zircon, apatite and liquid, Contrib. Mineral. Petrol., 94, 42-45.

Fyson, W. K., and Frith, R. A., 1979, Regional deformations and emplacement of granitoid plutons in the Hackett River greenstone belt, Slave Province, Northwest Territories, Can. J. Earth Sci., 16, 1187-1195.

Fyson, W. K., and Helmstaedt, H., 1988, Structural patterns and tectonic evolution of supracrustal domains in the Archean Slave Province, Canada, Can. J. Earth Sci., 25, 301-315.

Gariépy, C., and Allègre, C. J., 1985, The lead isotope geochemistry and geochronology of the late kinematic intrusives from the Abitibi greenstone belt, and the implications for late Archean crustal evolution, Geochim. Cosmochim. Acta, 49, 2371-2383.

Gerlach, D. C., Lallemant, H. G. A., and Leeman, W. P., 1981, An island arc origin for the Canyon Mountain Ophiolite Complex, eastern Oregon, U.S.A., Earth Planet. Sci. Lett., 53, 255- 265.

Gill, J. B., 1983, Mountain Building and Volcanism, *in* Hsu, K.J., ed., Mountain Building Processes, Academic Press, London, 13- 17.

Gill, J. B., 1981, Orogenic andesites and plate tectonics, Springer-Verlag, New York.

Gill, J. B., and Stork, A. L., 1979, Miocene low-K dacites and trondhjemites of Fiji, *in* Barker, F., ed., Trondhjemites, Dacites, and Related Rocks, Elsevier, Amsterdam, 629-250.

Goodwin, A. M., 1988, Geochemistry of the Slave Province volcanic rocks, *in* Contributions to the Geology of the Northwest Territories, Indian and Northern Affairs Canada, 3, 13-26.

Green, D. C., Baadsgaard, H., and Cumming, G. L., 1968, Geochronology of the Yellowknife area, Northwest Territories, Canada, Can. J. Earth Sci., 5, 725-735.

Green, D. C., and Baadsgaard, H., 1971, Temporal evolution and petrogenesis of an Archean crustal segment at Yellowknife, N.W.T., Canada, J. Petrology, 12, 177-217.

Green, D. H., 1973, Experimental melting studies on a model upper mantle composition at high pressure under water-saturated and water-undersaturated conditions, Earth Planet. Sci. Lett., 19, 37-53.

Green, D. H., 1976, Experimental testing of "equilibrium" partial melting of peridotite under water-saturated, high pressure conditions, Can. J. Earth Sci., 14, 255-268.

Green, T. H., 1982, Anatexis of mafic crust and high pressure crystallization of andesite, *in* Thorpe, R.S., ed., Andesites: Orogenic andesites and related rocks, John Wiley and Sons, New York, 465-487.

Green, T. H., 1976, Experimental generation of cordierite- or garnet-bearing granitic liquids from a pelitic composition, Geology, 4, 85-88.

Green, T. H., and Pearson, N. J., 1987, Rare-earth element partitioning between sphene and coexisting silicate liquid at high pressure and temperature, Chemical Geology, 55, 105-119.

Green, T. H., and Pearson, N. J., 1986, Ti-rich accessory phase saturation in hydrous mafic-felsic compositions at high P, T, Chemical Geology, 54, 185-201.

Green, T. H., and Ringwood, A. E., 1968, Genesis of the calc- alkaline igneous rock suite, Contrib. Mineral. Petrol., 18, 105-162.

Gromet, L. P., and Silver, L. T., 1983, REE distributions among minerals in a granodiorite and their petrogenetic implications, Geochim. Cosmochimica Acta, 47, 925-939.

Gromet, P. L., and Silver, L. T., 1987, REE variation across the Peninsular Ranges batholith: Implications for batholithic petrogenesis and crustal growth in magmatic arcs, J. Petrology, 28, 38-75.

Halliday, A. N., 1984, Coupled Sm-Nd and U-Pb systematics in late Caledonian granites and the basement under northern Britain, Nature, 307, 229-233.

Halliday, A. N., Stephens, W. E., Hunter, R. H., Menzies, M. A., Dickin, A. P., and Hamilton, P. J., 1985, Isotopic and chemical constraints on the building of the deep Scottish lithosphere, Scott. J. Geol., 21, 465-491.

Hargraves, R. B., 1986, Faster spreading or greater ridge length in the Archean?, Geology, 14, 750-752.

Harmon, R. S., Halliday, A. N., Clayburn, J. A. P., and Stephens, W. E., 1984, Chemical and isotopic systematics of the Caledonian intrusions of Scotland and northern England: a guide to magma source region and magma-crust interaction, Philos. Trans. R. Soc. London, A310, 709-742.

Harris, N. B. W., Imger, S., and Ronghua, X., 1990, Cretaceous plutonism in Central Tibet: an example of post-collision magmatism?, J. Volc. Geotherm. Res., 44, 21-32.

Harris, N. B. W., Pearce, J. A., and Tindle, A. G., 1986, Geochemical characteristics of collision-zone magmatism, Collision Tectonics, *in* Coward, M.P. and Ries, A.C., ed., Geological Society Special Publication 19, 67-81.

Hawkesworth, C. J., Van Calsteren, P., Rogers, N. W., and Menzies, M. A., 1987, Isotope variations in recent volcanics: a trace-element perspective. *in* Menzies, M.A. and Hawkesworth, C.J., ed., Mantle Metasomatism, Academic Press, London, 365-388.

Heaman, L. M., Bowins, R., and Crocket, J., 1990, The chemical composition of igneous zircon suites: implications for geochemical tracer studies, Geochim. Cosmochim. Acta, 54, 1597-1607.

Helmstaedt, H. Padgham, W.A., and Brophy, J., 1986, Multiple dikes in the lower Kam Group, Yellowknife Greenstone Belt: Evidence for Archean sea floor spreading?, Geology, 14, 562- 566.

Helmstaedt, H., and Padgham, W. A., 1986, A new look at the stratigraphy of the Yellowknife Supergroup at Yellowknife, N.W.T. - implications for the age of gold-bearing shear zones and Archean basin evolution, Can. J. Earth Sci., 23, 454-475.

Helz, R. T., 1976, Phase relations of basalt in their melting ranges at PH2O = 5 kb. Part II Melt compositions, J. Petrology, 17, 139-193.

Henderson, J. B., 1970, Stratigraphy of the Archean Yellowknife Supergroup, Yellowknife Bay Prosperous Lake area, District of Mackenzie, Geological Survey of Canada, Paper 70-26.

Henderson, J. B., 1981, Archean basin evolution in the Slave Province, Canada, *in* Kroner, A., ed., Precambrian Plate Tectonics, Elsevier, Amsterdam, 213-236.

Henderson, J. B., 1985, Geology of the Yellowknife-Hearne Lake Area, District of Mackenzie: A Segment Across an Archean Basin, Geological Survey of Canada, Memoir 414, 135.

Henderson, J. B., 1988, Geology, Keskarrah Bay area, District of Mackenzie, Northwest Territories, Geological Survey of Canada, Map 1679A.

Henderson, J. B., Loveridge, W. D., and Sullivan, R. D., 1982, A U-Pb study of zircon from granitic basement beneath the Yellowknife Supergroup, Point Lake, District of Mackenzie, *in* Rb-Sr and U-Pb Isotopic Age Studies, Report 5, Geological Survey of Canada, Paper 82-1C, 173-178.

Henderson, J. B., van Breemen, O., and Loveridge, W. D., 1987, Some U-Pb zircon ages from Archean basement, supracrustal and intrusive rocks, Yellowknife-Hearne Lake area, District of Mackenzie, *in* Radiogenic Age and Isotopic Studies, Report 1, Geological Survey of Canada, Paper 87-2, 111-121.

Hickey, R. L., Frey, F. A., and Gerlach, D. C., 1986, Multiple sources for basaltic rocks from the Southern Volcanic Zone of the Andes (34°-41°S): trace element and isotopic evidence for contributions form subducted oceanic crust, mantle and continental crust, J. Geophys. Res., 91, 5963-5983.

Hildreth, W., 1981, Gradients in silicic magma chambers: implications for lithospheric magmatism, J. Geophys. Res., 86, 10153-10192.

Hildreth, W., and Moorbath, S., 1988, Crustal contributions to arc magmatism in the Andes of central Chile, Contrib. Mineral. Petrol., 98, 455-489.

Hill, J. D., 1980, The Structural Development and Crystallization of the Kenoran Granitoid Plutons in the Nose Lake-Back River Area, Northwest Territories, unpublished PhD thesis, University of Western Ontario.

Hill, J. D., and Frith, R. A., 1982, Petrology of the Regan Intrusive Suite in the Nose Lake - Beechey Lake map area, District of Mackenzie, Geological Survey of Canada, Paper 82- 8, 1-26.

Hoffman, P. F., 1986, Crustal accretion in a 2.7-2.5 Ga "granite- greenstone" terrane, Slave Province, N.W.T.: a prograding arc-trench system?, *in* de Witt, M.J. and Ashwall, L.D., ed., Tectonic Evolution of Greenstone Belts, Report 86-10, Lunar and Planetary Institute, 120.

Hoffman, P. F., 1989, Precambrian geology and tectonic history of North America, *in* Bally, A.W. and Palmer, A.R., ed., The Geology of North America-An Overview, Geological Society of America, Boulder, Colorado, 447-512.

Hoisch, T. D., and Hamilton, W. B., 1990, Granite generation by fluid-induced anatexis, EOS, 71, 694.

Holloway, J. R., and Burnham, C. W., 1972, Melting relations of basalt with equilibrium water pressure less than total pressure, J. Petrology, 13, 1-29.

Houseman, G. A., McKenzie, D. P., and Molnar, P., 1981, Convective instability of a thickened boundary layer and its relevance for the thermal evolution of continental convergent belts, J. Geophys. Res., 86, 6115-6132.

Howell, D. G., Jones, D. L., and Scherner, E. R., 1985, Tectonostratigraphic terranes of the Circum-Pacific Rim, *in* Howell, D.G., ed., Tectonostratigraphic Terranes of the Circum-Pacific Region, Pacific Council for Energy and Mineral Resources, Earth Science Series, Number 1, 3-30.

Huang, W. L., and Wyllie, P. J., 1986, Phase relationships of gabbro-tonalite-granite-water at 15 kbar with applications to differentiation and anatexis, American Mineralogist, 71, 301- 316.

Hunter, D. R., Barker, F., and Millard, H. T., 1978, The geochemical nature of the Archean Ancient Gneiss Complex and granodiorite suite, Swaziland: a preliminary study, Precambrian Research, 22, 105-127.

Huppert, H. E., and Sparks, S. S. J., 1988, The generation of granitic magmas by intrusion of basalt into continental crust, J. Petrol., 29, 599-624.

Hyndman, D. W., and Foster, D. A., 1988, The role of tonalites and mafic dikes in the generation of the Idaho Batholith, J. Geol., 96, 31-46.

Irvine, T. N., and Baragar, R. A., 1971, A guide to the chemical classification of the common volcanic rocks, Can. J. Earth Sci., 8, 523-548.

Isachsen, C., and Bowring, S. A., 1989, U-Pb geochronology of the Yellowknife volcanic belt, N.W.T.: constraints on timing and duration of greenstone belt magmatism and deformation, *in* Exploration Overview, N.W.T. Geology Division, Indian and Northern Affairs, Yellowknife, 37-38.

Isachsen, C., Bowring, S. A., and Padgham, W. A., 1990, U-Pb zircon geochronology of the Yellowknife volcanic belt, N.W.T., Canada: new constraints on the timing and duration of greenstone belt magmatism, J. Geol., 99, 55-68.

Ishihara, S., 1977, The magnetite-series and ilmenite-series granitic rocks, Mining Geology, 27, 293-305.

Jahn, B. M., Glickson, A. Y., Peucat, J. J., and Hickman, A. H., 1981, REE geochemistry and isotopic data of Archean silicic volcanics and granitoids from the Pilbara Block, Western Australia: implications for early crustal evolution, Geochim. Cosmochim. Acta, 45, 1633-1645.

Jahn, B. M., Vidal, P. H., and Kroner, A., 1984, Multi-chronometric ages and origin of Archean tonalitic gneisses in Finnish Lapland: a case for long crustal residence time, Contrib. Mineral. Petrol., 86, 398-408.

James, D. T., 1990, Basement-cover relations between the Archean Sleepy Dragon Complex and the Yellowknife Supergroup in the Brown Lake area, Slave Province, Northwest Territories, *in* Current Research, Part C, Geological Survey of Canada, Paper 90-1c, 189-196.

James, D. T., and Mortensen, J. K., 1991, Basement-cover structural relations, southern Salve Province: geochronological constraints on Archean detachment faulting, Program with Abstracts, 16, A60.

Jenner, G. A., and Fryer, B. J., 1980, Geochemistry of the upper Snooks Arm Group basalts, Burlington Peninsula, Newfoundland: evidence against formation in an island arc, Can. J. Earth Sci., 17, 888-900.

Jenner, G. A., Fryer, B. J., and McLennan, S. M., 1981, Geochemistry of the Archean Yellowknife Supergroup, Geochim. Cosmochim. Acta, 45, 1111-1129.

Johnson, R. W., Mackenzie, D. E., and Smith, I. E. M., 1978, Delayed partial melting of subduction-modified mantle in Papua New Guinea, Tectonophysics, 46, 197-216.

Johnston, A. D., and Wyllie, P. J., 1988, Constraints on the origin of Archean trondhjemites based on phase relationships of Nuk gneiss with H2O at 15 kbar, Contrib. Mineral. Petrol., 100, 35-46.

Johnston, A. D., and Wyllie, P. J., 1986, Interaction of slab- derived melts with mantle peridotite: experimental constraints at 30 kbar with H_2O, EOS, 67, 405.

Kay, R. W., 1978, Aleutian magnesian andesites: melts from subducted Pacific Ocean crust, J. Volc. Geotherm. Res., 4, 117-132.

Kay, R. W., 1980, Volcanic arc magmas: Implications for a melting-mixing model for element recycling in the crust-upper mantle system, J. Geology, 88, 497-522.

Kelemen, P. B., 1990, Reaction between ultramafic rock and fractionating basaltic magma I. Phase relations, the origin of calc-alkaline magma series, and the formation of discordant dunite, J. Petrol., 31, 51-98.

Kelemen, P. B., Joyce, D. B., Webster, J. D., and Holloway, J. R., 1990, Reaction between ultramafic rock and fractionating basaltic magma II. Experimental investigation of reaction between olivine tholeiite and harzburgite at 1150-1050°C and 5 kb, J. Petrol., 31, 99-134.

Kempton, P. D., 1987, Metasomatism and enrichment in lithospheric peridotites, *in* M.A. Menzies and C.J. Hawkesworth, ed., Mantle Metasomatism, Academic Press, New York, 45-89.

King, J. E., Davis, W. J., Van Nostrand, T., and Relf, C., 1989a, Archean to Proterozoic deformation and plutonism of the western Contwoyto Lake map area, central Slave Province, District of Mackenzie, N.W.T., *in* Current Research, Part C, Geological Survey of Canada, Paper 89-1C, 81-93.

King, J. E., Davis, W. J., and Relf, C., 1989b, Comment and reply on "Accretion of the Archean Slave province", Geology, 17, 963-964.

King, J. E., Davis, W. J., Relf, C., and Avery, R. W., 1988, Deformation and plutonism in the western Contwoyto Lake map area, Slave Structural Province, District of Mackenzie, N.W.T., *in* Current Research, Part C, Geological Survey of Canada, Paper 88-1C, 161-176.

King, J. E., Davis, W. J., Relf, C., and van Nostrand, T., 1990, Geology of the Contwoyto-Nose Lakes map area, central Slave Province, District of Mackenzie, N.W.T., *in* Current Research, Part C, Geological Survey of Canada, Paper 90-1c, 177-188.

King, J. E., and Helmstaedt, H., 1989, Deformational history of an Archean fold belt, eastern Point Lake area, Slave structural province, N.W.T., Can. J. Earth Sci., 26, 106-118.

King, J. E., Van Nostrand, T., Bethune, K., Wingate, M. T., and Relf, C., 1991, Final preliminary report of the Contwoyto- Nose Lakes map area, central Slave Province, District of Mackenzie, N.W.T., *in* Current Research, Part C, Geological Survey of Canada, Paper 91-1C.

Kistler, R. W., and Peterman, Z. E., 1973, Variations in Sr, Rb, K, Na and 87Sr/86Sr in Mesozoic granitic rocks and intruded wall rocks in central California, Bull. Geol. Soc. America, 84, 3489-3512.

Kretz, R., Loop, J., and Hartree, R., 1989a, Petrology and Li-Be- B geochemistry of muscovite-biotite granite and associated pegmatite near Yellowknife, Canada, Contrib. Mineral. Petrol., 102, 174-190.

Kretz, R., Hartree, R., and Jones, P., 1989b, Metasomatic crystallization of muscovite in granite and tourmaline in schist related to pegmatite emplacement near Yellowknife, Canada, Contrib. Mineral. Petrol., 102, 191-204.

Krogh, T. E., and Gibbons, W., 1978, U-Pb isotopic ages of basement and supracrustal rocks in the Point Lake area of the Slave Structural Province, Canada, Program with Abstracts, 3, 438.

Kröner, A., 1991, Tectonic evolution in the Archean and Proterozoic, Tectonophysics, 187, 393-410.

Kusky, T. M., 1989a, Accretion of the Archean Slave province, Geology, 17, 63-67.

Kusky, T. M., 1989b, Reply on "Accretion of the Archean Slave province", Geology, 17, 964-966.

Kusky, T. M., 1990, Evidence for Archean ocean opening and closing in the southern Slave Province, Tectonics, 9, 1533- 1563.

Kusky, T. M., and De Paor, D. G., 1991, Deformed sedimentary fabrics in metamorphic rocks: Evidence from the Point Lake area, Slave Province, Northwest Territories, Geol. Soc. Amer. Bull., 103, 486-503.

Lambert, I. B., and Wyllie, P. J., 1972, Melting of gabbro (quartz eclogite) with excess water to 35 kbars, with geological applications, J. Geology, 80, 693-708.

Lambert, M. B., 1988, The Cameron River and Beaulieu River volcanic belts, District of Mackenzie, Northwest Territories, Geological Survey of Canada, Bulletin 382, 145.

Lambert, M. B., and Henderson, J. B., 1980, A U-Pb age of zircons from volcanics and sediments in the Back River Volcanic Complex, eastern Slave Province, District of Mackenzie, *in* Rb-Sr and U-Pb Isotopic Age Studies, Report 3, Geological Survey of Canada, 239-242.

Lambert, M. B., and van Staal, C. R., 1987, Archean granite- greenstone boundary relationships in the Beaulieu River volcanic belt, *in* Current Research, Part A, Geological Survey of Canada, Paper 87-1a, 605-618.

LeFort, P., Cuney, M., Deniel, C., France-Lanord, C., Sheppard, S. M. F., Upreti, B. N., and Vidal, Ph, 1987, Crustal generation of the Himalayan leucogranites, Tectonophysics, 134, 39-57.

LeMaitre, R. W., 1979, A new generalized petrological mixing model, Contrib. Mineral. Petrol., 71, 133-137.

Liew, T. C., and McCulloch, M. T., 1985, Genesis of granitoid batholiths of the Peninsular Malaysia and implications for models of crustal evolution: evidence from a Nd-Sr and U-Pb zircon study, Geochim. Cosmochim. Acta, 49, 587-600.

Liou, J. G., 1973, Synthesis and stability relations of epidote, $Ca_2Al_2FeSi_3O_{12}(OH)$, J. Petrol., 14, 381-413.

Loosveld, R. J. H., and Etheridge, M. A., 1990, A model for low- pressure facies metamorphism during crustal thickening, J. Metamorphic Geology, 8, 257-267.

Lopez-Escobar, L., Frey, F. A., and Vergara, M., 1977, Andesites and high-alumina basalts from the central-south Chile High Andes: geochemical evidence bearing on their petrogenesis, Contrib. Mineral. Petrol., 63, 199-228.

Lopez-Escobar, L., Frey, F. A., and Oyarzun, J., 1979, Geochemical characteristics of central Chile (33°-34°S) granitoids, Contrib. Mineral. Petrol., 70, 439-450.

Ludden, N. J., Gelinas, L., and Trudel, P., 1982, Archean meta-volcanics from the Rouyn-Noranda district, Abitibi Greenstone Belt, Quebec. 2. Mobility of trace elements and petrogenetic constraints, Can. J. Earth Sci., 19, 2276-2287.

Luhr, J. F., Carmichael, I. S. E., and Varekamp, J. C., 1984, The 1982 eruptions of El Chichon volcano, Chiapas, Mexico: mineralogy and petrology of the anhydrite-bearing pumices, J. Volc. Geotherm. Res., 23, 69-108.

Lux, D. R., DeYoreo, J. J., Guldotti, C. V., and Decker, E. R., 1986, Role of plutonism in low-pressure metamorphic belt formation, Nature, 323, 794-797.

Maaloe, S., and Aoki, K., 1977, The major element composition of the upper mantle estimated from the composition of lherzolites, Contrib. Mineral. Petrol., 63, 161-173.

Macfie, R. I., van Breemen, O., and Loveridge, W. D., 1990, Late Archean U-Pb zircon age for the Clinton-Colden gabbro- anorthosite intrusion, eastern Salve Province, District of Mackenzie, Northwest Territories, *in* Radiogenic Age and Isotope Studies, Report 3, Geological Survey of Canada, Paper 89-2, 45-48.

Machado, N., Brooks, C., and Hart, S. R., 1986, Determination of initial 87Sr/86Sr and 143Nd/144Nd in primary minerals from mafic and ultramafic rocks: experimental procedure and implications for the isotopic characteristics of the Archean mantle under the Abitibi greenstone belt, Canada, Geochim. Cosmochim. Acta, 50, 2335-2348.

Mackenzie, D. P., and Bickle, M. J., 1988, The volume and composition of melt generated by extension of the lithosphere, J. Petrol., 29, 625-679.

Mahood, G., and Hildreth, W., 1983, Large partition coefficients for trace elements in high-silica rhyolites, Geochim. Cosmochim. Acta, 47, 11-30.

Malpas, J., 1979, Two contrasting trondhjemite associations from transported ophiolites in western Newfoundland: Initial report, *in* Barker, F., ed., Trondhjemites, Dacites, and Related Rocks, Elsevier, Amsterdam, 465-484.

Martin, H., 1986, Effects of steeper Archean geothermal gradient on geochemistry of subduction-zone magmas, Geology, 14, 753- 756.

Martin, H., 1987, Petrogenesis of Archean trondhjemites, tonalites and granodiorites from eastern Finland: Major and trace element geochemistry, J. Petrology, 28, 921-953.

Martin, H., Chauvel, C., Jahn, B. M., and Vidal, P. H., 1983, Rb- Sr and Sm-Nd ages and isotopic geochemistry of Archean granodioritic gneisses from eastern Finland, PreCambrian Research, 20, 79-91.

Martin, H., and Querre, G., 1985, A 2.5 Ga reworked sialic crust: Rb-Sr ages and isotopic geochemistry of late Archean volcanic and plutonic rocks from Eastern Finland, Contrib. Mineral. Petrol., 85, 292-299.

McBirney, A. H., 1980, Mixing and unmixing of magmas, J. Volc. Geotherm. Res., 7, 357-371.

McCarthy, T. S., and Hasky, R. A., 1976, Trace element distribution patterns and their relationship to the crystallization of granitic melts, Geochim. Cosmochim. Acta, 140, 1351-1358.

McCulloch, M. T., and Wasserburg, G. J., 1978, Sm-Nd and Rb-Sr chronology of continental crust formation, Science, 200, 1003-1011.

McGlynn, J. C., and Henderson, J. B., 1970, Archean volcanism and sedimentation in the Slave Structural Province, *in* Baer, A.J., ed., Symposium on Basins and Geosynclines of the Canadian Shield, Geological Survey of Canada, Paper 70-40, 31-44.

Meintzer, R. E., 1987, The Mineralogy and Geochemistry of the Granitoid Rocks and Related Pegmatites of the Yellowknife Field, unpublished PhD thesis, University of Manitoba.

Menzies, M., Blanchard, D., and Xenophontos, C., 1980, Genesis of the Smartville arc-ophiolite, Sierra Nevada foothills, California, Am. J. Sci., 280-A, 218-224.

Miller, C. F., 1985, Are strongly peraluminous magmas derived from mature sedimentary (pelitic) sources?, J. of Geology, 93, 673-689.

Miller, C. F., and Barton, M. D., 1990, Phanerozoic plutonism in the Cordilleran Interior, U.S.A., Plutonism from Antartica to Alaska, *in* Kay, S.M. and Rapela, C.W., ed., Geological Society of America, Special Paper 241, 213-231.

Miller, C. B., and Mittlefehldt, D. W., 1984, Extreme fractionation in felsic magma chambers: a product of liquid- state diffusion or fractional crystallization?, Earth Planet. Sci. Lett., 68, 151-158.

Miller, C. F., Watson, E. B., and Harrison, T. M., 1988, Perspectives on the source, segregation and transport of magmas, Transactions Royal Society of Edinburgh, Earth Sciences, 79, 135-156.

Miyashiro, A., 1973, Metamorphism and metamorphic belts, John Wiley and Sons, New York.

Miyashiro, A., 1974, Volcanic rock series in island arcs and active continental margins, Am. J. Sci., 274, 321-355.

Moorbath, S., Taylor, P. N., and Goodwin, R., 1981, Origin of granitic magma by crustal remobilization: Rb-Sr and Pb-Pb geochronology and isotope geochemistry of the late Archean Qurqut Granite Complex of southern Greenland, Geochim. Cosmochim. Acta, 45, 1051-1060.

Mortensen, J. K., Thorpe, R. I., Padgham, W. A., King, J. E., and Davis, W. J., 1988, U-Pb zircon ages for felsic volcanism in the Slave Province, N.W.T., *in* Radiogenic Age and Isotopic Studies, Report 2, Geological Survey of Canada, 85-95.

Muecke, G. K., and Clarke, D. B., 1981, Geochemical evolution of the South Mountain Batholith, Nova Scotia: rare-earth-element evidence, Canadian Mineralogist, 19, 133-145.

Mueller, P. A., and Wooden, J. L., 1988, Evidence for Archean subduction and crustal recycling, Wyoming province, Geology, 16, 871-874.

Nelson, B. K., and DePaolo, D. J., 1985, Rapid production of continental crust 1.7-1.9 by ago: Nd and Sr isotopic evidence from the basement of the North American midcontinent, Geol. Soc. Am. Bull., 746-754.

Nicholls, I. A., 1974, Liquids in equilibrium with peridotitic mineral assemblages at high water pressures, Contrib. Mineral. Petrol., 45, 289-316.

Nikic, Z., Baadsgaard, H., Folinsbee, R. E., Krupicka, J., Leech, A. P., and Sasaki, A., 1980, Boulders from the basement, the trace of an ancient crust, Selected studies of Archean gneiss and lower Proterozoic rocks, southern Canadian Shield, *in* Morey, G.B. and Hanson, G.N., ed., Geological Society of America Special Paper 182, 169-175.

Nisbet, E. G., 1987, The Young Earth, an Introduction to Archean Geology, Allen and Unwin, Boston.

North American Commission on Stratigraphic Nomenclature, 1983, North American Stratigraphic Code, American Association of Petroleum Geologists Bulletin, 67, 841-875.

O'Conner, J. T., 1965, A classification of quartz-rich igneous rocks on feldspar ratios, U.S. Geological Survey, Prof. Paper, 525-B, 79-84.

Olafsson, M., and Eggler, D. H., 1983, Phase relations of amphibole-carbonate, and phlogopite-carbonate peridotite: petrologic constraints on the asthenosphere, Earth Planet. Sci. Lett., 64, 305-315.

Oversby, V. M., 1976, Isotopic ages and geochemistry of Archean acid igneous rocks from the Pilbara, Western Australia, Geochim. Cosmochim. Acta, 40, 817-829.

Padgham, W. A., 1981, Archean crustal evolution - a glimpse from the Slave Province, *in* Geological Society of Australia, Special Publication 7, 99-110.

Padgham, W. A., 1985, Observations and speculations on supracrustal sequences in the Slave Structural Province, *in* Ayres, L.D., Thurston, P.C., Card, K.C., and Weber, W, ed., Evolution of Archean Supracrustal Sequences, Geological Association of Canada Special Paper 28, 133-152.

Paradis, S., Ludden, J., and Gelinas, L., 1988, Evidence for contrasting compositional spectra in comagmatic intrusive and extrusive rocks of the late Archean Blake River Group, Abitibi, Quebec, Can. J. Earth Sci., 25, 134-144.

Patchett, P. J., and Bridgwater, D., 1984, Origin of continental crust of 1.9-1.7 Ga age defined by Nd isotopes in the Ketilidian terrain of South Greenland, Contrib. Mineral. Petrol., 87, 311-318.

Patino Douce, A. E., Johnston, A. D., and Humphreys, E. D., 1990b, Closed system anatexis in the Cordilleran Interior: the importance of initial lithologic structure, EOS, 71, 298- 299.

Patino Douce, A. E., and Johnston, A. D., 1990, Phase equilibria and melt productivity in the pelitic system: implications for the origin of peraluminous granitoids and aluminous granulites, Contrib. Mineral. Petrol., in press.

Peacock, M. A., 1931, Classification of igneous rock series, J. Geology, 39, 54-67.

Pearce, J. A., Bender, J. F., DeLong, S. E., Kidd, W S. F., Low, P. J., Guner, Y., Saroglu, F., Yilmaz, Y., Moorbath, S., and Mitchell, J. G., 1990, Genesis of collision volcanism in Eastern Anatolia, Turkey, J. Volc. Geotherm. Res., 44, 189-229.

Pearce, J. A., Harris, N. B. W., and Tindle, A. G., 1984, Trace element discrimination diagrams for the tectonic interpretation of granitic rocks, J. Petrology, 25, 956-983.

Pedersen, R. B., and Malpas, J., 1984, The origin of oceanic plagiogranite from the Karmoy ophiolite, Western Norway, Contrib. Mineral. Petrol., 88, 36-52.

Perkins, D., and Robinson, C., 1985, Archean geotherms and supracrustal assemblages - a discussion, Tectonophysics, 113, 367-370.

Phelps, D., 1979, Petrology, geochemistry and origin of the Sparta quartz diorite-trondhjemite complex, northeastern Oregon, *in* Barker, F., ed., Trondhjemites, Dacites, and Related Rocks, Elsevier, Amsterdam, 547-580.

Phelps, D., and Lallemant, H. G. Ave, 1980, The Sparta ophiolite complex, northeast Oregon: a plutonic equivalent to low-K2O island-arc volcanism, Am. J. Sci., 280-A, 345-358.

Pitcher, W. S., 1970, Ghost stratigraphy in intrusive granites: a review, *in* Newall, G. and Rast, N., ed., Mechanisms of Igneous Intrusion, Gallery Press, Liverpool, 123-140.

Pitcher, W. S., 1983, Granite type and tectonic environment, *in* Hsu, K.J., ed., Mountain Building Processes, Academic Press, London, 18-40.

Pitcher, W. S., 1987, Granites and yet more granites forty years on, Geologische Rundschau, 76, 51-79.

Puig, A., Herve, M., Suarez, M., and Saunders, A. D., 1984, Calc- alkaline and alkaline Miocene and calc-alkaline Recent volcanism in the southernmost Patagonian Cordillera, Chile, J. Volc. Geotherm. Res., 20, 149-163.

Rapp, R. P., and Watson, E. B., 1986, Monazite solubility and dissolution kinetics: implications for the thorium and light rare earth chemistry of felsic magmas, Contrib. Mineral. Petrol., 94, 304-316.

Relf, C., 1989, Archean deformation of the Contwoyto Formation metasediments, western Contwoyto Lake area, Northwest Territories, *in* Current Research, Part C, Geological Survey of Canada, Paper 89-1C, 95-105.

Relf, C., 1990, Archean deformation and metamorphism of metasedimentary rocks in the Contwoyto-Nose Lakes area, central Slave Province, N.W.T., *in* Current Research, Part C, Geological Survey of Canada, Paper 90-1c, 97-106.

Richter, F. M., 1985, Models for the Archean thermal regime, Earth Planet. Sci. Lett., 73, 350-360.

Robinson, P., Higgins, N., and Jenner, G. A., 1986, Determination of rare-earth elements, yttrium and scandium in rocks by an ion exchange-X-ray fluorescence technique, Chem. Geol., 55, 121-137.

Rogers, G., and Dunning, G. R., 1991, Geochronology of appinitic and related granitic magmatism in the W Highland of Scotland: constraints on the timing of transcurrent fault movement, J. Geological Society of London, 148, 17-27.

Rogers, G., and Hawkesworth, C., 1989, A geochemical traverse across the North Chilean Andes: evidence for crust generation from the mantle wedge, Earth Planet. Sci. Lett., 91, 271-285.

Rogers, G., and Saunders, A. D., 1989, Magnesian andesites from Mexico, Chile and the Aleutian Islands: implications for magmatism associated with ridge-trench collision, *in* Crawford, A.J., ed., Boninites and Related Rocks, Unwin Hyman Ltd, London, 417-445.

Rogers, J. J. W., and Greenberg, J. K., 1990, Late-orogenic, post-orogenic and anorogenic granites: distinction by major- element and trace-element chemistry and possible origins, J. of Geology, 98, 291-309.

Rudnick, R. L., and Taylor, S. R., 1986, Geochemical constraints on the origin of Archean tonalite-trondhjemite rocks and implications for lower crustal composition, The Nature of the Lower Crust, *in* Dawson, J.B., Carswell, D.A., Hall, J.A. and Wedepohl, K.H., ed., Geological Society Special Publication 24, 179-191.

Samson, S. D., Patchett, P. J., Gehrels, G. E., and Anderson, R. G., 1990, Nd and Sr isotopic characterization of the Wrangellia terran and implications for crustal growth of the Canadian Cordillera, J. Geol., 98, 749-762.

Sandiford, M., 1989, Secular trends in the evolution of metamorphic terrains, Earth Planet. Sci. Lett., 95, 85-96.

Saunders, A. D., Rogers, G., Marriner, G. F., Terrell, D. J., and Verma, S. P., 1987, Geochemistry of Cenozoic volcanic rocks, Baja California, Mexico: implications for the petrogenesis of post-subduction magmas, J. Volc. Geotherm. Res., 32, 223-245.

Sawka, M., 1988, REE and trace element variations in accessory minerals and hornblende from the strongly zoned McMurry Meadows pluton, California, Trans. R. Soc. Edinburgh Earth Sci., 157-168.

Schaltegger, U., and Krahenbuhl, U., 1990, Heavy rare-earth enrichment in granites of the Aar Massif (Central Alps, Switzerland), Chemical Geology, 89, 49-63.

Schärer, U., and Allègre, C. J., 1982, Investigations of the Archean crust by single grain ...ing of detrital zircon: a greywacke of the Slave Province, Canada, Can. J. Earth Sci., 19, 1910-1918.

Searle, M. P and Fryer, B. J., 1986, Garnet, tourmaline and muscovite-bearing leucogranites, gneisses and migmatites of the Higher Himalayas from Zanskar, Kulu Lahoul and Kashmir, *in* Coward, M.P. and Ries, A.C., ed., Collision Tectonics, Geological Society Special Publication 19, 185-202.

Sekine, T., and Wyllie, P. J., 1982a, The system granite- peridoite-H2O at 30 kbar, with applications to hybridization in subduction zone magmatism, Contrib. Mineral. Petrol., 81, 190-202.

Sekine, T., and Wyllie, P. J., 1982b, Phase relationships in the system $KAlSiO_4$-Mg_2SiO_4-SiO_2-H_2O as a model for hybridization between hydrous siliceous melts and peridotite, Contrib. Mineral. Petrol., 79, 368-374.

Shirey, S. B., and Hanson, G. N., 1986, Mantle heterogeneity and crustal recycling in Archean granite-greenstone belts: Evidence from Nd isotopes and trace elements in the Rainy Lake area, Superior Province, Ontario, Canada, Geochim. Cosmochim. Acta, 50, 2631-26511.

Shirey , S. B., and Hanson, G. N., 1984, Mantle-derived Archean monzodiorites and trachyandesites, Nature, 310, 222-224.

Sondor, L. J., England, P. C., Wernicke, B. P., and Christiansen, R. L., 1987, A physical model for Cenozoic extension of western North America, Continental Extensional Tectonics, *in* Coward, M.P., Dewey, J.F. and Hancock, P.L., ed., Geol. Soc. London, Special Publ. 28, 187-201.

Sparks, R. S. J., 1986, The role of crustal contamination in magma evolution through geological time, Earth Planet. Sci. Lett., 78, 211-223.

St. Seymour, K., Budkevitsch, P., and Kumarapeli, S., 1988, The petrotectonic environment of basalts of Point Lake and Redrock Lakes, Slave Province, NWT, *in* Contributions to the Geology of the Northwest Territories, Indian and Northern Affairs Canada, 3, 103-114.

Steiger, R. H., and Jager, E., 1978, Subcommission on Geochronology: Convention on the use of decay constants in geo- and cosmochronology, Earth Planet. Sci. Lett., 36, 359- 362.

Stern, C. R., 1991, Role of subduction erosion in the generation of Andean magmas, Geology, 19, 78-81.

Stern, C R., Futa, K., and Muehlenbachs, K., 1984, Isotope and trace element data for orogenic andesites from the Austral Andes, *in* R.S. Harmon and B.A. Barreiro, ed., Andean Magmatism, Chemical and Isotopic constraints, Shiva Publishing, Nantwich, England, 31-46.

Stern, C. R., and Wyllie, P. J., 1978, Phase compositions through crystallization intervals in basalt-andesite-H2O at 30 kb with implications for subduction zone magmas, American Mineralogist, 63, 641-663.

Stern, R. A., and Hanson, G. N., 1991, Archean high-Mg granodiorite: A derivative of light rare earth element- enriched Monzodiorite of mantle origin, J. Petrol., 32, 201- 238.

Stern, R. A., Hanson, G. N., and Shirey, S. B., 1989, Petrogenesis of mantle-derived, LILE-enriched Archean monzodiorites and trachyandesites (sanukitoids) in southwestern Superior Province, Can J. Earth Sci., 26, 1688- 1712.

Stockwell, C. H., 1933, Great Slave Lake-Coppermine River area, N W.T., Geological Survey of Canada, Summary Report 1932, Part C, 37-63.

Streckheisen, A., 1976, To each plutonic rock its proper name, Earth-Science Reviews, 12, 1-33.

Sun, S.-S., 1984, Geochemical characteristics of Archean ultramafic and mafic volcanic rocks: implications for mantle composition and evolution, *in* Kroner, A.F., Hanson, G.N. and Goodwin, A.M., ed., Archaean Geochemistry, Springer-Verlag, Berlin, 25-46.

Sun, S.-S., and Nesbitt, R. W., 1978, Geochemical regularities and genetic significance of ophiolitic basalts, Geology, 6, 689-693.

Sun, S.-S., Nesbitt, R. W., and McCulloch, M. T., 1989, Geochemistry and petrogenesis of Archean and early Proterozoic siliceous high-magnesian basalts, *in* Crawford, A.J., ed., Boninites and Related Rocks, Unwin Hyman Ltd, London, 149-173.

Swinden, H. S., Jenner, G. A., Fryer, B. J., Hertogen, J., and Roddick, J. C., 1990, Petrogenesis and paleotectonic history of the Wild Bight Group, an Ordovician rifted island arc in central Newfoundland, Contrib. Mineral. Petrol., 105, 219- 241.

Tarney, J., Dalziel, I. W. D., and de Wit, M. J., 1976, Marginal basin "Rocas Verde" complex from S. Chile: a model for Archean greenstone belt formation, The Early History of the Earth, 131-146.

Tatsumi, Y., 1981, Melting experiments on a high-magnesium andesite, Earth Planet. Sci. Lett., 54, 357-365.

Tatsumi, Y., 1989, Migration of fluid phases and genesis of basalt magmas in subduction zones, J. Geophys. Res., 94, 4697-4707.

Tatsumi, Y., 1982, Origin of high-magnesium andesites in the Setouchi volcanic belt, southwest Japan, II. Melting phase relations at high pressures, Earth Planet. Sci. Lett., 60, 305-317.

Tatsumi, Y., and Ishizaka, K., 1982a, Magnesian andesite and basalt form Shodo Shima island, southwest Japan and their bearing on the genesis of calc-alkaline andesites, Lithos, 15, 161-172.

Tatsumi, Y., and Ishizaka, K., 1982b, Origin of high-magnesian andesites in the Setouchi volcanic belts, southwest Japan, I. Petrological and chemical characteristics, Earth Planet. Sci. Lett., 60, 293-304.

Tatsumi, Y., and Maruyama, S., 1989, Boninites and high-Mg andesites: tectonics and petrogenesis, *in* Crawford, A.J., ed., Boninites and Related Rocks, Unwin Hyman Ltd, London, 50-71.

Tatsumi, Y., Hamilton, D. L., and Nesbitt, R. W., 1986, Chemical characteristics of fluid phase released from a subducted lithosphere and origin of arc magmas: evidence from high- pressure experiments and natural rocks, J. Volc. Geotherm. Res., 29, 293-309.

Taylor, S. R., and McLennan, S. M., 1985, The Continental Crust: Its Composition and Evolution, Blackwell, Oxford.

Theriault, R. J., 1990, Methods for Rb-Sr and Sm-Nd isotopic analyses at the geochronology laboratory, Geological Survey of Canada, *in* Radiogenic Age and Isotopic Studies, Report 3, Geological Survey of Canada, Paper 89-2, 3-6.

Thirwall, M. F., 1981, Implications for Caledonian plate tectonic models of chemical data from volcanic rocks of the British Old Red Sandstone, J. Geol. Soc. London, 138, 123-138.

Thirwall, M. F., 1982, Systematic variation in chemistry and Nd- Sr isotopes across a Caledonian calc-alkaline volcanic arc: implications for source materials, Earth Planet. Sci. Lett., 58, 27-50.

Thompson, A.B., and England, P. C., 1984, Pressure-temperature- time paths of regional metamorphism II. Their inference and interpretation using mineral assemblages in metamorphic rocks, J. Petrology, 25, 929-955.

Thompson, P. H., 1978, Archean regional metamorphism in the Slave Province - a new perspective on some old rocks, Metamorphism in the Canadian Shield, Geological Survey of Canada, Paper 78-10, 85-102.

Thompson, P. H., 1989, An empirical model for metamorphic evolution of the Archean Slave Province and adjacent Thelon Tectonic Zone, north-western Canadian Shield, *in* Daly, J.S., Cliff, R.A., and Yardley, B.W.D., ed., Evolution of Metamorphic Belts, Special Publication No. 43, Geological Society, 245-263.

Thurston, P. C., and Fryer, B. J., 1933, The geochemistry of repetitive cyclical volcanism from basalt through rhyolite in the Uchi-Confederation greenstone belt, Canada, Contrib. Mineral. Petrol., 83, 204-226.

Thy, P., Beard, J. S., and Lofgren, G. E., 1990, Experimental constraints on the origin of Icelandic rhyolites, J. Geol., 98, 417-421.

Tremblay, L. P., 1976, Geology of the northern Contwoyto Lake area, Geological Survey of Canada, Memoir 381.

van Breemen, O., and Bluck, B. J., 1981, Epsiodic granite plutonism in the Scottish Caledonides, Nature, 291, 113-117.

van Breemen, O., Davis, W. J., and King, J. E., 1991, Geochronology of granitoid rocks in the Archean Slave Province, N.W.T., Program with Abstracts, 16, A127.

van Breemen, O., Henderson, J. B., Sullivan, R. W., and Thompson, P. H., 1987a, U-Pb zircon and monazite ages from the eastern Slave Province, Healey Lake area, N.W.T., *in* Radiogenic Age and Isotopic Studies, Report 1, Geological Survey of Canada, Paper 87-2, 101-110.

van Breemen, O., Thompson, P. H., Hunt, P. A., and Culshaw, N., 1987b, U-Pb zircon and monazite geochronology from the northern Thelon Tectonic zone, District of Mackenzie, *in* Radiogenic Age and Isotopic Studies, Report 1, Geological Survey of Canada, Paper 87-2, 81-93.

van Breemen, O., and Henderson, J. B., 1988, U-Pb zircon and monazite ages from the eastern Slave Province and Thelon Tectonic Zone, Artillery Lake area, N.W.T., *in* Radiogenic Age and Isotope Studies, Report 2, Geological Survey of Canada, 73-83.

van Breemen, O., King, J. E., and Davis, W. J., 1990, U-Pb zircon and monazite ages from plutonic rocks in the Contwoyto-Nose lakes map area, central Slave Province, District of Mackenzie, Northwest Territories, *in* Radiogenic Age and Isotopic Studies, Report 3, Geological Survey of Canada, Paper 89-2, 29-38.

Vernon, R. H., 1983, Restite, xenoliths and microgranitoid enclaves in granites, Journal and Proceedings, Royal Society New South Wales, 116, 77-103.

Vidal, Ph, 1987, Use and misuse of radiogenic isotopes in granite petrology, *in* McReath, I., Sabate, P., and Sial, A.N., ed., International Symposium on Granites and Associated Mineralization, Salvador, Bahia, Brazil, 149-151.

Vidal, Ph, Bernard-Griffiths, J., Cocherie, A., LeFort, P., Peucat, J. J., and Sheppard, S. M. F., 1984, Geochemical comparison between Himalayan and Hercynian leucogranites, Physics of the Earth and Planetary Interiors, 35, 179-190.

Vidal, Ph Cocherie, A., and Lefort, P., 1982, Geochemical investigations of the origin of the Manaslu leucogranite (Himalaya, Nepal), Geochim. Cosmochim. Acta, 46, 2279-2292.

Vielzeuf, D., and Holloway, J. R , 1988, Experimental determination of the fluid-absent melting relations in the pelitic system, Contrib. Mineral. Petrol., 98, 257-276.

Walker, R. J., Hanson, G. N., Papike, J. J., and O'Neil, J. R., 1986, Nd, O and Sr isotopic constraints on the origin of Precambrian rocks, Southern Black Hills, South Dakota, Geochim. Cosmochim,. Acta, 50, 2833-2846.

Wall, V. J., Clemens, D., and Clarke, D. B., 1987, Models for granitoid evolution and source compositions, J. of Geology, 95, 731-749.

Wanless, R. K., and Loveridge, W. D., 1978, Rubidium-Strontium isotopic age studies, Report 2 (Canadian Shield), Paper 77- 14, Geological Survey of Canada, 7-12.

Watson, E. B., and Capobianco, C. J., 1981, Phosphorous and the rare earth elements in felsic magmas: an assessment of the role of apatite, Geochim. Cosmochim. Acta, 45, 2349-2358.

Watson, E. B., and Harrison, T. M., 1984, Accessory minerals and the geochemical evolution of crustal magmatic systems: a summary and prospectus of experimental approaches, Physics of the Earth and Planetary Interiors, 35, 19-30.

Watson, J., 1984, The ending of the Caledonian orogeny in Scotland, J. Geol. Soc. London, 191, 193-214.

Webb, D. R., and Kerrich, R., 1988, An Archean ultramafic lamprophyre, Yellowknife: Implications for tectonics and source regions, *in* Contributions to the Geology of the Northwest Territories, Indian and Northern Affairs Canada, 3, 115-122.

Wedepohl, K. H., and Muramatsu, Y., 1979, The chemical composition of kimberlites compared with the average composition of three basaltic magma types, *in* Boyd, F.R. and Meyer, H.O.A., ed., Kimberlites, diatremes and diamonds: Their geology, petrology and geochemistry, AGU, Washington, D.C., 300-312.

Wernicke, B. P., Christiansen, P. L., England, P. C., and Sondor, L. J., 1987, Tectono-magmatic evidence of Cenozoic extension in the North American Cordillera, Continental Extensional Tectonics, *in* Coward, M.P., Dewey, J.F. and Hancock, P.L., ed., Geol. Soc. London, Special Publ. 28, 203-221.

Whalen, J. B., 1989, The Topsails igneous suite, western Newfoundland: an Early Silurian subduction-related magmatic suite?, Can. J. Earth Sci., 26, 2421-2434.

Whalen, J. B., Currie, K. L., and Chappell, B. W., 1987, A-type granites: geochemical characteristics, discrimination and petrogenesis, Contrib. Mineral. Petrol., 95, 407-419.

White, A. J. R., and Chappell, B. W., 1983, Granitoid types and their distribution in the Lachlan fold belt, southeastern Australia, Geological Society of America, Memoir 159, 21-34.

White, A. J. R., Clemens, J. D., Holloway, J. R., Silver, L. T., Chappell, B. W., and Wall, V. J., 1986, S-type granites and their probable absence in southwestern North America, Geology, 14, 115.

Whitford, D. J., Nicholls, I. A., and Taylor, S. R., 1979, Spatial variations in the geochemistry of Quaternary lavas across the Sunda arc in Java and Bali, Contrib. Mineral. Petrol., 70, 341-356.

Wickham, S. J., 1987, The segregation and emplacement of granitic magmas, J. Geol. Soc. London, 144, 281-291.

Windley, B. F., 1976, New tectonic models for the evolution of Archean continents and oceans., *in* Windley, B.F., ed., The Early History of the Earth, J. Wiley and Sons, New York, N.Y., 105-102.

Wingate, M. T. D., 1990, Petrogenesis of Cordierite-bearing Migmatites of the Central Archean Slave Province, unpublished BSc. Thesis, Carleton University.

Wooden, J. L., and Mueller, P. A., 1988, Pb, Sr and Nd isotopic compositions of a suite of Late Archean, igneous rocks, eastern Beartooth Mountains: implications for crust-mantle evolution, Earth Planet. Sci. Lett., 87, 59-72.

Wyllie, P. J., 1984, Constraints imposed by experimental petrology on possible and impossible magma sources and products, Philos. Trans. R. Soc. London, Ser. A, 310, 439- 456.

Wyllie, P. J., and Sekine, T., 1982, The formation of mantle phlogopite in subduction zone hybridization, Contrib. Mineral. Petrol., 79, 375-380.

Zen, E-An, 1989, Wet and dry AFM mineral assemblages of strongly peraluminous granites, EOS, 70, 109-110.

Zen, E-An, and Hammarstrom, J. M., 1984, Magmatic epidote and its petrologic significance, Geology, 12, 515-518.

Zhou, J., 1985, The timing of calc-alkaline magmatism in parts of the Alpine-Himalayan collision zone and its relevance to the interpretation of Caledonian magmatism, J. Geol. Soc. London, 142, 309-317.

Zielinski, R. A., and Lipman, P. W., 1976, Trace element variations at Summer Coon volcano, San Juan Mountains, Colorado, and the origin of continental interior andesite, Geol. Soc. Amer. Bull., 87, 1477-1485.

Appendix 1

Geochemical Analytical Techniques

Rocks were sampled free of all visible weathering and alteration. Samples were scrubbed and ultrasonically cleaned in distilled water prior to crushing. 1 to 5 Kg of sample was coarsely crushed in a steel plated jaw crusher. A 150 to 250 g aliquot was then ground to a fine powder in a tungsten-carbide puck mill (TEMA).

Major element oxides were determined by atomic absorption spectrophotometry (G. Andrews, analyst). Accuracy and precision are given in Table A1.1

The trace elements Rb, Sr, Y, Zr, Nb (± Th) were determined by XRF using the REPEAT program on a Phillips 1450. Relative accuracy and precision for these elements determined from USGS standards are less than 5% for Rb, Sr, Zr and Y and less than 10% for Nb and Th (Table A1.2). Duplicate and replicate analyses of samples are presented in Table A1.3.

The trace elements Ga, Ba, Sc, V, Ni, Cu and Zn were determined by XRF using the Trace2 program at Memorial University. Relative accuracy and precision for these elements determined from replicate analyses of USGS standard samples are given in Table A1.4.

The rare earth elements (REE), Pb, U, Cs, Li and Th, were determined by ICP-MS at Memorial University (Longerich et al., 1990; Jenner et al., 1990). Two different sample preparation and analytical techniques were used: 1) HF-HNO_3 dissolution followed by analyses by standard addition (HF), and ; 2) Na_2O_2 sinter dissolution (Robinson et al., 1986) followed by analyses by internal standard (SIS) or standard addition (SSA). Duplicate and replicate analyses of both techniques are shown in Table A1.5. Relative accuracy and precision for the REE using the standard addition technique, based on replicate analyses of USGS standards are 3-5% (Jenner et al., 1990). Precision of the internal standard technique is slightly poorer, with RSD ranging from 4 to 6% (Table A1.5). Th is slightly poorer at 11%. These values were

determined from 22 sets of duplicate and replicate analyses of unknown samples (Table A1.5). Mean detection limits are generally less than 10 parts per billion (Table A1.5; Jenner et al., 1990) as were typical blanks.

Li, Cs, Tl, U and Pb were determined by ICP-MS only for those samples dissolved using the HF-HNO_3 technique.

Th was determined by XRF in those samples not analyses by ICP-MS. These samples can be recognized because they have Th data without REE data.

Table A1.1 Standard and Duplicate Analyses – Major Elements

Sample	Be-N Accepted	Be-N Avg 6	Be-N STD	Ma-N Accepted	Ma-N Avg 6	Ma-N STD
SiO2	38.2	38 5	0.18	66.6	65.6	0.08
TiO2	2.61	2.59	0.04	0.01	0	0.00
Al2O3	10.07	10.02	0.09	17.62	17.39	0.24
Fe2O3	12.84	12.84	0.11	0.47	0.45	0.005
MnO	0.2	0.19	0 00	0.04	0.04	0.00
MgO	13.15	13.14	0.07	0.04	0.045	0.005
CaO	13.87	13.91	0.05	0.59	0.58	0.007
Na2O	3.18	3.25	0.02	5.84	5.84	0.02
K2O	1.39	1.46	0.007	3.18	3.23	0.04

Sample	D40-89	D40-89	D41-89	D41-89	D283-89	D283-89	D153-89	D153-89	V308-88	V308-88
SiO2	77.3	75.4	74.6	74.6	55.9	57.7	71.7	72.5	72.8	72.1
TiO2	0 04	0.18	0.06	0.04	0.96	0.9	0.24	0.24	0.12	0.04
Al2O3	12.3	12.5	13.2	13.6	20	20.8	14.6	14.2	14.7	14.7
Fe2O3	1.24	1.29	0.9	0.92	7.95	8.42	1.67	1.57	0.82	0.79
MnO	0.02	0.02	0.01	0.02	0.1	0.1	0.02	0.02	0.01	0.02
MgO	0.11	0.12	0.13	0.13	4.2	4.28	0.53	0.55	0.28	0.29
CaO	0.72	0.68	0.82	0.9	1.4	1.48	0.78	0.8	0.86	0.88
Na2O	3.84	3 92	4.01	4.1	2.33	2.41	3.44	3.21	4.07	4.24
K2O	4.2	3.95	4.41	4.73	2.66	2.9	5.52	5.61	4.26	4.3
P2O5	0	0.01	0.02	0.01	0.09	0.06	0.15	0.16	0.24	0.23
LOI	0.55	0.23	0.24	0.47	1.46	1.15	0.88	0.56	0.97	0.86

Sample	D134-88	D134-88	D72B-87	D72B-87	D72B-87	D218-87	D218-87	D172b-87	D172b-87	D277-88
SiO2	74.0	75.0	70.9	71.3	71.4	58.1	58.4	52.7	53.8	63.5
TiO2	0.2	0.16	0.36	0.36	0.32	0.72	0.72	3.08	3.16	0.52
Al2O3	13.1	13	14.5	14.7	15.3	17.7	17.2	14.1	14.2	15.8
Fe2O3	1.43	1.41	2.86	2.78	2.98	6.04	5.87	13.54	13.1	4.76
MnO	0.01	0.01	0.05	0.04	0.04	0.08	0.07	0.14	0.13	0.08
MgO	0.34	0.33	0.74	0.69	0.71	3.8	3.52	3.59	3.56	2.47
CaO	0.84	0.84	2.8	2.96	2.96	5.48	5.72	5.9	6.16	4.64
Na2O	2.89	2.93	4.47	4.69	4.52	4.87	5.19	3.22	3.35	4.43
K2O	5.63	5.58	1 22	1.2	1.2	2.13	2.09	1.24	1.25	1.34
P2O5	0 07	0.02	0.11	0.08	0.11	0.38	0.3	0.33	0.28	0.28
LOI	0.55	0.7	0.38	0.5	0.4	0.39	0.54	0.66	0 83	1.23

Sample	D258-88	D258-88	D201a-87	D201a-87	D201a-87	D201a-87	D114-87	D114-87	D114-87	D114-87
SiO2	66.0	65.8	63.8	63.8	63.8	64.4	69.6	69.6	69.6	69.3
TiO2	0.56	0.56	0.48	0.52	0.52	0.48	0.52	0.48	0.52	0.52
Al2O3	15.8	15.8	15.7	15.8	15.9	15.8	14.4	14.5	14.4	14.4
Fe2O3	4.41	4.39	4.31	4.34	4.29	4.32	3.12	3.07	3.09	3.08
MnO	0.09	0.07	0.07	0.07	0.07	0.07	0.02	0.02	0.02	0.02
MgO	2.17	2.16	2.61	2.62	2.6	2.63	0.72	0.69	0.71	0.71
CaO	3.2	3.18	4.12	4.12	4.08	4.12	1.48	1.48	1.48	1.48
Na2O	4.55	4.52	4.83	4.8	4.79	4.75	2.98	3	2.99	2.99
K2O	2.11	2.16	1.96	1.99	1.99	1.99	5.85	5.8	5.8	5.75
P2O5	0.3	0.29	0.23	0.19	0.18	0.17	0.24	0.23	0.24	0.23
LOI	0.63	0.65	0.75	0.73	0.71	0.72	0.87	0.67	0.68	0.81

Table A1.2 XRF Precision and Accuracy – Repeat Program

		AGV-1	BCR-1	BCR-1	G-2	G-2	GSP-1	GSP-1	W-1	W-1	BHVO-
		1988	1988	1989	1988	1989	1988	1989	1988	1989	1988
Rb	AVG	67.8	47.7	47.7	163	164	247	247	21.8	21.3	9.0
	RSD	1.8%	2.1%	0.8%	1.3%	0.5%	0.7%	0.2%	3.3%	4.2%	5.9%
	ACC	67	46.6	46.6	169	169	250	250	21	21	11
	% Diff	1.2%	2.3%	2.3%	3.7%	3.1%	1.1%	1.3%	3.7%	1.5%	18.1%
Sr	AVG	677	335	338	471	474	233	232	189	189	397
	RSD	0.5%	0.6%	0.3%	1.1%	0.4%	0.5%	0.4%	0.7%	0.5%	0.5%
	ACC	660.0	330	330	479	479	240	240	190	190	403
	% Diff	2.5%	1.7%	2.4%	1.8%	1.0%	2.9%	3.5%	0.5%	0.5%	1.6%
Y	AVG	19.9	36.6	37.4	11.1	11.3	27.7	28.3	21.8	21.0	26.3
	RSD	4.3%	5.8%	2.1%	13.5%	2.0%	6.9%	1.7%	5.3%	5.4%	1.7%
	ACC	21.0	37	37	11.4	11.4	29	29	26	26	27.6
	% Diff	5.4%	1.2%	1.1%	2.6%	0.8%	4.4%	2.3%	16.2%	19.3%	4.9%
Zr	AVG	254	196	194	309	308	493	480	95.3	94.0	182
	RSD	1.5%	1.2%	0.5%	1.0%	0.3%	1.3%	0.8%	1.7%	1.3%	1.7%
	ACC	230.0	195	195	300	300	500	500	95	95	179
	% Diff	10.4%	0.3%	0.3%	3.0%	2.5%	1.4%	3.9%	0.3%	1.1%	1.9%
Nb	AVG	14.2	13.9	13.3	11.3	11.6	27.4	25.6	7.8	7.4	18.7
	RSD	3.8%	9.4%	2.6%	3.1%	1.9%	13.7%	1.8%	8.8%	10.6%	2.8%
	ACC	14.0	13.5	13.5	13	13	23	23	9	9	19
	% Diff	1.3%	2.7%	1.2%	12.7%	10.8%	19.3%	11.3%	13.8%	18.0%	1.7%
Th	AVG			5.4		24.4		97.1		1.9	
	RSD			7.0%		5.5%		1.1%		85.5%	
	ACC			5.9		24.6		106		2.4	
	% Diff			7.6%		0.8%		8.4%		19.6%	
	n	20	66	5	26	6	18	4	24	4	9

Table A1.3 Replicate XRF Analyses 1988

Sample	Run #	Rb	Sr	Y	Zr	Nb	Th
A294-87	RPT 203	122	117.4	26.4	131.0	6.8	
A294-87	RPT 195	121	118.8	27.1	132.2	6.9	
A294-87	AVERAGE	122	118.1	26.8	131.6	6.9	
A325-87	RPT 196	71.9	1352	20.1	96.9	4.6	
A325-87	RPT 189	72.9	1326	19.0	86.0	4.4	
A325-87	AVERAGE	72.4	1339	19.6	91.4	4.5	
A359-87	RPT 203	141	209	5.6	177	5.6	
A359-87	RPT 201	142	210	5.4	177	5.8	
A359-87	RPT 186	142	209	6.1	179	5.9	
A359-87	AVERAGE	142	209	5.7	177	5.7	
D023-87	RPT 191	81.3	1088	23.6	217	10.3	
D023-87	RPT 189	81.6	1112	23.9	229	11.4	
D023-87	AVERAGE	81.6	1100	23.8	223	10.8	
D029-87	RPT 198	56.8	765	18.1	152	7.7	
D029-87	RPT 185	58.5	766	15.5	154	7.2	
D029-87	AVERAGE	57.6	765	16.8	153	7.4	
D033-87	RPT 191	193	92.2	18.2	131.3	14.2	
D033-87	RPT 187	199	93.4	15.8	131.2	13.9	
D033-87	AVERAGE	196	92.8	17.0	131.2	14.0	
D057A-87	RPT 197	159	112.7	23.3	152	9.3	
D057A-87	RPT 186	162	110.4	21.0	152	10.7	
D057A-87	AVERAGE	161	111.6	22.1	152	10.0	
D059A-87	RPT 190	85.9	98.8	11.6	47.2	5.4	
D059A-87	RPT 183	84.5	97.8	10.4	46.6	5.1	
D059A-87	AVERAGE	85.2	98.3	11.0	46.9	5.2	
D072A-87	RPT 191	31.4	476	0.70	65.0	1.06	
D072A-87	RPT 187	31.8	479	0.39	64.8	1.35	
D072A-87	AVERAGE	31.6	478	0.54	64.9	1.21	
D072B-87	RPT 202	43.3	280	6.6	233	4.5	
D072B-87	RPT 201	43.0	281	6.8	234	5.5	
D072B-87	AVERAGE	43.2	280	6.7	234	5.0	
D081-87	RPT 203	200	70.9	10.5	39.2	9.2	
D081-87	RPT 195	200	71.4	10.6	39.6	9.4	
D081-87	AVERAGE	200	71.1	10.5	39.4	9.3	
D108A-87	RPT 197	35.8	20.8	49	163	27.0	
D108A-87	RPT 185	35.6	20.1	48	163	27.4	
D108A-87	AVERAGE	35.7	20.4	49	163	27.2	
D114C-1	RPT 196	201	115.9	17.0	392	12.2	
D114C-2	RPT 189	204	116.0	17.7	400	12.8	
D114C-3	RPT 195	208	125.1	17.7	411	11.1	
D114C-4	RPT 201	204	116.3	18.7	406	12.2	
D114c-87	AVERAGE	204	118.3	17.8	402	12.1	
D128A-87	RPT 202	275	37.3	7.0	23.6	5.2	
D128A-87	RPT 195	274	38.6	7.1	23.1	4.7	
D128A-87	AVERAGE	275	37.9	7.1	23.4	4.9	
D151-1-87	RPT 190	44.0	140.4	35	76.7	6.6	
D151-1-87	RPT 189	44.0	138.6	35	77.8	6.8	
D151-1-87	AVERAGE	44.0	139.5	35	77.3	6.7	
D152B-87	RPT 197	68.6	1351	22.5	85.2	3.6	
D152B-87	RPT 185	71.7	1348	22.5	81.2	2.12	
D152B-87	AVERAGE	69.2	1350	22.5	83.2	2.83	

D155-87	rpt 193	56.5	1082	9.6	161	4.7
D155-87	RPT 191	55.0	1056	8.7	159	4.7
D155-87	AVERAGE	55.7	1069	9.1	160	4.7
D169-87	RPT 196	56.8	352	14.8	172	9.4
D169-87	RPT 183	57.1	345	12.7	168	9.3
D169-87	AVERAGE	56.9	348	13.8	170	9.3
D172B-A	RPT 189	26.9	431	27.2	190	19.3
D172B-B	RPT 187	25.6	427	28.6	197	19.7
D172B-B*	RPT 204	25.8	430	28.7	197	19.7
D172B-87	AVERAGE	25.7	428	28.6	197	19.7
D201A-1	rpt 193	56.8	990	11.3	156	5.5
D201A-1	RPT 183	57.4	982	11.3	156	6.3
D201A-3	RPT 197	57.5	989	10.1	158	6.1
D201A-3	RPT 185	57.1	990	10.3	156	6.5
D201A-4	RPT 187	57.3	985	11.1	157	6.5
D201A-87	AVERAGE	57.2	987	10.8	157	6.2
D217-87	RPT 204	39.6	532	3.6	81.7	2.02
D217-87	RPT 203	38.5	523	3.5	80.9	1.90
D217-87	RPT 201	39.8	525	3.1	82.0	1.22
D217-87	RPT 186	38.1	525	2.93	82.2	2.50
D217-87	AVERAGE	39.0	526	3.3	81.7	1.91
D218-87	RPT 188	59.4	1098	19.0	231	8.7
D218-87	RPT 182	60.6	1124	18.6	232	9.4
D218-87	AVERAGE	60.0	1111	18.8	232	9.0
D221-87	RPT 202	11.3	39.0	126	225	35
D221-87	RPT 182	12.1	38.4	127	223	36
D221-87	AVERAGE	11.7	38.7	127	224	35
D237-87	RPT 203	-0.933	186.8	29.0	216	9.0
D237-87	RPT 197	0.752	187.5	29.3	215	9.9
D237-87	RPT 185	1.20	185.9	30	218	10.8
D237-87	AVERAGE	0.338	186.7	29.5	216	9.9
D265-87	RPT 191	131	164.9	6.4	126.2	5.7
D265-87	RPT 188	130	164.8	5.3	120.3	6.5
D265-87	AVERAGE	130	164.9	5.8	123.3	6.1
D316-87	RPT 203	277	6.72	12.1	25.6	12.5
D316-87	RPT 201	279	6.30	11.4	28.4	11.7
D316-87	RPT 185	279	6.26	12.5	29.0	13.3
D316-87	AVERAGE	278	6.43	12.0	27.7	12.5
D319C-87	RPT 199	14.7	718	-0.243	100.3	1.04
D319C-87	RPT 197	16.4	733	0.69	104.8	1.48
D319C-87	RPT 185	15.7	729	-0.409	102.5	1.39
D319C-87	AVERAGE	15.6	727	0.011	102.5	1.30
D335-87	RPT 204	223	69.3	35	204	16.3
D335-87	RPT 183	223	69.4	34	203	16.4
D335-87	AVERAGE	223	69.4	34	203	16.3
D338-87	RPT 201	258	138.1	9.0	66.9	7.2
D338-87	RPT 197	258	140.2	9.1	66.2	7.4
D338-87	RPT 186	258	139.3	9.9	65.6	7.1
D338-87	RPT 184	258	138.9	9.7	66.4	8.3
D338-87	AVERAGE	258	139.1	9.4	66.3	7.5
D350A-87	RPT 188	213	137.9	6.8	95.3	11.7
D350A-87	RPT 182	219	139.1	7.3	95.1	11.5
D350A-87	AVERAGE	216	138.5	7.1	95.2	11.6
D362-87	RPT 198	11.6	81	14.8	70.2	4.6
D362-87	RPT 188	13.2	485	15.0	71.8	5.2
D362-87	AVERAGE	12.4	483	14.9	71.0	4.9

D364A 87	RPT 202	33.7	509	44	125.5	13.6	
D364A-87	RPT 184	33.6	490	40	115.8	12.6	
D364A-87	AVERAGE	33.7	499	42	120.6	13.1	
D364B-87	rpt 193	51.9	603	7.4	278	9.5	
D364B-87	RPT 184	52.4	594	9.8	266	11.1	
D364B-87	AVERAGE	52.2	598	8.6	272	10.3	
D365-87	RPT 197	14.2	690	17.3	97.9	8.1	
D365-87	RPT 185	14.4	688	15.2	98.6	8.5	
D365-87	AVERAGE	14.3	689	16.3	98.2	8.3	
D375B-87	RPT 198	30.9	743	28.4	101.9	11.5	
D375B-87	RPT 186	30.4	745	28.9	102.3	13.3	
D375B-87	AVERAGE	30.6	744	28.6	102.1	12.4	
KO28B-87	RPT 201	191	89.8	23.9	125.7	11.0	
KO28B-87	RPT 188	190	90.5	24.3	126.4	12.0	
KO28B-87	RPT 182	191	89.3	23.9	124.8	11.6	
KO28B-87	AVERAGE	191	89.9	24.1	126.0	11.5	
K142-87	RPT 203	116	204	6.5	192	8.2	
K142-87	RPT 191	114	204	6.7	191	8.4	
K142-87	AVERAGE	115	204	6.6	191	8.3	
RO51-87	RPT 200	29.4	184.4	35	159	11.4	
RO51-87	RPT 186	30.3	185.8	34	158	12.2	
RO51-87	AVERAGE	29.9	185.1	34	158	11.8	

Duplicate Analyses 1989

		Rb	Sr	Y	Zr	Nb	Th
D105-88	RPT 425	72.5	957	18.0	194	8.9	7.1
D105-88	AVERAGE	71.8	937	18.1	187	9.3	6.2
D105-88D	RPT 430	71.0	917	18.2	179	9.7	5.4
D110-88	RPT 422	73.2	660	8.4	161	6.7	3.1
D110-88	AVERAGE	73.3	657	8.1	161	6.5	4.5
D110-88D	RPT 429	73.4	653	7.9	161	6.3	5.8
D136-88	RPT 423	37.0	538	0.32	87.3	0.87	2.7
D136-88	AVERAGE	36.9	531	0.58	87.3	1.11	0.63
D136-88d	RPT 427	36.8	525	0.85	87.4	1.35	-1.423
D168-88	RPT 422	162	526	18.6	177	12.7	14.2
D168-88	RPT 430	161	525	20.2	180	13.6	12.6
D168-88	AVERAGE	162	526	19.4	179	13.1	13.4
D205-88	RPT 427	70.7	360	6.3	167	3.9	5.4
D205-88	ROT 423	73.4	368	5.4	168	3.9	6.7
D205-88	AVERAGE	72.1	364	5.9	167	3.9	6.1
D273-88	RPT 424	112	774	12.4	186	6.6	3.8
D273-88	AVERAGE	113	777	12.7	184	6.6	2.6
D273-88D	RPT 429	114	780	12.9	182	6.7	1.33
D277-88	RPT 421	44.5	793	15.1	173	6.1	4.2
D277-88	AVERAGE	44.7	793	15.3	175	6.1	4.8
D277-88d	RPT 424	44.9	793	15.6	177	6.1	5.5

Repeat of samples analysed in 1988 in 1989

		Rb	Sr	Y	Zr	Nb	Th
D114C-1	1988	201	116	17.0	392	12.2	
D114C-2	1988	204	116	17.7	400	12.8	
D114C-3	1988	208	125	17.7	411	11.1	
D114C-4	1988	204	116	18.7	405	12.2	
D114C-4	AVERAGE	204	119	17.8	402	12.1	
D114C-3-87	rpt 427	206	124	18.0	410	12.8	29
D201A-1-87	1988	57.4	982.	11.3	156	6.258	
D201A-1-87	1988	56.8	990.	11.3	156	5.403	
D201A-3-87	1988	57.1	990.	10.3	156	6.493	
D201A-3-87	1988	57.5	989.	10.1	158	6.075	
D201A-4-87	1988	57.3	985.	11.1	157	6.507	
D201A	AVERAGE	57.2	987.	10.8	156.	6.2	
D201A4-87	1989	57.5	997.	11.8	158.	6.3	4

Table A1.4 XRF Precision and Accuracy – Trace2 Progra

		BCR-1 1988	BCR-1 1989	GSP-1 1988	GSP-1 1989	G-2 1988	G-2 1989	W-1 1988	W-1 1989
Ga	AVG	21	22	20	22	21		15	
	RSD	7.1%	6.9%	4.5%	3.8%	6.9%		8.7%	
	ACC	22	22	23	23	23	23	16	18
	% Diff	6.4%	0.5%	13.0%	4.9%	10.0%		3.8%	
Ba	AVG	704	672	1255	1287	1869	1938	188	173
	RSD	4.2%	7.3%	1.8%	2.3%	3.8%		12.9%	
	ACC	680	680	1300	1300	1900		160	
	% Diff	3.5%	1.2%	3.5%	1.0%	1.7%		17.3%	
Sc	AVG	31	32	5	6	3	3	34	37
	RSD	5.7%	6.9%	17.9%	21.7%	39.7%		5.8%	
	ACC	33	33	6.6	6.6	3.5		35	
	% Diff	6.9%	4.2%	24.2%	16.7%	2.9%		4.0%	
V	AVG		429	46	55	33	39	263	261
	RSD		0.8%	4.2%	4.6%	10.1%		1.3%	
	ACC		420	54	54	36		260	
	% Diff		2.2%	15.1%	1.4%	7.2%		1.3%	
Ni	AVG	17	18	9	7	7	5	78	77
	RSD	8.8%	13.6%	14.1%	20.5%	11.6%		2.1%	
	ACC	10	10	9	9	3.5		76	
	% Diff	72.0%	84.0%	0.0%	20.8%	94.3%		2.9%	
Cu	AVG	19	28	35	34	21	16	105	108
	RSD	7.5%	3.9%	2.6%	3.2%	6.3%		1.1%	
	ACC	16	16	33	33	10		110	
	% Diff	17.9%	71.9%	6.1%	1.9%	108%		4.9%	
Zn	AVG	130	129	103	101	88	86	97	94
	RSD	1.1%	1.4%	0.7%	1.1%	1.1%		0.9%	
	ACC	125	125	105	105	84		86	
	% Diff	4.0%	3.3%	1.7%	3.8%	5.2%		12.3%	
	n	15	9	6	8	10	2	5	1

Table A1.5 Duplicate and Replicate ICP–MS Analyses

Technique	Run	Sample	Li	Cs	La	Ce	Pr	Nd	Sm	Eu	Gd	Tb	Dy	Ho	Er	Tm	Yb	Lu	Pb	Th	U
HF	TR–122	D201A–1–87	94.9	5.4	31.01	70.10	8.38	33.51	5.47	1.48	4.98	0.49	2.39	0.44	1.10	0.16	1.06	0.15	9.2	5.9	2.35
HF	TR–123	D201A–2–87	98.8	5.5	29.42	66.01	7.92	31.65	5.42	1.35	4.45	0.46	2.45	0.45	1.06	0.15	0.99	0.15	9.3	5.4	2.21
HF	TR–123	D201A–3–87	101.6	5.4	30.27	68.10	8.05	31.37	5.28	1.36	4.60	0.47	2.37	0.43	1.02	0.16	0.96	0.15	9.6	5.4	2.10
SIS	SR–28	D201A–4–87			30.72	67.54	8.13	32.72	5.32	1.40	3.66	0.48	2.53	0.49	1.13	0.16	0.99	0.16		5.4	
SSA	TR–094	D201A–4–87		0.3	30.46	68.52	8.24	31.53	5.54	0.96	3.82	0.49	2.43	0.44	1.09	0.15	0.98	0.15	2.0	5.4	0.78
HF	TR–094	D218–87	41.4	2.0	42.73	103.11	12.61	48.60	7.90	1.83	6.18	0.68	3.48	0.64	1.53	0.21	1.33	0.20	10.3	6.5	1.98
SIS	SR–29	D218–87			51.23	111.60	14.38	56.32	9.52	2.56	6.08	0.77	3.84	0.72	1.86	0.23	1.75	0.25		8.1	
SSA	TR–094	D218–87		0.2	49.29	110.32	14.11	54.05	9.20	2.12	6.44	0.78	3.91	0.72	1.74	0.45	1.53	0.24	4.3	7.8	1.01
SSA	TR–094	D218–87		0.2	50.43	115.41	14.37	54.29	8.94	1.96	6.01	0.74	3.71	0.71	1.73	0.67	1.55	0.23	3.8	7.5	0.94
SIS	SR–29	D055–88			51.16	89.94	9.75	33.02	6.10	0.31	4.84	0.78	4.31	0.85	2.35	0.30	1.97	0.28		43.8	
SIS	SR–28	D055–88			51.20	96.94	10.43	36.18	6.64	0.43	5.70	0.96	5.51	1.02	2.85	0.36	2.35	0.34		33.0	
HF	TR–125	D065B–87	13.2	2.1	68.50	160.67	19.17	76.17	15.28	1.81	15.37	2.33	14.75	3.08	8.28	1.21	8.12	1.25	4.6	9.5	2.14
HF	TR–122	D065B–87	12.7	2.1	57.52	135.38	16.13	63.13	12.70	1.66	14.08	2.21	13.70	2.94	8.10	1.18	8.31	1.22	4.4	9.3	2.14
SIS	SR–29	D065B–87			62.58	135.69	17.51	70.54	14.06	1.67	13.01	2.27	14.31	3.15	8.72	1.29	8.45	1.28		9.0	
SSA	TR–098	D072A–87	0.7	0.0	6.64	13.05	1.44	5.36	0.82	0.31	0.54	0.07	0.33	0.06	0.16	0.02	0.15	0.03	1.5	0.9	0.55
SSA	TR–094	D072A–87	1.2	0.0	6.39	12.69	1.41	4.97	0.78	0.04	0.59	0.07	0.34	0.06	0.15	0.02	0.17	0.03	1.7	0.9	0.59
SSA	TR–111	D072A–87	–0.0	0.0	3.91	7.98	0.89	3.12	0.54	0.07	0.35	0.04	0.19	0.04	0.10	0.03	0.10	0.02	1.2	0.0	0.06
SIS	SR–29	D078A–88			52.95	101.18	10.61	35.55	6.20	0.47	4.47	0.76	4.34	0.83	2.23	0.27	1.84	0.27		39.3	
SIS	SR–28	D078A–88			54.76	102.18	10.20	35.23	5.72	0.44	4.37	0.73	4.06	0.78	1.94	0.27	1.58	0.22		46.6	
SIS	SR–29	D081–87			5.29	9.46	1.22	4.65	1.34	0.15	1.22	0.22	1.23	0.20	0.50	0.06	0.42	0.06		4.1	
SSA	TR–098	D081–87	4.7	0.3	6.09	12.33	1.43	5.21	1.44	0.18	1.49	0.27	1.48	0.25	0.59	0.08	0.48	0.08	4.9	4.8	1.02
SIS	SR–29	D108–88			46.25	95.74	11.63	46.50	8.04	1.60	5.13	0.77	3.92	0.69	1.83	0.23	1.44	0.25		9.0	
SIS	SR–29	D108–88			46.58	94.57	10.90	42.39	7.21	1.45	4.91	0.65	3.47	0.62	1.55	0.22	1.33	0.20		10.5	
SIS	SR–29	D110–88			47.43	96.45	11.13	42.73	7.02	1.31	3.31	0.39	1.73	0.26	0.64	0.08	0.50	0.06		5.9	
SIS	SR–28	D110–88			42.08	84.75	10.06	37.54	5.33	1.22	2.91	0.36	1.59	0.27	0.65	0.07	0.44	0.06		5.6	
SIS	SR–29	D110–88			44.74	90.93	10.78	40.51	5.89	1.33	3.12	0.39	1.74	0.30	0.72	0.08	0.48	0.07		5.3	
HF	TR–123	D154B–87	59.2	9.9	69.56	155.62	19.55	80.91	14.57	3.49	11.70	1.20	5.56	0.93	2.10	0.27	1.66	0.23	8.9	1.9	0.40
HF	TR–122	D154B–87	60.1	9.8	68.46	154.39	18.89	80.55	14.58	3.50	11.66	1.17	5.45	0.92	2.15	0.27	1.54	0.23	8.4	1.9	0.38
HF	TR–125	D172C–87	19.3	1.7	38.82	96.46	12.90	56.55	12.98	3.85	11.35	1.64	8.96	1.64	4.00	0.51	3.09	0.40	6.3	4.4	0.91
HF	TR–122	D172C–87	19.9	1.7	36.00	89.79	12.45	56.66	12.89	3.85	12.25	1.72	9.38	1.75	4.02	0.53	3.17	0.43	6.5	3.6	1.00
SSA	TR–111	D172C–87		0.0	35.41	88.91	12.02	54.57	12.41	3.46	10.56	1.49	8.12	1.55	3.99	0.51	3.13	0.43	0.3	0.0	0.01
HF	TR–123	D206–87	9.2	0.2	21.64	51.27	6.60	27.83	5.27	1.71	4.87	0.87	3.89	0.76	1.91	0.25	1.67	0.24	4.7	1.7	0.35
HF	TR–125	D206–87	11.1	0.3	26.45	64.02	8.13	34.37	6.36	2.00	5.50	0.79	4.44	0.88	2.37	0.32	2.13	0.30	6.0	2.1	0.46
SSA	TR–094	D217–87			4.90	10.15	1.14	4.31	0.87		0.78	0.10	0.57	0.11	0.29	0.04	0.28	0.04		4.4	
HF	TR–125	D217–87	15.4	1.2	5.81	12.37	1.38	5.23	0.88	0.17	0.96	0.09	0.42	0.08	0.25	0.04	0.22	0.03	7.8	7.7	0.41

Table A1.5 Duplicate and Replicate ICP–MS Analyses

Technique	Run	Sample	Li	Cs	La	Ce	Pr	Nd	Sm	Eu	Gd	Tb	Dy	Ho	Er	Tm	Yb	Lu	Pb	Th	U
HF	TR–123	D220–87	16.9	0.8	40.59	90.22	10.46	38.42	6.57	1.05	5.40	0.60	2.96	0.58	1.51	0.25	1.84	0.30	3.7	5.7	1.18
HF	TR–125	D220–87	17.4	0.8	42.47	95.29	10.68	38.95	6.74	1.04	5.58	0.62	2.98	0.56	1.65	0.26	1.94	0.30	3.4	6.7	1.21
SIS	SR–28	D221–87			73.22	156.48	20.27	80.85	17.29	2.49	18.14	3.23	19.94	4.17	11.00	1.56	10.69	1.52		8.3	
SIS	SR–28	D221–87			83.76	173.95	23.01	91.97	19.50	2.85	20.56	3.62	22.86	4.78	12.44	1.85	12.45	1.77		9.1	
HF	TR–094	D266–87	57.9	5.7	33.45	72.13	7.68	26.99	4.33	0.26	2.67	0.33	1.79	0.32	0.78	0.10	0.62	0.09	28.1	11.9	3.30
SSA	TR–094	D266–87		0.1	36.29	72.09	7.93	27.41	4.32	0.42	2.79	0.35	1.76	0.32	0.76	0.25	0.61	0.08	5.8	12.5	0.78
SSA	TR–094	D266–87		0.3	35.46	69.69	7.76	26.96	4.41	0.36	2.54	0.34	1.74	0.31	0.76	0.13	0.61	0.08	5.8	12.1	0.82
SIS	SR–28	D273–88			50.37	107.20	13.23	53.05	8.36	2.18	5.36	0.64	3.08	0.54	1.17	0.14	0.84	0.13		4.2	
SIS	SR–28	D273–88			54.11	114.39	14.03	55.76	9.06	2.38	6.19	0.71	3.44	0.54	1.38	0.15	1.08	0.14		4.3	
SIS	SR–28	D278–88			29.03	78.39	11.80	56.90	11.90	3.35	9.09	0.99	5.30	0.92	2.20	0.26	1.81	0.23		2.3	
SIS	SR–29	D278–88			29.28	78.46	11.87	56.33	11.66	3.25	8.14	1.00	4.76	0.86	1.98	0.24	1.54	0.25		2.5	
SIS	SR–28	D278–88			28.91	77.18	11.35	53.38	10.75	3.08	7.95	0.95	4.63	0.80	1.88	0.23	1.55	0.20		2.9	
SIS	SR–28	D280–88			35.87	74.59	9.95	40.18	6.66	1.84	4.34	0.49	2.38	0.39	0.99	0.12	0.73	0.12		2.4	
SIS	SR–28	D280–88			36.29	76.02	9.83	41.08	6.65	1.77	4.25	0.47	2.48	0.41	1.01	0.14	0.75	0.12		2.3	
HF	TR–123	D366–87	21.9	2.8	23.85	53.41	6.81	28.85	5.98	1.96	5.90	0.82	4.47	0.84	2.12	0.28	1.71	0.24	5.5	3.7	0.87
HF	TR–123	D366–87	27.4	3.4	29.90	67.[illegible]	8.54	36.36	7.72	2.56	7.66	1.04	5.68	1.11	2.61	0.35	2.18	0.32	6.9	4.5	1.11
HF	TR–123	K028A–87	5.9	2.9	6.45	13.67	1.57	6.03	1.38	0.19	1.58	0.32	2.22	0.49	1.37	0.21	1.51	0.23	20.3	8.1	3.53
HF	TR–122	K028A–87	5.8	3.1	6.54	14.02	1.62	5.97	1.44	0.25	1.59	0.32	2.14	0.48	1.39	0.22	1.61	0.23	20.3	8.6	3.53
HF	TR–125	K149A–87	37.7	7.7	36.10	77.79	8.80	33.65	6.11	1.55	5.53	0.72	3.72	0.70	1.72	0.23	1.47	0.20	9.5	7.1	1.75
SIS	SR–28	K149A–87			35.90	73.82	8.85	34.80	6.16	1.56	4.94	0.73	3.93	0.76	1.83	0.25	1.60	0.21		6.7	
	1	RSD (1 sigma)	3.1%	9.9%	4.0%	4.3%	4.5%	4.6%	5.1%	6.2%	6.0%	4.8%	5.5%	5.2%	4.8%	7.3%	4.9%	4.9%	8.7%	11%	8.0%
SIS	2	AGV–1			39.6	69.12	8.63	31.4	5.73	1.54	4.41	0.65	3.6	0.69	1.97	0.27	1.73	0.26		6.5	
HF	3	AGV–1	10.9	1.25	36.7	67.8	8	30.7	5.6	1.82	5.3	0.68	3.8	0.73	1.8	0.25	1.66	0.25	37.0	6.0	1.89
SIS	4	BCR–1			25.6	51.89	6.84	27.7	6.49	1.85	6.01	1.04	6.22	1.25	3.72	0.51	3.26	0.48		5.8	
HF	5	BCR–1	13.5	0.94	24.3	52.22	6.55	28.1	6.3	2.03	6.9	1.1	6.7	1.41	3.57	0.05	3.34	0.5	13.8	5.9	1.7
	6	LOD	0.4	0.02	0.011	0.009	0.009	0.040	0.030	0.009	0.030	0.006	0.018	0.006	0.020	0.007	0.020	0.006	0.07	0.013	0.014

1 Relative Standard Deviations (RSD) calculated from duplicate and replicate analyses by least–squares regression.
2. Average of 6 analyses of USGS standard AGV–1 by sinter and internal standard (SIS) (G A. Jenner, unpublished data)
3. Average of 6 analyses of USGS standard AGV–1 by HF–HNO3 dissolution and standard addition (Jenner et al. (1990)
4 Average of 7 analyses of USGS standard BCR–1 by sinter and internal standard (SIS) (G A. Jenner unpublished data)
5 Average of 6 analyses of USGS standard AGV–1 by HF–HNO3 dissolution and standard addition (Jenner et al. (1990)
6 Average limits of detection (LOD) reported by Jenner et al. (1990)

Appendix 2
Geochemical Data Base

1. Central Volcanic Belt, Coeval Plutonic Rocks and Metasedimentary Rocks of the Yellowknife Supergroup

Symbols

1 Gondor Plutonic Suite, Gondor Lake Area
2 Wishbone Plutonic Suite, Jaeger Monzogranite
3 Wishbone Plutonic Suite, Wishbone Dome Area
4 Olga Plutonic Suite, Olga Lake
5 Central Volcanic Belt (* designates intrusive rock)
6 Tuk Porphyry
7 Metasedimentary Rock - Turbidite
8 Metasedimentary Rock - Fe-stone
9 Epiclastic Volcanic Tuff within YKS Turbidites

Sample	D205A-87	D221-87	D205B-87	D215-87	D065B-87	D037-89	D038-89	D040-89	D041-89	D227-89	K180-89	D226-89	D327-87	D072A-87
Easting	461700	462000	461700	462000	458300	587500	587000	585500	585500	485300	478500	488000	478300	464000
Northing	7270500	7270000	7270500	7270100	7266700	7231500	7231000	7230000	7230000	7272000	7276300	7270100	7279000	7296000
Suite	Gondor	Gondor	Gondor	Gondor	Gondor	Wishbone	Wishbone	Wishbone	Wishbone	Wishbone	Wishbone	Wishbone	Wishbone	Olga
Symbol	1	1	1	1	1	2	2	2	2	3	3	3	3	4
SiO2	75.86	79.95	79.05	80.17	77.09	77.39	77.96	77.57	75.39	75.82	78.30	77.20	78.39	74.99
TiO2	0.21	0.08	0.12	0.08	0.24	0.08	0.08	0.04	0.04	0.36	0.08	0.22	0.32	0.04
Al2O3	11.72	11.55	11.44	11.25	12.28	12.25	12.23	12.34	13.74	12.86	12.00	12.61	11.46	15.12
FeO*	4.76	1.34	2.49	1.46	2.31	1.28	0.94	1.12	0.84	2.17	1.27	1.13	2.41	0.62
MnO	0.06	0.03	0.03	0.03	0.03	0.03	0.02	0.02	0.02	0.03	0.02	0.07	0.05	0.04
MgO	3.32	0.70	1.77	0.41	0.42	0.11	0.03	0.11	0.13	0.36	0.13	1.38	0.41	0.14
CaO	0.56	0.87	0.78	0.83	1.21	1.00	0.55	0.72	0.91	1.96	0.78	1.30	1.72	2.31
Na2O	2.34	4.81	3.30	5.25	4.62	4.00	4.07	3.85	4.14	4.13	3.64	4.37	4.03	5.33
K2O	1.16	0.67	1.01	0.51	1.79	3.84	4.12	4.21	4.78	2.27	3.76	1.68	1.19	1.40
P2O5						0.01			0.01	0.03	0.01	0.03	0.03	
LOI	2.15	0.80	1.39	0.58	0.91	0.45	0.48	0.55	0.47	0.82			0.42	0.68
Cr	<5	<5		<5	<5		<5	<5	14	<5			<5	<5
Ni	<3	<3		<3	<3		<3	<3	<3	<3			<3	<3
Sc	<3	<3		<3	3		<3	<3	5	<3			3	<3
V	<6	<6		<6	<6		<6	<6	<6	<6			<6	<6
Cu	<3	<3		<3	5		<3	<3	<3	<3			<3	<3
Pb					5									2
Zn	56	14		<9	13		10	<9	<9	<9			21	<9
Rb	19	12	17	8	43		132		131				37	32
Cs					2.19									
Ba	241	197		306	487		591	284	608	604			269	530
Sr	18	40	30	49	68		20		70				120	485
Ga	20	21		20	16		22		20				14	16
Li					13.56									
Nb	27.4	36.2	26.4	36.9	27.1		28.7	32.2	14.1	13.9			19.5	1.2
Zr	328	231	329	257	313		131		102				266	66
Y	77	131	98	105	84		79	101	140	34			50	1
Th		9.41			9.71		10.11	12.34	23.24				4.34	0.89
U					2.25		3.03		5.05					0.58
La		86.40			65.90			13.28		47.58			25.09	6.61
Ce		179.44			150.84			34.33		98.20			48.18	13.06
Pr		23.73			18.45			5.01		11.12			5.54	1.45
Nd		94.88			73.32			22.82		38.85			20.38	5.24
Sm		20.11			14.69			3.99		7.14			4.33	0.82
Eu		2.94			1.80			0.54		1.00			1.20	0.18
Gd		21.21			14.83			12.52		6.56			4.95	0.57
Tb		3.74			2.38			2.38		0.97			1.04	0.07
Dy		23.59			14.94			16.70		6.08			7.66	0.34
Ho		4.93			3.20			3.70		1.26			1.80	0.06
Er		14.33			8.77			11.43		3.72			5.35	0.16
Tm		1.91			1.29			1.75		0.56			0.81	0.02
Yb		12.84			8.69			11.36		3.62			5.29	0.16
Lu		1.82			1.31			1.64		0.52			0.70	0.03

Sample	D072B-87	D174-88	D072C-87	D173-88	D171-88
Easting	464000	464000	464000	464000	464000
Northing	7296000	7296000	7296000	7296000	7296000
Suite	Olga	Olga	Olga	Olga	Olga
Symbol	4	4	4	4	4
SiO2	72.52	73.43	73.51	73.01	76.43
TiO2	0.36	0.32	0.08	0.20	0.08
Al2O3	14.79	14.12	15.67	15.64	13.78
FeO*	2.66	2.78	1.05	1.10	0.71
MnO	0.04	0.04	0.02	0.03	0.01
MgO	0.72	0.65	0.41	0.40	0.13
CaO	2.86	2.78	2.14	2.33	2.09
Na2O	4.69	4.57	5.33	5.82	4.98
K2O	1.24	1.24	1.77	1.36	1.78
P2O5	0.12	0.07	0.02	0.11	0.01
LOI	0.50	0.53	0.39	0.61	0.48
Cr		<5	<5	<5	<5
Ni		<3	<3	<3	<3
Sc		<3	<3	<3	<3
V		22	7	16	<6
Cu		<3		<3	<3
Pb					
Zn		44	24	21	<9
Rb	43	31	49	42	32
Cs					
Ba		266	707	505	567
Sr	282	294	536	491	428
Ga		18	19	21	19
Li					
Nb	5.0	4.9	1.0	1.5	1.1
Zr	235	208	83	89	70
Y	7	6	2	3	3
Th	5.06		0.31		
U					
La	28.20		3.49		
Ce	52.64		7.04		
Pr	5.55		0.89		
Nd	18.29		3.64		
Sm	2.59		0.78		
Eu	0.68		0.23		
Gd	1.97		0.61		
Tb	0.24		0.09		
Dy	1.27		0.46		
Ho	0.27		0.10		
Er	0.68		0.24		
Tm	0.10		0.03		
Yb	0.69		0.20		
Lu	0.12		0.03		

D054B-87	D052-87	R051-87	D206-87	D237-87	D219-87	D052A-87	D084A-87
463300	463200	459800	461900	444600	460000	463200	455000
7261900	7261800	7266700	7270800	7275000	7270800	7261800	7266300
CVB	CVB	CVB	CVB	CVB	CVB	CVB	CVB
5*	5	5*	5	5	5	5	5
49.68	50.10	58.81	59.97	60.94	67.05	67.65	78.20
1.02	0.66	0.74	0.98	1.10	0.57	0.61	0.26
17.75	16.01	15.93	17.15	15.87	15.55	16.18	10.88
9.10	9.83	7.78	6.12	7.08	5.17	4.28	3.11
0.16	0.17	0.13	0.16	0.14	0.06	0.08	0.02
6.89	8.21	4.38	4.24	3.23	2.19	1.43	1.96
11.47	11.12	7.50	6.37	6.98	1.22	3.73	0.65
2.83	2.64	3.56	4.11	4.30	7.13	4.24	4.68
0.86	1.08	1.07	0.53	0.14	0.80	1.65	0.20
0.24	0.18	0.11	0.37	0.21	0.25	0.16	0.02
0.87	1.16	0.97	1.09	0.31	1.86	0.67	1.22
119	17		177	27	<5	<5	<5
121	42		90	16	<3	<3	<3
31	43		25	26	11	8	3
237	254		195	183	51	56	<6
<3			16	<3	<3	6	<3
		3	6	3	4	6	
82	84		78	87	66	62	29
16	25	31	8	0	11	90	3
		0.94	0.26	0.07	0.23	0.18	
93	53		91	14	201	302	30
329	282	193	161	192	144	235	53
18	15		15	16	15	19	13
		9.30	10.70	26.91	12.45	70.81	
6.7	1.1	12.3	10.0	10.2	13.8	8.4	16.0
72	35	165	173	222	265	189	338
18	13	36	24	30	29	11	36
0.40	0.43	3.06	2.01	3.21	3.82	3.24	4.32
		0.63	0.43	0.66	0.82	0.73	
12.53	20.92	21.15	25.36	24.94	30.50	15.83	25.17
29.05	51.61	49.61	60.80	55.91	70.49	34.75	52.65
3.98	8.09	6.33	7.77	6.94	8.48	4.11	7.41
16.68	39.23	26.35	32.80	28.41	33.52	16.04	28.99
3.64	10.08	5.81	6.73	5.79	5.97	2.95	6.05
1.23	5.17	1.13	1.96	1.66	1.69	0.94	1.12
3.29	10.38	6.28	5.47	5.98	5.32	2.79	5.65
0.51	1.67	1.00	0.77	0.91	0.74	0.38	0.87
3.20	10.31	6.33	4.39	5.63	3.80	2.09	5.33
0.67	2.18	1.35	0.87	1.18	0.74	0.43	1.05
1.76	5.74	3.71	2.26	3.24	2.01	1.10	2.99
0.26	0.81	0.55	0.30	0.46	0.31	0.16	0.42
1.67	5.53	3.71	2.01	3.15	2.20	1.03	2.70
0.24	0.82	0.56	0.29	0.47	0.33	0.16	0.40

Sample	D220-87	K299-87	K164-88
Easting	460000	489300	475400
Northing	7271300	7270300	7308500
Suite	CVB	CVB	CVB
Symbol	5	5	6
SiO2	78.93	81.63	68.85
TiO2		0.13	0 49
Al2O3	11.38	9.76	14.78
FeO*	1.98	1.53	4.54
MnO	0.03	0.02	0.05
MgO	2.30	1.59	1.58
CaO	1.05	0.39	4.54
Na2O	2.73	2.10	3.73
K2O	1.60	2.85	1.30
P2O5			0.13
LOI	2.93	1.21	0.64
Cr	<5	<5	15
Ni	<3	<3	<3
Sc	<3	<3	12
V	<6	<6	79
Cu	<3	<3	<3
Pb	4	1	
Zn	15		15
Rb	32	59	56
Cs	0.88	0.31	
Ba	199	624	284
Sr	53	137	266
Ga	21	11	18
Li	18.72	40.65	
Nb	19.8	22.4	7.3
Zr	267	272	156
Y	31	42	12
Th	6.78	7 22	
U	1.30	1.77	
La	45.28	30 52	
Ce	101 12	72.54	
Pr	11 52	8 59	
Nd	42.17	32.65	
Sm	7.25	5 89	
Eu	1.14	0.90	
Gd	5 99	5 65	
Tb	0 67	0 88	
Dy	3 24	5 05	
Ho	0 62	1 13	
Er	1.72	3 32	
Tm	0 28	0 51	
Yb	2 06	3.80	
Lu	0 33	0 59	

D300-89	D269-89	D271-89	D270-87	D268-87	D269-87	R231B-87	R231A-87	R252-87	D177-88
65°22'	490800	490800	476500	474500	474500	478000	478000	488600	490400
113°03'	7287000	7287000	7287000	7286200	7286200	7291000	7291000	7287000	7286600
YKS-SED	YKS-SED	YKS-SED	YKS-SED	YKS-SED	YKS-SED	YKS-FE	YKS-FE	YKS-FE	YKS-TUFF
7	7	7	7	7	7	8	8	8	9
58.65	61.97	47.20	73.05	60.71	60.40	53.52	42.63	51.19	59.36
0.81	0.51	2.03	0.62	0.80	0 73	0.50	0.24	2.06	0.43
20.97	16.90	14.12	14.32	18.83	21.79	10.66	15.50	12 88	12.11
9.09	12.03	13.24	4.81	10.30	7.82	26 27	27.16	14.88	7.97
0.09	0.07	0.20	0.04	0.10	0.05	0.04	0 07	0 22	0.14
4.09	3.55	9.77	2.34	4.28	3.80	4.93	2.63	5 89	12.98
0.83	1.15	12.72	0.56	0.80	0.37	2.67	9.24	9.68	4 84
1.51	0.91	0.52	1 76	1.11	0.73	0 13	0.36	2.45	1.83
3.83	2.74	0.02	2.44	2.96	4.11	1.20	0 18	0.60	0.18
0.13	0.16	0.18	0 06	0.11	0.19	0.08	1.98	0 15	0 16
4.19	3.70	5.43	1.29	4.94	2.96	-0 50	-1.15	0.27	4.04
			149	188	228				896
			49	18	85				269
			13	29	31				20
			123	239	237				192
			78	3	<3				49
		6	13	8	7		7		
			77	89	66				89
		1	80	109	142	111	4	17	4
		0.46	7.94	7 61	12.66		0.94		
			548	568	810				39
		429	183	95	126	53	279	220	612
			19	21	27				16
		67 12	77.32	73.47	165 29		19.96		
		15.8	7.2	8.3	8.2	6.0	6.0	12 4	6.6
		137	151	121	117	91	54	142	159
		19	14	17	17	13	15	33	19
8.58	6.60	1.60	7.61	8 24	8.57		2.81		
		0.34	2.49	2 31	2.32		1 05		
9.04	45.81	15.81	27 61	4.19	32 02		10 96		
19.88	58.71	36.85	58 63	9.23	71 16		24.85		
2.56	10.07	4 80	6 42	1.00	7 96		3 01		
10 21	38 73	21 32	24.40	4 06	31 73		12 67		
2 32	6.85	4 87	4 09	1 16	5 09		2 58		
0.76	1.53	1 89	1 04	0 41	0 99		1.34		
2.19	5 95	5 30	3 35	1.71	4 44		2 54		
0 40	0.76	0.78	0 39	0.35	0 50		0 38		
2.71	4 20	4 43	1 92	2 59	2 43		2 52		
0 57	0 79	0 90	0 32	0 59	0 42		0 56		
1 68	2 09	2 27	0 79	1 80	1 04		1 51		
0 23	0 28	0 30	0 10	0 27	0 16		0 22		
1 61	1 69	1 66	0 71	1 84	1 06		1 57		
0 25	0 25	0 26	0 12	0 29	0 16		0 24		

Appendix 2
Geochemical Data Base

2. Syn-Deformation Plutonic Suites
Concession and Siege Suites

Symbols

Concession Suite

1 North Eda Lake Area
2 Concession Pluton
3 West Fry Inlet Area
4 Southern Contwoyto Lake Area
5 Heckla Bay Area
6 East Yamba Lake Area
7 Sills South of Southern Diorite
8 Southern Diorite
9 Southeeast Concession Pluton
10 Harp Tonalite
11 Northern margin Woolverine Monzogranite
12 North of Ghurka Lake
13 Nose Lake Area
14 Cumulate Rocks
15 Lac de Gras Map Sheet
16 Pointless Batholith, Point Lake
17 Keskarrah Batholith, Point Lake

Siege Suite

18 Siege Tonalite

Sample	D169B-88	D168-88	D157-88	D167-88	D154B-87	D150-87	D194-89	A280-87	D203-87	D156-87	D155-87	D195-89	K202-87	D201A-87
Easting	460440	460483	459100	460095	463231	467300	466000	460898	470445	466998	463193	469800	468882	468959
Northing	7212986	7213137	7228400	7214648	7287674	7286500	7287900	7285548	7287714	7287872	7286837	7287800	7284609	7286484
Suite	Concess	Concess	Concess	Concess	Concess	Concess	Concess	Concess	Concess	Concess	Concess	Concess	Concess	Concess
Symbol	1	1	1	1	2	2	2	2	2	2	2	2	2	2
SiO2	64.83	65.25	65.54	67.10	53.35	57.08	58.04	60.38	64.72	64.85	65.05	65.07	65.30	65.33
TiO2	0.70	0.61	0.41	0.66	0.94	0.82	0.60	0.58	0.49	0.49	0.40	0.49	0.37	0.51
Al2O3	17.45	16.82	17.15	16.62	16.00	16.56	16.63	16.74	16.20	15.96	16.09	15.45	15.71	16.13
FeO*	4.03	4.20	4.17	3.50	8.26	7.90	6.36	5.11	4.20	4.33	3.96	4.19	4.19	3.97
MnO	0.05	0.07	0.04	0.05	0.13	0.13	0.10	0.09	0.07	0.07	0.07	0.08	0.08	0.07
MgO	1.88	2.17	1.85	1.79	6.38	4.68	4.20	4.23	3.18	3.10	2.92	3.24	2.86	2.67
CaO	4.11	3.85	3.94	3.65	7.67	6.17	5.51	5.35	4.24	4.05	4.19	4.29	4.80	4.20
Na2O	4.66	4.36	4.81	4.62	4.32	3.62	4.57	5.09	4.40	4.58	4.72	4.66	4.83	4.89
K2O	2.10	2.40	1.85	1.79	2.33	2.66	3.52	2.18	2.33	2.40	2.43	2.36	1.73	2.03
P2O5	0.20	0.27	0.25	0.24	0.61	0.37	0.46	0.25	0.16	0.17	0.16	0.17	0.14	0.19
LOI	1.06	0.62	0.63	0.54	0.70	0.75	0.71	0.69	0.65	1.01	0.80	1.09	0.66	0.73
Cr		27	7	11	113	46		102	95	89	65		91	55
Ni		7	<3	<3	75	14		68	50	39	30		40	32
Sc		10	3	6	24	24		15	11	11	11		11	9
V		107	78	81	231	224		123	106	102	94		117	91
Cu		35	<3	<3	54	32		<3	<3	<3	<3		<3	<3
Pb	7				9			8	9		9		6	10
Zn		84	72	62	97	83		66	56	48	51		61	56
Rb		165	76	104	62	68		54	52	64	56		32	58
Cs	4.7				10.1			4.0	2.5		2.2		1.4	5.5
Ba		221	280	467	1173	1002		1034	1078	1276	1014		1237	975
Sr		536	603	622	1535	1179		1243	1085	1050	1081		1008	1008
Ga		24	27	26	23	23		24	19	20	21		19	21
Li	74.9				61.2			53.0	43.8		35.6		30.3	100.5
Nb		13.4	13.1	8.4	6.6	8.0		5.5	5.2	5.1	4.8		4.6	6.3
Zr		182	185	150	143	160		174	163	156	162		157	160
Y		20	7	10	22	19		12	10	11	9		10	11
Th	4.56	14	6	6.93	1.93	7.17		4.59	6.40		7.02		4.32	5.59
U	0.73				0.40			1.03	0.98		1.83		0.81	2.26
La	14.15			41.05	70.80	45.74		32.48	30.92		32.90		29.36	31.01
Ce	33.56			86.10	159.02	102.31		72.32	66.89		68.77		63.62	69.47
Pr	4.18			10.81	19.71	12.96		8.66	7.73		8.02		7.47	8.31
Nd	18.09			43.21	82.82	53.43		34.63	29.89		30.87		29.22	32.83
Sm	4.26			7.25	14.96	9.35		6.02	4.76		5.09		5.07	5.52
Eu	1.45			1.35	3.59	2.19		1.24	1.21		1.03		1.27	1.43
Gd	4.15			4.34	11.98	6.41		5.06	4.20		4.27		4.75	4.39
Tb	0.56			0.56	1.22	0.79		0.51	0.38		0.40		0.41	0.49
Dy	3.03			2.71	5.65	4.00		2.44	2.00		1.99		2.23	2.48
Ho	0.57			0.47	0.95	0.76		0.47	0.38		0.37		0.41	0.46
Er	1.36			1.10	2.18	1.92		1.20	0.90		0.94		0.99	1.10
Tm	0.18			0.14	0.28	0.26		0.15	0.12		0.13		0.13	0.16
Yb	1.08			1.04	1.64	1.76		1.06	0.82		0.89		0.83	1.02
Lu	0.15			0.15	0.24	0.26		0.15	0.13		0.14		0.13	0.15

Sample	D180-89	D161-89	D242-89	D236-89	W176C-88	D253-88	D273-88	D254-88	D277-88	D282-88	D258-88	W171-88	D280-88	D260-88
Easting	527200	517000	513800	516400	542200	548000	543500	548100	543100	539600	548585	545800	542100	547136
Northing	7221700	7245000	7236600	7234400	7240600	7238500	7237400	7239000	7244200	7241200	7237091	7235700	7242300	7234496
Suite	Concess	Concess	Concess	Concess	Concess	Concess	Concess	Concess	Concess	Concess	Concess	Concess	Concess	Concess
Symbol	3	3	3	3	4	4	4	4	4	4	4	4	4	4
SiO2	61.45	61.64	66.54	67.40	63.46	64.41	64.50	64.94	65.32	66.44	66.81	66.89	68.36	69.86
TiO2	0.74	0.70	0.73	0.51	0.69	0.58	0.61	0.69	0.57	0.57	0.57	0.57	0.64	0.38
Al2O3	16.22	16.64	15.95	15.63	15.92	16.54	16.25	16.54	16.13	16.48	16.04	16.19	17.46	15.57
FeO*	5.75	5.21	3.83	3.69	4.75	4.47	4.76	4.27	4.34	3.80	4.01	3.92		2.90
MnO	0.09	0.08	0.05	0.06	0.08	0.07	0.07	0.07	0.08	0.06	0.07	0.05	0.05	0.06
MgO	3.58	2.95	2.33	2.08	3.87	2.90	2.76	2.67	2.54	2.13	2.19	2.30	2.39	1.53
CaO	5.43	3.53	3.82	3.64	5.38	4.58	4.05	4.44	4.78	4.18	3.23	3.76	4.51	2.45
Na2O	3.49	3.74	4.03	4.09	3.57	4.03	4.48	3.78	4.50	4.41	4.59	3.95	4.43	4.75
K2O	2.78	5.00	2.49	2.73	1.77	2.12	2.18	2.28	1.37	1.72	2.19	2.02	1.84	2.23
P2O5	0.45	0.50	0.23	0.17	0.49	0.31	0.35	0.30	0.37	0.20	0.29	0.35	0.32	0.24
LOI	0.90	0.95	0.84	0.25	0.85	0.89	1.04	0.79	1.15	0.85	0.65	0.64	0.64	0.81
Cr					26	51	34	43	40	<5	23	<5	35	<5
Ni					7	17	11	14	8	5	7	<3	10	<3
Sc					9	13	13	13	13	<3	7	4	11	4
V					89	440	107	107	104	41	91	47	88	167
Cu					<3	<3	<3	<3	<3	7	<3	<3	<3	18
Pb														
Zn					66	65	71	66	67	60	77	50	65	46
Rb					56	109	116	86	46	72	148	179	57	134
Cs														
Ba					757	892	528	732	632	589	326	481	813	688
Sr					1129	981	794	896	809	790	650	755	952	569
Ga					24	23	24	23	23	23	23	23	24	21
Li														
Nb					5.8	6.3	6.8	5.6	6.2	4.6	10.6	11.5	4.0	7.8
Zr					182	187	188	179	178	166	179	181	179	157
Y					21	16	13	15	16	12	15	17	13	14
Th					4.16	3.80	4.34	4	7.88	2.76		6.23	2.50	7.73
U														
La					50.58	47.07	53.39		70.41			54.29	38.41	43.20
Ce					119.63	105.73	113.25		141.87			114.85	80.18	87.61
Pr					15.63	13.65	13.93		17.18			14.45	10.53	10.73
Nd					67.75	56.39	55.61		65.92			58.24	43.26	41.75
Sm					12.47	9.45	8.90		9.92			9.44	7.09	7.09
Eu					3.28	2.48	2.33		2.19			2.19	1.92	1.38
Gd					8.21	5.54	5.90		5.60			5.85	4.57	4.46
Tb					0.94	0.69	0.69		0.66			0.70	0.51	0.60
Dy					4.52	3.37	3.33		3.27			3.33	2.59	2.69
Ho					0.78	0.57	0.55		0.56			0.54	0.43	0.42
Er					1.91	1.28	1.30		1.36			1.32	1.06	0.99
Tm					0.24	0.17	0.15		0.18			0.16	0.13	0.13
Yb					1.71	0.94	0.98		1.11			1.06	0.79	0.76
Lu					0.27	0.14	0.14		0.15			0.15	0.13	0.10

Sample	W163-88	D237-88	D292-88	V302A-88	D145-88	D142-88	D121A-88	V112B-88	V106-88	D334B-87	K104-88	K106-88	D105-88	K069-88
Easting	548500	502455	475800	515383	502200	501000	496000	497000	497500	421200	493102	491300	469700	471900
Northing	7241100	7305268	7301000	7302457	7213800	7216500	7211000	7209000	7210500	7212200	7211462	7212400	7240000	7238500
Suite	Concess	Concess	Concess	Concess	Concess	Concess	Concess	Concess	Concess	Concess	Concess	Concess	Concess	Concess
Symbol	4	5	5	5	6	6	6	6	6	6	6	6	7	7
SiO2	70.27	65.60	69.39	72.35	59.74	60.95	64.80	67.59	69.06	69.12	69.77	71.17	61.94	63.41
TiO2	0.40	0.54	0.49	0.16	0.95	0.69	0.69	0.53	0.53	0.41	0.37	0.32	0.65	0.53
Al2O3	15.65	17.25	15.72	15.96	17.26	16.94	17.37	16.51	15.98	15.71	15.94	15.21	16.55	16.54
FeO*	2.50	3.67	2.62	1.06	7.10	5.18	4.20	3.50	3.06	3.11	2.59	2.76	5.05	4.39
MnO	0.04	0.07	0.04	0.01	0.11	0.08	0.05	0.03	0.03	0.04	0.03	0.03	0.08	0.07
MgO	0.93	1.81	0.91	0.51	4.34	3.45	2.02	1.67	1.44	1.44	1.13	1.18	3.62	3.06
CaO	2.99	2.94	2.55	3.05	5.71	5.15	3.98	3.55	3.34	2.92	2.68	2.55	5.22	3.84
Na2O	5.21	5.10	4.72	5.96	1.30	4.54	4.50	4.55	4.55	3.80	4.32	4.29	4.60	4.74
K2O	1.89	2.88	3.26	0.90	3.08	2.70	2.08	2.01	1.86	3.27	2.77	2.34	2.01	3.03
P2O5	0.12	0.13	0.31	0.04	0.41	0.31	0.30	0.05	0.17	0.17	0.20	0.14	0.27	0.39
LOI	0.60	1.19	1.22	0.58	1.08	0.70	0.91	0.82	0.38	0.82	0.84	0.80	0.50	1.58
Cr	<5	36	<5	<5	38	28	10	<5	38	5	<5	10	84	
Ni	<3	7	<3	<3	4	12	<3	<3	<3	<3	<3	<3	30	
Sc	5	8	<3	<3	21	15	10	6	15	6	<3	4	16	
V	43	88	44	<6	173	116	92	74	187	59	49	50	138	
Cu	<3	7	<3	<3	<3	37	<3	<3	<3		<3	<3	4	
Pb														
Zn	43	62	64	15	94	65	70	52	57	51	34	43	72	
Rb	61	70	65	19	132	93	77	68	67	73	62	58	73	
Cs		1.0												
Ba	302	798	1759	231	987	1181	507	398	390	988	1014	558	993	
Sr	552	941	743	572	743	997	745	661	498	633	549	510	951	
Ga	20	22	22	21	23	23	24	23	21	20	21	19	25	
Li														
Nb	5.7	37.6	6.2	2.1	8.7	8.5	7.7	5.3	6.2	6.3	4.6	3.5	9.5	
Zr	149	211	190	88	145	231	151	149	136	141	143	121	190	
Y	7	12	9	3	22	20	10	5	7	9	8	4	18	
Th	2.01	5.62	6.44		4.39	10.53	5.79		8.26		8.21	5.29	8.16	14.39
U														
La	22.59	51.30	43.63		32.81	69.73	68.77		42.06		38.14	34.35	56.53	62.66
Ce	48.10	105.70	87.70		72.52	147.35	143.54		88.90		78.45	68.74	117.08	131.04
Pr	5.85	13.41	10.16		9.16	18.35	17.41		10.43		9.20	7.89	14.27	15.30
Nd	23.44	53.18	37.70		38.68	72.07	68.51		39.85		35.28	28.21	55.77	58.64
Sm	4.04	8.79	5.99		7.32	12.70	9.65		6.11		5.44	4.10	9.61	9.17
Eu	1.13	1.96	1.24		1.76	3.03	1.96		1.24		1.14	0.95	2.41	2.17
Gd	2.71	5.62	3.87		5.52	8.26	5.21		3.40		3.10	2.28	6.38	6.13
Tb	0.38	0.64	0.48		0.78	1.03	0.50		0.37		0.35	0.29	0.81	0.80
Dy	1.76	2.88	2.21		4.41	4.64	2.34		1.67		1.54	1.23	4.10	3.84
Ho	0.31	0.50	0.40		0.88	0.87	0.37		0.25		0.24	0.20	0.71	0.71
Er	0.75	1.16	0.94		2.21	2.01	0.62		0.60		0.61	0.50	1.88	1.67
Tm	0.09	0.16	0.11		0.34	0.26	0.08		0.07		0.06	0.07	0.26	0.22
Yb	0.51	0.96	0.79		1.96	1.75	0.41		0.40		0.36	0.44	1.59	1.55
Lu	0.09	0.14	0.10		0.32	0.26	0.05		0.05		0.06	0.06	0.25	0.22

Sample	D108-88	D023-87	D218-87	D127-87	D029-87	K294E-87	D364A-87	D172C-87	D173-87	D374-87	D169-87	K149A-87	D172-87	D184 88
Easting	469500	459170	460866	460504	459139	495598	496189	476763	475714	495910	478000	480800	477233	474990
Northing	7241500	7261621	7258037	7257922	7258475	7268740	7269671	7283054	7283533	7272089	7284500	7283500	72827?2	7313409
Suite	Concess	Concess	Concess	Concess	Concess	Concess	Concess	Concess	Concess	Concess	Concess	Concess	Concess	Concess
Symbol	7	8	8	8	8	9	9	9	9	9	9	9	9	10
SiO2	65.02	56.34	58.99	59.43	61.54	52.56	53.08	59.21	65 43	65 44	68.10	68.18	69.30	66 43
TiO2	0.61	0.86	0.73	0.66	0.58	1.78	1.40	1.65	0.78	0.85	0.70	0 61	0.62	0.61
Al2O3	16.18	17.96	17.97	16.73	17.60	18.14	17.66	14.36	16.33	16 34	15.77	15.72	15.50	14 85
FeO*	4.52	6.65	5.51	5.89	4.92	9.41	11.56	11.61	5 67	6.14	4.44	4.27	3.82	5.62
MnO	0.07	0.10	0.08	0.10	0.08	0.13	0.20	0.14	0.06	0.10	0.06	0 05	0 05	0 09
MgO	2.87	4.45	3.66	4.17	3.34	4.77	3.86	1.82	1.60	2.33	1 25	1.25	1.08	2.36
CaO	4.30	6.30	5.56	5.77	4.80	7.44	6.88	5.19	3.51	2.52	3.30	2.88	2.53	5.09
Na2O	4.16	4.53	4.94	4.35	4.80	3.53	3.71	3 59	4.14	3.51	4.30	4.06	4.14	3.70
K2O	2.08	2.32	2.16	2.42	2.09	1.91	1.50	1.58	2.20	2.69	1.94	2.82	2.82	1.16
P2O5	0.18	0.48	0.39	0.47	0.27	0.32	0.17	0.85	0.28	0.08	0.15	0 16	0.14	0.10
LOI	0.85	1.04	0.39	0.97	1.08	1.52	0.77	0.98	0.73	0.72	0.41	0.52	0.68	1.03
Cr	42	44	53	40	35			<5	6	102	8		<5	20
Ni	10	31	26	24	16			<3	<3	24	<3		<3	19
Sc	12	17	13	15	14			13	8	23	9		5	15
V	95	150	145	147	117			41	64	146	73		38	100
Cu	<3	43	24	33										4
Pb				15			6	7				10		
Zn	67	92	72	77	66			159	83	60	66		56	56
Rb	115	84	61	69	59	35	35	36	61	69	58	72	69	50
Cs			1.1	2.5			3.1	1.8				7.8		
Ba	672	781	911	1100	704			427	706	1010	659		599	170
Sr	610	1129	1128	1144	788	851	513	461	423	386	357	341	313	254
Ga	23	23	21	20	17			26	23	18	22		22	21
Li			42.0	46.6			30.0	20.3				36.5		
Nb	10.6	11.1	9.2	5.5	7.7	22.5	13.5	29.2	11.9	13.9	9.6	12.0	9.5	7.4
Zr	166	229	235	150	157	136	124	182	227	217	174	181	155	159
Y	18	24	19	21	17	24	43	45	16	29	14	18	19	15
Th	9.99	0.01	7.95	8.31	0.00			4.17	0.14		13.31	7.02	4.41	3.42
U				2.24				0.98				1.79		
La	47.53	63.36	51.39	63 44	49.49			37.96	38.29		50.09	36.74	23.89	20.90
Ce	97.44	149.57	114.17	140 92	106.69			94.09	81.90		94.10	77.37	51.32	39.0*
Pr	11.53	18.85	14.50	17.56	12.98			12 87	9.67		10.77	9.01	6.33	4.82
Nd	45.51	77.07	55.73	71.20	51.28			58.55	38 75		40.54	34 94	25.27	19.48
Sm	7.81	13.45	9.36	12.22	8.93			13.18	7.13		6.43	6.26	5.32	3.59
Eu	1.56	2.63	2.25	3.29	1.61			3.84	1.70		1.57	1.59	1.09	1.13
Gd	5.14	8.71	6.27	10.40	6.12			11.76	5 39		3.78	5.34	4.67	3 01
Tb	0.73	1.01	0.78	1.01	0.74			1.67	0 72		0.47	0.74	0 65	0 49
Dy	3.78	4.91	3.88	4.73	3.65			9.12	3.68		2.18	3.90	3.51	2.59
Ho	0.67	0.86	0.73	0.83	0.68			1.70	0 69		0.34	0.74	0.68	0.55
Er	1.73	2.14	1.80	1.93	1.80			4.13	1.71		1.04	1.81	1.54	1.38
Tm	0.23	0.29	0.46	0.25	0.24			0.54	0.22		0 14	0.24	0 20	0 20
Yb	1.41	1.81	1 64	1.50	1.57			3.23	1 32		0 85	1.56	1 29	1.25
Lu	0.23	0.28	0.24	0.25	0.25			0.43	0 18		0.08	0.21	0 20	0.20

Sample	V191-88	D201-88	D183-88	W141A-88	K144-88	V224-88	D110-88	K079-89	V233-89	D014-89	D029-89	D281-89	D280-89	D261A-89
Easting	473100	468557	475012	473000	479100	463742	468300	566800	592000	586800	588500	594600	594600	594000
Northing	7317100	7319051	7311856	7312500	7319200	7310903	7233800	7219000	7256500	7235300	7226600	7253200	7253200	7253500
Suite	Concess	Concess	Concess	Concess	Concess	Concess	Concess	Concess	Concess	Concess	Concess	Concess	Concess	Concess
Symbol	10	10	10	10	10	10	11	12	12	12	12	13	13	13
SiO2	67.78	68.41	69.89	71.73	71.84	72.40	66.94	64.86	65.09	65.21	70.97	54.80	56.85	57.38
TiO2	0.57	0.62	0.41	0.36	0.32	0.44	0.57	0.72	0.71	0.56	0.37	1.15	0.97	0.80
Al2O3	14.73	15.25	14.69	14.61	14.47	14.76	16.48	16.11	15.66	15.93	15.52	17.41	17.17	16.89
FeO*	5.04	3.96	4.18	3.01	3.26	2.78	3.79	5.22	5.26	4.15	2.06	9.13	7.61	7.36
MnO	0.08	0.08	0.06	0.04	0.05	0.04	0.05	0.09	0.08	0.06	0.03	0.14	0.12	0.12
MgO	2.04	1.69	1.52	0.96	1.10	0.83	1.82	2.76	2.31	2.49	0.83	4.24	4.66	4.62
CaO	4.23	4.41	3.59	3.24	2.71	2.75	3.87	4.54	4.23	4.43	2.96	7.81	7.32	6.88
Na2O	3.98	4.34	4.23	4.76	4.44	4.65	4.42	3.65	3.31	4.62	5.27	3.32	3.13	3.42
K2O	1.41	1.14	1.34	1.21	1.67	1.26	1.84	1.89	3.17	2.31	1.89	1.68	1.97	2.37
P2O5	0.13	0.10	0.09	0.08	0.13	0.09	0.21	0.15	0.17	0.23	0.10	0.32	0.20	0.15
LOI	1.10	1.07	0.77	0.62	0.85	0.53	0.69	0.41	0.55	0.58	0.19	0.82	1.05	0.50
Cr	<5	<5	9	<5	<5	<5	<5							
Ni	<3	<3	<3	<3	<3	<3	<3							
Sc	<3	7	7	<3	5		8							
V	<6	88	79	13	55	18	74							
Cu	<3	<3	<3	<3	<3	<3	<3							
Pb														
Zn	9	46	37	9	35	30	61							
Rb	61	45	61	42	60		75							
Cs							1.0							
Ba	206	242	364	708	307	430	328							
Sr	255	327	208	227	174		672							
Ga	16	22	21	17	21	21	25							
Li														
Nb	6.5	8.9	7.7	6.5	7.6		6.7							
Zr	159	177	138	143	116		165							
Y	12	13	13	9	11		8							
Th	5	2.97	6.95	3.72	9		5.72							
U														
La		18.34	24.03	25.17			45.81							
Ce		40.95	45.27	47.06			92.85							
Pr		5.13	4.67	5.14			10.91							
Nd		21.23	16.57	18.64			41.21							
Sm		3.85	2.79	3.06			6.22							
Eu		1.36	0.75	0.71			1.32							
Gd		2.94	2.28	2.03			3.19							
Tb		0.42	0.37	0.28			0.39							
Dy		2.53	2.06	1.50			1.72							
Ho		0.51	0.42	0.26			0.26							
Er		1.36	1.06	0.71			0.69							
Tm		0.19	0.16	0.09			0.08							
Yb		1.21	1.00	0.63			0.48							
Lu		0.20	0.17	0.08			0.07							

Sample	D262B-89	D279-89	D262A-89	K281-87	D154A-87	D151-1-8	D192-89	D365-87	D151-2-8	D375C-87	D152B-87	D375B-87	D319-87	D362-87
Easting	594500	594500	594500	474000	463231	465744	464500	496338	465744	496437	465523	496437	503000	496059
Northing	7252800	7253200	7252800	7286400	7287674	7288179	7287600	7269486	7288179	7273500	7287981	7273500	7255600	7269402
Suite	Concess	Concess	Concess	Concess	Concess	Concess	Concess	Concess	Concess	Concess	Concess	Concess	Concess	Concess
Symbol	13	13	13	13	14	14	14	14	14	14	14	14	14	14
SiO2	60.27	64.86	67.59	63.91	43.54	43.86	44.43	45.90	46.27	47.31	48.63	48.75	49.43	50.75
TiO2	0.69	0.68	0.50	0.63	1.49	1.58	1.47	1.95	0.71	0.87	1.03	1.48	1.82	0.90
Al2O3	17.47	16.06	16.10	19.14	11.56	11.09	10.22	16.72	6.07	9.61	15.53	18.92	13.75	13.05
FeO*	6.81	5.13	4.18	6.09	13.10	14.02	13.67	15.93	12.92	11.75	11.10	11.47	16.32	10.00
MnO	0.12	0.08	0.07	0.05	0.20	0.19	0.19	0.18	0.17	0.19	0.17	0.15	0.20	0.16
MgO	2.73	2.34	1.87	3.51	12.84	14.15	13.26	6.28	24.13	14.74	7.92	5.36	5.20	11.20
CaO	5.76	4.08	3.80	0.92	12.90	11.36	13.44	9.55	8.23	13.83	10.30	8.87	8.83	11.59
Na2O	3.88	3.46	3.55	2.60	1.70	1.38	1.53	2.40	0.38	1.07	2.74	3.33	3.22	1.64
K2O	2.10	3.13	2.22	3.05	1.51	1.85	0.97	0.97	1.08	0.57	2.02	1.36	0.99	0.65
P2O5	0.15	0.18	0.13	0.10	1.18	0.52	0.82	0.11	0.04	0.06	0.57	0.31	0.23	0.06
LOI	0.73	0.63	0.73	3.39	0.79	0.75	0.88	1.28	3.58	1.58	1.14	0.81	0.44	1.00
Cr				199	226			<5	379	785	118	<5	<5	116
Ni				25	96			<3	233	165	39	<3	29	21
Sc				28	43			38	54	69	39	27	42	53
V				191	434			680	215	434	370	309	519	292
Cu				20				20		106	111	17		12
Pb				11	3	4						4		2
Zn				73	136			122	92	58	100	89	105	61
Rb				86	22	46		15	46	10	71	31	11	13
Cs				3.6	5.7	5.3						1.9		0.5
Ba				984	377			209	132	124	1233	267	92	90
Sr				225	714	145		716	121	213	1388	765	191	497
Ga				20	22			24	9	12	22	22	20	15
Li				55.3	57.8	73.4						31.7		6.2
Nb				7.4	7.9	7.0		8.6	2.4	4.5	2.9	12.8	6.8	5.1
Zr				151	128	80		102	40	51	86	105	75	73
Y				16	40	36		17	12	16	23	29	26	15
Th				7.20	3.25	1.39					0.55	1.11		1.64
U				2.25	0.63	0.33						0.33		0.34
La				21.91	73.31	27.58					40.04	25.40		11.40
Ce				49.57	196.35	90.24					96.74	72.44		27.03
Pr				5.67	27.62	15.03					13.26	10.47		3.50
Nd				22.52	128.58	77.00					58.30	47.36		15.22
Sm				4.12	24.54	17.42					11.37	9.76		3.25
Eu				1.09	5.78	3.96					2.47	2.62		1.06
Gd				3.80	19.05	13.83					8.37	8.81		3.32
Tb				0.48	2.16	1.64					0.98	1.15		0.49
Dy				2.99	9.80	8.09					4.83	6.57		2.84
Ho				0.59	1.67	1.44					0.88	1.28		0.58
Er				1.73	3.64	3.37					2.02	3.21		1.56
Tm				0.24	0.44	0.43					0.26	0.43		0.21
Yb				1.64	2.72	2.55					1.68	2.68		1.34
Lu				0.26	0.37	0.34					0.24	0.41		0.19

Sample	D282-89	A325-87	D278--88	D103-88	D172B-87	D123-88	D191-89	D334D-87	D366-87	D119-88	D201B-87	D044 -89	D364B-87	D045-89
Easting	596000	462900	542900	465900	477064	493872	464500	421200	496714	492711	468959	585600	496189	585600
Northing	7253100	7249300	7244100	7236100	7282881	7212633	7287500	7212200	7269453	7211922	7286481	7234500	7269671	7234500
Suite	Concess	Concess	Concess	Concess	Concess	Concess	Concess	Concess	Concess	Concess	Concess	Concess	Concess	Concess
Symbol	14	14	14	14	14	14	14	14	14	14	14	14	14	14
SiO2	51.75	53.24	53.59	54.56	54.72	55.01	55.13	55.84	56.74	57.40	57.52	57.56	58.75	58 98
TiO2	1.29	0.87	0.96	1.08	3.15	0.82	0.76	0.86	2.14	0.85	0 65	0 72	0.05	0 67
Al2O3	14.27	17.93	13.11	19.95	14.69	21.74	14.78	21.51	15.62	16.47	12 75	15.58	18 97	15.25
FeO*	11.24	7.89	7.07	6.81	12.45	5.50	7.62	5.27	10.30	6.59	8 61	6.52	7.35	6.11
MnO	0.17	0.14	0.12	0.08	0.14	0.05	0.12	0.06	0.12	0.09	0 18	0 10	0.16	0 09
MgO	7.14	5.54	10.81	3.97	3.72	2.74	6.15	2.77	3.79	6.30	7 57	5.46	2.14	5 66
CaO	9.45	7.64	9.84	6.57	6.19	4 22	7.88	4.73	6.23	6.18	7 81	6.81	4.91	6.73
Na2O	2.37	4.17	2.89	4.07	3.34	5.93	3 72	5 45	3.22	2.85	3.49	3.57	4 36	3.71
K2O	2.05	1.94	1.21	2.53	1.26	3.20	3.39	2.98	1.60	2.91	1 34	3 00	2.09	2.46
P2O5	0.26	0.64	0.39	0.38	0.33	0.77	0 44	0 52	0 23	0.35	0.28	0 68	0.32	0 33
LOI	1.31	0.76	1.77	0.93	0.67	0.84	0.64	0.90	0.67	1.74	0.74	0.82	0.70	1.03
Cr		58	617	46	<5			<5	<5	232	356		12	
Ni		36	214	22	<3			4	<3	94	74		<3	
Sc		23	35	20	23			13	5	21	30		5	
V		200	263	150	255			101	57	156	194		63	
Cu			10		5					<3				
Pb		5							6		9		5	
Zn		101	75	105	133			103	88	74	138		91	
Rb		75	42	76	27	114		108	37	105	33		54	
Cs		3.1							3.2		2.6		1.4	
Ba		410	264	888	252			716	603	1105	347		626	
Sr		1380	601	1321	445	832		672	473	696	690		617	
Ga		22	19	30	22			27	19	23	18		19	
Li		38.4							25.3		78 8		23 8	
Nb		4.7	5 7	13 9	20.4	11.0		10 1	14 5	9.0	7 0		10 6	
Zr		94	103	329	204	122		87	179	165	110		281	
Y		20	20	28	30	29		18	24	23	24		9	
Th		1 59	2.70	15.16	2 72	0 24			4 20	8 60	2 56		1 65	
U		0.87							1.01		2 73		0 61	
La		46.67	30 25	84 86	25.65	19 92			27 63	48.48	2: 74		24 06	
Ce		113 26	81 18	175.95	60 38	47 41			62 29	102 10	70 41		67 90	
Pr		14.75	12 15	22 46	8 21	6 51			7 89	13 32	11 31		9 84	
Nd		65 42	57 79	90 09	35 98	26 78			33 52	54 51	54 79		45 77	
Sm		11 93	11 30	15 57	8 25	6 06			7 04	10 43	11 61		10 30	
Eu		4 09	3.36	3 49	2 61	1 59			2 32	2 42	2 98		2 48	
Gd		9.21	8 74	10 50	7 61	5 45			6 97	7 83	9 16		9 45	
Tb		1 00	1 02	1 35	1 14	0 95			0 95	1 12	1 09		1 40	
Dy		4 74	5.10	6 84	6 17	5 47			5 21	5 85	5 56		8 49	
Ho		0 83	0 89	1.20	1 17	0 99			1 00	1 04	1 04		1 76	
Er		1.97	2 10	2 93	2 78	2 76			2 43	2 64	2 50		4 81	
Tm		0 24	0 25	0 35	0 37	0 36			0 32	0 35	0 34		0 68	
Yb		1 52	1.70	2 31	2 34	2 18			2 00	2 55	2 26		4 68	
Lu		0 21	0 23	0 32	0 34	0 31			0 29	0 34	0 34		0 68	

Sample	D363B-87	W008-87	D154-88	D218-88	D219-88	D222-88
Easting	496385	458400		113°37'	113°36'	113°03'
Northing	7269877	7213800		65°21'	65°21'	65°04'
Suite	Concess	Concess				
Symbol	14	14	15	16	16	17
SiO2	59.99	63.94	67.72	70.41	72.25	69.33
TiO2	0.86	0.69	0.53	0.36	0.28	0.40
Al2O3	19.01	17.59	16.67	14.59	14.51	15.60
FeO*	6.23	4.41	3.28	2.76	2.39	3.30
MnO	0.09	0.07	0.04	0.04	0.02	0.06
MgO	2.25	2.30	1.63	1.22	0.81	1.09
CaO	4.39	4.68	3.44	2.41	2.26	3.26
Na2O	4.53	3.92	4.48	3.70	3.58	4.68
K2O	2.40	2.12	1.99	4.36	3.82	2.14
P2O5	0.25	0.27	0.22	0.15	0.09	0.13
LOI	0.79	0.73	0.90	0.47	0.57	0.61
Cr	33	7	8	12	<5	<5
Ni	12	3	<3	<3	<3	<3
Sc	8	6	7	6	4	6
V	117	109	74	39	45	52
Cu	5	9	<3	<3	<3	<3
Pb						
Zn	80	85	60	34	15	43
Rb	63	95	128	108	82	66
Cs						
Ba	830	1175	365	1953	1642	409
Sr	603	905	696	606	370	345
Ga	19	21	24	19	18	21
Li						
Nb	9.4	5.1	5.3	10.2	7.0	10.4
Zr	258	171	145	171	142	176
Y	7	11	5	23	10	15
Th	0.01	8.56	2	19.65	42.70	6.61
U						
La	21.57	57.15		77.11	84.36	44.21
Ce	43.15	120.02		147.55	149.21	82.07
Pr	4.84	14.80		17.46	15.31	9.92
Nd	17.85	58.23		67.26	54.06	38.43
Sm	2.75	9.31		11.70	7.35	6.42
Eu	1.52	2.07		1.94	1.18	1.56
Gd	2.09	5.52		8.21	4.36	4.55
Tb	0.26	0.59		1.12	0.53	0.63
Dy	1.45	2.57		6.03	2.35	3.59
Ho	0.29	0.40		1.04	0.37	0.68
Er	0.85	0.88		2.55	0.68	1.88
Tm	0.12	0.10		0.35	0.10	0.25
Yb	0.88	0.61		2.30	0.48	1.81
Lu	0.15	0.09		0.29	0.08	0.27

V284-88	D319C-87	D104-88	D119-87	D217-87	D044-87	D136-88
486000	503000	468500	471300	469524	465000	465511
7256800	7255600	7242900	7256600	7248189	7252900	7244014
Siege	Siege	Siege	Siege	Siege	Siege	Siege
18	18	18	18	18	18	18
71.43	72.34	71.96	73.01	72.46	74.02	72.52
0.16	0.08	0.16	0.04	0.10	0.08	0.16
16.79	16.84	16.45	15.68	16.22	15.53	16.10
1.06	0.67	1.22	0.93	0.93	0.66	1.01
0.02	0.01	0.02	0.02	0.03	0.02	0.01
0.41	0.22	0.41	0.36	0.29	0.22	0.40
3.15	2.69	2.79	2.34	2.89	1.94	3.26
6.06	6.23	5.52	5.41	5.45	4.98	5.34
0.90	0.87	1.44	2.16	1.57	2.43	1.20
0.02	0.04	0.02	0.05	0.05	0.12	
0.54	0.73	0.54	0.31	0.31	0.55	0.69
<5	<5	<5	<5	<5	<5	<5
<3	<3	<3	<3	<3	<3	<3
<3	<3	<3	<3	<3	<3	<3
<6	<6	13	<6	<6	<6	10
<3	<3	<3	<3	<3	<3	<3
				8		
13	15	11	18	11	10	<9
27	16	31	41	39	63	37
				1.3		
332	202	674	984	712	484	337
540	742	512	548	531	469	538
20	19	20	17	16	16	18
				15.7		
2.3	1.3	1.7	0.8	1.9	2.4	1.1
86	105	101	83	83	71	88
<2	<2	<2	<2	3	3	<2
			0.41	6.11	0.14	0.50
				0.41		
	3.35		3.83	5.43	2.15	3.10
	6.46		6.71	11.41	3.71	5.37
	0.68		0.71	1.28	0.40	0.54
	2.44		2.58	4.84	1.52	1.97
	0.50		0.54	0.88	0.38	0.35
	0.19			0.17	0.16	0.15
	0.33		0.39	0.67	0.36	0.21
	0.04		0.05	0.10	0.07	0.03
	0.22		0.23	0.50	0.48	0.18
	0.05		0.04	0.10	0.10	0.04
	0.14		0.13	0.28	0.31	0.14
	0.02		0.02	0.04	0.05	0.02
	0.14		0.14	0.25	0.36	0.13
	0.03		0.03	0.04	0.06	0.02

Appendix 2
Geochemical Data Base

3. Post-Deformation Plutonic Suites
Contwoyto and Yamba Suites

Symbols

Contwoyto Suite

1 Heckla Bay Area
2 East of Yamba Lake
3 Contwoyto Monzogranite
4 North of Ghurka Lake
5 Olga Lake Area
6 Pellatt Lake Area
7 Southeast of the Wishbone Dome

Yamba Suite

8 Pellatt Monzogranite
9 Northern Wolverine Monzogranite (Low Y Group)
10 Wolverine Monzogranite
11 Olga Lake Area
12 Cordierite-granite, migmatite north of Wolverine
13 Itchy Lake
14 Wolverine Monzogranite - Lac de Gras Map Sheet

Sample	D241-88	V252-88	V283-88	V308-88	D295-88	D231-89	K124-88	W059-88	D207-88	D208-88	D254-87	D128A-87	D180-87	D182-88
Northing	508227	529379	527722	515565	518815	50 415	500119	504000	491204	490141	458700	481116	471594	476600
Easting	7307988	7289064	7299610	7304169	7306602	7240888	7229426	7223500	7297885	7296320	7312800	7291586	7290901	7311100
Suite	Contwoyto	Contwoyto	Contwoyto	Contwoyto	Contwoyto	Contwoyto	Contwoyto	Contwoyto	Contwoyto	Contwoyto	Contwoyto	Contwoyto	Contwoyto	Contwoyto
Symbol	1	1	1	1	1	2	2	2	3	3	3	3	3	3
SiO2	72.53	71.83	75.46	74.23	74.01	72.54	73.21	74.03	72.93	73 63	72.79	75.69	71.61	74 38
TiO2	0.32	0 24	0.16	0.12	0.08	0.41	0.12	0 12	0.24	0 25	0.24	0 08	0.36	0 08
Al2O3	15.32	15.73	14.19	14.99	14.82	15.06	15.03	14.74	14 77	14.91	14.84	13.98	15.15	14 69
FeO*	1.77	1.41	0.86	0.75	0.85	1.75	0.99	0.87	2.13	1 51	1 56	0.40	2 26	0 99
MnO	0.04	0 03	0 01	0.01	0.01	0.02	0.01	0.01	0.03	0 03	0 02	0.02	0.03	0.01
MgO	0.75	0.47	0.29	0.29	0.28	0.58	0.37	0.29	0.67	0.48	0 50	0 07	0 95	0.27
CaO	1.38	1.86	0.35	0.88	0.63	1.81	0.67	0.72	1.01	0.88	0 81	0 63	2.10	0.83
Na2O	4.92	5.58	3 83	4.15	4.07	4.09	3.77	3 86	3.85	4.05	3.50	4.59	5.10	4.21
K2O	2.92	2.69	4.69	4.34	4.84	3.66	5.57	5.17	4.19	4.12	5.64	4.25	2.31	4 39
P2O5	0.05	0.16	0.16	0.24	0.40	0.08	0 26	0.19	0.18	0.14	0.08	0 28	0.12	0.16
LOI	0.69	0.51	0.83	0.95	0.87	0.52	0.68	0.60	0.82	1.05	0 43	0.49	0.43	0.58
Cr	6	<5	<5	<5	<5		<5	<5	31	<5	<5	<5	<5	<5
Ni	<3	<3	<3	<3	<3		<3	<3	<3	<3	<3	<3	<3	<3
Sc	<3	5	<3	<3	<3		<3	<3	8	<3	<3	<3	4	<3
V	28	41	19	11	6		8	13	<6	8	<6	<6	35	11
Cu	<3	<3	<3	<3	<3		<3	<3	<3	<3	<3	<3	<3	<3
Pb											27			
Zn	15	44	29	<9	32		22	15	26	26	27	14	42	13
Rb	112	64	182	151	290		191	169	180	194	157	280	92	154
Cs											3.4			
Ba	613	283	946	314	314		476	497	511	349	787	153	571	617
Sr	232	876	87	150	87		119	118	139	107	142	39	311	100
Ga	22	21	21	19	26		27	18	23	23	19	17	22	17
Li											44.7			
Nb	4.9	3.7	10.1	6.6	4.7		5.7	6.8	9.3	8.8	12 4	5 0	5.5	6.3
Zr	121	157	72	55	69		76	61	114	81	90	24	146	72
Y	6	6	6	8	8		6	6	14	13	14	7	7	7
Th	7.20	6	21	2.39	6.22		6		7.63	5.97	9.90	1.04	4.66	7
U											3.12			
La	21.67			10.05	12.69				22.29	18.11	18.82	2.63	22.09	
Ce	37.97			19.77	26.39				48.25	41.00	39 90	6 00	43.58	
Pr	4.43			2 41	3.44				6.09	4.80	4.68	0.77	4.66	
Nd	15.86			9.20	12.85				24.25	18.89	17.10	2 94	16 97	
Sm	2.68			2.20	2.82				4.77	4.08	3.53	0 79	2.85	
Eu	0.44			0.55	0.35				0.87	0.69	0.53	0.13	0.72	
Gd	1.92			1.75	1.48				3.45	2.86	2.81	0.66	2 06	
Tb	0.25			0.30	0.13				0.49	0.43	0.32	0.11	0 23	
Dy	1.30			1.38	0.41				2 41	2.21	1.48	0.56	1.06	
Ho	0.22			0.16	0.07				0.43	0.40	0.26	0.10	0 19	
Er	0.58			0.38	0.14				1.03	1.03	0.64	0.29	0.45	
Tm	0.07			0 04	0.02				0.12	0.13	0 08	0 04	0.06	
Yb	0.51			0.18	0.12				0.76	0.97	0 49	0.35	0.36	
Lu	0.07			0.03	0.01				0.11	0.11	0.07	0 05	0.05	

Sample	D190-87	D199-88	D200-88	D202-88	D205-88	D212-88	D213-88	D262-87	D265-87	D266-87	D267-87	K159-88	K181-88	K193-88
Northing	481320	468929	471411	483645	465485	484344	482723	455004	463800	465500	466500	475656	470812	480362
Easting	7293045	7303761	7300580	7305869	7293258	7291614	7292598	7302548	7301800	7301000	7300300	7302343	7309824	7300458
Suite	Contwoyto	Contwoyto	Contwoyto	Contwoyto	Contwoyto	Contwoyto	Contwoyto	Contwoyto	Contwoyto	Contwoyto	Contwoyto	Contwoyto	Contwoyto	Contwoyto
Symbol	3	3	3	3	3	3	3	3	3	3	3	3	3	3
SiO2	73.70	72.85	72.92	75.16	71.17	73.37	73.76	69.71	72.71	70.86	71 65	74.87	75.25	72.77
TiO2	0.20	0.28	0.24	0.04	0.41	0.20	0.25	0.44	0.32	0.32	0.32	0.08	0.08	0.12
Al2O3	14.90	14.91	15.09	14.40	15.54	14.94	14.32	16.12	15.21	16.03	15 32	14.73	14.59	15.50
FeO*	0.97	1.76	1.51	0.68	2.36	1 48	1.90	2.09	1.73	2.14	2 47	0.51	0.87	1.27
MnO	0.01	0.02	0.02	0.01	0.03	0.03	0.03	0.02	0.02	0.03	0.02	0.01	0 01	0.02
MgO	0.41	0.54	0.55	0.33	0.87	0 52	0.51	1.56	0.65	0.90	0.98	0.16	0.26	0.43
CaO	0.61	1.11	1.30	0.45	2.29	1.17	0.96	3.22	1.27	1.35	1.30	0.62	0.58	1.09
Na2O	3.39	4.13	4 05	3.69	5.26	4.16	3.82	4.45	4.10	4.26	4.18	3.69	4.33	4.41
K2O	5.43	4.21	4.13	5.13	1.97	3.97	4.26	2.27	3.87	3.77	3.62	4.95	3.89	4.14
P2O5	0.39	0.18	0.18	0.10	0.10	0.15	0.19	0.11	0.12	0.34	0.13	0.38	0.15	0.26
LOI	0.77	0.66	0.81	0.90	0.62	0.81	0.78	0.54	0.49	0.57	0.68	0.77	0.61	0.83
Cr		8	5		<5	<5	<5		<5	8	<5		<5	<5
Ni		<3	<3		<3	<3	<3		<3	<3	<3	<3	<3	<3
Sc		<3	<3		<3	<3	<3		4	<3	4	<3	<3	<3
V		13	12		34	79	13		19	32	38	<6	<6	9
Cu		<3	<3		<3	<3	<3		<3	<3	<3	<3	<3	<3
Pb								11		28	19			
Zn	14	20	18		29	13	27		33	24	30	<9	<9	11
Rb	[illegible]	112	143		74	200	200	42	131	92	103	128	78	124
Cs								4.9		5.7	4.6			
Ba	[illegible]	612	489		542	549	375		546	795	692	296	459	411
Sr	81	158	138		372	149	111	425	166	214	199	89	89	124
Ga	21	24	24		24	25	25		22	18	19	16	20	21
Li								48.4		58 4	47.4			
Nb	5.7	7 3	8 0		4.0	7.3	8.5	2.2	6.2	7.2	6.7	4 1	2.9	5 0
Zr	79	144	109		171	114	103	180	124	156	181	42	63	97
Y	5	10	9		6	10	12	2	6	9	10	11	6	8
Th	8.00	8.05	8.03		6	6	7	4.32	0.15	12.26	10.45	6	6	6 81
U								1.13		3 32	2 95			
La	15 25	24.98	20.75					21 25	26.99	35.35	26 66			19 06
Ce	34.77	47 08	41.30					39.22	55.15	71.87	54.30			37 86
Pr	4.27	6.06	4.60					4 09	5 96	7 85	5 71			4 30
Nd	16.75	22.78	16.75					14 68	20.66	27.33	19 95			15 48
Sm	3.69	4.16	3 01					2 07	3 49	4 39	3.16			2 79
Eu	0 35	0.63	0 50					1 03	0 24	0 35	0 57			0 45
Gd	2 42	2.60	1.60					1 63	2.22	2 69	2 55			1.89
Tb	0 23	0.34	0.24					0 15	0 21	0 34	0 26			0 27
Dy	0 67	1 55	1.34					0 60	0 93	1.78	1 26			1 42
Ho	0 08	0 25	0 23					0 10	0.15	0 32	0 23			0 25
Er	0 16	0.64	0 59					0.21	0.40	0 77	0.53			0 67
Tm	0 02	0 07	0 10					0.02	0 06	0 12	0 07			0 10
Yb	0 14	0 47	0 62					0 16	0 34	0 62	0 40			0 63
Lu	0.02	0 05	0 11					0 03	0 06	0 08	0 06			0 09

3/4

Sample	R159C-87	V195-88	V203-88	V221-88	K195-88	R037-89	D114-89	D033-87	D035B-87	D057A-87	D059A-87	D081-87	D216-87	K142-87
Northing	475600	481149	478495	466000	479793	584430	579800	457215	457493	463865	463700	455148	469404	475800
Easting	7291500	7305506	7305405	7316500	7294831	7231809	7227400	7257894	7258856	7262069	7262800	7257707	7261381	7226000
Suite	Contwoyto	Contwoyto	Contwoyto	Contwoyto	Contwoyto	Contwoyto	Contwoyto	Contwoyto	Contwoyto	Contwoyto	Contwoyto	Contwoyto	Contwoyto	Contwoyto
Symbol	3	3	3	3	3	4	4	5	5	5	5	5	5	5
SiO2	73.00	73.98	73.27	74.01	74.18	75.79	74.15	73.82	73.45	74.51	76.19	74.58	75.17	72.90
TiO2	0.29	0.08	0.32	0.16	0.16		0.12	0.16	0.12	0.16	0.08	0.04	0.12	0.24
Al2O3	15.23	14.68	14.65	14.72	14.86	14.07	14.41	14.21	15.22	14.07	14.28	14.92	14.48	14.80
FeO*	2.18	0.81	1.75	1.68	0.96	0.34	0.90	1.27	0.99	1.33	0.40	0.77	0.95	1.72
MnO	0.03	0.01	0.02	0.02	0.02	0.01	0.01	0.02	0.02	0.02	0.02	0.02	0.02	0.02
MgO	0.84	0.39	0.59	0.47	0.34	0.12	0.31	0.41	0.32	0.31	0.13	0.22	0.23	0.55
CaO	1.88	0.97	1.26	1.92	0.66	0.99	0.66	1.04	0.63	0.79	1.22	0.70	0.88	1.73
Na2O	5.15	4.22	4.05	4.92	3.60	4.28	3.51	3.51	3.35	3.55	5.08	3.99	3.79	4.24
K2O	1.34	4.49	3.87	2.06	4.94	4.35	5.66	5.34	5.68	5.18	2.60	4.52	4.30	3.63
P2O5	0.06	0.17	0.20	0.03	0.30	0.04	0.27	0.21	0.21	0.07	0.01	0.23	0.04	0.16
LOI	0.60	0.72	0.70	0.54	0.91	0.52	0.47	0.61	0.67	0.57	0.23	0.61	0.63	0.37
Cr	<5		15	<5	<5			<5	<5	<5		<5	<5	<5
Ni	<3		9	<3	<3			<3	<3	<3		<3	<3	<3
Sc	<3		10	<3	<3			<3	<3	<3		<3	<3	<3
V	30		88	13	<6			<6	<6	<6		<6	<6	22
Cu	<3		12	<3	<3			<3	<3	<3		<3	<3	<3
Pb	14									42	25			15
Zn	32		55	25	14			36	19	22		20	16	44
Rb	40	100	107	42	166			201	192	162	85	207	191	116
Cs	7.0									2.2	1.9			0.9
Ba	556		278	408	388			519	551	848	260	290	291	838
Sr	268	133	129	204	75			95	104	113	98	74	119	206
Ga	20		19	21	22			20	17	16	18	18	18	21
Li	73.8									24.8	14.7			29.4
Nb	6.2	3.3	9.3	5.3	7.5			14.4	10.3	10.1	5.2	9.9	13.3	8.4
Zr	153	68	146	113	67			134	69	154	47	41	58	193
Y	6	7	13	5	7			17	14	22	11	11	22	7
Th	6.84	7	14	4	4.31	3.02		0.38		65.26	3.58	4.93	13.47	13.29
U	1.87									13.06	5.35			2.36
La	27.11				10.41	6.83		46.26		55.96	4.10	6.22	13.42	29.25
Ce	51.98				21.49	13.27		93.15		99.30	7.32	12.59	26.32	56.80
Pr	5.35				2.92	1.47		10.32		9.46	0.75	1.46	2.99	5.93
Nd	19.08				12.19	5.34		36.54		30.74	2.56	5.32	10.35	21.02
Sm	3.12				2.78	1.30		7.11		5.73	0.74	1.47	2.48	3.13
Eu	0.63				0.24	0.30		0.14		0.34	0.36	0.19	0.20	0.65
Gd	2.57				2.01	1.08		4.67		5.29	0.87	1.52	2.28	2.65
Tb	0.25				0.22	0.13		0.65		0.73	0.16	0.28	0.45	0.24
Dy	1.23				0.96	0.72		3.10		3.64	1.01	1.52	2.85	1.13
Ho	0.21				0.13	0.13		0.52		0.62	0.21	0.26	0.57	0.20
Er	0.48				0.31	0.37		1.36		1.47	0.60	0.61	1.46	0.55
Tm	0.06				0.04	0.04		0.18		0.19	0.10	0.08	0.20	0.07
Yb	0.31				0.23	0.28		1.13		1.24	0.70	0.49	1.27	0.47
Lu	0.04				0.04	0.04		0.17		0.19	0.11	0.08	0.18	0.07

Sample	D107-89	A359-87	D315-87	D316-87	D350A-87	D350B-87	D051-89	D056-89	D153-89	D066-89	D182-89	D095-88	D338-87
Northing	566586	454400	492900	492800	491422	491425	555561	551286	559914	508852	523991	468923	469000
Easting	7211475	7291200	7260900	7260900	7260361	7260361	7231017	7223701	7226569	7209436	7223583	7231345	7231000
Suite	Contwoyto	Contwoyto	Contwoyto	Contwoyto	Contwoyto	Contwoyto	Yamba	Yamba	Yamba	Yamba	Yamba	Yamba	Yamba
Symbol	6	7	7	7	7	7	8	8	8	8	8	9	9
SiO2	74.60	71.93	74.36	75.21	73.55	74.14	74.80	73.16	72.80	72.96	73.90	70.55	73.16
TiO2	0.07	0.20	0.08	0.04	0.08	0.12	0.20	0.16	0.24	0.30	0.26	0.04	0.12
Al2O3	13.84	15.59	14.65	14.74	15.14	14.73	13.83	14.81	14.82	14.85	14.42	13.31	14.53
FeO*	1.30	1.83	0.87	0.72	1.17	1.14	1.18	1.03	1.53	1.91	1.90	0.35	0.90
MnO	0.02	0.01	0.01	0.13	0.02	0.03	0.01	0.01	0.02	0.03	0.02	0.01	0.01
MgO	0.43	0.62	0.18	0.10	0.38	0.35	0.39	0.35	0.54	0.71	0.71	0.08	0.24
CaO	1.18	1.39	0.55	0.24	0.98	0.89	0.61	0.67	0.79	2.01	1.98	0.78	0.75
Na2O	3.58	4.33	3.89	4.76	3.86	4.35	3.32	3.51	3.49	4.28	4.53	2.86	2.91
K2O	4.87	3.91	4.94	3.89	4.65	4.13	5.46	6.19	5.61	2.85	2.11	5.98	7.29
P2O5	0.10	0.19	0.47	0.16	0.17	0.12	0.20	0.11	0.15	0.10	0.16	0.04	0.10
LOI	0.33	0.45	0.65	0.55	0.46	0.51	0.53	0.57	0.87	0.42	0.65	0.38	0.33
Cr	<5	<5	<5	16	<5	<5	21	6	<5	9		<5	<5
Ni	<3	<3	<3	<3	<3	<3	<3	<3	<3	<3		<3	<3
Sc	<3	3	<3	<3	<3	<3	<3	<3	<3	<3		<3	<3
V	<6	19	<6	<6	<6	<6	<6	13	9	32		<6	<6
Cu	<3		<3	<3	<3	<3	<3	<3	<3	<3		<3	<3
Pb	18	21			21	20	21	40	34	15			
Zn	34	49	15	<9	27	29	51	22	48	51		<9	9
Rb	130	143	195	283	219	238	207	125	252	105		157	260
Cs		8.3			20.4	18.0							
Ba	983	782	417	23	678	547	367	476	596	738		604	1211
Sr	184	211	89	7	141	118	87	100	136	323		115	140
Ga	19	24	15	23	21	19	21	18	23	21		13	16
Li		101.7			116.2	167.0							
Nb	6.3	5.8	6.2	12.7	11.8	11.3	6.6	2.4	10.7	7.8		2.0	7.6
Zr	147	179	43	28	97	93	87	119	137	139		26	67
Y	4	6	3	12	7	7	1	6	2	6		6	10
Th	11	13.62		3.39	16.12	16.50	13	15.12	28.43	7.03		4.64	16.08
U	4	4.45			6.34	12.42	12	7.05	3.05	4.01			
La		34.73		2.37	26.61	26.34		28.72	32.43	31.86	42.61	8.19	20.98
Ce		72.16		5.75	50.28	49.91		62.92	77.42	67.90	80.98	13.43	36.45
Pr		7.93		0.72	5.12	5.04		7.53	9.80	7.75	8.31	1.39	3.77
Nd		28.74		2.47	17.52	16.62		28.16	37.14	27.50	28.14	4.76	12.72
Sm		4.84		0.84	3.01	2.98		5.18	8.03	4.42	3.77	1.06	2.35
Eu		0.60		0.01	0.33	0.43		0.50	0.54	0.88	0.95	0.34	0.41
Gd		3.15		0.81	2.55	2.66		3.12	4.67	2.87	2.46	0.66	1.94
Tb		0.27		0.21	0.26	0.24		0.31	0.44	0.28	0.20	0.10	0.26
Dy		1.13		1.47	1.10	1.05		1.47	1.53	1.34	0.91	0.58	1.25
Ho		0.18		0.28	0.17	0.16		0.23	0.21	0.20	0.16	0.14	0.21
Er		0.41		0.78	0.4.	0.36		0.59	0.50	0.50	0.38	0.36	0.49
Tm		0.06		0.13	0.05	0.06		0.07	0.06	0.10	0.05	0.05	0.06
Yb		0.33		1.02	0.35	0.33		0.41	0.26	0.40	0.45	0.30	0.32
Lu		0.05		0.14	0.05	0.06		0.06	0.05	0.06	0.09	0.04	0.05

Sample	V022-88	W001-88	D007A-88	D007B-88	D081-88	R051E-88	D055-88	D063-88	D077-88	D078A-88	D117-88	D132-88	D134-88	D135-88
Northing	476882	473404	465159	465159	467700	464629	476695	471868	472539	472035	488500	474616	469884	470310
Easting	7236021	7235945	7230007	7230007	7232800	7227342	7225414	7226178	7230937	7230058	7216000	7218075	7218016	7218106
Suite	Yamba	Yamba	Yamba	Yamba	Yamba	Yamba	Yamba	Yamba	Yamba	Yamba	Yamba	Yamba	Yamba	Yamba
Symbol	9	9	9	9	9	9	10	10	10	10	10	10	10	10
SiO2	74.07	75.27	73.30	69.49	70.16	70.05	74.19	75.26	75.12	74.29	72.95	72.28	75.65	74.29
TiO2	0.24	0.16	0.28	0.45	0.24	0.37	0.20	0.24	0.16	0.20	0.28	0.36	0.16	0.24
Al2O3	13.95	13.50	14.17	15.93	16.60	15.69	13.83	12.88	13.68	13.88	13.68	14.17	13.11	13.82
FeO*	1.57	1.17	1.59	2.18	1.82	2.42	1.49	2.00	1.07	1.38	2.51	2.58	1.28	1.68
MnO	0.02	0.01	0.02	0.02	0.02	0.03	0.02	0.02	0.02	0.01	0.02	0.03	0.01	0.02
MgO	0.36	0.29	0.52	0.92	1.01	0.81	0.31	0.40	0.24	0.30	0.51	0.84	0.33	0.36
CaO	1.37	1.17	1.92	2.78	1.32	2.17	0.87	1.39	1.08	1.20	1.17	1.30	0.85	1.14
Na2O	3.40	3.49	3.53	4.67	3.21	4.24	3.15	3.07	3.57	3.34	2.76	3.05	2.96	3.29
K2O	4.94	4.82	4.58	3.38	5.54	4.06	5.91	4.72	5.00	5.35	6.05	5.35	5.63	5.13
P2O5	0.07	0.12	0.09	0.19	0.07	0.16	0.03	0.02	0.04	0.04	0.08	0.04	0.02	0.02
LOI	0.44	0.44	0.77	0.75	0.94	0.40	0.42	0.55	0.40	0.54	0.79	0.83	0.75	0.46
Cr	<5	<5	<5	10	29	<5	<5	<5	<5	<5	<5	16	<5	<5
Ni	<3	<3	<3	<3	8	<3	<3	<3	<3	<3	<3	<3	<3	<3
Sc	<3	<3	<3	<3	<3	<3	<3	<3	<3	<3	<3	4	<3	<3
V	12	10	30	39	44	43	11	15	8	10	27	42	9	16
Cu	<3	<3	<3	<3	<3	<3	<3	<3	<3	<3	<3	<3	<3	<3
Pb														
Zn	17	14	18	43	17	45	11	19	<9	<9	26	34	10	16
Rb	165	109	87	82	108	85	173	165	189	186	198	223	209	185
Cs							1.0							
Ba	737	667	1450	1471	2357	871	475	535	465	680	909	786	554	688
Sr	107	131	412	437	457	342	63	74	67	85	101	137	70	80
Ga	18	17	19	22	17	19	16	16	16	18	18	19	15	17
U														
Nb	13.1	4.7	3.4	4.3	4.9	2.9	12.0	14.9	9.9	10.4	12.2	18.1	12.7	14.1
Zr	162	127	171	236	141	246	112	175	101	143	302	258	126	176
Y	12	10	6	6	8	5	28	15	25	23	23	31	30	18
Th	43	24	15.72	16	7	35.89	18.98	59	27	43.56	85.17	74.84	43	58.98
U														
La			40.88			67.31	1.01			54.58	119.23	107.63		67.12
Ce			77.78			139.76	1.01			103.05	215.41	206.99		128.65
Pr			8.75			15.76	1.01			10.55	22.94	23.17		13.13
Nd			31.58			55.67	1.01			35.87	78.14	79.49		44.09
Sm			4.68			8.04	1.01			6.04	11.49	13.60		7.26
Eu			0.77			1.17	1.01			0.46	0.62	0.96		0.54
Gd			2.67			4.09	1.01			4.48	7.10	9.92		5.54
Tb			0.25			0.31	1.01			0.76	0.87	1.40		0.84
Dy			0.98			1.08	1.01			4.25	4.33	6.92		4.23
Ho			0.15			0.15	1.01			0.82	0.74	1.18		0.72
Er			0.31			0.34	1.01			2.11	1.67	2.43		1.63
Tm			0.03			0.05	1.01			0.27	0.22	0.28		0.18
Yb			0.24			0.26	1.01			1.73	1.40	1.71		1.23
Lu			0.03			0.06	1.01			0.25	0.20	0.24		0.18

Sample	D162-88	D164-88	D169A-88	D170-88	D335-87	K094-88	K105-88	K135-88	K226-88	H028-88	V035-88	V099-88	V102-88	V120-88
Northing	462193	463292	460440	465537	480095	487492	493043	467424	481626	473690	469100	482000	479646	464503
Easting	7219885	7216757	7212986	7211584	7219287	7221967	7212444	7212528	7242087	7228690	7226600	7221600	7224271	7223581
Suite	Yamba	Yamba	Yamba	Yamba	Yamba	Yamba	Yamba	Yamba	Yamba	Yamba	Yamba	Yamba	Yamba	Yamba
Symbol	10	10	10	10	10	10	10	10	10	10	10	10	10	10
SiO2	75.55	74.21	73.1[illegible]	75.12	72.14	74.21	69.30	76.93	73.07	75.20	73.66	73.71	75.01	75.55
TiO2	0.20	0.28	0.24	0.16	0.24	0.20	0.61	0.04	0.37	0.12	0.25	0.24	0.20	0 16
Al2O3	13.27	13.77	14.01	13.56	14.71	13.79	14.96	13.11	14.33	13.44	13.89	14.11	13.62	13.00
FeO*	1.27	1.65	2.11	1.41	2.26	1.64	3.71	0.57	1.68	1.18	1 90	1.54	1.12	1.39
MnO	0.01	0.02	0 03	0.01	0.04	0.03	0.04		0.02	0.01	0.01	0.01	0.02	0.02
MgO	0.28	0.39	0.50	0.36	0.53	0.39	0.88	0 07	0.60	0.29	0 48	0.31	0.23	0 50
CaO	0.86	1.11	1.32	1.28	1 28	1.19	2.26	1.13	0 94	0 98	1.08	1.12	0.94	0.31
Na2O	3.43	3.03	2.99	3.35	3.19	3.62	3.01	3.39	3.10	3.28	2 97	3.17	3.18	2.37
K2O	5.08	5.48	5.54	4.68	5.54	4.81	4.99	4.73	5.77	5.34	5.69	5.71	5 64	6.40
P2O5	0.05	0 05	0 11	0.06	0.07	0.11	0.24	0.04	0.12	0 15	0 06	0 08	0.04	0.30
LOI	0.42	0.70	0.56	0.40	0.59	0.55	0.89	0.28	0.73	0.43	0.49	0.47	0.54	0.87
Cr	<5	<5		<5	<5	<5	<5	<5	<5	<5	<5	<5	<5	<5
Ni	<3	<3		<3	<3	<3	<3	<3	<3	<3	<3	<3	<3	<3
Sc	<3	<3		<3	3	<3	6	<3	<3	<3	<3	<3	<3	
V	7	12		12	18	15	48	6	14	10	20	<6	6	14
Cu	<3	<3		<3	<3	<3	<3	<3	<3	<3	<3	<3	<3	<3
Pb														
Zn	11	12		14	23	33	42	<9	23	<9	18	9	10	10
Rb	184	169		239	226	193	150	160	144	169	165	199	216	208
Cs														
Ba	446	785		605	590	704	1433	403	571	507	717	697	717	547
Sr	63	100		86	70	111	190	66	131	79	91	82	86	78
Ga	16	16		20	18	19	19	17	17	14	17	20	17	16
Li														
Nb	12 2	19.4		18.5	16.6	14 5	16.4	4 7	5.9	9.4	12.3	11.6	11.8	17.5
Zr	124	183		139	206	145	509	51	172	117	200	162	108	164
Y	25	13		24	35	21	22	17	16	17	20	20	20	83
Th	34	59		40		35	50.91	17	54	38	54	60	36	60 73
U														
La							136.65							63.05
Ce							259.73							127.44
Pr							27.34							13 31
Nd							91 31							45 87
Sm							13.38							9.53
Eu							1 32							0 55
Gd							8.15							8 79
Tb							1.00							1.75
Dy							4 89							12 50
Ho							0 86							3 03
Er							1 95							8 92
Tm							0 24							1 24
Yb							1 47							7 [illegible]7
Lu							0 20							1 07

Sample	V126-88	V132-88	V157-88	V168-88	V169-88	W025-88	W080-88	D060-88	D238-87	A294-87	K028B-87	K028A-87	D114-87	K022-88
Northing	467606	465602	464700	475000	474589	480095	481141	471871	452505	454427	460021	460021	473300	462705
Easting	7222396	7219650	7220000	7256000	7208769	7219289	7209641	7223493	7269943	7313219	7260359	7260359	7254000	7228258
Suite	Yamba	Yamba	Yamba	Yamba	Yamba	Yamba	Yamba	Yamba	Yamba	Yamba	Yamba	Yamba	Yamba	Migmatite
Symbol	10	10	10	10	10	10	10	10	11	11	11	11	11	12
SiO2	75.85	75.38	73.82	74.55	75.85	75.50	74.67	73.25	74.71	74.56	74.05	78.32	70.63	75.19
TiO2	0.16	0.16	0.29	0.16	0.16	0.20	0.16	0.20	0.16	0.16	0.16	0.04	0.53	0.08
Al2O3	13.33	13.61	13.97	13.64	13.36	12.90	13.78	14.63	13.84	14.11	14.44	12.30	14.61	13.62
FeO*	0.94	1.16	1.56	1.53	1.13	1.76	1.50	1.70	1.45	1.25	1.22	0.26	2.82	0.84
MnO	0.02	0.01	0.02	0.03	0.01	0.02	0.01	0.03	0.05	0.01	0.02	0.01	0.02	0.01
MgO	0.23	0.29	0.34	0.31	0.19	0.33	0.31	0.39	0.32	0.44	0.33	0.07	0.72	0.41
CaO	0.85	0.71	1.14	0.78	0.82	1.03	1.15	0.89	1.12	0.81	0.65	0.12	1.50	0.52
Na2O	3.06	3.23	3.22	3.10	3.47	2.90	3.28	3.38	3.45	3.61	3.47	3.33	3.03	2.60
K2O	5.51	5.39	5.61	5.86	4.96	5.28	5.00	5.49	4.89	4.93	5.63	5.55	5.89	6.63
P2O5	0.04	0.04	0.04	0.04	0.05	0.07	0.13	0.04	0.01	0.13	0.03		0.24	0.09
LOI	0.45	0.75	0.49	0.59	0.47	0.60	0.41	0.65	0.54	0.48	0.57	0.41	0.85	0.72
Cr	<5	<5	<5	<5	<5	<5	<5	<5	<5	<5	<5		<5	<5
Ni	<3	<3	<3	<3	<3	<3	<3	<3	<3	<3	<3		<3	<3
Sc	<3	<3	<3	<3	<3	<3	<3	<3	<3	<3	3		<3	<3
V	<6	<6	12	12	9	12	<6	15	<6	<6	<6		26	15
Cu	<3	<3	<3	<3	<3	<3	<3	<3	<3	<3	<3		<3	<3
Pb										28	39	20	36	
Zn	<9	<9	16	16	20	14	11	14	17	14	31		53	<9
Rb	167	224	234	295	181	201	196	221	198	122	194	175	207	137
Cs										2.9	4.8	3.0	0.8	
Ba	405	490	608	610	501	835	415	658	619	595	654	299	1090	1238
Sr	68	73	81	67	34	68	92	87	82	119	91	67	120	268
Ga	16	19	17	17	18	17	21	18	15	16	17	12	19	14
Li										31.6	25.9	5.9	17.0	
Nb	8.3	14.7	17.3	23.6	12.7	13.5	11.3	21.1	15.1	6.9	11.7	6.8	12.3	5.6
Zr	108	118	172	124	135	160	139	156	133	133	128	23	408	98
Y	22	19	36	50	58	19	16	26	18	27	25	21	18	37
Th	30	37	63	53	34.20	57	23	41.44	53.40	22.24	41.19	8.46	120.02	119.79
U										5.22	15.19	3.56	3.97	
La					36.68			52.48	48.62	40.05	40.52	6.54	122.87	126.25
Ce					73.60			103.72	75.53	87.26	82.88	13.96	250.94	275.21
Pr					8.12			9.27	6.75	9.56	9.00	1.61	27.21	31.63
Nd					28.33			30.32	20.70	35.04	31.90	6.05	95.15	113.03
Sm					6.00			5.19	3.22	6.67	6.48	1.42	14.84	22.83
Eu					0.29			0.39	0.34	0.74	0.31	0.22	0.95	1.39
Gd					6.28			3.71	2.88	6.04	5.22	1.60	10.62	19.03
Tb					1.29			0.51	0.41	0.75	0.69	0.32	0.97	17.74
Dy					8.85			2.55	2.54	3.70	3.44	2.20	4.05	2.24
Ho					2.00			0.43	0.54	0.62	0.62	0.49	0.67	9.66
Er					5.91			0.98	1.48	1.47	1.62	1.39	1.51	1.33
Tm					0.60			0.12	0.23	0.19	0.22	0.22	0.19	2.49
Yb					6.06			0.82	1.61	1.32	1.49	1.57	1.00	0.8[illegible]
Lu					0.90			0.12	0.26	0.18	0.21	0.23	0.16	0.12

Sample	D224-88	D152-88	D153-88	D155-88	D156-88
Northing	65°28'	Lac des	Lac des	Lac des	Lac des
Easting	112°28'	Gras Sheet	Gras Sheet	Gras Sheet	Gras Sheet
Suite	Yamba	Yamba	Yamba	Yamba	Yamba
Symbol	13	14	14	14	14
SiO2	73.38	75.06	72.11	75.60	75.60
TiO2	0.32	0.33	0.37	0.24	0.24
Al2O3	13.95	13.85	14.77	13.11	13.11
FeO*	2.20	1.63	1.54	1.59	1.59
MnO	0.05	0.01	0.02	0.01	0.01
MgO	0.50	0.44	0.63	0.47	0.47
CaO	1.46	1.32	1.49	0.67	0.67
Na2O	3.30	3.86	3.35	2.86	2.86
K2O	4.75	3.46	5.65	5.41	5.41
P2O5	0.10	0.04	0.07	0.05	0.05
LOI	0.54	0.87	0.80	0.75	0.75
Cr	<5	<5	<5	<5	<5
Ni	<3	<3	<3	<3	<3
Sc	<3	<3	<3	<3	<3
V	16	26	20	23	13
Cu	<3	<3	<3	<3	7
Pb					
Zn	27	27	17	16	12
Rb	178	67	110	134	193
Cs					
Ba	993	642	798	878	474
Sr	137	211	205	250	64
Ga	18	18	16	18	20
Li					
Nb	12.4	5.0	5.4	3.3	13.7
Zr	211	147	217	183	141
Y	16	5	5	8	18
Th	42	22.91	64.37	19	46
U					
La		33.65	16.45		
Ce		73.46	31.15		
Pr		8.62	3.86		
Nd		32.73	15.27		
Sm		6.57	2.84		
Eu		0.68	1.29		
Gd		3.67	1.84		
Tb		0.31	0.21		
Dy		1.10	0.90		
Ho		0.16	0.15		
Er		0.32	0.45		
Tm		0.04	0.05		
Yb		0.34	0.36		
Lu		0.05	0.07		

Appendix 2
Geochemical Data Base
Pre–Yellowknife Supergroup
Acasta Gneiss

Sample	D217–88	D214–88	D216–88	D215–88
	115°36'	115°36'	115°36'	115°36'
	65°25'	65°25'	65°25'	65°25'
RockType	Pre–YKS	Pre–YKS	Pre–YKS	Pre–YKS
SiO2	46.22	75.92	49.29	72.27
TiO2	3.03	0.08	2.85	0.36
Al2O3	16.70	13.46	12.30	14.15
FeO*	14.74	1.05	18.50	2.32
MnO	0.28	0.02	0.33	0.03
MgO	4.68	0.39	4.68	0.62
CaO	8.32	2.85	7.79	1.66
Na2O	2.84	4.27	1.96	3.73
K2O	1.85	0.96	1.07	3.75
P2O5	0.01	0.00	0.06	0.05
LOI	1.32	0.39	1.16	1.06
Cr	<5	<5	<5	<5
Ni	<3	<3	<3	<3
Sc	48	<3	10	<3
V	13	<6	652	23
Cu	<3	<3	68	<3
Pb				
Zn	88	<9	103	24
Rb	38	15	13	46
Cs				
Ba	245	202	341	1747
Sr	225	331	104	385
Ga	23	18	23	17
Li				
Nb	5.2	2.5	11.0	4.5
Zr	38	104	127	229
Y	12	1.5	27	5
Th	0.68	3.35	1.36	13.29
U				
La	3.95	19.75	17.84	89.88
Ce	8.62	30.21	39.22	147.62
Pr	1.13	2.77	4.87	14.07
Nd	4.99	8.74	20.81	45.01
Sm	1.44	1.03	4.79	5.03
Eu	0.85	0.75	1.53	0.98
Gd	1.64	0.68	4.71	2.66
Tb	0.28	0.10	0.84	0.29
Dy	2.02	0.42	5.52	1.27
Ho	0.43	0.09	1.19	0.23
Er	1.22	0.21	2.96	0.55
Tm	0.16	0.04	0.42	0.08
Yb	1.09	0.20	2.84	0.39
Lu	0.17	0.05	0.41	0.06

Appendix 3

Nd Isotopic Techniques and Data Presentation

Chemical separations were carried out in clean laboratory conditions using reagents doubly distilled in quartz or two-bottle Teflon stills at Memorial University. Approximately 100-300 mg of sample was dissolved in HF-HNO_3 in two stages: 1) initial open beaker dissolution, followed by; 2) 5 days at 220°C in high pressure Teflon bombs. Fluorides were converted to perchlorates which were than dissolved in HCL in two evaporations. Samples were then taken up in 6N HCl, heated to homogenization and split for Nd isotope composition (2/3) and Nd and Sm isotope dilution (1/3) analyses. A mixed ^{150}Nd-^{147}Sm spike was mixed with the ID fraction of the solution which was then evaporated to dryness.

Nd and Sm were separated using a three stage ion exchange procedure. The REE were initially separated in HCl, using 10 ml of Amberlite CG-120 cation exchange resin in 30 cm quartz columns. Ba was then separated from the REE in a small HNO_3 column. Nd and Sm were separated in quartz columns using Teflon powder coated with di-2-ethylhexyl orthophosphoric acid. Typical procedural blanks for Nd and Sm at MUN are less than 200 and 100 picograms (Swinden et al., 1990). Some samples were analyzed by E. Hegner at the Geological Survey of Canada (samples indicated in Table 7.1). Analytical techniques at the G.S.C. are described by Theriault (1990).

Samples were analyzed in static mode on a Finnigan Mat 261 multi-collector mass spectrometer at the G.S.C. in Ottawa. Determinations of LaJolla during the course of analyses yielded $^{143}Nd/^{144}Nd = 0.511862 \pm 19$ (2 SEM, n=69). The two sigma error of the mean for an individual determination of an unknown sample was always less than $15 * 10^{-6}$ on individual ratios; better than the stated external precision.

Epsilon Nd Notation

The notation for Sm-Nd isotopic data used in this thesis follows the notation of DePaolo and Wasserburg (1976). Initial epsilon Nd values ($\epsilon_{Nd(t)}$) compare the initial $^{143}Nd/^{144}Nd$ value of a sample to that of the chondritic uniform reservoir.

$$\epsilon_{Nd(I)} = [(^{143}Nd/^{144}Nd_{(I)\ sample}/^{143}Nd/^{144}Nd_{(I)\ CHUR})-1]*10^4,$$

where the subscript (*I*) indicates the time of formation of the sample. $\epsilon_{Nd(I)}$ were calculated using the following reference values for the chondritic reservoir (CHUR): $^{147}Sm/^{144}Nd = 0.1967$; present day $^{143}Nd/^{144}Nd = 0.512638$.

The notation $f_{Sm/Nd}$ compares the $^{147}Sm/^{144}Nd$ ratio of a sample to the CHUR value (0.1967).

$$f_{Sm/Nd} = [^{147}Sm/^{144}Nd_{sample}/0.1967]-1.$$

The one sigma uncertainty in the $\epsilon_{Nd(I)}$ values determined from estimated errors in the relevant isotopic ratios is considered to be less than 1 ϵ_{Nd} unit. A duplicate analyses of one sample yielded a one sigma error in the $\epsilon_{Nd(I)}$ value of ± 1.3, slightly higher than the error assuming only analytical errors. All the error in this case was in the $^{147}Sm/^{144}Nd$ ratio (Table A3.1) and this may in part be attributable to problems in the splitting process. $^{147}Sm/^{144}Nd$ values determined by ICP-MS for selected samples are shown in Table A3.2. The values determined by this method compare favourably with those determined by ID (within 3%) and result in absolute differences in the calculated $\epsilon_{Nd(I)}$ values of less than 1.5 units. The $\epsilon_{Nd(I)}$ values for 5 samples were calculated using the ICP-MS values.

Table A3.1. Duplicate Analyses of Sample D201a-87

Sample	$^{147}Sm/^{144}Nd$ ICP-MS	$^{147}Sm/^{144}Nd$ ID-TIMS	$^{143}Nd/^{144}Nd$	$\epsilon_{Nd(I)}$
D201a-87	-	0.1019	0.511118	+2.2
D201a-87	-	0.1073	0.511118	+0.4
D201a-87	0.1061*	-	-	+0.8

* average of 6; $\sigma = .0036$

Table A3.2 $^{147}Sm/^{144}Nd$ Determined by ICP-MS Compared to TIMS by ID

Sample	$^{147}Sm/^{144}Nd$ ICP-MS	$^{147}Sm/^{144}Nd$ ID-TIMS	Rel Diff	$\epsilon_{Nd(i)}$
D216-87	.1473	.1434	+2.7%	-1.3
	.1434		0.0%	0.0
D072a-87	.0969	.0972	-0.3%	+0.1
	.0988		+1.6%	-0.5
D218-87	.1010	.1045	-3.3%	+1.2
	.1006		-3.7%	+1.4
	.1031		-1.3%	+0.5
	.1045		0.0%	0.0
D278-87	.1307	.1264	+3.4%	-1.5
	.1244		-1.5%	+0.7
	.1293		+2.3%	-1.0

Nd Depleted Mantle Model Ages The Nd depleted mantle model age (T_{DM}) refers to the time at which a sample would have the same ϵ_{Nd} value as the contemporaneous depleted mantle. The depleted mantle has a $^{147}Sm/^{144}Nd$ ratio greater than the chondritic uniform reservoir (CHUR) and evolves to higher ϵ_{Nd} with time. In contrast, samples of the continental crust have $^{147}Sm/^{144}Nd$ ratios less than CHUR and evolve to lower ϵ_{Nd} values with time. The point in time in the past at which the two evolution lines intersect (ie. had the same values) yields the depleted mantle model age. In the simplest case this estimates the integrated average time of separation of the Nd and Sm in the sample from the depleted mantle reservoir (ie. time of crust-mantle differentiation). The age cannot be uniquely interpreted as it may reflect a mixture of crustal material separated from the mantle at various times (e.g. Arndt and Goldstein, 1987). Furthermore, the calculation of $T_{(DM)}$ values assumes that the $^{147}Sm/^{144}Nd$ ratio has not been fractionated by crustal processes (e.g. weathering, sedimentation, partial melting). $T_{(DM)}$ were calculated assuming a linear evolution for the depleted mantle from a CHUR value at earth formation (4.5 Ga) to a present ϵ_{Nd} value of +10 (Goldstein and O'Nions, 1984). T_{DM} values were calculated by projecting from the initial $^{143}Nd/^{144}Nd$ value of a sample along an evolution line of typical crustal $^{147}Sm/^{144}Nd$ (0.1100) to intersect the depleted mantle evolution line. This was done

because the $^{147}Sm/^{144}Nd$ ratio in some of the granites may have been fractionated by high level processes (e.g. pegmatite formation and fluid and mineral fractionation processes).

Appendix 4

Calculation of Bulk D Values for Batch Partial Melting Models and Tables of Kd Values

In quantitative partial melting modelling one of the most sensitive but least constrained parameters is the calculation of the Bulk D value for the residual assemblage. This is largely owing to the difficulty in predicting individual Kd values for, and percentages of residual minerals under varying physical conditions (e.g P, T, volatile content, composition). For this reason partial melting models have been tested using an inverse method (e.g. Smith et al., 1979). The standard batch equilibrium melting equation of Arth (1976) is inverted to solve for D at various degrees of melting (F), using reasonable estimates of source compositions and measured liquid compositions. This method makes no assumptions about individual Kd values or the residual assemblage. This can impose limits on the possible mineralogy of the residual assemblage by comparing D values to those calculated from published Kd values and experimentally determined mineralogy of the source rocks. It is particularly effective for determining the importance of residual phases which strongly fractionate the REE (e.g. garnet). The aim of this modelling is not to advocate the details of a specific model but to demonstrate permissible or non-permissible source rocks and mineralogies.

In other cases standard forward modelling techniques were used (Arth, 1976) utilizing the published Kd values listed in Tables A4.1 to 3. The values were compiled by Dr G.A. Jenner from the following sources: Pearce and Norry (1979); Frey et al., (1978); Nicholls and Harris (1980); Arth and Hanson (1975); Shimizu (1980); Hanson (1978). Values for accessory mineral phases (apatite, zircon, titanite, allanite) are

based on values given by: Fujimaki (1986); Luhr et al. (1984), Brooks et al. (1981). The values used are low relative to some reported values (e.g. Sawka, 1988; Mahood and Hildreth, 1984).

Table A4.1. Partition coefficients (Kd) for basaltic compositions

	Oliv	Opx	Cpx	Amph	Garnet	Plag
K	0.007	0.015	0.03	0.6	0.015	0.17
Rb	0.006	0.02	0.05	0.25	0.02	0.1
Ba	0.006	0.013	0.02	0.09	0.02	0.16
Sr	0.016	0.016	0.165	0.57	0.014	1.8
Th	0.005	0.005	0.02	0.54	0.1	0.01
Nb	0.01	0.15	0.02	0.8	0.1	0.01
Zr	0.01	0.03	0.1	0.5	0.3	0.01
La	0.0005	0.0005	0.02	0.16	0.001	0.18
Ce	0.0008	0.0009	0.04	0.22	0.0033	0.12
Pr	0.001	0.0013	0.062	0.31	0.0075	0.097
Nd	0.0013	0.0019	0.09	0.42	0.0184	0.081
Sm	0.0019	0.0028	0.14	0.75	0.0823	0.067
Eu	0.0019	0.0036	0.16	0.8	0.133	0.34
Gd	0.0019	0.0045	0.18	0.9	0.18	0.063
Dy	0.0019	0.0074	0.193	1.0	0.51	0.055
Y	0.01	0.02	0.5	1.0	2.0	0.025
Er	0.0022	0.013	0.2	1.0	1.6	0.063
Yb	0.004	0.0286	0.2	0.77	4.0	0.067
Lu	0.0048	0.038	0.19	0.66	7.0	0.06
Ni	14	4	3	7	0.8	0.04
Cr	2.1	10	8.4	3	0.1	0.04

Abbreviations: Oliv = olivine; OPX = orthopyroxene; CPX = clinopyroxene; Amph = amphibole; Biot = biotite; Plag = plagioclase.

Table A4.2. Partition coefficients (Kd) for Andesitic compositions

	Oliv	Opx	Cpx	Amph	Biot	Garnet	Plag	Apat	Titan	Zircon	Allan
K	0.01	0.02	0.02	0.33	2.7						
Rb	0.01	0.02	0.02	0.05	0.01	0.01	0.07				
Ba	0.01	0.02	0.02	0.09	1.1	0.02	0.16	0.1			
Sr	0.02	0.02	0.08	0.23	0.08	0.02	1.8	1.8	1.		
Th	0.003	0.15	0.13	0.22	0.31	0.1	0.01	2	17	7	68
Nb	0.01	0.35	0.3	1.3	1.0	0.17	0.025	0.25	142	5	2
Zr	0.01	0.08	0.25	1.4	0.6	0.5	0.03				
La	0.008	0.028	0.25	0.4	0.035	0.28	0.35	14.5	45	1.14	820
Ce	0.009	0.038	0.3	0.51	0.034	0.35	0.24	21.1	87	1.17	635
Pr	0.01	0.048	0.38	0.8	0.033	0.43	0.2	27	120	1.2	550
Nd	0.01	0.058	0.49	1.2	0.032	0.53	0.17	32.8	152	1.38	463
Sm	0.011	0.1	0.7	2.	0.031	2.66	0.13	46.	204	2.03	205
Eu	0.01	0.079	0.87	1.7	0.036	1.5	2.11	25.5	181	0.85	81
Gd	0.012	0.171	0.96	2.5	0.03	10.5	0.09	43.9	220	6.41	130
Dy	0.014	0.293	1.2	3.5	0.03	28.6	0.084	34.8	220	31.4	65
Y	0.01	0.45	1.5	2.5	0.03	11	0.06	20.	104	120	8.9
Er	0.017	0.46	1.2	2.75	0.034	42.8	0.084	22.7	210	64.6	20
Yb	0.023	0.67	0.9	2.	0.042	39.9	0.077	15.4	104	128	8.9
Lu	0.026	0.84	0.8	1.7	0.046	29.6	0.062	13.8	92	196	7.7
Ni	49	8	6	8	20	0.6	0.04				
Cr	4.2	13	30	30	12.6	22	0.04				

Abbreviations: Oliv = olivine; OPX = orthopyroxene; CPX = clinopyroxene; Amph = amphibole; Biot = biotite; Plag = plagioclase; Apat = Apatite; Titan = titanite; Allan = allanite

Table A4.3 Partition coefficients (Kd) for felsic compositions

	Oliv	Opx	Cpx	Amph	Biot	Garnet	Plag	K-spar	Apat	Titan	Zircon	Allan
K	0.0	0.002	0.037	0.08	4	0.01	0.1	1.4				
Rb	0.01	0.003	0.032	0.014	2.24	0.01	0.04	0.366				
Ba	0.01	0.003	0.13	0.04	9.7	0.02	0.31	6.12	0.1			
Sr	0.02	0.085	0.516	0.22	0.12	0 02	4.4	9.4	1.8	1		
Th	0.003	0.16	0.15	0.22	0.31	0.1	.0001	.0001	2	17	7	68
Nb	0.01	0.5	0.4	4	2.3	0.01	0.001	0.001	0.25	142	5	2
La	0.008	0.22	0.32	0.7	28	0.39	0.32	0.05	14.5	45	1.14	820
Ce	0.009	0.15	0.5	1.52	0.32	0.62	0.27	0.04	21.1	87	1.17	635
Nd	0.01	0.22	1.11	4.26	0.29	0.63	0.21	0.025	32.8	152	1.38	463
Zr	0.01	0.15	0.3	4	1.5	1.2	0.1	0.001				
Sm	0.011	0.27	1.67	7.77	0.26	2.2	0.13	0.018	46	204	2.03	205
Eu	0.01	0.17	1.56	5.14	0.24	0.7	2.15	1.13	25.5	181	0.85	81
Gd	0.012	0.34	1.85	10	0.28	7.7	0.097	0.011	43.9	220	6.41	130
Dy	0.014	0.46	1.93	13	0.29	20	0.064	0.006	34.8	220	31.4	65
Y	0.01	0.8	2	6	1.5	35	0.1	0.001	20	104	120	8.9
Er	0.017	0.65	1.66	12	0.35	35	0.055	0.006	22.7	210	64.6	20
Yb	0.023	0.86	1.58	8.4	0.44	43	0.049	0.012	15.4	104	128	8.9
Lu	0.026	0.9	1.54	5.5	0.33	38	0.046	0.006	13.8	92	196	7.7

Abbreviations: Oliv = olivine; Opx = orthopyroxene; Cpx = clinopyroxene; Amph = amphibole; Biot = biotite; Plag = plagioclase; K-spar = alkali feldspar; Apat = Apatite; Titan = titanite; Allan = allanite

Appendix 5

Trace Element Normalizing Values

Normalizing values used for primitive mantle, chondrite and mid-ocean reservoirs are given in Table A5.1. The primitive mantle and MORB values are from data compiled by G.A. Jenner (unpublished). The subscript $_N$ refers to chondrite normalized values.

Table A5.1. Normalizing Values Used in this Thesis

	Primitive Mantle	Chondrite (Taylor and Mclennan, 1985)	MORB
Rb	.55	3.45	1.12
Ba	6.27	3.41	14.3
Th	0.088	0.0425	.185
K	267.	854	955
Nb	0.65	.375	3.58
La	0.63	.367	3.96
Ce	1.59	.957	11.97
Sr	18.9	11.9	122
Pr	0.251	.137	
Nd	1.21	.711	10.96
Zr	9.8	5.54	90
Sm	0.399	0.231	3.62
Eu	0.15	0.087	1.31
Gd	0.533	.306	4.78
Tb	0.0974	0.058	
Ti	1134	654	9000
Dy	0.661	0.381	5.98
Y	3.9	2.25	34.2
Ho	0.148	0.0851	
Er	0.432	0.249	3.99
Tm	0.0676	0.0356	
Yb	0.442	0.248	3.73
Lu	0.066	0.0381	0.56